UNCLASSIFIED

AD NUMBER
AD383738
CLASSIFICATION CHANGES
TO: unclassified
FROM: confidential
LIMITATION CHANGES
TO: Approved for public release, distribution unlimited
FROM: Distribution authorized to U.S. Gov't. agencies and their contractors; Administrative/Operational Use; AUG 1967. Other requests shall be referred to Air Force Rocket Propulsion Lab., Edwards AFB, CA.
AUTHORITY
31 Aug 1979, DoDD 5200.10; AFRPL ltr, 5 Aug 1986

THIS PAGE IS UNCLASSIFIED

THIS REPORT HAS BEEN DELIMITED AND CLEARED FOR PUBLIC RELEASE UNDER DOD DIRECTIVE 5200.20 AND NO RESTRICTIONS ARE IMPOSED UPON ITS USE AND DISCLOSURE.

DISTRIBUTION STATEMENT A

APPROVED FOR PUBLIC RELEASE; DISTRIBUTION UNLIMITED.

GENERAL DECLASSIFICATION SCHEDULE

IN ACCORDANCE WITH
DOD 5200.1-R & EXECUTIVE ORDER 11652

THIS DOCUMENT IS:

CLASSIFIED BY DDC

Subject to General Declassification Schedule of Executive Order 11652-Automatically Downgraded at 2 Years Intervals- DECLASSIFIED ON DECEMBER 31, 73.

BY

Defense Documentation Center
Defense Supply Agency
Cameron Station
Alexandria, Virginia 22314

AD 383 738

AUTHORITY:
AFRPL ltr 5 Feb 66

SECURITY MARKING

The classified or limited status of this report applies to each page, unless otherwise marked.
Separate page printouts MUST be marked accordingly.

THIS DOCUMENT CONTAINS INFORMATION AFFECTING THE NATIONAL DEFENSE OF THE UNITED STATES WITHIN THE MEANING OF THE ESPIONAGE LAWS, TITLE 18, U.S.C., SECTIONS 793 AND 794. THE TRANSMISSION OR THE REVELATION OF ITS CONTENTS IN ANY MANNER TO AN UNAUTHORIZED PERSON IS PROHIBITED BY LAW.

NOTICE: When government or other drawings, specifications or other data are used for any purpose other than in connection with a definitely related government procurement operation, the U. S. Government thereby incurs no responsibility, nor any obligation whatsoever; and the fact that the Government may have formulated, furnished, or in any way supplied the said drawings, specifications, or other data is not to be regarded by implication or otherwise as in any manner licensing the holder or any other person or corporation, or conveying any rights or permission to manufacture, use or sell any patented invention that may in any way be related thereto.

AFRPL-TR-67-75

August 1967

19

AD383738

(TITLE UNCLASSIFIED)
ADVANCED ROCKET ENGINE--STORABLE
PHASE I INTERIM FINAL REPORT

Part 2 of three parts

Sections V through VIII

Prepared by

AEROJET-GENERAL CORPORATION

ADVANCED STORABLE ENGINE PROGRAM DIVISION

LIQUID ROCKET OPERATIONS

SACRAMENTO, CALIFORNIA

Prepared for

AIR FORCE ROCKET PROPULSION LABORATORY

RESEARCH AND TECHNOLOGY DIVISION

AIR FORCE SYSTEMS COMMAND

UNITED STATES AIR FORCE

EDWARDS, CALIFORNIA

DDC

SEP 12 1967

Best
Available
Copy

Report 10830-F-1, Phase I

LEGAL NOTICE

"When U.S. Government drawings, specifications, or other data are used for any purpose other than a definitely related Government procurement operation, the Government thereby incurs no responsibility nor any obligation whatsoever, and the fact that the Government may have formulated, furnished, or in any way supplied the said drawings, specifications, or other data, is not to be regarded by implication or otherwise, or in any manner licensing the holder or any other person or corporation, or conveying any rights or permission to manufacture, use, or sell any patented invention that may in any way be related thereto."

AFRPL-TR-67-75

August 1967

(TITLE UNCLASSIFIED)
ADVANCED ROCKET ENGINE--STORABLE
PHASE I INTERIM FINAL REPORT

Part 2 of three parts

Sections V through VIII

Prepared by

AEROJET-GENERAL CORPORATION

ADVANCED STORABLE ENGINE PROGRAM DIVISION

LIQUID ROCKET OPERATIONS

SACRAMENTO, CALIFORNIA

Prepared for

AIR FORCE ROCKET PROPULSION LABORATORY

RESEARCH AND TECHNOLOGY DIVISION

AIR FORCE SYSTEMS COMMAND

UNITED STATES AIR FORCE

EDWARDS, CALIFORNIA

GROUP 4

DOWNGRADED AT 3 YEAR INTERVALS; DECLASSIFIED AFTER 12 YEARS

"THIS DOCUMENT CONTAINS INFORMATION AFFECTING THE NATIONAL DEFENSE OF THE UNITED STATES WITHIN THE MEANING OF THE ESPIONAGE LAWS, TITLE 18, U.S.C., SECTIONS 793 AND 794. ITS TRANSMISSION OR THE REVELATION OF ITS CONTENTS IN ANY MANNER TO AN UNAUTHORIZED PERSON IS PROHIBITED BY LAW"

6798T

AEROJET-GENERAL CORPORATION

A SUBSIDIARY OF THE GENERAL TIRE & RUBBER COMPANY

Report 10830-F-1, Phase I

FOREWORD

This report reviews the technical accomplishments of the ARES Advanced Development Program, Contract AF 04(611)-10830, from 1 July 1965 through 27 January 1967. The work during this period was directed primarily toward demonstrating the feasibility of advanced components and subsystems considered critical to the integrated engine module design. Analysis, design, fabrication, and test activities are summarized.

All work was performanced by Liquid Rocket Operations of Aerojet-General Corporation for the Air Force Rocket Propulsion Laboratory at Edwards Air Force Base, California. Mr. R. Beichel is the Aerojet Program Manager, and Mr. C. W. Hawk is the Air Force Program Manager.

This report has been divided into three separate parts for ease of handling.

This technical report has been reviewed and is approved.

C. W. Hawk
USAF Program Manager

Report 10830-F-1, Phase I

UNCLASSIFIED ABSTRACT

(U) This report summarizes the Phase I work on Contract AF 04(611)-10830 through 27 January 1967.

(U) The objective of the program was to demonstrate in two phases the engineering practicality and performance characteristics of a high chamber pressure, staged combustion engine module. Before the complete engine can be assembled and tested in Phase II, a Phase I effort must demonstrate the feasibility of several features considered critical to the engine design.

(U) The Phase I program to date has accomplished the following:

a. Established master layouts for both an advanced engine design and for a relatively more conservative back-up version of the engine.

b. Established a master layout for a very large thrust propulsion system utilizing 20 engine modules in a cluster, with all modules exhausting into a single large forced deflection nozzle.

c. Detail designed all the engine components.

d. Demonstrated a successful primary injector and combustion chamber for production of the turbine drive gas.

e. Demonstrated transpiration cooled chambers that can apparently meet contractual performance goals when a suitable secondary injector is evolved.

f. Demonstrated the feasibility of lubricating turbopump bearings with the storable propellants used in the engine.

UNCLASSIFIED ABSTRACT (cont.)

g. Demonstrated pump wear ring designs that permit operation at very close clearance with little or no explosion hazard from pump rub.

h. Demonstrated the suitability of high pressure multiple purpose housings for the turbopump and primary combustion chamber assembly.

i. Developed and demonstrated satisfactory propellant flow control components for the full-scale engine.

j. Completed several supporting studies that provide additional design criteria in such areas as nozzle Aerodynamics, low frequency stability, fluid flow characteristic of propellant and turbine drive-gas passage, and design changes required for conversion to advanced storable propellants.

(U) Remaining Phase I technical goals are conclusion of 60 sec of simulated engine operation with the hydrostatic combustion seal, and three 20-sec firings of a cooled combustion chamber at contractually required specific impulse or higher. The current effort to achieve a high performance, streak free secondary injector must be completed before the cooled thrust chamber demonstration can take place.

Report 10830-F-1, Phase I

TABLE OF CONTENTS

Part 1

		Page
I.	Introduction	I-1
II.	Summary	II-1
	A. Engine and Propulsion System Design	II-1
	B. Turbopump Assembly	II-1
	C. Thrust Chamber Assembly	II-8
	D. Controls	II-16
	E. Supporting Studies	II-18
III.	Module	III-1
	A. Objective and Approach	III-1
	B. Propulsion System	III-5
	C. Engine Module, Advanced Turbopump	III-8
	D. Engine Module, Conservative Turbopump	III-15
IV.	Turbopump Assembly	IV-1
	A. Summary	IV-1
	B. T-Design Turbopump	IV-7
	C. Engine Housing, T-Configuration	IV-41
	D. Backup Turbopump	IV-79
	E. Engine Housing, In-line Configuration	IV-112
	F. Boost Pump	IV-124
	G. Propellant - Lubricated Bearings	IV-136
	H. Pump Wear Rings	IV-158
	I. Combustion Seal	IV-183

Part 2

V.	Primary Combustor Assembly	V-1
	A. Objective	V-1
	B. Summary	V-1
	C. Component Design	V-2
	D. Development Testing	V-7

TABLE OF CONTENTS (cont.)

Part 2 (cont.)

		Page
VI.	Secondary Combustion Program	VI-1
	A. ICP Residual Hardware Program	VI-1
	B. Modular Secondary Injector Program	VI-25
	C. Modular-Cooled Chamber Program	VI-52
	D. Uncooled Two-Dimensional Nozzle Program	VI-116
VII.	Controls	VII-1
	A. Introduction	VII-1
	B. Suction Valve	VII-2
	C. Fuel Controls	VII-15
	D. Suction and Feed Lines	VII-29
	E. Conclusions	VII-31
VIII.	Supporting Studies	VIII-1
	A. Module Fluid Dynamic Testing	VIII-1
	B. Subscale Nozzle Program	VIII-11
	C. Advanced Propellants	VIII-29
	D. Analytical Models	VIII-32
	E. Reliability	VIII-47

Part 3 (APPENDIXES)

	Appendix
ARES Engine Handbook	I
Suction Valve Storage Seal and Cutter Development	II
Advanced Propellants	III

TABLE LIST

	Table
Test Requirements and Results of the Suction Valve	VII-1

FIGURE LIST

	Figure
Propulsion System, 20-Module Forced Deflection Nozzle	III-1
Advanced Storable Engine--Demonstrator	III-2
ARES Module Subassembly	III-3
ARES Module, External View	III-4
ARES System Staged Combustion Cycle	III-5
"C" Design TPA Layout	IV-1
Oxidizer Pump Design Data	IV-2
Fuel Pump Design Data	IV-3
TPA Water Test Sequence	IV-4
Turbine Design Data	IV-5
Air Test Turbine Photos	IV-6
Turbine Mod. I and Mod. II Configurations	IV-7
Air Test Setup	IV-8
Turbine Weight Flow & Effeciency vs Pressure Ratio	IV-9
Turbine Efficiency vs Pressure Ratio and Speed	IV-10
Mod. I Rotor Discharge Survey	IV-11
Ball Bearing Life vs Load	IV-12
Bearing Thrust Load vs Time - Engine Start Transient	IV-13
Roller Bearing Life vs Misalignment	IV-14
TPA Filter Pressure Drop Data	IV-15
Metal Model I	IV-16a
Metal Model II	IV-16b
Metal Model Bearing Axial Displacement	IV-16c
Metal Model Diametral Expansion	IV-16d
Metal Model I Test Results	IV-17
Photo Elastic Model Longitudinal and Lateral Section Stresses (Four Views)	IV-18

FIGURE LIST (cont.)

	Figure
Housing A	IV-19
Housing A Rib Pattern	IV-20
Housing A Hydrotest Pressure Zones	IV-21
Housing A Hydrotest Assembly	IV-22a
Stress at Test, View 1; Pressure Test, View 2	IV-22b
Housing A Pressure and Thrust Proof Test Results	IV-23
Vibration Test Results	IV-24a
Vibration Test Results	IV-24b
Two Walled Housing	IV-25
Housing B	IV-26
Oxidizer Dome Parameter vs Displacement	IV-27
Housing C Rib Pattern	IV-28
Configuration Survey	IV-29
Pump Efficiency vs Specific Speed	IV-30
Turbine Efficiency vs Design Speed	IV-31
Inline TPA Weight vs Design Speed	IV-32
Inline TPA Cross Section	IV-33
Turbine Cross Section	IV-34
Inline Turbopump (Two Views)	IV-35
Inline Turbopump Housing	IV-36
Inline Turbopump Housing Hydrotest Assembly	IV-37
Inline Turbopump Housing (Pressure Zones and Test Setup)	IV-38
Location of Displacement of Inline Turbopump Housing Bearing, (Pressure Diagram and Pressure and Thrust Proof Curves)	IV-39
Inline Turbopump Housing Vibration Test Results	IV-40

FIGURE LIST (cont.)

	Figure
Boost Pump Operation Requirements	IV-41
Oxidizer Boost Pump Layout	IV-42
Fuel Boost Pump Layout	IV-43
Oxidizer Boost Pump Axial Thrust	IV-44
25,000 rpm Posttest Bearings Cages - N_2O_4 Lubricated	IV-45
Summary of 25,000 rpm Bearing Tests in N_2O_4	IV-46
40,000 rpm Bearing Tester	IV-47
Ball Bearing Cage Designs	IV-48
Roller Bearing Cage Designs	IV-49
Summary of 40,000 and 31,250 rpm Bearing Tests in N_2O_4	IV-50
31,250 rpm Posttest Bearings - N_2O_4 Lubricated	IV-51
Summary of 40,000 and 31,250 rpm Bearing Tests in AeroZINE 50	IV-52
31,250 rpm Posttest Bearings - AeroZINE 50 Lubricated	IV-53
Test Data Plot - 40,000 rpm N_2O_4 Lubricated Bearing Test 1.2-03-WAW-006B	IV-54
40,000 rpm Posttest Bearings - N_2O_4 Lubricated	IV-55
40,000 rpm Posttest Bearings - AeroZINE 50 Lubricated	IV-56
Wear-Ring Configurations Selected for Propellant Testing	IV-57
Oxidizer-Pump Efficiency Loss as a Function of Wear-Ring Radial Clearance	IV-58
Retention Mechanisms for Straight-Labyrinth Inert Inserts	IV-59
Design Parameters of the Hydrostatic Face Wear-Ring Seal	IV-60
Design Parameters of the Hydrostatic Journal Wear-Ring Seal	IV-61
Wear-Ring Tester	IV-62
Typical Wear-Ring Test Installation and Nomenclature	IV-63
N_2O_4 Wear-Ring Test Summary -- Hydrostatic Face Seal and Vespel SP-21 Labyrinth Insert	IV-64
AeroZINE 50 Wear-Ring Test Summary-Kynar and Kel-F Labyrinth Inserts	IV-65
Water-Flow Data from Nonrotating and Rotating Straight-Labyrinth Tests	IV-66
Stepped-Labyrinth Water-Flow Data	IV-67
Water and N_2O_4 Flow Data for Hydrostatic Face Seal with Correlation with Estimated Flows	IV-68

FIGURE LIST (cont.)

	Figure
Post-Test Photograph of Hydrostatic Journal Seal and Water-Test Data	IV-69
Water-Flow Data for Hydrostatic Journal Seal Correlated with Estimated Flows	IV-70
Stiffness and Clearance of Hydrostatic Face Seal as a Function of Impeller Angular Deflections	IV-71
Combustion Concept of Seal	IV-72
Bellow Stresses Under Operative Condition	IV-73
2-D Seal Tester and Flow Diagram	IV-74a
2-D Test Segment	IV-74b
2-D Test Summary	IV-75
2-D Test Data -- Test 030	IV-76
Flow Diagram, Hot Tests	IV-77
Cold Rotating Test Summary	IV-78
Start Transient Simulation	IV-79
Data Plots Test 14	IV-80
Hydrostatic Combustion Seal in Tester	IV-81
Hot Testing Test Summary	IV-82
Post-Test Photograph of Seal Test 14	IV-83
Purge Seal in ARES TPA	IV-84
ARES Purge Seal Flowrate & Temperature Rise vs Viscosity (changed)	IV-85
Purge Fluid Viscosity vs Pressure	IV-86
Purge Seal in Tester	IV-87
Flow Diagram	IV-88
Test Summary	IV-89
Purge Seal Test Data (added)	IV-90
Final Configuration of the Primary Combustor	V-1
Work Statement Requirement and Experimental Test Results	V-2
Primary Combustor Components	V-3
Full-flow and Quadlet Injectors	V-4
Pentad Injector	V-5
Primary Combustor Housing and Combustion Chamber Liner	V-6

FIGURE LIST (cont.)

	Figure
Primary Combustor Burnoff Stack Duct and Injector	V-7
Test Configuration and Data Summary	V-8
Primary Combustor Test Setup	V-9
Typical Oscillograph, Start Transient and Steady State	V-10
Quadlet Injector and Liner Vane Assembly Posttest 1.2-04-WAG-006	V-11
Turbulator Ring, Vane Assembly Pretest 1.2-04-WAG-008	V-12
Chamber Pressure Oscillation Characteristic 1.2-03-WAG-007, -008, -009, -010	V-13
Injector and Turbulator Vane Assembly Posttest 1.2-04-WAG-010	V-14
Quadlet Injector Posttest 1.2-04-WAG-012	V-15
Canted Blade Turbulators	V-16
Full Flow Injector-Turbulator Vane Assembly Posttest 1.2-04-WAG-017	V-17
Quadlet Injector Posttest 1.2-04-WAG-018	V-18
Turbulator-Solid Triangular Inner Ring, Notched Triangular Outer Ring	V-19
Combustion Loss Versus Chamber L*	VI-1
Film Cooling Performance Degradation Versus Film Coolant Flow	VI-2
Mark 32 Secondary Injector	VI-3
Mark 125 Secondary Injector	VI-4
Mark 20 Primary Injector	VI-5
Uncooled Ablative Chambers, 20 and 45 L*	VI-6
Photograph of Regenerative Chamber Installed on Test Stand H-2	VI-7
Capillary Tube Chamber	VI-8
Hydraulic Test of Regenerative Chamber SN R-6	VI-9
Multiple Orifice Film Coolant Ring	VI-10
Multiple Tube Film Coolant Ring	VI-11
Pump-Feed Staged-Combustion Test Engine	VI-12
Intensifier System Schematic with Sector Engine	VI-13
ICP Residual Hardware Program Performance Summary	VI-14

FIGURE LIST (cont.)

	Figure
Postfire Condition Mark 32 Injector	VI-15
Postfire Condition Mark 125 Injector	VI-16
Injector Chamber Configuration L* Evaluation Series	VI-17
Prefire Photograph of Film Coolant Ring - Looking Upstream Through the Nozzle Throat	VI-18
Postfire Photographs of SN4 Regenerative Test	VI-19
Thermocouple Data from ICP Film-Cooled, Ablative Chamber Tests (Test Series 1.2-07-WAM)	VI-20
Test Parameters for ICP Chamber Tests	VI-21
Chamber Wall Temperatures for Test 1.2-07-WAM-009	VI-22
Chamber Wall Temperatures for Test 1.2-07-WAM-010	VI-23
Chamber Wall Temperatures for Test 1.2-07-WAM-011	VI-24
Regenerative Coolant Bulk Temperature, Test 1.2-08-WAM-002	VI-25
Regenerative Coolant Bulk Temperature, Test 1.2-08-WAM-003	VI-26
Modular Configuration--Mark 125 Injector	VI-27
Turbopump-Injector-Cooled Chamber Interface	VI-28
Fuel Swirl Rake Injector	VI-29
Uncooled Ablative Thrust Chambers of Different L*'s	VI-30
Uncooled Instrumented Thrust Chamber Schematic	VI-31
Test Stand Adapter	VI-32
Modular Secondary Injector Performance Summary	VI-33
Typical Oscillograph, Secondary Injector Test	VI-34
Injector-Chamber Interface Development	VI-35
Mixture Ratio Distribution Effects	VI-36
Effect of Characteristic Length on Combustion Loss	VI-37
Mark 125 Injector Vanes	VI-38
Mark 125 Secondary Injector Performance Certification	VI-39
Effects of Oxidizer Film Coolant on the Performance of the ARES Thrust Chamber	VI-40
Modified Rake Injector	VI-41
Thermocouple Data for Test No. 1.2-11-WAM-018	VI-42
Thermocouple Data for Test No. 1.2-11-WAM-019	VI-43

FIGURE LIST (cont.)

	Figure
Film Temperatures for Test No. 1.2-11-WAM-018	VI-44
Cooled Chamber Predicted Temperatures	VI-45
Regeneratively Cooled Combustion Chamber	VI-46
Regeneratively Cooled Combustion Chamber	VI-47
Flow Characteristics of Capillary Regenerative Chambers	VI-48
Flow Characteristics of Noncapillary Regenerative Chambers	VI-49
Capillary Tube Installation	VI-50
Total Pressure Distribution for ARES Regenerative Chambers	VI-51
Regenerative Coolant Capability	VI-52
ARES Chamber Heat Load	VI-53
ARES Chamber Wall Temperatures	VI-54
Film Cooling Requirements for ARES Chambers	VI-55
Performance Potential in ARES Chambers	VI-56
Uncoated 0.040-in. Capillary Tube Heat Flux Capability	VI-57
Uncoated 0.045-in. Capillary Tube Heat Flux Capability	VI-58
Uncoated 0.050-in. Capillary Tube Heat Flux Capability	VI-59
Typical Inconel 718 Tubing Defect	VI-60
Typical Inconel 718 Tubing Defect	VI-61
Selection of Transpiration Chamber Wall Material	VI-62
Transpiration Cooled Combustion Chamber	VI-63
Transpiration Cooled Combustion Chamber	VI-64
Layout of Transpiration Cooled Chamber	VI-65
Sectional Washer Pairs for Transpiration Chambers	VI-66
Summary of ARES Transpiration Cooled Chamber Assembly (Flow Rates, Supply Pressure and Wall Temperatures)	VI-67
Advanced Thermal Model	VI-68
Transpiration Coolant Flow Rates vs Axial Distance (1500°F Wall)	VI-69
Throat Wall and Coolant Temperatures vs Transpiration Coolant Flow Rates	VI-70
Transpiration Coolant Flow Rates vs Axial Distance (1900°F Wall)	VI-71

FIGURE LIST (cont.)

	Figure
Transpiration Chamber Wall Temperatures vs Coolant Flow Rate (Compartment 1-4)	VI-72
Transpiration Chamber Wall Temperatures vs Coolant Flow Rate (Compartment 5-7)	VI-73
Transpiration Chamber Wall Temperatures vs Coolant Flow Rate (Compartment 8-10)	VI-74
Transpiration Chamber Wall Temperatures vs Coolant Flow Rate (Compartment 11 and 12)	VI-75
Radial Wall Temperature Distribution in ARES Transpiration Cooled Chamber	VI-76
Radial Wall Temperature Distribution in ARES Transpiration Cooled Chamber	VI-77
Transpiration Chamber Flow Data Summary (Chamber SN 001)	VI-78
Transpiration Chamber Flow Data Summary (Chamber SN 002)	VI-79
Transpiration Chamber Test Data and Performance Summary	VI-80
Transpiration Cooled Chamber Intensifier Fed Test Schematic	VI-81
Transpiration Chamber Postfire Conditions (Test 1.2-12-WAM-002)	VI-82
Transpiration Chamber Postfire Conditions (Test 1.2-12-WAM-012)	VI-83
Transpiration Chamber Postfire Conditions (Test 1.2-12-WAM-024)	VI-84
Transpiration Chamber Postfire Conditions (Test 1.2-12-WAM-030)	VI-85
Regenerative Chamber Postfire Conditions (Test 1.2-14-WAM-002)	VI-86
Regenerative Chamber Postfire Conditions (Test 1.2-14-WAM-005)	VI-87
Predicted ARES Performance	VI-88
Percent Film Coolant Loss vs Percent Coolant Flow (Test Series 1.2-12-WAM)	VI-89
Injector-Chamber Configuration for Transpiration Chamber SN-001 (Test Series 1.2-12-WAM)	VI-90
Injector-Chamber Configuration for Transpiration Chamber SN-002 (Test Series 1.2-12-WAM)	VI-91
Regenerative Chamber Test Data and Performance Summary	VI-92
Transpiration Chamber SN 001 Temperature Summary	VI-93
Transpiration Chamber SN 002 Temperature Summary	VI-94
Transpiration Chamber SN 002 Surface Temperatures (Tests 1.2-12-WAM-016 to 018)	VI-95

FIGURE LIST (cont.)

	Figure
Measured and Predicted Temperatures for Test 1.2-12-WAM-016	VI-96
Measured and Predicted Temperatures for Test 1.2-12-WAM-017	VI-97
Measured and Predicted Temperatures for Test 1.2-12-WAM-018	VI-98
Plasma Thermal Shock/Oxidation Test Results	VI-99
Shroud Types	VI-100
Brazed Bonded Laminated Tungsten Cermet Thermal Barrier	VI-101
Brazed Bonding Microstructure	VI-102
Transpiration Laboratory Program, Subscale Washers	VI-103
Photograph of Transparent Scale Model Simulating Diffusion Area	VI-104
Two-Dimensional Nozzle Design	VI-105
Two-Dimensional Nozzle Assembly	VI-106
Chamber-Nozzle Instrumentation Schematic	VI-107
Test Data Summary	VI-108
Condition of Nozzle after Test 1.2-11-WAM-025	VI-109
Nozzle Temperature Data, Test 1.2-11-WAM-023	VI-110
Nozzle Temperature Data, Test 1.2-11-WAM-025	VI-111
Suction Valve Configuration	VII-1
Electron Beam Welding Parameters	VII-2
PCFCV Flow Characteristics	VII-3
PCFCV Control Port Configurations	VII-4
SCFCV Flow Characteristics	VII-5
SCFCV Exploded View	VII-6
Suction Valve Selective Control Circuit	VII-7
Fuel Valve Servo Controller (schematic)	VII-8
Air Test Facility Schematic	VIII-1
Oxidizer Discharge Model	VIII-2
Oxidizer Discharge Housing Rib Pattern	VIII-3
Pressure Drop Parameter vs Hole Number	VIII-4
Flow Distribution Parameter vs Hole Number	VIII-5
Oxidizer Return Housing Rib Pattern	VIII-6

FIGURE LIST (cont.)

	Figure
Pressure Drop Parameter vs Inlet Hole Number	VIII-7
Flow Distribution Parameter vs Injector Hole Number	VIII-8
Turbine Inlet Model	VIII-9
Instrumentation Planes	VIII-10
Turbine Inlet Passage	VIII-11
Flow Pitch Angle at Turbine Inlet	VIII-12
Total Pressure Distribution at Turbine Inlet	VIII-13
Turbine Exhaust Model	VIII-14
Flow Distribution Concepts	VIII-15
Flow Distribution	VIII-16
Nozzle Performance Program Summary	VIII-17
Nozzle Design Parameters	VIII-18
Nozzle Performance Models	VIII-19
Subscale Nozzle Performance	VIII-20
Full-scale Nozzle Performance	VIII-21
Ambient Base Bleed Effects	VIII-22
IES Area Ratio Effects	VIII-23
Module Skirt Merging Angle Effects	VIII-24
Skirt Length Effects	VIII-25
Module Cant Angle Effects	VIII-26
Module-Out Effects on Performance	VIII-27
Module-Out Effects on Thrust Vector Angle	VIII-28
Engine Throttling by Module Shutdown	VIII-29
Model 2-D	VIII-30
Heat Transfer Test Conditions	VIII-31
Model 2-D Shadowgraphs	VIII-32
Model 2-D Heat Transfer Coefficients	VIII-33
Heat Transfer Model 1a, Skirt	VIII-34
Heat Transfer Model 1a, Heat Shield	VIII-35
Heat Transfer Model 2	VIII-36

FIGURE LIST (cont.)

	Figure
Time from Initial Valve Motion to Partial Outflow from Injector Manifold	VIII-37
Engine Model Flow Chart	VIII-38

V.

PRIMARY COMBUSTOR ASSEMBLY

V.

PRIMARY COMBUSTOR ASSEMBLY

A. OBJECTIVE

(C) The objective of the primary combustor program was to develop a unit which would satisfy the following three criteria: (1) produce a homogenous oxidizer-rich turbine drive gas at a temperature of approximately 1225°F, (2) operate at a chamber pressure of approximately 4700 psia, (3) operate with less than ± 5% chamber pressure oscillations during steady-state operating.

B. SUMMARY

(U) The basic purpose of the primary combustor on the modular engine is to generate a high-temperature oxidizer-rich gas and supply this gas as an energy source to drive the modular turbine assembly. Liquid N_2O_4 and Aero-ZINE 50 are mixed at a ratio of approximately 11.5:1 to generate the desired gas. The turbine, in turn, drives the oxidizer and fuel pumps, and the turbine exhaust gases pass to the secondary combustor for final burning. In the modular engine, the primary combustor assembly consists simply of two components, the injector and the combustion chamber thermal-barrier liner (or some other thermal barrier device).

(U) The Phase I task for the primary combustor was the development of the flight-weight modular configuration primary injector. To conduct development tests with candidate injectors before integration into the modular engine turbopump housing, it was necessary to test these components in a simulated environment. To accomplish this, a "workhorse" housing was used. This housing employed the same interface dimensions and gas passage configuration as the flight-weight modular housing. It was designed in a heavy-weight configuration to permit easy removal of injectors and liners and to provide for extensive instrumentation to facilitate evaluation of the performance and operating characteristics of the injectors.

V, B, Summary (cont.)

(U) Five injector concepts were studied early in the program, from which three were selected for detailed design, fabrication, and test evaluation. A combustion chamber liner to reduce heat transfer to the modular turbopump housing was also designed and evaluated. The test program was designed to provide a detailed evaluation of these components. Based on the test data obtained and the posttest condition of the hardware following each test, an iterative type development program was conducted until a satisfactory injector and combustion chamber configuration was derived.

(C) The primary combustor configuration developed during the test program met or exceeded all requirements. The test program consisted of 31 tests: one cold-flow test and 30 hot-fire tests. The average temperature obtained on the three certified work statement tests was 1340°F; the average pressure obtained was 4650 psia; the chamber pressure oscillations at steady state averaged ± 1.27%. The average mixture ratio during these tests was 11.63:1. The development program proved the pentad injector superior to both the quadlet and the full-flow injectors. The final configuration which ultimately satisfied all contract work statement requirements is shown in Figure V-1. The developed assembly consisted of the pentad injector with a chamber configuration incorporating five axial vanes to inhibit tangential instability, and two turbulators to provide mechanical mixing of the propellants. The contractual work statement requirements and experimental test results are summarized in Figure V-2.

C. COMPONENT DESIGN

(U) Major components of the primary combustor included the injectors, the workhorse housing, the combustion chamber liner, and the burnoff stack. Design descriptions for each of these components are given in this section. A photograph showing all hardware which comprised a typical primary combustor assembly, including the minor integrating components, is shown in Figure V-3.

V, C, Component Design (cont.)

1. Injectors

(U) Three injector configurations were selected for test evaluation. These designs were designated the full flow, the quadlet, and the pentad. The full flow injector was based on an injection concept used successfully on the High Chamber Pressure Rocketry Program, AF 04(611)-8191. The quadlet design was based on the primary injector concept developed in the Integrated Components Program, AF 04(611)-8548. The pentad was a new injector concept to be evaluated as an alternative to the full-flow and quadlet patterns.

(U) The body design of all three injectors was identical. The body was an annular configuration having an outside diameter of 10.500 in. and an inside diameter of 6.255 in. The injector face outside and inside diameter dimensions are approximately 10 and 7 in., respectively, resulting in a total face area of 40 $in.^2$ The outer diameter interfaces with the workhorse housing, where oxidizer is fed through matching holes in the housing and injector body. The oxidizer circuit is sealed from external leakage and combustion zone leakage by metal piston-type rings on both sides of the feed holes. The inner diameter interfaces with a turbine simulator nozzle which simulates the pressure drop through the modular turbine assembly. The fuel is fed into the inner injector manifold through a 1 in. dia tube. The entire injector body is fabricated from Inconel 718 material.

(U) The total design propellant flow rate is 233 lb/sec at an oxidizer-to-fuel ratio of 11.5:1. Nominal design pressure drops were 400 psi for the fuel circuit and 300 psi for the oxidizer circuit.

Each of the three injectors patterns is described in the following paragraphs.

V, C, Component Design (cont.)

a. Full-Flow Injector

(U) The full-flow injector consists of 28 fuel spray elements uniformly spaced around the centerline of the annular injector face. The remaining face area comprises the oxidizer injection circuit, which consists of a porous metal sheet (Rigimesh) 0.125 in. thick. The porosity was calibrated to 3900 gpm/ft^2 of 70°F water at a pressure drop of 100 psi. The oxidizer injection velocity is very low and was not specifically defined. The fuel injection velocity is 150 ft/sec. The injector is shown in Figure V-4.

b. Quadlet Injector

(U) The quadlet injector concept was based on the successful "Mod H" injector developed during the AF 04(611)-8548 program. The concept was incorporated into the annular injector body by uniformly spacing 28 injection elements around the center of the annulus. The element consists of three oxidizer streams impinging on a fuel-spray nozzle (the same one as used in the full-flow injector). The fuel discharge produces a 60° conical spray when flowed to atmosphere. The injector face is protected from erosion by a porous face plate (Rigimesh) through which approximately 4% of the oxidizer is flowed. The oxidizer orifice injection velocity is 94 ft/sec and the fuel injector velocity is 177 ft/sec. The injector is shown in Figure V-4.

c. Pentad Injector

(U) The pentad injector, shown in Figure V-5, has 180 elements uniformly spaced about the injector annulus. The elements are arranged in three rows of 60 elements each. The element consists of four oxidizer streams impinging at 45° upon a single central fuel element. The entire element is recessed in a hemispherical cup machined into the combustion face side. Injector

velocity is 220 ft/sec for the fuel and 100 ft/sec for the oxidizer. No supplemental face cooling is used on this concept because of the great number of elements.

2. Workhorse Housing

(U) The workhorse primary combustor housing is a heavy duty unit used to develop the injector for the modular engine. The housing was fitted with pulse guns and high-frequency transducer capability to evaluate stability characteristics of the developed injector.

(U) The workhorse housing, shown in Figure V-6, simulated the module engine housing geometrically, hydraulically, and aerodynamically. Oxidizer enters the housing through a 4-in. oxidizer inlet flange and is fed through transfer passages in the housing wall into the manifold of the injector body. The fuel is fed through a 2-in. inlet flange mounted on the housing which interfaces with the 1-in. tube on the injector. The propellants are injected in the direction of the oxidizer pump (of the modular engine); the propellants combust and turn 180°, passing through the center of the injector, which houses a turbine simulator nozzle. After leaving the nozzle, the gases turn 90° and enter the burnoff duct. (The oxidizer circuit for the secondary combustor would replace the burnoff duct on the modular engine.)

(U) The propellants are admitted to the primary housing from the high-pressure intensifiers of the test facility. These units are capable of delivering 6000 psia at the required engine flow rates. The propellants are fed through their respective feedlines, through high pressure "ball type" control valves into the housing inlets. The start and shutdown transients, balance and mixture ratio requirements are provided by computerized programing of the intensifier control system.

V, C, Component Design (cont.)

3. Combustion Chamber Liner

(U) The combustion chamber liner, shown in Figure V-6, is made from 0.040-in.-thick Hastelloy X sheet. This liner follows the contour of the combustion chamber, with an allowance for a stagnant gas space to protect the TPA housing wall. The ends of the toroidal liner, securely held in place, permit thermal growth without inducing additional stresses. A pair of flexible support members are spot-welded to the outside of the chamber liner to control vibration. Adequate pressure equalizing holes are provided to vent the stagnant side of the liner during rapid pressure transients.

4. Burnoff Stack

(U) The burnoff stack, shown in Figure V-7, consists of a duct, a hot-gas orifice used as a back-pressure device for the turbine simulator nozzle, and a burnoff injector. This unit was used to prevent the toxic oxidizer rich gas generated in the primary combustor from being directly released to the atmosphere. The injector was designed originally as a tripropellant unit, with the oxidizer rich gas and RP-1 as the main propellants and AeroZINE 50 used for ignition purposes. The unit was incapable of reducing the toxicity to a tolerable level for very short duration tests because of the ignition delay of the propellants; therefore the fuel was converted from RP-1 to AeroZINE 50. Approximately 20 lb/sec of AeroZINE 50 was injected into the supersonic gas stream.

V, Primary Combustor Assembly (cont.)

D. DEVELOPMENT TESTING

1. Summary

(U) The overall objective of the test program was to develop a primary combustor assembly capable of providing a homogenous oxidizer rich gas at proper temperature, pressure, and mass flow conditions to the ARES TPA turbine. The success criteria for the primary combustor test program was that the temperature of the primary combustor exhaust gas, as measured by three thermocouples at the entrance to the turbine nozzle ring, must not exceed 1600°F, and the variation between each thermocouple must not exceed 400°F. Also, chamber pressure oscillations must not exceed ± 5% of the average chamber pressure value and must not be divergent with time when measured during the steady-state portion of the test firing. Compliance with these conditions was to be demonstrated in three tests, each having a minimum duration of 1-sec of steady-state operation. The primary combustor must be in refireable condition following the demonstration test series.

(U) Three injector configurations, together with various configurations of the combustion chamber and thermal barrier liner, were evaluated in the test program. Thirty-one tests were conducted. The first test was a cold flow test to ascertain basic hydraulic characteristics and to check out the test facility computer and intensifier systems. Of the remaining 30 tests, 29 yielded valid data; one malfunction (Test 1.2-04-WAG-015) occurred when the fuel flow control valve of the test facility failed to ramp properly. The test program was initiated on 6 June 1966 and was completed successfully on 6 October 1966.

V, D, Development Testing (cont.)

(C) The test program objectives for the primary combustor assembly were fully achieved. The mixture ratio ranged from an intentionally high 40.0:1 to a low of 10.77:1. A spectrum of measured temperatures was obtained over a range of mixture ratios from 10.77:1 to 12.71:1 and chamber pressures from 4602 to 4723 psia. The finalized data shows that the combustion temperatures in this range of pressures and mixture ratios are slightly higher than the theoretical temperatures predicted by the thermo-chemical model for partial equilibrium. Test data showed that a mixture ratio of approximately 12.5:1 corresponds to the target design temperature of 1225°F.

2. Detailed Test Program

(U) The tests conducted with the primary combustor are grouped into eight test series. Each of these series is discussed in the following sections. The various configurations tested and final test data are shown in Figure V-8. The test set-up, which included the primary combustor assembly, valves, frame, and burn-off stack, is shown in Figure V-9. Representative oscillographs showing characteristic start transient and steady-state operation are shown in Figure V-10.

a. Test Series 1 (1.2-04-WAG-001 through -005)

(U) The objective of this test series was to verify manifold fill times, structural integrity of hardware components, and test facility operation, as well as to initiate evaluation of the quadlet injector and the thermal barrier combustion chamber liner (see Figures V-4 and V-6).

(U) Test 001 was a cold-flow test to determine the oxidizer manifold fill characteristics and to verify intensifier ramp characteristics for both the oxidizer and fuel systems. A blank orifice plate was installed

V, D, Development Testing (cont.)

between the fuel thrust chamber valve and the primary combustor fuel inlet manifold, which prevented fuel from entering the primary combustor. Test data showed that the oxidizer manifold fill time occurred 35 millisec earlier than predicted by the computerized transient model. Based on this information, the proper correction was made to the computer program.

(C) The remaining three tests in this series were of very short duration to evalute the start-transient characteristics of the primary combustor. The first of these tests, in which a chamber pressure of 1820 psig was achieved, exhibited a feed-system-coupled high-amplitude oscillation in the 600 cps range. No hardware damage was incurred however. In the next test, the duration was increased to determine if the oscillations would attenuate on approaching steady-state operation. In this test, a chamber pressure of 3020 psig was reached. The oscillations continued to diverge. Posttest inspection showed that the combustion chamber liner was bent and torn and indicated that the oscillatory force was oriented primarily in a tangential direction. The liner was removed and the test repeated to determine if there was any connection between the combustion chamber liner configuration and the oscillations. The test data very closely approximated that of the previous tests, which eliminated the liner as being receptive to the oscillations.

(U) A detailed study was then made to determine causes for the feed system coupled oscillations. One suspected cause was that the resistance across the oxidizer injector circuit was very low. It had been intended that the pressure drop across the oxidizer orifice would be in the range of 250 to 300 psi; however, a design error in assuming the orifice discharge coefficient resulted in an actual pressure drop of only 77 psi. It was postulated that increasing the resistance of the oxidizer circuit to its intended value might correct the problem. A second possibility as to the cause of the oscillations was also considered. Because of the three dimensional 180°

V, D, Development Testing (cont.)

bend configuration of the combustion chamber, it is natural for the gas flow to assume a tangential direction as it flows around the bend. This change in flow direction then sets up pressure perturbations which could couple with the system. Mechanical baffles or turning vanes could be installed in the combustion chamber to compartmentize the gas flow and thus prevent a gross tangential rotation of the gases as they passed through the 180° bend.

(U) It was decided to evaluate each of these potential solutions to the oscillation problem. The test hardware was removed from the stand and the injector was reworked to increase the pressure drop across the oxidizer orifice.

b. Test Series 2 (1.2-04-WAG-005 and 006)

(U) The objective of this test series was to determine if the feed-system-coupled oscillations could be attentuated or eliminated by either the increased oxidizer system resistance or through the use of mechanical turning vanes. The first test evaluated the new injector configuration but did not incorporate the turning vanes. The pressure drop across the oxidizer orifice was increased to 240 psi. The test results still showed the oscillations present; however, the amplitude was slightly reduced from the previous tests. The combustion chamber liner fitted with five axial vanes was then installed in the primary combustor and the test was repeated. This change eliminated the tangential oscillations and reduced chamber pressure perturbations from approximately 70% P_c to 6% P_c (peak-to-peak). However, the aerodynamic mixing which had been generated by the tangential oscillations was eliminated with the incorporation of the vanes, and fuel-rich striations were noted in the combustion zone. Localized erosion of both the injector and liner resulted. The posttest condition of the injector and liner-vane assembly is shown in Figure V-11.

V, D, Development Testing (cont.)

This condition precipitated a design analysis to provide mechanical mixing by means of turbulator rings.

(U) Since the quadlet injector required repair because of the erosion sustained, the program was continued with the evaluation of the pentad injector.

c. Test Series 3 (1.2-04-WAG-007 through 010)

(C) The objective of this series was to evaluate the pentad injector (see Figure V-5). The five axial vanes used in the previous series were incorporated in this assembly also. In the first test, in which a chamber pressure of 2480 was reached, minor erosion on the liner-vane assembly occurred. However, operation from the stability point of view was completely satisfactory. No abnormal oscillations of any type were noted. Prior to the next two tests, turbulators were added to the liner-vane assembly to promote better mixing. This configuration is shown in Figure V-12. The turbulators proved to be successful in eliminating the erosion characteristics, but a new 100 cps oscillation was observed. The oscillation was attentuated as the unit approached steady state operation, and when no damage occurred, the test program was continued. On the fourth test however, the oscillations diverged not only through the state transient but into steady state operation. The chamber pressure characteristics recorded in each of these tests are shown in Figure V-13. During this test the magnitude of oscillations reached 34% of chamber pressure. Mixture ratio excursions toward fuel-rich conditions followed and gross damage to all test hardware was experienced (Figure V-14).

(U) A detailed combustion stability analysis was performed to determine the cause of the oscillations. It was concluded that the

V, D, Development Testing (cont.)

the oscillations were most probably produced by a "fluid oscillator" condition within the combustion chamber itself resulting from interaction between the injector face and the turbulator ring nearest the face. It was recommended that the configuration of the turbulators be changed to eliminate the problem.

d. Test Series 4 (1.2-04-WAG-011 and 012)

(U) The objective of this series was to continue the evaluation of the quadlet injector in conjunction with a modified turbulator configuration. In Test Series 2, erosion had occurred on the injector skirt and on the thermal barrier liner. In addition to the incorporation of mechanical turbulating vanes, the quadlet injector was modified for this test series by the addition of film cooling holes around the inner and outer periphery of the injector. The film cooling holes each had a diameter of 0.040 in. There were 84 holes located on the inner injector face diameter and 112 holes on the outer injector face diameter. The total film cooling weight flow was calculated to be 17.4 lb/sec.

(U) The turbulator configuration used in this test series was similar to that used in Test Series 3 except that the turbulator ring nearest the injector was machined to a saw-tooth configuration. The saw-tooth turbulator was designed to promote better mixing and also to prevent a pressure wave interaction between the turbulator ring and the injector face. Another change made for this test series was the replacement of the turbine simulator nozzle with a turbine simulator orifice of substantially less pressure drop. This change was made because the nozzle was destroyed in Test 010, and an orifice was much less expensive and more readily fabricated. Overall system back-pressure was maintained by decreasing the diameter of the sonic nozzle in the turbine exhaust duct.

V, D, Development Testing (cont.)

(U) Test results showed no evidence of the 100 cps oscillation encountered in Test Series 3. It is thought that the saw-tooth turbulator most probably caused the elimination of the oscillation. The turbine simulator change could have effected the system stability; however, since no evidence of 100 cps has been evident in tests with either the nozzle or orifice, except for the one test series with the pentad injector and annular ring turbulator, the probability that this change caused the elimination of the oscillation problem is considered remote. However, neither the film cooling from the injector face nor the saw-tooth turbulator configuration eliminated erosion. Burning was sustained both on the combustion chamber liner as well as the injector skirt, as shown in posttest photograph, Figure V-15.

(U) Based on these test results, a further design study was initiated to improve the effectiveness of mechanical turbulators. It was concluded at this point that the quadlet pattern, if it were to be successful, would require a more sophisticated approach to turbulator design. While new designs were being prepared, it was decided to continue the program with the evaluation of the third injector concept, as yet untested.

e. Test Series 5 (1.2-04-WAG-013 through 017)

(U) The objective of this test series was to evaluate the full-flow injector concept (see Figure V-4). The initial test in this series incorporated the five axial vanes to prevent tangential oscillations but did not include any mechanical turbulators. Because of the erosion experienced in previous tests, the thermal barrier combustion chamber liners available were in poor condition. It was therefore decided to continue the test program with the vanes incorporated directly into the end-cap closure of the housing assembly. The geometry of this configuration is almost identical to that of the liner, the only difference being the slightly increased volume caused

V, D, Development Testing (cont.)

by the 1/8 in. gap between the liner and the end-cap closure. Inspection of the hardware following the first test showed that all five vanes had failed structurally in the parent metal adjacent to the weld interface. Therefore, prior to the next test, a reinforcing band was added to the outer periphery of the vanes to give improved structural rigidity. Minor erosion of the vanes was experienced on this test, indicating the need for mechanical turbulators with this injector pattern also.

(C) At the time, a new configuration turbulator assembly became available with two rows of canted blades similar to a turbine nozzle (see Figure V-16). These turbulators were used in conjunction with the five axial vanes for the next three tests. The first of these tests resulted in a malfunction shutdown when the fuel flow control valve failed to ramp; the second test, which was of very short duration, resulted in no damage; the third test, which was of longer duration in which a chamber pressure of 4878 psig was reached, resulted in local erosion on the downstream side of the turbulator rings. Posttest conditions of the injector and end-cap is shown in Figure V-17.

(U) Because of the minor nature of the erosion sustained, it was decided to continue the evaluation of these turbulators with one of the other injector patterns. In addition, it was decided to continue the design study for improved turbulator configurations.

f. Test Series 6 (1.2-04-WAG-018 and 019)

(U) The objective of this series was to evaluate the quadlet injector modified for film cooling in conjunction with the combustion chamber configuration with the five axial vanes and the canted blade turbulators. Two tests were performed, both of which resulted in random local erosion of the

V, D, Development Testing (cont.)

injector skirt. Posttest condition of the hardware is shown in Figure V-18. It was concluded at this point that the quadlet and full-flow injectors would require considerable additional development effort before streak-free operation could be obtained. It was decided to continue with the evaluation of the pentad injector with which incidents of erosion and degree of damage had been substantially less than with the other two patterns.

g. Test Series 7 (1.2-04-WAG-020 through 024)

(U) The objectives of this series was to continue the evaluation of the pentad injector. In Test Series 3, in which this injector together with the continuous angular turbulator configuration was tested, 100 cps oscillations were present. These oscillations were eliminated in test series 4 by interrupting the continuous angular surface by saw-tooth cuts; however, erosion on the underside of the tubulator blades occurred. Based on this experience, a new turbulator configuration was designed and used in this test series. The angular turbulators were changed to solid triangular rings (see Figure V-19) to provide streamlined gas flow on the trailing edge of the turbulator and thus prevent erosion-causing turbulance on the underside of the turbulator. To prevent oscillations, the turbulator surface was interrupted by milling scalloped slots in the outer ring at the top of the axial vanes. The lower turbulator was attached directly to the injector skirt. Photographs of this configuration are shown in Figure V-1.

(U) Five tests were conducted with this configuration. Test durations were successively increased from 1.081 sec to 2.598 sec. The latter two tests provided steady-state durations in excess of 1.0 sec, which were sufficient to meet work statement requirements. No damage of any kind was incurred during these tests. Operation was stable and normal in every respect. It was concluded that this configuration was therefore satisfactory and authorization was obtained to proceed with work statement compliance demonstration tests.

V, D, Development Testing (cont.)

h. Test Series 8 (1.2-04-WAG-025 through 031)

(U) This test series was designed for all work statement compliance tests for the primary combustor program. These included three tests of 1-sec-minimum duration at engine design mixture ratio, one test at low mixture ratio, one test at high mixture ratio, and one test in which the primary combustor assembly was to be shocked with a pulse gun during steady-state operation.

(U) Posttest inspection of the hardware following the first test, which was the low mixture ratio demonstration test, revealed minor erosion of one of the single pentad elements. Further investigation showed that this was caused by a metal chip lodged in the oxidizer feed manifold to that element. In all other respects, the test was satisfactory. The chip was formed during fabrication of the workhorse housing and was passed into the injector during the test. Normal flushing and back flushing of the housing had failed to remove all the chips. The housing was removed from the stand and flushed with high-pressure gaseous nitrogen in an attempt to remove any residual chips. The unit was then returned to the stand and testing was resumed. Following the next test, additional chips were found in the oxidizer injector manifold. Because of the difficulty experienced in removing all of the chips from the housing, it was decided to place a screen between the injector and housing manifold. The injector was reworked to incorporate the screen, after which the test program was resumed. Following a checkout test, the three design mixture ratio tests were performed. Finally, the high mixture ratio demonstration test was performed, which included pulsing the unit just prior to shutdown with an 80 grain charge. The test therefore also fulfilled the work statement requirements for the shock test.

V, D, Development Testing (cont.)

(U) Following Test 031, a cold pulse test was performed to obtain the ring frequency of the primary combustor assembly. It was desired to compare this frequency to those combustion frequencies noted during normal and excited operation to see if any relationship existed. The 80 grain charge used to pulse the assembly induced a 4600 cps oscillation which damped in 7 millisec. This compared to a 1900 cps oscillation damped in 3 millisec when the chamber was pulsed under hot firing conditions with the same charge size. Random frequencies noted on hot fire tests using the same hardware configuration ranged from 1300 cps to 3000 cps. It was concluded that since the ring frequency was well outside the range of frequencies observed in operation, no interreaction between the two frequencies existed.

(U) Operation during all work statement demonstration tests was completely satisfactory. Formal data sheets were prepared for each of the tests and were submitted to the Air Force Project Officer to indicate satisfactory completion of the test program.

(U) The Phase I work statement requirements for the primary combustor, together with the specified values of the work statement and the test values obtained, are summarized in Figure V-2. Also shown in this figure are the temperature data for each of the work statement compliance demonstration tests together with other valid test data which help define the relationship between exhaust gas temperature and mixture ratio. Using this data, it is seen that a mixture ratio of approximately 12.5 corresponds to the target design temperature of about 1225°F. The theoretical mixture ratio based on partial decomposition of N_2O_4 had predicted a mixture ratio of 11.5:1. The experimental data showed the actual mixture ratio to be slightly higher than that which had been predicted for a given gas temperature. Engine analyses in Phase II will incorporate the temperature-mixture ratio relationship obtained from the Phase I experimental test program.

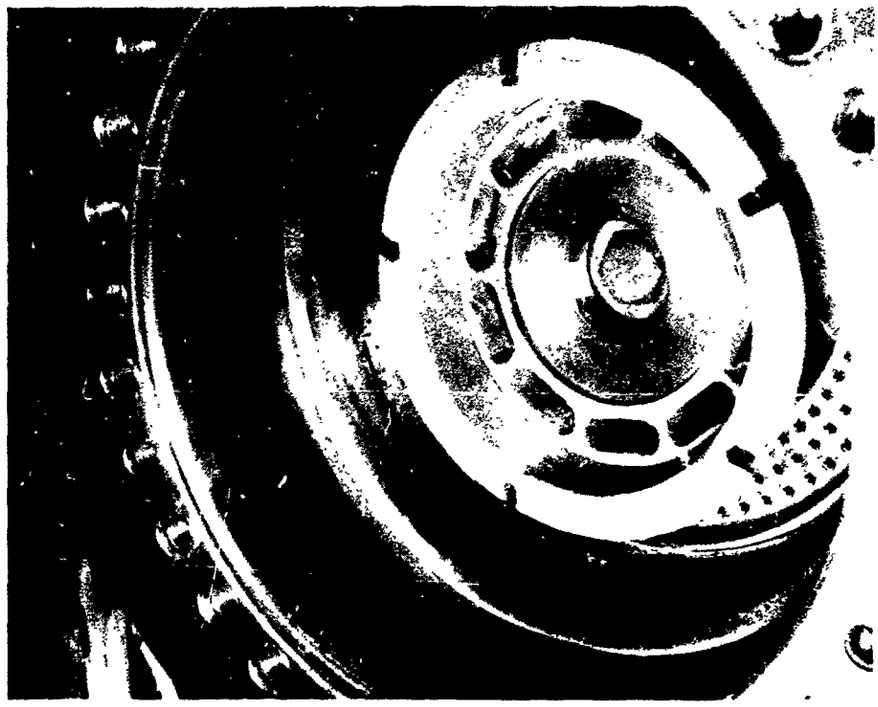

View Looking Toward Injector

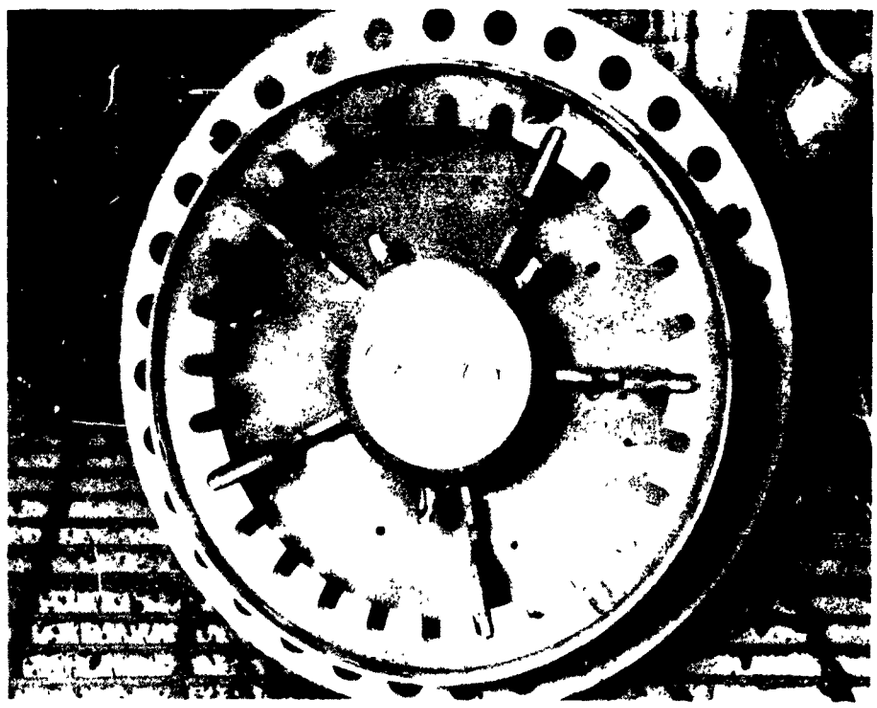

View Looking Toward End Cap Assembly

Final Configuration of the Primary Combustor

Figure V-1

PHASE I WORK STATEMENT REQUIREMENTS

REQUIREMENT	SPECIFIED VALUE	TEST VALUE
EXHAUST GAS TEMP	1650°F MAX	1486°F MAX
TEMP VARIATION BETWEEN THREE THERMOCOUPLES	400°F MAX	200°F MAX
P_C OSCILLATIONS FROM AVERAGE VALUE	± 5% MAX	1.29% MAX
STEADY-STATE DURATION	1.0 SEC, MIN	1.06 SEC, MIN
STABILITY PULSE TEST	NONE	80 GRAIN CHARGE 640 PSI PEAK-TO-PEAK .003 SEC DURATION

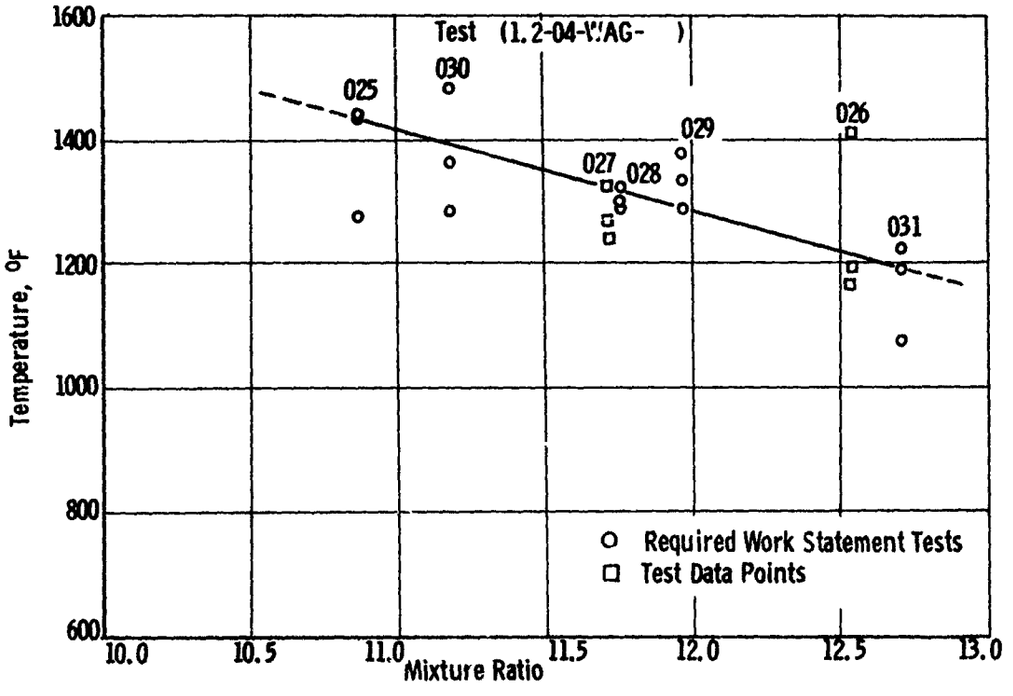

Work Statement Requirement and Experimental Test Results

Figure V-2

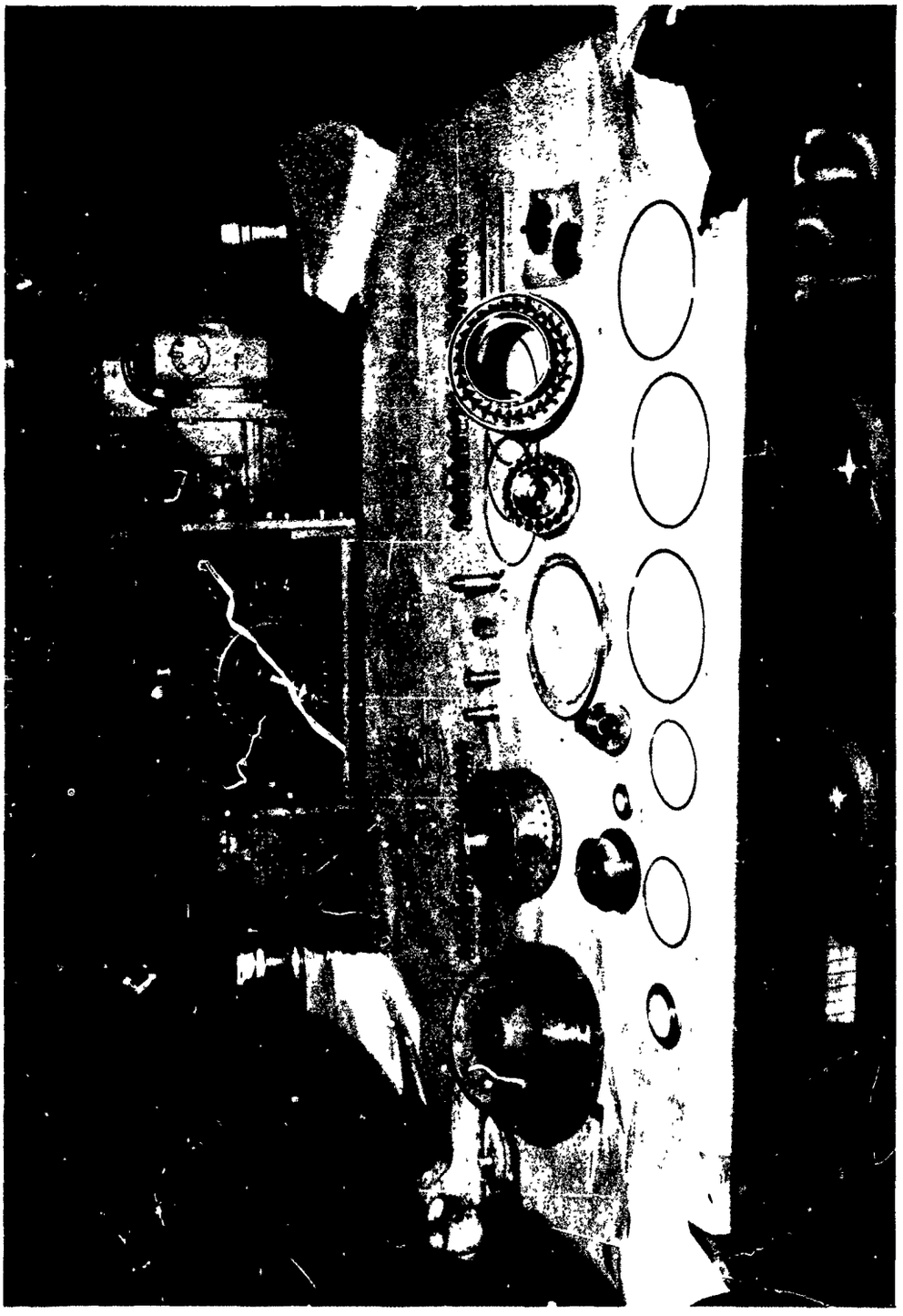

Primary Combustor Components

Figure V-3

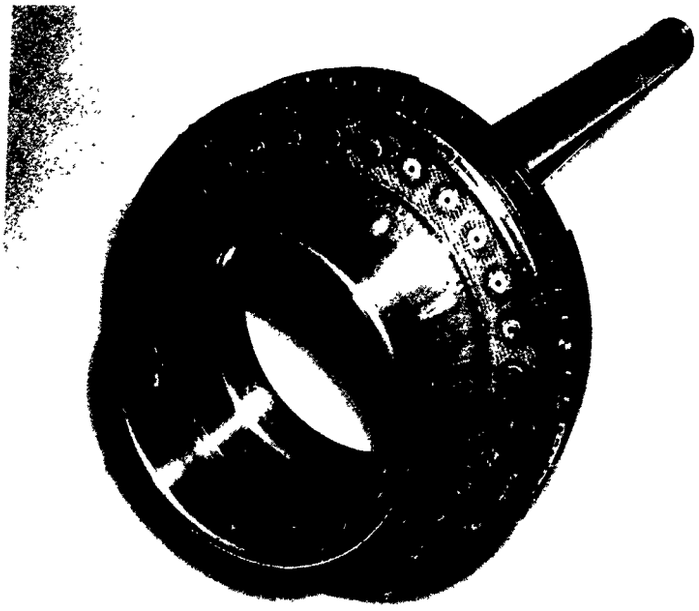

Full Flow Injector

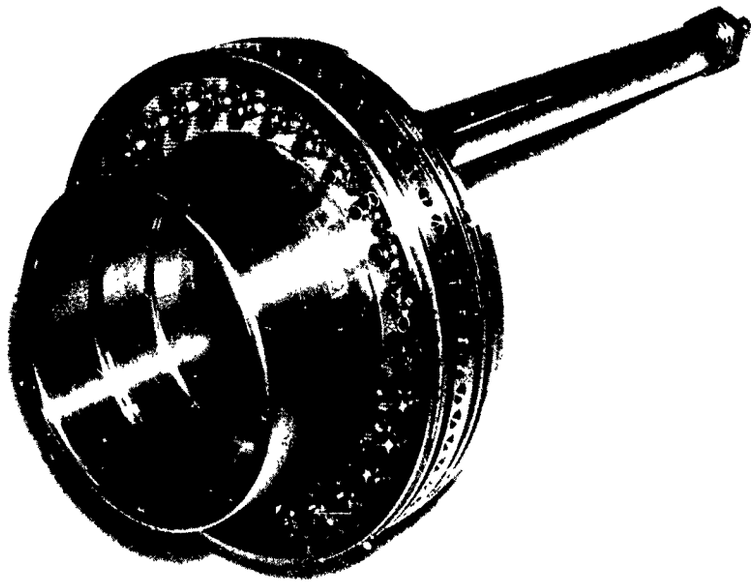

Quadlet Injector

Full-Flow and Quadlet Injectors

Figure V-4

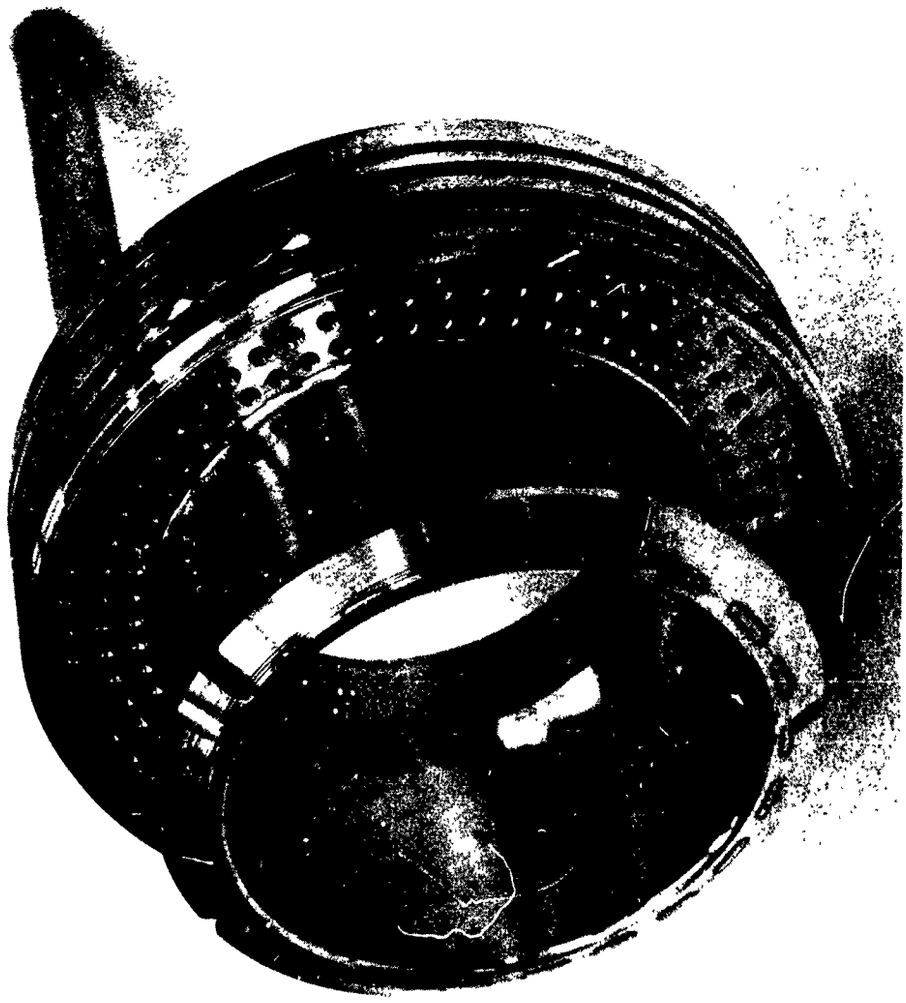

Pentad Injector

Figure V-5

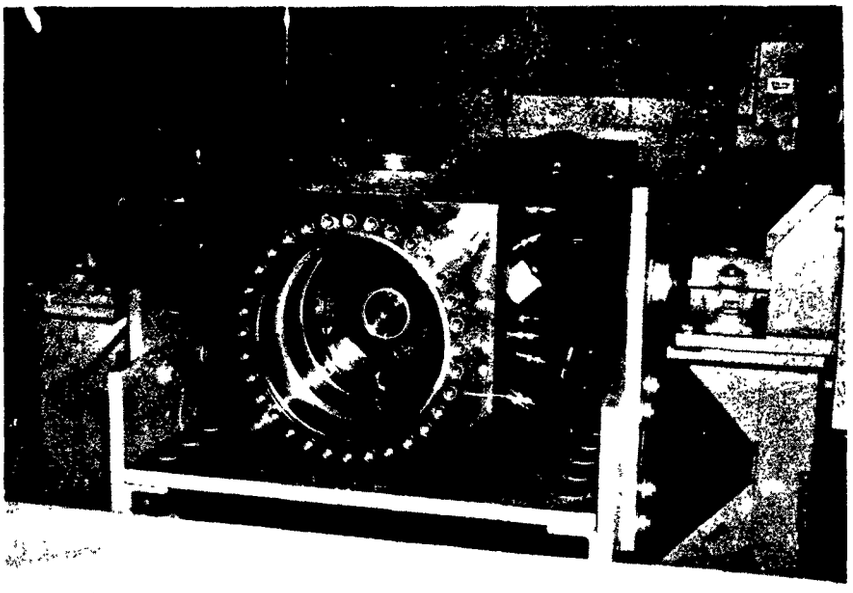

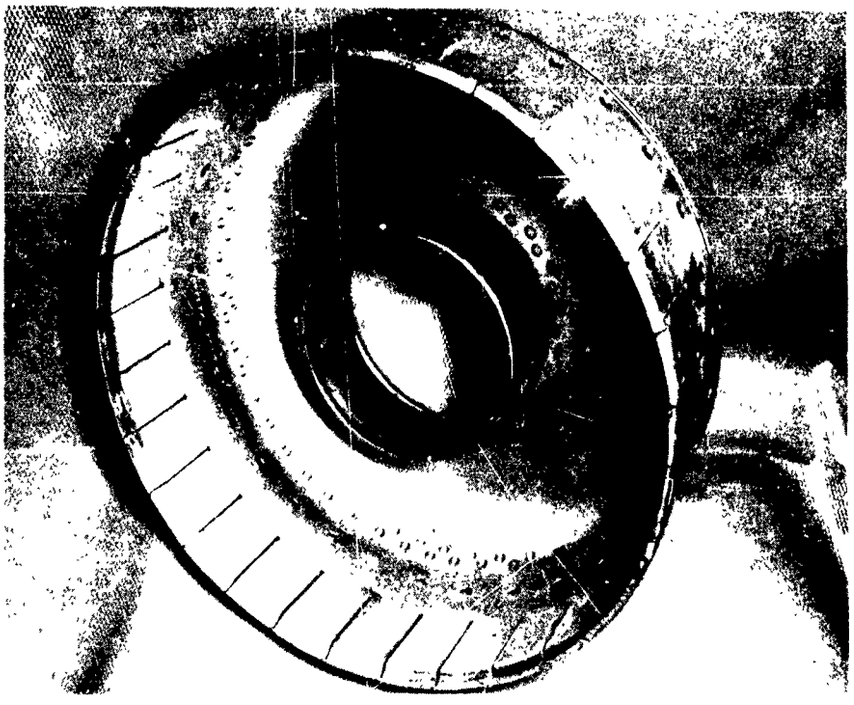

Primary Combustor Housing and Combustion Chamber Liner

Figure V-6

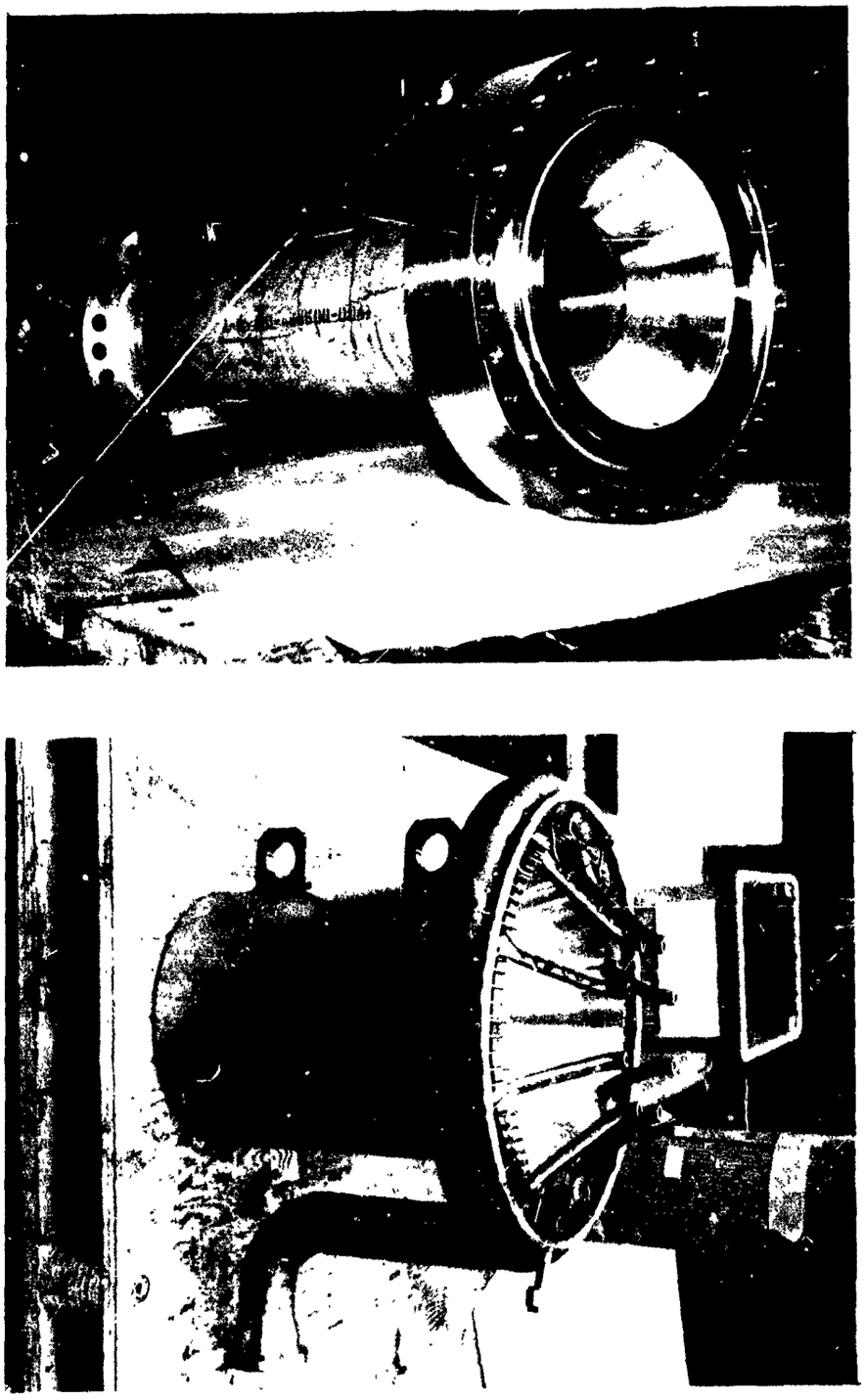

Primary Combustor Burnoff Stack Duct and Injector

Figure V-7

TEST No. 1.2-04-WAG-001	DATE 6-7-66	
Hardware Housing P/N 1121674 S/N 002 Injector Type Quadlet Injector P/N 1122112-9 S/N 001 Liner P/N 1122111 Turbulator P/N N/A Turbine Simulator P/N 1122363 Temperature Rake P/N N/A End Cap P/N 1121594 Burnoff Injector P/N 1121502 Adapter Burnoff P/N 1121499	**Test Data** $\dot{W}_o$ (lbm/sec) 365 $\dot{W}_f$ (lbm/sec) N/A P_c (psia) N/A MR N/A TtTi-1B (°F) N/A TtTi-2C (°F) N/A TtTi-3A (°F) N/A ΔPc (%) N/A Duration (sec) 1.700	**Remarks** 1. Cold flow test to determine oxidizer fill times and characteristics. 2. No damage to hardware. 3. No erosion noted.
TEST NO. 1.2-04-WAG-002	DATE 6-8-66	
Hardware Housing P/N 1121674 S/N 002 Injector Type Quadlet Injector P/N 1122112-9 S/N 001 Liner P/N 1122111 Turbulator P/N N/A Turbine Simulator P/N 1122363 Temperature Rake P/N N/A End Cap P/N 1121594 Burnoff Injector P/N 1121502 Adapter Burnoff P/N 1121499	**Test Data** $\dot{W}_o$ (lbm/sec) 170 $\dot{W}_f$ (lbm/sec) 4 P_c (psia) 1820 MR > 40 TtTi-1B (°F) N/A TtTi-2C (°F) N/A TtTi-3A (°F) N/A ΔPc (%) 10 Duration (sec) 0.917	**Remarks** 1. The tangs on the sheet metal liner showed signs of a tangential force. 2. No erosion noted.
TEST NO. 1.2-04-WAG-003	DATE 6-9-66	
Hardware Housing P/N 1121674 S/N 002 Injector Type Quadlet Injector P/N 1122112-9 S/N 001 Liner P/N 1122111 Turbulator P/N N/A Turbine Simulator P/N 1122363 Temperature Rake P/N N/A End Cap P/N 1121594 Burnoff Injector P/N 1121502 Adapter Burnoff P/N 1121499	**Test Data** $\dot{W}_o$ (lbm/sec) 240 $\dot{W}_f$ (lbm/sec) 10 P_c (psia) 3020 MR 24 TtTi-1B (°F) N/A TtTi-2C (°F) N/A TtTi-3A (°F) N/A ΔPc (%) 22.8 Duration (sec) 1.115	**Remarks** 1. The tangs on the sheet metal liner were torn and bent from a tangential oriented force. 2. No erosion noted.

365 N/A N/A N/A N/A N/A N/A N/A 1.700	**Remarks** 1. Cold flow test to determine oxidizer fill times and characteristics. 2. No damage to hardware. 3. No erosion noted.	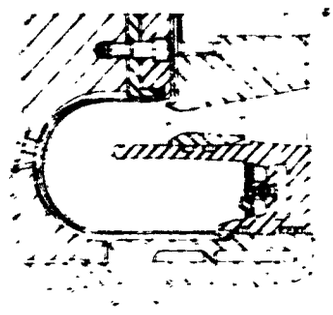
170 4 1820 > 40 N/A N/A N/A 10 0.917	**Remarks** 1. The tangs on the sheet metal liner showed signs of a tangential force. 2. No erosion noted.	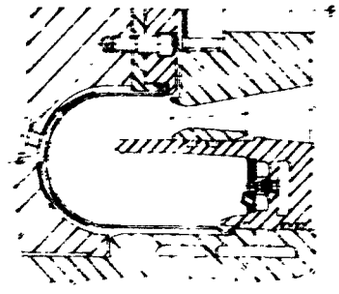
240 10 3020 24 N/A N/A N/A 22.8 1.115	**Remarks** 1. The tangs on the sheet metal liner were torn and bent from a tangential oriented force. 2. No erosion noted.	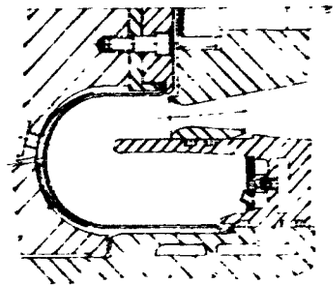

CONFIDENTIAL

Test Configuration and Data Summary (u)

Figure V-8, Sheet 1 of 11

TEST No. 1.2-04-WAG-004	DATE 6-14-66	
Hardware	**Test Data**	**Remarks**
Housing P/N 1121674 S/N 002	$\dot{W}_o$ (lbm/sec) 250	1. This test run without a liner.
Injector Type Quadlet	$\dot{W}_f$ (lbm/sec) 11	2. No damage to hardware.
Injector P/N 1122112-9 S/N 001	P_c (psia) 3400	3. No erosion noted.
Liner P/N N/A	MR ~23	
Turbulator P/N N/A	TtTi-1B (°F) N/A	
Turbine Simulator P/N 1122363	TtTi-2C (°F) N/A	
Temperature Rake P/N N/A	TtTi-3A (°F) N/A	
End Cap P/N 1121594	ΔPc (%) 83.3	
Burnoff Injector P/N 1121502	Duration (sec) 1.211	
Adapter Burnoff P/N 1121499		

TEST NO. 1.2-04-WAG-005	DATE 6-27-66	
Hardware	**Test Data**	**Re**
Housing P/N 1121674 S/N 002	$\dot{W}_o$ (lbm/sec) 150	1. No damage to hardware.
Injector Type Quadlet Mod "A"	$\dot{W}_f$ (lbm/sec) 8	2. No erosion noted.
Injector P/N 1122112-9 S/N 001	P_c (psia) 2600	3. The Mod "A" quadlet was a rework which increased the pressure drop in the oxidizer circuit by welding tube inserts into the existing 84 oxidizer triplet tubes.
Liner P/N N/A	MR 18.75	
Turbulator P/N N/A	TiTi-1B (°F) N/A	
Turbine Simulator P/N 1122363	TtTi-2C (°F) N/A	
Temperature Rake P/N N/A	TtTi-3A (°F) N/A	
End Cap P/N 1121594	ΔPc (%) 70	
Burnoff Injector P/N 1121502	Duration (sec) 1.010	
Adapter Burnoff P/N 1121499		

TEST NO. 1.2-04-WAG-006	DATE 6-28-66	
Hardware	**Test Data**	**Remarks**
Housing P/N 1121674 S/N 002	$\dot{W}_o$ (lbm/sec) 180	1. Minor erosion on injector skirt and liner.
Injector Type Quadlet Mod "A"	$\dot{W}_f$ (lbm/sec) 11	
Injector P/N 1122112-9 S/N 001	P_c (psia) 3280	2. Turning vanes installed.
Liner P/N 1130144	MR 16.5	
Turbulator P/N N/A	TiTi-1B (°F) N/A	
Turbine Simulator P/N 1122363	TtTi-2C (°F) N/A	
Temperature Rake P/N N/A	TtTi-3A (°F) N/A	
End Cap P/N 1121594	ΔPc (%) 6	
Burnoff Injector P/N 1121502	Duration (sec) 1.112	
Adapter Burnoff P/N 1121499		

250 11 3400 ~.23 N/A N/A N/A 83.3 1.211	**Remarks** 1. This test run without a liner. 2. No damage to hardware. 3. No erosion noted.	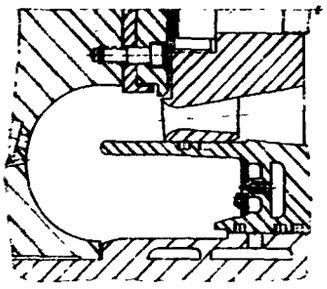
150 8 2600 18.75 N/A N/A N/A 70 1.010	**Remarks** 1. No damage to hardware. 2. No erosion noted. 3. The Mod "A" quadlet was a rework which increased the pressure drop in the oxidizer circuit by welding tube inserts into the existing 84 oxidizer triplet tubes.	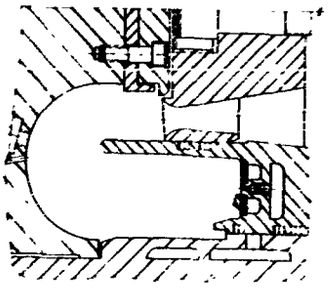
180 11 3280 16.5 N/A N/A N/A 6 1.112	**Remarks** 1. Minor erosion on injector skirt and liner. 2. Turning vanes installed.	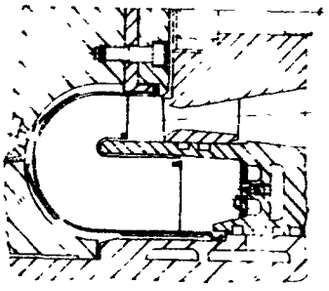

CONFIDENTIAL

Test Configuration and Data Summary (u)

Figure V-8, Sheet 2 of 11

TEST No. 1.2-04-WAG-007	DATE 7-1-66	
Hardware Housing P/N 1121674 S/N 002 Injector Type Pentad Injector P/N 1121895 S/N 002 Liner P/N 1130144 Turbulator P/N N/A Turbine Simulator P/N 1122363 Temperature Rake P/N N/A End Cap P/N 1121594 Burnoff Injector P/N 1121502 Adapter Burnoff P/N 1121499	**Test Data** $\dot{W}_o$ (lbm/sec) 180 $\dot{W}_f$ (lbm/sec) 8 P_c (psia) 2480 MR 22.5 TtTi-1B (°F) N/A TtTi-2C (°F) N/A TtTi-3A (°F) N/A ΔPc (%) 7.6 Duration (sec) 1.017	**Remarks** 1. Minor erosion on injector face between two orifice elements in middle row.
TEST NO. .2-04-WAG-008	DATE 7-7-66	
Hardware Housing P/N 1121674 S/N 002 Injector Type Pentad Injector P/N 1121895 S/N 002 Liner P/N 1130241-19 Turbulator P/N 1130241-19 Turbine Simulator P/N 1122363 Temperature Rake P/N N/A End Cap P/N 1121594 Burnoff Injector P/N 1121502 Adapter Burnoff P/N 1121499	**Test Data** $\dot{W}_o$ (lbm/sec) 240 $\dot{W}_f$ (lbm/sec) 17 P_c (psia) 4520 MR 14.1 TiTi-1B (°F) N/A TtTi-2C (°F) N/A TtTi-3A (°F) N/A ΔPc (%) 6 Duration (sec) 1.504	**Remarks** 1. Minor erosion on the liner 2. Turbulators added
TEST NO. 1.2-04-WAG-009	DATE 7-7-66	
Hardware Housing P/N 1121674 S/N 002 Injector Type Pentad Injector P/N 1121895 S/N 002 Liner P/N 1130241-19 Turbulator P/N 1130241-19 Turbine Simulator P/N 1122363 Temperature Rake P/N N/A End Cap P/N 1121594 Burnoff Injector P/N 1121502 Adapter Burnoff P/N 1121499	**Test Data** $\dot{W}_o$ (lbm/sec) 190 $\dot{W}_f$ (lbm/sec) 16 P_c (psia) 4460 MR 11.88 TiTi-1B (°F) N/A TtTi-2C (°F) N/A TtTi-3A (°F) N/A ΔPc (%) 6.4 Duration (sec) 1.627	**Remarks** 1. No damage to hardware 2. No erosion noted

Test (

180 8 2480 22.5 N/A N/A N/A 7.6 1.017	**Remarks** 1. Minor erosion on injector face between two orifice elements in middle row.	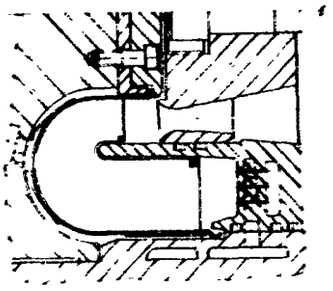
240 17 4520 14.1 N/A N/A N/A 6 1.504	**Remarks** 1. Minor erosion on the liner 2. Turbulators added	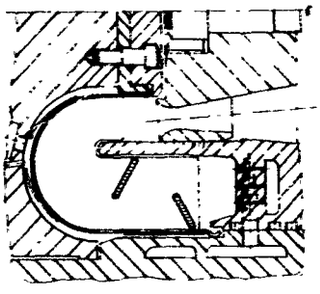
190 16 4460 11.88 N/A N/A N/A 6.4 1.627	**Remarks** 1. No damage to hardware 2. No erosion noted	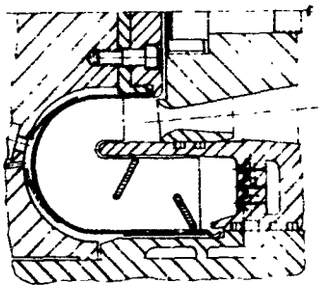

Test Configuration and Data Summary (u)

Figure V-8, Sheet 3 of 11

TEST No. 1.2-04-WAG-010	DATE 7-8-66	
Hardware Housing P/N 1121674 S/N 002 Injector Type Pentad Injector P/N 1121895 S/N 002 Liner P/N 1130241-19 Turbulator P/N 1130241-19 Turbine Simulator P/N 1122363 Temperature Rake P/N N/A End Cap P/N 1121594 Burnoff Injector P/N 1121502 Adapter Burnoff P/N 1121499	**Test Data** $\dot{W}_o$ (lbm/sec) invalid $\dot{W}_f$ (lbm/sec) invalid P_c (psia) 4800 MR invalid TtTi-1B (°F) N/A TtTi-2C (°F) N/A TtTi-3A (°F) N/A ΔPc (%) 34 Duration (sec) 2.277	**Remarks** 1. All test hardware and some stand equipment damaged. 2. Severe erosion on injector, nozzle, housing, end cap, burnoff stack, burnoff injector and stand plumbing and purge check valves.
TEST NO. 1.2-04-WAG-011	DATE 8-13-66	
Hardware Housing P/N 1121674 S/N 003 Injector Type Quadlet Mod "B" Injector P/N 1122112-9 S/N 001 Liner P/N 1130241-9 Turbulator P/N 1130241-9 Turbine Simulator P/N 1130436 Temperature Rake P/N N/A End Cap P/N 1121594 Burnoff Injector P/N 1121502 "A" Adapter Burnoff P/N 1130340	**Test Data** $\dot{W}_o$ (lbm/sec) 197.6 $\dot{W}_f$ (lbm/sec) 10.4 P_c (psia) 3300 MR 19.4 TiTi-1B (°F) N/A TtTi-2C (°F) N/A TtTi-3A (°F) N/A ΔPc (%) 3 Duration (sec) 1.105	**Remarks** 1. Erosion noted on the injector skirt, flow nozzle and liner 2. Both injector and housing oxidizer feed holes were full of metal chips. 3. Housing and injector were sent back thru more rigorous cleaning. 4. The Mod "B" quadlet incorporated additional film cooling on inner and outer primary walls by drilling coolant holes thru the regimesh face. 5. Turbine simulator orifice changed.
TEST NO. 1.2-04-WAG-012	DATE 8-19-66	
Hardware Housing P/N 1121674 S/N 003 Injector Type Quadlet Mod "B" Injector P/N 1122112-9 S/N 001 Liner P/N 1130241-9 Turbulator P/N 1130241-9 Turbine Simulator P/N 1130436 Temperature Rake P/N N/A End Cap P/N 1121594 Burnoff Injector P/N 1121502A Adapter Burnoff P/N 1130340	**Test Data** $\dot{W}_o$ (lbm/sec) 220 $\dot{W}_f$ (lbm/sec) 9.8 P_c (psia) 2910 MR 22.5 TiTi-1B (°F) N/A TtTi-2C (°F) N/A TtTi-3A (°F) N/A ΔPc (%) 3 Duration (sec) 1.102	**Remarks** 1. Erosion noted on the injector skirt, flow nozzle and liner.

invalid invalid 4800 invalid N/A N/A N/A 3 2.277	**Remarks** 1. All test hardware and some stand equipment damaged. 2. Severe erosion on injector, nozzle, housing, end cap, burnoff stack, burnoff injector and stand plumbing and purge check valves.	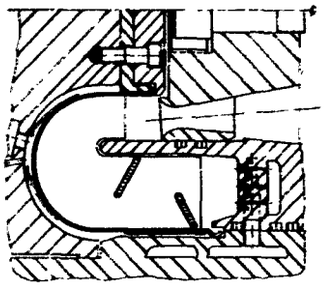
197.6 10.4 3300 19.4 N/A N/A N/A 3 1.105	**Remarks** 1. Erosion noted on the injector skirt, flow nozzle and liner 2. Both injector and housing oxidizer feed holes were full of metal chips. 3. Housing and injector were sent back thru more rigorous cleaning. 4. The Mod "B" quadlet incorporated additional film cooling on inner and outer primary walls by drilling coolant holes thru the regimesh face. 5. Turbine simulator orifice changed.	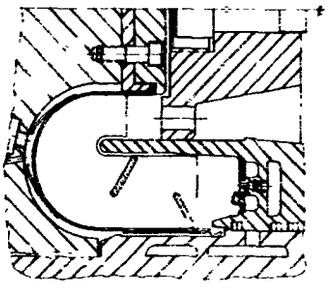
220 9.8 2910 22.5 N/A N/A N/A 3 1.102	**Remarks** 1. Erosion noted on the injector skirt, flow nozzle and liner.	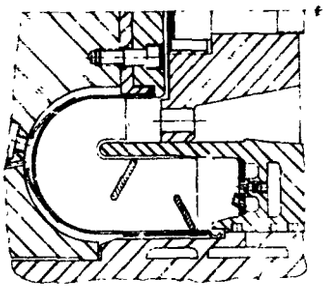

TEST No. 1.2-04-WAM-013	DATE 8-23-66	
Hardware Housing P/N 1121674 S/N 003 Injector Type Full flow Injector P/N 1122112-19 S/N 001 Liner P/N N/A Turbulator P/N N/A Turbine Simulator P/N 1130436 Temperature Rake P/N N/A End Cap P/N 1131400 Burnoff Injector P/N 1121502 Mod"A" Adapter Burnoff P/N 1130340	**Test Data** $\dot{W}_o$ (lbm/sec) 200 $\dot{W}_f$ (lbm/sec) 12 P_c (psia) 3050 MR 16.7 TtTi-1B (°F) N/A TtTi-2C (°F) N/A TtTi-3A (°F) N/A ΔPc (%) 98 Duration (sec) 1.105	**Remarks** 1. All 5 vanes which were welded to the end cap failed structurally next to weld.
TEST NO. 1.2-04-WAG-014	DATE 8-25-66	
Hardware Housing P/N 1121674 S/N 003 Injector Type Full flow Injector P/N 1122112-19 S/N 001 Liner P/N N/A Turbulator P/N N/A Turbine Simulator P/N 1130436 Temperature Rake P/N N/A End Cap P/N 1131400 Burnoff Injector P/N 1121502 Mod "A" Adapter Burnoff P/N 1130340	**Test Data** $\dot{W}_o$ (lbm/sec) 200 $\dot{W}_f$ (lbm/sec) 10.5 P_c (psia) 3150 MR 19 TiTi-1B (°F) N/A TtTi-2C (°F) N/A TtTi-3A (°F) N/A ΔPc (%) 2 Duration (sec) 1.103	**Remarks** 1. Minor erosion noted on two of the five axial vanes.
TEST NO. 1.2-04-WAG-015	DATE 8-26-66	
Hardware Housing P/N 1121674 S/N 003 Injector Type Full flow Injector P/N 1122112-19 S/N 001 Liner P/N N/A Turbulator P/N 1130825 Turbine Simulator P/N 1130436 Temperature Rake P/N N/A End Cap P/N 1130825 Burnoff Injector P/N 1121502 Mod "A" Adapter Burnoff P/N 1130340	**Test Data** $\dot{W}_o$ (lbm/sec) $\dot{W}_f$ (lbm/sec) P_c (psia) MR TiTi-1B (°F) N/A TtTi-2C (°F) N/A TtTi-3A (°F) N/A ΔPc (%) Duration (sec) Malfunction	**Remarks** 1. The intensifier fuel flow control valve did not ramp, causing the malfunction. 2. Prior to this test the injector fuel orifice opposite the fuel inlet tube was plug welded to eliminate possible start transient MR excursions. 3. Turbine nozzle type turbulators added.

Test Con

Fi

200 12 3050 16.7 N/A N/A N/A 98 1.105	**Remarks** 1. All 5 vanes which were welded to the end cap failed structurally next to weld.	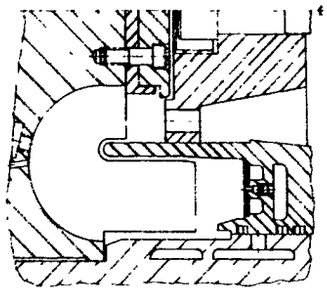
200 10.5 3150 19 N/A N/A N/A 2 1.103	**Remarks** 1. Minor erosion noted on two of the five axial vanes.	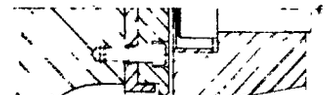
N/A N/A N/A Malfunction	**Remarks** 1. The intensifier fuel flow control valve did not ramp, causing the malfunction. 2. Prior to this test the injector fuel orifice opposite the fuel inlet tube was plug welded to eliminate possible start transient MR excursions. 3. Turbine nozzle type turbulators added.	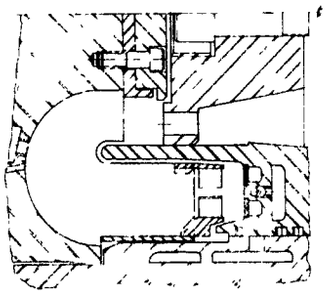

CONFIDENTIAL

Test Configuration and Data Summary (u)

Figure V-8, Sheet 5 of 11

TEST No. 1.2-04-WAG-016	DATE 8-26-66	
Hardware	**Test Data**	**Remarks**
Housing P/N 1121674 S/N 003	$\dot{W}_o$ (lbm/sec) 200	1. No damage to hardware
Injector Type Full flow	$\dot{W}_f$ (lbm/sec) 10	2. No erosion noted.
Injector P/N 1122112-19 S/N 001	P_c (psia) ~3100	
Liner P/N N/A	MR 20	
Turbulator P/N 1130825	TtTi-1B (°F) N/A	
Turbine Simulator P/N 1130436	TtTi-2C (°F) N/A	
Temperature Rake P/N N/A	TtTi-3A (°F) N/A	
End Cap P/N 1130825	ΔPc (%) 45	
Burnoff Injector P/N 1121502 Mod "A"	Duration (sec) 1.102	
Adapter Burnoff P/N 1130340		

TEST NO. 1.2-04-WAG-017	DATE 8-27-66	
Hardware	**Test Data**	**Remarks**
Housing P/N 1121674 S/N 003	$\dot{W}_o$ (lbm/sec) 225	1. Random erosion noted on the downstream side of the turbulators and at the turn around section of the axial vanes.
Injector Type Full flow	$\dot{W}_f$ (lbm/sec) 17.5	
Injector P/N 1122112-19 S/N 001	P_c (psia) 4878	
Liner P/N N/A	MR 12.9	
Turbulator P/N 1130825	TiTi-1B (°F) N/A	
Turbine Simulator P/N 1130436	TtTi-2C (°F) N/A	
Temperature Rake P/N N/A	TtTi-3A (°F) N/A	
End Cap P/N 1130825	ΔPc (%) 4	
Burnoff Injector P/N 1121502 MOD "A"	Duration (sec) 1.492	
Adapter Burnoff P/N 1130340		

TEST NO. 1.2-04-WAG-018	DATE 8-31-66	
Hardware	**Test Data**	**Remarks**
Housing P/N 1121674 S/N 003	$\dot{W}_o$ (lbm/sec) 230	1. Prior to this test the injector fuel orifice opposite the fuel inlet tube was plug welded.
Injector Type Quadrijet Mod "B"	$\dot{W}_f$ (lbm/sec) 9.9	
Injector P/N 1122112-9 S/N 001	P_c (psia) 2880	2. Random heat marks noted on the injector skirt and turbine simulator orifice.
Liner P/N N/A	MR 23	
Turbulator P/N 1130825	TiTi-1B (°F) N/A	3. Oily carbon deposits noted on the turbine simulator orifice.
Turbine Simulator P/N 1130436	TtTi-2C (°F) N/A	
Temperature Rake P/N N/A	TtTi-3A (°F) N/A	4. Turbulators moved downstream away from injector face.
End Cap P/N 1130825	ΔPc (%) 1.58	
Burnoff Injector P/N 1121502 Mod "A"	Duration (sec) 1.096	
Adapter Burnoff P/N 1130340		

Test Confi

Fi

200 10 ~3100 20 N/A N/A N/A 45 1.102	**Remarks** 1. No damage to hardware 2. No erosion noted.	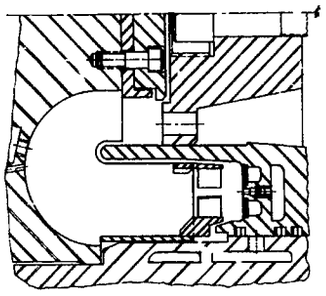
225 17.5 4878 12.9 N/A N/A N/A 4 1.492	**Remarks** 1. Random erosion noted on the downstream side of the turbulators and at the turn around section of the axial vanes.	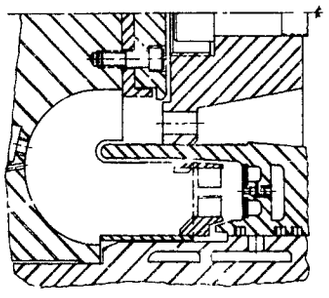
230 9.9 2880 23 N/A N/A N/A 1.58 1.096	**Remarks** 1. Prior to this test the injector fuel orifice opposite the fuel inlet tube was plug welded. 2. Random heat marks noted on the injector skirt and turbine simulator orifice. 3. Oily carbon deposits noted on the turbine simulator orifice. 4. Turbulators moved downstream away from injector face.	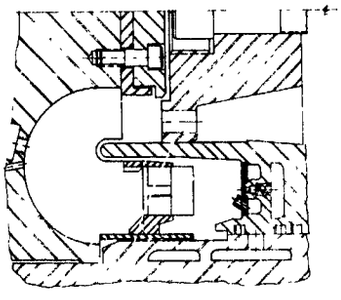

TEST No. 1.2-04-WAG-019 **DATE** 9-8-66

Hardware

- Housing P/N 1121674 S/N 003
- Injector Type Quadlet Mod "B"
- Injector P/N 1122112-9 S/N 001
- Liner P/N N/A
- Turbulator P/N 1130825
- Turbine Simulator P/N 1130436
- Temperature Rake P/N N/A
- End Cap P/N 1130825
- Burnoff Injector P/N 1121502 Mod"A"
- Adapter Burnoff P/N 1130340

Test Data

$\dot{W}_o$ (lbm/sec)	220
$\dot{W}_f$ (lbm/sec)	9.6
P_c (psia)	2900
MR	22.9
TtTi-1B (°F)	N/A
TtTi-2C (°F)	N/A
TtTi-3A (°F)	N/A
ΔPc (%)	
Duration (sec)	1.082

Remarks

1. Random heat marks noted on the injector skirt and turbine simulator orifice
2. Thermocouple rakes were installed for this test.

TEST NO. 1.2-04-WAG-020 **DATE** 9-19-66

Hardware

- Housing P/N 1121674 S/N 003
- Injector Type Pentad Mod "A"
- Injector P/N 1121895 S/N 002
- Liner P/N N/A
- Turbulator P/N 1130820
- Turbine Simulator P/N 1130436
- Temperature Rake P/N N/A
- End Cap P/N 1130820
- Burnoff Injector P/N 1121502 Mod "A"
- Adapter Burnoff P/N 1130340

Test Data

$\dot{W}_o$ (lbm/sec)	~ 200
$\dot{W}_f$ (lbm/sec)	~ 10
P_c (psia)	3040
MR	~ 20
TiTi-1B (°F)	N/A
TtTi-2C (°F)	N/A
TtTi-3A (°F)	N/A
ΔPc (%)	
Duration (sec)	1.081

Remarks

1. No damage to hardware
2. No erosion noted
3. Thermocouple rakes removed for redesign.
4. The mod "A" pentad incorporates shields over the fuel orifices opposite the end of the fuel inlet tube to prevent transient MR excursions.
5. Triangular cross section turbulators added.

TEST NO. 1.2-04-WAG-021 **DATE** 9-19-66

Hardware

- Housing P/N 1121674 S/N 003
- Injector Type Pentad Mod "A"
- Injector P/N 1121895 S/N 002
- Liner P/N N/A
- Turbulator P/N 1130820
- Turbine Simulator P/N 1130436
- Temperature Rake P/N N/A
- End Cap P/N 1130820
- Burnoff Injector P/N 1121502 Mod"A"
- Adapter Burnoff P/N 113034C

Test Data

$\dot{W}_o$ (lbm/sec)	~220
$\dot{W}_f$ (lbm/sec)	~15.5
P_c (psia)	4040
MR	14.2
TiTi-1B (°F)	N/A
TtTi-2C (°F)	N/A
TtTi-3A (°F)	N/A
ΔPc (%)	
Duration (sec)	1.293

Remarks

1. No damage to hardware
2. No erosion noted

Test (

220 9.6 2900 22.9 N/A N/A N/A 1.082	**Remarks** 1. Random heat marks noted on the injector skirt and turbine simulator orifice 2. Thermocouple rakes were installed for this test.	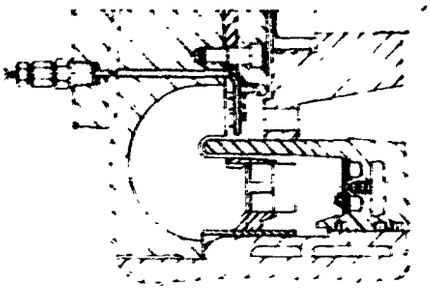
~200 ~ 10 3040 ~ 20 N/A N/A N/A 1.081	**Remarks** 1. No damage to hardware 2. No erosion noted 3. Thermocouple rakes removed for redesign. 4. The mod "A" pentad incorporates shields over the fuel orifices opposite the end of the fuel inlet tube to prevent transient MR excursions. 5. Triangular cross section turbulators added.	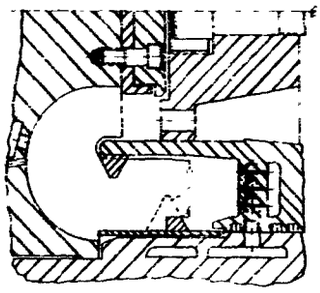
~220 ~15.5 4040 14.2 N/A N/A N/A 1.293	**Remarks** 1. No damage to hardware 2. No erosion noted	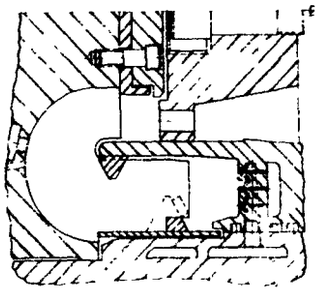

CONFIDENTIAL

Test Configuration and Data Summary (u)

Figure V-8, Sheet 7 of 11

TEST No. 1.2-04-WAG-022	DATE 9-19-66	
Hardware	**Test Data**	**Remarks**
Housing P/N 1121674 S/N 003	$\dot{W}_o$ (lbm/sec) 232.5	1. No damage to hardware
Injector Type Pentad Mod "A"	$\dot{W}_f$ (lbm/sec) 18.1	2. No erosion noted
Injector P/N 1121895 S/N 002	P_c (psia) 4526	
Liner P/N N/A	MR 12.85	
Turbulator P/N 1130820	TtTi-1B (°F) N/A	
Turbine Simulator P/N 1130436	TtTi-2C (°F) N/A	
Temperature Rake P/N N/A	TtTi-3A (°F) N/A	
End Cap P/N 1130820	ΔPc (%)	
Burnoff Injector P/N 1121502 Mod"A"	Duration (sec) 1.559	
Adapter Burnoff P/N 1130340		

TEST NO. 1.2-04-WAG-023	DATE 9-22-66	
Hardware	**Test Data**	**Remarks**
Housing P/N 1121674 S/N 003	$\dot{W}_o$ (lbm/sec) 228.6	1. Thermocouple rakes reinstalled.
Injector Type Pentad Mod "A"	$\dot{W}_f$ (lbm/sec) 18.9	2. No damage to hardware
Injector P/N 1121895 S/N 002	P_c (psia) 4666	3. No erosion noted
Liner P/N N/A	MR 12.1	
Turbulator P/N 1130820	TiTi-1B (°F) 1237	
Turbine Simulator P/N 1130436	TtTi-2C (°F) 1220	
Temperature Rake P/N 1123032	TtTi-3A (°F) 1142	
End Cap P/N 1130820	ΔPc (%)	
Burnoff Injector P/N 1121502 Mod "A"	Duration (sec) 1.554	
Adapter Burnoff P/N 1130340		

TEST NO. 1.2-04-WAG-024	DATE 9-23-66	
Hardware	**Test Data**	**Remarks**
Housing P/N 1121674 S/N 003	$\dot{W}_o$ (lbm/sec) 227.3	1. No damage to hardware
Injector Type Pentad Mod "A"	$\dot{W}_f$ (lbm/sec) 18	2. No erosion noted
Injector P/N 1121895 S/N 002	P_c (psia) 4636	
Liner P/N N/A	MR 12.6	
Turbulator P/N 1130820	TiTi-1B (°F) 900	
Turbine Simulator P/N 1130436	TtTi-2C (°F) 1273	
Temperature Rake P/N 1123032	TtTi-3A (°F) 1160	
End Cap P/N 1130820	ΔPc (%)	
Burnoff Injector P/N 1121502 Mod "A"	Duration (sec) 2.598	
Adapter Burnoff P/N 1130340		

Te

232.5 18.1 4526 12.85 N/A N/A N/A 1.559	**Remarks** 1. No damage to hardware 2. No erosion noted	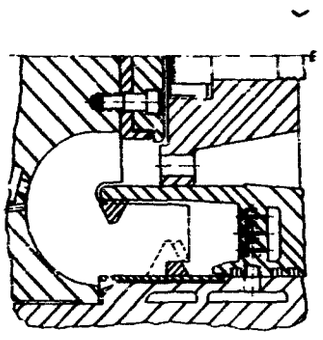
228.6 18.9 4666 12.1 1237 1220 1142 1.554	**Remarks** 1. Thermocouple rakes reinstalled. 2. No damage to hardware 3. No erosion noted	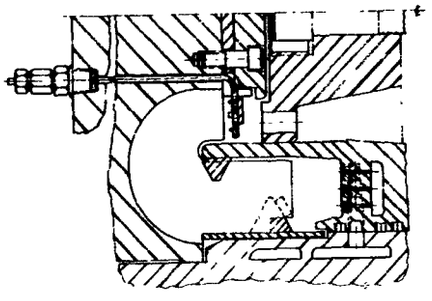
227.3 18 4636 12.6 900 1273 1160 2.598	**Remarks** 1. No damage to hardware 2. No erosion noted	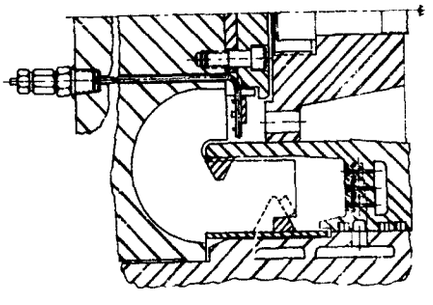

CONFIDENTIAL

Test Configuration and Data Summary (u)

Figure V-8, Sheet 8 of 11

TEST No. 1.2-04-WAG-025	DATE 9-23-66		
Hardware	**Test Data**		**Remarks**
Housing P/N 1121674 S/N 003	$\dot{W}_o$ (lbm/sec)	212.5	1. Erosion noted on the turbulators and turbine simulators orifice. This could be traced to oxidizer orifices plugged by metal chips in one case, and oxidizer orifices plugged partially by beam welding during repair in the other case.
Injector Type Pentad Mod "A"	$\dot{W}_f$ (lbm/sec)	19.73	
Injector P/N 1121895 S/N 002	P_c (psia)	4723	
Liner P/N N/A	MR	10.77	
Turbulator P/N 1130820	TtTi-1B (°F)	1431	
Turbine Simulator P/N 1130436	TtTi-2C (°F)	1437	
Temperature Rake P/N 1123032	TtTi-3A (°F)	1278	
End Cap P/N 1130820	ΔPc (%)		
Burnoff Injector P/N 1121502 Mod "A"	Duration (sec)	2.594	
Adapter Burnoff P/N 1130340			

TEST NO. 1.2-04-WAG-026	DATE 9-30-66		
Hardware	**Test Data**		**Remarks**
Housing P/N 1121674 S/N 003	$\dot{W}_o$ (lbm/sec)	229.5	1. Erosion noted on the turbulators and axial vane. This was traced to weld slag in the oxidizer feed holes.
Injector Type Pentad Mod "A"	$\dot{W}_f$ (lbm/sec)	18.3	
Injector P/N 1121895 S/N 002	P_c (psia)	4670	
Liner P/N N/A	MR	12.54	
Turbulator P/N 1130820	TtTi-1B (°F)	1410	
Turbine Simulator P/N 1130436	TtTi-2C (°F)	1193	
Temperature Rake P/N 1123032	TtTi-3A (°F)	1167	
End Cap P/N 1130820	ΔPc (%)		
Burnoff Injector P/N 1121502 Mod"A"	Duration (sec)	2.583	
Adapter Burnoff P/N 1130340			

TEST NO. 1.2-04-WAG-027	DATE 10-5-66		
Hardware	**Test Data**		**Remarks**
Housing P/N 1121674 S/N 003	$\dot{W}_o$ (lbm/sec)	223	1. Erosion noted on the injector face between two orifice elements.
Injector Type Pentad Mod "B"	$\dot{W}_f$ (lbm/sec)	19.1	2. The fuel orifices at the affected elements are welded closed for run 028.
Injector P/N 1121895 S/N 002	P_c (psia)	4691	3. The Mod "B" pentad incorporates a screen over the oxidizer feed holes to eliminate the chip plugging problem.
Liner P/N N/A	MR	11.72	
Turbulator P/N 1130820	TtTi-1B (°F)	1242	
Turbine Simulator P/N 1130436	TtTi-2C (°F)	1325	
Temperature Rake P/N 1123032	TtTi-3A (°F)	1267	
End Cap P/N 1130820	ΔPc (%)		
Burnoff Injector P/N 1121502 Mod"A"	Duration (sec)	2.608	
Adapter Burnoff P/N 1130340			

Test Co

212.5 19.73 4723 10.77 1431 1437 1278 2.594	**Remarks** 1. Erosion noted on the turbulators and turbine simulators orifice. This could be traced to oxidizer orifices plugged by metal chips in one case, and oxidizer orifices plugged partially by beam welding during repair in the other case.	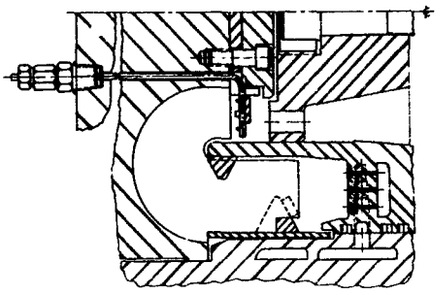
229.5 18.3 4670 12.54 1410 1193 1167 2.583	**Remarks** 1. Erosion noted on the turbulators and axial vane. This was traced to weld slag in the oxidizer feed holes.	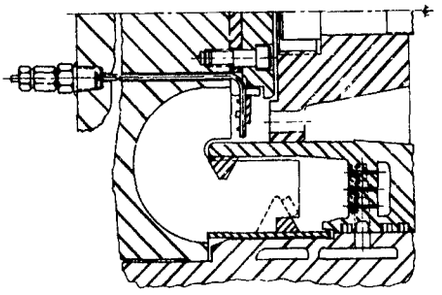
223 19.1 4691 11.72 1242 1325 1267 2.608	**Remarks** 1. Erosion noted on the injector face between two orifice elements. 2. The fuel orifices at the affected elements are welded closed for run 028. 3. The Mod "B" pentad incorporates a screen over the oxidizer feed holes to eliminate the chip plugging problem.	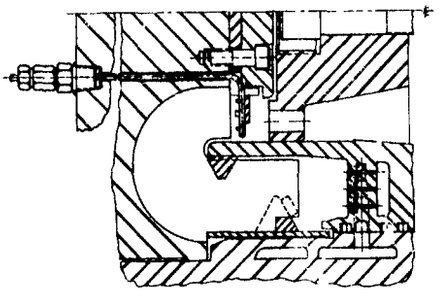

TEST No. 1.2-04-WAG-028	DATE 10-5-66			
Hardware	**Test Data**		**Remarks**	
Housing P/N 1121674 S/N 003	$\dot{W}_o$ (lbm/sec)	223	1. No damage to hardware	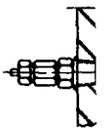
Injector Type Pentad Mod "B"	$\dot{W}_f$ (lbm/sec)	18.97	2. No erosion noted	
Injector P/N 1121895 S/N 002	P_c (psia)	4654		
Liner P/N N/A	MR	11.76		
Turbulator P/N 1130820	TtTi-1B (°F)	1297		
Turbine Simulator P/N 1130436	TtTi-2C (°F)	1329		
Temperature Rake P/N 1123032	TtTi-3A (°F)	1302		
End Cap P/N 1130820	ΔPc (%)	1.24		
Burnoff Injector P/N 1121502 Mod "A"	Duration (sec)	2.606		
Adapter Burnoff P/N 1130340				

TEST NO. 1.2-04-WAG-029	DATE 10-6-66			
Hardware	**Test Data**		**Remarks**	
Housing P/N 1121674 S/N 003	$\dot{W}_o$ (lbm/sec)	226	1. No damage to hardware	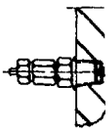
Injector Type Pentad Mod "B"	$\dot{W}_f$ (lbm/sec)	18.9	2. No erosion noted	
Injector P/N 1121895 S/N 002	P_c (psia)	4632		
Liner P/N N/A	MR	11.97		
Turbulator P/N 1130820	TiTi-1B (°F)	1378		
Turbine Simulator P/N 1130436	TtTi-2C (°F)	1331		
Temperature Rake P/N 1123032	TtTi-3A (°F)	1288		
End Cap P/N 1130820	ΔPc (%)	1.29		
Burnoff Injector P/N 1121502 Mod "A"	Duration (sec)	2.619		
Adapter Burnoff P/N 1130340				

TEST NO. 1.2-04-WAG-030	DATE 10-6-66			
Hardware	**Test Data**		**Remarks**	
Housing P/N 1121674 S/N 003	$\dot{W}_o$ (lbm/sec)	216.4	1. No damage to hardware	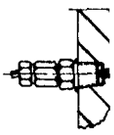
Injector Type Pentad Mod "B"	$\dot{W}_f$ (lbm/sec)	19.35	2. No erosion noted	
Injector P/N 1121895 S/N 002	P_c (psia)	4664		
Liner P/N N/A	MR	11.18		
Turbulator P/N 1130820	TiTi-1B (°F)	1369		
Turbine Simulator P/N 1130436	TtTi-2C (°F)	1486		
Temperature Rake P/N 1123032	TtTi-3A (°F)	1286		
End Cap P/N 1130820	ΔPc (%)	1.29		
Burnoff Injector P/N 1121502 Mod "A"	Duration (sec)	2.609		
Adapter Burnoff P/N 1130340				

Test Confi

Fi

223 18.97 4654 11.76 1291 1329 1302 1.24 2.606	**Remarks** 1. No damage to hardware 2. No erosion noted	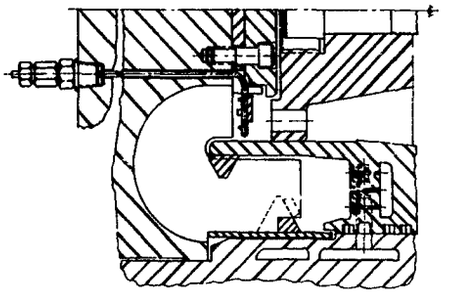
226 18.9 4632 11.97 1378 1331 1288 1.29 2.619	**Remarks** 1. No damage to hardware 2. No erosion noted	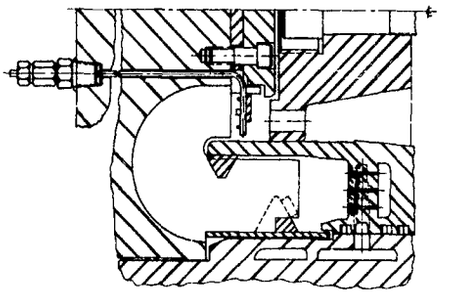
216.4 19.35 4664 11.18 1369 1486 1286 1.29 2.609	**Remarks** 1. No damage to hardware 2. No erosion noted	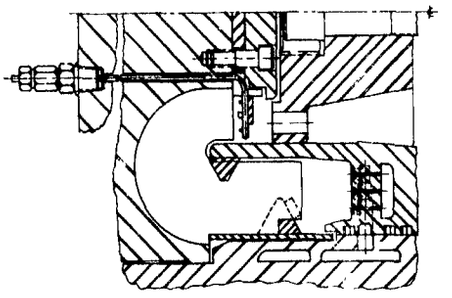

TEST No. 1.2-04-WAG-031	DATE 10-6-66	
Hardware	**Test Data**	**Remarks**
Housing P/N 1121674 S/N 003	$\dot{W}_o$ (lbm/sec) 234	1. No damage to hardware
Injector Type Pentad Mod "B"	$\dot{W}_f$ (lbm/sec) 18.4	2. No erosion noted
Injector P/N 1121895 S/N 002	P_c (psia) 4602	3. Pulsed with an 80 grain charge at FS_2
Liner P/N N/A	MR 12.71	
Turbulator P/N 1130820	TtTi-1B (°F) 1079	
Turbine Simulator P/N 1130436	TtTi-2C (°F) 1224	
Temperature Rake P/N 1123032	TtTi-3A (°F) 1191	
End Cap P/N 1130820	ΔPc (%)	
Burnoff Injector P/N 1121502 Mod "A"	Duration (sec) 2.609	
Adapter Burnoff P/N 1130340		

TEST NO. 1.2-04-WAG-032	DATE 10-6-66	
Hardware	**Test Data**	**Remarks**
Housing P/N 1121674 S/N 003	$\dot{W}_o$ (lbm/sec) N/A	1. Cold pulse test with 80 grain charge to determine pulsing characteristics to assist in stability analysis.
Injector Type Pentad Mod "B"	$\dot{W}_f$ (lbm/sec) N/A	
Injector P/N 1121895 S/N 002	P_c (psia) N/A	2. No damage to the hardware.
Liner P/N N/A	MR N/A	
Turbulator P/N 1130820	TtTi-1B (°F) N/A	
Turbine Simulator P/N 1130436	TtTi-2C (°F) N/A	
Temperature Rake P/N 1123032	TtTi-3A (°F) N/A	
End Cap P/N 1130820	ΔPc (%)	
Burnoff Injector P/N 1121502 Mod "A"	Duration (sec) 2.609	
Adapter Burnoff P/N 1130340		

TEST NO.	DATE	
Hardware	**Test Data**	**Remarks**
Housing P/N S/N	$\dot{W}_o$ (lbm/sec)	
Injector Type	$\dot{W}_f$ (lbm/sec)	
Injector P/N S/N	P_c (psia)	
Liner P/N	MR	
Turbulator P/N	TtTi-1B (°F)	
Turbine Simulator P/N	TtTi-2C (°F)	
Temperature Rake P/N	TtTi-3A (°F)	
End Cap P/N	ΔPc (%)	
Burnoff Injector P/N	Duration (sec)	
Adapter Burnoff P/N		

Test Cc

234 18.4 4602 12.71 1079 1224 1191 2.609	**Remarks** 1. No damage to hardware 2. No erosion noted 3. Pulsed with an 80 grain charge at 78_c	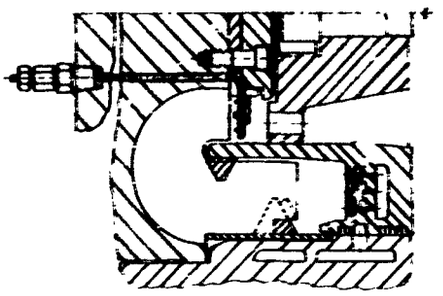
N/A N/A N/A N/A N/A N/A N/A 2.609	**Remarks** 1. Cold pulse test with 80 grain charge to determine pulsing characteristics to assist in stability analysis. 2. No damage to the hardware.	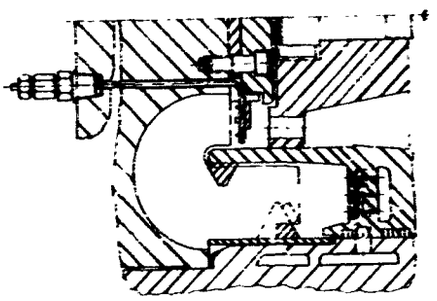
	Remarks	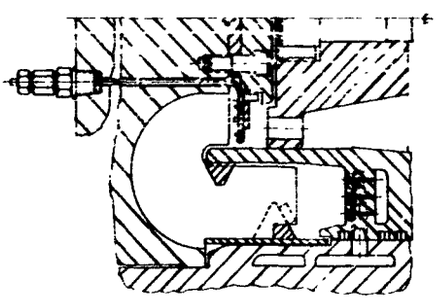

CONFIDENTIAL

Test Configuration and Data Summary (u)

Figure V-8, Sheet 11 of 11

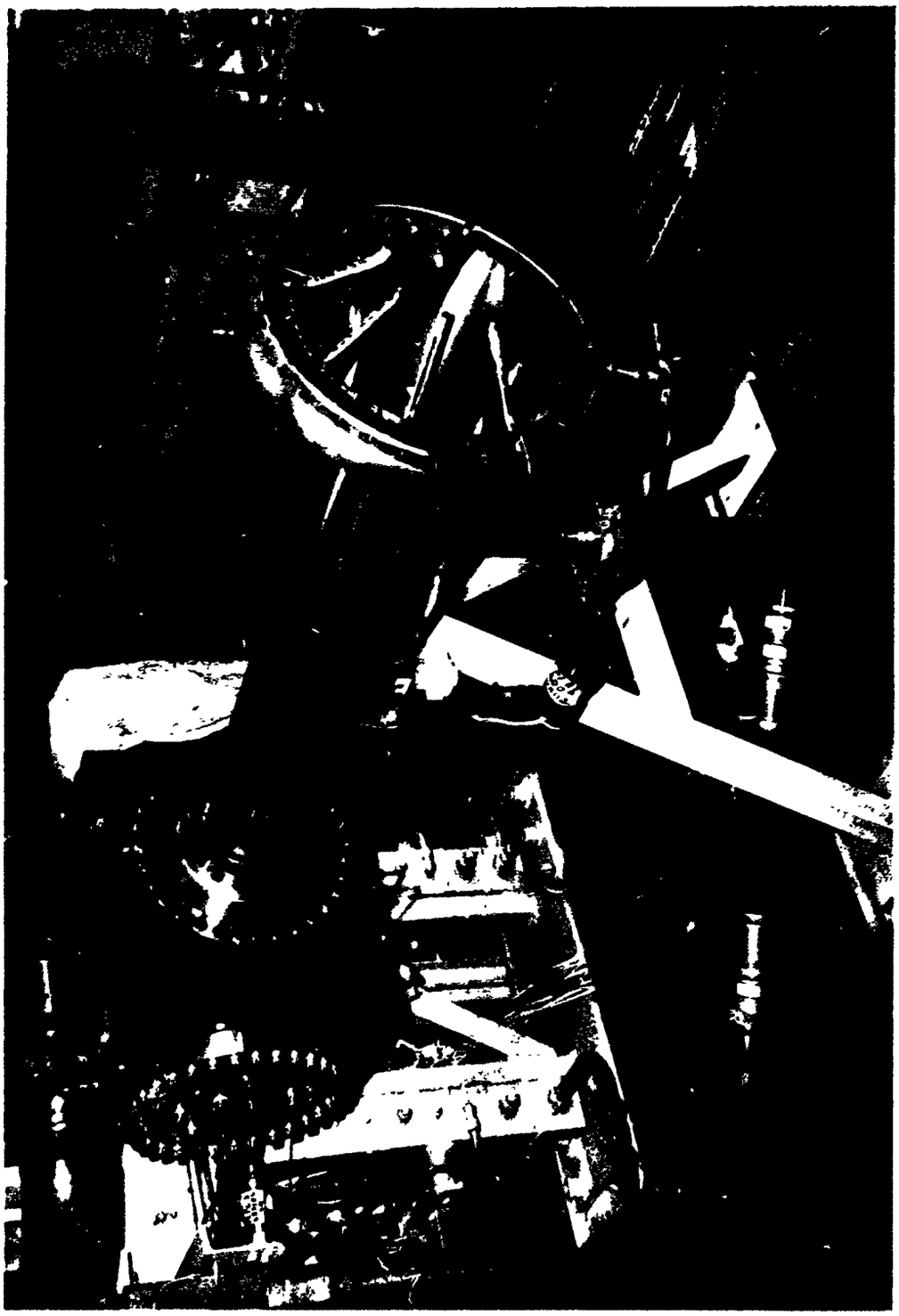

Primary Combustor Test Setup

Figure V-9

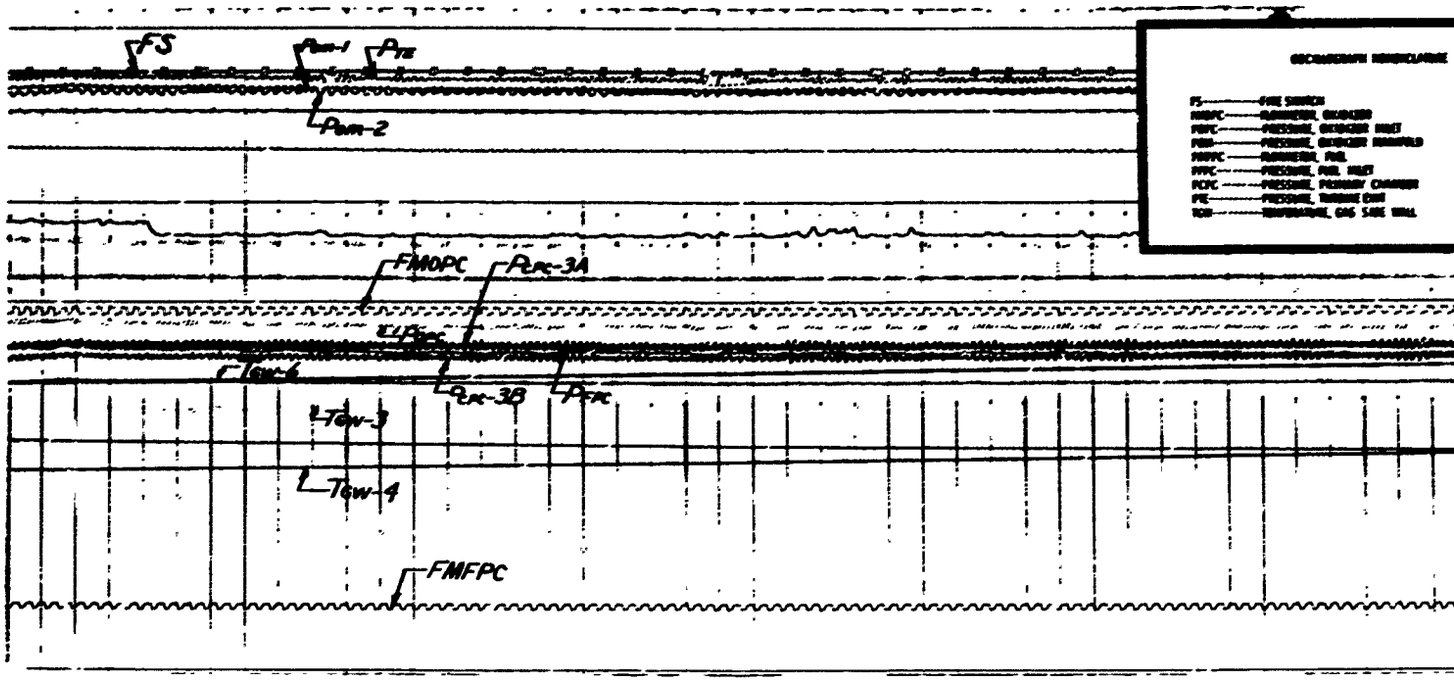

Start Transient

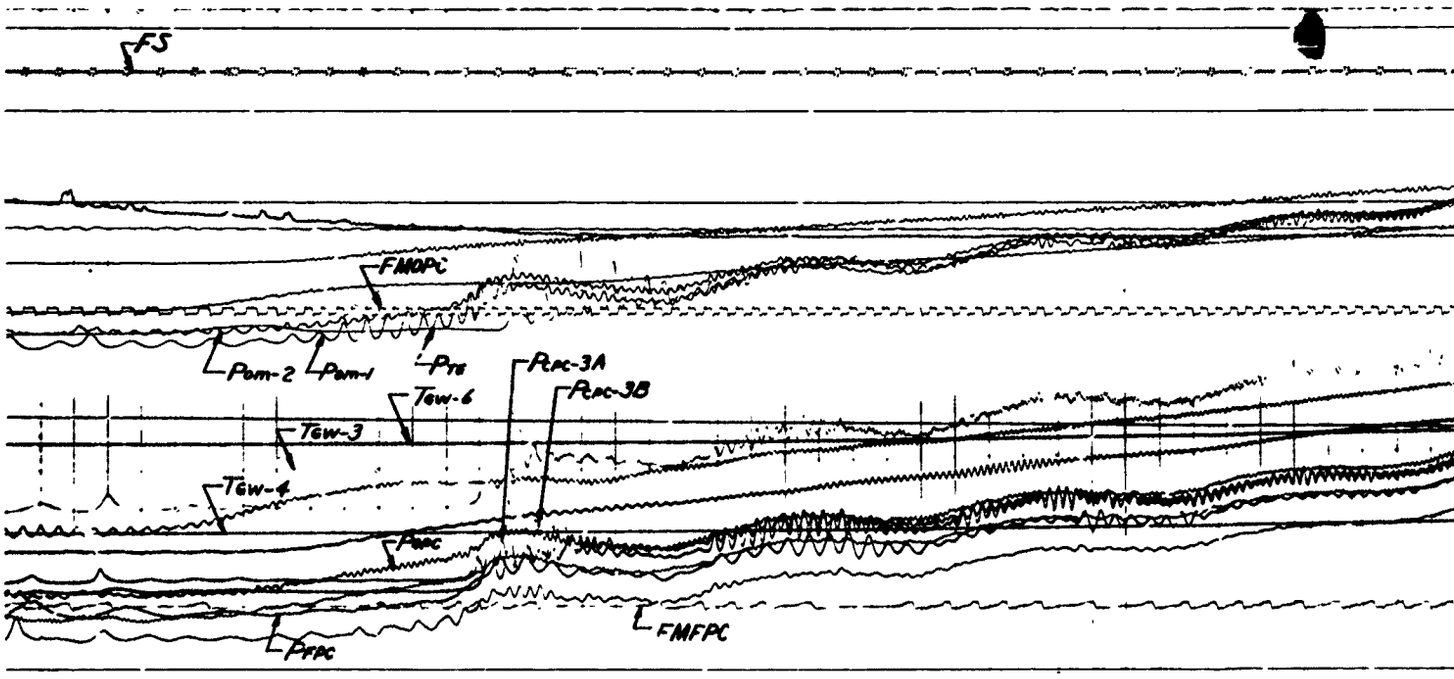

Steady State

Typical Oscillograph, Start Transient

Figure V-10

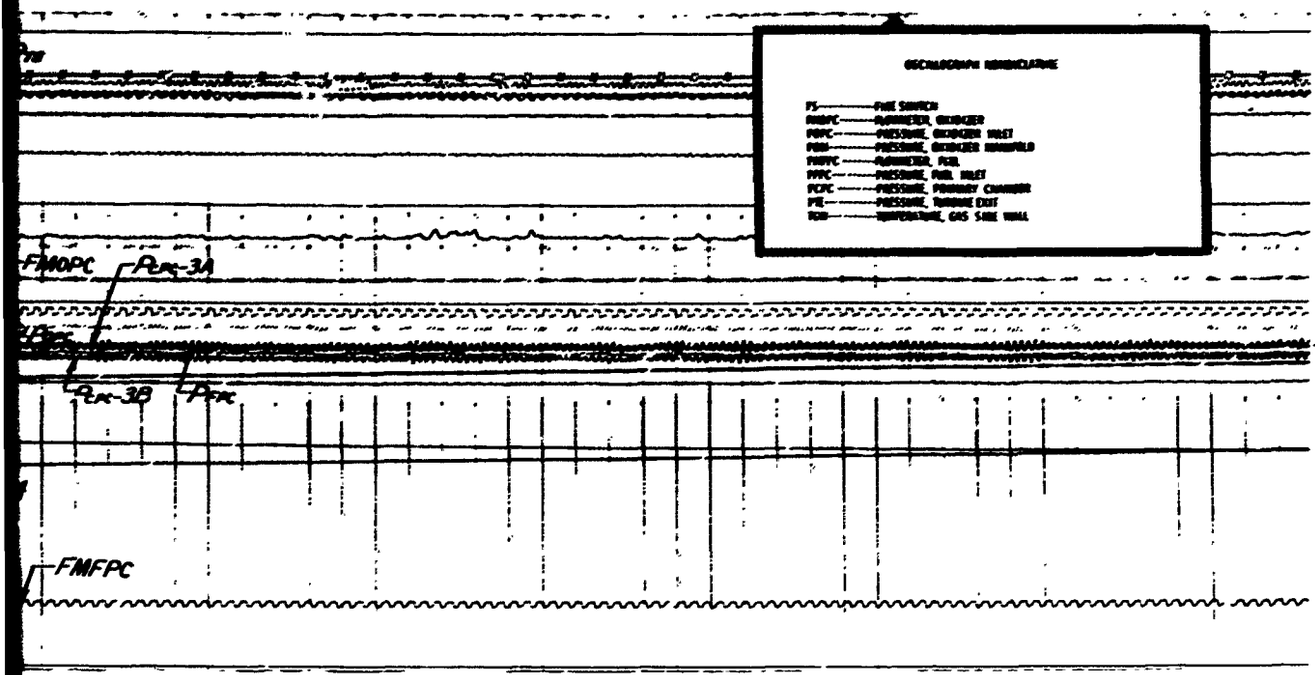

Start Transient

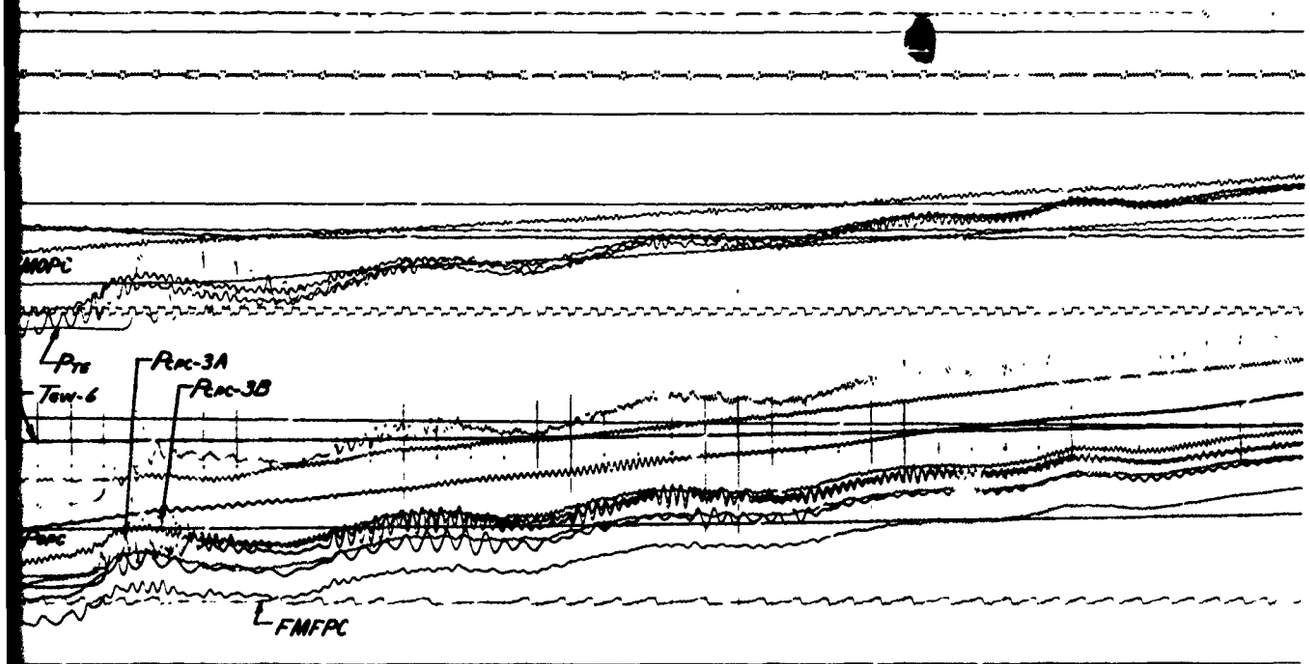

Steady State

Typical Oscillograph, Start Transient and Study State

Figure V-10

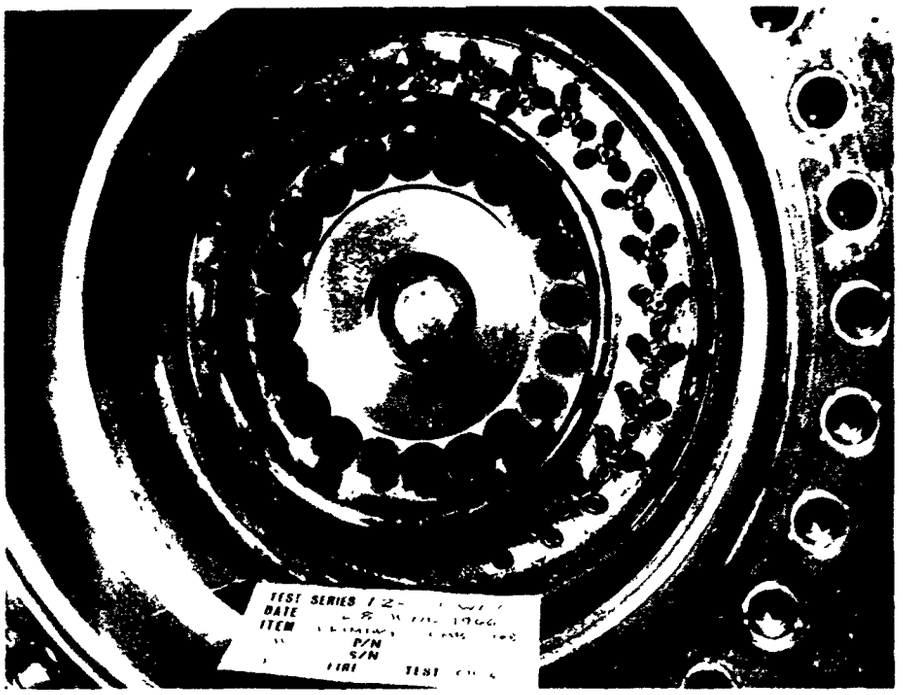

View Looking Toward Injector

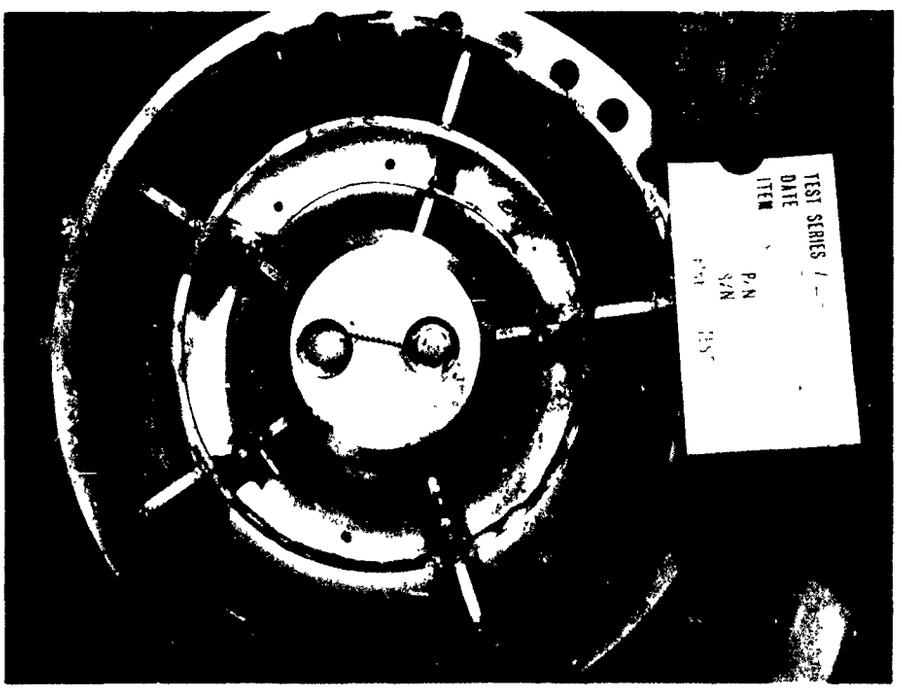

View Looking Toward Vane Assembly

Quadlet Injector and Liner Vane Assembly Posttest 1.2-04-WAG-006

Figure V-11

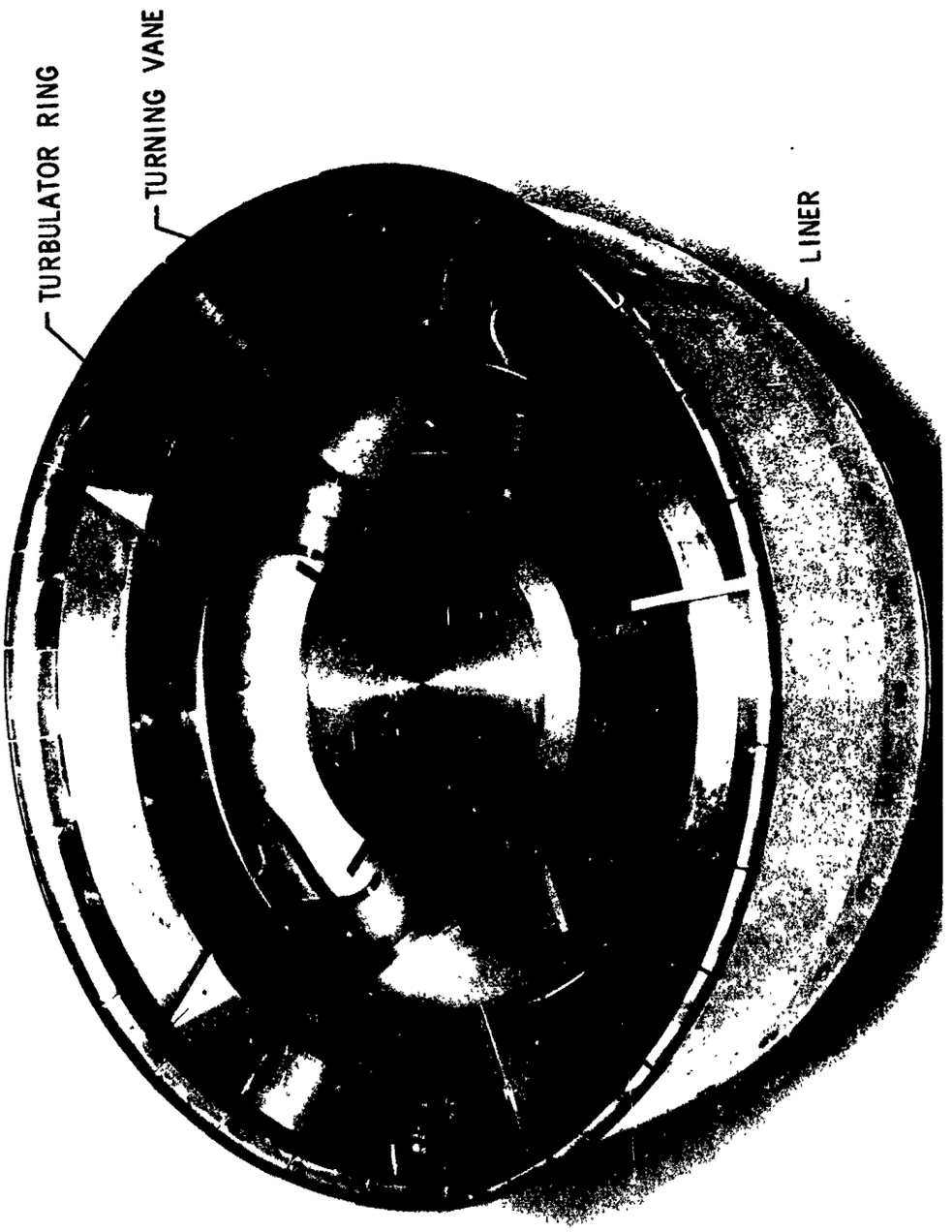

Turbulator Ring, Vane Assembly Pretest 1.2-04-WAG-008

Figure V-12

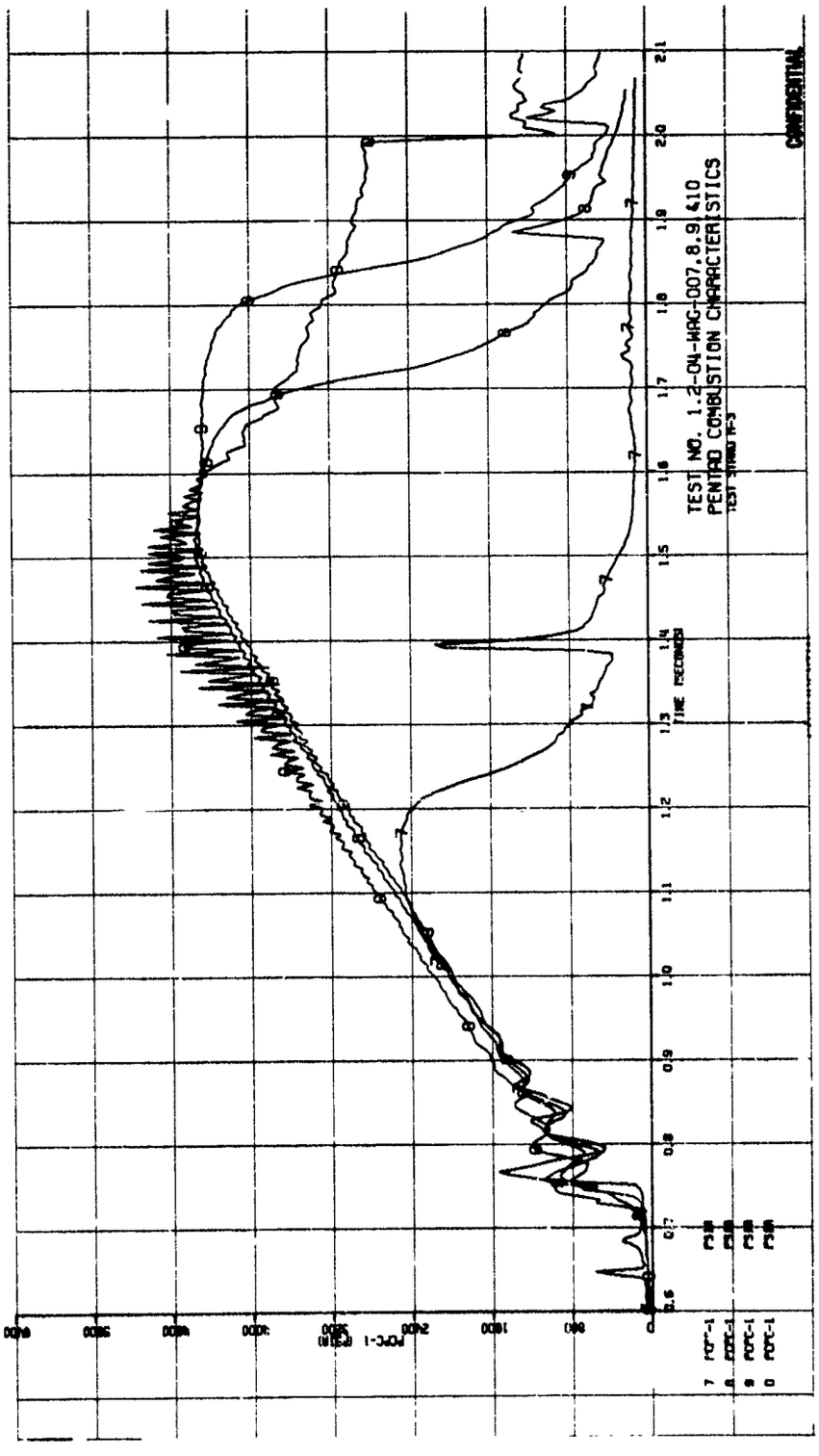

Chamber Pressure Oscillation Characteristic 1.2-03-WAG-007, -008, -009, -010 (u)

Figure V-13

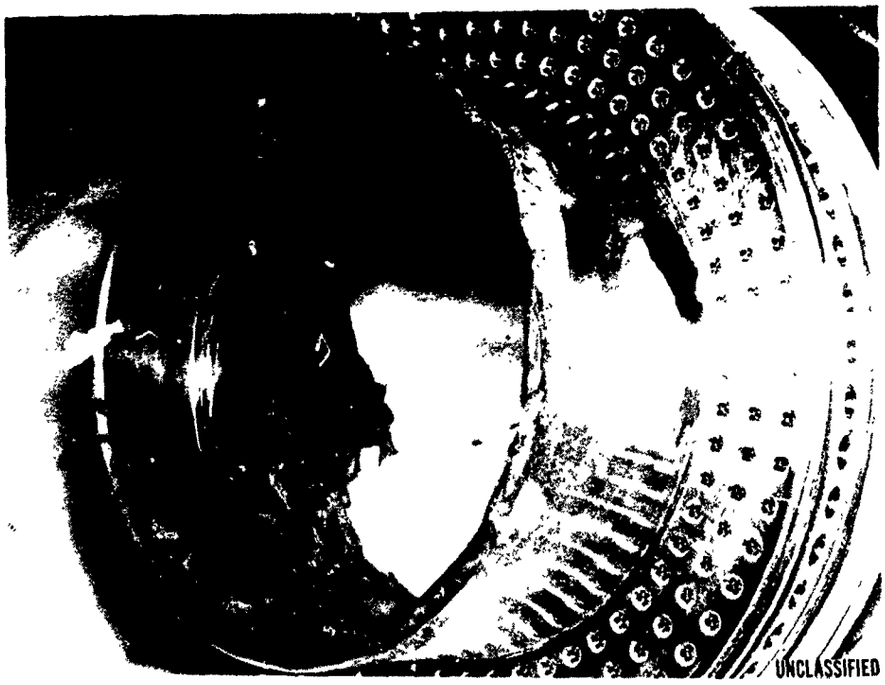

View Looking Toward Injector

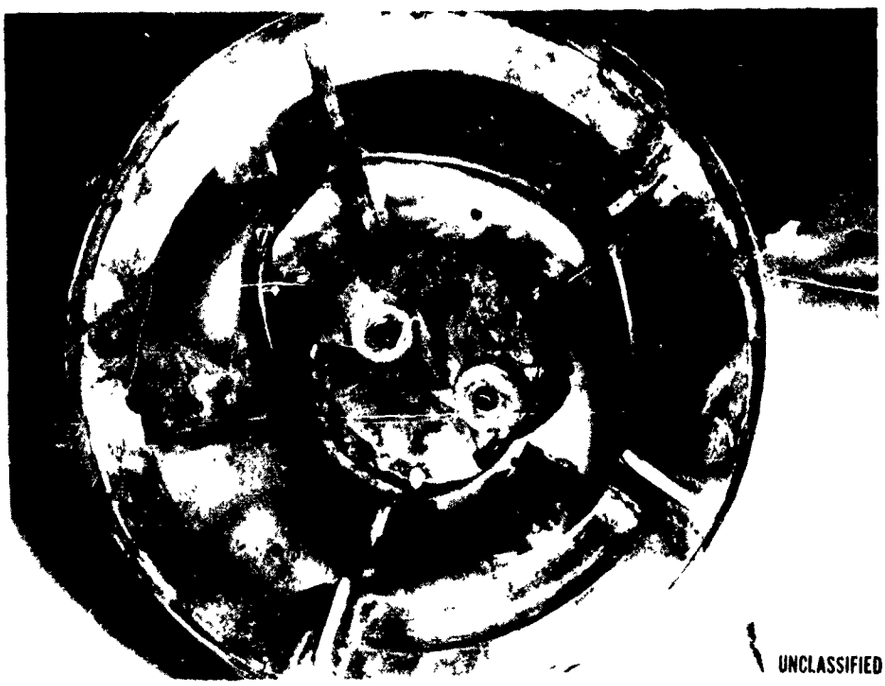

View Looking Toward Vane Assembly

Pentad Injector and Turbulator Vane Assembly Posttest 1.2-04-WAG-010

Figure V-14

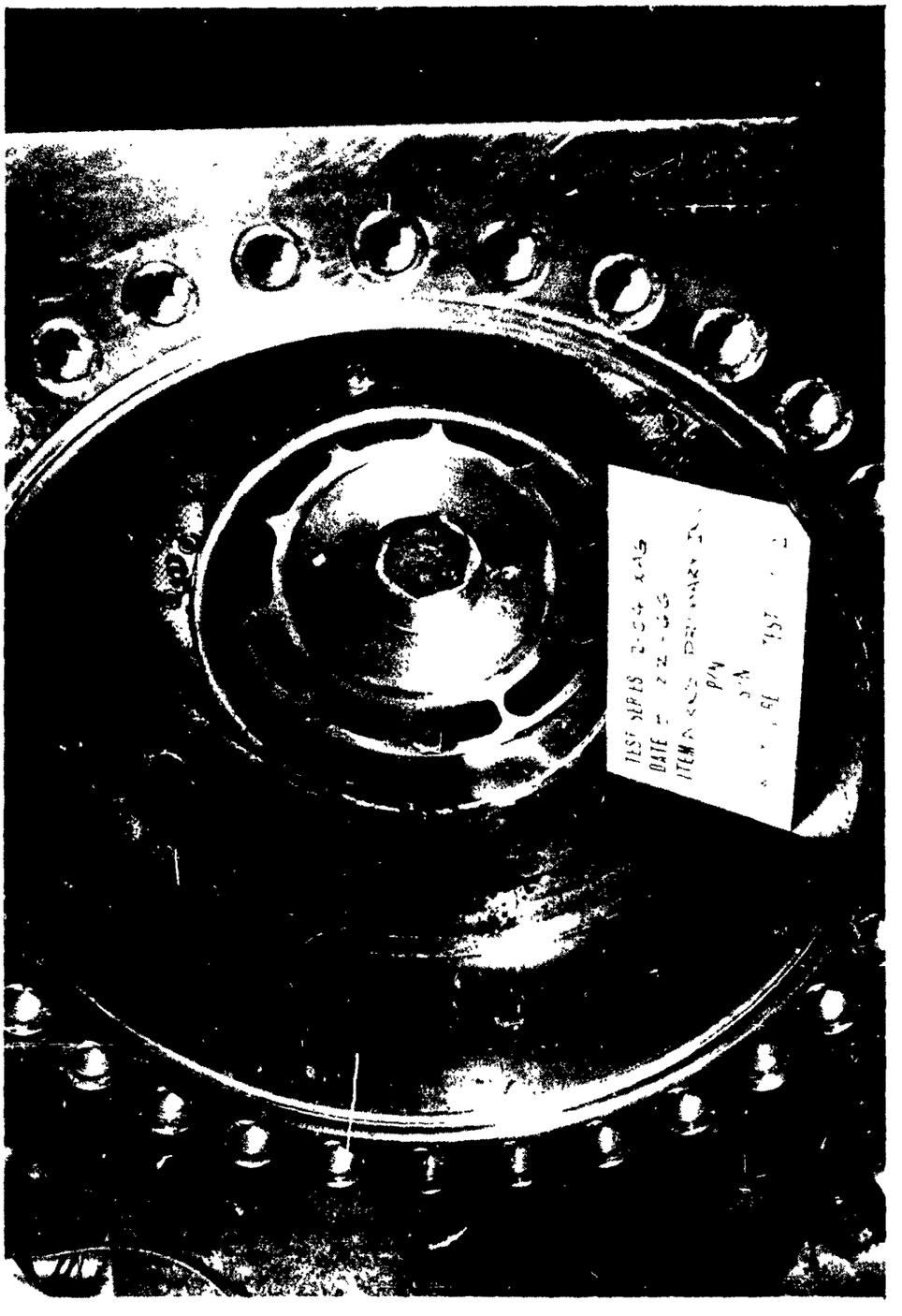

Quadlet Injector Posttest 1.2-04-WAG-012

Figure V-15

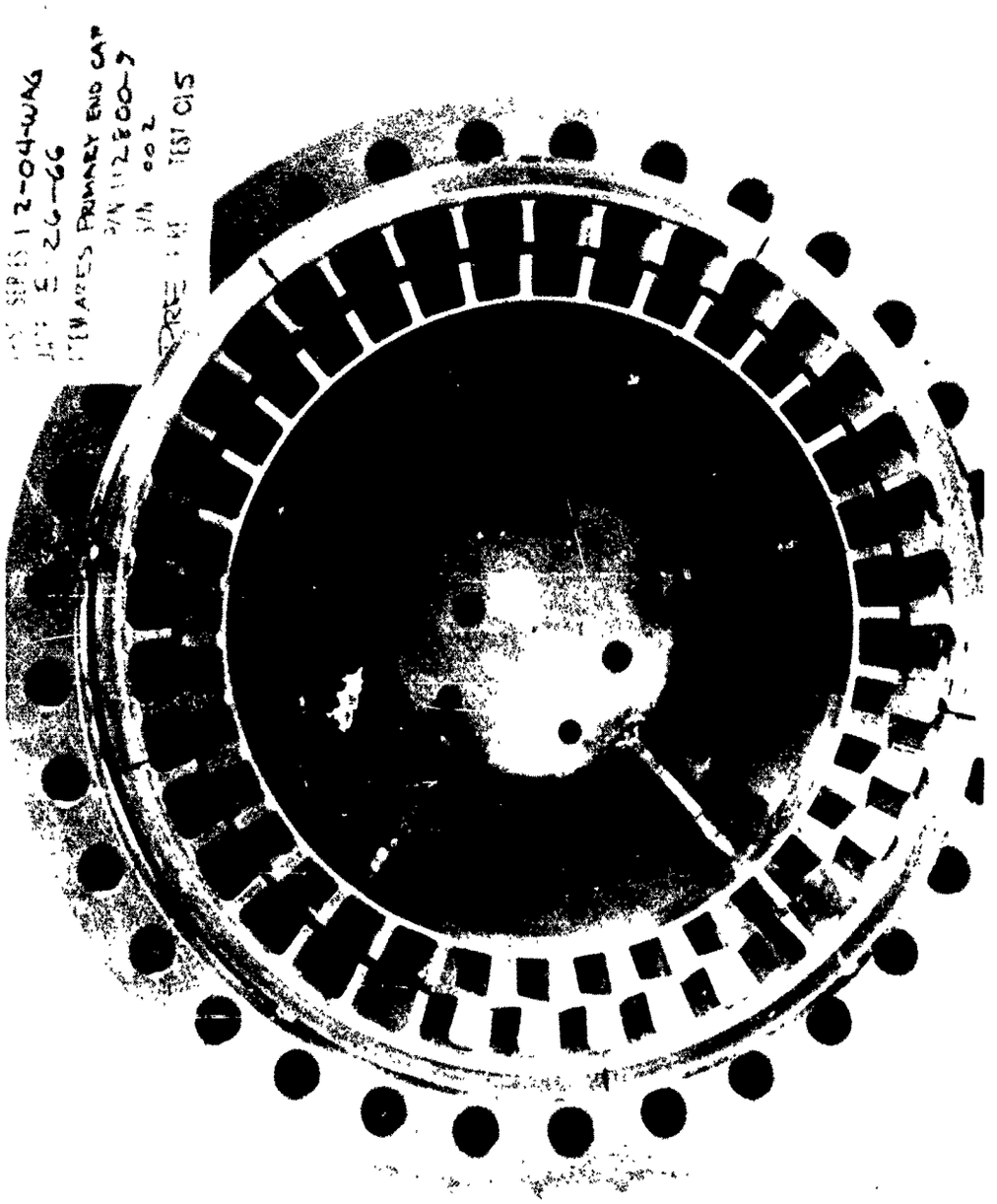

Canted Blade Turbulators

Figure V-16

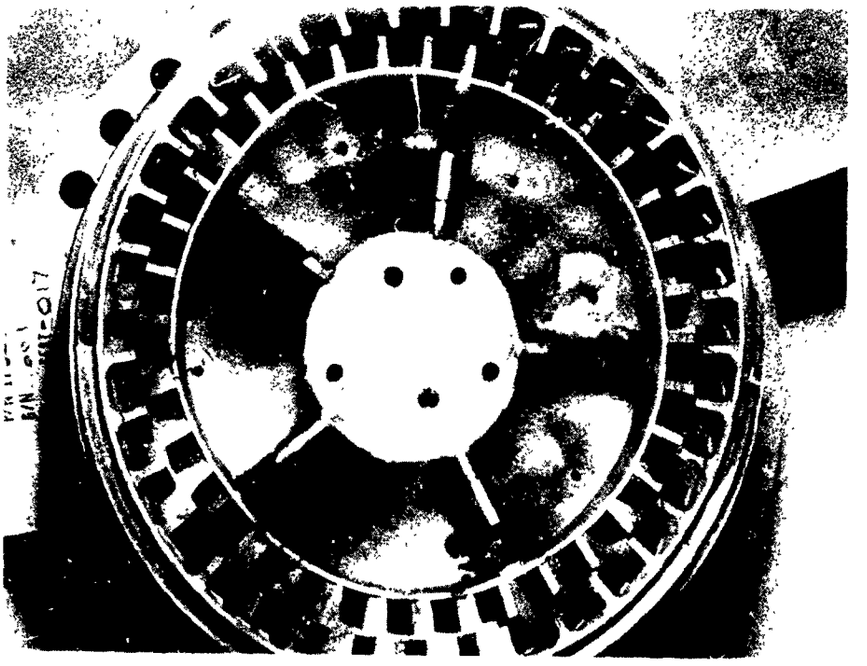

View Looking Toward Vane Assembly

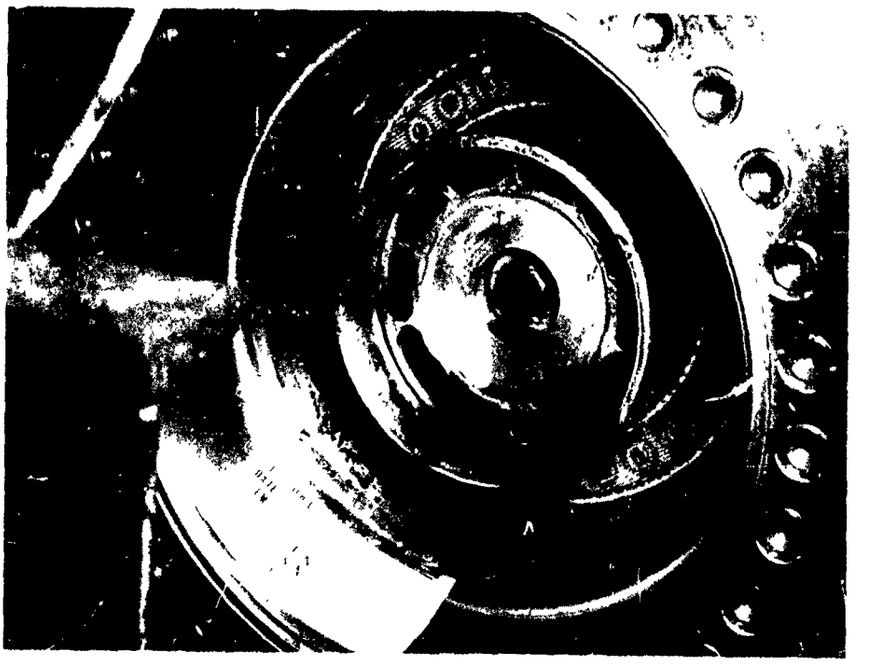

View Looking Toward Injector

Full Flow Injector-Turbulator Vane Assembly Posttest 1.2-04-WAG-017

Figure V-17

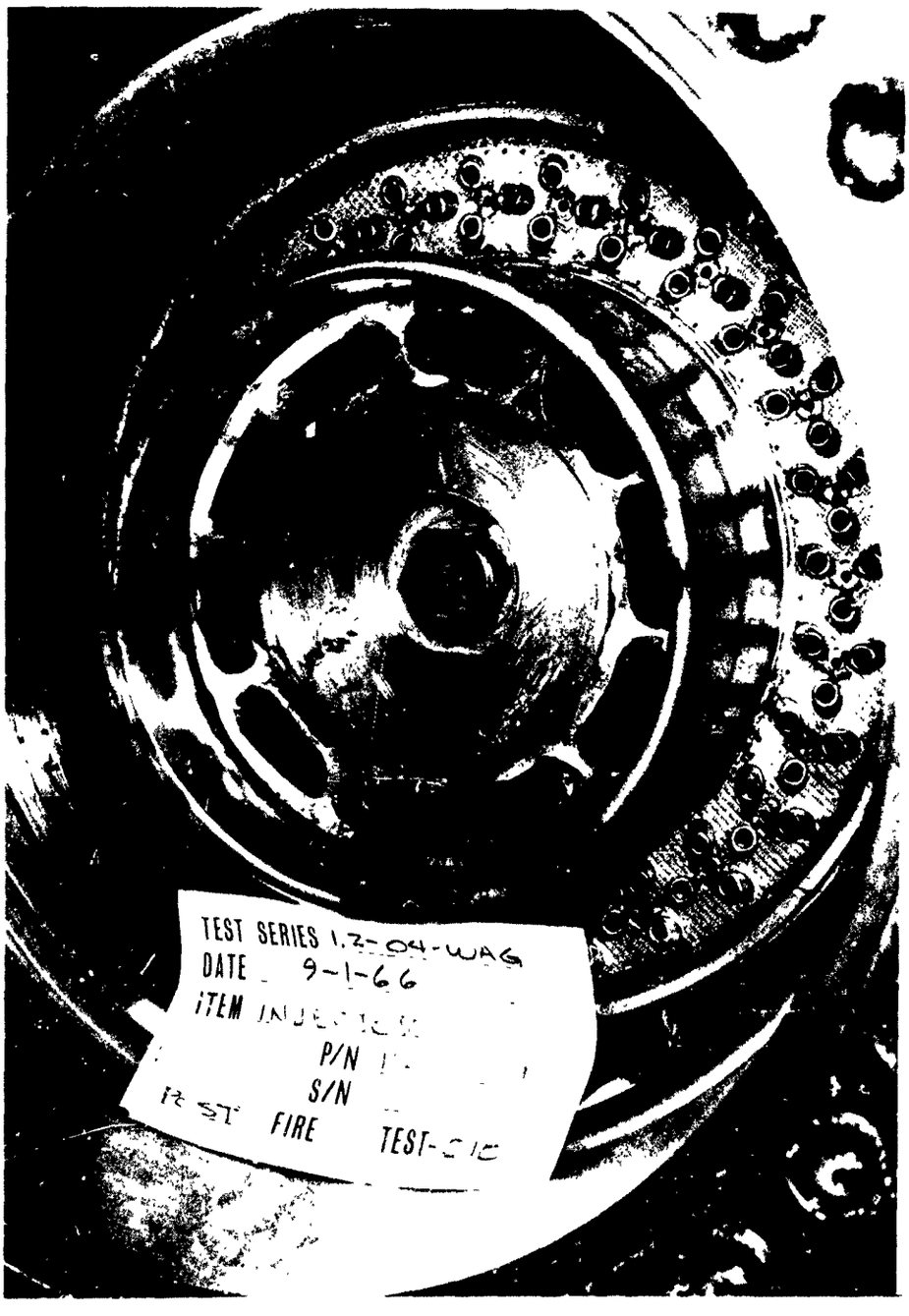

Quadlet Injector Posttest 1.2-04-WAG-018

Figure V-18

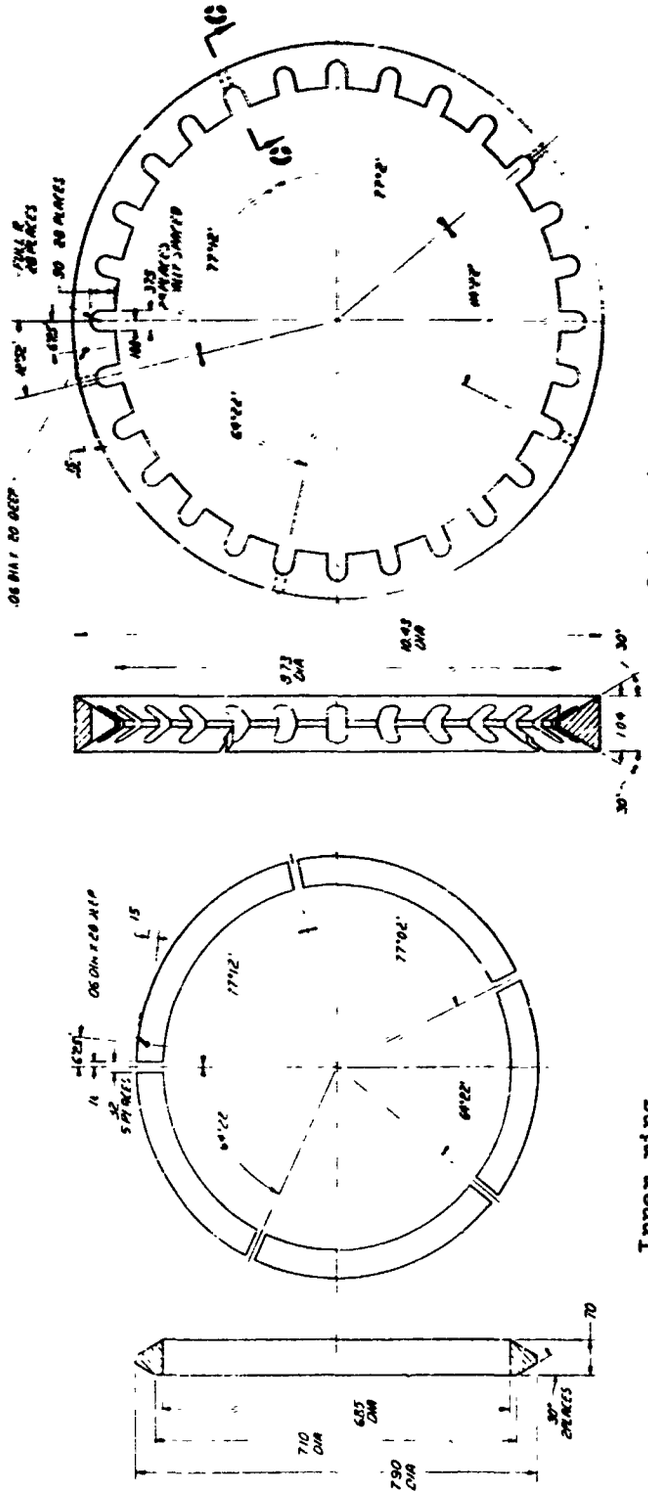

Outer ring

Inner ring

Turbulator-Solid Triangular Inner Ring, Notched Triangular Outer Ring

Figure V-19

VI.

SECONDARY COMBUSTOR ASSEMBLY

VI.

SECONDARY COMBUSTOR PROGRAM

A. ICP RESIDUAL HARDWARE PROGRAM

1. Objective

(U) The objective of the ICP residual hardware program was to supply design data for modular injector and chamber designs of Phase I as well as to demonstrate regenerative cooling with supercritical N_2O_4. Specifically, this program would evaluate (1) the performance potential of two candidate secondary injector patterns, (2) the effects on injector performance with variation in characteristic length, (3) the performance loss attendant with oxidizer film cooling injected at the injector face over a wide range of flow, (4) the heat transfer capability and mechanical integrity of regenerative cooled chambers, and (5) the operating characteristics of an intensifier pressurization system to replace the turbopump pressurization system of the original ICP program.

2. Summary

(U) At the completion of the Integrated Components Program (ICP), Contract AF 04(611)-8548, significant amounts of hardware remained which could be used to obtain early design data for modular hardware as well as demonstrate the feasibility of supercritical N_2O_4 cooling in regeneratively cooled chambers. Realizing such information would not be available for a considerable period of time using new ARES-configuration hardware, this program was initiated to evaluate these residual components.

(U) The remaining components included two single pass regenerative cooled chambers, one with single point film coolant injection (Chamber SN R-4) and the other with two-point capillary tube injection (Chamber SN R-5).

(This page is Unclassified)

VI, A, ICP Residual Hardware Program (cont.)

The capillary tube chamber was approximately 90% fabricated while the other was ready for test. Two flameholder injector designs were also available, designated the Mark 32 and Mark 125 configurations. The Mark 32 injector was partially fabricated, while the Mark 125 injector required a small amount of remaining design effort. The staged-combustion test engine, with its high pressure pumping system, was completely available to do all required testing.

(C) The test program, which included 13 valid data point hot-firing tests, consisted of four test series. The first series was a basic evaluation of the Mark 32 and Mark 125 injectors. The thrust chamber used in these tests was an ablative-lined uncooled design having a nominal L* of 45 in. and an area ratio of 14.5. The measured vacuum specific impulse efficiencies of the assemblies using these two injectors were 86.4% and 86.3%, respectively. A substantial portion of the specific impulse loss in these tests is attributed to two losses not connected to the inherent performance of the injector. The first was a friction loss approximately 4.5% higher than normally experienced; this resulted from the very rough exit nozzle used in these tests. The second was a mixture ratio distribution loss of about 4% resulting from oxidizer gas from the primary combustor escaping into the secondary combustion chamber through a peripheral gap between the chamber and injector. Both of these excess losses were eliminated in subsequent tests (though not in the same test). When the friction and mixture ratio distribution losses, together with the calculated nozzle geometry loss, are subtracted from the measured specific impulse, the difference is the combustion loss, which represents the inherent performance of the injector. Using this method, the resulting calculated combustion loss efficiencies of the Mark 32 and Mark 125 injectors were 97.5% and 97.6% I_s, respectively. However, the Mark 32 injector experienced erosion on the trailing edge of its vanes and was therefore dropped from further consideration. The Mark 125 injector experienced no erosion, was very stable, and showed sufficiently high performance to be subjected to cooled chamber testing. Therefore, further investigations (Test Series 2 and 3 of the test program) were initiated.

VI, A, ICP Residual Hardware Program (cont.)

(U) The second test series was directed toward defining the characteristics of the Mark 125 injector when subjected to changes in chamber volume and the addition of supplementary film cooling. First, the effect of chamber characteristic length (L*) on injector performance was determined from chambers having L*'s from 17 to 38-in. (Figure VI-1). The data are shown corrected to an area ratio of 20:1 to be indicative of the ARES configuration. Second, the performance degradation due to oxidizer film cooling was established at film cooling flow rates of 0 to 15% of total engine flow. The results are shown in Figure VI-2. This series also determined that the friction loss of ablative nozzles can be as high as 5.5% of theoretical specific impulse.

(U) The third test series evaluated two regenerative chamber concepts, with two tests performed on each. The single-point injection chamber (SN R-4) was tested twice; spalling of the coating and pinhole leaks in the throat area resulted. The capillary tube chamber (SN R-5) was then tested, and gave excellent results while completing its desired duration with no erosion. During the second test with chamber SN R-5, an oxidizer supply hose ruptured, terminating the oxidizer flow to the primary combustor and causing it to go fuel-rich, which resulted in excessive engine and chamber damage. Based on the limited test data with these two chambers, the two-point capillary tube injection appears to be a more effective coolant injection technique than single-point injection. This failure cut short the planned eleven tests of the cooled chamber test program.

(U) The fourth series was directed toward developing the intensifier pressurization system to replace the turbopumps for the modular injector and chamber checkout testing. The intensifier system has the advantage of rapid turn-around testing by avoiding the sometimes lengthy service procedures of the turbopumps and gas generating supply system. A series of 22 cold flow tests and 3 hot firing tests were performed to develop this system.

(U) The test program also yielded a number of engine operational characteristics which were employed during the entire Phase I program. The fuel-side resistance requirement necessary to eliminate feed-coupled instabilities with the combustion process was defined. The phasing and termination of propellants to both primary and secondary injectors to obtain erosion-free engine operation were determined. Analytical representations of computerized engine operation simulation models for start, steady state, and shutdown were verified. These models allowed the prediction and elimination of numerous potential operational problems prior to testing.

(U) With the completion of this program, a foundation was available for design and development of all injector and chamber designs of the modular engine configuration.

3. Component Design

a. Injectors

(U) Two secondary injectors and one primary injector were test fired during the ICP Residual Hardware Program. They included the Mark 32 secondary injector, the Mark 125 secondary injector, and the Mark 20 primary injector.

(1) Mark 32 Secondary Injector

(U) The Mark 32 secondary injector was a flameholder design with 32 vanes of fuel jets suspended in the primary gas stream. With the oxidizer completely vaporized, the resulting reaction is only dependent on complete vaporization of the fuel. Since vaporization is dependent on droplet size, it is beneficial to increase the fuel dispersion to promote

rapid vaporization. A measure of this dispersion is termed the fuel perimeter, the summation of all fuel injection element perimeters. For the Mark 32, this perimeter was 110 in., somewhat greater than other injectors previously developed on the Integrated Components Program, Contract AF 04(611)-8548. (The Mark 19 and Mark 16 injectors of the ICP program had fuel exposure areas of 46 in. and 91 in., respectively.) The injector was designed on the previous program but fabricated on this program.

(U) The Mark 32 injector consisted of 16 long and 16 short evenly spaced radial vanes cantilevered into the hot gas stream, and in a plane perpendicular to the centerline of the combustor. Hot gas flows around each vane, in which fuel tubes are brazed at angles to the vane centerlines. The final assembly is shown in Figure VI-3. Each long vane has twenty-two 0.060-in. tubes spaced alternately on each side with one 0.120-in. tube on the end at the point of maximum circumference. Each short vane had seven 0.060-in. tubes spaced alternately on each side and one 0.105-in. tube on the outboard end. The pattern was designed to produce an even fuel distribution across the face.

(2) Mark 125 Secondary Injector

(U) This flameholder injector utilizes the same dispersion process as that of the Mark 32 injector with a slightly larger fuel perimeter (125 in.) and aerodynamically shaped vanes. The injector has 32 identical vanes with 20 tubes per vane. Each tube is 0.063-in. ID and extends, as shown in Figure VI-4, in such a manner to cover the entire face equally. The vanes are cantilevered from the fuel manifold and suspended so that the trailing edges are in a plane just downstream of the point of optional film coolant injection. Injector diameter was 8.5 in. so that the outboard tip of the vanes nearly touched the conical regenerative chamber wall when suspended within the chamber.

VI, A, ICP Residual Hardware Program (cont.)

(3) Mark 20 Primary Injector

(U) This injector was designed and fabricated on Contract AF 04(611)-8548 as a back-up to the Mod H design. The design includes 19 major elements, as shown in Figure VI-5. Fuel is injected from each element by eight radial tubes in a plane perpendicular to the combustor axis. Liquid oxidizer flows across these tubes from an annulus at the injector face as well as from eight holes at each element base. Seventy-two peripheral oxidizer injection holes were included for wall film cooling in the conical portion of the injector, which is in the combustion zone.

b. Combustion Chambers

(U) Two types of combustion chambers remained from Contract AF 04(611)-8548, ablative and regeneratively cooled. Both types were tested on this program.

(1) Ablative Chambers

(U) Residual ablative chambers were flanged pressure vessels lined with phenolic-impregnated refrasil material, MX2646, and were cemented at the joints with room-temperature-vulcanizing silicone rubber (RTV-60). Two chamber configurations were tested, cylindrical and conical. The conical chambers were of identical geometry to the regenerative chambers and of the same L* (17-in.). For increases in L*, a 27-in. L* cylindrical spool was employed ahead of the conical zone. Sectioned drawings of both configurations are shown in Figure VI-6.

VI, A, ICP Residual Hardware Program (cont.)

(2) Regeneratively Cooled Chambers

(U) Three different regeneratively cooled thrust chambers were assembled from components remaining from Contract AF 04(611)-8548. The basic regenerative circuit was the same for all of the three chambers. The difference between the individual units is the way in which supplemental film coolant was added into the combustion zone.

(U) The tube bundles were of single-pass design. Oxidizer entered the chamber through the inlet manifold at the expansion section end, area ratio seven, and flowed toward the injector through 176 tapered Inconel 718 tubes. Oxidizer was then collected in an outlet manifold and routed to the primary combustor externally around the secondary injector. The chamber contour approximated two intersecting cones intersecting at the throat. The entrance half angle was 7 degrees 45 minutes, while the exit half angle was 15 degrees. The tube bundles were externally reinforced with alternate layers of epoxy-impregnated glass cloth and roving. For performance testing at short durations an uncooled steel exit nozzle was used which extended the area ratio from 7 to 17 at the same exit 15 degree exit half angle. Tests of 5 sec or more would be performed without the extension. Detailed design descriptions are given in the Integrated Components Program Final Report, Contract AF 04(611)-8548. A photograph of a chamber assembled on the test engine is shown in Figure VI-7.

(C) Chamber SN R-4 was coated to a depth of 0.056-in. with a thermal barrier material composed of 85% W, 12% ZrO_2, and 3% Si. It contained no orifices for distribution of oxidizer film coolant. In testing of this chamber, film coolant was injected into the combustion chamber by a separate film-cooling ring located just above the chamber (see paragraph VI,C,3, below).

VI, A, ICP Residual Hardware Program (cont.)

(C) On Chamber SN R-5 a film-coolant distribution manifold at the injector end of the chamber was added. This manifold was supplied with oxidizer from the tube-bundle discharge manifold through ten drilled passages. Film coolant entered the combustion chamber through 176 small bleed holes drilled into the manifold and through 176 capillary tubes, supplied by the manifold and discharging just upstream of the throat. Figure VI-8 illustrates this construction and also the basic tube bundle shape. This chamber was coated with 0.020 to 0.025 in. of 82% W, 12 ZrO_2, 3% Si, and 3% Cu.

(U) Chamber SN R-6 was built exactly the same as SN R-4, without a film coolant supply manifold. However, the tube crowns contained twenty-five 0.005 in. dia holes cut into each tube at the convergent section of the chamber with an electron beam to supply film coolant to the gas-side tube wall. Starting at the throat, the holes were spaced 0.264-in. apart to a distance 3.69 in. above the throat. From that point up to a total distance of 6.84 in. above the throat, the spacing was 0.315 in. Figure VI-9 shows this chamber in the hydraulics laboratory flowing water from the crown holes of the tube. During the flow test, approximately 15% of the film coolant holes became plugged with contaminates from the laboratory water, which would have to have been removed prior to committing the chamber to an engine test. At that point in time, ARES configuration secondary injector hardware became available for testing, and it was decided to proceed with that test program in lieu of additional ICP configuration cooled chambers. As a result, chamber SN R-6 was never test-fired in the program.

c. Film Coolant Rings

(U) The first film-coolant ring used on the residual hardware program contained a projecting shoulder on the inside diameter. Three hundred and sixty holes of 0.031-in. dia were drilled into this shoulder at an

VI, A, ICP Residual Hardware Program (cont.)

8° angle, discharging film coolant parallel to the ablative walls. Every fourth hole in this ring had been welded shut for testing under Contract AF 04(611)-8548. The ring was tested in this condition in Tests 1.2-07-WAM-007 and -008. Figure VI-10 is a photograph of this ring.

(U) The second film-coolant ring tested on the residual hardware program was composed of 360 tubes and their supply manifold. The tubes were 0.065-in. OD and had a 0.015-in. wall. The tubes entered the combustion zone at an angle of nearly 90 degrees with the chamber centerline so that the film coolant was discharged along the conical ablative wall. The upper surface of the coolant ring was protected during firings with a contoured collar of refrasil material. Figure VI-11 is a photograph of this coolant ring.

(U) Although the film coolant ring was sandwiched between the injector manifold and the combustion chamber, the film coolant and secondary fuel discharged in about the same plane as a result of axial displacement of the injector elements below the injector supply manifold.

d. Engine System

(U) Nineteen tests were conducted on the residual hardware program using the staged-combustion test engine developed during the Integrated Components Program. High-pressure propellants were supplied by pumps for 16 tests and by intensifiers for three tests. The basic engine configuration was not altered when the pressure source was changed.

VI, A, ICP Residual Hardware Program (cont.)

(1) Staged-Combustion Test Engine

(U) In the test engine, oxidizer is routed from the pump discharge through the regenerative chamber circuit (if used), through the primary oxidizer valve, and injected into the Mod-H primary combustor, which was developed on Contract AF 04(611)-8548. Film coolant, if required, was tapped off the main oxidizer line at the pump discharge location.

(U) Fuel was routed two ways from the pump discharge. Approximately 20% was supplied to the primary combustor through a small line and valve. Secondary fuel, the remaining 80%, flows in a larger pipe through the secondary combustor fuel valve, balance orifice, and is then injected into the secondary chamber. Figure VI-12 is a schematic drawing of this engine.

(2) Pumping System

(U) The turbopump system was completely developed on Contract AF 04(611)-8548. In this system, hot gas from a single large LO_2-RP_1 gas generator was supplied to two turbopumps through a Y-manifold. Power balance was obtained by orificing the fuel turbine hot gas inlet. A number of supporting subsystems were required such as a gas generator valve, switches, LO_2 and RP_1 supply vessels and valves, purge lines and valves, and lube-oil supply. As a result of this added complexity, the pumping system was responsible for four of the six test malfunction obtained during engine testing. In a number of cases, rated chamber pressure could not be attained because of turbine power limitations.

(3) Intensifier System

(U) The last three tests performed on the Residual Hardware Program employed gas-liquid pressure intensifiers to replace the turbopumps.

VI, A, ICP Residual Hardware Program (cont.)

Each intensifier is composed of a cylinder, within which operates a shaft with pistons at either end. The pistons have an area ratio of 5:1; therefore, the gas side pressure, which is supplied at up to 1250 psig, produces a pressure five times greater on the liquid side (6,200 psig max).

(U) Control of gas pressure and subsequently liquid pressure is maintained by two gas flow control systems to the low-pressure side of the intensifier. Servo-control for the flow control valves is supplied by a logic system with a proportional and integral error system programed in an analog computer located in the control room at the test stand. This system can control to any desired time base pressure profile for flow rates of 10 to 280 lb/sec of oxidizer and 1 to 105 lb/sec of fuel. Maximum discharge pressure is 6200 psia. Run time is limited to 5 sec at rated engine flows.

(U) Pressure control on the gas side of the intensifiers permits small leaks in the engine from effecting pressure and flows; thus, proper mixture ratio is always maintained. This is not the case in a pump-fed system where pressure and flow are regulated to a set of values commensurate to the balanced gas horsepower.

(U) The intensifiers, being single-stroke positive-displacement pumps, allow propellant consumption to be measured directly by piston position. A schematic of the intensifier system is shown in Figure VI-13.

4. Development Testing

(U) The test program was divided into four parts. The first part defined the base injector performance characteristics. The second part defined the injector-chamber performance characteristics effects of chamber volume and film cooling. The third part of the program evaluated the

VI, A. ICP Residual Hardware Program (cont.)

feasibility of supercritical N_2O_4 cooling by testing the remaining regenerative chambers. The fourth part developed the intensifier pressurization system to a point of operational acceptance for Phase I modular testing.

a. Uncooled Injector Performance, Stability and Erosion Evaluation (Tests 1.2-07-WAM-001 through 005)

(U) This series evaluated the base performance, erosive characteristics, and stability of the two injector patterns. Performance interpretation is shown in Figure VI-14 and is discussed under Test Data Evaluation VI,E,1.

(1) Mark 32 Injector

(U) The series was initiated with testing of the Mark 32 in an uncooled chamber of 44-in. L*. Postfire evaluation of the hardware indicated several split fuel tubes and minor erosion of the vane trailing edges. Performance was satisfactory as shown in the performance summary of Figure VI-14. Postfire hardware condition is shown in Figure VI-15. Detailed data analysis revealed the erosion was partly a result of transient temperature excursions in the primary combustor and vane aerodynamic characteristics.

(2) Mark 125 Injector

(U) Superior overall operation was demonstrated by the Mark 125 injector as compared to the Mark 32 injector tested previously. The test data and performance of this injector is shown in Figure VI-14. No incidence of instability was recorded. Postfire hardware condition was excellent, as shown in Figure VI-16.

VI, A, ICP Residual Hardware Program (cont.)

b. Effects of L* and Film Cooling (Tests 1.2-07-WAM-006 through 012)

(U) This series of tests was conducted to produce data allowing optimization of the modular Phase I TCA chamber design. As generally recognized, significant performance increases are available by increasing the chamber length (L*). This performance increase, however, usually results in increases in the heat transfer requirements because of larger exposed surface area. Additional amounts of supplementary cooling are then required. Therefore, increases in chamber L* must be limited to that which yields performance gains above the performance losses of supplementary coolant. The empirical data gained from this series would allow optimization of the design taking into account these factors.

(U) Using the Mark 125 secondary injector the L* evaluation series was conducted first. At 17-in. L* the injector demonstrated significant performance over that encountered at 38-in. L*. Detailed analysis indicated this effect was a result of reduction of primary gas flow about the injector periphery. In the 38-in. L* configuration, a gap of approximately 3/8 in. existed between the outermost fuel tube and the chamber wall. At 17-in. L*, however, the gap was completely eliminated by the intersection of the injector diameter on the conical wall of the chamber. A sketch of the injector in the two tested configurations is shown in Figure VI-17. Graphic representation of the performance effect as a result of L* changes defined the combustion loss as given in Figure VI-1.

(U) Four tests were conducted with ablative chambers to establish the effect of film coolant on engine performance and heat transfer in the chamber and nozzle. All tests were conducted with the Mark 125 secondary injector. In the first two tests ablative nozzles were used. The last

VI, A, ICP Residual Hardware Program (cont.)

two tests were run with a Rockide-coated steel nozzle to verify shear-drag losses calculated for the rough ablative nozzles. The first three tests produced film coolant percentages of 15, 10, and 8% of total engine flow, respectively, with the last test of the series conducted without film coolant for base-point injector performance. Figure VI-18 is a prefire photograph of the tube-type film coolant ring combined with the modified Mark 125 injector and ablative chamber. Performance data obtained in this series appears in Figure VI-14. Performance loss as a result of these percentages of film cooling appear in Figure VI-2 with detailed analysis in Section VI,A,5a. Evaluation of temperature data obtained, giving measures of the heat transfer through the coolant, is given in Section VI,A,5,6.

c. Regenerative Chamber Evaluation (Tests 1.2-08-WAM-001 through 004)

(U) Two of the three regenerative chambers fabricated on the program were fired during this series. They were Serial Numbers (SN) R-4 and R-5.

(U) Chamber SN R-4 was tested with the multi-tube film-coolant ring and steel extension skirt. Shutdown of the test was signalled prematurely by an erroneous malfunction detection system signal. The gas generator shut down, but the thrust chamber valves did not. As a result, the chamber was fired for 87 sec at pump suction pressures until the test stand safety valves were closed. This sequence of events was attributed to a misconnected electrical control system.

(U) All hardware was undamaged and refired on Test 1.2-08-WAM-002. Film coolant flow rate during the test was 49.6 lb/sec, or 8.9% of total engine propellant flow. Postfire examinations of this duration test revealed a large number of pinhole leaks in the throat area and spalling of

the thermal barrier coating at the upper chamber flange and below the throat. Figure VI-19 illustrates these conditions.

(U) Chamber SN R-5 had two point film coolant injection and was tested twice. Test 1.2-08-WAM-003, which was performed with a film coolant flow rate of 40 lb/sec (8.1% total flow), was completely successful and no tube erosion or spalling of thermal barrier material was evident. The chamber was in excellent condition and completely satisfactory for repeat testing. It should be noted that the two point injection chamber operated successfully at substantially less coolant flow than was used in the erosive test of SN R-4 chamber.

(U) Test 1.2-08-WAM-004 was performed on chamber SN R-5 in an attempt to extend the firing duration from 2.0 to 3.25 sec. A malfunction detection system terminated the test after the flexible hose of an oxidizer inlet ruptured.

(U) Interpretation of the performance and cooling data obtained is discussed in Section VI,A,5.

d. Intensifier Checkout Series (Tests 1.2-09-WAM-001 through 003)

(U) Checkout of the intensifier pressurization system was conducted in three tests establishing operational capability. The original checkout engine comprised the back-up Mark 20 primary injector and back-up Mark 32 secondary injector. Following a malfunction, the second test gave excellent pressurization system operation. Hardware inspection, however, yielded severe erosion of the primary combustor injector, chamber and secondary injector. Detailed data analysis indicated this condition was a result

VI, A, ICP Residual Hardware Program (cont.)

of recirculations on the uncooled primary injector peripheral face area reacting exothermically with the highly oxidizing atmosphere of primary gases, and was no fault of the intensifier.

(U) The third test used the Mod H primary injector and the Mark 125 secondary injector and gave completely satisfactory operation. Performance data appears in Figure VI-14. Twenty water tests preceded this testing, the results of which established loop control settings for the computer logic system.

5. Test Data Evaluation

a. Performance

(1) Method of Determination

(U) Thrust chamber assembly performance for each test of the residual program was calculated using Performance Interaction Theory developed by Aerojet-General. These calculations were made as follows:

(U) First, specific impulse efficiency is calculated from test data.

$$\%I_{sv} = \frac{F + Pa \cdot Ae}{\dot{W}_T} / I_{s\ theor} \times 100$$

where:
- F = corrected sea level thrust, lbf
- Pa = ambient atmospheric pressure, psia
- Ae = measured nozzle exit area, $in.^2$
- $\dot{W}_T$ = total propellant weight flow, lbm

VI, A, ICP Residual Hardware Program (cont.)

(U) Next, losses are calculated for those factors which degrade performance. These losses are then subtracted from the theoretical specific impulse for the same mixture ratio and expansion ratio as the test. The remainder is then the loss associated with combustion performance for the particular injector-chamber combination, termed energy release loss. The validity of the loss calculations method has been verified from analyses of data produced by this and other Aerojet rocket programs.

(U) The end product of the foregoing series of computations is the loss associated with the injector on uncooled chamber tests. When film coolant is added to the thrust chamber, the energy release loss is then an established input, and the remaining loss is attributed to film cooling.

(U) The following paragraphs discuss losses associated with rocket engine performance.

(U) NOZZLE GEOMETRY or DIVERGENCE loss is a result of hot gas exiting the nozzle plane at an angle with the thrust axis.

(U) NOZZLE FRICTION loss is that loss associated with the viscous or shear drag in the boundary layer and at the nozzle wall.

(U) MIXTURE RATIO DISTRIBUTION loss is a result of propellant mass distribution at the injector face. The model considers that no appreciable mixing occurs between reacting "stream tubes" established at the injector because of the short stay time in the combustor. Therefore, the total performance is actually a summation of the performances of all of the individual "stream tubes." Most injectors are designed to operate at a mixture ratio corresponding to maximum specific where impulse losses are

incurred on either side of this mixture ratio. By having some areas fuel rich and some areas oxidizer rich, it is possible to operate an injector at optimum overall mixture ratio and yet deliver less than optimum performance. This loss in combustor performance is amplified in the nozzle because of the presence of less energetic gases in the nozzle expansion process.

(U) ENERGY RELEASE OR COMBUSTION loss results from the fact that even those propellants in the same "stream-tube" do not react completely as a result of the lack of sufficient chamber residence time. It also follows that this loss is amplified in the nozzle expansion process.

(U) FILM COOLANT loss occurs because the film coolant does not contribute to the combustion process, and in fact, reduces the average enthalpy of the exiting chamber gases. This loss is likewise amplified in the nozzle expansion process.

(U) An advantage attached to this method of data analysis lies in the assignment of losses to specific causes. In this manner, effort can be directed toward correction of those causes most amenable to improvement.

(2) Interpretation of Test Results

(U) For the tested configurations, the performance losses which apply are those of nozzle friction, nozzle exit geometry, mixture ratio distribution, combustion and oxidizer cooling. The tabulated losses for all tests appear in Figure VI-14.

VI, A, ICP Residual Hardware Program (cont.)

(a) Mixture Ratio Distribution Losses

(U) Mixture Ratio Distribution (MRD) losses for the tested injectors were created by two mechanisms: injector-to-chamber gap and irregular fuel distribution. The gap allowed primary combustor gas to escape without mixing with fuel, giving a low stream-tube performance. This mechanism was held responsible for the largest percentage of the MRD losses. Irregular fuel distribution was present on all Mark 125 injectors after Test 1.2-07-WAM-009 to reduce the cooling loads at the injector gas-to-film cooling interface. This condition was promoted by reducing the fuel flow area to 60% of its former value in the four outermost rows of the injector. This condition was incorporated to minimize interface reactions of injector gases with oxidizer film coolant.

(U) The MRD losses for each test were different for two reasons, injector-to-chamber gap distance and expansion area ratio. The gap loss changed on each buildup, since the distance from injector to chamber was different. Expansion area changes the MRD loss since the loss is expanded or magnified by area ratio.

(U) Test 1.2-07-WAM-006 was the only test that did not have any MRD losses. Test 1.2-09-WAM-003 was the only test other than 006 that did not have a chamber-to-injector gap MRD loss. All Mark 125 injector tests, except Tests 1.2-07-WAM-005 and 006, had the outer four rows of fuel tubes pinched to 60% of their normal fuel flow area. The variation in the recorded losses is a result of hardware changes and difference in operating point together with the magnifying effect of area ratio.

VI, A, ICP Residual Hardware Program (cont.)

(b) Friction Losses

(U) Four of the analyzed tests were conducted using ablative nozzles and one with an uncooled steel nozzle (Test 1.2-07-WAM-012) extending from area ratio 2 to 17. Postfire examination of the ablative nozzles indicated a rough wall had developed during the firing. A comparison with overall performance with ablative and steel nozzles indicated a performance decrement of about 4% occurring on the ablative nozzles. The ablative nozzle friction loss, determined by use of the Schlichting resistance formula for a rough wall, (Reference 16), was also 4% greater than the smooth-wall steel-nozzle friction loss determined using the extended Frankl-Voishel expression (Reference 17).

(U) The calculated friction loss for each test appears in the performance summary in Figure VI-14.

(c) Nozzle Divergence

(U) The nozzle divergence loss for tests with the ICP residual hardware was calculated for nozzles having 15 degree exit half angles. Variances in the results of these calculations result from the changes in mixture ratio of the gas and the nozzle area ratio. These results are also shown in the performance summary, Figure VI-14.

(d) Combustion Loss

(U) The five uncooled chamber tests allowed calculation of the combustion loss for the various characteristic lengths (L*) tested. They were 1.2-07-WAM-004, 006, 009, 012, and 1.2-09-WAM-003. Figure VI-1 shows these losses normalized to an area ratio of 20:1. These losses were calculated by taking the measured performance, subtracting it from

VI, A, ICP Residual Hardware Program (cont.)

theoretical and reducing the remainder by the three aforementioned loss calculations. At an L* of 39 in., the ARES design point, a loss of 25% results; therefore, the combustion loss efficiency for the Mark 125 injector is taken as 97.5%. The computed losses for the test area ratio and L* appear in the performance summary, Figure VI-14.

(e) Cooling Loss

(U) Five of the tests conducted (see Figure VI-14) were fired with various amounts of oxidizer film coolant. The chamber used for these tests had an L* approximately equal to the L* used on Test 012, which had a steel nozzle and no film cooling. Thus, by using the combustion loss from Test 012, it was possible to estimate the performance degradation from oxidizer film cooling. This correlation normalized to area ratio 20 appears in Figure VI-2. The effect of oxidizer film coolant on performance approximates 0.6% reduction in vacuum specific impulse for every percent film coolant used (percent of total engine flow).

b. Cooling

(1) Ablative Chamber Testing

(U) In the film cooled, ablative chamber testing, it was desired to examine the validity of the analytical model which describes the film cooling effectiveness of N_2O_4 in the ARES thrust chamber, in addition to measuring the performance loss associated with various amounts of film cooling.

VI, A, ICP Residual Hardware Program (cont.)

(U) Three tests, 1.2-07-WAM-009 through 011, were conducted to investigate the effect of different film-coolant flow rates on the temperature profile along the ablative chamber wall. The chamber was instrumented with Chromel-Alumel thermocouples. The tips of the thermocouples were installed flush with the wall to minimize flow disturbances in this region.

(U) Tests -009 and -010 used a fully ablative chamber and nozzle which had been tested previously on the ICP contract. Its degree of erosion and glassing over before these tests obscured any significant conclusions that otherwise could have been drawn from postfire inspection. The thermocouples were located in two rows (A and B) displaced 45 degrees radially and at ten stations along the chamber wall. The station locations with respect to the film coolant ring are presented in Figure VI-20.

(U) In Test -011 a new ablative chamber with a Rockide-coated steel skirt attached at an area ratio of 2:1 was used. The thermocouples were located circumferentially around the chamber at eight axially spaced stations. The axial locations of these thermocouples are presented in Figure VI-20.

(C) All tests were conducted at rated conditions of thrust, chamber pressure, and mixture ratio. The specific test parameters are presented in Figure VI-21. The stagnation temperatures of the mainstream gases were calculated on the basis of injector mixture ratio, chamber pressure, and combustion efficiency. The combustion efficiency associated with the Mark 125 injector was taken as 97.1%. This value was obtained from data of Test 1.2-07-WAM-012, which was uncooled. The stagnation temperatures were then calculated assuming they were proportional with the square of combustion efficiency.

VI, A, ICP Residual Hardware Program (cont.)

(U) The temperature data, shown in Figure VI-20, compare favorably with that data obtained from previous ICP tests. The only notable difference between the two is that the more recent temperatures are generally lower. This difference can be attributed to two factors: improved injector/chamber compatibility and a higher injector mixture ratio. The experimental data are compared to the analytical predictions in Figures VI-22 through 24.

(U) The predicted wall temperatures were based on a heat transfer coefficient determined by the well-known Bartz equation. Because of the dependence of the heat transfer on the combustion phenomena in the vicinity of the injector, a multiplication factor of 1.5 is applied to the heat transfer coefficient in the combustion chamber. This factor, hereafter referred to as the Bartz factor, decreases with contraction ratio to a value of 1.0 at the throat. This distribution was chosen for this comparison because it has been the basis of all ARES design work. As shown in the figures, the selected distribution produces reasonably close, but conservative, predictions for thrust chamber wall temperatures. The experimental data can be nearly matched by a distribution of 1.0 at the injector face and 1.2 at the throat. However, for clarity, this curve has been omitted from these figures.

(U) An additional factor to consider is the potential effect of outgassing of the ablative liner on the measured film coolant recovery temperature. Using semi-empirical relationships, the outgassing flow rate for the case of one-dimensional ablation can be determined as a function of time. At one second firing time with 20 lb/sec of film cooling it can be shown that the outgassing flow rate is only 3% of the film cooling flow rate and would not, therefore, significantly influence the film cooling temperature. Because of the uncertainties in this determination, however, it should be pointed out that the gases generated in the charring process, when introduced into the oxidizer film coolant will exothermically react, at least in part, with the

VI, A, ICP Residual Hardware Program (cont.)

film coolant. The extent of this reaction and its effect on film coolant temperatures cannot be realistically determined. However the effect will be conservative, i.e., higher film coolant temperatures will exist than would if the reaction did not occur.

(U) Examination of the chamber after Test-011 showed a definite pattern of black and white streaks. The white streaks began in 16 locations about 2 in. downstream of the film coolant ring. These white streaks flared out until they merged about 2 in. above the throat. Since the thermocouples were staggered circumferentially, some were in black areas and some were in white areas.

(U) The thermocouple data shows a significant disparity between the temperatures in the two areas. Thermocouples A-1, A-2, and A-4 are in black areas, whereas thermocouples A-3 and A-5 are in white areas. The black, or cooler, areas were observed to fall in line with 16 posts inserted between alternate pairs of injector vanes. It was surmised that the posts effectively forced the oxidizer-rich gas to flow parallel to the chamber wall. The absence of the posts appeared to allow this gas to impinge sharply on the film coolant, disrupting this stream and resulting in the white, or higher temperature, area. The need was therefore defined for a modified injector with diffuser vanes to control and direct the oxidizer flow.

(U) An attempt was made to evaluate selected thermocouple traces to define the heat-transfer coefficient and the true film-recovery temperature. It was recognized that steady-state thermocouple readings are not necessarily equal to gas temperature, even when the thermocouples are located at the surface of a nearly adiabatic wall. Several attempts with simplified conduction models were unsuccessful; therefore, an alternative approach was developed to be utilized on future tests involving high-response thermocouples sheathed in the same material as that which comprises the chamber wall (i.e., Nanmac thermocouples).

VI, A, ICP Residual Hardware Program (cont.)

(U) Evaluation of this data as it applies to regenerative and film-cooled chamber design resulted in the decision to continue using the present analytical model with the 1.5-1.0 Bartz factor. This assumption is sufficiently conservative to cover the degree of inaccuracy in the measured film temperatures while not being so conservative as to jeopardize the prospects of any design concept.

(2) Regeneratively Cooled Chamber Testing

(U) Data from two Tests, 1.2-08-WAM-002 and -003, contributed to the evaluation of supercritical N_2O_4 as a regenerative coolant while verifying the analytical model upon which the design of the modular cooled chambers was based. Both tests were conducted with chambers consisting of a single-pass tube bundle in which the regenerative coolant flowed countercurrent to the main-stream gas.

(U) Test -002 was conducted with Chamber R-4 which was film-cooled by injection at the secondary-injector face plane. A capillary tube chamber, R-5, was used in Test -003. It was film-cooled by injection at two locations: at the secondary-injector face plane and at a distance of 12.25 in. downstream of the injector face. The latter location was designed to film cool the throat region where the heat loads are greatest. The capillary tubes were located in the convolutions between the regenerative coolant tubes.

(U) The test parameters for both tests are presented in Figure VI-21. The stagnation temperatures of the mainstream gases were calculated on the same basis as that used for the ablative chamber testing described previously.

VI, A, ICP Residual Hardware Program (cont.)

(U) The experimental measurements of regenerative coolant inlet and outlet bulk temperature are compared to the analytical predictions in Figures VI-25 and 26. As in the ablative chamber analysis, the predicted temperatures are based on a Bartz factor distribution of 1.5 at the injector face and 1.0 at the throat. The predicted temperatures for Test -003 (the capillary tube chamber test) are based on the assumption that only 17% of the heat rejected by the chamber gas in the capillary tube region is absorbed in the regenerative cooling tubes. The 17% value represents that portion of the regenerative coolant tube surface area which is exposed to the combustion gases. The remaining heat load is handled by the coolant flowing through the capillary tubes for subsequent injection as film coolant.

(U) The placement of the capillary tubes necessitated an additional assumption. In all previous film-cooling tests, the film cooling effectiveness (η) was assumed to be constant downstream of the throat, based on earlier test data (ICP, Contract AF 04(611)-8548 (Reference 18). However, this assumption is unrealistic for Test -003, since film coolant was introduced from the capillary tubes only 1 in. from the throat. Therefore, for Test -003 only, constant film-cooling effectiveness (η) was assumed to begin at a point somewhat downstream of the throat. This point occurs at a location where the predicted temperature of the film downstream of the throat is equal to the predicted temperature of the film at the throat in Test -002.

(U) In Test -002 an oxidizer leakage of about 8 lb/sec occurred in the chamber prior to the data period. This leakage rate was not included in either the regenerative or film-coolant flow rates used for predicting temperatures.

(U) The predicted temperature rise of the regenerative coolant agreed well with the measured value for Test -003, as may be seen from Figure VI-26. However, in Test -002 the predicted temperature rise was

VI, A, ICP Residual Hardware Program (cont.)

7 degrees, about 25%, less than measured. Accuracy of the bulk rise values is $\pm$ 4°F due to the $\pm$ 2°F accuracy on each measurement. This discrepancy may be attributed to a loss of coating at several locations in the throat region where the heat flux is maximum. In addition, the film cooling effectiveness (η) may have been reduced because of a local loss of coating near the injector face. This loss of coating resulted in a severe (0.056 in.) discontinuity on the wall near the film-coolant tubes, possibly causing disruption of the boundry layer and increased mixing of the coolant with the mainstream gases.

VI, Secondary Combustor Program (cont.)

B. MODULAR SECONDARY INJECTOR PROGRAM

1. Objective

(U) The main objective of the Modular Seconary Injector Program was to develop a high performance, stable, mechanically sound injector suitable for use with the modular cooled secondary combustion chamber. The success criteria for this effort, as defined in the contractual work statement, was that the injector selected for test with cooled thrust chambers must have achieved a minimum duration of 0.5 sec of steady-state operation in an uncooled thrust chamber with steady-state chamber pressure oscillations which shall not have exceeded ±5% of the average chamber pressure value. Additionally, the hardware must be in refirable condition at the conclusion of the test.

(U) A second objective of the program was to supply design data for the cooled chamber design task. Included were the relationship of injector performance to chamber L*, the performance loss attendant with supplemental film cooling, and the heat transfer conditions in the thrust chamber.

2. Summary

(U) At the conclusion of the ICP Residual Hardware Program, the Mark 125 injector had been proven a high performance, stable, mechanically sound injector. Therefore, this injector concept was selected as the primary approach in the Modular Secondary Injector Program. The injector was redesigned to a flight-weight configuration, and the injector face diameter increased from 8.5 to 9.5 in. to be compatible with the modular cooled thrust chamber configuration. To provide a backup injector for the test program, an injector design study was performed in which several new injector concepts were evaluated. From this study, a new design designated the "fuel swirl rake"

VI, B, Modular Secondary Injector Program (cont.)

was selected for fabrication and test evaluation. In this injector, fuel is introduced into the secondary combustion chamber through 109 spray nozzles located in a near uniform pattern over the injector face.

(C) The test program consisted of 24 tests, of which 18 yielded valid data. All testing was performed with uncooled ablative lined combustion chambers, the inner contour of which was identical to the modular cooled combustion chamber. Basic evaluation tests were first performed with both the Mark 125 and the fuel swirl rake injectors. In these tests, the rake injector showed slightly higher performance than the Mark 125, but the performance of both units was significantly below that obtained with the ICP configuration Mark 125 injector. Subsequent review of the test data and the injector designs showed that oxidizer was escaping into the combustion chamber around the periphery of the injector before being combusted with the fuel. To eliminate this problem, a circular shroud was installed around each injector to contain the oxidizer within the fuel injection evelope. With this change, the Mark 125 injector proved to be the higher performer and demonstrated a delivered performance of 93.5% I_s. Based on the result of that test, evaluation of the rake injector was discontinued.

(U) Additional testing was then performed with the Mark 125 injector to determine the relationship between injector performance and chamber L*, and to determine the effect of various amounts of supplemental film cooling on the overall injector/chamber performance. In two of these tests, the uncooled combustion chamber was instrumented with thermocouples to provide heat transfer data. Concurrently, investigations were performed with various cooled configurations of the performance-improving shroud to make it suitable for use in extended-duration cooled chamber firings. A satisfactory design was obtained and subsequently incorporated into the regeneratively cooled chamber design.

VI, B, Modular Secondary Injector Program (cont.)

(U) All secondary injector requirements prior to cooled chamber testing, as set forth in the contractual work statement, were achieved during Test 1.2-11 WAM-018, performed on 28 July 1966. Following this test, work statement compliance data sheets were prepared and submitted to the USAF project officer. Coordination was subsequently effected to proceed with cooled thrust chamber testing using the Mark 125 injector.

(U) Cooled chamber testing was then initiated in which five tests were conducted with the regeneratively cooled chambers and 30 tests were performed with transpiration-cooled chambers. Testing with the transpiration cooled chamber revealed that a compatibility problem existed between injector and chamber. When the transpiration coolant was reduced in successive steps to increase secondary chamber performance, a streaking condition became evident on the chamber wall, which during two tests, progressed to metal erosion and subsequent destruction of the transpiration-cooled chambers. The streaks were attributed to the injector by which fuel is impinged on the wall. It was decided that the Mark 125 injector, in its present configuration, was not suitable for further testing with cooled chambers. The Rake injector was modified in an attempt to improve its performance and ensure compatibility by maintaining an oxidizer-rich condition around the injector periphery. Two tests were conducted; however, performance was not improved and the effort was abandoned.

(U) Two approaches are currently being pursued to solve the compatibility problem. The first is to modify the Mark 125 injector to give a finer distribution at the injector periphery and to eliminate any impingement of the fuel onto the chamber wall by directing the outer fuel axially. The second approach is to design and test new injector concepts designed specifically for optimum injector and chamber compatibility, while maintaining high performance. This effort is being conducted in the extended Phase-I Program which

VI, B, Modular Secondary Injector Program (cont.)

was initiated 2 February 1967. It is planned to test evaluate these new injectors in the near future, after which cooled-chamber testing will be resumed.

3. Component Design

(U) The major components used in the Modular Secondary Injector Program included two secondary injectors and uncooled thrust chambers of several configurations. These components were tested on Test Stand H-2 using the sector engine system. It was necessary to design an adapter to accommodate the modular configuration hardware to the sector engine, which was originally used with ICP configuration hardware. Design descriptions for the injectors, uncooled chambers, and test-stand adapter are given in this section.

a. Injectors

(U) Two injector configurations were selected for test evaluation: the Mark 125 and fuel swirl rake. The Mark 125 injector was based on the successful Mark 125 injector developed in the ICP Residual Hardware Program. The fuel swirl rake injector was based on a liquid-liquid injection concept used successfully on the High Chamber Pressure Rocketry Program, AF 04(611)-8191. Each of the injectors is described in the following paragraphs.

(1) Mark 125 Injector

(C) The modular Mark 125 injector was patterned very closely to the ICP configuration Mark 125 injector. The most significant change was an increase in diameter from 8.5 to 9.5 in. to be compatible with the ARES modular cooled chamber. The injector is composed of 32 tapered vanes each

VI, B, Modular Secondary Injector Program (cont.)

having a step-drilled fuel-feed manifold on the leading edge and fuel discharge holes on the trailing edge. Twenty 0.093-in.-dia x 0.015-in. wall tubes are brazed into the fuel discharge holes on the trailing edge of each vane for a total of 640 fuel injection points. These tubes are bent in a manner to give a uniform fuel injection pattern over the entire face of the injector, as can be seen in Figure VI-27. The total fuel exposure perimeter of this injector is 125 in. The fuel injection velocity is 126 ft/sec; the fuel circuit pressure drop is 315 psi. Oxidizer flows from the primary combustor and passes between the fuel vanes of the secondary injector at a velocity of 94 ft/sec (at the trailing edge of the vane). The oxidizer-circuit pressure drop is very low and is on the order of 25 psi. The injector is designed to operate at a chamber pressure of 2800 psia and at a mixture ratio of 2.2:1, which are the engine specification values.

(U) The modular injector body was designed as a flight-weight configuration to fit the modular engine, and as such represents one of the major interfaces of the ARES engine, connecting the turbopump, injector, and thrust chamber. The flight-weight interface requirement imposed many design considerations for the injector body in addition to the function of simply manifolding fuel to the injector vanes. Design criteria established for the body design included the following:

(a) The engine was to include no external main oxidizer lines. Therefore, all oxidizer used for regeneratively cooling the chamber must pass internally through the injector body.

(b) The oxidizer coolant passages through the injector body must be sufficiently large to give a very low pressure drop through the injector body.

VI, B, Modular Secondary Injector Program (cont.)

(c) The injector, chamber, and turbopump will be separable from one another during the predevelopment program to ease interchangeability of components during development testing.

(d) The injector must be attached to the turbopump within a bolt circle diameter of 13.2 in. (diameters in excess of this result in significant increases in turbopump weight).

(e) The number of interpropellant welds and seals should be kept between minimum because small leakage can result in destruction of the entire assembly.

(f) The injector flange should have sufficient stiffness to ensure the compression of all interface propellant seals.

(U) Following extensive studies of several designs, a final design was established. The selected body and interface configuration are shown in Figure VI-28. Oxidizer coolant for the regeneratively cooled chamber passes from the turbopump housing flange through the injector flange and into the chamber coolant tubes. The coolant is then routed through the chamber and back through the injector body where it is returned to the turbopump housing. These oxidizer passages are slotted rather than round to allow low oxidizer velocity while still minimizing the size of the injector. Sealing is accomplished at the two interfaces by six Omniseals. All seal grooves are machined into the injector body, which is made of CRES 347 stainless steel.

(U) Fuel passes into the injector body through a constant cross-sectional torus, externally fed. The fuel then passes into the injector manifold through radially slotted passages in the body. The individual injector element then carries fuel from this manifold to the combustion zone.

VI, B, Modular Secondary Injector Program (cont.)

(U) The outside diameter of the injector vane assembly is 9.5 in. whereas the cooled chamber diameter is 10.5 in. The 9.5 in. dimension was the largest diameter which could be contained within the 13.2-in.-dia bolt circle of the TPA housing. As can be seen in Figure VI-28, three interface seals are located inboard of the bolt circle; the injector element assembly had to be contained within this envelope to be removable from the chamber. Once the injector diameter was established by the TPA bolt circle and seals, the top chamber flange design was allowed to extend inward to the 9.5-in.-dia dimension. The resulting 1/2 in. step between the injector and cooled chamber proved to be a major problem in the injector development program; oxidizer-rich gas from the primary combustor escaped through this gap into the secondary chamber without being combusted with fuel, which lowered performance. This problem is discussed fully in Section VI,B,4, below.

(2) Fuel Swirl Rake Injector

(C) The fuel swirl rake injector shown in Figure VI-29, consists of 12 tapered pods, from each of which protrude nine 3/8-in.-dia tubes. The tubes are interconnected by steel ribs to provide a rigid construction for eliminating vibration in the tubular legs of the assembly. Modified commercial spray nozzles are welded into the end of each tube, giving a total of 109 elements located uniformly across the injector face. When fuel is introduced through these nozzles, it forms overlapping spray cones through which the oxidizer gas must pass. The pressure drop in the fuel circuit is 266 psi, while the oxidizer pressure drop is again very low, about 25 psi. This injector was designed for the same operating condition as was the Mark 125 (i.e., 2800 psi chamber pressure and 2.2 mixture ratio).

VI, B, Modular Secondary Injector Program (cont.)

(U) The injector body design is identical to that of the Mark 125 injector.

b. Uncooled Thrust Chamber

(U) The purpose of the uncooled thrust chamber was to provide a device with which injectors could be test fired, developed, and from which base-line thrust chamber performance data could be obtained for cooled chamber testing. A second purpose was to provide a device for experimentally obtaining heat transfer data in the modular-configuration secondary combustion chamber and nozzle.

(U) To accomplish these purposes most effectively, a segmented chamber design, shown in Figure VI-30 was selected. This chamber is composed of a chamber segment and an exit nozzle segment which are removable from each other. The chamber segment is of heavy-wall steel construction and was fabricated in several lengths to allow an evaluation of injector performance vs chamber L*. The chamber segment contains a two-piece ablative liner fabricated from high silica Refrasil material. The first piece, used in the convergent and throat section of the chamber, is made from compression-molded material and is common to chambers of all lengths. The other piece is used in the cylindrical section of the chamber and is of 1/2-in.-thick taped-wrapped construction. The liner piece varies in length depending on the particular chamber L* for which the assembly was made. The expansion nozzle segment also consists of a steel pressure vessel lined with ablative material. It is attached to the chamber segment at an area ratio of 2:1 and extends to an area ratio of 12:1. This ablative liner is also of taped-wrapped construction 1/2-in.-thick.

(U) An alternative expansion nozzle liner was also designed and used in the test program. Testing with the ablative expansion nozzle

resulted in severe roughening of the liner wall, which caused a considerable performance loss because of the increased friction. The precise determination of this loss was very difficult because the roughness varied considerably from test to test. Therefore, in tests where injector performance determination was the primary test objective, the ablative expansion nozzle liner was replaced with a Rockide-coated steel liner. The wall of the steel liner remained smooth and made the determination of injector performance much easier.

(U) One 40-in. L^* chamber was modified specifically for obtaining heat transfer data. In this chamber, 24 high response 0.040-in. chromel/alumel thermocouples were installed through the chamber and nozzle walls. In addition, seven flush-mounted Nanmac thermocouples, including five Pt/Pt - 10 Rh and two W/W - 26 Re, were installed to measure higher film temperatures than the 2500°F capability of the C/A thermocouples. The instrumented chamber is shown in Figure VI-31.

3. Test-Stand Adapter

(U) The staged-combustion test engine, which was used for all secondary combustor test evaluations, was designed for ICP configuration injectors and chambers. To facilitate the modular configuration hardware, it was necessary to design and fabricate an adapter connecting the ICP primary combustor to the ARES secondary injector.

(U) The adapter design is shown in Figure VI-32. It is a cone-shaped part approximately 17 in. long and is fabricated from stainless steel. It is designed to allow passages of oxidizer coolant from the secondary combustor injector to the secondary regeneratively cooled chamber, from which it is returned to the primary combustor injector. The adapter also provided a thrust-take-out ring which connected the thrust chamber to the existing test stand interface.

VI, B, Modular Secondary Injector Program (cont.)

4. Development Testing

a. Test Program Summary

(U) The primary objective of the Modular Secondary Injector Test Program was to evaluate the Mark 125 and rake injectors, and using the best of these designs, to perform any additional development testing necessary to ensure high performance, stable, and mechanically sound operation. A second objective of the test program was to provide test data for the design of cooled secondary combustion chambers. Included in this task were the determination of the effects of chamber L* on injector performance, the performance loss attendant with various amounts of supplemental film cooling, the heat transfer characteristics of the secondary combustion chamber, and the development of a transition section between the secondary injector and the cooled secondary combustion chamber.

(U) The test program was initiated on 25 March 1966 and was concluded on 30 Nov 1966. Twenty-four tests were conducted during this period, of which 17 yielded valid data. The Mark 125 injector was fired successfully 12 times in uncooled ablative-lined chambers ranging in L* from 20.0 to 46.8 in; the rake injector was fired successfully six times in chambers ranging in L*'s from 19.7 to 46.5 in. Nominal injector pressure and mixture ratio for these tests were 2800 psia and 2.2, respectively. A cumulative summary for all testing is shown in Figure VI-33. A representative oscillograph showing the major test parameters is given in Figure VI-34.

(This page is Unclassified)

VI, B, Modular Secondary Injector Program (cont.)

(C) Both injectors performed satisfactorily with regard to combustion stability, freedom from erosion, and structural integrity. The combustion loss as a function of L* was determined for each injector. The performance of the Mark 125 injector proved to be 1-1/2% higher than that of the rake design in comparable configurations. At the L* of the ARES cooled chamber, it has been computed that the modular Mark 125 injector has a combustion loss of 3.6%, resulting in a combustion loss efficiency of 96.4% at a nozzle area ratio of 20:1.

(C) Additional testing was then conducted with the Mark 125 injector to determine the effect of supplemental film cooling on thrust chamber performance. It was determined that a performance loss of approximately 0.51% specific impulse occurs for each percent of oxidizer film cooling introduced into the secondary combustor chamber. These data, when combined with the data from the injector performance tests, indicate that performance with cooled chambers was sufficiently high to meet the Phase-I ARES performance requirement. On this basis, the Mark 125 injector was selected for cooled-chamber testing; the rake injector, while performing satisfactorily, was relegated to back-up status.

(C) The success criteria for the modular secondary injector program, as defined in the contractual work statement, was that the injector selected for testing with cooled thrust chambers must have achieved a minimum duration of 0.5 sec of steady-state operation with steady-state chamber pressure oscillations not exceeding $\pm$ 5% of the average chamber pressure. Also the injector was to be in refireable condition following the test. The work statement requirements were fulfilled in Test 1.2-11-WAM-018 with the Mark 125 injector. In this test, the injector operated at steady-state for 0.89 sec, at an average chamber pressure of 2818 psia. Chamber pressure oscillations during the test did not exceed $\pm$ 1.07% of average chamber pressure. The injector was in perfect condition following the test.

VI, B, Modular Secondary Injector Program (cont.)

(U) Subsequent testing with the Mark 125 injector with the transpiration cooled chamber revealed a compatibility problem between the injector and the chamber. This condition has caused additional injector development effort to be performed, which is being done in the extended Phase-I Program. This effort was initiated in February 1967 and is scheduled for completion by July 1967.

b. Detailed Test Program

(U) The tests performed in the modular secondary injector program are logically grouped into four test series, including the Mark 125 injector evaluation, the rake injector evaluation, the film-cooling and cooled-shroud evaluations (performed concurrently), and the modified rake injector evaluation. Each of these test series is discussed below. Performance and heat-transfer data obtained in these test series are summarized in Section VI,B,5, below.

(1) Mark 125 Injector Evaluation: Tests 1.2-11-WAM-001 through 003, 007 through 011, and 015 through 018

(U) The objective of this test series was to evaluate the Mark 125 injector. The injector configuration used in this test series is shown in Figure VI-27. The initial injector and chamber interface configuration, which proved to be very important in the test program, is illustrated in Figure VI-35.

(U) Twelve tests were conducted, of which nine were development tests producing valid data, two were test-stand malfunctions, and one was a work statement compliance demonstration test. In these tests, evaluation criteria included injector performance, structural integrity, erosion characteristics, and combustion stability characteristics. Each of these is discussed in the following paragraphs.

VI, B, Modular Secondary Injector Program (cont.)

(a) Injector Performance

(U) Performance was determined using Aerojet-General's Interaction Theory, previously described in Section VI,A,5, above. For the ARES sector engine test system, the total measured performance loss is distributed between combustion or energy release loss, mixture ratio distribution loss, nozzle friction loss, nozzle geometry loss, and film-cooling loss (in tests in which supplementary film cooling is used). Of these losses, the combustion loss and mixture ratio distribution loss establish the inherent performance of the injector and were therefore of primary concern in this test series.

(U) The performance obtained in initial tests (002 and 003) was substantially lower than expected. The Mark 125 injector in the ICP configuration had yielded very high combustion efficiency, and the modular configuration was sufficiently similar that a large performance difference was not expected. After a careful study of the test data and injector and chamber interface configuration, it was determined that most of the performance loss was caused by a poor mixture ratio distribution around the periphery of the injector. The transition section between the injector and chamber was subsequently modified in two steps by incorporation of a steel ring and shroud which effectively eliminated the mixture ratio distribution (MRD) loss. These configurations are shown in Figure VI-36, Configurations B and C. The resolution of the MRD problem is given in detail in the Performance Analysis Discussion, Section VI,B,5, below.

(C) With the mixture ratio distribution loss eliminated, tests were then performed to determine the combustion loss of the injector as a function of chamber L*. Data from tests 007, 008, 010, and 011, in which chamber L* was varied between 20.0 and 46.8 was used to establish this relationship. The results are shown, corrected to the modular engine

area ratio of 20:1, in Figure VI-37. At the ARES design L*, the combustion loss is 3.6%. Comparison of this performance with the ICP Mark 125 and rake injectors is discussed in the performance analysis section.

(b) Mechanical Integrity

(U) The Mark 125 injector proved to be mechanically sound. Two small problems did arise and were corrected during the course of the test program. First, the fuel tubes on the Mark 125 vane were originally hand brazed into each of the vanes. On Test 014, fuel leaks developed in the tube-vane braze joint, which caused local erosion of the vane. It was established that the poor braze joint was caused by braze-flux inclusions; the problem was corrected by furnace brazing the vanes instead of the hand-brazing method. Figure VI-38 shows typical vanes brazed by the two methods. Tests 016 and 017 were conducted with the primary objective of demonstrating the revised braze procedure. The tests were completely satisfactory; no erosion occurred.

(U) The second structural problem encountered was an occurrence of cracking of the weld which joins the injector vane to the injector body. This was corrected by modifying the joint design and extending the weld completely around the vane-body joint. No further difficulties occurred.

(c) Erosion Characteristics

(U) The Mark 125 injector operated completely free from erosion. In the two instances where local erosion occurred, it was caused by the poor tube-vane braze joint and was not an inherent characteristic of the injector.

VI, B, Modular Secondary Injector Program (cont.)

(d) Combustion Stability Characteristics

(U) Injector operation was completely stable in all tests. There was no evidence of either low-frequency or high-frequency combustion instability.

(U) The test evaluation of the Mark 125 injector was satisfactorily concluded and the injector selected for additional testing to provide film cooling performance loss data for the cooled chamber program. This test series is described in paragraph VI,B,4,b,(3), below. One of these tests, 018, was declared a demonstration test for the modular injector selection for cooled chamber testing. The injector was in perfect condition following the test. The chamber pressure characteristics for this test, together with the allowable oscillation band as given in the work statement, are shown in Figure VI-39.

(2) Rake Injector Evaluation: Tests 1.2-11-WAM-004 through 006, 012 and 013

(U) Concurrently with the evaluation of the Mark 125 injector, the rake injector (reference Figure VI-29) was evaluated. Five tests were conducted, of which four yielded valid data and one was a malfunction. Evaluation criteria were identical to those in the Mark 125 evaluation, namely injector performance, structural integrity, erosion characteristics, and combustion stability characteristics.

(a) Injector Performance

(C) The basic performance of the Rake injector was first evaluated in an uncooled chamber having an L* of approximately 46 in. In these tests, 004 and 005, measured performance of 89.8 and 89.9% specific

VI, B, Modular Secondary Injector Program (cont.)

impulse were achieved. This performance was higher than that obtained in the initial tests with the Mark 125 injector but was still below an acceptable value. The successful shrouding technique used to eliminate the mixture ratio distribution loss in the Mark 125 injector test series was then used with the rake injector. A ring and shroud of identical configuration were installed at the injector-chamber interface to prevent primary oxidizer gas from escaping to the chamber wall prior to combustion. Two tests were conducted with this configuration using chambers of 19.7 and 42.9-in. L*, respectively. Performance improved significantly, reaching 91.5% of specific impulse when tested with the 42.9-in. L* chamber.

(C) The relationship of injector combustion loss and chamber L*, corrected to an area ratio of 20:1, is shown in Figure VI-37. It is seen that the rake injector performance, although high, is approximately 1.4% lower than the Mark 125 injector at the ARES design L*.

(b) Mechanical Integrity

(U) The rake injector was mechanically sound in all respects. At no time during any of the tests performed did a structural problem arise.

(c) Erosion Characteristics

(U) No injector erosion was experienced on any test with the rake injector. Some pitting did occur in the recessed cups in some of the fuel injection pods directly adjacent to the point where the fuel is injected into the combustion chamber. It is possible that the pitting could have developed into erosion if the injector had been tested in extended durations. For this reason, the pod design was modified in the evaluation of the modified rake injector, described in paragraph VI,B,4,b,(4), below.

VI, B, Modular Secondary Injector Program (cont.)

(d) Combustion Stability Characteristics

(U) Injector operation was stable in all tests. During the start transient, oscillations are present in any rocket engine system. These oscillations were significantly higher with the rake injector than had been experienced with the Mark 125 injector. As steady state was approached, however, the oscillations damped out and operation was normal.

(U) Following this test series, the rake injector was relegated to back-up status, since its performance was not as high as the Mark 125 injector. When, during the course of cooled-chamber testing, a compatibility problem became evident with the Mark 125 injector, additional testing was performed with a modified rake injector in an attempt to raise its performance to that of the Mark 125. This testing is discussed in Section VI,B,4,b,(4).

(3) Film-Cooling and Cooled-Shroud Evaluations: Tests 1.2-11-WAM-015 through 022

(U) This test series was designed to provide design information for the regeneratively cooled chamber program. The test series included two separate investigations, performed concurrently. The first was to develop a cooled transition section between the injector and the cooled chamber to eliminate the mixture ratio distribution loss experienced in the an injector evaluation test series. The second was to determine the effect of supplementary film cooling on overall thrust chamber performance. The Mark 125 injector, which had been selected for cooled chamber testing, was used exclusively in this test series.

VI, B, Modular Secondary Injector Program (cont.)

(a) Cooled-Transition-Section Evaluation

(U) In the basic injector evaluation, a ring-shroud transition section was developed that effectively eliminated the mixture ratio distribution loss. This transition section was used only as a development tool and no attempt was made at that time to design around the obvious buring problem associated with inserting uncooled metal hardware into the 6000°R combustion environment. As a result, surface erosion was evidenced on the ring-shroud in all tests. Having successfully eliminated the MRD loss, the attention now focused on modifying the design so that it would not burn during testing. A further requirement was that this design must be such that it could be incorporated into both the single point and capillary tube regeneratively cooled thrust chambers, which were partially fabricated at the time.

(U) The first attempt was to contour the inner surface of the shroud into a smooth transition section and depend upon primary oxidizer gas to film cool the shroud. This configuration, evaluated in Test 015, is shown in Figure VI-35. Severe erosion of the shroud was experienced; it was concluded that the design was unsatisfactory.

(U) The shroud design was then changed to provide liquid-oxidizer film cooling of the shroud. The coolant was injected around the inside of the shroud through 21 tangentially drilled holes of 0.031-in. diameter located above the plane of injector fuel injection. To prevent the possibility of this coolant from entering the main gas stream, thin tabular shrouds were welded between each injector vane around the periphery. Also, the main chamber film coolant was manifolded down through the shroud allowing the film coolant to be injected at the base of the shroud at high velocity through 104 0.040-in.-dia holes. This configuration, evaluated in Test 018, is shown in Figure VI-35. Erosion was experienced near the base of the shroud. However, the condition of the hardware was sufficiently satisfactory to indicate that increased shroud film cooling could solve the buring problem.

VI, B, Modular Secondary Injector Program (cont.)

(U) Concurrently, a second-configuration cooled shroud was being fabricated. The cooled shroud design used in Test 018 is not suitable for capillary tube regenerative chambers because the capillary tubes enter the top chamber flange in such a way that there is no room to incorporate the main coolant circuit in the shroud. Therefore, a separate design was prepared in which the shroud is film cooled by liquid oxidizer in a manner identical to that used in the previous shroud design; however, the main film coolant is not manifolded within the shroud. In this design, the main film coolant is injected behind the shroud through 104 0.028-in.-dia holes, located between each capillary tube. Based on the results of Test 018, the number of shroud film-cooling holes was increased from 21 to 51. This capillary-tube shroud design was evaluated in Test 019. Minor erosion was experienced, but was much less than that occurring in Test 018. The shroud design was then further modified to incorporate 104 0.028-in.-dia shroud film-cooling holes. This configuration was fired with the capillary tube shroud design in Tests 020 and 022. No burning occurred during these tests and the shroud design was termed satisfactory.

(U) Based on this test series, final designs for cooled shrouds were established for the regeneratively cooled chambers. For the single-point injection chambers, the final design incorporates 104 0.028-in.-dia, shroud film-cooling holes as well as 208 0.028-in.-dia main film-cooling holes which inject fuel at the base of the shroud. The capillary-tube chamber shroud uses the same shroud film-cooling circuit, but introduces the main film coolant through 104 0.028-in.-dia holes behind the shroud, in addition to the coolant introduced through 104 capillary tubes.

(b) Film Cooling Evaluation

(C) Concurrently with the evaluation with the cooled shroud designs, the effect of film cooling on thrust chamber performance

VI, B, Modular Secondary Injector Program (cont.)

was determined. Performance data from Tests 018, 019, 020, and 022 were used to establish this relationship, which is shown in Figure VI-40. It was determined that for every percent of film coolant introduced into the chamber, a specific impulse loss of 0.51% occurs.

(4) Modified Rake Injector Evaluation: Tests 1.2-11-WAM-024 and 026

(U) When the compatability problem between the Mark 125 injector and the transpiration-cooled chamber became evident, further testing of the Mark 125 injector with cooled chambers was suspended. At this point the only short-range possibility for demonstrating cooled chamber performance was with the rake injector, which had been relegated to backup status. However, the performance of the rake injector was not considered high enough to meet cooled chamber performance requirements. Therefore, an attempt was made to modify the injector to improve its performance while maintaining an oxidizer-rich boundary around the periphery of the injector to ensure compatibility with the transpiration cooled chamber. A Rigimesh plate was attached to the injector face, in which 109 holes had been drilled to align with the injector pods. The pattern was such that a concentric sheet of oxidizer was impinged on each of the fuel spray cones. The face was transpiration cooled with primary oxidizer gas through the porus Rigimesh plate. Also, the fuel pod tip was modified slightly to eliminate the pitting experienced in the earlier rake injector tests.

(U) The two tests conducted with the modified rake injector, 024 and 026, showed no increase in performance. In fact, performance was reduced. Furthermore, slight burning occurred around the periphery of the Rigimesh face as shown in the postfire photographs of the injector, Figure VI-41. No further testing was attempted with this injector.

VI, B, Modular Secondary Injector Program (cont.)

5. Test Data Evaluation

(U) In this section, the performance and heat-transfer results of the modular injector test program are given in a consolidated discussion. The Mark 125 injector performance is compared to that of the Rake injector as well as the ICP configuration Mark 125 injector. Performance parameters common to both injectors are also discussed.

a. Performance

(U) Engine performance was evaluated using the Interaction Theory described in Section VI,A,5, above. Significant elements of performance loss in the ARES-sector-engine test system include mixture ratio distribution loss, combustion or energy release loss, nozzle friction loss, nozzle geometry loss, and film cooling loss. Each of these losses experienced in the modular engine test program is discussed in the paragraphs below.

(1) Mixture Ratio Distribution Loss

(C) Initial testing with the Mark 125 injector yielded significantly lower performance than had been anticipated on the basis of the test results to the ICP configuration Mark 125 injector. Performance data analysis of these tests, 002 and 003, revealed that the low performance was caused largely by poor mixture ratio distribution (MRD) around the periphery of the injector. This loss was calculated to be 18.9 and 27.5 sec, respectively, for the two tests (the difference in MRD loss between these tests was a result of changes in primary and secondary mixture ratio, which effect the MRD loss). The loss was caused by the 0.5-in. discontinuity at the injector-chamber interface which allowed the oxidizer to flow in a path as shown in Figure VI-36, Configuration A. The oxidizer bypassed the injector fuel elements and passed essentially uncombusted into the outer chamber region forming

VI, B, Modular Secondary Injector Program (cont.)

an annulus of relatively high mixture ratio gas. When expanded through the nozzle, this gas gives low specific impulse. Furthermore, the loss of the oxidizer gas to the outside of the chamber caused the core of the combustor to operate fuel-rich, again producing low specific impulse.

(C) To prevent the oxidizer gas from escaping through the wall before combustion could occur, a steel ring was inserted below the injector face (Figure VI-36, Configuration B). Tests 007, 008, 009, and 010 were conducted with this configuration. Test results showed a marked improvement in performance; however, an MRD loss of 10 sec was still evident. Closer inspection of the injector and chamber interface showed a 0.1-in. tolerance gap between the secondary injector vanes and the chamber through which oxidizer gas from the primary combustor could flow. To stop gas flow in this small annulus, a cylindrical shroud was installed about the secondary injector (shown in Figure VI-36, Configuration C). In this configuration, the oxidizer was contained entirely within the injector diameter to a point 1/2-in. downstream of the point of fuel injection, which allowed sufficient combustion of the propellants before expansion of the primary gas to the chamber wall could occur. This configuration was evaluated in Test 011, in which performance was substantially improved (93.5% of specific impulse was achieved on this test). For purposes of comparative analysis, the mixture ratio distribution loss was assumed to be 0 for secondary injectors tested with this final interface configuration.

(U) The rake injector showed higher performance than the Mark 125 injector when tested without the ring and shroud. It is believed that this resulted from the fuel-swirl concept of this injector, which permits fuel to be injected into the oxidizer-rich gas in the outer chamber annulus. This results in a lower MRD loss in the annulus than with the Mark 125 injector. When the rake injector was subsequently tested with the ring and shroud (Tests 012 and 013) performance was improved approximately 1%. However, the overall

VI, B, Modular Secondary Injector Program (cont.)

performance was lower than that achieved with the Mark 125 injector in the shrouded configuration. The performance analyses for Tests 012 and 013 considered the MRD loss to be zero.

(U) It was concluded that the initial low performance with both injectors was definately attributable to the MRD loss and that the incorporation of the ring and shroud combination effectively eliminated the loss.

(2) Combustion or Energy Release Loss

(U) The combustion loss for the modular Mark 125 and rake injectors are shown in Figure VI-37. This data is presented corrected to an area ratio 20:1 making it directly applicable to the ARES engine design. For reference, the ICP configuration Mark 125 injector combustion loss is also shown.

(C) At the ARES chamber design L*, the combustion loss of the modular Mark 125 injector is 3.4%. This loss, added to the other performance loss of geometry friction and film cooling, still provides a delivered performance sufficient to meet the Phase-I performance goals. It was for this reason that the Mark 125 injector was selected for cooled-chamber testing.

(C) Figure VI-37 shows that the combustion loss of the rake injector is approximately 1 to 1-1/2% greater than that of the Mark 125 injector for all chamber L*'s. On the other hand, the ICP-configuration Mark 125 injector performed approximately 1% better than the modular Mark 125 injector. This difference is probably the result of the difference in the two configurations, e.g., 9.5 vs 10.5-in. chamber diameter, conical vs cylindrical chamber shape, etc.

VI, B, Modular Secondary Injector Program (cont.)

(3) Nozzle Friction Loss

(U) Many of the test firings were conducted with ablative expansion nozzles. In repeat tests with the same nozzle, the nozzle wall becomes progressively rougher causing an increase in friction loss. To determine the combustion and mixture ratio distribution losses, it is necessary to know rather precisely the nozzle friction loss. A method of calculating nozzle friction for rough ablative walls was developed during the program on the basis of analytical model developed by Schlichting (Reference 16) for gas flow over rough surfaces. The data summarized in Figure VI-33 reflects the adjustment made in nozzle friction loss to account for the varying degree of nozzle surface roughness. To provide a more accurate evaluation of injector performance, some tests were performed with smooth steel nozzles, the friction loss for which can be precisely calculated.

(4) Nozzle Geometry Loss

(U) In any given rocket nozzle, a performance loss is generated by a non-axial flow component of the supersonic gas stream at the point leaves the nozzle. As this radial flow cannot contribute to thrust, a loss is produced. A magnitude of this loss is reflected in Figure VI-33.

(5) Film Cooling Loss

(C) When supplementary film coolant is introduced into the combustion chamber, an additional loss occurs. The magnitude of this loss was determined for the modular configuration thrust chamber; the results are tabulated in Figure VI-33 and graphically represented in Figure VI-40. It was determined that a 0.51% loss in specific impulse is incurred for every percent of film coolant introduced into the chamber. A similar test series had been previously performed with the ICP-configuration thrust chamber, and the results

VI, B, Modular Secondary Injector Program (cont.)

of that test series are also shown for reference. The performance loss for the two configurations are in reasonable agreement; geometry variations between the two hardware configurations probably account for the difference.

b. Heat Transfer

(U) Two film-cooled ablative chamber tests were conducted with thermocouple instrumentation. The objective of these tests, 1.2-11-WAM-018 and 019, was to evaluate the performance of the film cooling as coolant in the modular configuration to verify the cooled chamber design and analysis which was based on data solely from the ICP configuration. This was in addition to the evaluation of the effect of the film coolant on overall thrust chamber performance.

(U) Both tests were conducted with a 40-in.L* ablative chamber having a conical ablative exit section described earlier. Test -018 utilized a shroud to blend from the 9.5-in. injector diameter to the 10.5-in. chamber diameter from which the film coolant was injected at high velocity along the wall through 104 0.040-in.-dia holes in the tip of the shroud (see Figure VI-35). Additionally, there were twenty-one 031-in.-dia holes to cool the face of the shroud in the area adjacent to the main stream combustion. This test was conducted with 26.5 lb/sec of film cooling of which 2.8 lb/sec was shroud coolant. Test -019 utilized a similar shroud except that the film coolant was injected from 104 0.040-in.-dia holes behind the shroud which fit to the chamber with a nominal 0.015-in. gap (see Figure VI-35). The shroud cooling was accomplished through fifty-one 0.028-in. holes which flowed 5.5 lb/sec of the total 28.2 lb/sec coolant.

(U) Both of these instrumented film-cooled tests were conducted at effective film cooling flow rates less than ever tested on an ICP

chamber. Consequently, while there were two rows of twelve 0.040-in. chromel-alumel thermocouples, one axial and the other staggered circumferentially, only the first thermocouple in each row gave data within the 2500°F limit of the C/A thermocouples in either test. Additional thermocouple instrumentation consisted of a row of five "Nanmac" Pt/Pt-10Rh thermocouples and a row of two "Nanmac" W/W-26 Re thermocouples. These thermocouples are located axially in stations 2 through 6 for the platinum and in 5 and 6 for the tungsten. The stations are located as shown in Figure VI-31. These thermocouples, besides having the higher temperature limitation of 3200°F and 5000°F, respectively, for the platinum and tungsten, consist of foil-type junctions sheathed in the same ablative material comprising the chamber wall and hence, minimize conduction losses away from the junction. The junctions are exposed and continually remake as the surface erodes. Traces of these thermocouple readings versus time are shown in Figure VI-42 for Test -018 and Figure VI-43 for Test -019.

(U) The gas film coolant temperature recorded by thermocouple C-5 (TGFC-C5 on Figure VI-42) indicates the results of severe oxidation of the tungsten by N_2O_4 invalidating the readings of both C5 and C6. In Figure VI-43, the three thermocouples remaining from the previous test are shown. The record of B2 in particular, due to its proximity to the film coolant shroud, and the record of B3, to a much lesser extent, show the result of both closure or near-closure of the nominal 0.015-in. gap through which the coolant flows from behind the shroud and the burning of the shroud which occurred in line with each fuel injection point. This closure and the burning were observed on postfire examination of the hardware. The steady-state values prior to the rise in temperature are considered valid.

(U) Consideration of the apparent steady-state readings represented by Figure VI-42 and VI-43 and conversion to a scale of axial distance from the injector face results in Figure VI-44, which shows the film

VI, B, Modular Secondary Injector Program (cont.)

profile observed on the two tests together with a predicted profile. This predicted profile is for a test which averages the film coolant flow rates experimentally measured, assuming partial effectiveness for the shroud coolant. Without attempting to explain the difference in the shapes of the two curves, it is possible to show that the result of a film temperature profile such as that observed in Test -018 would present no hardship to a regeneratively cooled chamber. Figure VI-45 shows the coating and tube wall temperature of the cooled chamber, which would result from the imposition of such a film temperature profile.

(U) Any further attempt to rationalize this data would be presumptuous with only two tests conducted. The life of the thermocouples used proved to be sufficiently short so that thermocouple instrumentation on subsequent film cooled tests was impossible. The tests, however, verified the cooled-chamber design and analysis sufficiently to show that the Phase I allowable film-cocling flow rate should satisfactorily cool a regeneratively cooled chamber th t is fully compatible with its injector.

VI, Secondary Combustor Program (cont.)

C. MODULAR-COOLED CHAMBER PROGRAM

1. Objective

(C) The objective of the Phase I Modular Cooled Chamber Program was to demonstrate high performance and structural integrity of a full-scale modular configuration cooled combustion chamber and nozzle. The success criterion for this effort, as specified in the contractual work statement, was that the cooled thrust chamber must demonstrate a minimum delivered specific impulse at sea level of 280 sec during each of three or more tests each of 20 sec minimum duration. At the conclusion of each test, the thrust chamber must be in refireable condition. Refurbishment of the chamber coating (if used) between duration tests is acceptable.

2. Summary

(U) Two basic cooling concepts were evaluated in the Cooled-chamber development program: (1) regenerative cooling supplemented with film cooling and a thermal-barrier coating, and (2) transpiration cooling. The two cooling systems represent alternative approaches; either concept can be used to satisfy program performance and duration requirements.

(U) The feasibility of regenerative cooling at high chamber pressures was indicated in the ICP Residual Hardware Program. Based on these results, a new flight-weight modular configuration regeneratively cooled chamber was designed for test evaluation in the Modular Cooled Chamber Program. The chamber design included two alternative configurations of the film-cooling system: one in which all the film coolant is introduced from the face plane of the thrust chamber injector, and one which has an additional injection point in the convergent section of the chamber. A high-temperature thermal-barrier coating was applied to the gas-side tube wall of the chamber to reduce required supplemental film coolant.

CONFIDENTIAL

VI, C, Modular-Cooled Chamber Program (cont.)

(U) Since the state-of-the-art of transpiration cooling was not as advanced as that of regenerative cooling at the beginning of the modular program, the transpiration-cooled chamber was designed to allow a wide flexibility in coolant flow rates used in various portions of the chamber. The design was not complicated by the addition of a cooled nozzle skirt, which can be cooled by conventional techniques of regenerative cooling. The cooled portion of the chamber ends at an area ratio of 4:1, at which point an uncooled skirt is attached, extending to the exit area ratio of 20:1. In accordance with the contract, performance demonstration for the transpiration-cooled chamber during Phase I may be conducted in two parts: three tests of 1 sec duration will be made with the uncooled skirt attached to demonstrate specific impulse, and three additional 20-sec tests will be made with the skirt removed, but at the same coolant flow rates, to demonstrate satisfactory cooling and chamber durability. If the transpiration-cooled chamber concept is proved successful in Phase I, the chamber will be redesigned in Phase II to a flight-weight configuration with an integral regeneratively cooled skirt.

(U) Four regeneratively cooled chambers and three transpiration-cooled chambers were fabricated for test evaluation. Two additional regeneratively cooled chambers were scrapped during fabrication as a result of fabrication problems associated with the Inconel 718 material of the tube bundle.

(U) The modular cooled test program was initiated on 4 August 1966 with the transpiration-cooled chamber. Testing with the regeneratively cooled chamber began on 4 November 1966. Thirty tests were performed with two transpiration-cooled chambers, and five tests were performed with three regeneratively cooled chambers.

(U) The technical approach used in the testing of both chamber concepts was to first evaluate the basic design and operation of the concept. In these tests, the maximum amount of chamber coolant was used to ensure the

VI, C, Modular-Cooled Chamber Program (cont.)

most conservative heat-transfer conditions possible. Performance was then to be increased to the required level by successively reducing chamber film or transpiration coolant. Once performance was obtained, test duration would then be extended steps until the three required 20-sec tests were achieved.

(U) The feasibility of the transpiration chamber concept was demonstrated in the test program. Actual attainment of the required performance has not been demonstrated to date, however, because of the incompatibility problem associated with the Mark 125 injector which became apparent during the transpiration cooling test series. Because of this incompatibility problem, testing with cooled chambers has been temporarily suspended pending improvement of the secondary injector to eliminate this problem. Improved injectors are now being tested in the Extended Phase I program; cooled chamber testing will be resumed as soon as a streak-free injector becomes available.

(C) In the transpiration-cooled chamber test series, the lowest transpiration coolant flow rate attained without chamber burnout was 36.6 lb/sec (Test 022). The measured sea-level specific impulse during this 3-sec test was 267.6 sec. The injector used in this test was Mark 125 SN-003, which, based on its diameter and the resulting injector-chamber interface gap, was considered to have a 6 sec mixture ratio distribution loss. The highest specific impulse recorded in the test program was 271.1 sec, obtained in Test 023. This test, which had a coolant flow rate of 40.8 lb/sec, used high performing SN-002 injector. Because of the very short steady state test duration (0.1 sec), the data will not be relied upon until substantiating data are obtained.

(C) Performance obtained with the regeneratively cooled chamber was significantly lower, the maximum obtained being 237 sec. This performance was low for two reasons: (1) the injector used in the test series had a large mixture ratio distribution loss, and (2) no significant amount of film cooling reduction was achieved before the chambers were damaged.

VI, C, Modular-Cooled Chamber Program (cont.)

(U) The design and fabrication efforts performed for each of the cooled chambers are discussed in Section VI,C,3. The development test program, together with the analyses of the performance and heat-transfer data obtained, are discussed in Sections VI,C,4, and VI,C,5.

3. Cooled Chamber Components

a. Regeneratively Cooled Chamber

(1) Concept Selection and Design Criteria

(U) The regenerative cooling concept was selected on the basis of the regenerative cooling investigation at high chamber pressures in the ICP Residual Hardware Program. Also, this cooling technique is the widest used and best understood of all cooling concepts used in current operational engines. The criteria established for regeneratively cooled chamber design included the ARES modular engine thrust level, chamber pressure, nozzle contour, and nozzle area ratio. In addition, the chamber must be of flight-weight configuration, interface with the modular secondary injector and turbopump housing, and require no external lines for the regenerative cooling circuit.

(2) Design Description

(U) The regeneratively cooled combustion chamber, shown in Figures VI-46 and VI-47, is a double-pass oxidizer-cooled tube bundle configuration with an ID of 10.50 in. The nozzle has a throat diameter of 5.214 in. and expands to an area ratio of 20. The nozzle contour is an 80% bell configuration. The overall chamber length is 41.7 in. Chamber L* is 40 in. (the injector protrudes 1/4 in. into the chamber, reducing the effective L* to 39 in.).

VI, C, Modular-Cooled Chamber Program (cont.)

(U) The regenerative coolant circuit is composed of 104 tubes fabricated from Inconel 718 material. Fifty-two tubes carry the down flow and an equal number the return flow. The velocity profile through the tubes varies axially. Flow velocity is 85 ft/sec in the cylindrical section, 205 ft/sec in the throat, and 26 ft/sec in the aft end. The coolant pressure drop is approximately 857 psi (measured). Each tube is fabricated in two sections: one has a wall thickness of 0.015 in. and extends from the injector face down to an area ratio of 8:1, whereas the other has a wall thickness of 0.026 in. and extends from that point to the exit area ratio of 20:1. The two sections are joined by inserting the aft tube into the forward tube and induction-brazing the two together.

(U) The full length tubes are joined in pairs: one down and one return. The tube pairs are first TIG-welded together at the aft end and then fitted with an individual hemispherical cup fitting which comprises the coolant turnaround manifold. During the course of the program the design of this fitting was modified twice to ease fabrication problems and improve reliability.

(U) The chamber mounting flange, shown in Figure VI-28, has a three-fold function: it serves as the TPA-TCA interface attachment point, as a coolant transfer passage, and as the film coolant injector. The tube bundle is inserted into the flange body and is furnace-brazed concurrently with the brazing of the tubes to each other. The coolant enters the flange from the pump housing through 32 oval slots which split into 52 down-flow tubes. The coolant returns through 52 up-flow tubes and is rejoined inboard through 32 oval slots. There are 32 bolts 1/2-in. in diameter which mount the chamber. The film coolant circuit is composed of an outside manifold which feeds an inner manifold through 24 radial ports located between the regenerative coolant circuit inlet and outlet feed ports and bolting holes. There are two alternative film cooling injector configurations: one for single-point film cooling

VI, C, Modular-Cooled Chamber Program (cont.)

and one for two-point film cooling (called the "capillary tube" design). These injectors were developed during the Modular Secondary Injector Program as part of the cooled shroud investigation. Both designs include a smooth transition contour from the 9.5-in.-dia injector to the 10.5-in.-dia chamber. In the single-point injection design, film coolant is injected through 208 holes 0.028-in. in diameter, which exit from the base of the transition section or shroud. In addition, the shroud itself is film cooled by liquid oxidizer through 104 tangentially drilled holes 0.028 in.-in diameter. In the capillary tube design, chamber film coolant is introduced in both the plane of the injector face and in the convergent section of the chamber at a point 5 in. above the chamber throat. The coolant is injected in the upper station through 104 holes 0.028-in. in diameter located behind the transition shoud. The remainder of the coolant is introduced through the capillary tubes which are located in the valleys between the main tubes. The shroud itself is film cooled in an identical manner to that of the single-point injection design, i.e., through 104 tangentially drilled holes 0.028 in. in diameter. The flow characteristics of the chamber and shroud film coolant circuits for both designs are shown in Figures VI-48 and VI-49. The capillary tube installation is shown in Figure VI-50.

(U) The chamber structure is composed of alternate layers of glass cloth to provide longitudinal support and hoop-wound glass roving to provide additional hoop strength. The wrap terminates just above the base of the chamber. Epoxy resin is used to fill the convolutions between the tubes, thereby forming a smooth contour which eliminates point contact and stress concentrations between the wrap and tube crowns. An antiseize compound is placed over the epoxy surface so that the wrap will not bond to, and restrict axial growth of, the coolant tubes.

VI, C, Modular-Cooled Chamber Program (cont.)

(U) One of the capillary tube chambers built during this program was weighed at various intervals during fabrication to establish actual chamber weight. The total weight of the coated chamber was found to be 176 lb, composed of the following elements: brazed tube bundle, 55 lb; mounting flange, 60 lb; glass wrap, 38 lb; and coating, 23 lb.

(3) Design Analysis

(U) This section discusses in detail the design analysis effort performed in support of the regeneratively cooled chamber design. Included are the areas of coolant jacket design, heat-transfer studies, and capillary tube design. In addition, a new computer program was developed for evaluating regenerative and film coolant rocket thrust chambers. This program represents an improvement to the program previously used in that it includes test data from the ICP and ARES thrust chamber firings.

(a) Coolant Jacket Design

(C) Certain constraints, which fall into two general categories, were established for the design: (1) those that result directly from the program work statement and engine specifications such as thrust and cooling jacket pressure loss, and (2) those established during the course of the design effort.

1 Engine Specifications

Thrust at sea level, lb	100,000
Chamber pressure, psia	2800
Propellants	N_2O_4/AeroZINE 50
Mixture ratio (secondary injector)	2.2
Total flow rate (secondary combustor), lb/sec	351

VI, C, Modular-Cooled Chamber Program (cont.)

2 Thrust Chamber Specifications (Regeneratively Cooled Double Pass, Axial Tube Bundle)

Regenerative coolant flow rate, lb/sec	222.1
Target regenerative coolant pressure drop including turn-around, psi	775
Regenerative coolant inlet static pressure, psia	6000
Regenerative coolant inlet temperature, °R	550
Throat diameter, in.	5.214
Nozzle area ratio	20:1
Nozzle contour	80% Bell

(U) The N_2O_4 was selected as the regenerative and film coolant because of its superior heat capacity and convective heat-transfer properties over AeroZINE 50 at supercritical conditions.

(U) Studies conducted on Contract AF 04(611)-10827 showed that a 10.5-in.-dia chamber represented the minimum size that would allow the possibility of eliminating film cooling in the cylindrical portion of the chamber.

(U) The contour of the convergent portion of the chamber was that shape used previously on Titan thrust chambers. This shape consists of two radii connected by a 30-degree convergent angle. Each of the radii is equal to the throat diameter thus providing smooth transitions from the cylindrical portion and to the divergent nozzle.

(U) An L* of 50 in. was selected initially after considering all aspects of uncooled chamber performance as well as losses associated with film cooling. Subsequent film-cooling studies (discussed in the following section) provided the bases for optimizing L* at approximately 40 in.

VI, C, Modular-Cooled Chamber Program (cont.)

(U) Inconel 718 was chosen as the tube material on the basis of Contract AF 04(611)-8548 experience. Of the other materials considered (Hastelloy, CRES 347, and Inconel X), only Inconel X had sufficient strength for this application. However, its ductility at the desired operating temperatures is inferior to that of Inconel 718.

(U) A tube wall thickness of 0.015 in. was selected for use in the chamber and throat regions. Although it is readily apparent that a minimum thickness is desirable from a heat-transfer standpoint, there is a limitation imposed by maximum allowable stress level due to internal pressure. Fabrication considerations dictated a two-piece tube because of the large variation in desired diameter. Therefore, a 0.026-in. tube wall thickness was selected for the low heat flux portion of the nozzle where the potential stress levels are high due to the large tube diameter.

(U) A limiting tube aspect ratio (overall inside length divided by average inside diameter) of two was selected. This selection was made following a study of data on the effect of tube aspect ratio on local or minimum velocity (Reference 19). This effect is important, because velocity directly affects the liquid-side heat-transfer coefficient which, in turn, affects the heat flux capability of the tube. These data indicated no reduction in local velocity at an aspect ratio of two, whereas severe reductions in local velocity occurred at aspect ratios greater than three.

(U) A minimum flat length on the tube of 1/32 in. was selected to provide sufficient contact surface for brazing.

(U) These criteria resulted in the design of a double pass, regenerative-coolant jacket consisting of 104 tubes. The total pressure drop through this jacket at rated flow was predicted to be approximately 600 psi, which was well under the allowable value of 775 psi (Figure VI-51).

VI, C, Modular-Cooled Chamber Program (cont.)

(U) In addition to satisfying the previously stated ground rules, this design provided the potential of minimum film-cooling requirements due to the high regenerative coolant velocities and associated heat flux capabilities in the critical throat region. The regenerative coolant heat flux capabilities of this design are presented in Figure VI-52. The heat flux values are based on the outside surface area of the tube.

(b) Heat-Transfer Studies

(U) The heat loads in the chamber were calculated for gas-side surface temperatures of 1500 and 3500°F (Figure VI-53). These temperatures are the maximum operating values based on strength and/or oxidation-resistant properties for the Inconel 718 tube material and a tungsten-based coating, respectively. This thermal barrier was selected on the basis of successful laboratory tests and demonstrated potential in cooled thrust chamber tests on the ICP contract where N_2O_4 film cooling was used. A detailed discussion of the thermal barrier program is presented in Section VI,C,6,a. The heat loads were based on 100% c* and on a Bartz factor which was considered to decrease linearly with area ratio from 1.5 at the injector to 1.0 at the throat. The 1.5 factor was used in the cylindrical portion to account for turbulence in the combustion zone. The heat-transfer coefficients for these heat loads were based on free-stream gas conditions.

(U) The effect of coating thickness is presented in Figure VI-54. The curve shows the allowable outside tube wall and coating temperatures as well as an allowable average wall temperature of 1200°F. The data are shown only for the cylindrical portion of the chamber with no supplemental film cooling. Examination of this figure shows that very minimal amounts of film cooling will be required to bring the chamber operating point within all three temperature limits.

VI, C, Modular-Cooled Chamber Program (cont.)

(C) To select the ARES chamber L*, film cooling requirements were determined for each of six chamber configurations (uncoated and coated surface conditions in 17.4, 30, and 50 L* chambers). These film-cooling requirements, which were established as those that would limit the surface temperatures to their allowable values, are presented in Figures VI-55 for both single-point injection (at the injector) and two-point injection (at the injector and from unheated capillary tubes). The performance losses associated with these film coolant flow rates were combined with those experimentally determined losses due to mixture ratio distribution, combustion, nozzle friction, and nozzle geometry. The resulting performance potential of these six chamber configurations was calculated and plotted as a function of L* in Figure VI-56. Phase I and Phase II requirements of 90 and 91.6% of sea-level specific impulse, respectively, also are shown in this figure. Trading off the performance potential of the coated and uncoated configurations to retain the maximum flexibility for ultimate selection of either concept, the 39 L* chamber was selected as the best choice. The predicted allowable film-coolant flow rates are 29.2 and 25.2 lb/sec for Phases I and II, respectively.

(c) Capillary Tube Design

(U) The chamber was analyzed for 104 capillary tubes, one in each valley between the regenerative coolant tubes. Each capillary tube was considered to extend from the injector face plane to a point 5 in. upstream of the throat. A point closer to the throat would have required slightly less film-coolant flow; however, the shorter tube allowed greater flexibility of flow rates for development testing. Additionally, this injection point is in a region of significantly lower heat flux, and consequently the tubes had a greater margin of safety.

VI, C, Modular-Cooled Chamber Program (cont.)

(U) Parametric studies were conducted for three sizes of uncoated stainless-steel capillary tubes; inside diameters of 0.040, 0.045, and 0.050 in., each with a wall thickness of 0.005 in. Figures VI-57, 58, and 59 present the heat flux capability of these tubes as a function of coolant velocity in the capillary tubes for film-coolant flow rates of 13.8, 20, 30, and 40 lb/sec. The dashed lines reflect the tube heat fluxes at the capillary tube ends. These lines show that the heat flux is lower at the tube inlet for 13.8 and 20 lb/sec and at the tube exit for 30 and 40 lb/sec. These changes in heat flux for a given weight flow may be attributed to the combined effects of variations in fluid transport properties that result from changes in pressure and temperature. A design burnout heat flux line is also shown on these figures. This line limits the film-coolant flow rates to minimum values of about 15, 19.5, and 24 lb/sec for the 0.040-, 0.045-, and 0.050-in.-dia tubes, respectively.

(U) Initial pressure drop calculations for the three tube sizes indicated maximum flow rate capabilities of 27, 37, and 48 lb/sec for the 0.040, 0.045, and 0.050-in.-dia tubes respectively. These factors led to the selection of the 0.045-in.-dia tube, because it had a capability range which encompassed the high flow rates desired for initial tests as well as the flow rate associated with the total of 29.2 lb/sec for Phase I. However, following water flow tests with residual ICP tubes (discussed in succeeding paragraphs), the revised pressure drop calculations indicated that this 0.045-in. dia tube would have to be coated. The maximum capability of uncoated tubes was determined to be 22 lb/sec, whereas 24.7 lb/sec was required for cooling. Therefore, a coating was required to reduce the heat input to the capillary tubes and consequently to reduce the film-coolant requirements.

(U) The experimental investigation of two modified ICP capillary tubes was conducted to ascertain their capabilities of satisfying ARES design criteria. One tube had an inside diameter of 0.044 in. and

a uniform wall thickness of 0.004 in.; the other had an inside diameter of 0.055 in. and a similar wall thickness. The investigation consisted of water flow tests to determine their absolute roughness values and associated friction factors. The test data revealed absolute roughness values of about 90 microinches for the 0.044-in.-dia tube and 200 to 300 micro in. for the 0.055-in.-dia tube. These values, which correspond to friction factors from about 0.023 to 0.032, indicated that the larger tube with its 0.035-in. nozzle exit would be the better selection for use in the first capillary tube chamber (SN 003). This tube provided a capability range which encompassed the high flow rates desired for initial tests as well as the flow rate associated with the total allowable flow for Phase I. Additionally, the nozzle exit provided the high injection velocities desired for increasing film cooling effectiveness. The only limitation on the use of this tube was the condition that it be coated to avoid tube burnout.

(d) Computer Program Development

(U) A new computer program (AGC 8083) was developed to evaluate the effectiveness of regenerative and film cooling in liquid rocket thrust chambers. This program is basically similar to the 8037 program used on the ICP contract, AF 04(611)-8548, but incorporates several improvements which give results more closely approxima ing actual ICP and ARES test data. The improvements include:

1 A new relationship for the calculation of the liquid-side heat-transfer coefficient, i.e.,

$$h_1 = 0.0087 \frac{K}{d} R_e^{0.9} Pr^{0.4}$$

where k = liquid-side coefficient, Btu/in.^{2}-sec-°R
K = Fluid thermal conductivity, Btu/in.-sec-°R
d = Hydraulic diameter of tube, in.
Re = Reynolds number, dimensionless
Pr = Prandtl number, dimensionless

VI, C, Modular-Cooled Chamber Program (cont.)

This equation was determined experimentally for N_2O_4 coolant for properties evaluated at fluid-bulk temperature and pressure.

(U) 2 A new method of calculating the interface temperatures based on radial heat flow through the coating and/or tube wall. This method was found to yield temperatures which closely approximate maximum surface temperatures calculated two-dimensionally.

(U) 3 A new method of calculating the film-coolant carryover effect for multiple-point film-coolant injection. This is accomplished in a two-step procedure. Initially, only the first injection point is considered to establish adiabatic film temperatures downstream of the second injection point. Subsequently, these temperatures were input as the mainstream gas temperatures in a second computer run, since it is these temperatures that effectively heat the film coolant injected at the second injection point. The heat-transfer coefficient at the interface between the two film streams was calculated using the Colburn equation, i.e.,

$$h_g = 0.027 \frac{K}{D} RE^{0.8} Pr^{0.4}$$

Where h_g = Gas-side film coefficient between two film streams, Btu/in.^{2}-sec-°R

K = N_2O_4 thermal conductivity at average temperature of of two film streams, Btu/in.-sec-°R

D = Chamber diameter, in.

Re = N_2O_4 Reynolds Number at average temperature of two film streams, dimensionless

Pr = N_2O_4 Prandtl Number at average temperature of two film streams, dimensionless

(U) 4 A new relationship for the calculation of pressure drop due to friction in the regenerative coolant tubes. Previously, the pressure drop in the tubes was calculated based on a constant relative (ε/D)

in the tubes of 0.00001. With this modification, the absolute roughness (ϵ) is input and held constant throughout the tubes. The relative roughness is calculated for each tube-length increment based on the local tube hydraulic diameter. The corresponding friction factor (f) is then calculated based on an algebraic representation of the Moody diagram (Reference 20), i.e.,

$$f = 0.0055 \left[1 + \left(2 \times 10^4 \, \epsilon/d + 10^6/Re\right)^{1/3}\right]$$

where f = Friction factor, dimensionless
ϵ = Absolute roughness of tube, in.
d = Hydraulic diameter of tube, in.
Re = Reynolds Number, dimensionless

(U) 5 A new reference temperature for the evaluation of the mainstream gas and film-coolant convective heat-transfer coefficients. These coefficients were previously referenced to the mainstream gas and film-coolant bulk temperatures, respectively. The reference temperature for the gas coefficient now is a film temperature equal to the arithmetic mean between the mainstream gas and film-coolant temperature; for the film-coolant coefficient, the reference temperature is the arithmetic mean between the film-coolant and wall temperatures.

(4) Fabrication

(U) Six regeneratively cooled chambers were to be fabricated during the program, including three single-point film cooling injection chambers and three capillary tube chambers. Substantial difficulty was experienced during the fabrication of these chambers, which resulted in scrapping of two of the single-point chambers and truncating the third at an area ratio of 2:1. A summary of the problems encountered is given in the

VI, C, Modular-Cooled Chamber Program (cont.)

following paragraphs. The four completed chambers were coated with a tungsten-base thermal barrier liner to reduce film cooling requirements (the coating is discussed in Section VI,C,6,a). Chamber SN 002 was the small area ratio chamber having single point film cooling injection, and chambers SN 003, 004 and 005 were the capillary tube chambers.

(U) It was known from the program beginning that thin-gage Inconel 718 is a very difficult material to work; however, the pressure and heat load requirements of the ARES engine are so severe that no other material exists which has the desired combination of workability and required structural properties. During the course of this program, a great amount of knowledge was gained concerning the problems associated with this material and successful techniques for overcoming these problems. Because of the widespread interest for this information, a special report entitled "Inconel 718 Thrust Chamber Fabrication" has been written covering in detail the fabrication problems of the ARES regeneratively cooled Inconel chambers. This report, TR-67-74, is available through the Government. Since the fabrication of the ARES chamber is covered in a special report, a detailed discussion is not presented in this final report. However, a brief account of the problems encountered is given.

(U) (a) At the beginning of the ARES program, no specification existed for ordering thin-gage Inconel 718 material from the mill. The tubing was therefore ordered to a sheet stock specification together with supplemental instructions to cover known changes between sheet and tubing requirements. When the initial order of tubing was received, the tubing was found to be of substandard quality. All tubing contained surface discontinuities, visible to the naked eye, which could propagate during the forming operation and be detrimental to the mechanical properties of the tubes. The flaws were circumferential depressions on the outside diameter of the tubes (see Figures VI-60 through VI-61) and were present on all tubes. A very

detailed metallurgical analysis, performed on "random" and "worst" samples of tubing, established that all properties met the requirements to which the tubes had been procured. The surface depressions were found to have a depth of less than 0.001 in. Further, when typical depressions were sectioned, mounted, and examined at magnifications from 50 to 205X the depressions were judged not to be cracks because their root radii were large. These surface flaws were probably introduced during a grinding operation. Based on the results of the metallurgical examinations, it was decided that forming operations on part of the tubing should be continued. During the ARES program, Specification AGC 44204A was developed from which all future 718 tubing will be procured.

(U) (b) Immediately at the beginning of forming operations, the tubes were found to crack. This cracking was not altogether caused by a propagation of the circumferential flaws, as might be expected, but predominately from excessive cold working of the tubing. The vendor had been restricted to an anneal temperature of 1800°F. This low anneal temperature is desirable because it permits uniform elongation properties of the Inconel 718 tubing in the operating range of 1200 to 1400°F. If annealing temperatures exceed this 1800°F limit, the elongation properties at elevated temperatures are noticeably reduced. After extensive attempts at fabricating formed tubes, it was decided to form the tubes in a four-phase operation. The tubes are partially formed, annealed at 1925 $\pm$ 25°F, further formed, annealed, formed to within 90% of final shape, annealed and final formed. The higher temperature yields a softer material and the step forming minimized the cold work induced into the tube. Approximately 40% of the material annealed at 1800°F and drawn in a two-phase operation was scrapped. The new four-phase forming operation cut the scrap rate to a negligible amount.

(U) (c) Considerable difficulty was encountered during the brazing operation of the tube bundle. The tube-to-tube braze joint had several leaks even after repair furnace braze cycles were run. Similar leakage,

VI, C, Modular-Cooled Chamber Program (cont.)

which occurred on the Integrated Component and Improved Titan programs, was stopped by applying soft solder with an oxyacetelene torch to the joints. This was done and, as the joints cooled, cracks would appear in the parent tube material. Extensive repair attempts were made to the chamber but repeated failure resulted in scrapping the unit. Metallographic analysis of the cracking resulted in changing the solder material and applying it with a large soldering iron. No further cracks developed from that time on.

(U) (d) Each regenerative tube was fabricated in two pieces and brazed together with an induction coil. This two-piece configuration was necessary because the tube forming supplier was unable to form the convergent-divergent configuration beyond a diameter ratio of 2:1 on a single tube, whereas the design called for a ratio of 3.9:1. The joint, when placed next to an adjoining tube, formed a void between tubes of up to 0.020 in. square. This void was too excessive for braze alloy to fill and cling to by surface tension alone. Nickel wire and shim stock were used with partial success to fill the void and seal the joint.

(U) The induction-brazed joint produced another related problem in that when a local high temperature (1950 to 2000°F) was applied to the joint, the tube would expand in width in an effort to seek its original round shape prior to flattening. This condition became apparent during tube bundle layup where gaps up to 0.015 in. were noted. This condition was partially alleviated by placing light gage CRES 347 shim stock in the gaps and swaging the tubes to fit.

VI, C, Modular-Cooled Chamber Program (cont.)

b. Transpiration-Cooled Chamber

(1) Concept Selection and Design Criteria

(U) The most important criteria in the design of a transpiration-cooled chamber are: (1) the ability of its porous wall to eject a prescribed amount of coolant at a specific zone on the chamber surface, and (2) permeability only in the radial direction. Attempts to use sintered and woven materials have been unsuccessful because directional coolant flow could not be controlled and because the distribution hydraulics were dependent upon the thermodynamics. Figure VI-62 summarizes the advantages and disadvantages of several materials for a transpiration-cooled wall. Among the possibilities investigated, the photographically etched, chemically milled, ultrathin washer concept was chosen for the ARES combustion chamber because it best satisfied the design criteria.

(U) N_2O_4 was selected as the transpiration coolant because it is available to the engine system at high pressure, and does not contain constituents which leave wall plugging deposits, nor will it detonate. Furthermore, N_2O_4 undergoes two endothermic decomposition reactions upon heating which enhance its cooling capacity.

(C) The transpiration-cooled chamber was designed to meet the ARES modular engine operation specifications of 100,000 lb/thrust and 2800-psia chamber pressure. Because the state-of-the-art of transpiration cooling is not as advanced as that of regenerative cooling, it was decided to allow as much flexibility as possible in the coolant flow rates used in various portions of the chamber. At area ratios greater than 4:1, conventional regenerative cooling is sufficient to cool the exit nozzle and needs no feasibility demonstration. On the basis of these considerations, the design criteria for

VI, C, Modular-Cooled Chamber Program (cont.)

the Phase I transpiration-cooled chamber differed from that of the regeneratively cooled chamber. Thick-walled workhorse type construction of the pressure vessel was allowed, as was an uncooled skirt extension extending from the area ratio of 4:1 to the module exit ratio of 20:1. With these allowances, maximum opportunity was afforded to demonstrate the washer transpiration cooling concept. After Phase I performance and durability requirements are successfully demonstrated, the chamber will then be redesigned into a flight-weight configuration having an integral regeneratively cooled skirt. This effort will be performed during Phase II.

(2) Design Description

(U) The ARES transpiration-cooled combustion chamber, shown in Figures VI-63 and VI-64, is a workhorse design. The chamber is composed of 12 individual compartments, as shown in Figure VI-65, which are housed in a 1-1/2-in.-thick steel shell forming a cylinder with a diameter of about 18 in. Each compartment is manifolded individually to allow external control of gross pressure-drop and flow rate. Thus, coolant flow rate may be varied within the compartments from test to test in an effort to achieve optimum operation. Special instrumented washers, each containing six high-response thermocouples, are located between compartments to measure surface temperatures.

(U) Each compartment is composed of a stack of "washer pairs," as shown in Figure VI-66. These pairs consist of a 0.001-in.-thick flow-control washer and of a flow-diffusion washer, 0.010 in. thick in the throat region and 0.020 in. thick in the chamber region. The passages in the flow-control washer are etched through the 0.001-in. thickness, whereas the channels in the flow-diffusion washers are 0.0025 in. deep.

VI, C, Modular-Cooled Chamber Program (cont.)

(U) Precise metering of the coolant is achieved in the flow-control channels. The flow-diffusion channels provide peripheral distribution of the coolant and allow the coolant to diffuse into the chamber through the thermal influence zone. All heat is exchanged in the thermal influence zone; coolant flow into this zone is controlled by the previously mentioned flow-control channels and is independent of the heat input. Coolant flow within the washer passages is confined to the laminar region, permitting accurate flow-control predictions to be made.

(U) As mentioned previously, each compartment's total flow rate can be regulated externally. However, the flow rate within the washer pairs themselves is further controlled by the manner in which they are assembled. Because flow rate is directly proportional to flow-channel length in the laminar flow regime, the washers were designed to be assembled in six possible positions, each providing a different channel length and, hence, different flow rate.

(U) The aft flange and the aft retainer are designed as an integral unit. The forward end of the chamber incorporates a 1/4-in. plate which extends from the chamber ID to the retainer OD. Both the 1/4-in. plate and the aft flange are keyed to their respective adjacent retainers by means of a shear ring in addition to the two dowel locating pins, which are used to locate all retainers in the entire assembly. An adapter flange was designed for the forward end of the transpiration-cooled chamber to permit installation to the secondary injector. The entire chamber is held in compression by 32 high-strength studs 5/8 in. in diameter.

(3) Design Analysis

(U) This section discusses the design analysis effort performed in support of the transpiration-cooled chamber design. The effort included: (1) the necessary analyses to establish transpiration coolant flow rate requirements for two conditions of ARES operation, i.e., a conservative first-test schedule and an optimized design schedule, and (2) the development of analytical models for evaluating transpiration coolant effectiveness in high heat flux regions.

(a) Design Considerations

(U) Constraints similar to those established for the regeneratively cooled chamber design were used for this design. In addition to the engine specifications listed in Section VI,C,3,a,(3), the design was based on a 10.5-in., 40 L* chamber with a throat diameter of 5.214 in. The chamber diameter was selected to be the same as that of the regeneratively cooled chamber to maintain as much geometrical similarity as possible. Oxidizer transpiration cooling was used from the injector face to an exit area ratio of 4.0. A temperature of 1900°F was selected as the maximum operating wall temperature. The ignition temperature of CRES 347 steel in this pressure range is approximately 2500°F (Reference 22).

(U) The design selection was strongly influenced by several factors associated with the platelet material. These factors included: thermal conductivity, availability, compatibility with N_2O_4, cost, and the ability to fabricate and handle. The thermal analyses showed that the most efficient use of the coolant can be realized by employing a thin platelet with high thermal conductivity, since these two aspects tend to promote internal heat transfer. CRES 347 was selected because of its availability, low cost, and moderately good oxidation resistance at high temperatures, even

though its thermal conductivity is poorer than would be desired. From a strictly thermal viewpoint, nickel, copper, beryllium, or laminated plate containing these materials as a core would have been better selections, but potential compatibility problems strongly outweighed the advantages of their higher conductivities. Distribution plate thicknesses of 0.010 and 0.020 in. were selected mainly on the basis of cost and ability to handle. Thinner distribution platelets, although desirable, were considered impractical. The use of 0.001-in. stock for metering platelets was accepted in spite of potential handling difficulties, because technical considerations left no alternative choice.

(U) A scale drawing showing the chamber subdivided into 12 hydraulically isolated compartments is presented in Figure VI-65. Figure VI-67 completely defines the assembly of the chamber circuitry. This figure contains a summary listing the length of each compartment, the number and thickness of platelets in each compartment, and a primary metering groove indexing position for each platelet. Also given for each compartment is a tabulation of the required weight flow, its coolant supply pressure, and resulting wall temperature at both the optimized operating condition and at the high initial coolant flow rates. Maximum temperatures were predicted to occur in Compartments 5 and 6.

(b) Method of Analysis

(U) The thermal analysis of this chamber was an evolutionary process. The early analysis was based on a simple energy balance which assumed that the transpiration coolant leaves the wall at the wall temperature. This method, however, made no allowance for platelet thermal conductivity and thickness or alterations to the thermal, hydrodynamic and transport property profiles caused by the mass addition to the boundary layer.

VI, C, Modular-Cooled Chamber Program (cont.)

(U) In an attempt to account for the effect of mass transfer on the boundary layer, a modified form of the Rannie correlation was employed (Reference 22). This method considers changes in the temperature and velocity profiles within the laminar sublayer, but it assumes that the two profiles are unchanged within the turbulent core. These considerations made the analysis less conservative than the simple energy balance, and they introduced a more involved computational procedure. Additionally, this method also did not take into account flow geometry, metal conductivity and other boundary layer effects associated with mass addition to the boundary layer.

(U) Following these analyses, the design was frozen to initiate fabrication. Liberal allowances were made, however, in the platelet designs to accommodate changes in coolant flow rates by at least a factor of two, either up or down.

(U) A more representative model (referred to as the advanced thermal model) was developed later. This model (shown schematically in Figure VI-68) developed from a one-dimensional fin conduction model with imposed boundary conditions which are analogous to a platelet cooled on its sides and heated at the tip. Contact area between the platelet and the coolant within the wall and appropriate wall-to-coolant heat-transfer coefficients were introduced as parameters. Because flow between the plates is laminar throughout the entire systems under all anticipated flow conditions, wall coolant heat-transfer coefficients could be reasonably predicted by assuming either a uniform wall temperature or uniform heat flux boundary condition and constant fluid properties.

(U) To properly evaluate the effects of mass addition to the boundary layer and its resultant effect upon the gas-side surface energy exchange, several simplifying assumptions were made. One assumption was that the external region of coolant influence is confined to

the single platelet from which the coolant is ejected. This, in essence, means that there is no thermal and hydrodynamic influence on the mainstream boundary layer as a result of mass transfer to the boundary layer from platelets upstream of the platelets of interest. This is, of course, not necessarily correct and in actuality such "carryover" effects may be quite significant.

(U) Two film cooling models were used to predict temperature profiles over the thin platelets. One was the Hatch and Papell model (Reference 23), the other was a boundary layer mixing model advanced by Stollery and El-Ehwany (Reference 24). A comparison of these models is presented at the end of this section. The film cooling model utilized for determining coolant flow requirements is the model set forth by Hatch and Papell.

(U) The platelet gas-side surface boundary condition was represented by a constant temperature due to the limitations inherent in the one-dimensional platelet conduction model. Therefore, regardless of which film cooling model is used an average temperature must be obtained. This was accomplished by using an integrated average of the temperature profile over the platelet gas-side surface.

(U) Analysis based on this model indicated that the transpiration coolant would leave the wall at a temperature considerably below the wall temperature under the high heat fluxes in the ARES chamber. Thus, the estimated coolant requirements were increased over those calculated using either of the two previous methods. This method placed greater dependence on the film cooling aspect to control wall temperatures, and less on the transfer of heat within the wall. The initial conservatism in the platelet design along with increased coolant supply pressure and the flexibility in

selecting metering groove resistances on assembly permitted the higher coolant flow rates without difficulty.

(U) Figure VI-69 is a plot of coolant specific flow requirements for the three analytical models. It is quite apparent from this plot that the simple energy balance approach deviates radically from the advanced thermal model in the high flux regions. At the throat, the predicted flow rate difference amounts to over a factor of two.

(U) The Rannie and the simple energy balance methods are quite comparable. The greatest deviation between these two models occurs from the injector face to the throat. The two models are virtually identical in the divergent region.

(U) When the advanced thermal model is compared to the energy balance model, quite close agreement is found for cases of equivalent Bartz factors in the chamber. Again, in the divergent region, near the terminus of the transpiration section, the two models begin to converge on equivalent flow rates. Remembering that the assumption of equal wall and coolant temperatures is fundamental to the energy balance analysis, it is of interest to consider the degree of violation of this assumption indicated by the advanced thermal model. In the nominal design case of 1.5 Bartz factor in the cylindrical chamber region, for a 1500°F wall temperature, a coolant wall temperature difference of about 550°F exists. At the throat section a temperature difference of 1240°F is predicted for a wall temperature of 1500°F. This means that there is only an increase of 160°F in the coolant temperature through the platelets located within the throat region. Figure VI-70 shows the temperature predicted for the coolant and wall at the throat section using the Hatch and Papell technique in the advanced thermal model. This is shown as individual plots of wall temperature and initial film-coolant

injection temperature (the temperature of the coolant as it emerges from the platelet) as a function of coolant flow rate. Wall and coolant temperature for a single flow rate is shown for the boundary layer mixing model. It is now quite apparent that within the high flux region the equal wall-coolant temperature assumption is a poor one for the combination of material and plate thickness employed.

(U) At the divergent end of the transpiration-cooled portion of the chamber, i.e., at area ratio of 4.0, a coolant-wall temperature difference of about 230°F is predicted at a wall temperature of 1500°F.

(U) The effect of platelet thickness on the predicted coolant requirements in high heat flux regions is significant. In the convergent section a step reduction of 26.5% in predicted coolant flow is obtained by changing from 0.021- to 0.011-in. platelets.

(U) It is inappropriate to consider whether the boundary layer mixing model is more realistic than the Hatch and Papell film cooling model in predicting the wall temperatures which will occur for a given flow rate because neither analysis includes the effect of coolant carryover. It is believed that if the total boundary layer history, including carryover, were considered, the boundary layer mixing model would provide the most realistic approach to the problem's solution. Some treatment of the effect of coolant carryover similar to that which is advanced by Sellers (Reference 20) would be a good first approach to the problem. Ultimately, a comprehensive boundary layer analysis is required which will consider the total boundary layer history of mass transport and chemical reaction. The other and perhaps more expedient approach is to obtain valid data and empirically determine correlative relationships between the mass transfer to the boundary layer

and the resultant wall temperatures. Hopefully, valid data in conjunction with more realistic hydrodynamic, thermal, and chemical reactive models will provide the best solution to the heat-transfer analysis of this advanced cooling concept.

(U) The design philosophy of the platelet hydraulic distribution system was to provide a uniform and adequate coolant flow at the heated surface in such a way that the rate and location of the heat addition to the wall will not affect the coolant flow rates. This is accomplished by means of a three-part series circuit containing primary and secondary fluid metering channels and thermally influenced distribution channels. Nominal pressure drop through the distribution channels is on the order of a few psi, and that through the metering grooves is in the order of hundreds of psi. Therefore, the coolant flow rates will not be altered appreciably by large density and viscosity changes due to the heat addition within the metering channels.

(c) Instrumentation

(U) The thermal instrumentation consisted of six 0.010-in.-dia chromel/alumel thermocouples in the downstream platelet of Compartments 1 through 11. These thermocouples were oriented 60-degree intervals peripherally with one exception, i.e., the platelet separating Compartments 2 and 3. The reason for this anomaly was to obtain midpoint and onpoint spacing of the thermocouples with respect to the fuel discharge pattern of either the Mark 32 or Mark 125 injector. This was done to detect possible hot streaks caused by fuel injection.

(U) The thermocouple junctions were nominally located at three radial locations: at the gas-side surface, 0.010 in. below

VI, C, Modular-Cooled Chamber Program (cont.)

the surface, and 0.050 in. below the surface. The majority of the junctions were placed at the surface so that hot spots or streaks could be detected. The other junctions were to provide the experimental data necessary to verify the fin heat conduction model.

(d) Results

(U) A total transpiration coolant flow rate of 14.1 lb/sec is required to maintain a uniform wall temperature of 1900°F. This ideal distribution, which was calculated using the advanced thermal model, is presented in Figure VI-71. The estimated distribution of 14.8 lb/sec which can be achieved utilizing the six available discrete indexing positions is presented in this figure also. The criteria employed in the flow rate matching was a nominal +7% excess and -5% deficit deviation from the predicted ideal curve.

(U) The predicted ranges of surface temperatures within the flow control compartments are presented in Figures VI-72 through -75 as functions of flow rate. The ranges result from variations in chamber pressure and platelet indexing location.

(U) The predicted radial temperature gradients are presented in Figures VI-76 and -77 for the 0.021- and 0.011-in. platelets, respectively. These gradients, which are shown for various gas-side surface temperatures, are pronounced in that the temperatures drop rapidly as the distance from the surface increases. For example, the 0.021-in. platelet temperature drops from 1500°F at the surface to [illegible] at 0.029 in. below the surface and to 105°F at 0.220 in. below the surface; the same temperature variations occur in only 0.021 and 0.135 in. below the surface, respectively, in the 0.011-in. platelet.

VI, C, Modular-Cooled Chamber Program (cont.)

(U) The 0.021 and 0.011-in. platelets have thermal influence zones of approximately 0.250- and 0.150-in., respectively. These relatively thin zones mean that the internal coolant heat exchange must occur in a very short time. This delineates the need for a higher conductivity material so that the radial temperature gradients will be less steep and consequently will extend further into the platelets for greater thermal effectiveness.

(U) Figure VI-77 also shows the radial temperature gradient for a 0.021-in. instrumented platelet which is located at the throat. This platelet experiences the same effective gas-recovery temperature as adjacent 0.011-in. flow-metering platelets that are operating at a surface temperature of 1900°F. The corresponding surface temperature of the 0.021-in. instrumented platelet is 2175°F. An even higher surface temperature would be experienced in a similar platelet if it were thermally isolated from the cooler 0.011-in. platelets.

(4) Fabrication

(U) Three transpiration-cooled chambers were fabricated during Phase I, of which two were used in the test program. As a result of the supporting laboratory program, no major problems were encountered during the fabrication phase. The basic design of all three chambers was similar. However, the inside diameter contour at the forward end of each chamber differed slightly. The first two chambers each had a divergent transition section from 9.5 to 10.5 in. ID immediately downstream of the injector as shown in Figure VI-65. This transition section was necessitated by the fact that the secondary injector diameter was 9.5 in. whereas the chamber was 10.5 in. to maintain the same geometry as the regenerative chamber. The transition section of the first chamber was rather abrupt, occurring within

VI, C, Modular-Cooled Chamber Program (cont.)

the short length of the first compartment. Posttest hardware inspection indicated that chamber wall streaking appeared to be accentuated downstream of the divergent transition section. In an effort to minimize chamber wall streaking, the transition section of the second chamber was machined to be more gradual, extending over the entire length of the second compartment as shown in phantom line of Figure VI-65. However, continued chamber wall streaking occurred; therefore the third chamber was fabricated at a constant inside diameter of 9.5 in., thereby eliminating the transition section altogether.

(U) Fabrication of the transpiration chamber retainers and flanges was accomplished by conventional machining operations. The fabrication sequence employed in building the transpiration washer compartments is as follows. Both the flow-control and flow-diffusion washers were fabricated by vendors specializing in chemical etching. The completed washers were then assembled on a vacuum-operated washer orienting-and-unitizing fixture. Orientation was accomplished by means of the indexing tab; unitizing was accomplished by means of six mirco-spot welds equally spaced at the outer periphery. Unitized washer compartments were then machined on the OD tabs to conform to the ID of the retainer rings. The final washer compartment machining operation was that of machining the ID contour. Upon completing the machining operations, individual washer compartments were flow-evaluated.

(U) Final assembly of the first chamber was then accomplished. A special assembly fixture compressed the compartments, including the 11 instrumentation washers, until all parts bottomed out. Twelve circumferential seal welds were then made to join the outer retainers and the forward and aft flanges into one unitized chamber.

VI, C, Modular-Cooled Chamber Program (cont.)

(U) Concurrently, laboratory experiments had demonstrated the effectiveness of electrochemical deburring. Thus, a cathode mandrel was designed and fabricated to deburr the machined ID contour. The transpiration-cooled chamber was mounted over the cathode mandrel to permit the entire ID chamber contour to be electrochemically deburred in one operation. The resultant porous surface was entirely free of burrs.

(U) Because the instrumented washers in the first chamber required careful masking during the electropolishing operation, successive chambers were electropolished prior to having the thermocouples brazed into the instrumentation washers.

VI, C, Modular-Cooled Chamber Program (cont.)

4. Development Testing

(U) The objectives of the modular-cooled chamber test program were to evaluate the ARES configuration transpiration- and regeneratively cooled secondary combustion chambers and, using either of these concepts, to demonstrate Phase I performance and durability requirements.

(U) Detailed discussions of the transpiration- and regeneratively cooled test series are given in the following sections. The performance and heat-transfer data are discussed in Section VI, C, 5.

a. Transpiration-Cooled Chamber Testing

(U) The transpiration-cooled chamber test program consisted of two test series; the first using transpiration-cooled chamber SN 001 and the second using transpiration-cooled chamber SN 002. The test data obtained in these tests are shown in Figures VI-78 -79 and -80.

(1) Test Series 1--Tests 1.2-12-WAM-001 through 012

(U) This test series was devoted to the initial evaluation of the transpiration-cooled chamber concept. The purpose of this series was to (1) establish the basic feasibility of N_2O_4 transpiration cooling at supercritical pressures, (2) demonstrate the mechanical integrity of the test system, (3) verify the selected method of coolant control for the 12 transpiration compartments (and the skirt film cooling compartment), (4) develop a suitable start and shutdown technique, and (5) selectively reduce the coolant flow in the compartments to attain the ARES I performance goals.

VI, C, Modular-Cooled Chamber Program (cont.)

(U) The transpiration chamber was tested using the intensifier-fed sector engine shown schematically in Figure VI-81. The 13 compartments were connected to a common feed manifold with flex lines having metering (and balancing) orifices installed at the downstream end. Pressure measurements at inlets to the lines and outlets of the calibrated orifices allowed calculation of the individual compartment weight flows on each of the tests conducted.

(U) Balance orifices for the desired flow in each compartment were calculated using the resistance characteristics of the compartments obtained in the flow laboratory, the isentropic chamber static wall back pressure at each station, and the pressure at the common supply manifold calculated from the intensifier feed pressure for the total flow required.

(U) The operating sequence for the tests was calculated using the intensifier-fed sector-engine analytical simulation computer program. The resulting sequence was identical to previous uncooled testing with two additions. First, a 6-sec fill time for filling of the chamber was used to ensure complete priming of the platelet diffusion zones prior to chamber ignition. Second, a low-pressure water purge was applied on shutdown to evacuate the secondary fuel at a high flow rate.

(U) The initial tests were balanced to give maximum coolant flow rate in each of the compartments. The predicted wall temperatures for this condition was below 1500°F in all cases and substantially less in most of the compartments. Analysis of the chamber design indicated that erosion-free operation could be maintained with the chamber operating at a maximum wall temperature of 1900°F.

VI, C, Modular-Cooled Chamber Program (cont.)

(U) Results from the first two tests (001 and 002) indicated several problems: (1) heat marks started abruptly in Compartment 6, (2) minor erosion of the chamber throat and exit section regions occurred, concentrated at the 7 o'clock position of the horizontally mounted chamber, and (3) a rough pressure transient was present in the secondary chamber during shutdown. Figure VI-82 shows the postfire condition of the chamber. The chamber was subsequently repaired by grinding out the eroded areas and electropolishing the surface to restore the coolant openings.

(U) Correction of the first problem on subsequent testing was effected by modifying the metering grooves in chamber Compartments 6, 7, 8, and 9 to allow twice the coolant flow. The chamber erosion at 7 o'clock was attributed to an unequal primary gas distribution across the secondary injector face that was caused by the turbulators of the primary combustor. This effect was removed by placing a multihole flow distribution orifice above the secondary injector face. To eliminate the rough shutdown, the water purge was dropped since its pressure level was inadequate to sustain the expulsion of fuel. The adequacy of these steps to correct these initial problems was demonstrated by the successful completion of the remaining nine tests of this test series during which none of the above problems recurred.

(U) The first four tests used Mark 125 injectors SN 002 and 004. Both of these injectors were of large diameters and were high performing. In Test 003, which was a malfunction, the oxidizer intensifier failed to ramp, which caused the primary combustor to operate extremely hot and resulted in damaging the fuel tubes of the secondary injector. Following the next test (004), the condition of the injector was considered marginal for further testing. This injector was therefore replaced by injector SN 001, which was of small diameter and known to have a large MRD loss. Tests 005 and 006 were performed with this injector; in Test 006 the film coolant used to cool the uncooled extension was eliminated with no detrimental effects on the hardware.

VI, C, Modular-Cooled Chamber Program (cont.)

(U) At this time, a new higher performing injector SN 003 became available, and Tests 007 through 010 were performed using this new injector. During these tests, transpiration coolant reductions were made in Compartments 3, 4, 11, and 12. While the coolant performance loss decreased as coolant was reduced, the overall performance was below that previously demonstrated. This occurred because SN 003 injector, while significantly higher performing than SN 001, was not as high as SN 002 or SN 004. In an effort to obtain high overall specific impulse, it was decided to resume testing with injector SN 004.

(U) Tests 011 and 012 were performed using injector SN 004. In Test 012, the injector was displaced back 1/2-in. in the chamber by adding a spacer between the injector and chamber to reduce the MRD loss to zero by providing the highest performing transition configuration as determined in the Modular Injector Evaluation Program. Postfire inspection following Test 012 revealed massive erosion of the chamber at the 3 o'clock position directly in line with three fractured injector tubes. The fractured tubes had allowed a local high concentration of fuel, which combined with the coolant on the wall and ignited the steel, causing it to burn exothermically. Once the ignition temperature of the steel is reached (approximately 2500°F, Reference 22), the metal burns progressively with N_2O_4. Figure VI-83 shows the postfire condition. The chamber was not repairable and the test series was suspended pending the receipt of chamber SN 002.

(C) Two conclusions were drawn from this first test series: (1) in order to achieve the required specific impulse of 280 sec, large diameter injectors having close to zero MRD loss must be used, and (2) the wall of the transpiration chamber is sensitive to fuel streaks; therefore, all possible precautions should be taken to prevent excessive fuel contact with the wall.

VI, C, Modular-Cooled Chamber Program (cont.)

(2) Test Series 2--Tests 1.2-12-WAM-013 through 030

(U) In an attempt to increase thrust chamber performance, transpiration chamber SN 002 was fabricated with the chamber-injector transition section configuration which was found to give the highest performance in the modular injector test program. In this chamber, Compartment 1 had a constant 9.6-in. diameter. Compartment 2 formed the transition section and was uniformly tapered over its entire length from the 9.6-in. diameter to the 10.5-in. chamber diameter. The configuration is shown in Figure VI-65.

(U) On the basis of the compatibility problem experienced in Test 012, a more conservative approach was used in the second test series. Each time a major change was made (such as a change of injector serial number or a significant reduction in transpiration coolant) a short-duration test of approximately 1.3 to 1.8 sec was conducted, after which a 3.0-sec test was made. By this method, it was hoped to spot any damaging erosion in the short test before the entire chamber was lost. Testing was initiated with Mark 125 SN 003; injectors 002 and 005 were also used in this test series. Transpiration coolant was reduced in successive tests from 56.2 to 38.8 lb/sec in tests 013 to 018. At this time, the instrumentation in the throat showed that the chamber was operating at a marginally hot condition. Therefore, the chamber was removed and the throat compartment modified to allow an increase in flow rate in that compartment.

(C) Testing was resumed with the flow rate in throat Compartment 8 increased from 1.3 lb/sec to approximately 2.2 lb/sec. Transpiration coolant flows were adjusted in subsequent tests in an effort to reach required performance level. The highest sustained performance obtained was during Test 022 in which a delivered specific impulse of 267.6 sec was measured. Injector SN 002 was used in Tests 023 and 024. During Test 023,

VI, C, Modular-Cooled Chamber Program (cont.)

a specific impulse of 271.1 sec was measured. This test, however, was of very short duration and the data is therefore considered questionable and will not be relied upon until further substantiating data become available. Slight chamber erosion was experienced in Test 024 as shown in Figure VI-84. It was found that this erosion aligned with two vanes of injector SN 002 that were spaced very close together. Therefore, testing was resumed with a new injector, SN 005. Tests 025 through 030 were performed using injector SN 005. On Test 030, the chamber suffered gross erosion very similar to that experienced in Test 012 with chamber SN 001. Erosion was initiated in Compartment 2, as shown in Figure VI-85, a photo of Compartment 2 taken after disassembly of the chamber.

(U) A posttest, examination of injector SN 005 revealed no abnormalities or failure of the injector. It was concluded that the Mark 125 injector in its present configuration allows too much concentrated fuel to contact the transpiration-cooled wall, which results in burning of the coolant and subsequent burnout. Therefore, further testing of transpiration chambers was suspended until an injector having better compatibility is developed.

b. Regeneratively Cooled Chamber Testing--Tests 1.2-14-WAM-001 through 005

(U) Five hot test firings were made during the Phase I program with regeneratively cooled chambers. Two of these were with chamber SN 002, two with chamber SN 003, and one with chamber SN 004. Chamber SN 002 had been terminated at an area ratio of 2:1 during fabrication as a result of cracks which developed on the lower portion of the chamber skirt. In this condition, it became a logical checkout chamber for initial testing. The inside of the tube bundle was coated with a tungsten-base thermal barrier

VI, C, Modular-Cooled Chamber Program (cont.)

coating. Chambers SN 003 and SN 004 were both capillary tube chambers extending to the design area ratio of 20:1. Each of these chambers was also coated with the thermal barrier coating.

(U) A first regeneratively cooled test was performed on 4 November 1966 with chamber SN 002. The injector used with this testing was Mark 125 SN 001, which was known to have a small diameter and therefore a large MRD loss. This injector was selected for the initial tests since it would provide the most conservative heat-transfer conditions on the chamber wall, and was expendable in the event a chamber failure was encountered. Two tests were performed with this chamber and injector, Tests 001 and 002. The first test was a short checkout test to confirm the structural adequacy of the chamber and to check out the test system operation with regeneratively cooled chambers. The test was completely satisfactory; no damage or abnormal operation of any type was encountered. In the next test, the duration was extended to 2 sec; the film cooling flow rate in this test was 49.5 lb/sec. Again, no problems were encountered. The hardware was in excellent condition following the test. A postfire photo of the chamber as shown in Figure VI-86. It was therefore decided to continue the program with the evaluation of the full area ratio capillary tube chamber.

(U) The next two tests (003 and 004) were performed using capillary tube chamber SN 003 and the Mark 125 injector SN 001. The initial test was again a short-duration checkout test. Postfire condition of the hardware was excellent. No damage of any type occurred. The next test was then performed for 2 sec at a film coolant flow rate of 56.9 lb/sec. Just following the test, detonations occurred in the chamber which were traced to propellant leakage past the injector-chamber seal. These detonations were in no way connected with the design or operation of the chamber; however, they caused several of the chamber capillary tubes to break and the thermal barrier coating to spall in several places. This damage was subsequently repaired. While repairs were being made, testing was continued with chamber SN 004.

VI, C, Modular-Cooled Chamber Program (cont.)

(U) Because of the successful operation of chamber SN 003, it was decided to replace the low-performance SN 001 Mark 125 injector with high-performance SN 002 Mark 125 injector. In the first test with the chamber (test 005), a malfunction detection system sensed a chamber leakage of 25 lb/sec and aborted the programed 2.25-sec test at 1.734 sec. Postfire inspection revealed severe damage to the chamber throat, secondary injector, and primary combustor barrels. Loss of oxidizer from the chamber reduced primary injector flow and shifted the primary mixture ratio to the fuel-rich side, severely damaging the entire hot-gas system. The postfire condition of the chamber is shown in Figure VI-87. Careful examination of the motion picture records showed that the beginning of burnout occurred at the 7 o'clock position. It is not conclusively known whether this was caused by tube failure, or a fuel-rich zone in the boundary layer. Detailed investigation indicated severe erosion in 32 locations directly in line with the fuel injector vanes. This condition could be the result of either of two occurrences: first, local high heat transfer during normal run conditions, and second, following loss of oxidizer flow, the injector operated fuel-rich, which burned the chamber coolant and raised the temperature beyond tolerable limits. Additional discussion on this failure is given in the Test Data Analysis section.

(U) Testing with the transpiration-cooled chamber has shown that the Mark 125 injector was not sufficiently streak-free to allow continued transpiration chamber testing. Since fuel streaking was a major possibility as the cause of failure in regenerative Test 005, further testing with regeneratively cooled chambers was suspended until more compatible injectors are available.

VI, C, Modular-Cooled Chamber Program (cont.)

5. Test Data Analysis

a. Performance

(C) This section discusses the thrust chamber performance obtained with the transpiration- and regeneratively cooled chambers. Using the injector performance determined in the Modular Secondary Injector Program, together with calculated performance losses associated with nozzle friction and geometry, it was determinated that a supplemental cooling loss of 4.2% I_s is allowable in Phase I to meet the overall performance requirement of 90% I_s. Using the performance data from the film cooling test series of the injector program for the regeneratively cooled chamber, and the performance data of the transpiration-cooled testing, Phase I target supplemental cooling flow rates of 29.2 and 25.2 lb/sec were established for the two chambers, respectively. The predicted ARES performance at the Phase I 90% I_s level is summarized in Figure VI-88. Also shown is the predicted performance for Phase II. The Phase II tabulation was prepared assuming that injector performance would be improved 1% during Phase II over the value demonstrated in Phase I uncooled testing.

(U) Detailed discussions of the performance data obtained in the test program are given in the following sections.

(1) Transpiration-Cooled Chamber

(U) The performance data of the transpiration-cooled chamber were analyzed using the performance interaction theory to define the magnitudes of mixture ratio distribution, nozzle friction, nozzle geometry, combustion and film cooling losses. A summary of the transpiration coolant flow rates and the test data results is presented in Figures VI-78, 79, and 80.

VI, C, Modular-Cooled Chamber Program (cont.)

(a) Mixture Ratio Distribution Losses (M_1)

(C) Testing with modular injectors on uncooled ablative and film-cooled ablative chambers disclosed mixture ratio distribution losses were present on all Mark 125 injectors with the exception of SN 004. This was primarily due to the basic injector diameters being different. The diameter of the first ARES Mark 125 injector was undersize as a result of distortion which occurred during welding of the element assembly into the body. For subsequent injectors, special tooling was made to minimize this distortion. During the course of the development program, reworking of the injectors required removing the element assembly from the body and then rewelding them together, which caused minor changes in the injector diameter.

(C) The following table gives the losses associated with each injector when shrouded and tested in the transpiration configurations of Figures VI-90 and VI-91. All presented losses are corrected to the design area ratio of 20:1.

Mark 125 Injector SN	SN 001 Chamber MRD Loss, sec	SN 002 Chamber MRD Loss, sec
001	10	Never tested
002	10	0
003	12	6
004	0	Never tested
005	Never tested	3

(U) Mark 125 injector SN 001 was tested twice at mixture ratios above design. The losses depicted in Figure VI-80 reflect the effects due to mixture ratio, area ratio, and duration.

VI, C, Modular-Cooled Chamber Program (cont.)

(U) Mark 125 injector SN 002 was tested four times, with two tests on each chamber. With chamber SN 001 (Figure VI-90) the fuel tubes extended to a point even with the angled portion of the chamber, giving a MRD loss. The condition causes the primary gas to expand out in a semiradial direction from the outer fuel row giving the effect of a radial gap about the injector. With chamber SN 002, a transpiration boundary exists at the point of fuel injection for an axial distance of 0.875 in. This containment theoretically eliminates the mixture ratio distribution loss.

(U) With injector SN 003, the MRD loss in chamber SN 001 was greater than with any other injector. This condition occurred because the injector's fuel tubes were longer than in any other unit. This extra length caused the semi-radial tap to appear larger to the exiting primary gas, giving a larger MRD loss (12 sec). Tests 007, 008, and 009 with this injector reflect an out of tolerance orientation of the fuel tubes across the face giving an additional MRD loss. When used with transpiration chamber SN 002 the loss drops to 3 sec due to containment of primary combustor gas about the fuel injection points.

(U) Injector SN 004 has a large outer fuel tube diameter, which allows a minimum of gas flow in the semiradial direction. This injector therefore was assumed to have a zero MRD loss for its four tests with chamber SN 001.

(U) Injector SN 005 became available late in the testing of chamber SN 002. In its tested configuration, a low 3-sec MRD loss resulted (Figure VI-91). Since area ratio, mixture ratio, and duration were nearly constant on the tests conducted, the loss remains constant.

(b) Nozzle Friction Loss (NFL)

(U) The performance losses which result due to friction along the smooth steel nozzle wall are summarized in Figure VI-80 and are nearly constant. Any variations reflect changes in mixture ratio and area ratio.

(c) Nozzle Geometry Loss (NGL)

(U) Losses due to nonaxial components of the exhaust velocity for the 80% bell contour transpiration chamber are tabulated in Figure VI-80. Differences in the presented values are properties of change in area ratio and base enthalpy differences at the point of exit.

(d) Combustion Losses

(U) The tabulated combustion losses reflect the combustion loss characteristics established during the modular injector development program (see Figure VI-37). Variations in the presented losses are due to mixture ratio and chamber characteristic length (L*).

(e) Film Cooling Loss (FCL)

(U) The film cooling loss for each of the transpiration chamber tests was calculated by summing the previously discussed losses, adding the sum to the measured vacuum specific impulse and subtracting this total from the theoretical impulse for the actual test injector mixture ratio. The remainder becomes that loss associated with the heat removal from the core gas and the inefficient expansion of the warm N_2O_4 coolant. This resulting loss is tabulated in Figure VI-80 and graphically represented in Figure VI-89.

VI, C, Modular-Cooled Chamber Program (cont.)

(C) As can be seen in Figure VI-89, the data reflect an average loss of approximately 0.6% I_s for each percent of film coolant used. However, the data have some scatter, with the tests reflecting two bands of losses, a 0.66% band and a 0.50% band. This variation is the result of four factors: (1) the differences in coolant performance for each of the 12 compartments, (2) normal data scatter, (3) accuracy of mixture ratio distribution losses, and (4) the fact that any inaccuracies in the four other losses are included in the film coolant loss calculation.

(C) 1 The first effect, differences in coolant performance for each compartment, results from the changes in coolant temperature at the throat and during expansion for each of the 13 injection points. Analysis predicts that the performance loss per pound of coolant injected will increase by 20% comparing Compartment 1 to Compartment 13. The tests summarized in Figure VI-89 reflect random reductions in different compartments making the loss factor as applied to the total flow dependent on the compartments that are varied. This effect can account for a $\pm$ 0.6% impulse variation for the presented data.

(U) 2 The presented loss can also be affected by normal data scatter and instrumentation accuracies. This effect is generally considered to be $\pm$ 0.5%.

(U) 3 The third effect is a result of inaccuracies in the MRD calculations. As previously discussed under secondary injector testing, the mixture ratio distribution loss is difficult to calculate since the primary gas is compressible while the fuel is incompressible. Therefore, the amount of primary gas which escapes uncombusted varies with mixture ratio, geometry, and fuel vaporization. As shown in Figure VI-89, the cooling performance loss data can be grouped in association with each

VI, C, Modular-Cooled Chamber Program (cont.)

SN chamber. This grouping is believed to result from inaccuracies in MRD loss calculations which arise because of marked differences in injector-chamber geometry. The injector-chamber configurations for SN 001 and SN 002 are shown in Figures VI-90 and VI-91, respectively. A complete discussion of MRD loss calculations and the geometry characteristics is given in Section VI,B,5,a,(1).

(U) 4 The fourth effect is a result of the method used in analyzing the data. Since the film coolant loss includes any errors in previously discussed loss calculations, the errors of MRD, combustion, friction and geometry could easily account for another ± 0.5% accuracy in the film coolant loss calculation.

(U) Considering these four factors the data correlation as presented in Figure VI-89 is considered satisfactory.

(C) Using the transpiration coolant performance data gained from this testing, the total coolant required to meet Phase I performance requirements is 25 lb/sec. The value is obtained by using the 0.6 I_s loss/% film cooling obtained in Figure VI-89 and applying it to the allowable 4.2% cooling loss as shown in Figure VI-88.

(2) Regeneratively Cooled Chamber

(U) The performance of the regeneratively-cooled chamber was analyzed using performance interaction theory previously discussed in Section VI,A,5,a,(1). The losses which apply to the regeneratively cooled chamber tests were those of: mixture ratio distribution, geometry, friction, film cooling, and combustion. Figure VI-92 summarizes these losses together with pertinent test data for each of the five tests conducted.

VI, C, Modular-Cooled Chamber Program (cont.)

(U) Five regeneratively cooled chamber tests were conducted, of which two yielded valid steady-state performance data. (Tests 1.2-14-WAM-002 and 004.) The loss calculations together with the explanation of the results are described under each of the loss subsections.

(a) Mixture Ratio Distribution Loss (MRD)

(C) The two valid performance tests utilized Mark 125 secondary injector SN 001. This injector had previously demonstrated a high mixture ratio distribution loss on both the uncooled secondary injector test series and the transpiration-cooled chamber test series. The loss was produced by the expansion of an annulus of primary combustor gas between the outer fuel tubes of the secondary injector and the chamber wall. At 20:1 area ratio, this low performance stream yields an impulse of approximately 160 sec versus 329 sec of the core gas stream. When the weighted average of the two streams is applied, a significant loss over the impulse for a homogeneous mixture ratio condition results. On Test 1.2-14-WAM-002, this loss was calculated to be 5.2 sec since the area ratio was only 2:1. On Test 1.2-14-WAM-004, which had a chamber with an area ratio of 21.75:1, the MRD loss was amplified to 14.1 sec.

(b) Nozzle Friction Loss (NFL)

(C) The nozzle friction losses (NFL) for the two tests reflect the area ratio change as did the MRD losses. With chamber SN 003 at 21.75 area ratio, the loss increases from 0.2 to 2.8 sec because of the larger surface area in contact with the supersonic gas stream.

(c) Nozzle Geometry Loss (NGL)

(C) The 80% bell nozzle of the regenerative chamber has a varying nozzle geometry loss at each area ratio due to the constantly

changing wall angle. (In the 15-degree conical nozzle of uncooled testing the angle was constant at all nozzle stations.) For the truncated chamber SN 002 this divergence angle was approximately 30 degrees and gave a divergence loss of 13.5 sec. At the 21.75:1 area ratio of chamber SN 003 the exit angle is 9.6 degrees giving a loss of only 2.3 sec.

(d) Combustion Loss

(C) Combustion losses for the regenerative chamber tests with chambers SN 001 and 003 reflect the difference in L* of each chamber at 40 and 42.3, respectively. These loss calculations are derived from Figure VI-37 and result in 6.4 and 9.6 sec for the two chambers when the difference in area ratio is applied.

(e) Film Cooling Loss (FCL)

(C) Film coolant performance was deduced by summing the losses previously mentioned, adding the result to the measured value, and subtracting the sum from theoretical. The remainder gives that loss experienced due to film cooling heat removal from the core gas. The results from chamber SN 001 with single-point film cooling give a loss slope of 0.60% impulse/% coolant as compared to 0.51 demonstrated during the film cooling evaluation testing as described in Section VI,B. With chamber SN 003 the loss slope is 0.582 and is indicative of the increase loss slope for two-point version single-point injection. The correlations are considered in reasonable agreement on the basis of the limited test data obtained with the regenerative chamber.

VI, C, Modular-Cooled Chamber Program (cont.)

b. Cooling

(1) Transpiration-Cooled Chamber

(U) The thermocouple instrumentation for the ARES transpiration-cooled chamber had as its primary objective the identification of potential hot spots subject to early burnout. Evaluation of the near-surface (0 to 0.010 in. in depth) thermocouple readings from test to test as the coolant flow is successively reduced in the particular compartment results in a guide for subsequent flow reduction. Comparison of these thermocouple readings, adjusted approximately for depth, to the analytical surface temperature prediction enables qualitative evaluation of the performance potential of the chamber. The character of the advanced thermal model is such that, while rapid and exact determination of the experimental surface temperatures is not possible, the near surface temperature gradients are approximately constant for a given compartment when the temperatures approach the area of interest, that is 1500 to 1900°F. These gradients are ∿35°F/Mil in the chamber and ∿ 50°F/mil throat (see Figures VI-76 and 77). Clearly, when the temperatures are much lower the gradients near the surface will be somewhat less and the thermocouple readings themselves can be used for guidance. Use of the predicted wall temperature versus compartment coolant flow curves shown in Figures VI-72 through VI-75 beyond the range of those curves should be discouraged.

(U) The tests conducted on chamber SN 001, on which there was significant thermocouple instrumentation, were limited to two: 1.2-12-WAM-001 and -002. In these tests, there was considerable erosion in the lower half of the horizontally mounted chamber starting at Compartment 6 and extending downstream. Consideration of the temperature data in the first five compartments and in the unaffected areas downstream, however, in light of the

discussion in the preceding paragraph, indicates some safety margin in these areas. But it must be recognized that both of these tests were only transient engine tests, with the combustion chamber having no duration of steady-state operation. The thermocouple data then represent an early time in the thermal transient. A summary of the temperature values observed on the tests of SN 001 together with the measured thermocouple depths and compartment flows are shown in Figure VI-93. Tests where the engine did not reach design operating conditions are not shown. Tests on SN 001 conducted after repair (SN 001a) contained no working thermocouples.

(U) Testing of the second transpiration-cooled chamber (SN 002) began with Test 1.2-12-WAM-013. In this series there were ten valid tests conducted which had useful thermocouple instrumentation. Data from these tests is summarized in Figure VI-94. Tests -013 to -016 comprised a series with successively increasing duration from 1.3 to 3.0 sec, all at the same nominal balance point. Tests -017 and -018 were conducted at the final 3.0-sec duration with coolant flow reduction in selected compartments. Tests -016 to -018, then, represent the bulk of steady-state thermal data acquired to that time. Figure VI-95 shows the maximum thermocouple readings for these three tests. Thermocouples 0.010 in. and less from the surface are shown with the correction factors discussed above applied. Since the majority of these temperature readings are fairly low, use of these full correction factors results in values that are somewhat high. Thermocouples that are more than 0.010 in. deep are not examined here because their primary purpose is to aid in verifying or improving the conduction model and corrections to surface values cannot be made simply. With the massive failure of SN 001 at the 3 o'clock position of the chamber, there is some interest in observing any geometrical effect which may be readily apparent in the thermocouple readings. For this reason, Figure VI-95 also shows the clock location represented by each thermocouple reading. Figures VI-96, 97, and 98 summarize these adjusted

thermocouple readings on plots of approximate surface temperature versus compartment location for the three tests. Wherever available, predicted surface temperatures are also shown in these figures, the limitation being the range of the predictions as discussed above.

(U) The first aspect of these data to consider are those temperatures which greatly exceed the predicted values. These generally occur in Compartments 2, 8, and 9. In Compartment 2, one thermocouple is the offender in all three tests. Although this thermocouple is at the 2:30 o'clock location, an adjacent thermocouple at 3:00 shows much lower values which are more consistent with those of other clock locations. It must be surmised that the high thermocouple readings at this point are erroneous (or that a streak existed). In Compartments 8 and 9 it must first be remembered that in these, as in 6, 7, 10, and 11, the temperature values represent surface conditions on the 0.021-in. instrumentation platelet whereas the compartment is comprised of 0.011-in. platelets that will run somewhat cooler (see discussion of instrumentation in Paragraph VI,C,3,b,3). The consistency of the thermocouples in Compartments 8 and 9 with the exception of TCSC-48 (see Figure VI-95) demonstrates the validity of these values and indicates a degree of optimism in the analysis in the area of the throat. This is true even with the maximum 300°F correction for platelet thickness (see Figure VI-77). This apparent variance in the region of the throat is not sufficient to compromise the performance potential of the chamber, particularly when one considers the degree of apparent analytical conservatism in the area of the chamber and expansion regions. A scan of the temperature values in the other compartments shows no obvious geometrical effect but the effect is probably within normal data scatter at these overcooled conditions.

VI, C, Modular-Cooled Chamber Program (cont.)

(U) After Test 1.2-12-WAM-018, the chamber was removed from the test stand for maintenance and the associated handling eliminated the majority of the useful instrumentation for subsequent tests.

(U) The near surface thermocouple instrumentation has successfully fulfilled its primary objective of identifying potential hot spots and guiding the flow reduction program. The accumulation of further data on subsequent tests will result in sufficient data being available to verify or improve the analytical model as well as aiding the evaluation of film coolant "carryover".

(2) Regeneratively Cooled Chamber

(U) A series of five regeneratively cooled chamber tests was conducted in this program. In each case, instrumentation providing any cooling data consisted of manifold measurements of the regenerative coolant bulk temperature at inlet and outlet.

(C) The first test was conducted on chamber SN 002 which had been cut off at an area ratio of 1.86. This chamber was film-cooled by N_2O_4 injected through 208 holes (0.028 in. dia) in the tip of a cooled shroud. The shroud coolant amounts to one-third of the total coolant flow rate. The chamber is coated with a 0.005-in. basecoat of tungsten and Nicoro 80, 0.020 in. of thermal barrier consisting of 82% tungsten, 12% zirconia, 3% silicon, and 3% Nicoro 80. Test 1.2-14-WAM-001 was a short-duration checkout run that yielded no cooling test data. Test -002 had about 0.3 sec of steady-state operation and had an experimentally measured bulk temperature rise of 16°F with 49.5 lb/sec of supplementary coolant. The analytical prediction for these test conditions, assuming a 1.5 Bartz factor in the chamber decreasing to 1.0 at the throat and all areas downstream, ranged from 8 to 18°F. The two

VI, C, Modular-Cooled Chamber Program (cont.)

values represent the assumptions of total cooling effectiveness from the shroud coolant to no cooling effectiveness, respectively. Since the chamber and the coating were in perfect refireable condition after the test, the data can be taken to be totally representative of the demonstrated heat flux conditions. Discussion of apparent wall temperatures or heat fluxes is not appropriate at this point because of the flexibility between effective coolant flow rate and Bartz factors to predict the observed regenerative coolant bulk temperature rise. It is only pertinent at this point to say that the assumptions utilized in the design analysis of the ARES regeneratively cooled chambers are reasonable on the basis of this test.

(U) Tests -003 and -004 were conducted on Chamber SN 003, which was similar to SN 002 except that the main film coolant was split between the injector face and capillary tubes that extended to a point 5 in. upstream of the throat. This chamber has a design area ratio of 20:1 and was coated similarly to SN 002 but acquired a slightly undersize throat during fabrication. The first test was again a transient test and the second a 2-sec test providing about 0.3 sec of steady-state engine operation. In this test, however, the thermocouple measurement of the regenerative coolant outlet temperature did not reach steady state. This is, perhaps, attributable to the greatly increased length of the chamber and the associated higher temperature rise. For this reason, no comparison to predicted values will be made on this test. Postfire detonations damaged both the thermal barrier and a number of capillary tubes. The causes of these detonations are discussed in Section VI,C,4,a, but are not in any way associated with integrity of the chamber cooling concept.

(U) The fifth test in the series was conducted on chamber SN 004, which is similar to SN 003 except in the size of the capillary tubes. This test provided no coolant data because the chamber failed during the start transient. Three areas were investigated in detail in search of the probable cause of the failure: structure, heat transfer, and test data.

VI, C, Modular-Cooled Chamber Program (cont.)

(U) Structural failure due to transient pressure loads, severe thermal loads, manufacturing difficulties or basic material failure were all ruled out as primary causes of failure because of insufficient evidence. A secondary contributing cause not ruled out was a weld repair in a tube crown just upstream of the throat. This repair could not be found in postfire examination of the chamber.

(U) Heat-transfer analysis over a wide range of conditions was performed in an attempt to predict a chamber failure. It was not reasonably possible to predict a failure with uniform circumferential gas and coolant distribution. A possible contributing cause could be the partial blockage of the capillary tube exits during the coating operation. Even complete tube blockage, however, could not have been the primary cause of failure as the measured film coolant flow rate is sufficient to cool the chamber under even the most adverse assumptions if all of the coolant was injected at the injector face.

(U) Detailed review of the millisadic and oscillograph records of the test failed to show any irregularity other than a slight knee in the fuel ramp between 1.19 and 1.23 sec after PS_1. Review of the motion picture records, however, revealed hot streaks at several clock locations with the most severe at 7 and at 3 o'clock. The streak at 7 o'clock started at 0.992 sec and appeared intermittently and successively brighter until what appeared to be a piece of coating was ejected at 1.365 sec. The tube failed at 1.399 sec and the failure subsequently propagated around the periphery of the chamber. Postfire examination of the chamber showed the most severe erosion in all areas in line with the injector vanes (see Section C,4,a). The chamber failure had as its primary cause, then, a fuel-rich streak at the 7 o'clock position which created combustion in the boundary layer and subsequent failure of the tube bundle.

VI, C, Modular-Cooled Chamber Program (cont.)

6. Supporting Laboratory Programs

a. Thermal Barrier Coatings

(1) Approach and Summary

(C) The thermal barrier development program was conducted in two phases. The overall objective of the program was to develop a thermal barrier suitable for ARES conditions which would allow a reduction in film cooling requirements and associated performance losses. The approach in the first phase was to upgrade the tungsten-zirconia-silicon thermal barrier by (1) improving oxidation resistance by various siliconizing methods and (2) enhancing mechanical properties by new plasma position techniques and composition modifications. The second phase of study included evaluation of braze bonding, investigation of further plasma process improvements, and evaluation of plasma-sprayed Hastelloy X.

(C) The accomplishments of this laboratory program included the following: Cyclic oxidation resistance at 3500°F was improved by a factor of 30 by adding 3% copper to the 85W-12ZrO_2-3Si composition, hereafter referred to as I, and by inclusion of a nondiffused silicon topcoat. This thermal barrier was utilized with residual chamber R-5 and suffered no erosion or spalling during a test run. It should be noted, however, that the chamber was overcooled during this test. The substitution of 3% Nicoro 80 for 3% copper was found to provide equivalent oxidation resistance and will resist corrosion attack between firings from residual N_2O_4 absorbed into the liner. The bond strength of the thermal barrier is increased through use of a 95W-5 Nicoro 80 primer coat. This addition was included in the thermal barriers applied to ARES modular-cooled chambers. This thermal barrier demonstrated no erosion or spalling on several test firings, all of which were overcooled to some degree. The various aspects of each phase of this program are

summarized below. More detailed discussion of these studies is available in the following Aerojet-General Corporation Materials R&D reports: LRD 65-362, 6 January 1966; NRD 6212, 29 March 1966; and NRD 6285, 18 July 1966.

(2) Oxidation Resistance

(C) Static-oxidation tests of a variety of plasma-sprayed coatings on disc coupons in predominantly oxygen atmosphere were conducted. Coatings were run at 3700°F for about 500 sec. The I composition, which was first tested on the ICP program, demonstrated a regression rate of about 0.015 mils/sec. The addition of 3% copper (97I-3 Cu) reduced the static oxidation test regression rate to zero.

(C) As a final evaluation of some of the more promising combinations, three-tube Inconel 718 specimens were sprayed and tested for both thermal shock and cyclic oxidation resistance with repeated 20-sec exposure cycles. The 97I-3Cu coating with a nondiffused silicon topcoat showed a 30-fold improvement over I and became the basis for the selection of this thermal barrier for ICP chamber R-5. A summary of these results is shown in Figure VI-99.

(C) The role of the copper in the success of this coating is three-fold: (1) it melts and fills pores, reducing surface area exposed to oxidation, (2) it alloys with silicon and feeds silicon to the surface, and (3) it helps prevent breakaway of the oxide protection film under cyclic conditions. The as-sprayed silicon topcoats contribute to the coating protection by melting at 2550°F during engine startup and forming a disilicide with the tungsten. Attempts at diffusion of the silicon topcoat into the thermal barrier through furnace cycling or torch fusing were unsuccessful.

VI, C, Modular-Cooled Chamber Program (cont.)

(U) Other techniques considered but not pursued further included thermal treatments, which showed enough success to warrant further investigation; pack cementation, which proved feasible but offered no advantage over sprayed and diffused silicon; infiltration; use of slurries; and use of the metallo-organic silicon process.

(3) Application Techniques

(C) Several application parameters were shown to have effects on the bend and bond strength of the thermal barriers. It was found that it is desirable to minimize the number of passes utilized to build up the thermal barrier. This is due to the contamination in the overspray region which becomes spread out in the layers in the multi-pass liners. Use of a tube type shroud rather than the ring shroud (see Figure VI-100) on the plasma nozzle increased the bend strength of the I coating by 55% due to reduction in feed port blockage and oxygen contamination. The 97I-3Cu composition was also shown to have superior bend flexure strength to other compositions tested.

(4) Braze Bonding

(C) Braze bonding of the tungsten cermet thermal barriers to Inconel 718 was accomplished in a braze treatment of 2 hr in vacuum at 1750°F. The resulting microstructures are illustrated in Figures VI-101 and 102. An excellent bond is achieved by diffusion of the gold through the pores of the thermal barrier or liner into the surface of the Inconel 718. An additional layer of liner, shown in Figure VI-101 which is desiliconized was found necessary for preventing embrittlement of the bond zone during the braze cycle. Unfortunately, the Inconel 718 cannot be aged prior to braze bonding the liner, and, in the compositions studied, the aging treatment of 8 hr at 1350°F, furnace cooling to 1200°F, and 20 hr total time, caused embrittlement of the

VI, C, Modular-Cooled Chamber Program (cont.)

bond zone between the prime layer and the thermal barrier. Consequently, braze bonding was not recommended for ARES Inconel 718 chambers. Considerable development will be required to solve the embrittlement problem during aging. It is believed that braze bonding on stainless steel or Hastelloy X chambers, which require no aging, will be practical with moderate additional development.

(5) Further Plasma Process Improvements

(U) A number of experiments were conducted with the objective of increasing the strength of the deposit. Various powder feed port injection methods were tried which fed the powder into the plasma at angles close to the direction of the flame rather than the conventional right-angle injection. The objective was to raise the initial velocity of the particles. Also, a tungsten nozzle shroud was used to restrict the expansion of the plasma to raise impingement velocities and to reduce overspray. The near parallel injection had a secondary purpose of eliminating deposit buildup on the tungsten nozzle by aiming the powder down the center line.

(U) Powder buildup on the tungsten nozzle was a major problem that was not solved. In bend flexure strength tests, the strongest coating was sprayed using a water-cooled feed tube which had a 16-degree impingement angle and injection about 0.150 in. from the center line of the flame. However, the deposition efficiency with this arrangement was too low.

(U) A means for cleaning part of the overspray contamination on a continuous basis was devised which consists of a copper tube bent into a 1.5-in.-ID ring mounted 1/2 in. from the chamber surface, and drilled with a series of holes pointed at the coating at a 45-degree angle away from the flame. Argon gas at 100 psig continuously blows loose powder and dust from the region of the flame. Bend tests showed some strength improvement from this technique.

VI, C, Modular-Cooled Chamber Program (cont.)

(6) Hastelloy X

(U) The thermal shock resistance of plasma-sprayed Hastelloy X on Inconel 718 tubing was found to be poor. Spalling-type thermal shock failures occurred in two to seven 20-sec cycles due to insufficient adherence. Apparently, the bond between Hastelloy X and Inconel 718 is mechanical, whereas the bond between tungsten and Inconel 718 is a diffusion type which accounts for the superior results with tungsten-based coatings.

(U) Metallographic examination of the plasma-sprayed Hastelloy X showed that thermal shock failures initiated at the bond zone and that the sprayed material had very little porosity.

(C) Braze bonding did not consistently improve the thermal shock resistance of the sprayed Hastelloy X. The mechanism for braze bonding of the tungsten coatings utilizes the fact that gold is insoluble. Diffusion of gold into the Inconel 718 causes concentration of gold at the bond zone. In the case of the Hastelloy X-Nicoro 80 mixtures, the gold diffuses into the matrix of Hastelloy X as readily as into the substrate and no bond zone improvement was evident. If a primer layer of tungsten or molybdenum with 5% Nicoro 80 were used, diffusion of gold to the Inconel 718 substrate as well as into the Hastelloy X thermal barrier could be expected.

b. Transpiration Cooling Investigations

(U) The supporting laboratory program for the transpiration-cooled chamber included three areas of investigation: hydraulic investigation, fabrication techniques investigation; and development of special thermal instrumentation. Each of these are discussed in the following paragraphs.

VI, C, Modular-Cooled Chamber Program (cont.)

(1) Hydraulic Investigation

(U) To provide early required design data, subscale washers, shown in Figure VI-103, were designed and fabricated to investigate washer sealing load requirements and leakage rates.

(U) Hydraulic tests with water proved that leakage rates can be predicted by approximate solution of the fully developed laminar flow equation for rectangular ducts, as long as the clamping pressure exceeds 1250 psi. An increase beyond this pressure will not alter the leakage rate until the washer fails in shear by extruding into the flow passages. Tests indicated that under the worst conditions, leakage will be less than 2% of the coolant flow between the compartment manifold and the individual platelet.

(U) Design of the diffusion area was accomplished by constructing a ten times size transparent scale model which simulated momentum and Reynolds number. The model was flowed with water and a dye ejectant to visually evaluate various distribution concepts. A 16-mm movie sequence of the flow distribution characteristics of various diffusion patterns was taken to aid in the final selection of the pattern. Figure VI-104 is a color reproduction of the flow process for the best design shortly after the dye injectants were activated. Dye was injected both upstream and downstream of the dots. The path of the fluid flow through the dots is revealed by the upstream injection ports. The fluid velocity profile downstream of the dots is revealed by the distance the dye, which is introduced through the secondary ports, has traveled when the picture is taken. The approximately uniform travel length indicates an acceptable flow distribution.

VI, C, Modular-Cooled Chamber Program (cont.)

(2) Fabrication Techniques Investigation

(U) Fabricating the full-scale transpiration-cooled chamber required detailed knowledge of all fabrication problems and their solution well in advance so that proper tooling and procedures could be available when required. To provide this information, the supporting laboratory program investigated washer surface finish requirements, washer tolerance buildup, washer and compartment unitizing techniques, and washer machining (contouring) techniques.

(U) Using the same subscale washers as used in the Hydraulic Investigation, it was determined that washer tolerance buildup is a problem but can be circumvented by machining the retainer heights after the washer stack has been compressed and its height accurately measured. Surface finish requirements of approximately 8 microinches are readily met by the raw material coil stock from which the washers are fabricated.

(U) Sample flow control washers were spot-welded to sample flow diffusion washers with exceptionally good results. Spot welds prevent washers from shifting with respect to each other without affecting stack compressibility or coolant flow rate.

(U) Additional laboratory tests were conducted to determine the best method of unitizing the spot-welded washers into unitized compartments. Each of these methods was to be limited to unitizing the washers on the outer periphery. Methods considered for unitizing the washers included brazing, electron-beam welding, soldering, and TIG welding. The first two methods were eliminated in favor of the last two because of the potential warpage that may be experienced with a high-temperature braze and the problem associated with keeping the braze out of the flow-control washer entrances

VI, C, Modular-Cooled Chamber Program (cont.)

and passages; electron-beam welding required a development program to achieve the proper length and intensity of the beam and posed further problems in possibly causing craters and weld spattering at the weld junctions.

(U) Soldering and TIG welding appeared promising. Of the various solders investigated, Eutectic-157 exhibited the best characteristics. Two-in.-dia sample washers were spot-welded into pairs and bolted between two 3/4-in.-thick plates. The assembly was preheated to about 400°F after which the Eutectic-157 was applied to the outer periphery. Further testing revealed that the Eutectic-157 solder and all other solders investigated were not compatible with nitric acid. All solder samples immersed in beakers of various concentrations of nitric acid were chemically attacked, leaving a heavy precipitate. Electroless gold plating of a solder sample proved unsatisfactory. Although precautions could be taken to prevent moisture from contaminating the nitrogen tetroxide coolant, it was considered an unnecessary risk if a more reliable unitizing method could be developed.

(U) TIG welding proved to be the final solution. Welds were located axially along the periphery of the sample compartment. Initially, weld shrinkage at the edge of the first and last washer of the compartment appeared to be a problem; however, it was later determined that a small weld bead (about 1/16 in. wide) could be obtained without appreciable shrinkage if the arc was struck on a copper plate located at the top and bottom of the compartment assembly and then moved toward the center of the stack using a minimum of current. Six axial welds, equally spaced around the periphery proved to be sufficient to unitize the compartment.

(U) Obtaining a satisfactory porous chamber wall contour posed the greatest challenge in fabricating the transpiration-cooled chamber. Electrochemical machining (ECM), electrical discharge machining (EDM), and conventional machining were seriously considered. Because of the

VI, C, Modular-Cooled Chamber Program (cont.)

size of the chamber, both the ECM and EDM processes required extensive tooling and special equipment not available at Aerojet. Vendors specializing in these machining processes were overtaxed with existing parts and had considerable backlogs. Thus, conventional machining offered the quickest solution at least cost, provided the machined porous wall was acceptable.

(U) A preliminary machining trial of the inside diameter of three full-scale washers without visibly affecting the porsity of the flow-diffusion area was demonstrated by using a modified cutting tool which would peel the metal off. Microscopic examination of the washer pores revealed tiny fissures or hairs at the leading edge but no clogged passages.

(U) An experimental prototype compartment composed of rejected washers was fabricated to demonstrate the unitizing and machining operations to be performed on each compartment. To determine the effect of machining the porous wall contour, the compartment was water-flow tested before and after machining the inside diameter. Hydraulic laboratory data revealed that pressure-drop-versus-flow-rate values were not affected by machining.

(U) It was not until the first chamber was assembled that further laboratory experiments were conducted to improve the appearance of the porous wall. Two sample machined compartments were prepared to be electrochemically deburred. The first compartment was sent to a vendor who specializes in electropolishing. The second compartment to be deburred was attempted in-house. Both attempts were entirely successful. The porous wall surface was entirely free of burrs. This method has been selected to be used in the final contouring operations of all future chambers. The contour will initially be machined, and electropolishing used to produce the final surface finish.

VI, C, Modular-Cooled Chamber Program (cont.)

(3) Special Instrumentation Development

(U) One of the original objectives of the cooled chamber laboratory program was to obtain heat-transfer data for the washer or "platelet" concept of transpiration cooling by building and hot-firing a low-pressure subscale chamber. At the time when this effort was to be initiated, the feasibility of this chamber concept had already been demonstrated on other programs. Therefore, confidence was sufficiently high to substitute the subscale chamber with a highly instrumented full-scale chamber to obtain this heat-transfer data. The data would be much more valuable in that it would be obtained at the full thrust level and pressure of the ARES engine. To this end, the first two transpiration-cooled chambers tested in the program were modified to include extensive temperature instrumentation. Specifically, special spacer washers, each incorporating six thermocouples, were inserted between each washer stack of the chamber, giving a total of 66 thermocouples in each chamber.

(U) The method of installing the thermocouples in the spacers was determined by laboratory investigation. Several sample instrumentation washers were machined in an effort to obtain a satisfactory 0.012-in.-wide by 0.014-in.-deep radial groove in a 0.020-in.-thick flow diffusion washer into which a 0.010-in.-dia chromel-alumel thermocouple could be brazed. Difficulty was obtained in machining these grooves because of their small size. Electric-discharge machining (elox) was then used to make the groove. Results were excellent and the grooves in the full-size washers were fabricated by this method.

(U) The heat-transfer data obtained with the special instrumentation are presented in Section VI,C,5,b,(1).

VI, C, Modular-Cooled Chamber Program (cont.)

7. Conclusions and Recommendations

(U) a. The feasibility of the transpiration-cooled chamber has been demonstrated, and all indications are that this chamber concept is capable of meeting the ARES performance and duration specifications when coupled with a high performing nonstreaking injector.

(U) b. Work statement performance requirements have not been met to date because of an incompatibility problem which existed between the Mark 125 injector and the transpiration-cooled chamber. Fuel streaks from the injector reacted with the oxidizer transpiration coolant on the chamber wall on two occassions, resulting in burnout of the chambers. The streaking condition was aggravated by a 1-in. (diametral) transition section in the chamber where its diameter changes from 9.5 to 10.5 in., which promotes recirculation of the combustion gases.

(U) c. The recommended action for achieving fulfillment of the work statement contractual requirements are three-fold: First, develop a high performing injector which is compatible with the chamber wall. This effort should include both improvement of the fuel distribution of the Mark 125 injector, as well as evaluation of new injector concepts designed for better inherent compatibility. Secondly, the transpiration-cooled chamber diameter should be changed to a constant 9.5 in., thereby removing gas recirculation tendencies near the injector-chamber interface. Third, a backup approach should be pursued whereby the cylindrical portion of the chamber is replaced by a 9.5-in.-dia regeneratively cooled tube bundle section, which may be less sensitive to injector combustion irregularities. (No regenerative-cooled chamber burnouts have occurred in this region of the chamber). The regeneratively cooled L* section would be used in conjunction with a transpiration-cooled convergent and throat segment; this concept is called the "composite chamber".

VI, Secondary Combustion Program (cont.)

D. UNCOOLED TWO-DIMENSIONAL NOZZLE PROGRAM

1. Objective

(U) The objective of the two-dimensional nozzle program was to determine the effects that controlled amounts of supplementary film coolant have on temperature distribution of a two-dimensional expansion nozzle attached to an ARES configuration axisymmetric combustion chamber and throat. These characteristics were to be obtained using uniform and tailored film-coolant injection from a film coolant ring attached to the chamber-to-injector flange. Thermocouples on both the curved and flat sides of the nozzle were to record sufficient heat-transfer data to aid in the design of a cooled nozzle during the Phase II effort of the ARES program.

2. Summary

(U) The ARES engine module is designed so that modules can be used separately or in clusters to provide thrust at incremental levels of 100,000-lb thrust. When used in large numbers, they can be arranged to discharge through a common nozzle such as a plug or a forced-deflection nozzle. When modules are clustered in this manner, a nozzle transition section called the "internal expansion section" is used from the throat to expansion ratios in the range of 5:1 to 8:1. One task in the ARES Phase I program was the design and analysis of a propulsion system incorporating twenty 100,000-lb-thrust engine modules clustered within a forced-deflection nozzle. Phase II of the ARES program includes the design and test evaluation of a cooled two-dimensional internal expansion section nozzle. To provide heat-transfer design data for this nozzle design, test evaluation of an instrumented uncooled two-dimensional nozzle was included in the Phase I program.

VI, D, Uncooled Two-Dimensional Nozzle Program (cont.)

(U) The uncooled two-dimensional thrust chamber assembly consisted of a full scale 30 in. L* axisymetric combustion chamber and a conical two-dimensional nozzle contained in a heavy-steel pressure shell. The entire assembly was lined with ablative Refrasil material. The two-dimensional portion of the chamber extended from the throat to an area ratio of 5:1. Thermocouples were provided through the ablative wall in axial rows on both the curved and flat sides, with two additional rows occupying additional space on the flat sides to provide thorough temperature coverage.

(U) The test plan was designed to first evaluate the two-dimensional nozzle temperature characteristics with film cooling injected uniformly at the injector face. If the temperature distribution proved to be non-uniform, tailored film-coolant injection would then be investigated in an attempt to achieve uniform temperature distribution. A final test was planned to evaluate the base nozzle performance with no film coolant.

(U) Two tests were conducted with the two-dimensional nozzle thrust chamber. Temperature data from the first test, which was an evaluation with uniform film-coolant injection, showed the temperature distribution was uneven, with higher temperatures occurring on the flat side of the nozzle. A second test was then performed in which the film cooling was tailored to provide relatively greater amounts on the flat side of the nozzle. Temperature data from this test showed the temperature distribution around the nozzle to be substantially uniform. The accumulative erosion of the ablative material just downstream of the throat sustained from these two tests, however, was so high that further testing with this chamber could not be safely conducted. Since the primary objectives of the test program had been achieved and since a replacement ablative two-dimensional liner was not available, the uncooled base performance test was not performed and the test program was concluded.

VI, D, Uncooled Two-Dimensional Nozzle Program (cont.)

3. Component Design

(U) The contour of the two-dimensional nozzle, as originally designed, was identical to an optimized contour corresponding to the 20-module propulsion system design (discussed in Section III,B). This nozzle had a slight "hot dog" shape and was contoured along its curved sides (shown in Figure VI-105). Fabrication and tooling cost estimates obtained for this design indicated that the cost would be prohibitive. Therefore, a design analysis was performed to determine what modifications could be incorporated without significantly changing the heat-transfer characteristics of the nozzle. On the basis of this study, the configuration was changed to a contour approximating an isosceles trapezoidal prism having a two-dimensional half angle of 23° 36 minutes. The changes in heat-transfer characteristics imposed accuracy of the temperature instrumentation. The final design is shown in Figure VI-106.

(U) The two-dimensional nozzle was designed to be attached directly to the combustion chamber of the ARES uncooled combustion chamber. A chamber of 30-in.-L*, which was the shortest ARES chamber fabricated, was selected for the two-dimensional nozzle assembly so that the distance between the injected film coolant and the two-dimensional nozzle section would be minimal and thus provide the greatest amount of coolant to the nozzle section. The ablative liner for the chamber and throat sections was fabricated from MX 2646 chopped Refrasil.

(U) The two-dimensional nozzle pressure shell was of rectangular cross section and was composed of 1-in.-thick plates of 347 stainless steel (see Figure IX-2). The ablative material in the two-dimensional nozzle section was fabricated from trapezoidal blocks of ablative high char silica material.

These blocks were resin-bonded in laminations at cure temperature and pressure. The ablative liner was retained in the steel pressure shell by means of an end retainer plate 1/2-in. thick. Sealing of the liner to the pressure shell was effected by RTV 60 rubber adhesive. Pressure and temperature bosses were located on the nozzle assembly as shown in Figure VI-107.

4. Development Testing

(U) Two tests were performed with the two-dimensional nozzle in which the wall temperature characteristics on both the curved and flat sides of the nozzle were evaluated for both uniform and tailored film cooling injection.

(U) The first test, 1.2-11-WAM-023, was conducted 18 October 1966 at a film coolant flow rate of 55 lb/sec. This coolant was introduced into the chamber through 208 0.04-in.-dia injection orifices uniformly located around the periphery of the chamber. The engine test data is shown in Figure VI-108. Test duration was 3.012 sec, of which 1.3 sec were at a steady-state pressure. Recorded thermocouple data are discussed in Section VI,D,5 below, Test Data Evaluation.

(U) Posttest hardware inspection revealed that the ablative material had fractured just below the injector face in a 2-in.-wide area extending over 300 degrees. Subsequent review of the motion picture of the test firing showed the fractured section was expelled during the start transient just after secondary combustor ignition.

(U) The nozzle exhibited severe erosion just below the chamber-to-nozzle joint. Material removal characteristic was indicative of axisymmetric expansion being restricted by the two-dimensional walls. On the flat

sides of the nozzle, in which the laminated ablative sheets were parallel with the nozzle velocity vector, the ablation was greater than has been experienced in the past with nozzles having oriented ablative grain. On the curved sides, where the edges of the laminated sheets were exposed, erosion was moderate with material removal along the bond liner being more prominent.

(U) The test temperature data showed a more severe wall temperature condition on the flat sides of the nozzle. Therefore, it was decided to tailor the film cooling during the next test in an attempt to make the temperature distribution around the nozzle uniform. This was accomplished by plug welding every third hole in the film coolant injection ring in line with the curved sides of the nozzle.

(U) The second test, 1.2-11-WAM-025, was conducted on 18 November 1966. Since nearly all thermocouples evidenced an overscale condition in the first test, the engine was rebalanced to give the highest obtainable film-coolant flow for this test, which was 62 lb/sec. Further flow increases would require increases in the intensifier pressures beyond safe operating limits or a reduction in chamber pressure. The engine test data is shown in Figure VI-108. The test duration was 2.263 sec, of which 0.7 sec were at steady-state pressure.

(U) Hardware examination following the test revealed the same erosion characteristics on the two-dimensional nozzle as in the previous test. The combustion chamber however was in excellent condition. Posttest condition of the hardware is shown in Figure VI-109.

(U) The cumulative erosion of the flat sides of the chamber liner for the 5.25 sec run time was such that it was considered unsafe to subject this nozzle to any additional testing. With satisfactory tailoring

of the film coolant, which equalized the temperature profiles of the curved and flat sides of the nozzle, the primary objectives of this program were achieved. It was decided that the risk of test-stand damage that could be incurred with additional testing outweighed the obtaining of the base performance which would require an additional test. Therefore, the test series was concluded.

5. Test Data Evaluation

(U) The thermocouple data from Tests 1.2-11-WAM-023 and 025 are shown in Figures VI-110 and VI-111. Evaluation of this data showed that the nozzle temperature distribution during the first test was not uniform and that the tailoring of film cooling in the second test corrected the nonuniformity.

(U) The test data evaluation was dependent upon the transient thermocouple data in that the 55 lb/sec film-cooling flow rate of the first test was insufficient to keep a significant number of the chromel-alumel thermocouples within their 2500°F operating range. Previous experiences with similar coolant flow rates using axisymmetric nozzles had, however, been successful in maintaining thermocouple continuity at all points except in the immediate area of the throat. A major influencing factor in Test -023 was the loss of the ablative liner near the injector face. This failure contributed to loss of cooling effectiveness in downstream areas. Additionally, all thermocouples that remained in their normal operating range exhibited the same characteristis of a very rapid rise in temperature and then a distinct falling off. This is attributed to the ablating characteristics of the chamber and nozzle material. The tape wrapped liners used in axisymmetric ablative chambers have shown a much lower charring and ablation rate.

I, D, Uncooled Two-Dimensional Nozzle Program (cont.)

(U) The effect of the ablation through the many laminations of material in the flat (A row) side of the nozzle can be seen from the results of the first test, where all nozzle thermocouple readings lose meaning late in the steady-state portion of the test. On the second test, the only valid readings after the start transient are in the convergent section of the combustion chamber. The curved side (C row) thermocouples were in a line coincident with the joint in the laminated nozzle. Post-fire examination of this region showed the ablative material removed to a maximum depth of about 1 in. in the immediate area of the thermocouples. This row, then, can also be considered valid only in the very early stages of each test.

(U) As a result of the factors discussed above, qualitative comparison between the flat and curved sides during the thermal transient was required. Comparison of the two rows in Test -023 show a definite tendency for the A row, or flat side, to seek higher steady-state temperature values. On this basis, the second test was conducted with every third film-coolant hole plugged in line with the curved side of the nozzle. The chamber portion of the ablative liner remained intact and, hence, was of no influence in this test. Examination of the resulting temperature traces of Test -025 indicated very near matching of the temperature transients in the flat and curved sides of the nozzle. Therefore, the capability of tailoring film cooling to achieve equal nozzle temperature distribution was demonstrated in this test series.

(U) Design of a regeneratively cooled two-dimensional nozzle, with the knowledge that a nonuniformity in heat-flux distribution does exist, can be approached in several ways. Uniform injection at the injector face of sufficient film coolant to cool the hottest portion of the nozzle represents the alternative giving the greatest performance loss. Tailored injection of film coolant at the injector face results in over-cooling part of the combustion chamber with its attendant performance loss. Utilization of capillary tubes

to inject tailored film cooling near the throat is the most desirable of these alternatives from a performance standpoint. With the knowledge of the relative heat loads in the flat and curved sides acquired in this test program, it is possible to further improve the nozzle design by tailoring the regenerative cooling capability of the tube bundle to minimize the necessity of tailoring supplementary cooling.

(U) Beyond these possibilities, the success of transpiration cooling in the ARES Phase I program makes it reasonable to consider this concept for cooling of internal expansion section. Tailoring of the transpiration coolant is no problem, since the concept inherently allows control of the coolant distribution circumferentially as well as axially.

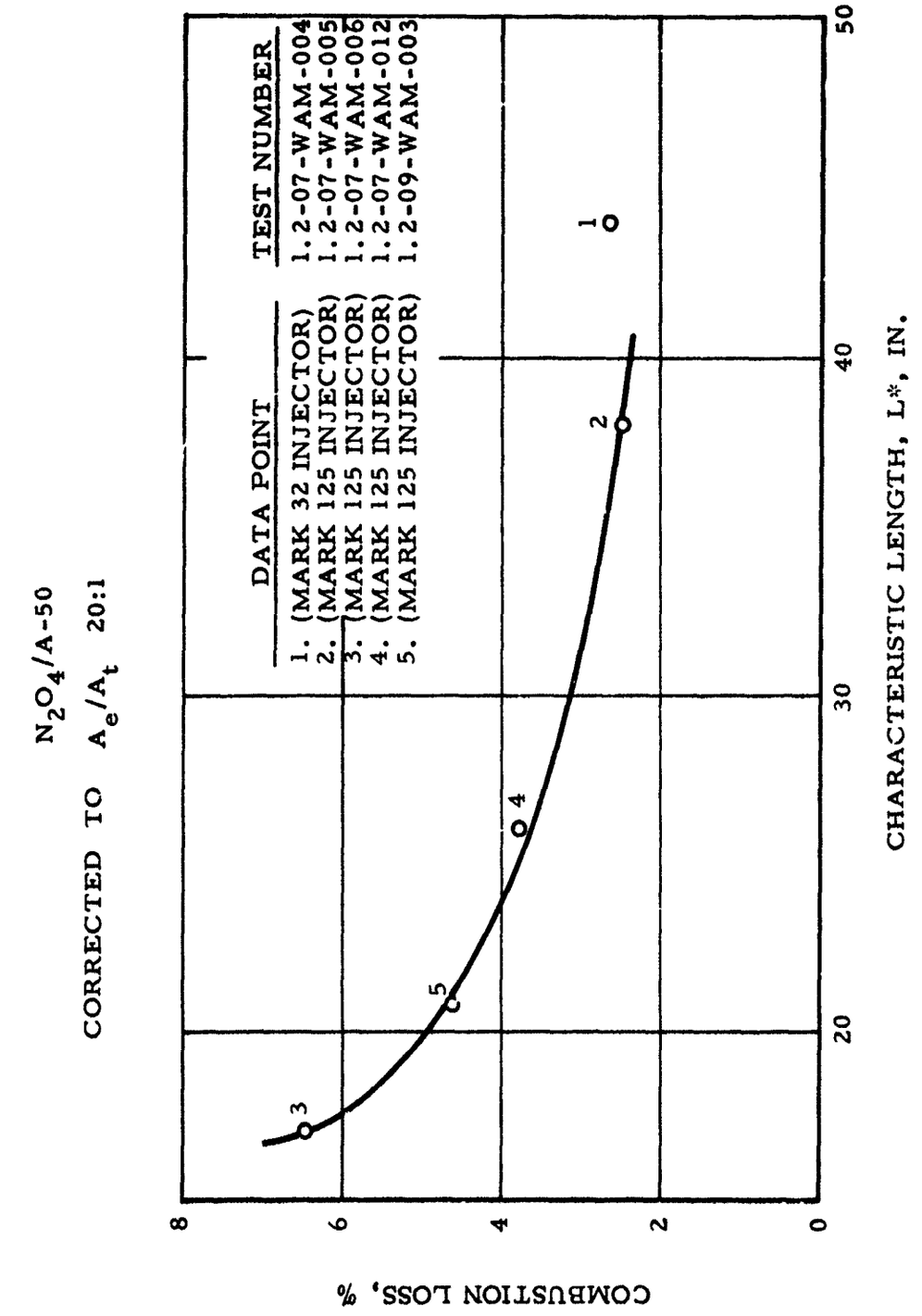

Combustion Loss vs Chamber L* (u)

Figure VI-1

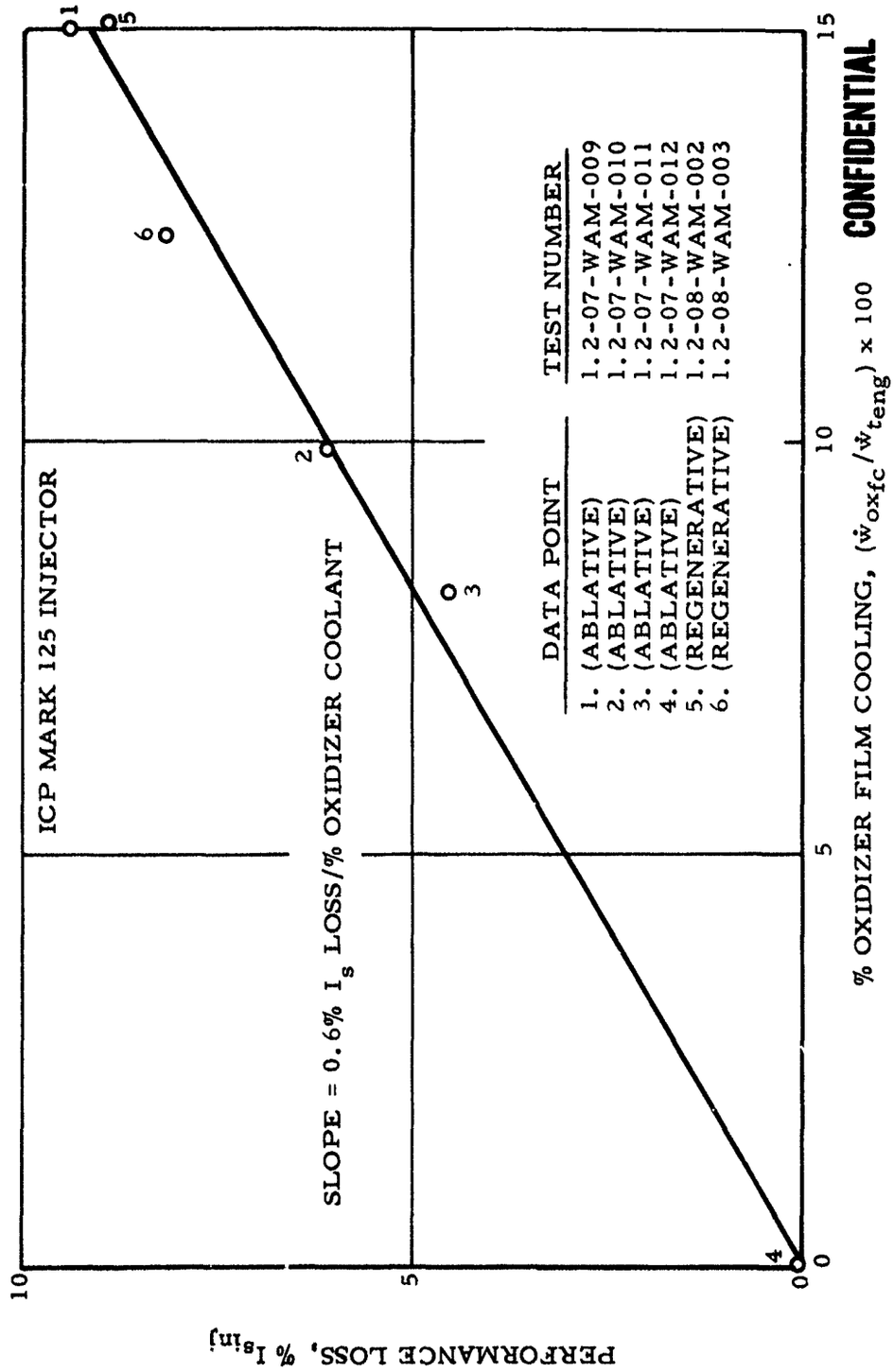

Film Cooling Performance Degradation vs Film Coolant Flow (u)

Figure VI-2

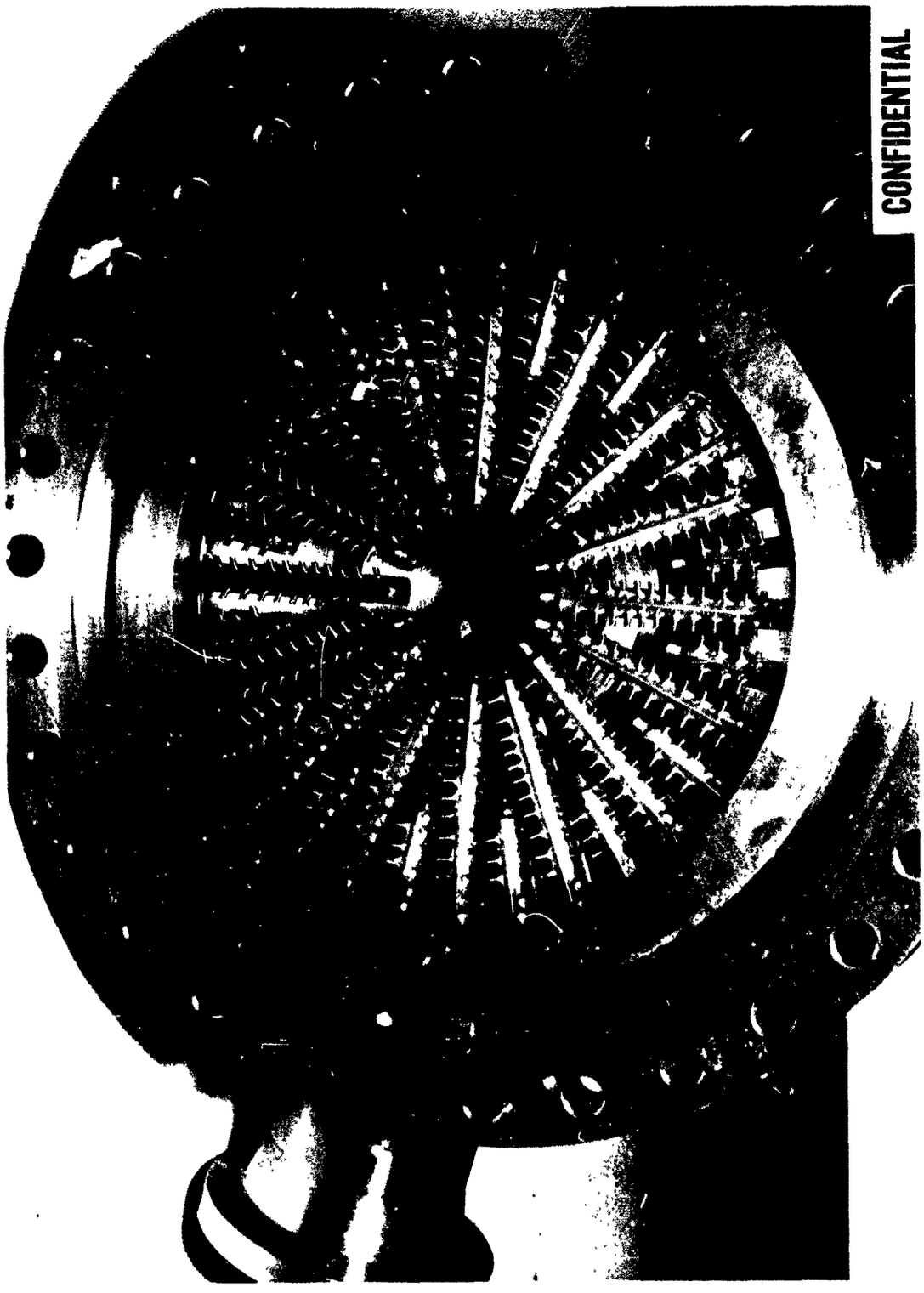

Mark 32 Secondary Injector (u)

Figure VI-3

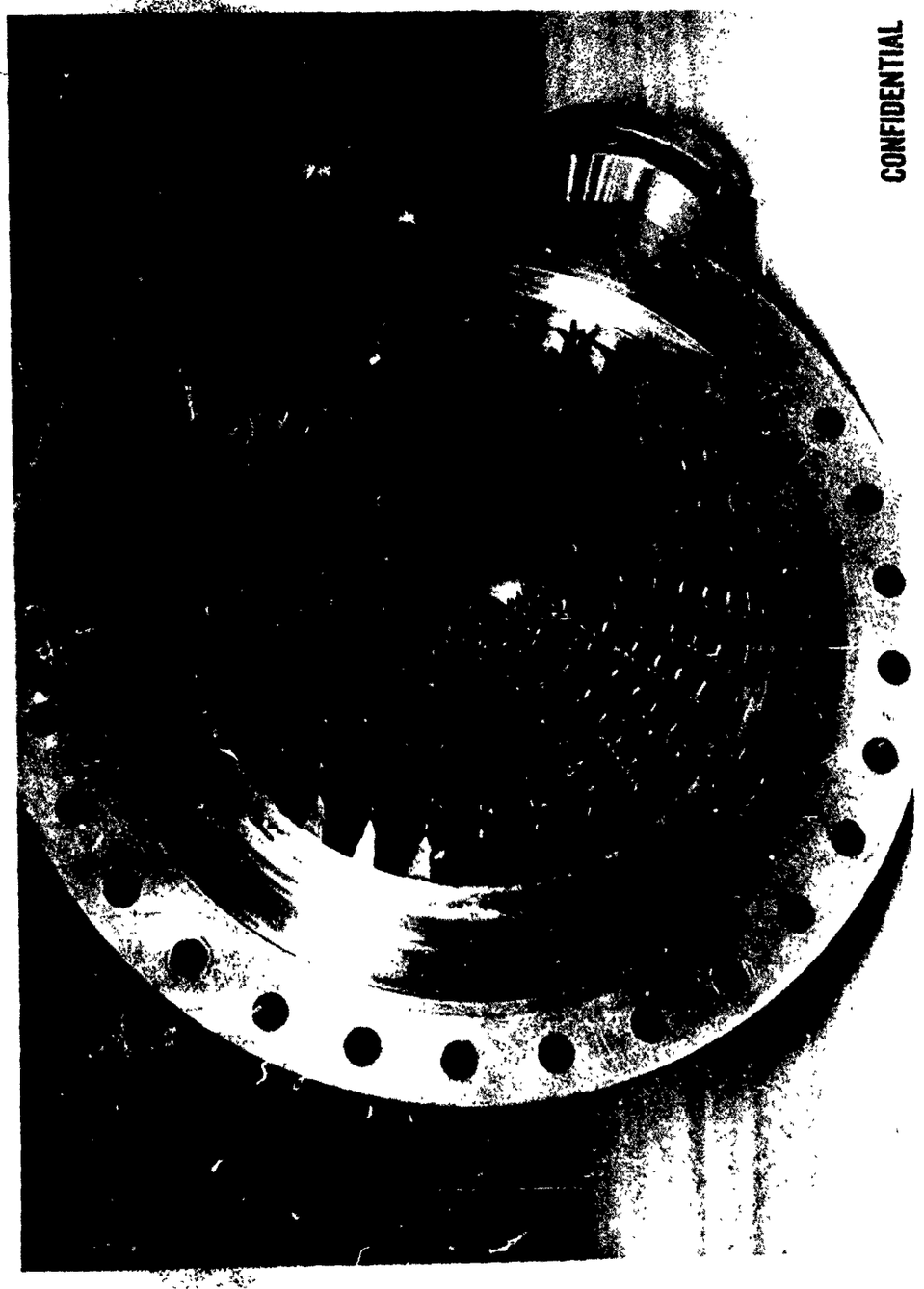

Mark 125 Secondary Injector (u)

Figure VI-4

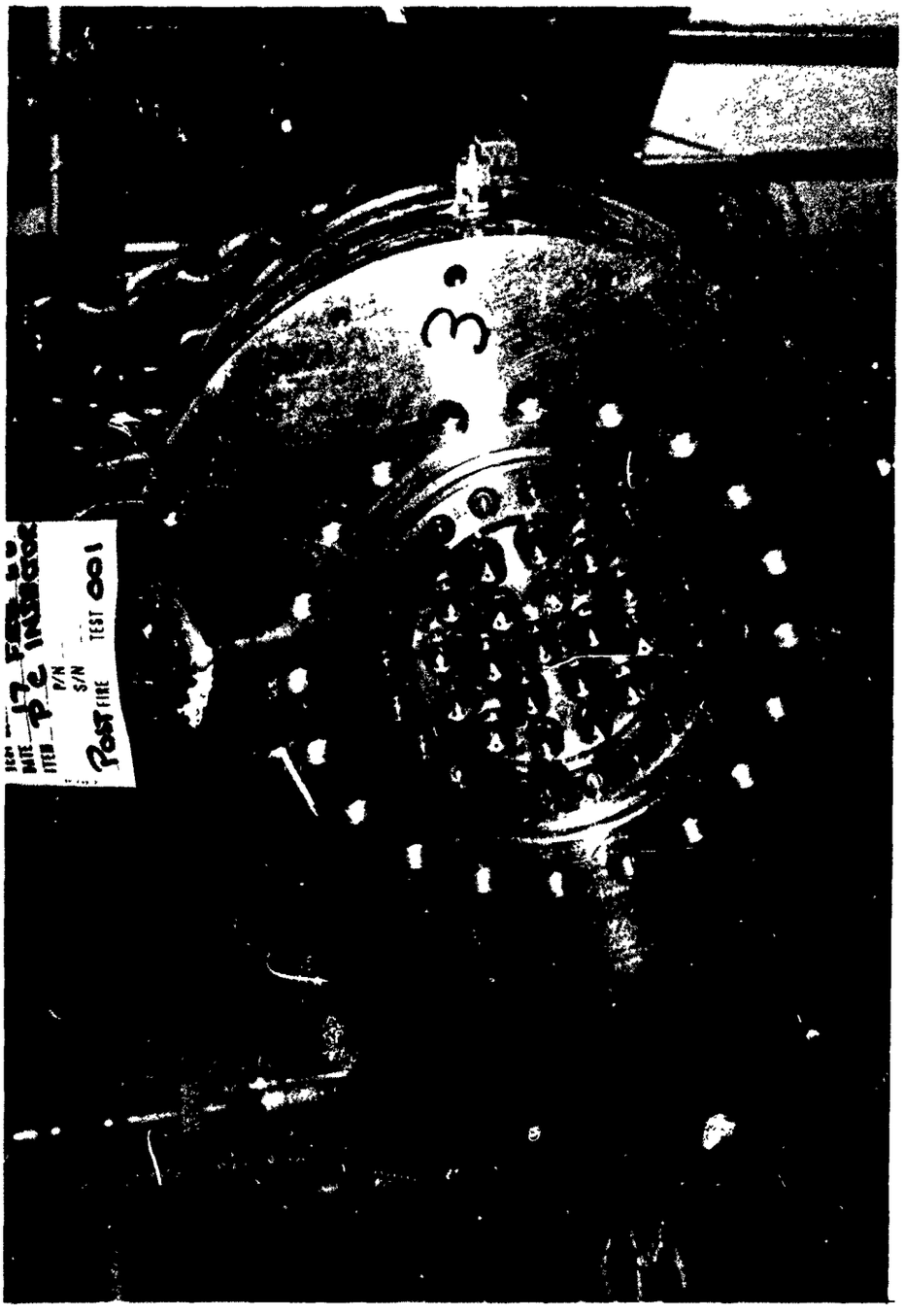

Mark 20 Primary Injector

Figure VI-5

20 L* DESIGN

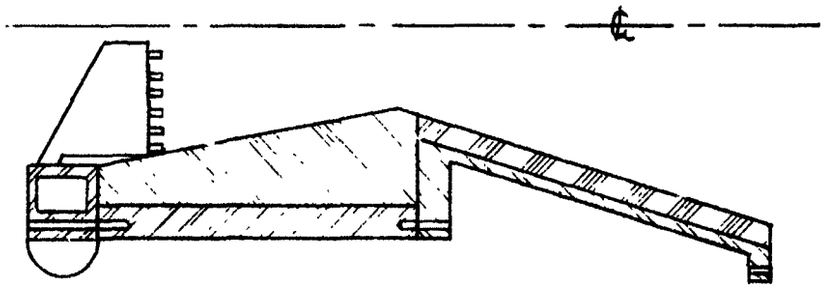

45 L* DESIGN

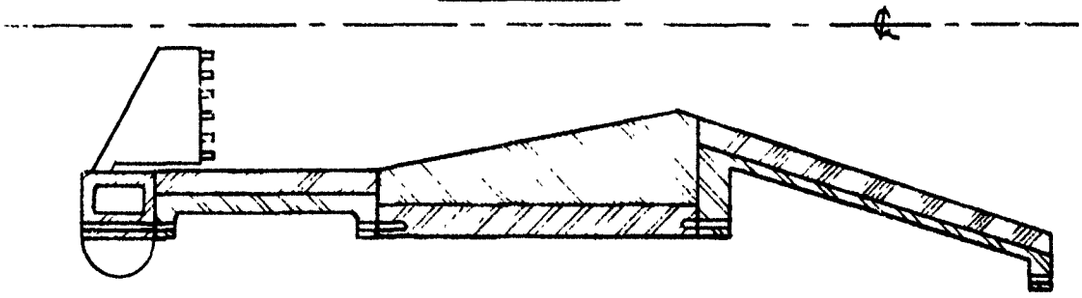

Uncooled Ablative Chambers, 20 and 45 L*

Figure VI-6

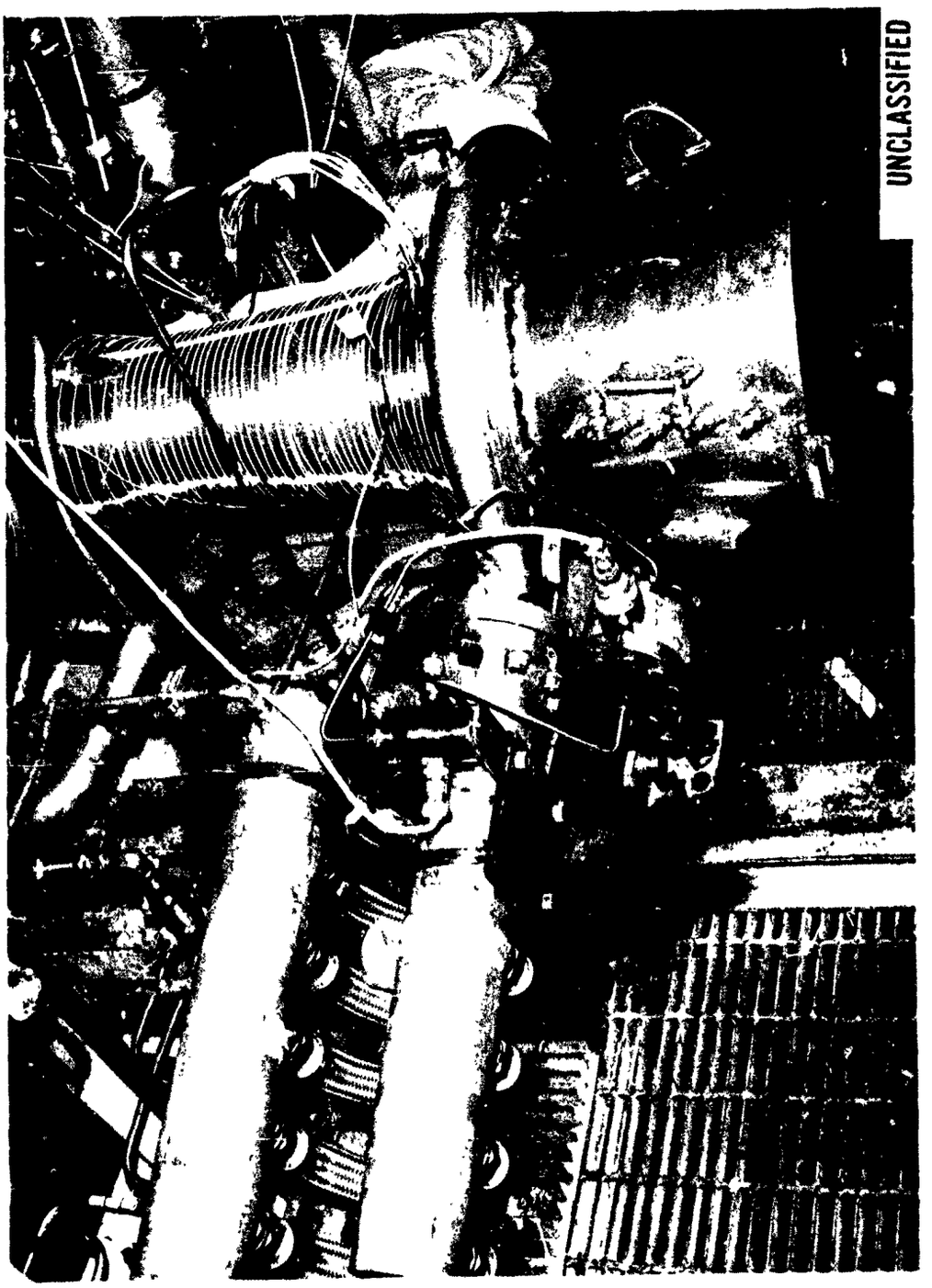

Photograph of Regenerative Chamber Installed on Test Stand H-2

Figure VI-7

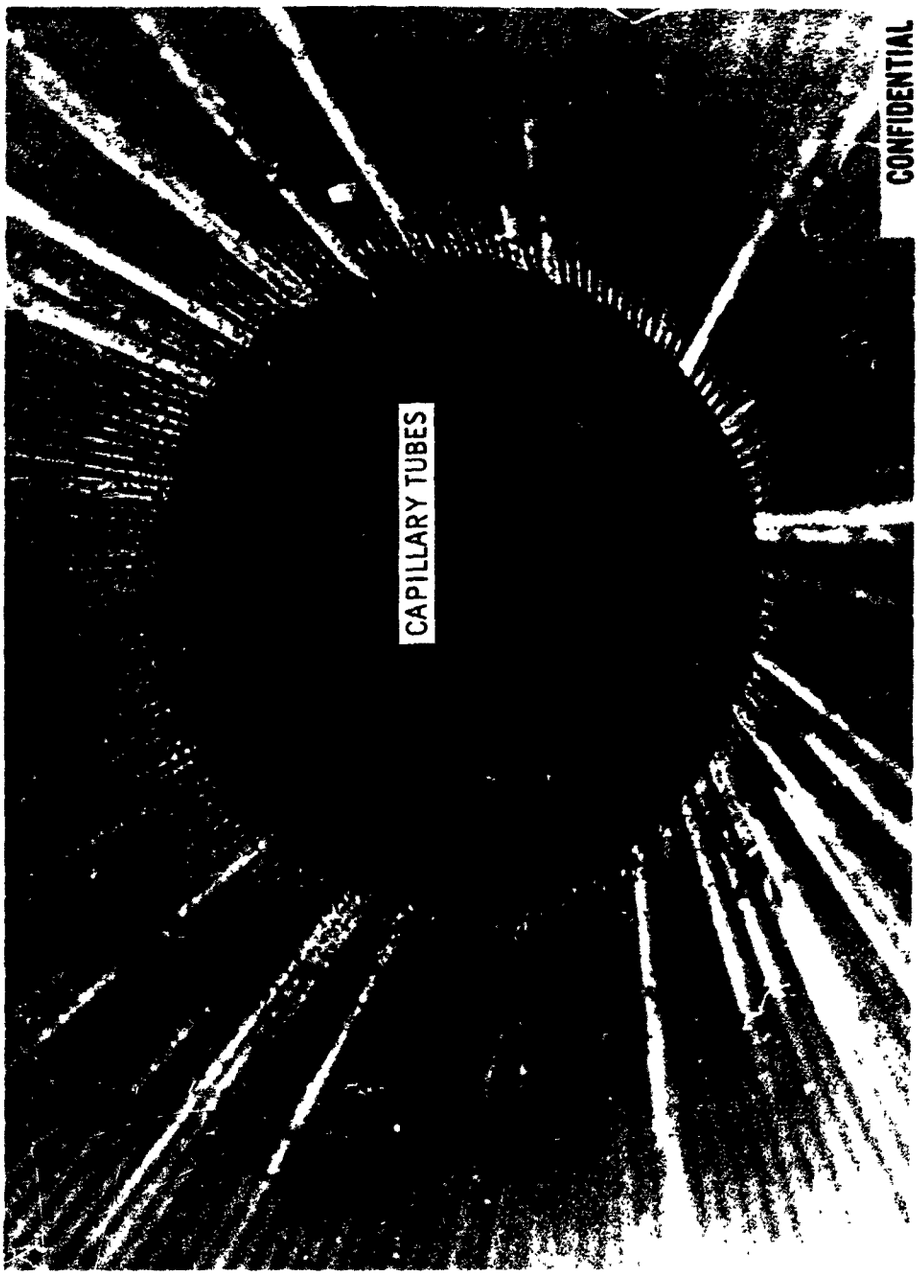

Capillary Tube Chamber (u)

Figure VI-8

Hydraulic Test of Regenerative Chamber SN R-6

Figure VI-9

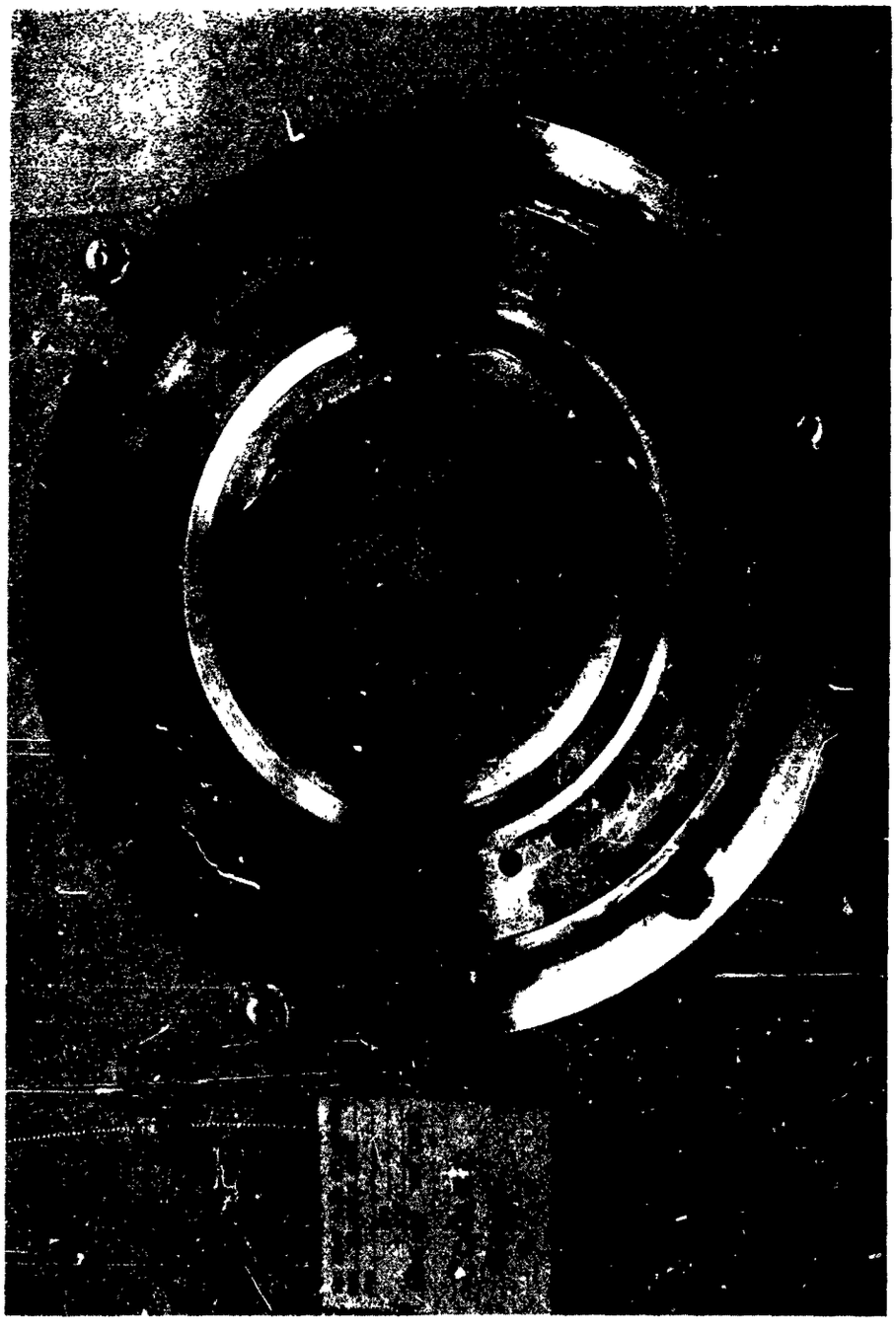

Multiple Orifice Film Coolant Ring

Figure VI-10

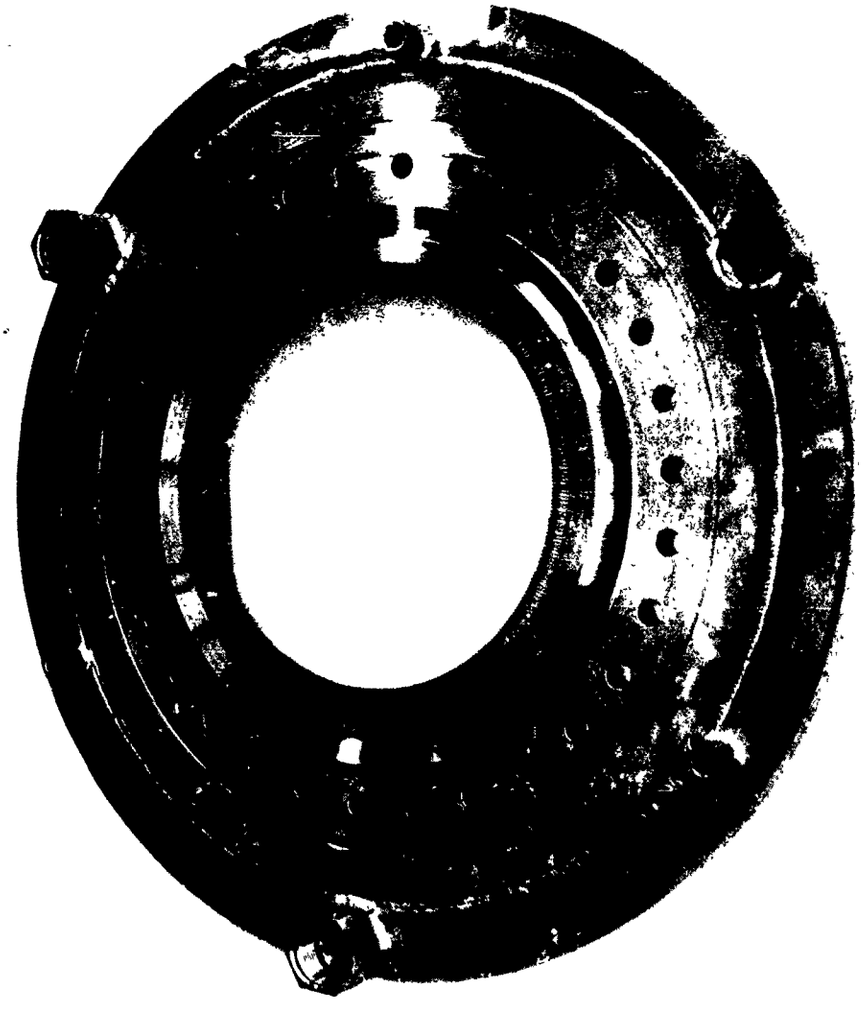

Multiple Tube Film Coolant Ring

Figure VI-11

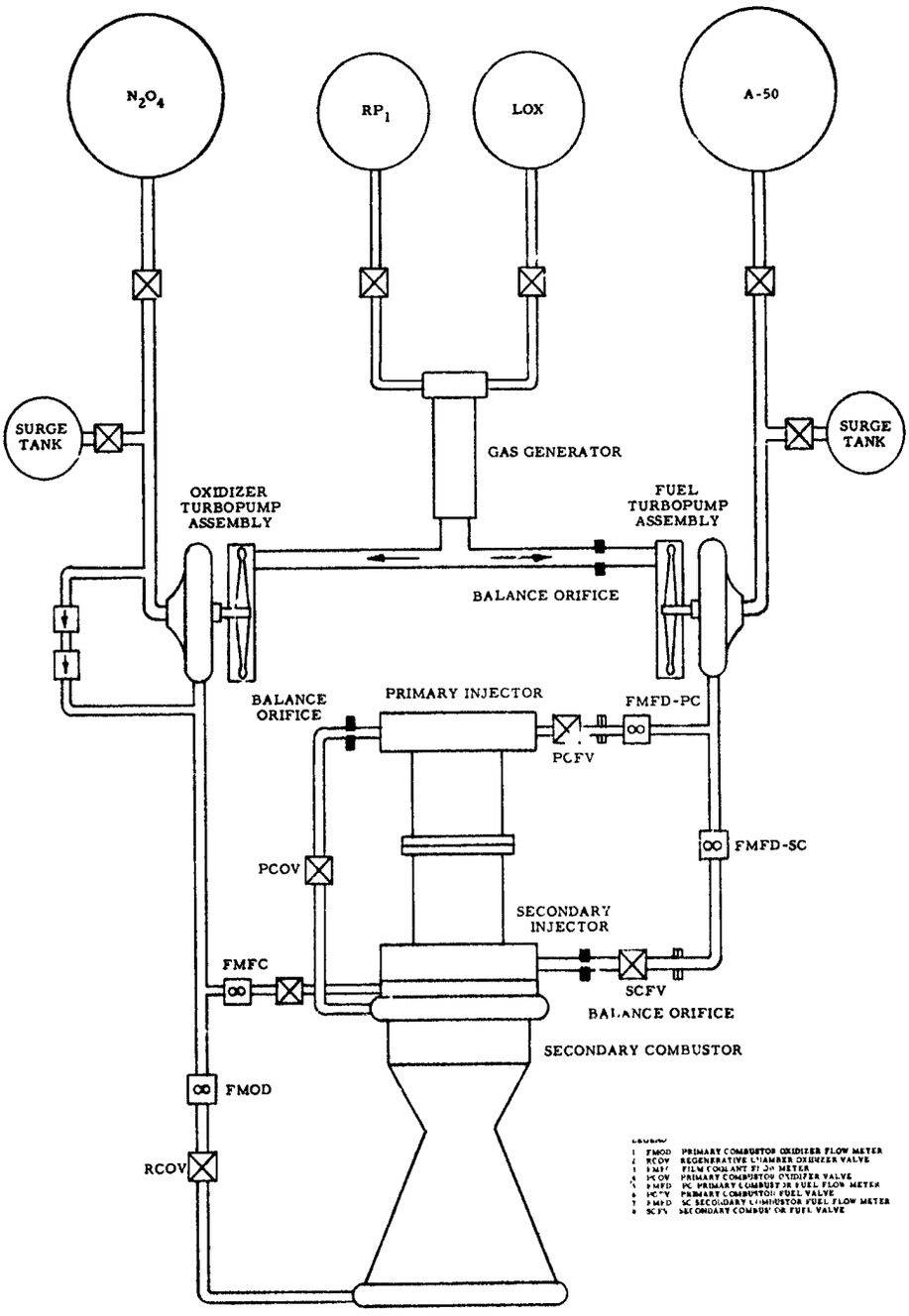

Pump-Fed Staged-Combustion Test Engine

Figure VI-12

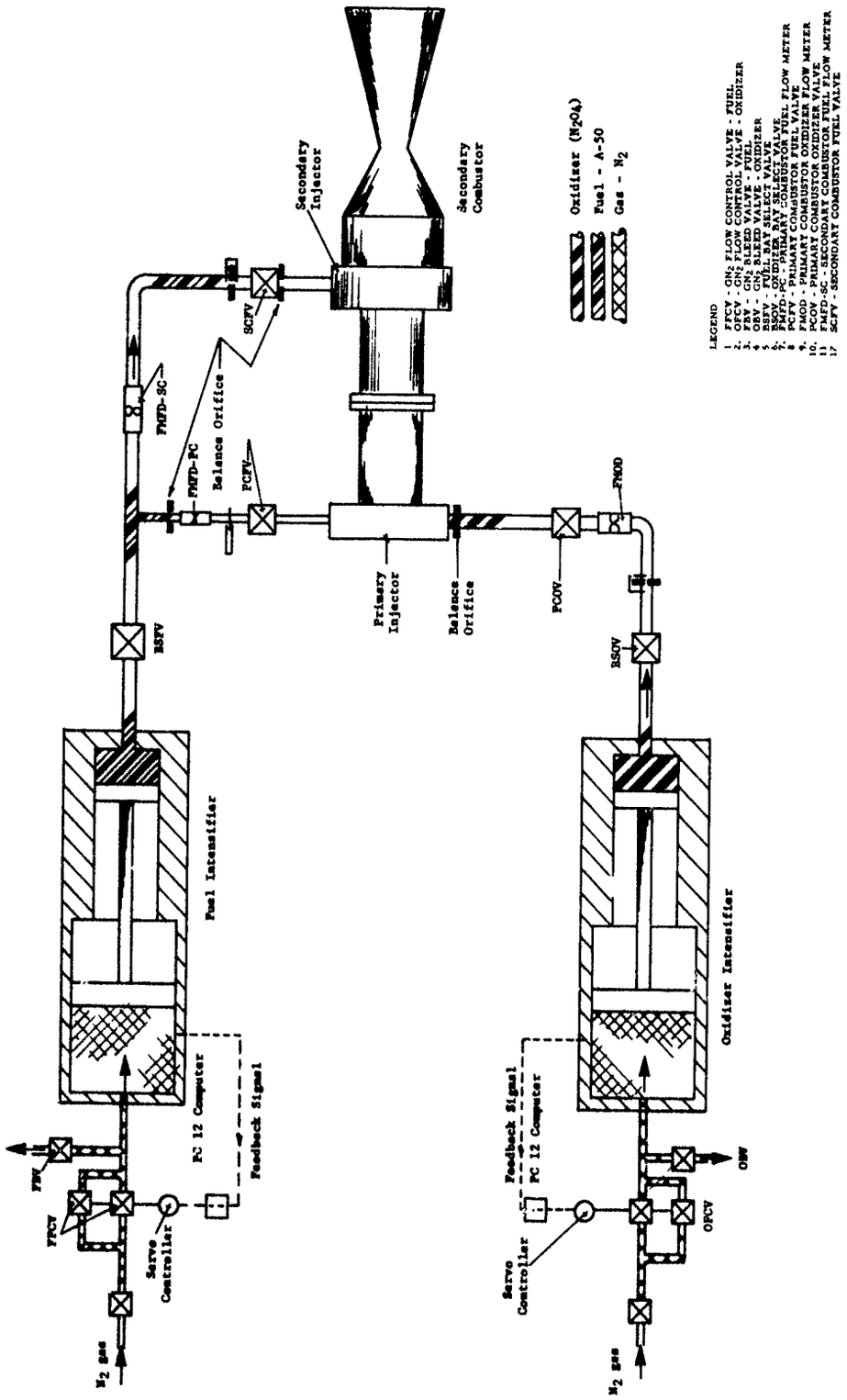

Intensifier System Schematic with Sector Engine

Figure VI-13

ICP RESIDUAL HARDWARE PI
TEST DATA AND PERFORMANCE S

	GENERAL DATA								MEASURED DATA					
	DATE	DUR. FS_1-FS_2	DATA PERIOD FS_1 +	INJECTOR	CHAMBER NOZZLE	THROAT AREA	AREA RATIO	CHAR. LENGTH	CHAMBER PRESS.	INJECTOR MIXTURE RATIO	FILM COOLANT FLOW RATE	VACUUM THRUST	ENGINE WEIGHT FLOW	N SI S
SYMBOLS						A_t		L*	Pc	MR_j	WOFC	F_v	W_t	
UNITS	---	sec.	sec.	---	---	$in.^2$	---	in.	psia	---	lbs/sec	lbs	lbs/sec	
TEST														
1.2-07-WAM-001	9-1-65	.496	None	Mk 32	Ablative	24.76	14.54	44	Malfunction - excessive gas generator valve op					
-002	9-8-65	.478	None	Mk 32	Ablative	24.76	14.54	44	Malfunction - excessive gas generator valve op					
-003	9-8-65	.552	None	Mk 32	Ablative	24.76	14.54	44	Malfunction - excessive gas generator valve op					
-004	9-9-65	1.65	1.42-1.62	Mk 32	Ablative	24.76	14.54	44	2595	2.347	0	109,017	395.07	26
-005	9-21-65	1.66	1.43-1.63	Mk 125A	Ablative	24.88	14.47	38	2642	2.178	0	109,002	390.82	26
-006	9-24-65	1.68	1.43-1.63	Mk 125A	Ablative	24.98	14.41	17	2682	2.132	0	111,042	394.3	26
-007	10-28-65	.560	None	Mk 125A	Ablative	21.8	15.52	26	Malfunction - primary combustor fuel valve mic					
-008	10-29-65	2.013	None	Mk 125A	Ablative	23.2	15.52	26	Measured and performance data compromised due					
-009	11-10-65	2.029	1.38-1.98	Mk 125A	Ablative	23.20	15.22	26	2315	2.43	53.6	89,654	357.25	23
-010	11-11-65	2.00	1.35-1.95	Mk 125A	Ablative	23.65	15.22	26	2600	2.41	38.7	102,027	390.45	24
-011	11-17-65	2.037	1.39-1.99	Mk 125B	Ablative	21.43	16.80	26	2535	2.605	27.7	90,102	339.80	24
-012	11-18-65	1.717	1.47-1.67	Mk 125B	ABL/STL	21.43	16.80	26	2640	2.645	0	96,930	348.55	26
1.2-08-WAM-001	12-2-65	87.0	None	Mk 125A	R-4	19.86	18.05	27	Malfunction - erroneous chamber leakage signal					
-002	12-7-65	2.274	1.72-2.22	Mk 125A	R-4	19.86	18.05	27	2465	2.56	49.6	88,339	329.90	23
-003	12-14-65	2.042	1.69-1.99	Mk 125A	R-5	20.95	17.15	24.6	2240	2.74	40.0	79,615	315.5	23
-004	12-17-65	1.836	None	Mk 125A	R-5	20.95	17.15	24.6	Measured and performance data compomised due c					
1.2-09-WAM-001	2-15-66	1.543	None	Mk 32	Ablative	21.8	17.3	18.0	Malfunction - open primary combustor fuel valv					
-002	2-23-66	2.30	None	Mk 32	Ablative	21.8	17.3	18.0	Measured and performance data compromised due					
-003	3-3-66	2.514	1.46-1.96	Mk 125AB	Ablative	21.82	17.3	20.8	2845	2.60	0	106,298	376.7	26

ICP RESIDUAL HARDWARE PROGRAM
TEST DATA AND PERFORMANCE SUMMARY

RED DATA				PERFORMANCE							PERCENT PERFORMANCE		
FILM COOLANT FLOW RATE	VACUUM THRUST	ENGINE WEIGHT FLOW	MEASURED SEA-LEVEL SPECIFIC IMPULSE	VACUUM SPECIFIC IMPULSE	MIXTURE RATIO DISTR. LOSS	NOZZLE GEOMETRY LOSS	NOZZLE FRICTION LOSS	FILM COOLING LOSS	COMB. LOSS	THEO. VACUUM SPECIFIC IMPULSE	PERCENT COOLANT	PERCENT COOLANT LOSS	PERCENT VACUUM SPECIFIC IMPULSE
WOFC	F_v	W_t	$Is_{S.L.}$	Is_V	MRDL	NGL	NFL	FCL	ERL	IsV_t	% WOFC	% Is_{FC}	% Is_V
lbs/sec	lbs	lbs/sec	sec.	sec.	sec.	sec.	sec.	sec.	sec.	sec.	%	%	%
sive gas generator valve opening time - no measured or performance data.													
sive gas generator valve opening time - no measured or performance data.													
sive gas generator valve opening time - no measured or performance data.													
0	109,017	395.07	261.6	275.9	12.7	4.8	17.9	0	8.1	319.4	0	0	86.4
0	109,002	390.82	265.6	278.9	14.6	4.8	17.2	0	7.7	323.2	0	0	86.3
0	111,042	394.3	268.1	281.6	0	4.9	17.2	0	20.0	323.7	0	0	87.0
ry combustor fuel valve microswitch failed to open - no measured or performance data.													
ance data compromised due to feed-coupled-combustion instability.													
53.6	89,654	357.25	236.2	251.0	19.0	4.3	3.2	29.9	11.3	318.7	15.0	9.38	78.8
38.7	102,027	390.45	247.7	261.3	18.9	4.5	3.2	19.3	11.3	318.5	9.9	6.06	82.0
27.7	90,102	339.80	249.2	265.2	15.8	4.5	3.3	14.5	11.5	314.8	8.15	4.61	84.2
0	96,930	348.55	262.9	278.1	16.1	4.9	3.3	0	11.5	313.8	0	0	88.6
ous chamber leakage signal - no measured or performance data													
49.6	88,339	329.90	236.4	252.5	16.6	4.3	3.4	28.2	11.6	316.6	15.05	8.91	79.7
40.0	79,615	315.5	235.7	252.5	14.1	4.3	3.3	25.2	12.0	311.4	12.68	8.09	81.0
ance data compomised due chamber oxidizer supply flex hose failure.													
rimary combustor fuel valve microswitch - no measured or performance data.													
ance data compromised due to excessive erosion of Mark 32 primary combustor.													
0	106,298	376.7	267.2	282.0	6.7	4.9	7.3	0	14.5	315.5	0	0	89.4

ICP Residual Hardware Program Performance Summary (u)

Figure VI-14

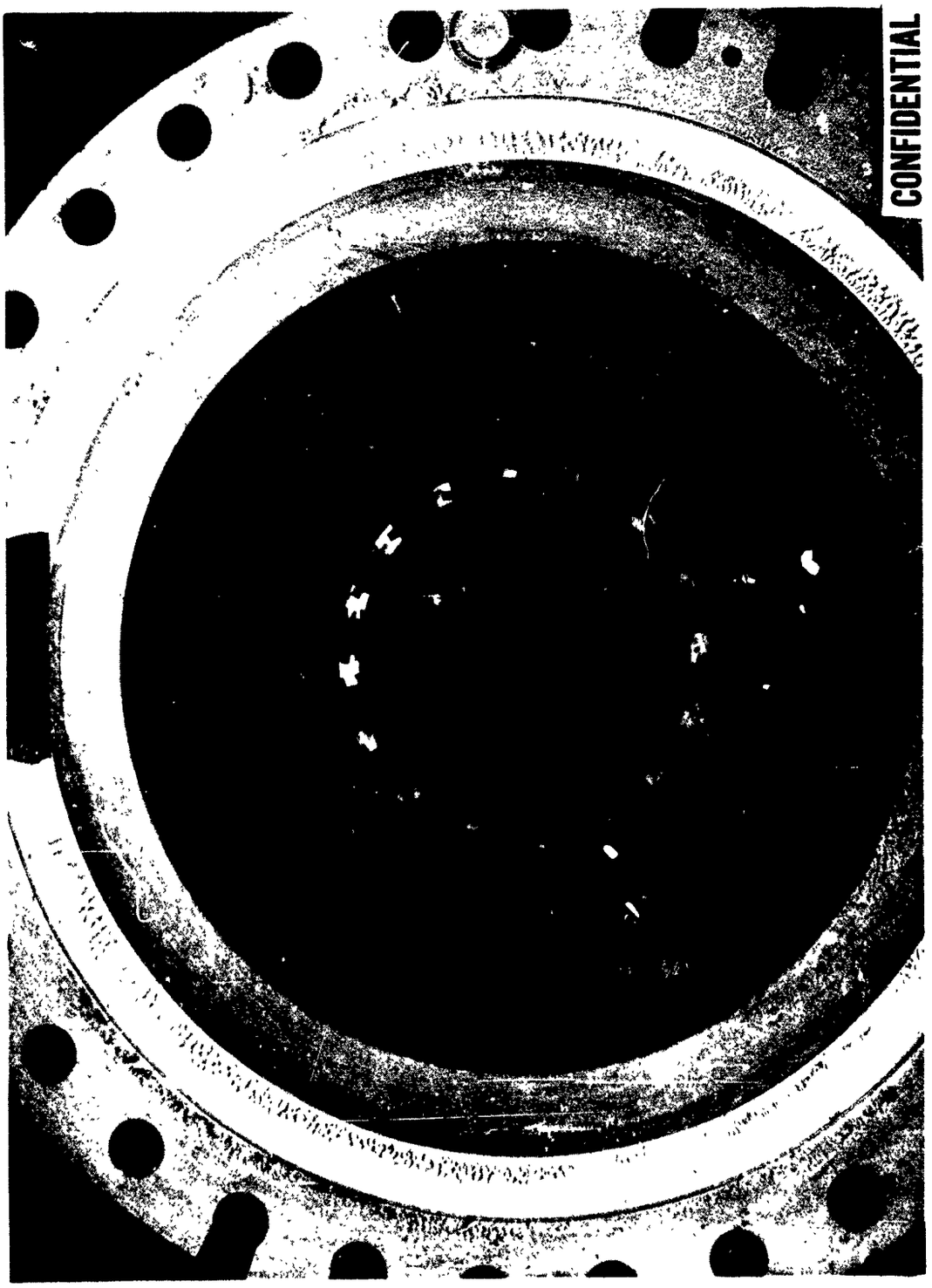

Postfire Condition Mark 32 Injector (u)

Figure VI-15

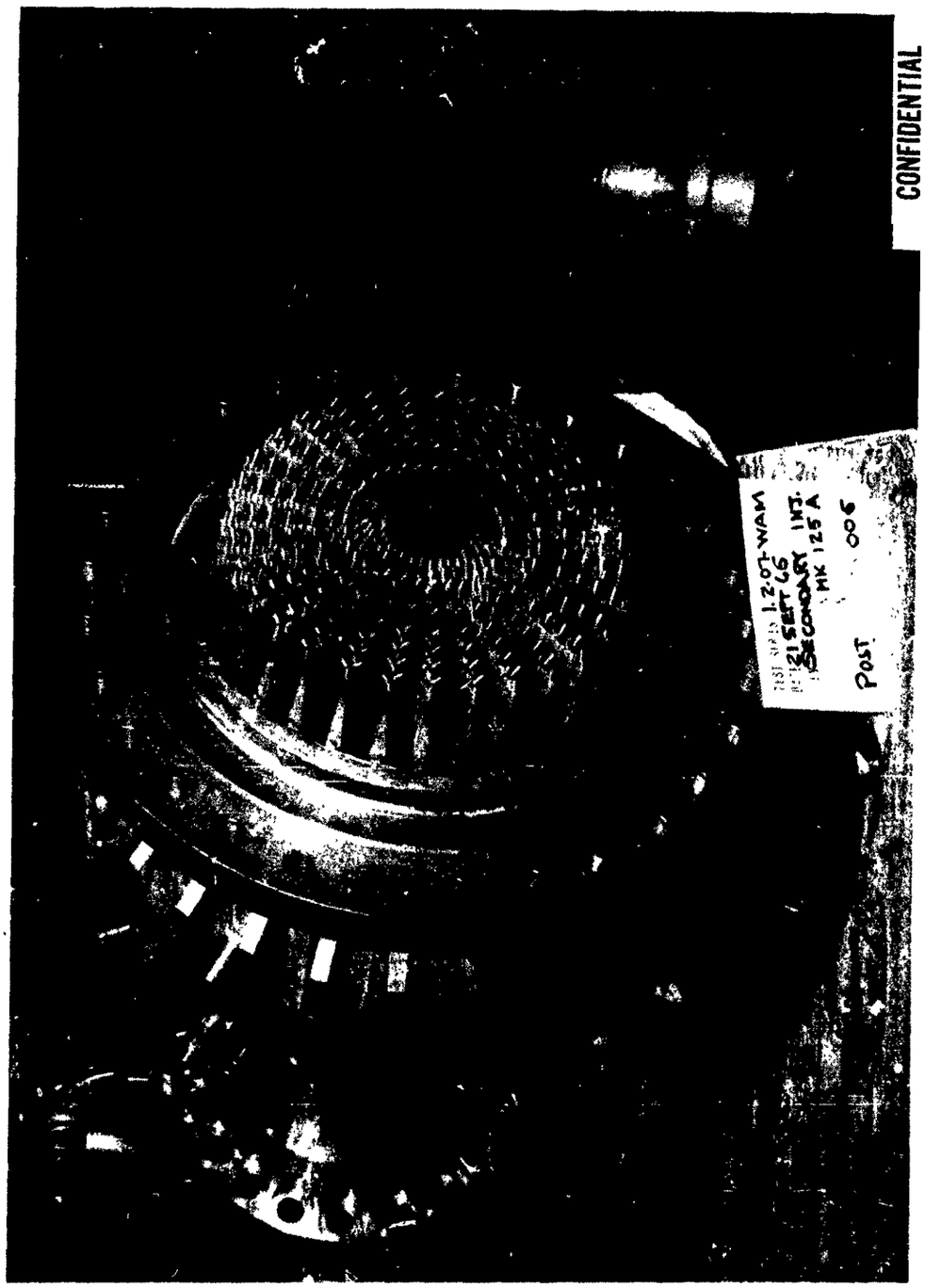

Postfire Condition Mark 125 Injector (u)

Figure VI-16

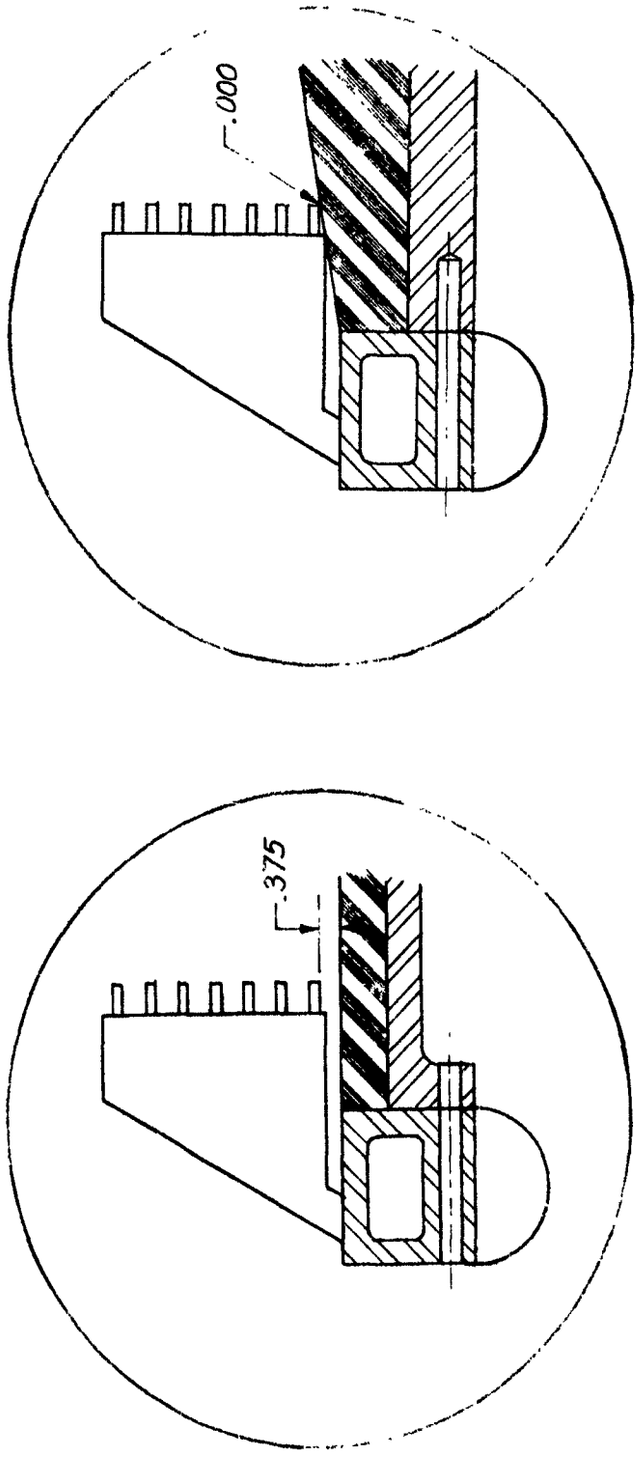

UNCLASSIFIED

Injector Chamber Configuration L* Evaluation Series

Figure VI-17

Prefire Photograph of Film Coolant Ring Looking Upstream Through the Nozzle Throat (u)

Figure VI-18

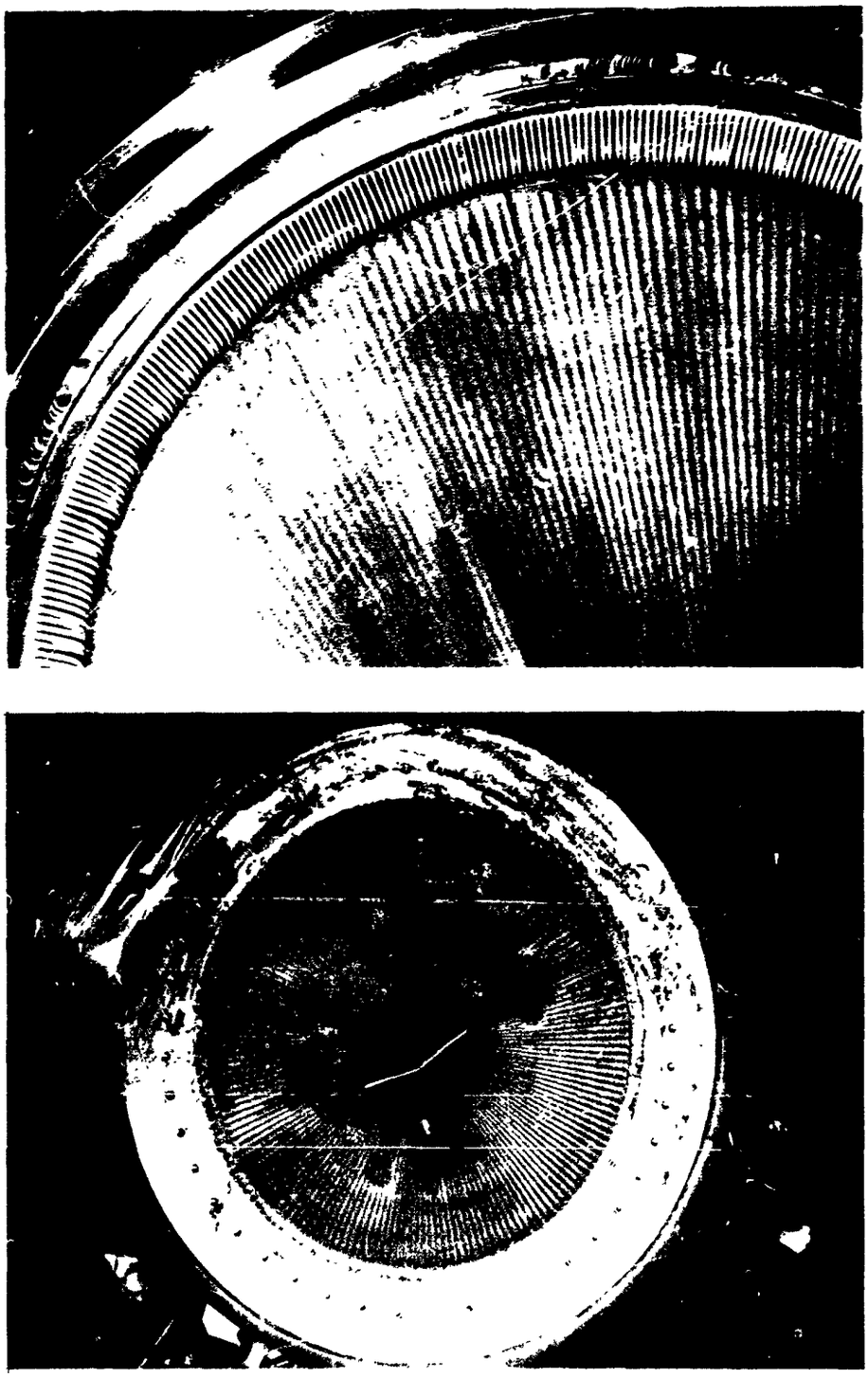

Postfire Photographs of SN 4 Regenerative Test

Figure VI-19

THERMOCOUPLE	TEST -009 AND -010 *DISTANCE FROM FILM COOLANT RING, IN.	MAX. TEMPERATURE, °F -009	-010	TEST -011 *DISTANCE FROM FILM COOLANT RING, IN.	MAXIMUM TEMPERATURE, °F
TCA-1	2.00	340	360	2.00	360**
-2	4.75	400	700	3.87	380
-3	7.50	770	1350	5.74	1500
-4	10.25	1150	1900	7.61	1370
-5	13.00	1600	2500	9.48	2500
-6	16.00	1780	BURNOUT	11.35	---
-7	19.50	INVALID	OVERSCALE	13.22	BURNOUT
-8	22.90	OVERSCALE	BURNOUT	16.00	OVERSCALE
-9	26.30	1500	OVERSCALE	NOT RECORDED	
TCB-1	2.00	340	370	NOT RECORDED	
-2	4.75	420	770	NOT RECORDED	
-3	7.50	820	1400	NOT RECORDED	
-4	10.25	1320	2140	NOT RECORDED	
-5	13.00	1700	OVERSCALE	NOT RECORDED	
-6	16.00	1900	BURNOUT	NOT RECORDED	
-7	19.50	1830	2450	NOT RECORDED	
-8	22.90	2050	2060	NOT RECORDED	
-9	26.30	980	QUESTIONABLE	NOT RECORDED	
-10	29.70	1310	1620	NOT RECORDED	

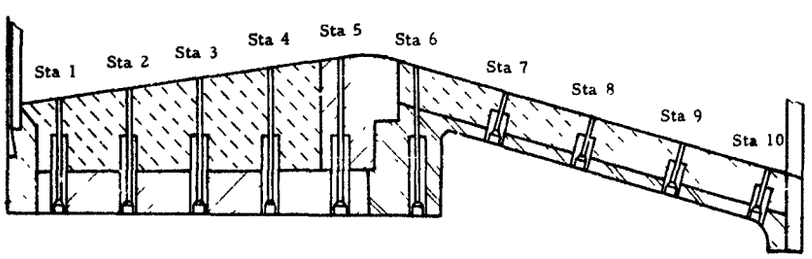

* THROAT IS 13.86 IN. FROM FILM COOLANT RING
**HIGH RESPONSE THERMOCOUPLE

Thermocouple Data from ICP Film-Cooled, Ablative Chamber Tests
(Test Series 1.2-07-WAM)

Figure VI-20

TEST NO.	COATING THICKNESS IN.	COATING COND. B/IN.-SEC°R	WALL THICKNESS IN.	WALL COND. B/IN.-SEC°R	W_{REG} LB/SEC	$W_{MAIN\ STREAM}$ LB/SEC	W_{f_c} LB/SEC	X_{f_c} IN.	INLET VEL. (fc) FT/SEC	INLET TEMP (fc) °R	STAGNATION TEMP (MAINSTREAM) °R
1.2-07-WAM -009	-	-	-	-	-	303.6	53.6	0	410.	545.	5500.
1.2-07-WAM -010	-	-	-	-	-	351.3	38.7	0	410.	545.	5540.
1.2-07-WAM -011	-	-	-	-	-	312.6	27.7	0	410.	545.	5460.
1.2-08-WAM -002	.056	.00016	.012-.02	.00026	193.5	272.4	49.5		346.	518.	5478.
1.2-08-WAM -003	.025	.00012	.012-.020	.00026	202.0	275.5	24.	0	476.	521.	5407.
*	.025	.00012	.004	.00026	16.	275.5	16.	12.25	187.	581.	

*CAPILLARY TUBE DATA FOR TEST 1.2-08-WAM-003

Test Parameters for ICP Chamber Tests

Figure VI-21

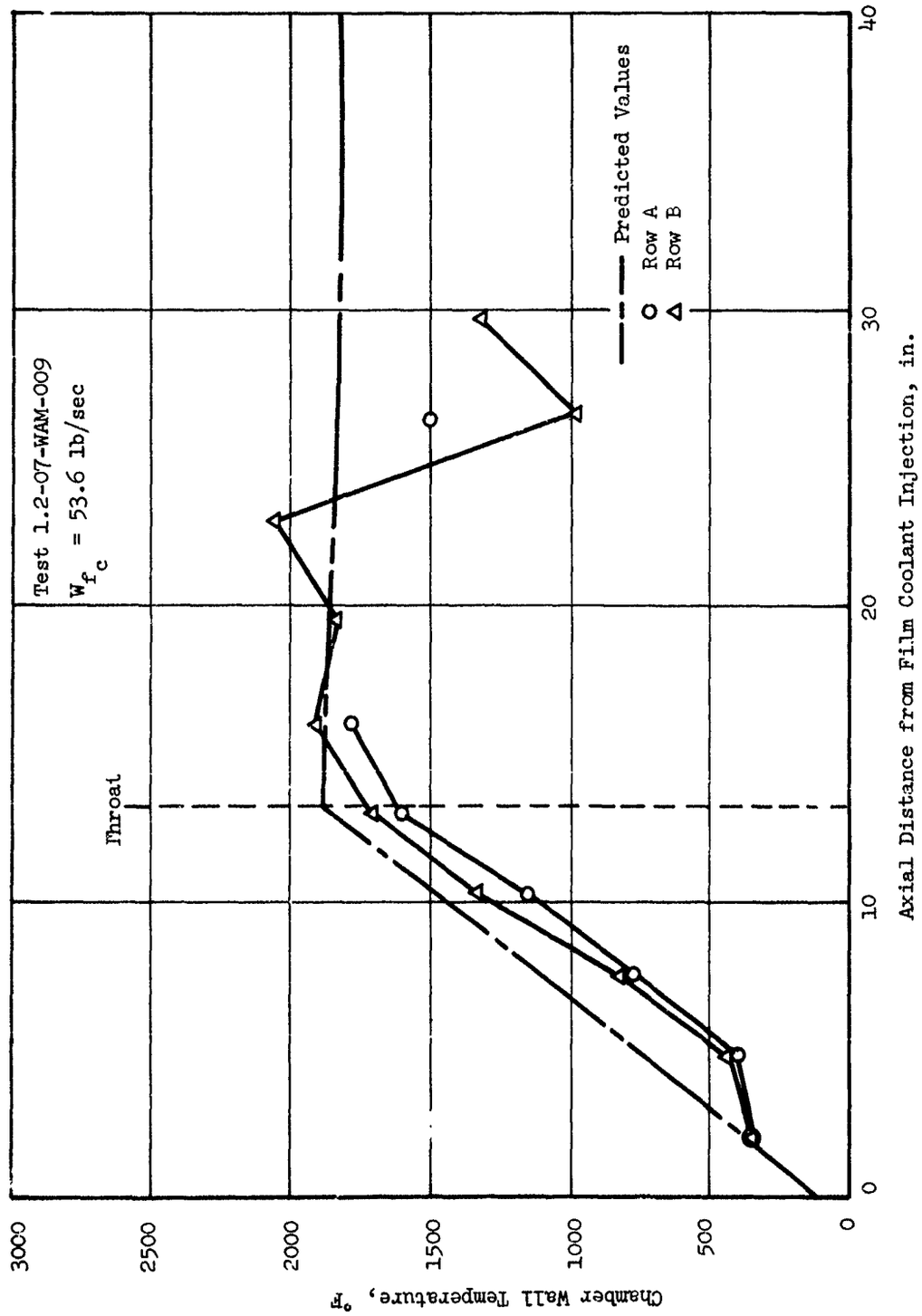

Chamber Wall Temperatures for Test 1.2-07-WAM-009

Figure VI-22

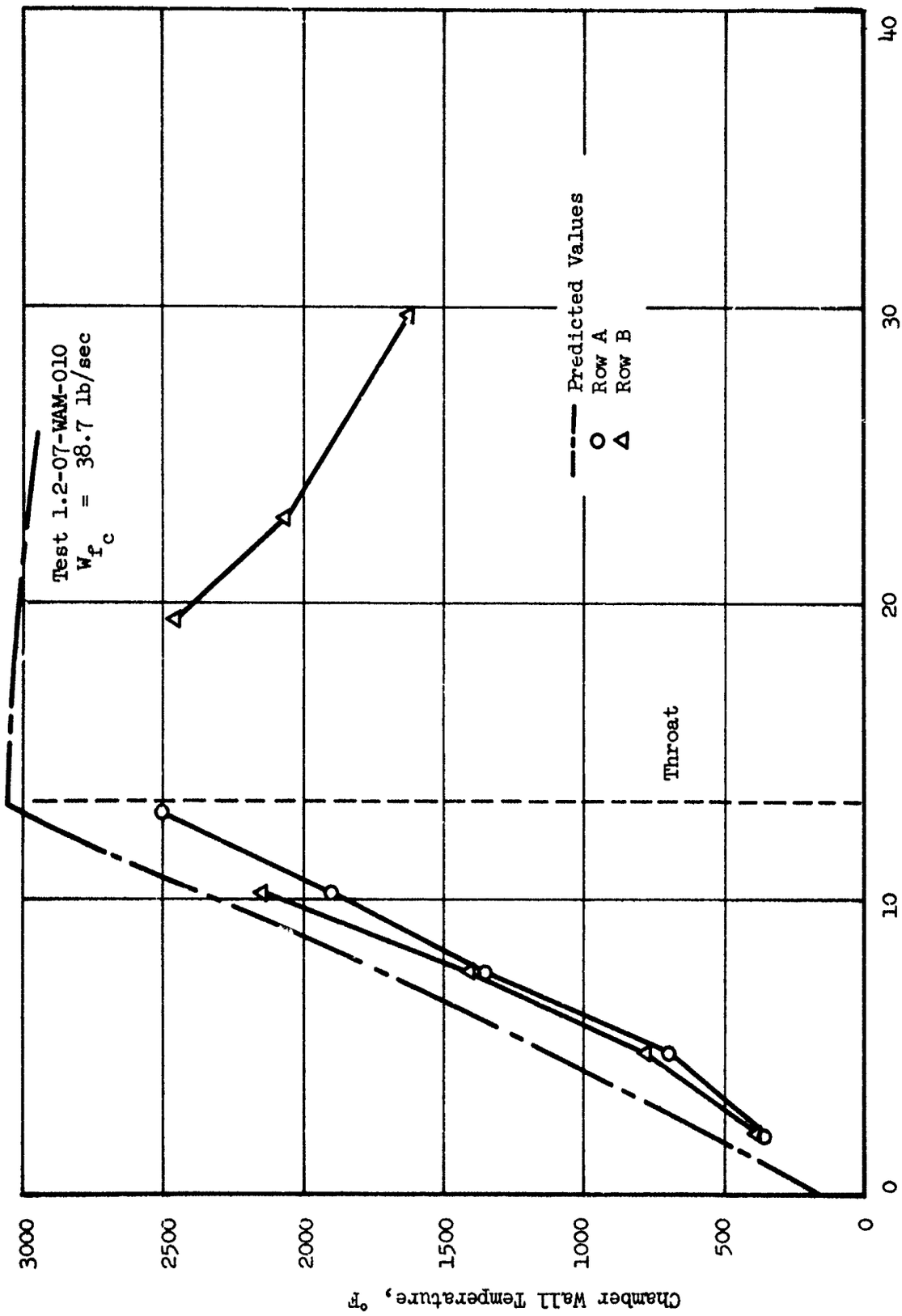

Chamber Wall Temperatures for Test 1.2-07-WAM-010

Figure VI-23

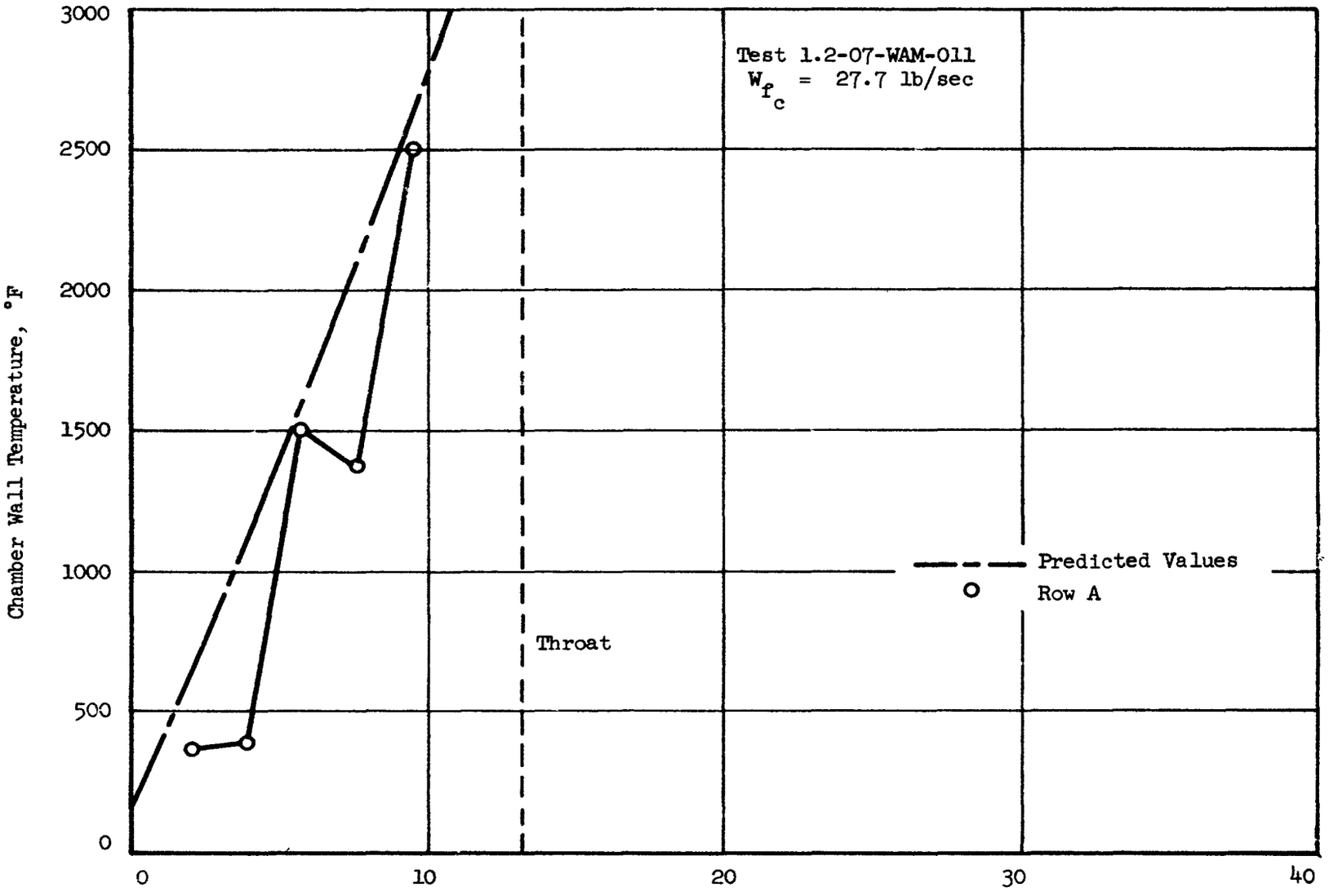

Figure VI-24

Chamber Wall Temperatures for Test 1.2-07-WAM-011

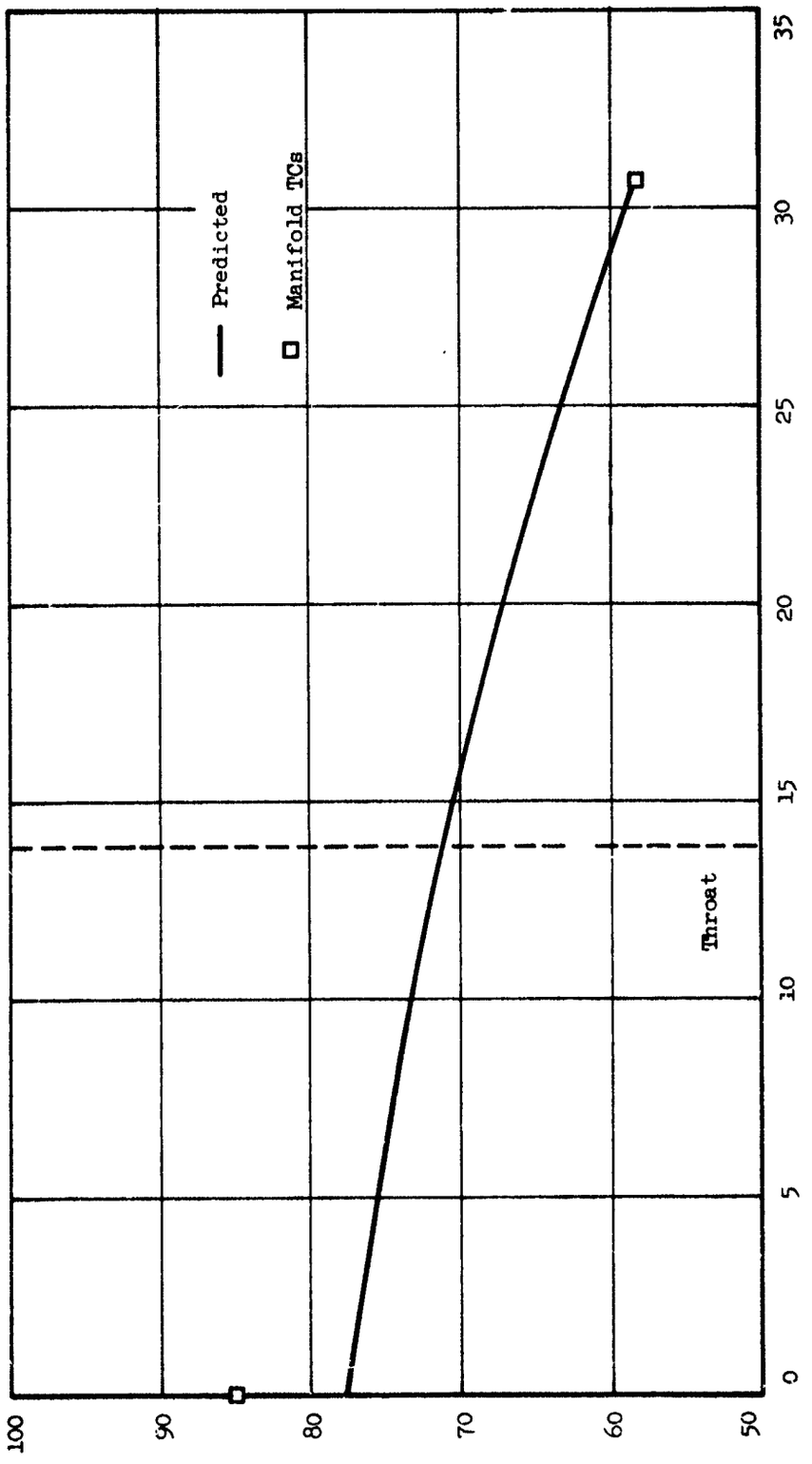

Regenerative Coolant Bulk Temperature, Test 1.2-08-WAM-002

Figure VI-25

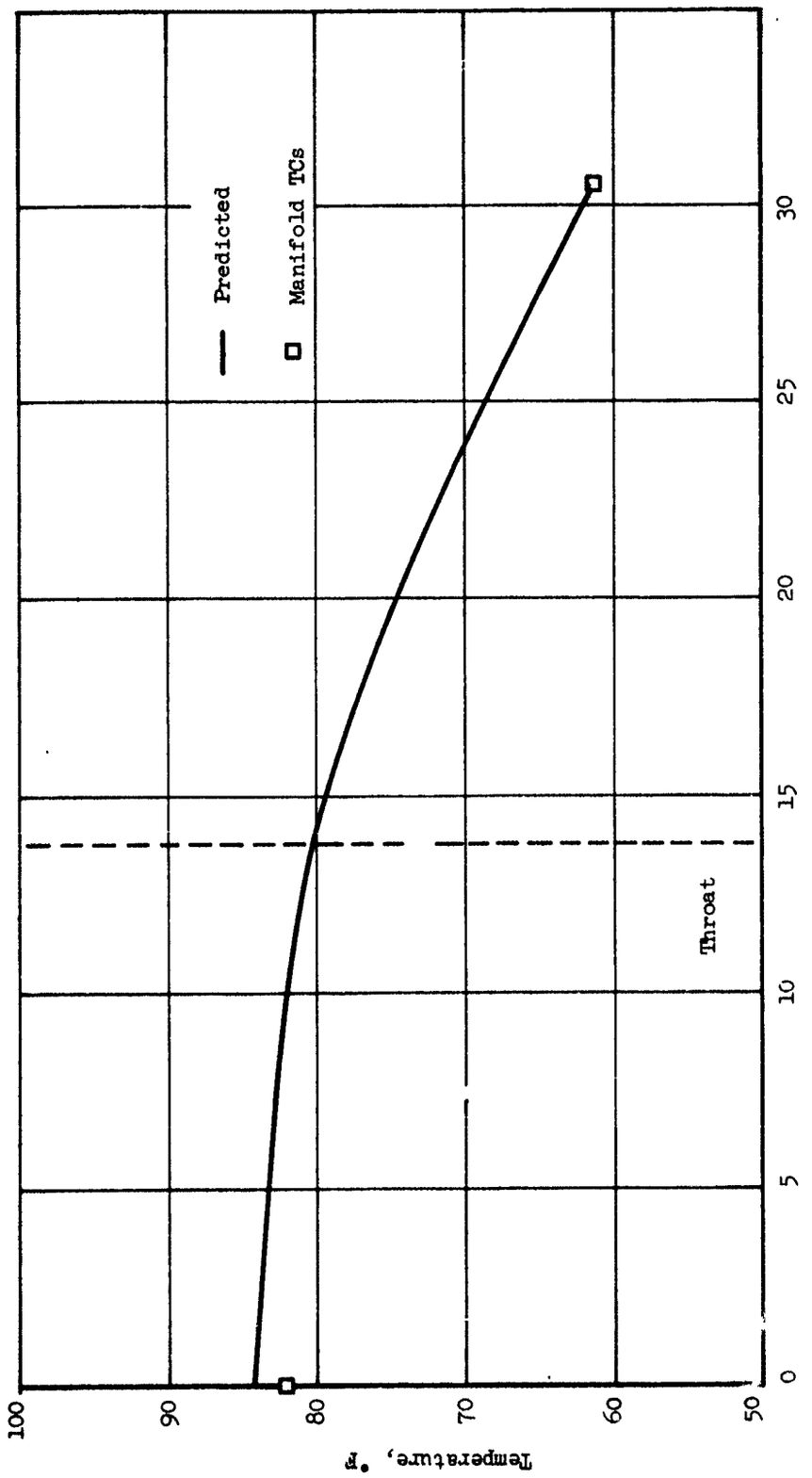

Regenerative Coolant Bulk Temperature, Test 1.2-08-WAM-003

Figure VI-26

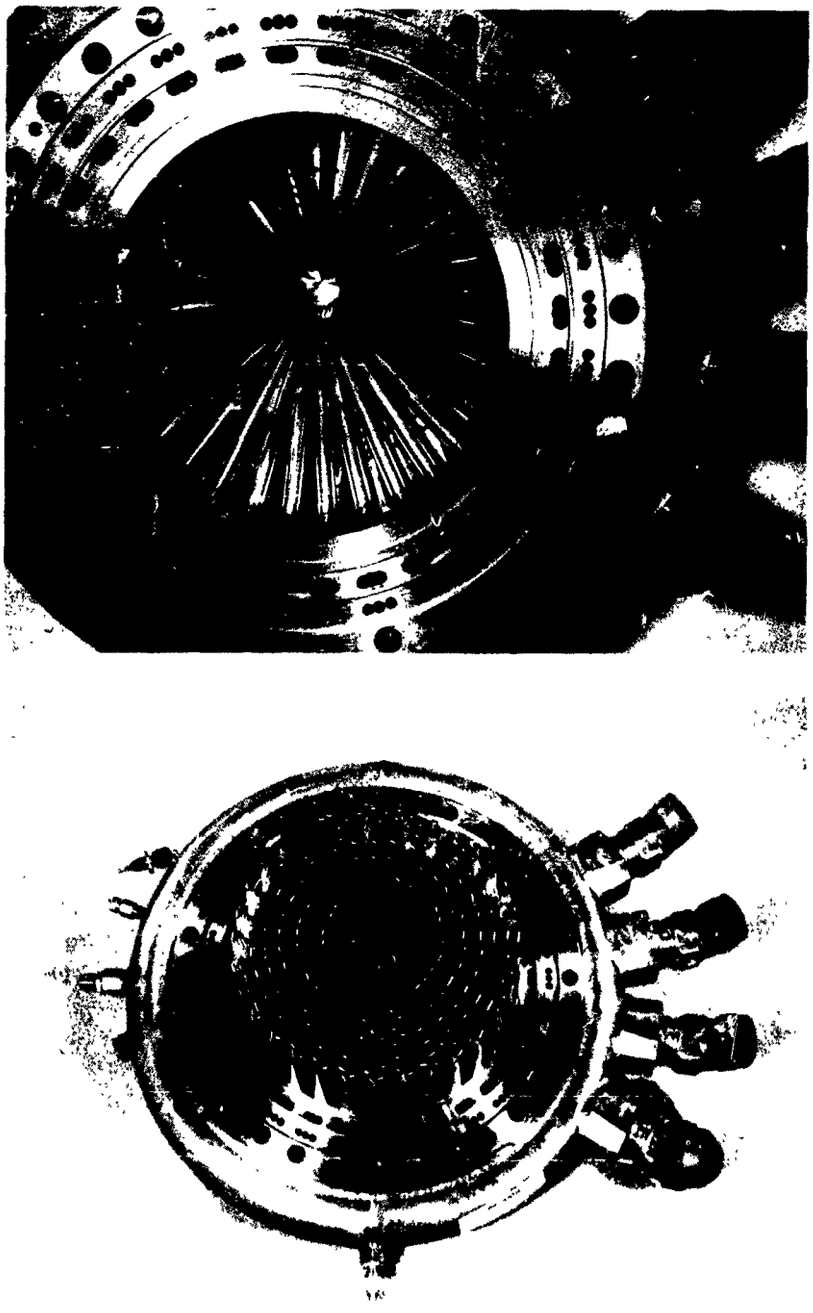

CONFIDENTIAL

Modular Configuration--Mark 125 Injector (u)

Figure VI-27

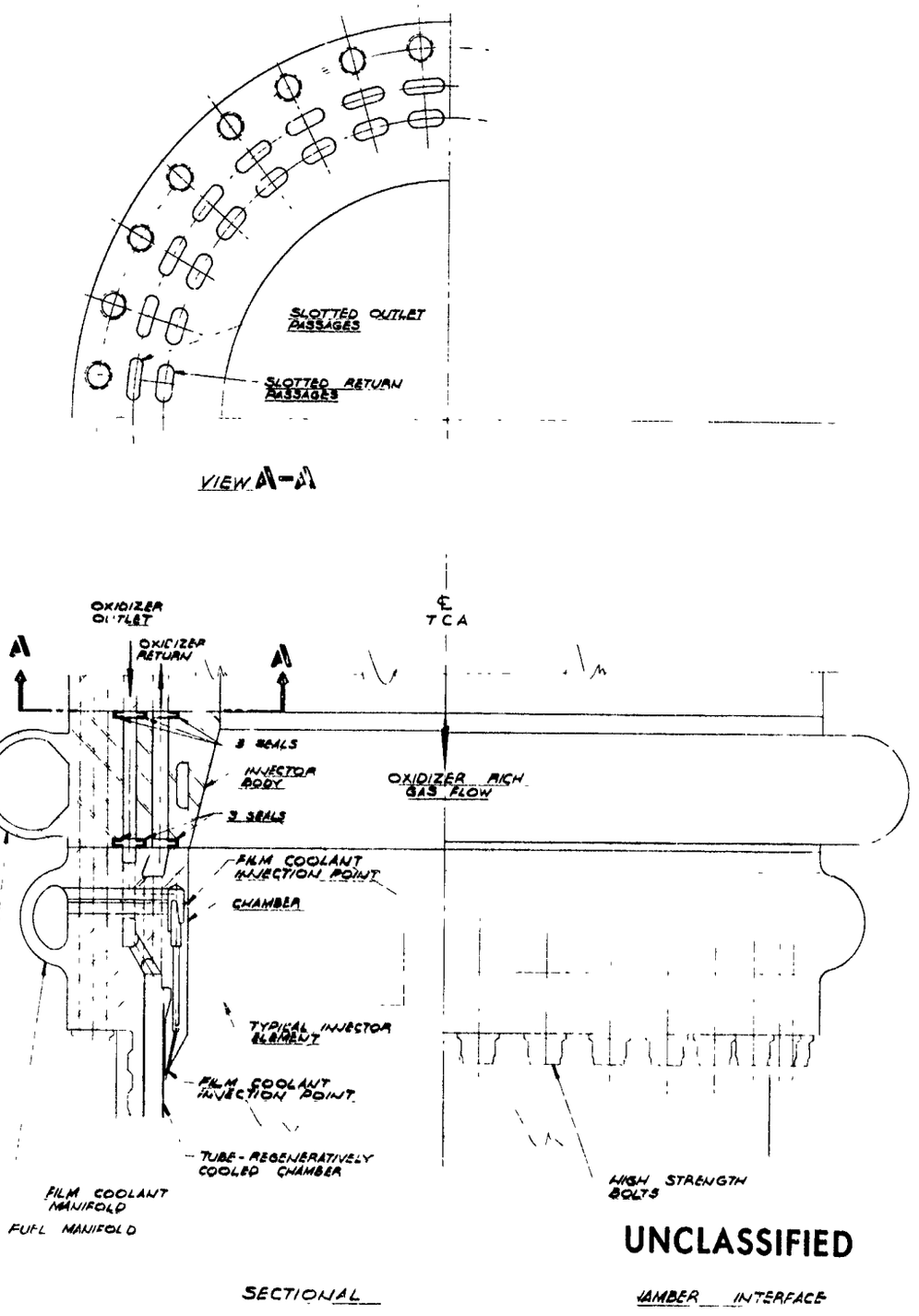

UNCLASSIFIED

Turbopump-Injector-Cooled Chamber Interface

Figure VI-28

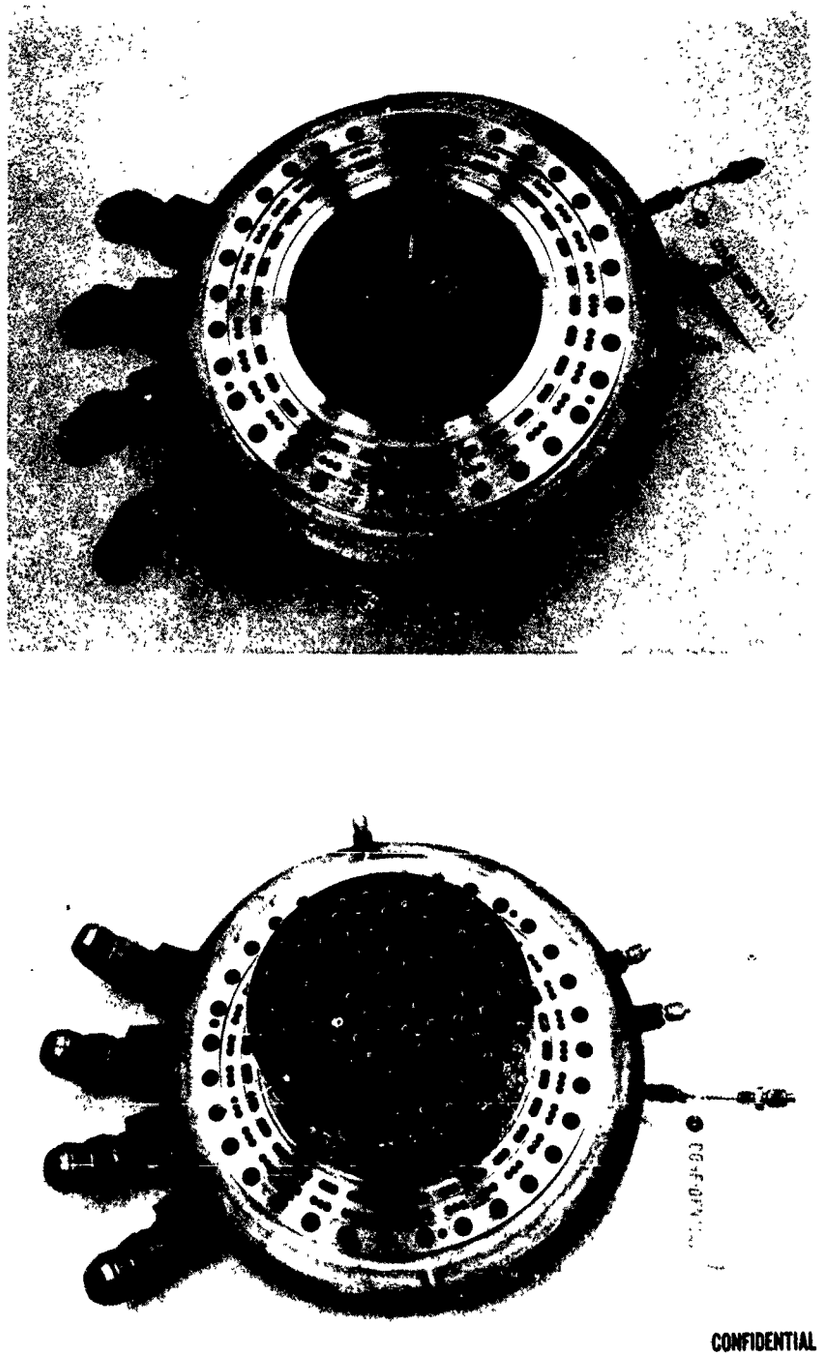

CONFIDENTIAL

Fuel Swirl Rake Injector (u)

Figure VI-29

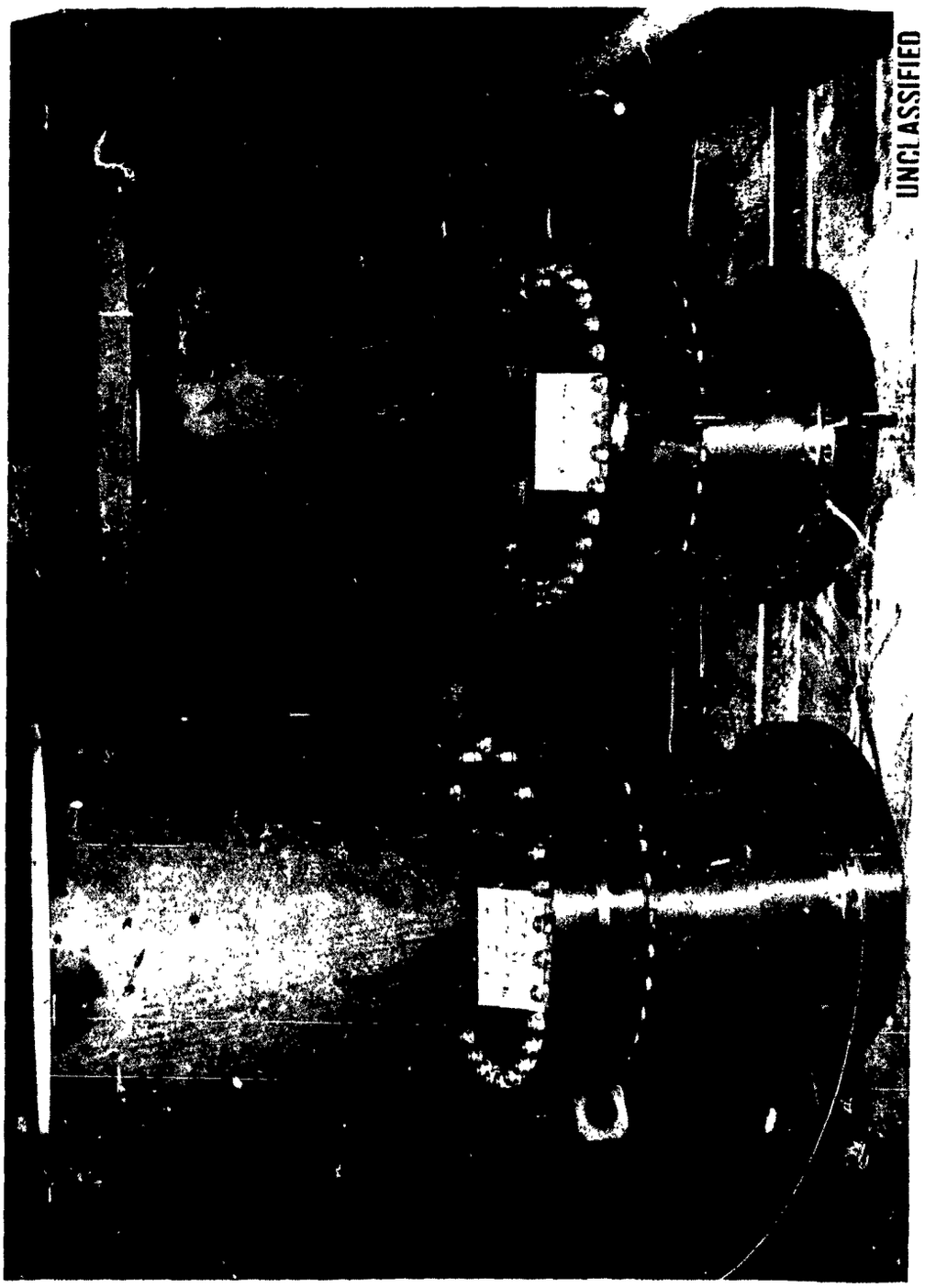

Uncooled Ablative Thrust Chambers of Different L*'s

Figure VI-30

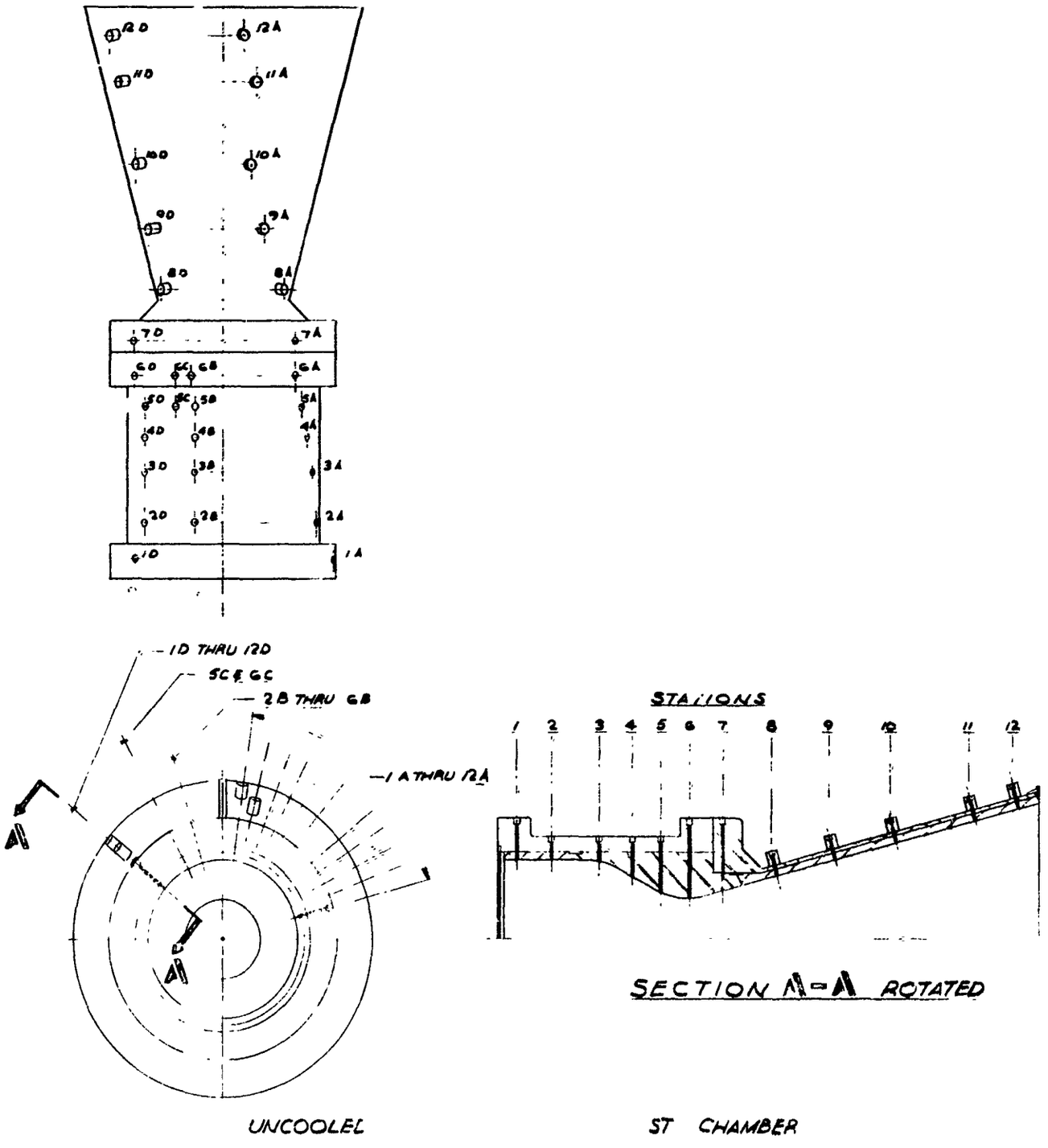

Uncooled Instrumented Thrust Chamber Schematic

Figure VI-31

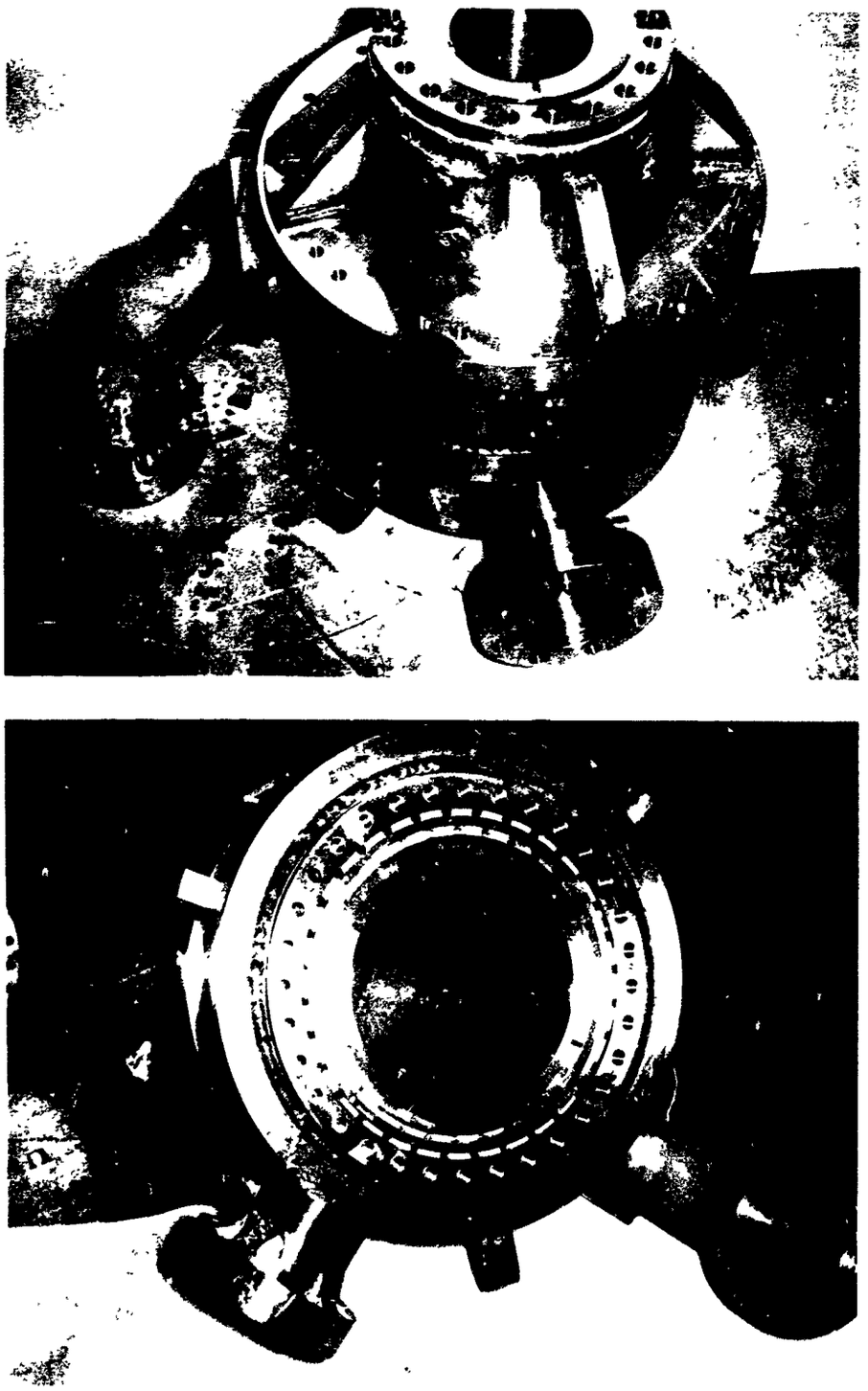

Test Stand Adapter

Figure VI-32

	GENERAL DATA							MEASURED DATA						
	DATE	DURATION FS_1	FS_2	DATA PERIOD FS_1 +	INJECTOR SERIAL NUMBER	THROAT AREA	AREA RATIO	CHAR-ACTERISTIC LENGTH	CHAMBER PRESSURE	INJECTOR MIXTURE RATIO	FILM COOLANT FLOW RATE	VACUUM THRUST	ENGINE WEIGHT FLOW	MEASURED SEA LEVEL SPECIFIC IMPULSE	VACUU SPECIF IMPULS
SYMBOLS						A_T		L^*	P_C	MR_J	$\dot{W}_{OFC}$	F_V	$\dot{W}_T$	Is_{SL}	Is_V
UNITS	---	SEC		SEC	---	$IN.^2$	---	IN.	PSIA	---	LB/SEC	LB	LB/SEC	SEC	SEC
TEST															
1.2-11-WAM-001	3-25-66	0.903	NONE		125-SN-1	21.12	11.92	46.8	MALFUNCTION - NO VALID PERFORMANCE DATA						
002	3-29-66	1.909	1.76-1.86		125-SN-1	21.12	11.92	46.8	2848	2.57	0	99.850	370	260	270
003	3-30-66	2.313	1.86-2.26		125-SN-1	21.0	11.96	46.8	2811	2.03	0	97,530	357	263	273
004	3-30-66	2.026	1.78-1.98		RAKE	21.0	11.92	46.5	2850	2.22	0	99,630	350	274	285
005	3-30-66	2.309	1.76-2.26		RAKE	21.2	11.87	46.1	2820	2.21	0	99,370	350	274	285
006	4-1-66	1.728	NONE		RAKE	21.2	11.87	46.1	MALFUNCTION - NO VALID PERFORMANCE DATA						
007	4-19-66	2.010	1.76-1.96		125-SN-1	22.3	11.32	43.2	2854	2.27	0	102,290	362	273	283
008	4-20-66	2.011	1.76-1.96		125-SN-1	21.2	11.70	35.0	2891	2.27	0	103,420	362	276	286
009	4-20-66	0.410	NONE		125-SN-1	21.2	11.7	35.0	MALFUNCTION - NO VALID PERFORMANCE DATA						
010	4-20-66	2.009	1.76-1.96		125-SN-1	21.9	11.53	20.0	2841	2.26	0	100,310	360	269	279
011	5-2-66	2.003	1.65-1.95		125-SN-4	22.6	10.96	32.9	2828	2.18	0	105,520	357	286	296
012	5-3-66	2.002	1.55-1.95		RAKE	21.2	11.35	19.7	2821	2.19	0	101,310	359	272	282
013	5-3-66	2.006	1.56-1.96		RAKE	22.9	11.02	42.1	2771	2.27	0	103,530	362	276	286
014	5-11-66	2.010	NONE		125-SN-1	22.9	11.02	42.1	STEEL NOZZLE LINER EXPULSION - NO VALID PERFORM						
015	6-13-66	2.000	1.55-1.95		125-SN-4	23.3	10.78	42.0	2660	2.34	0	104,850	360	281	291
016	6-29-66	1.396	NONE		125-SN-4	24.6	10.21	45.0	SHORT DURATION - NO VALID PERFORMANCE DATA						
017	6-30-66	2.506	1.76-2.45		125-SN-4	24.9	10.78	39.0	2720	2.31	0	113,730	396	279	288
018	7-28-66	2.090	1.9-2.0		125-SN-2	21.5	11.81	34.5	2820	2.32	26.5	100,396	348	278	288
019	8-31-66	3.242	2.49-3.19		125-SN-2	22.2	11.40	32.3	2740	2.28	28.2	99,760	356	269	279
020	9-2-66	2.013	1.76-1.96		125-SN-2	23.4	10.55	31.6	2730	2.28	46.3	103,110	377	263	273
021	10-12-66	1.764	NONE		125-SN-3	23.4	10.55	31.6	MALFUNCTION - NO VALID PERFORMANCE DATA						
022	10-12-66	2.011	1.94-1.98		125-SN-3	24.2	10.55	30.4	2800	2.30	40.5	107,630	402	259	268
024	11-16-66	2.155	1.91-2.11		MOD RAKE	21.6	11.75	34.4	2840	2.32	0	102,210	354	279	289
026	11-30-66	3.030	NONE		MOD RAKE	21.6	11.75	34.4	INVALID FLOW DATA - NO VALID PERFORMANCE DATA						

ASURED DATA				PERFORMANCE							PERCENT PERFORMANCE		
FILM R COOLANT FLOW RATE	VACUUM THRUST	ENGINE WEIGHT FLOW	MEASURED SEA LEVEL SPECIFIC IMPULSE	VACUUM SPECIFIC IMPULSE	MIXTURE RATIO DISTRIBU- TION LOSS	NOZZLE GEOMETRY LOSS	NOZZLE FRICTION LOSS	FILM COOLING LOSS	COMBUSTION LOSS	THEORETICAL VACUUM SPECIFIC IMPULSE	PERCENT COOLANT	PERCENT COOLANT LOSS	PERCENT VACUUM SPECIFIC IMPULSE
$\dot{W}_{OFC}$	F_V	$\dot{W}_T$	Is_{SL}	Is_V	MRDL	NGL	NFL	FCL	ERL	Is_{VT}	$\%\dot{W}_{OFC}$	$\%Is_{FC}$	$\%Is_V$
LB/SEC	LB	LB/SEC	SEC	SEC	SEC	SEC	SEC	SEC	SEC	SEC	%	%	%
- NO VALID PERFORMANCE DATA													
0	99,850	370	260	270	18.9	4.7	4.0	0	9.2	307	0	0	88.0
0	97,530	357	263	273	27.3	4.7	4.2	0	9.6	319	0	0	85.6
0	99,630	350	274	285	14.0	4.9	4.2	0	23.2	317	0	0	89.8
0	99,370	350	274	285	13.7	4.9	4.2	0	22.9	317	0	0	89.9
- NO VALID PERFORMANCE DATA													
0	102,290	362	273	283	10.5	4.9	7.3	0	10.0	315	0	0	89.6
0	103,420	362	276	286	10.3	4.9	3.0	0	11.7	316	0	0	90.5
- NO VALID PERFORMANCE DATA													
0	100,310	360	269	279	9.7	4.8	4.2	0	18.1	316	0	0	88.4
0	105,520	357	286	296	0	5.1	3.0	0	12.5	316	0	0	93.5
0	101,310	359	272	282	0	4.9	7.3	0	22.7	317	0	0	89.0
0	103,530	362	276	286	0	5.0	7.3	0	15.8	314	0	0	91.1
LINER EXPULSION - NO VALID PERFORMANCE DATA													
0	104,850	360	281	291	0	5.0	7.9	0	10.5	314	0	0	92.6
- NO VALID PERFORMANCE DATA													
0	113,730	396	279	288	2.3	5.0	7.8	0	8.5	311	0	0	92.4
26.5	100,396	348	278	288	0	5.0	3.0	9.5	9.1	315	7.63	3.02	91.2
28.2	99,760	356	269	279	0	4.8	6.3	13.2	11.6	315	7.71	3.87	88.6
46.3	103,110	377	263	273	0	4.7	3.0	20.1	12.2	313	12.30	6.42	87.2
NO VALID PERFORMANCE DATA													
40.5	107,630	402	259	268	7.7	4.7	3.0	17.0	12.2	313	10.10	5.92	85.6
0	102,210	354	279	289	EROSION PRECLUDES VALID LOSS BREAKOUT						0	0	91.7
TA - NO VALID PERFORMANCE DATA													

Modular Secondary Injector Performance Summary (u)

Figure VI-33

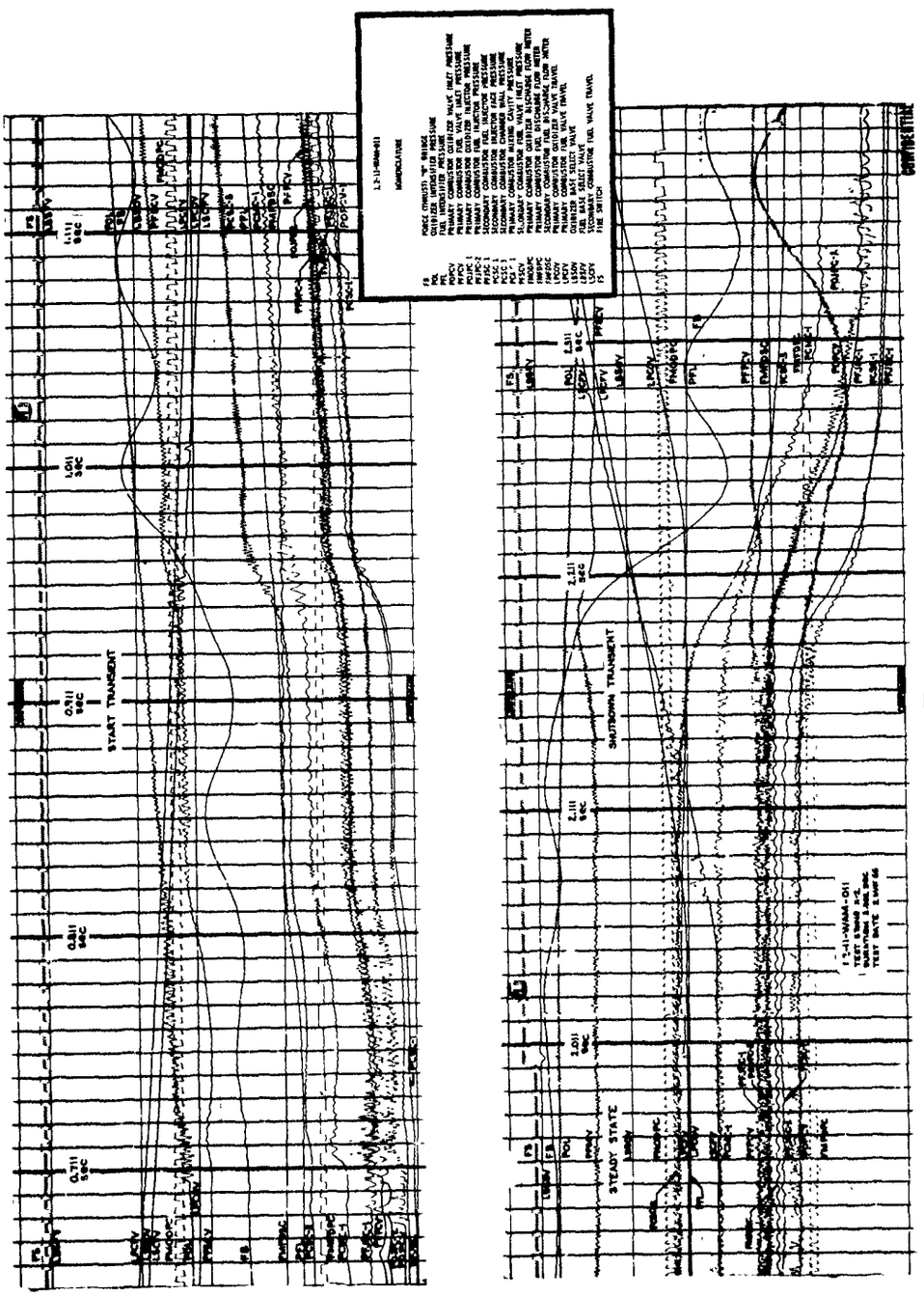

Typical Oscillograph, Secondary Injector Test (u)

Figure VI-34

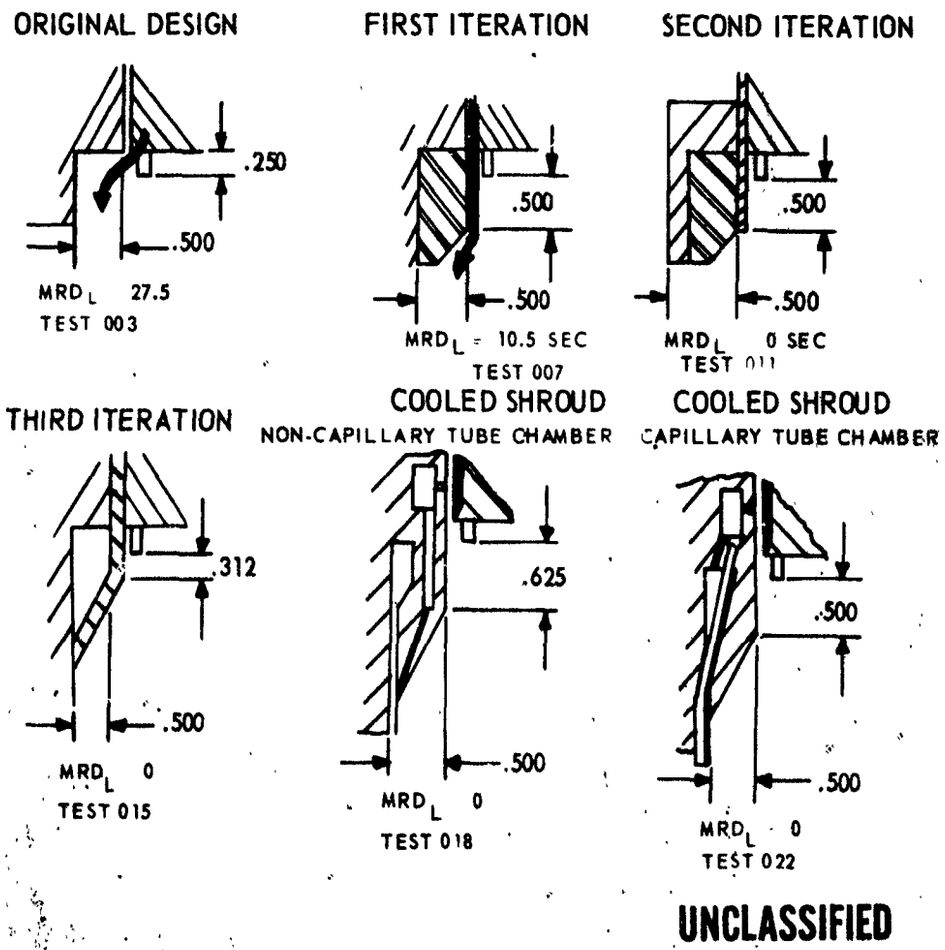

UNCLASSIFIED

Injector-Chamber Interface Development

Figure VI-35

CONFIGURATION C
CONFIGURATION B
CONFIGURATION A
OXIDIZER FLOW
FUEL FLOW
UNCLASSIFIED
Mixture Ratio Distribution Effects

Figure VI-36

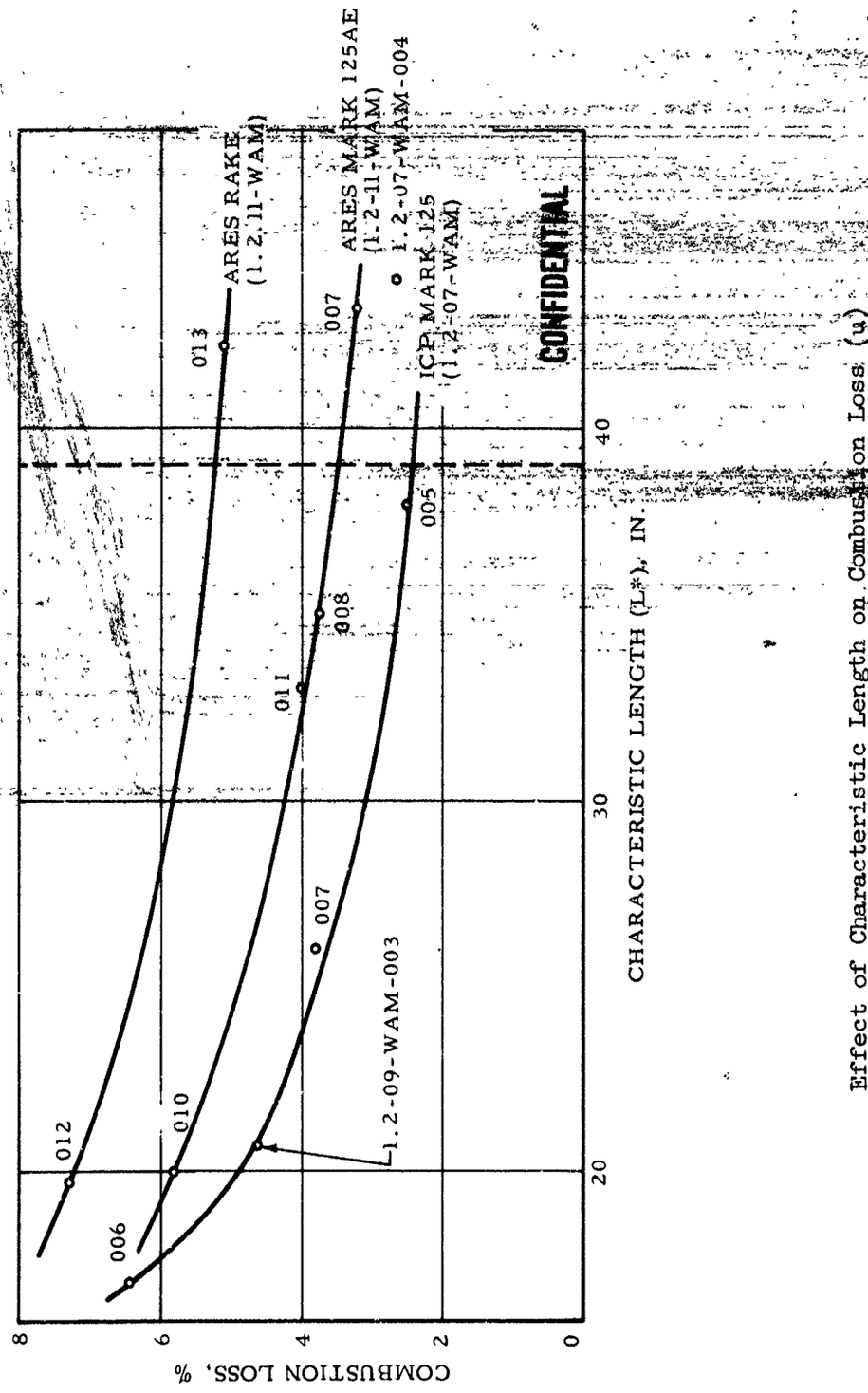

Effect of Characteristic Length on Combustion Loss (u)

Figure VI-37

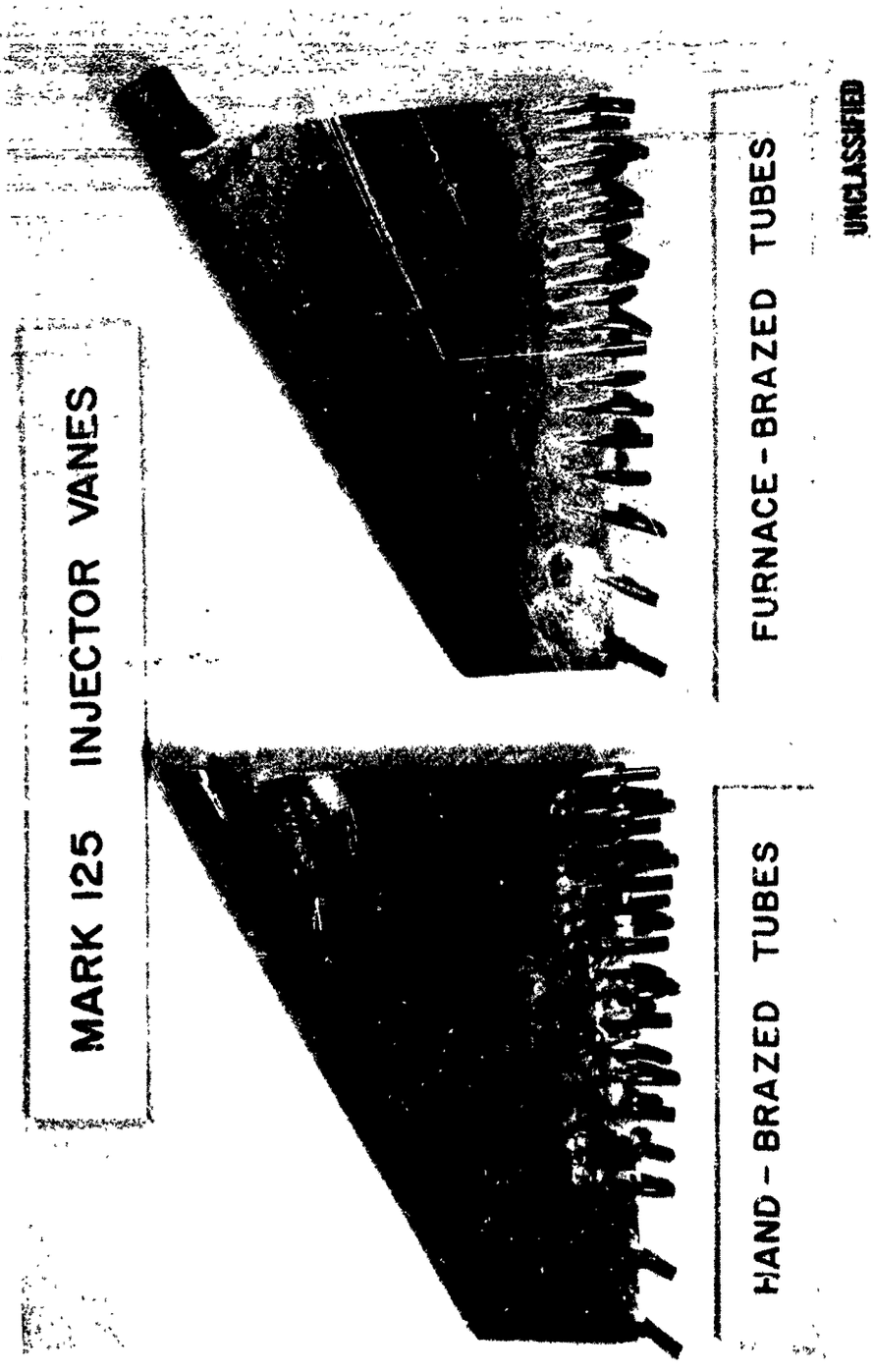

Mark 125 Injector Vanes

Figure VI-38

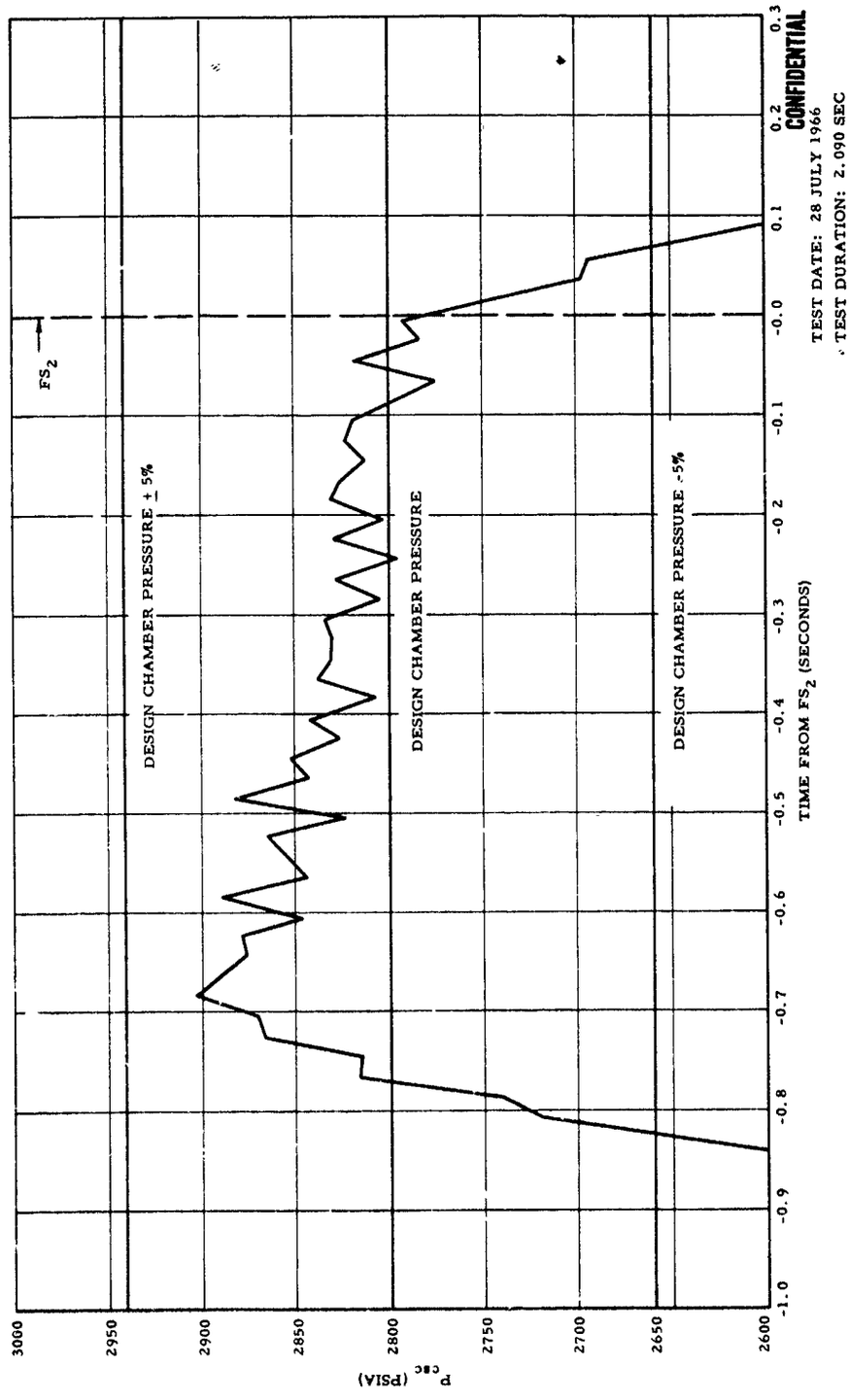

Mark 125 Secondary Injector Performance Certification (u)

Figure VI-39

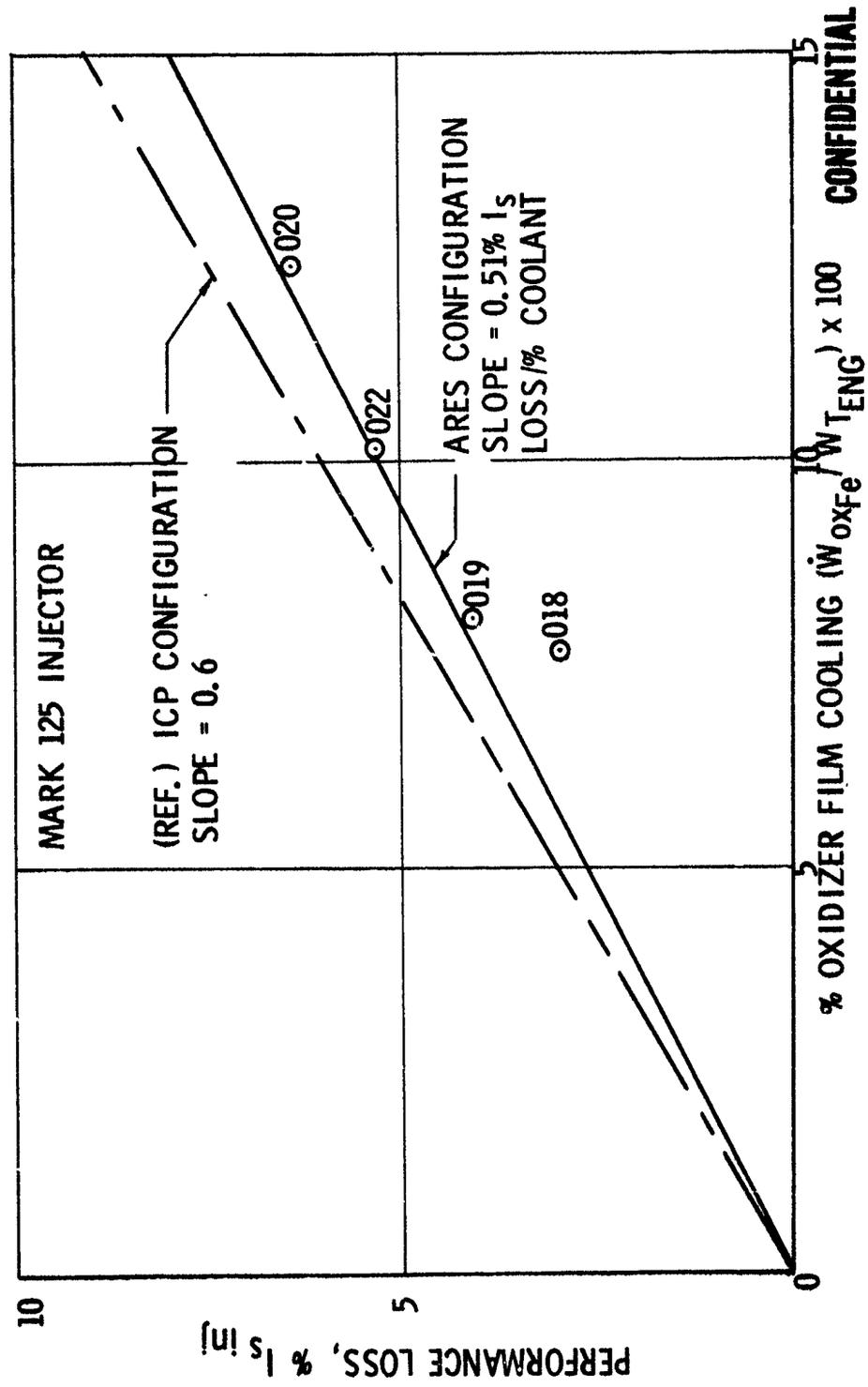

Effect of Oxidizer Film Coolant on the Performance of the ARES Thrust Chamber (u)

Figure VI-40

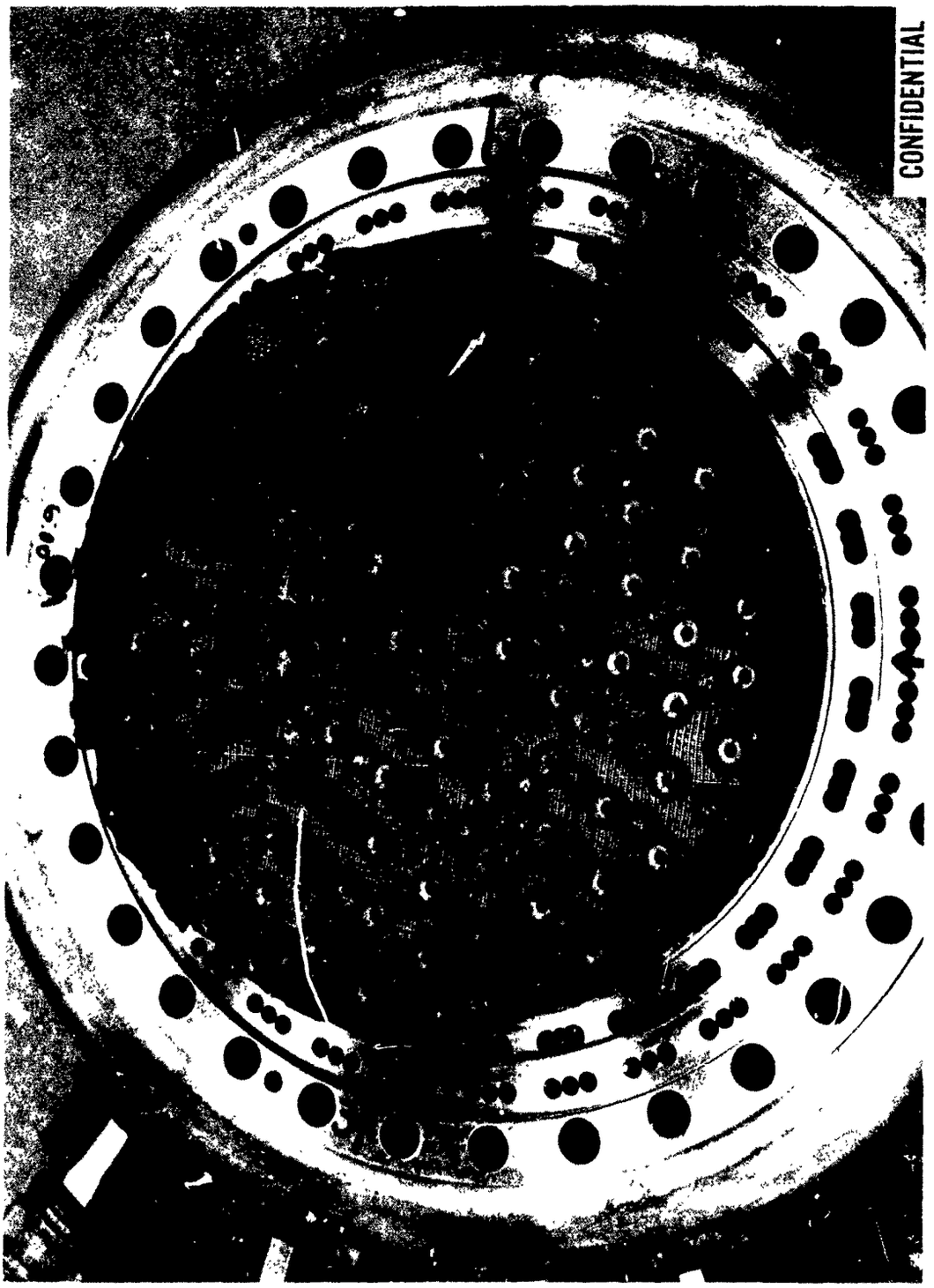

Modified Rake Injector (u)

Figure VI-41

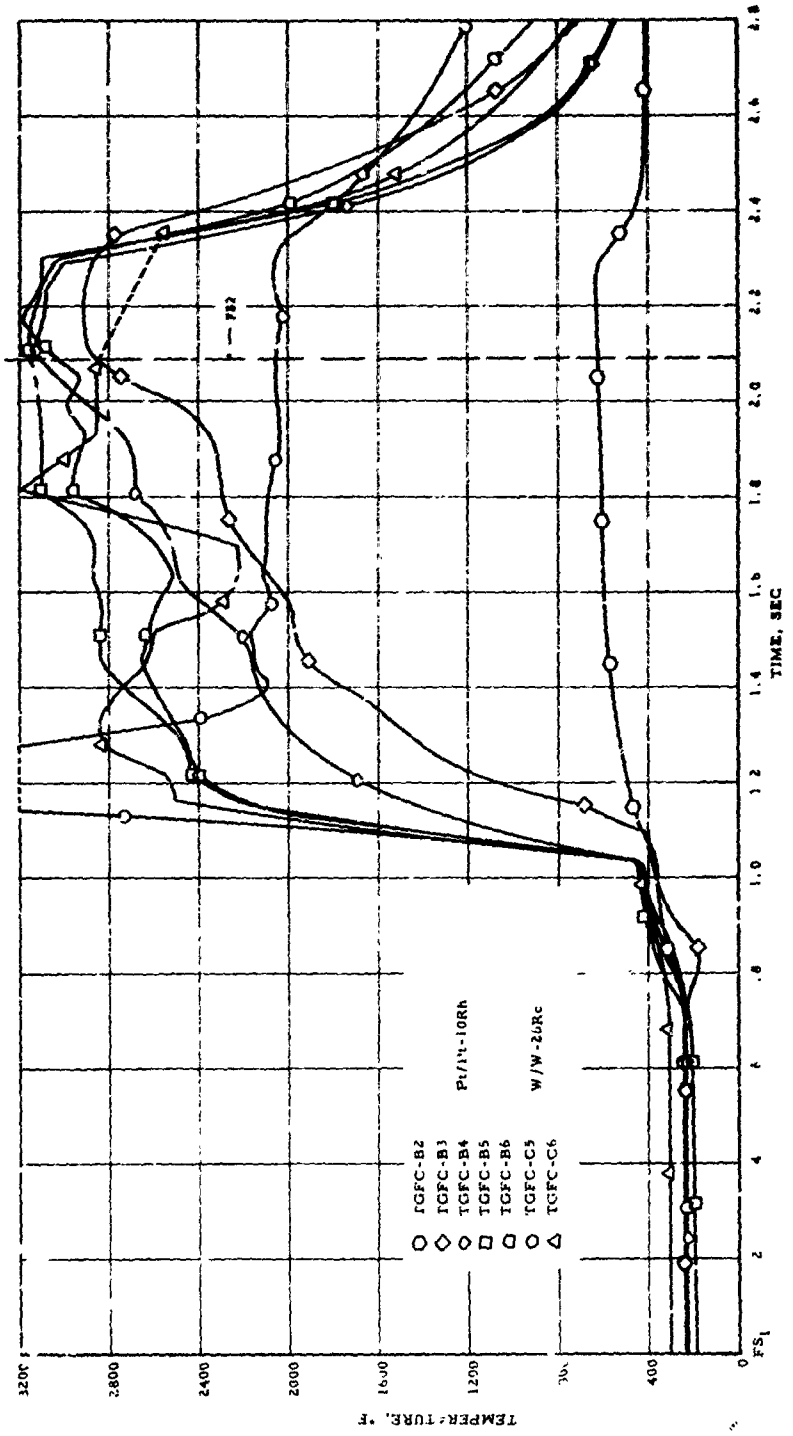

Thermocouple Data for Test 1.2-11-WAM-018

Figure VI-42

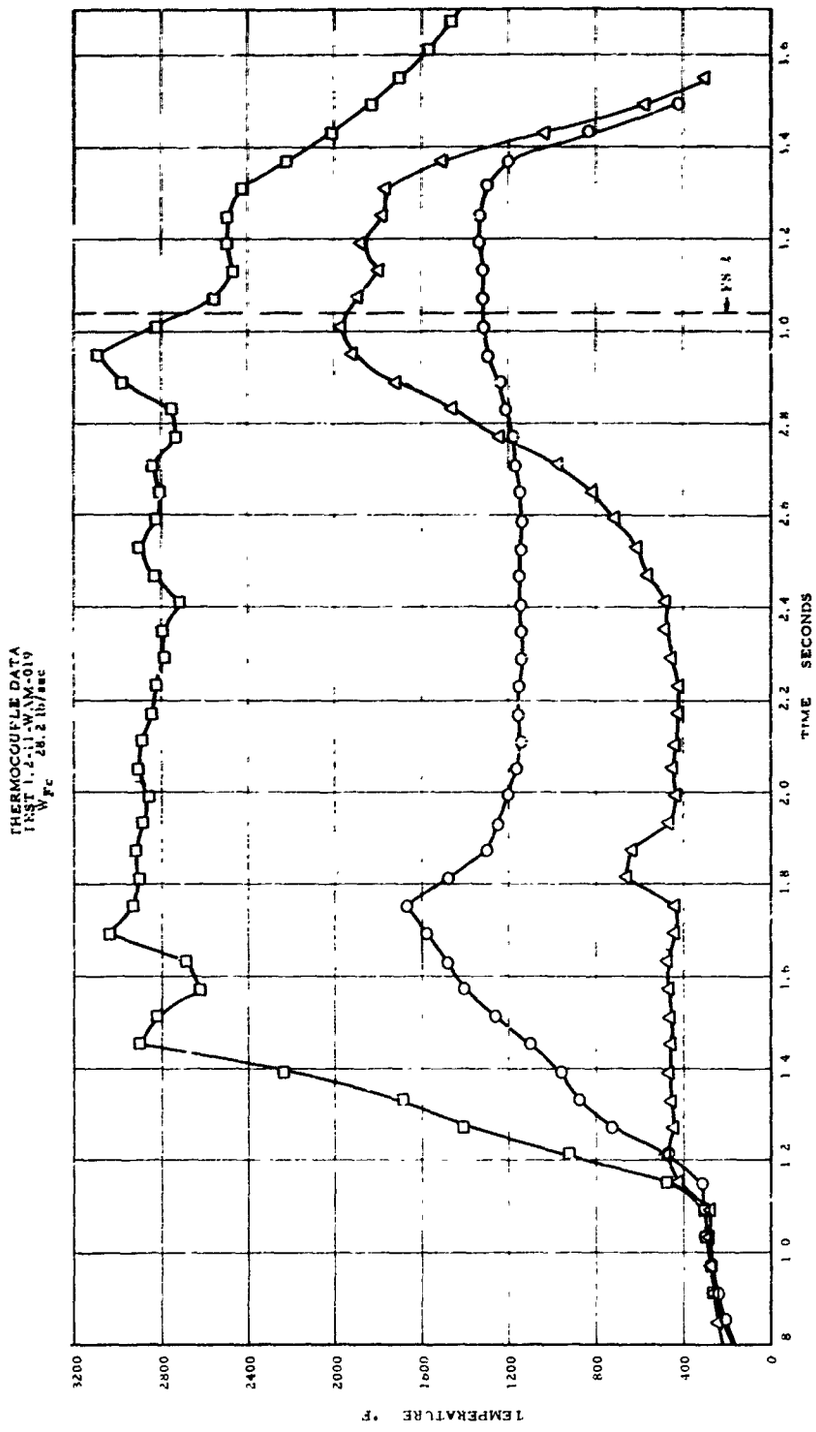

Thermocouple Data for Test 1.2-11-WAM-019

Figure VJ-43

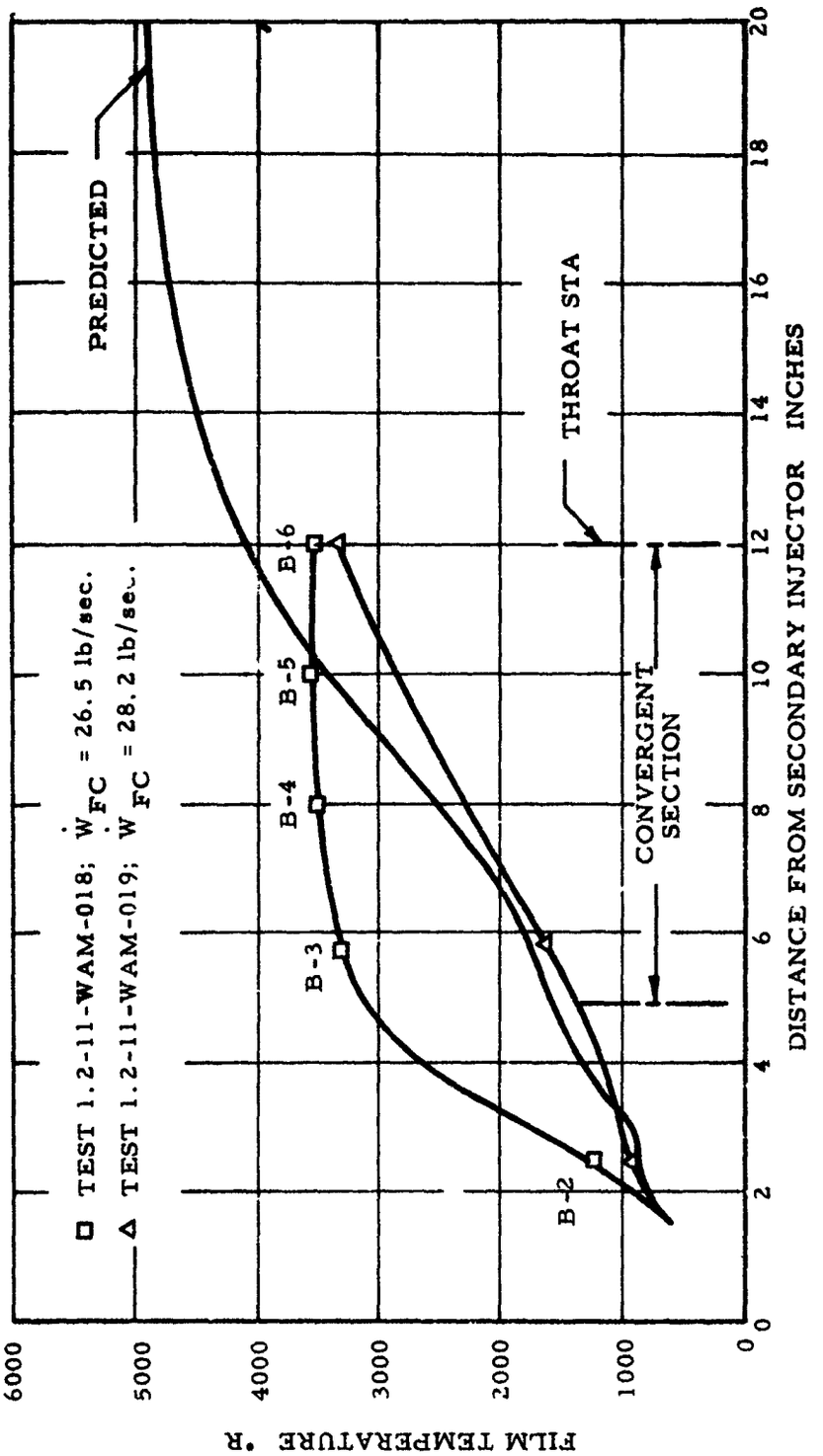

Film Temperatures for Test 1.2-11-WAM-018

Figure VI-44

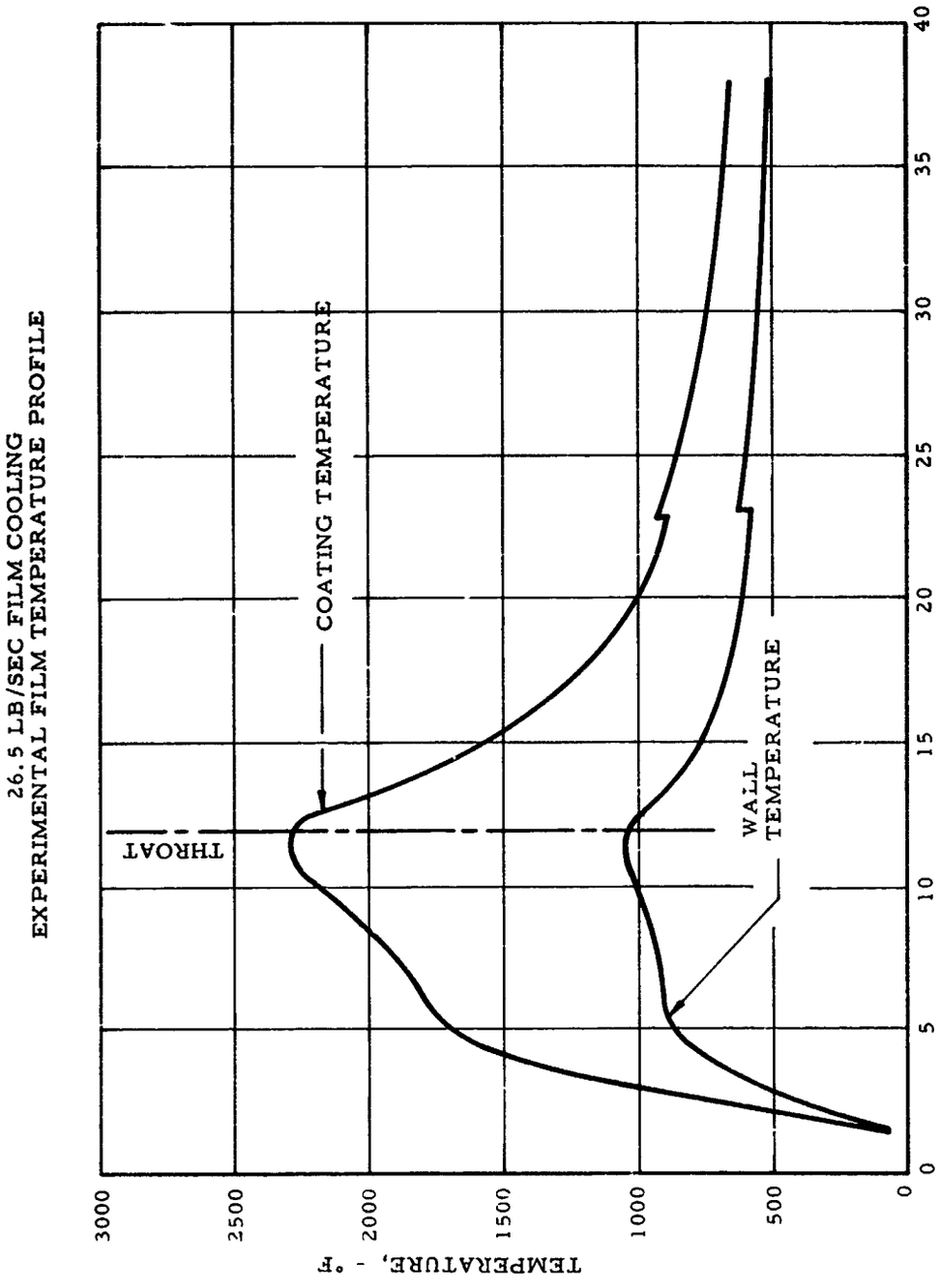

Cooled Chamber Predicted Temperatures

Figure VI-45

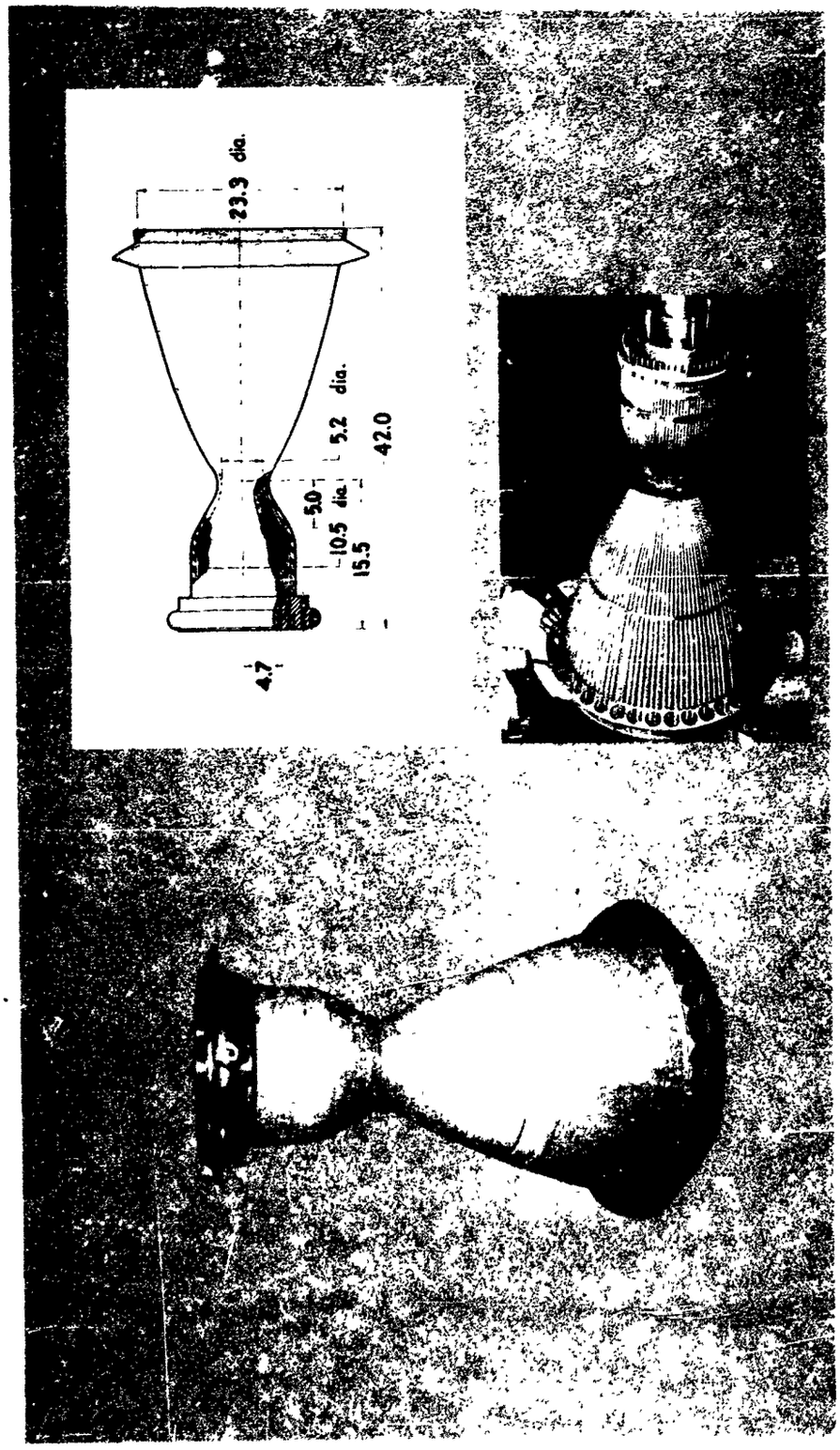

Regeneratively Cooled Combustion Chamber

Figure VI-46

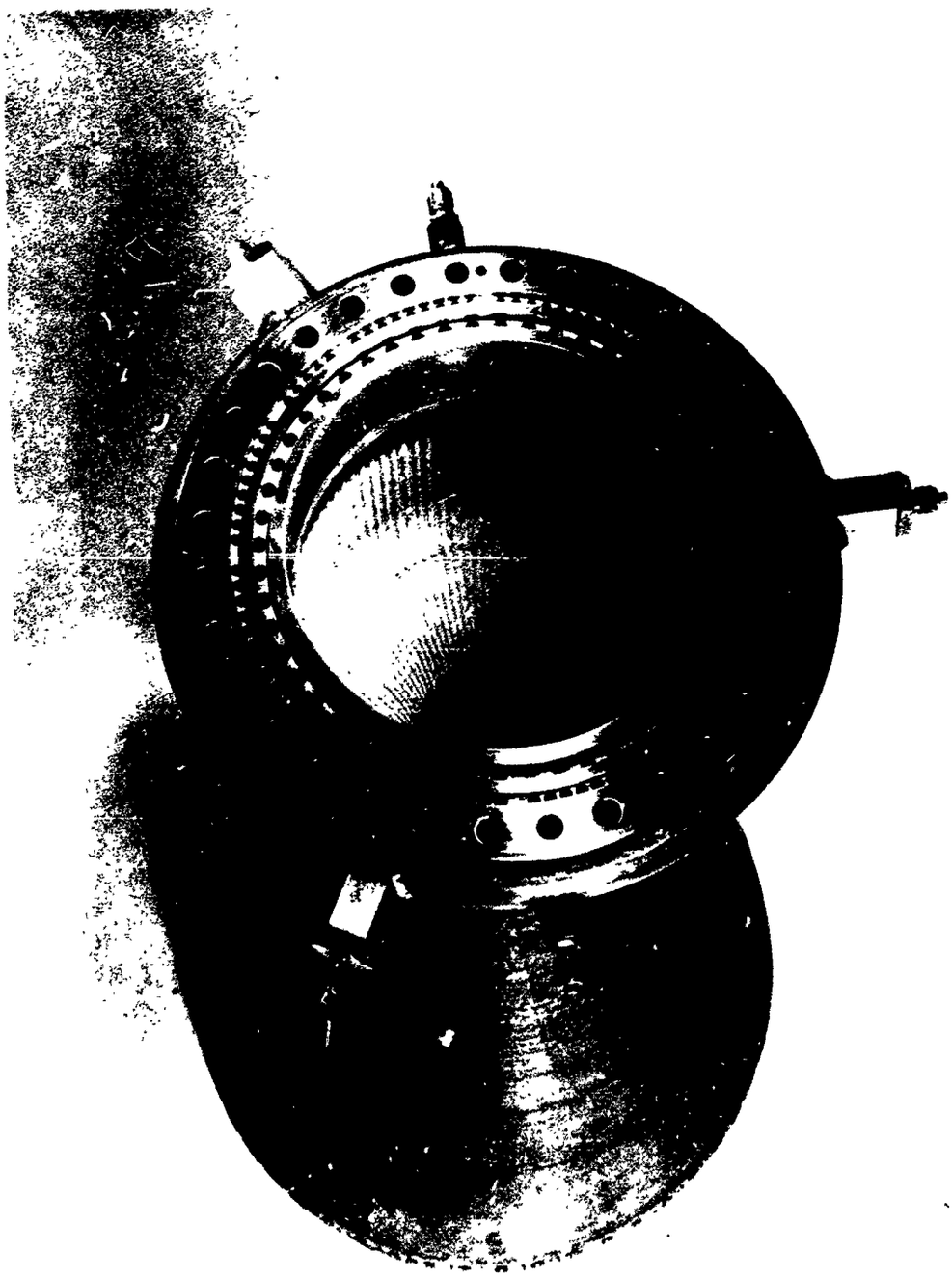

Regeneratively Cooled Combustion Chamber

Figure VI-47

REGEN. CHAMBERS S/N's 3, 4, & 5
(CAPILLARY TUBE CONE)

CONFIGURATION
104 EA. .028 IN. DIA CHAMBER COOLANT HOLES
104 EA. CAPILLARY TUBES
104 EA. .028 IN. DIA SHROUD COOLANT HOLES

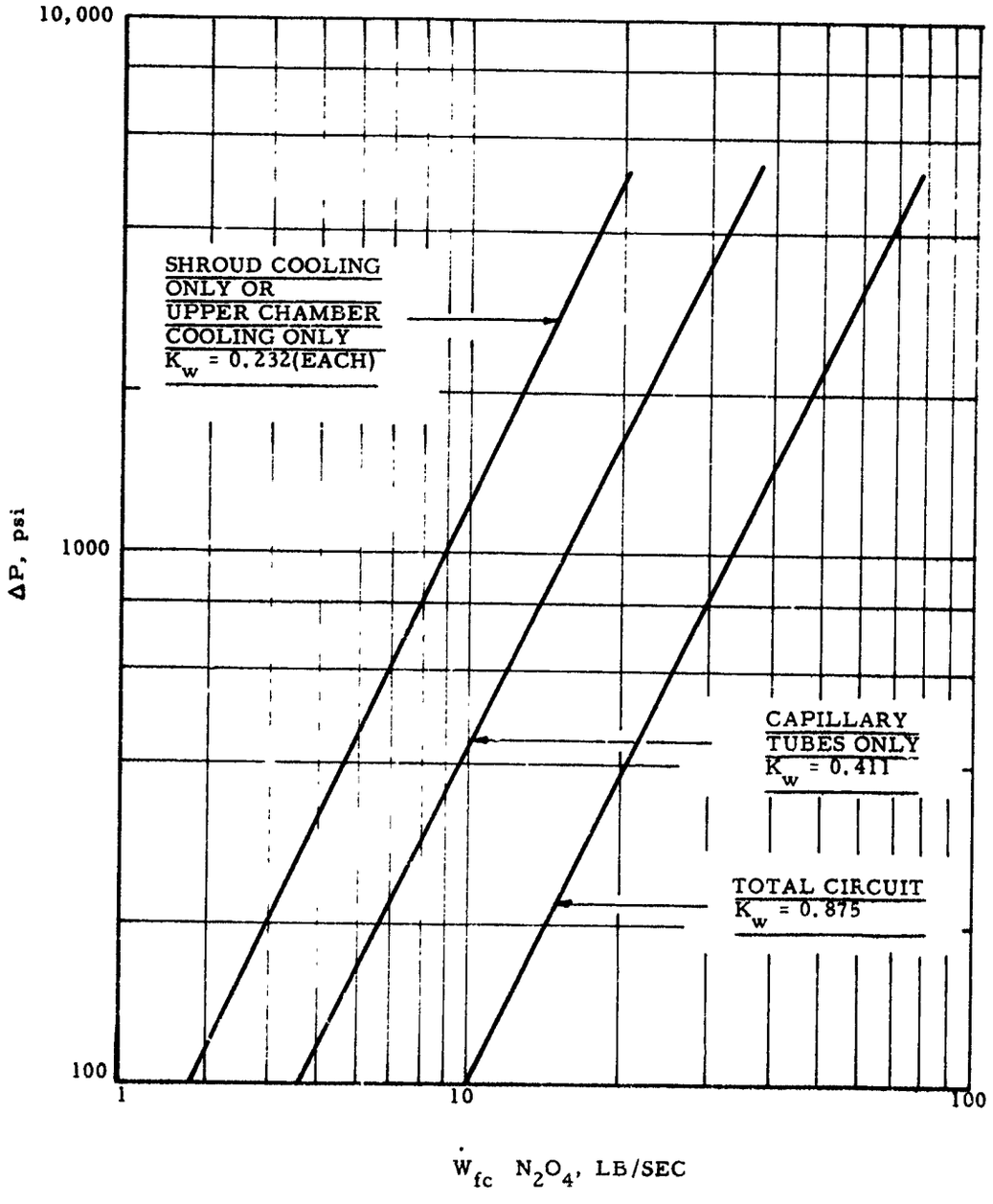

Flow Characteristics of Capillary Regenerative Chambers

Figure VI-48

Report 10830-F-1, Phase I

REGEN. CHAMBERS S/N's 1, 2, & 6
(NON-CAPILLARY TUBE)

CONFIGURATION
208 EA. .028 IN. DIA CHAMBER COOLANT HOLES
104 EA. .028 IN. DIA SHROUD COOLANT HOLES

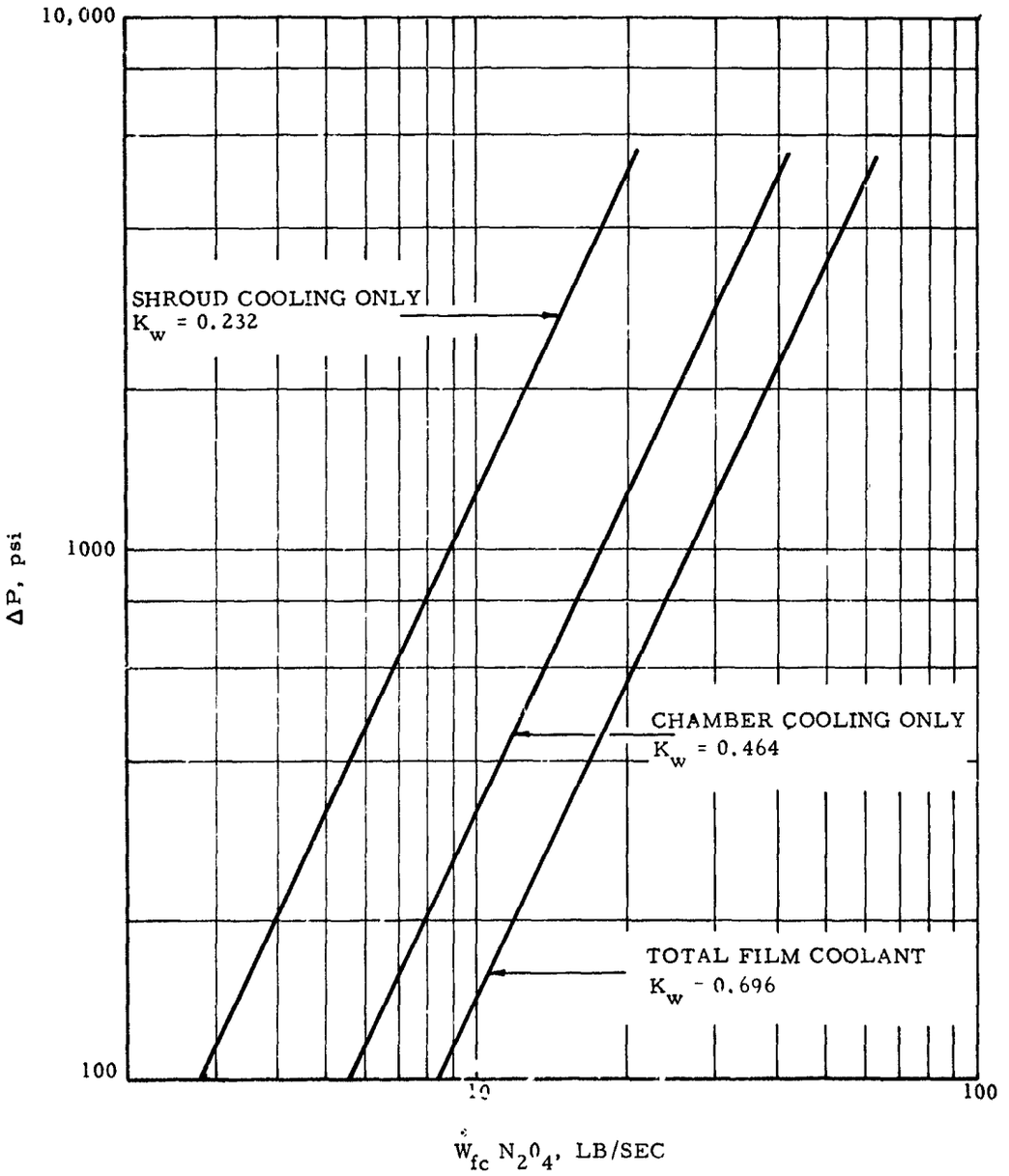

Flow Characteristics of Noncapillary Regenerative Chambers

Figure VI-49

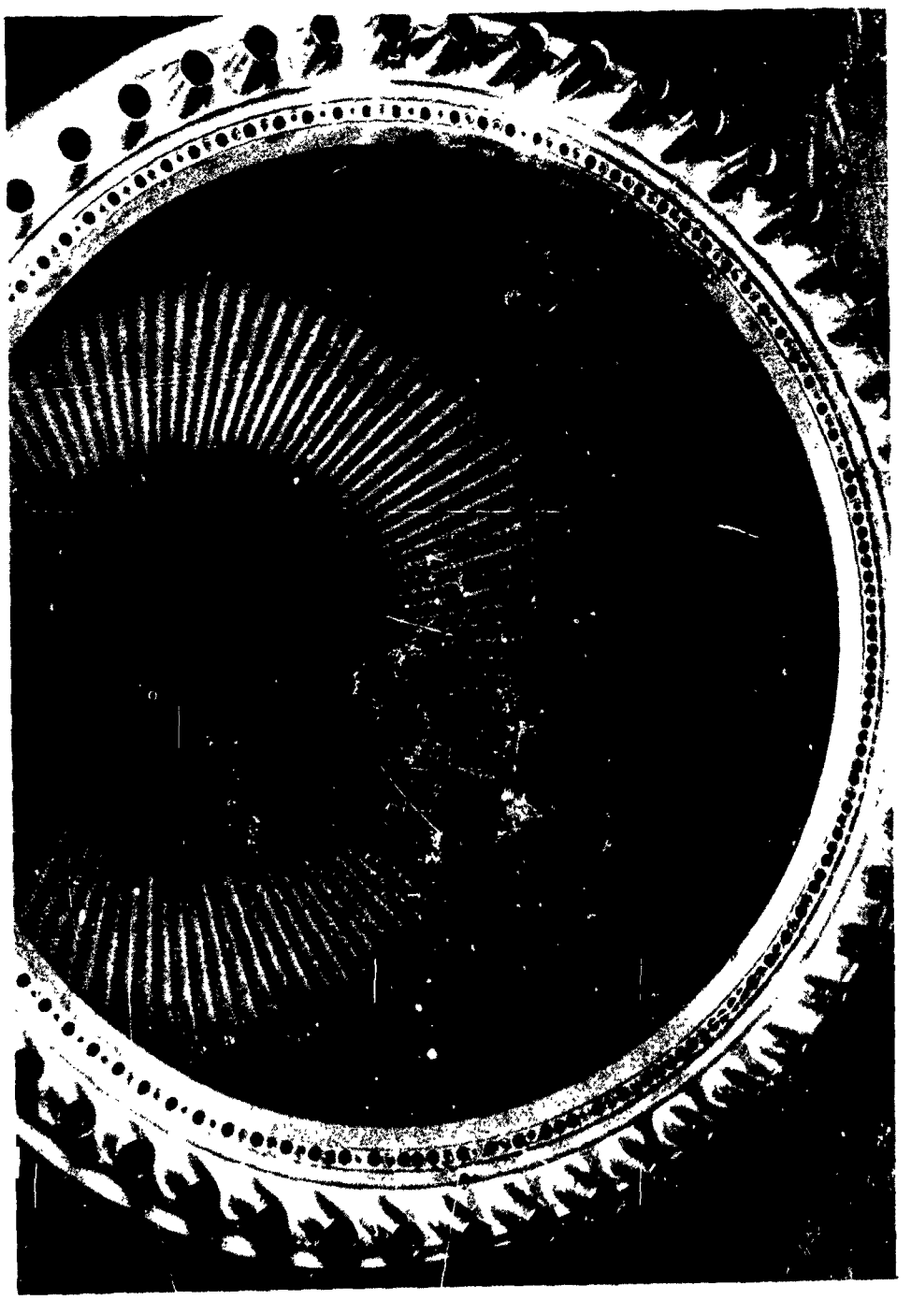

Capillary Tube Installation

Figure VI-5

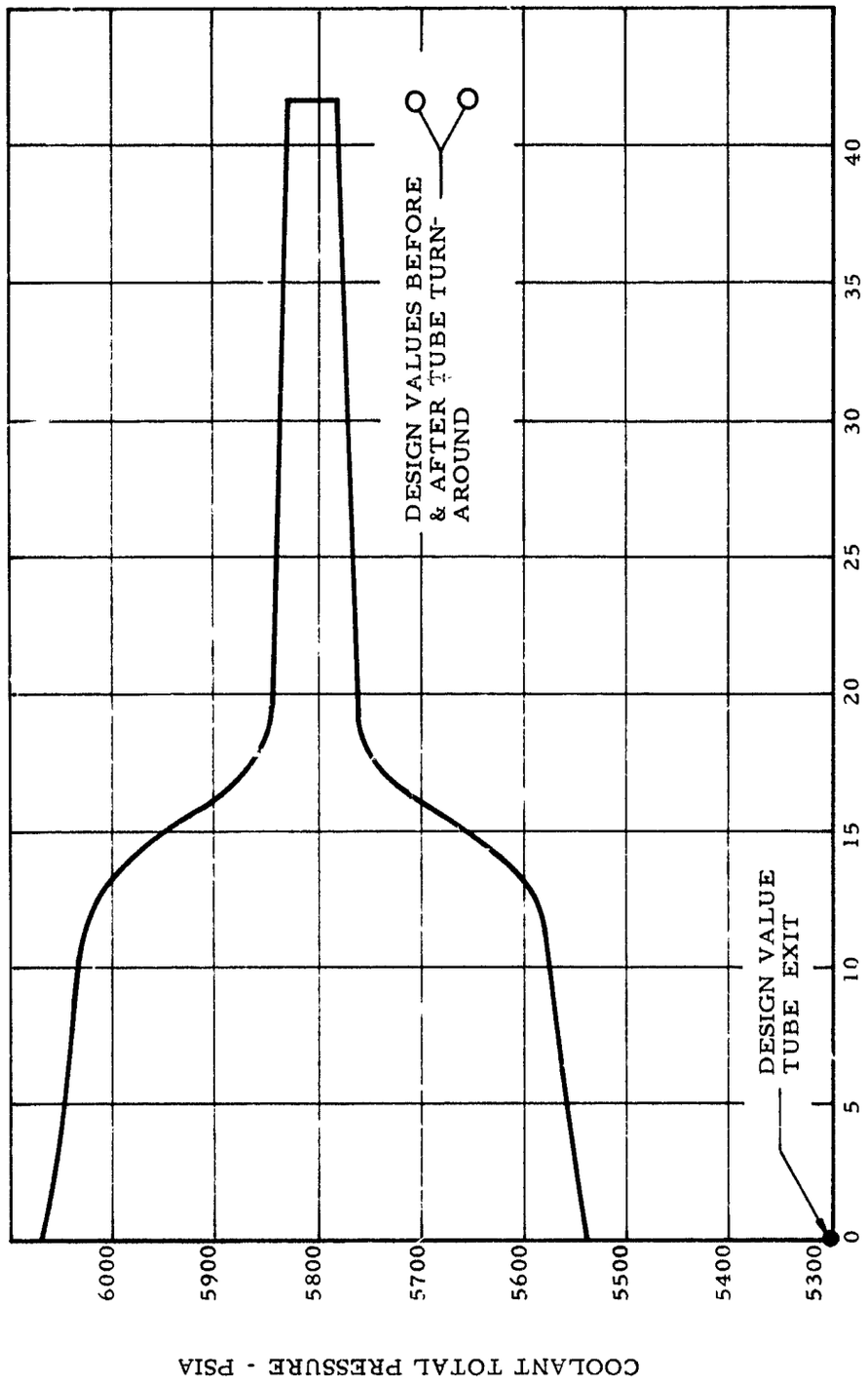

Total Pressure Distribution for ARES Regenerative Chambers

Figure VI-51

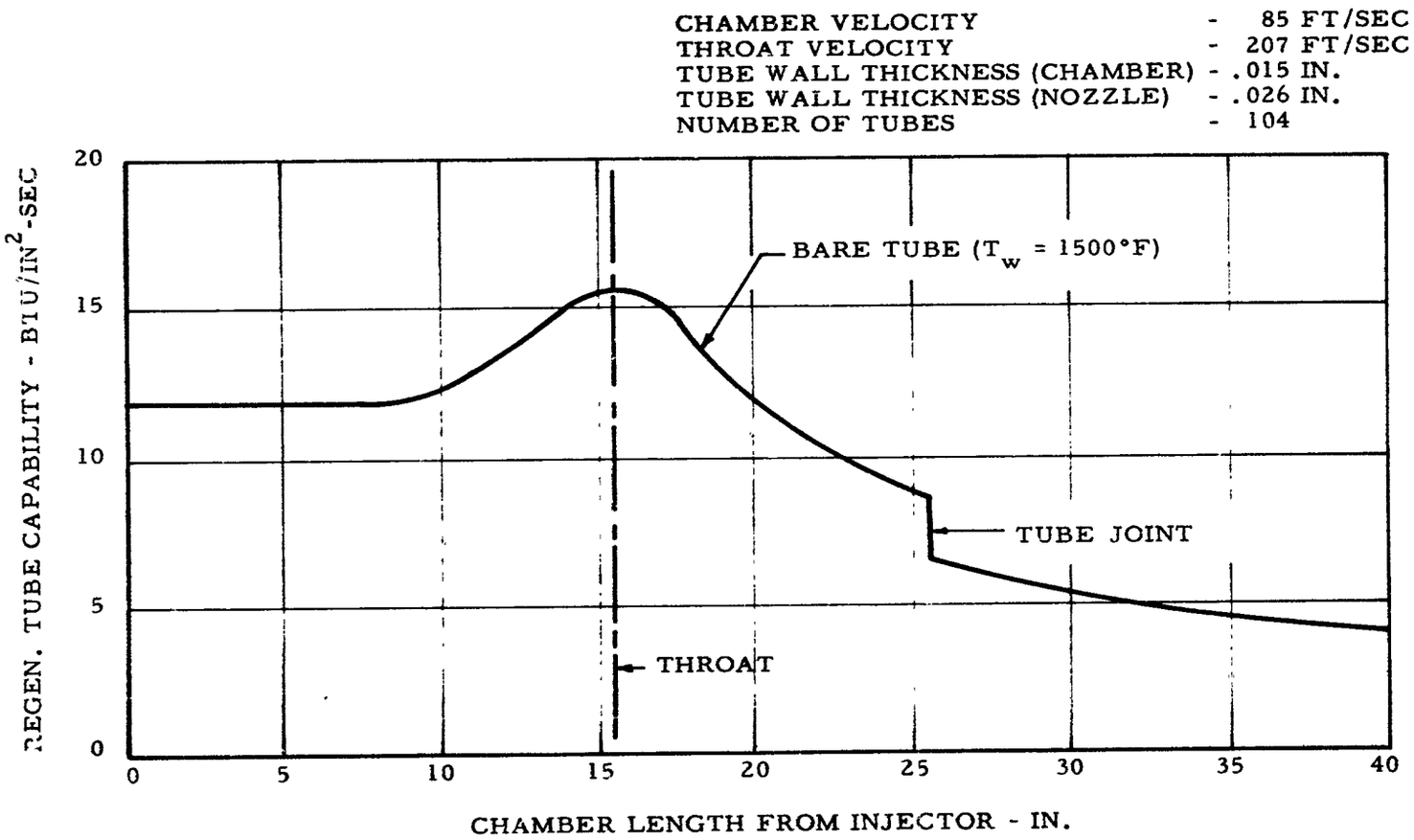

Figure VI-52

Regenerative Coolant Capability

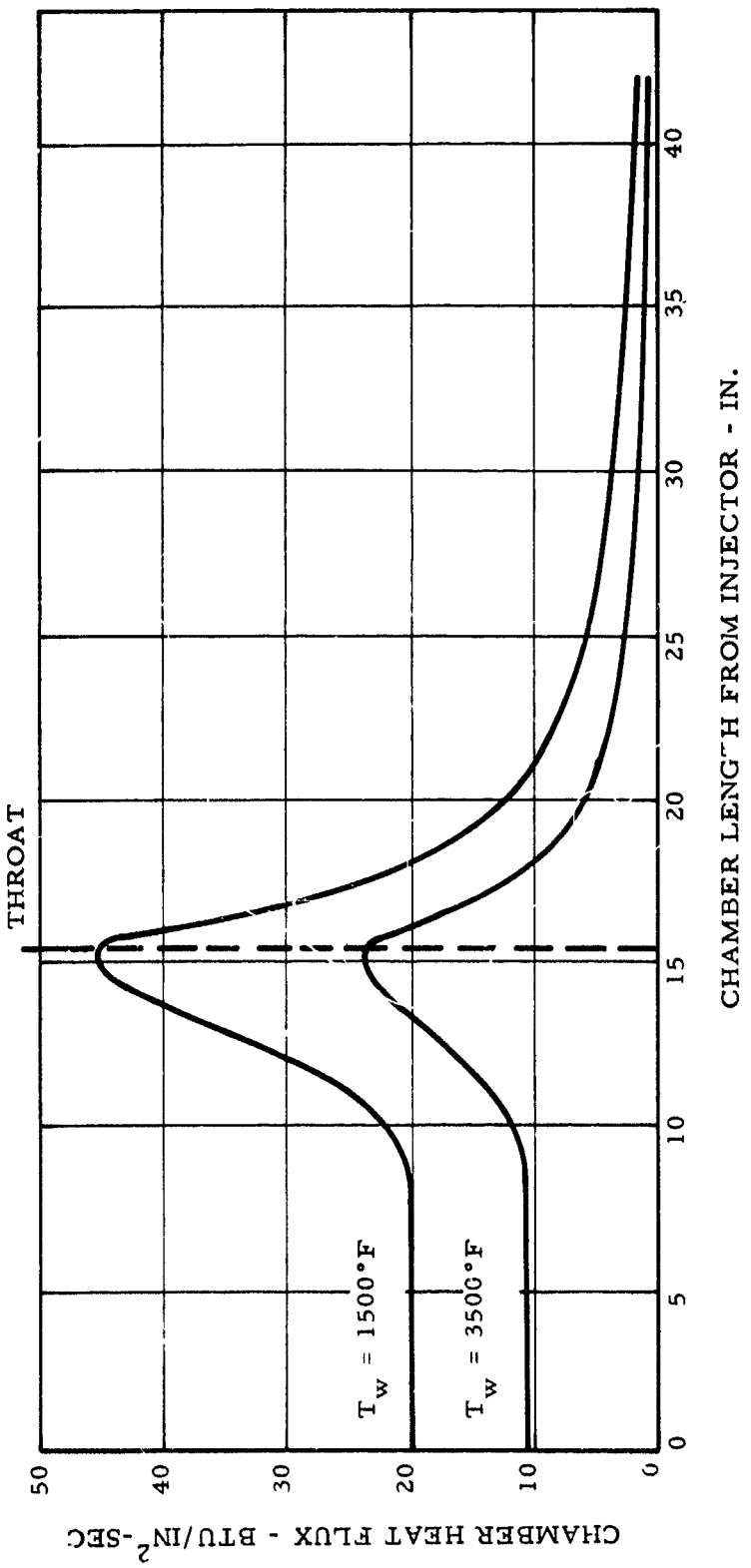

ARES Chamber Heat Load

Figure VI-53

REGEN. CHAMBERS S/N's 3, 4, & 5
(CAPILLARY TUBE CONE)

CONFIGURATION
104 EA. .028 IN. DIA CHAMBER COOLANT HOLES
104 EA. CAPILLARY TUBES
104 EA. .028 IN. DIA SHROUD COOLANT HOLES

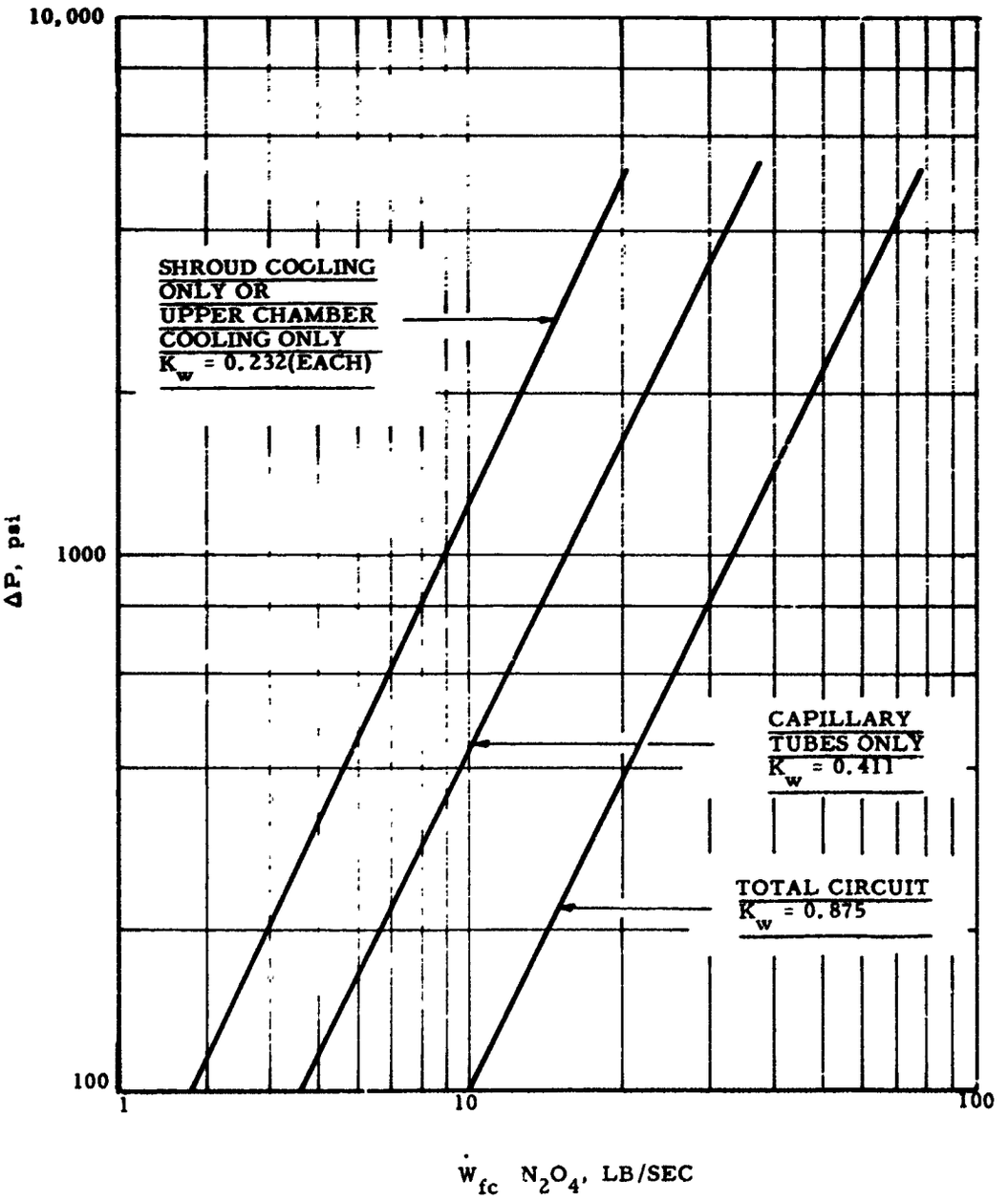

Flow Characteristics of Capillary Regenerative Chambers

Figure VI-48

REGEN. CHAMBERS S/N's 1, 2, & 6
(NON-CAPILLARY TUBE)

CONFIGURATION
208 EA. .028 IN. DIA CHAMBER COOLANT HOLES
104 EA. .028 IN. DIA SHROUD COOLANT HOLES

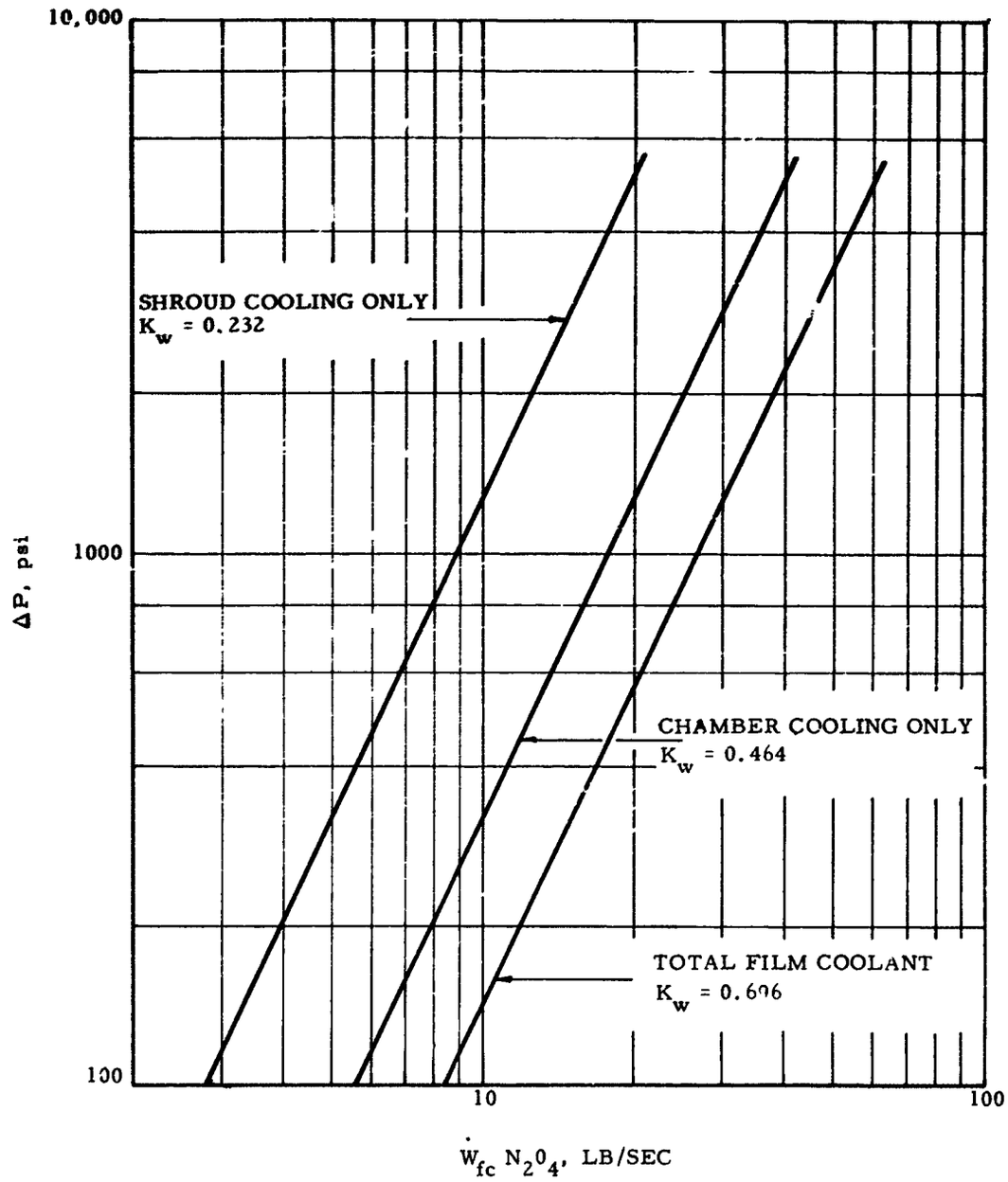

Flow Characteristics of Noncapillary Regenerative Chambers

Figure VI-49

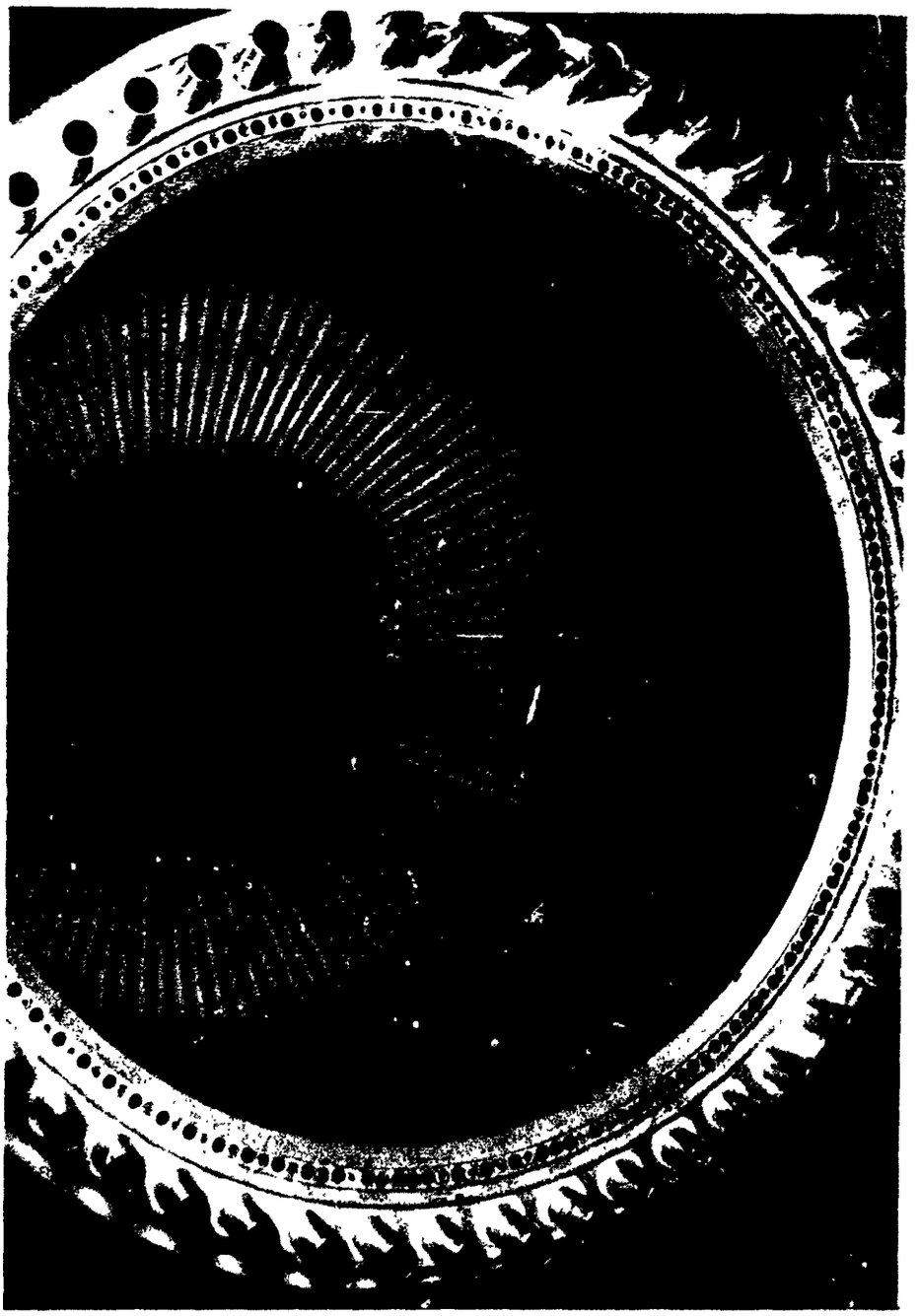

Capillary Tube Installation

Figure VI-50

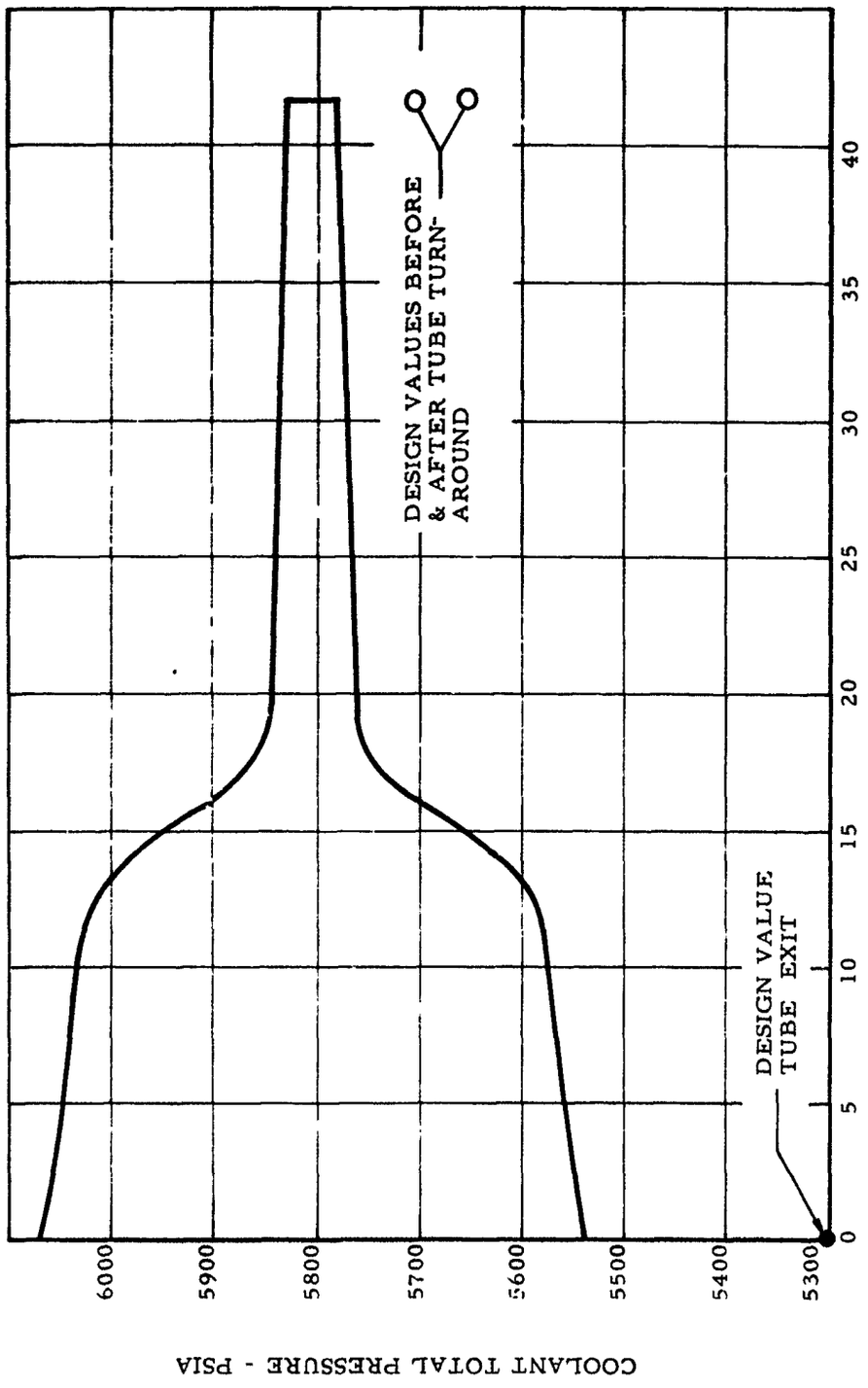

Total Pressure Distribution for ARES Regenerative Chambers

Figure VI-51

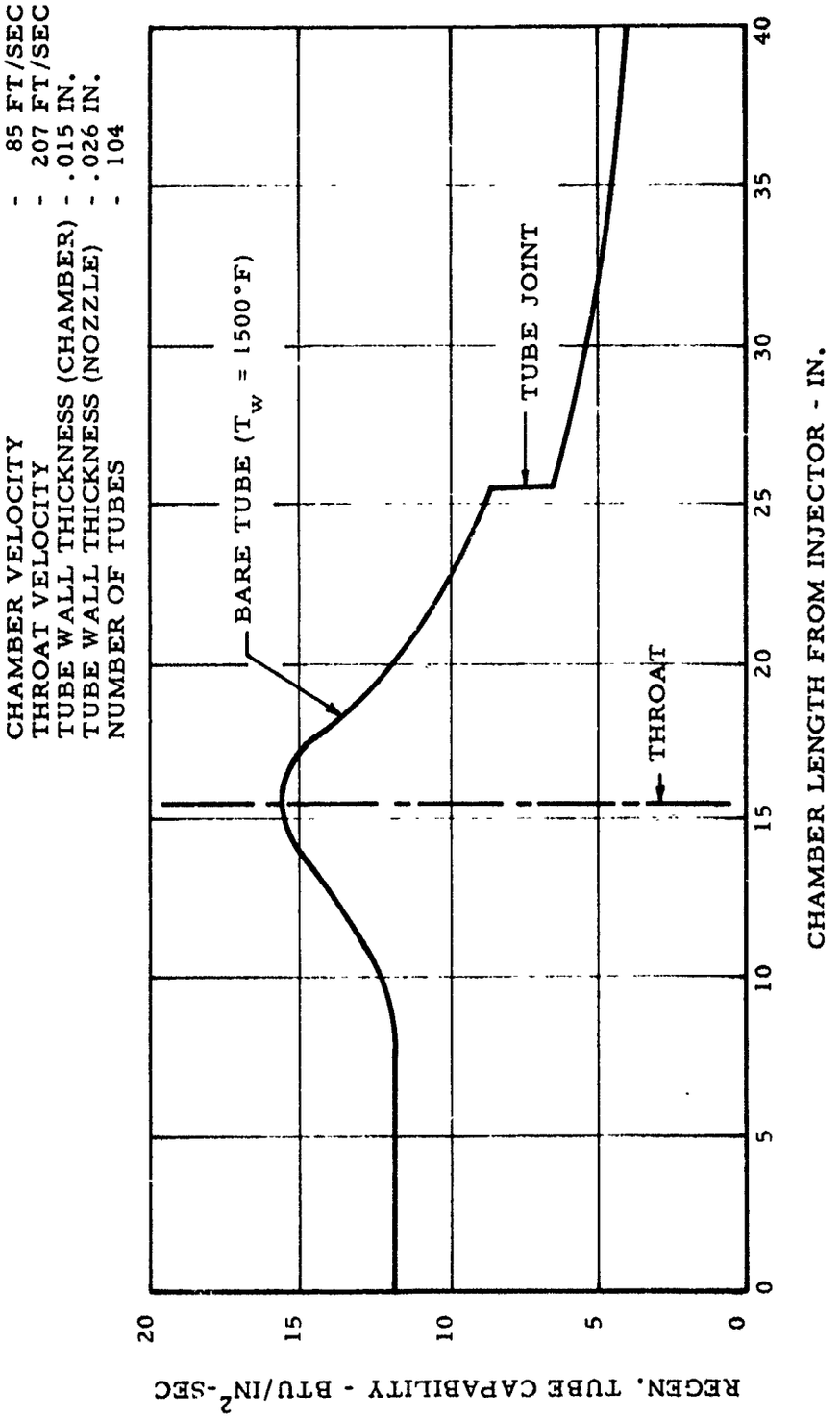

Regenerative Coolant Capability

Figure VI-52

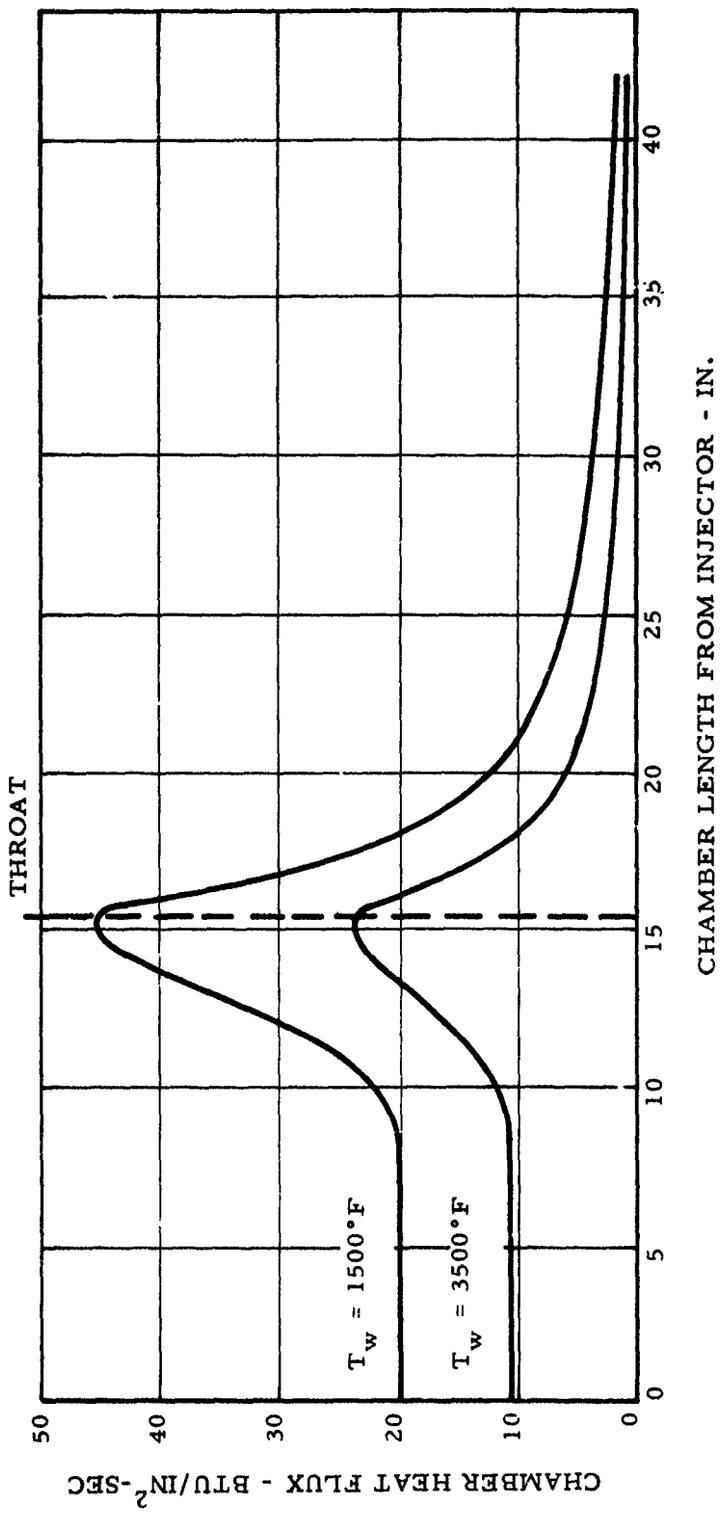

ARES Chamber Heat Load

Figure VI-53

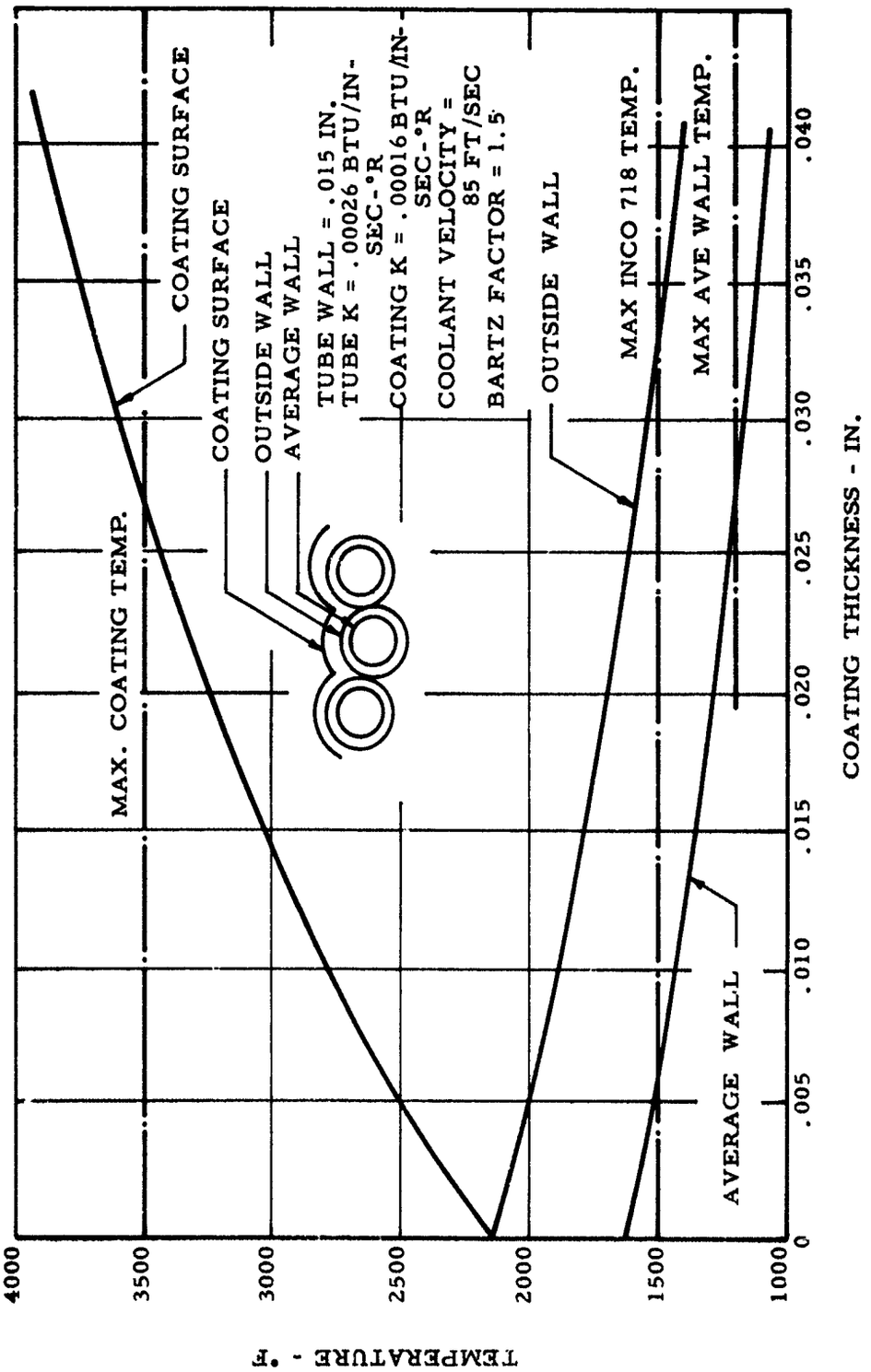

ARES Chamber Wall Temperatures

Figure VI-54

	Uncoated			Tungsten Coated		
Surface Temperature Limits, °F						
Outside tube wall		1500			1500	
Coating surface					3500	
Characteristic Length (L*), in.	17.4	30	50	17.4	30	50
Minimum Film-Cooling Requirements, lb/sec						
Single-point injection	20.6	31.0	46.0	7.2	10.7	16.2
Two-point injection	14.0	17.9	21.0	5.4	5.8	8.4
Injector face plane	4.0	6.1	6.4	2.4	2.4	4.2
Capillary tubes (unheated)	10.0	11.8	14.6	3.0	3.4	4.2

Film-Cooling Requirements for ARES Chambers

Figure VI-55

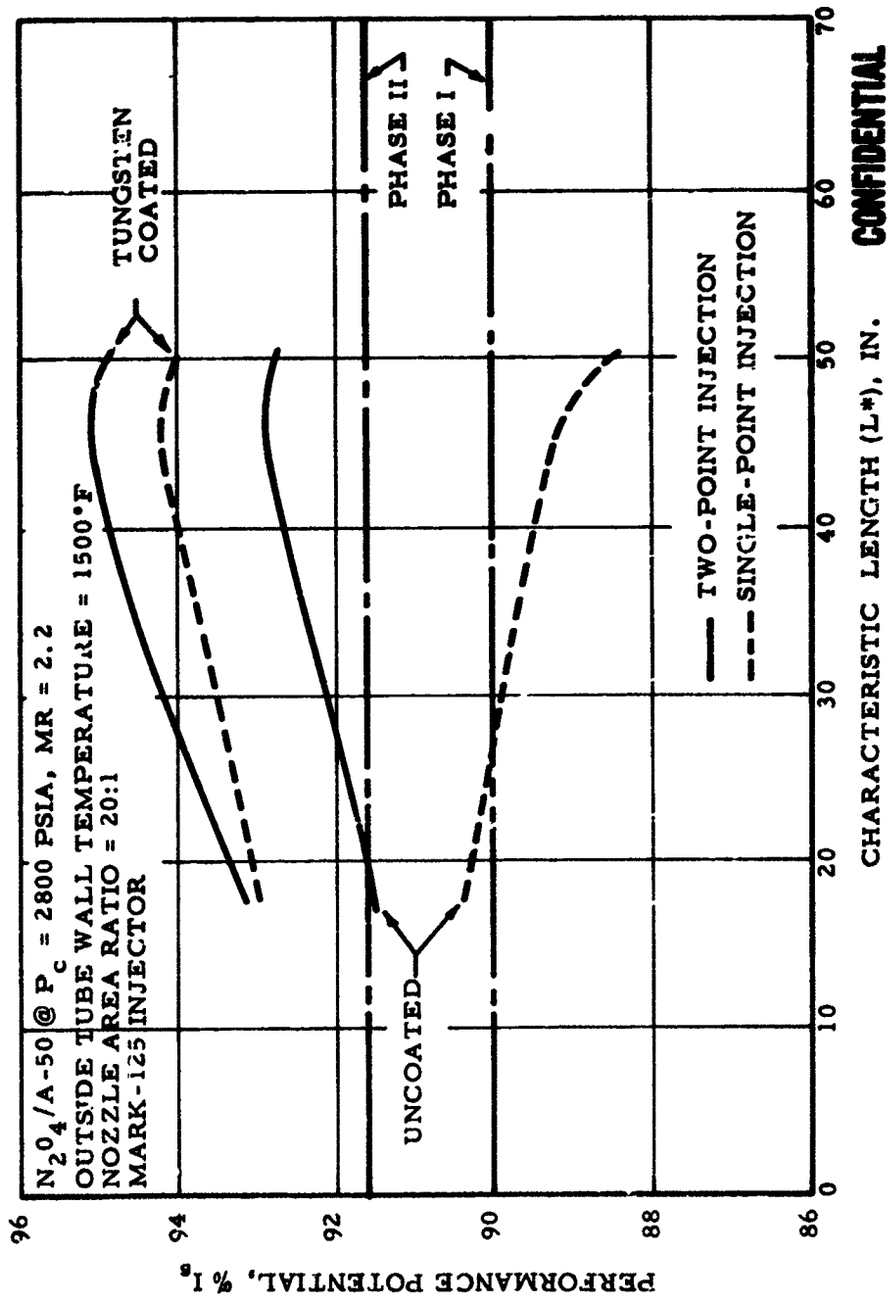

Performance Potential in ARES Chambers (u)

Figure VI-56

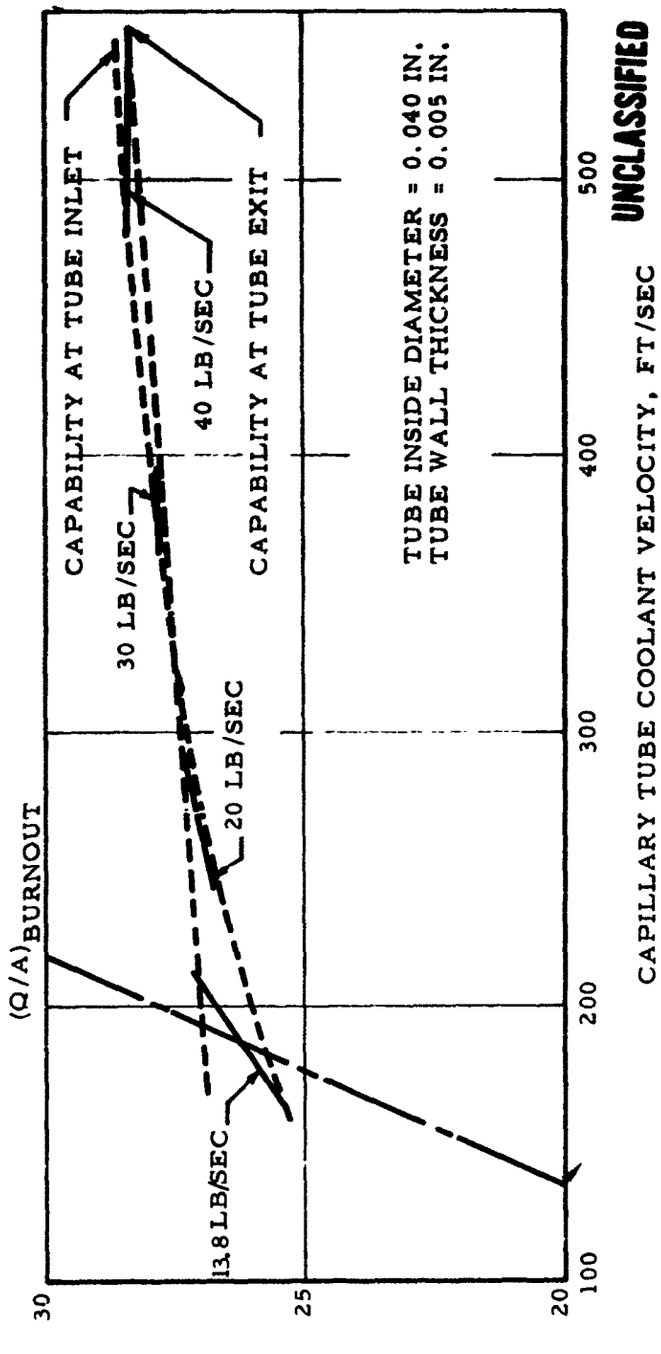

Uncoated .040-in. Capillary Tube Heat Flux Capability

Figure VI-57

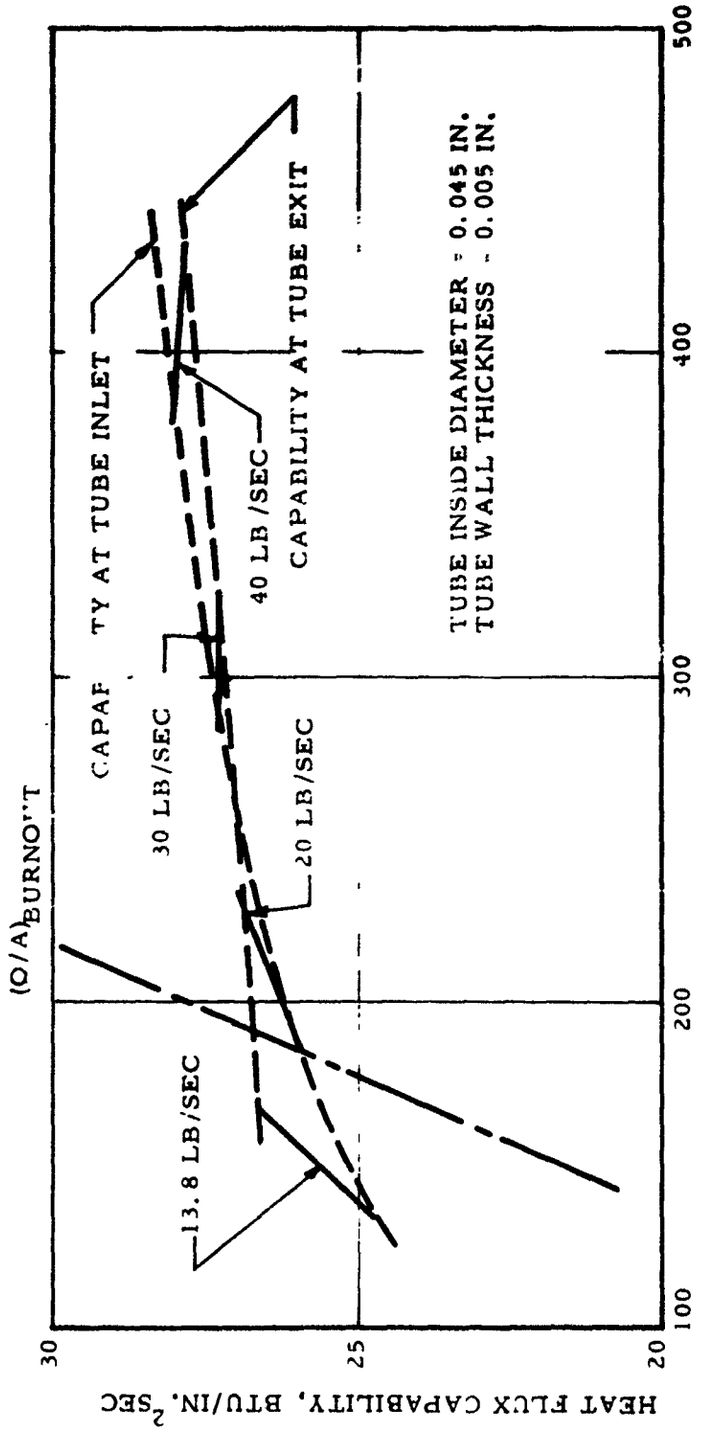

Uncoated .045-in. Capillary Tube Heat Flux Capability

Figure VI-58

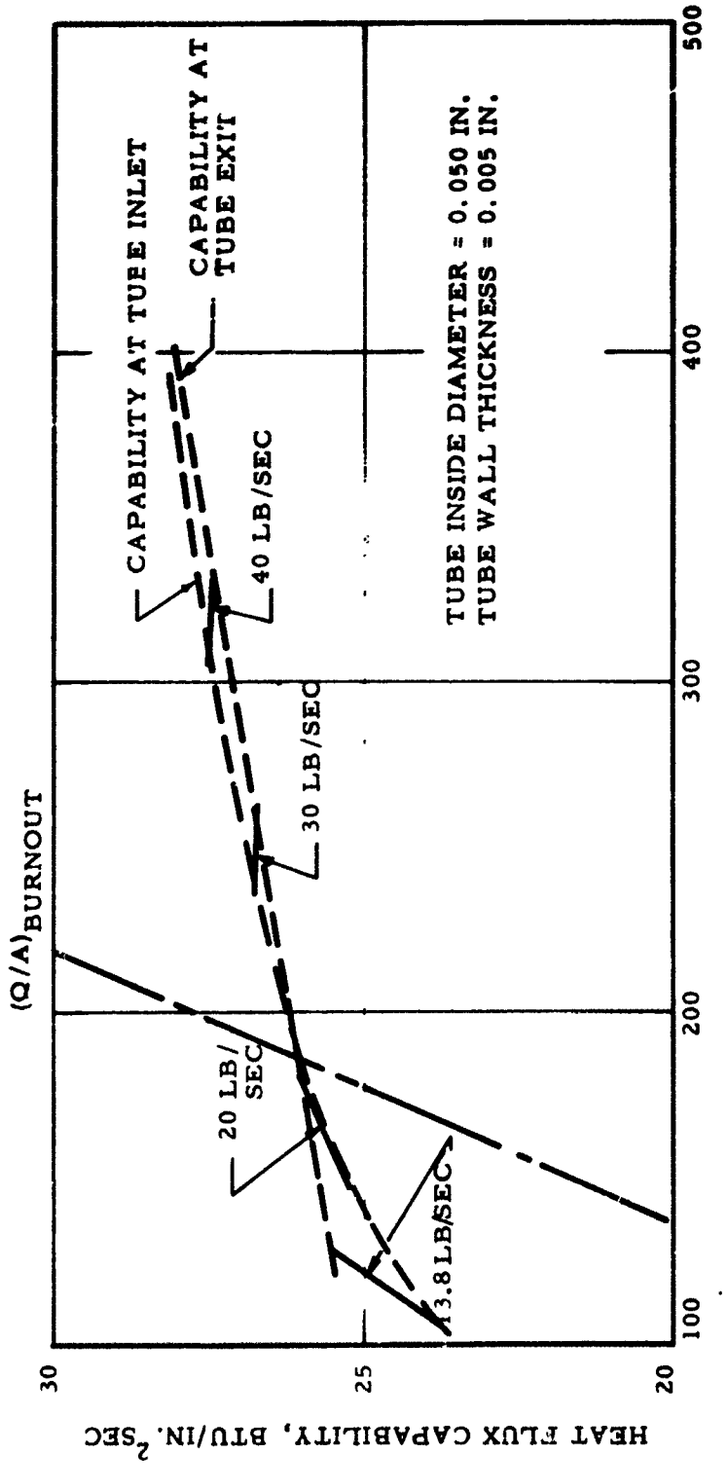

Uncoated .050-in. Capillary Tube Heat Flux Capability

Figure VI-59

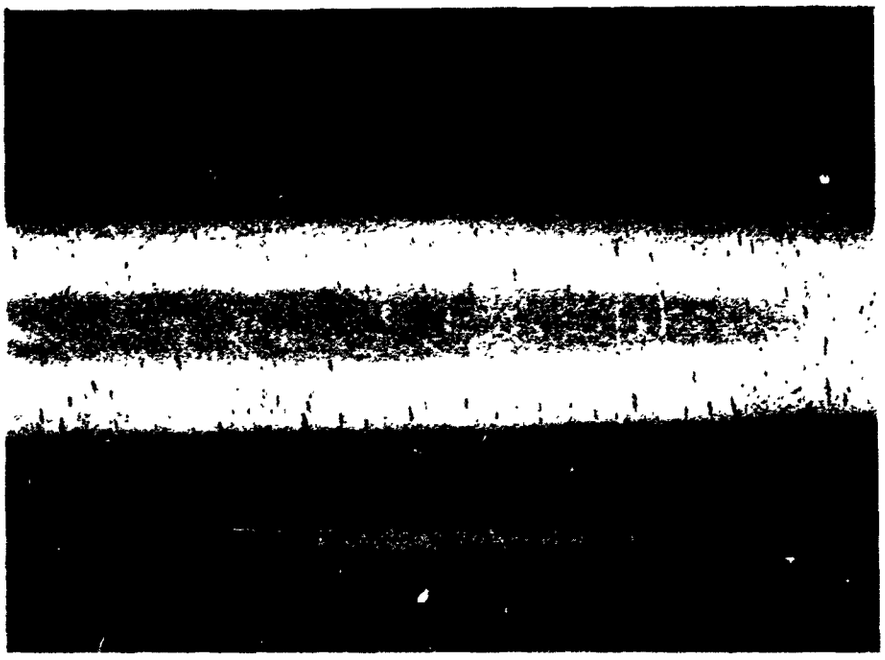

Tubing .488 O.D.X 0.015 Wall Inconel 718-Typical Defect 10X

Section View Above Tube - 100X

Typical Inconel 718 Tubing Defect

Figure VI-60

Tubing .778 O.D.X. 026 Wall Inconel 718-Typical Defect 3X

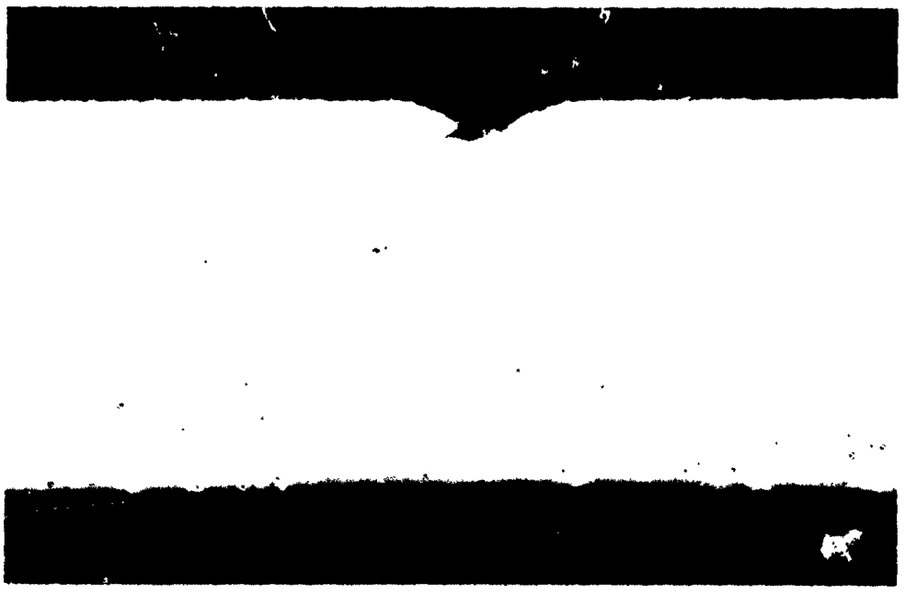

Section View-Above Defect 100X

Typical Inconel 718 Tubing Defect

Figure VI-61

WALL MATERIAL	ADVANTAGE	DISADVANTAGE
1. WOVEN METAL CLOTH (REGIMESH)	1. UNIFORM POROSITY	1. MUST BE FABRICATED IN CONICAL AND CYLINDRICAL SHAPES AND WELDED. 2. DOES NOT HAVE UNIDIRECTIONAL RADIAL FLOW. 3. DOES NOT HAVE LARGE PERMEABILITY VARIATION OVER SHORT DISTANCE.
2. WOUND WIRE (POROLOY)	1. UNIFORM POROSITY	1. CAN BE CONSTRUCTED IN ONLY LIMITED SHAPES. 2. DOES NOT HAVE UNIDIRECTIONAL RADIAL FLOW. 3. DOES NOT HAVE LARGE PERMEABILITY VARIATION OVER SHORT DISTANCE.
3. POWERED SINTERED METAL	1. CAN BE FABRICATED TO DESIRED GEOMETRICAL SHAPE.	1. UNIFORM POROSITY IS NOT ALWAYS ACHIEVED. 2. DOES NOT HAVE UNIDIRECTIONAL RADIAL FLOW. 3. DOES NOT HAVE LARGE PERMEABILITY VARIATION OVER SHORT DISTANCE.
4. SINTERED-FELTED SHORT METAL FIBERS.		
5. SINTERED FOAM METALS		
6. PHOTO-ETCHED WASHERS	1. CONTROLLED POROSITY 2. ACCURATE FLOW DISTRIBUTION 3. PERMEABILITY ONLY IN RADIAL FLOW DIRECTION. 4. FLEXIBILITY IN CHOICE OF MATERIALS, FLOW PATTERNS AND WASHER THICKNESS. 5. CAPABILITY OF REPLACING INDIVIDUAL WASHERS OR WASHER SECTIONS.	1. WEIGHT 2. INITIAL COST WILL BE HIGH. 3. CLOSE TOLERANCES COMPLICATE FABRICATION.

Selection of Transpiration Chamber Wall Material

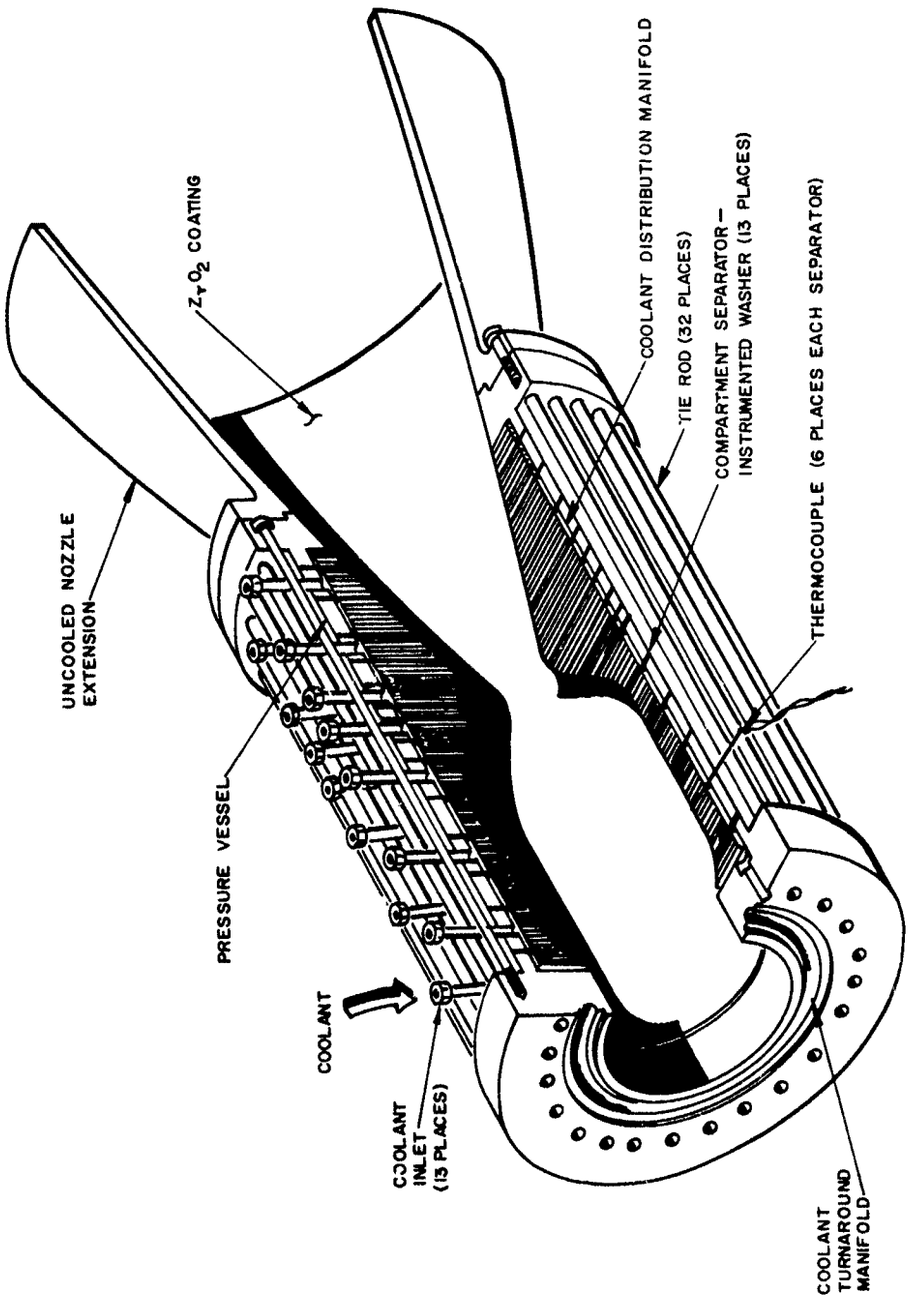

Transpiration-Cooled Combustion Chamber

Figure VI-63

Transpiration-Cooled Combustion Chamber

Figure VI-64

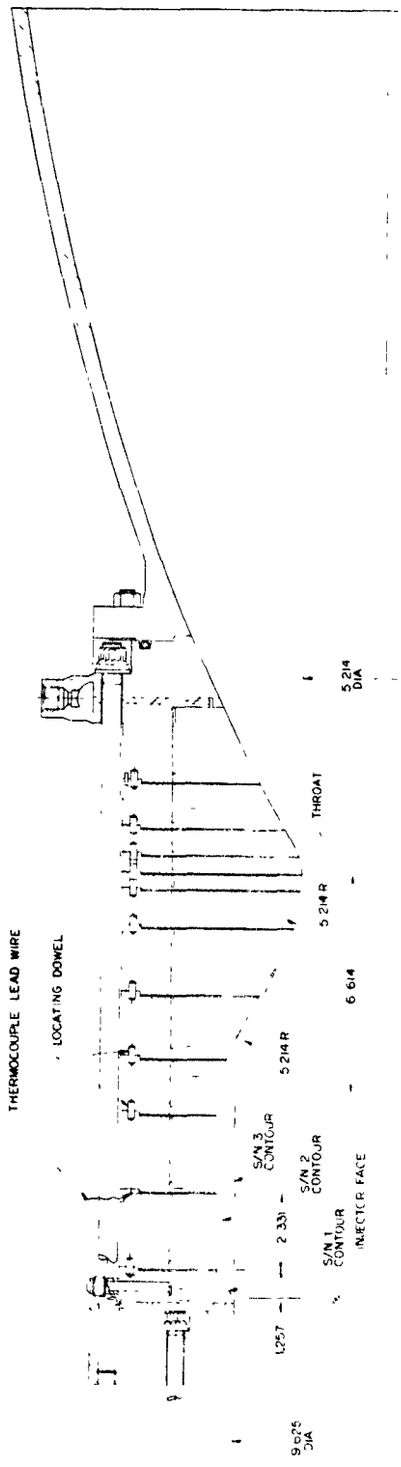

Layout of Transpiration-Cooled Chamber

Figure VI-65

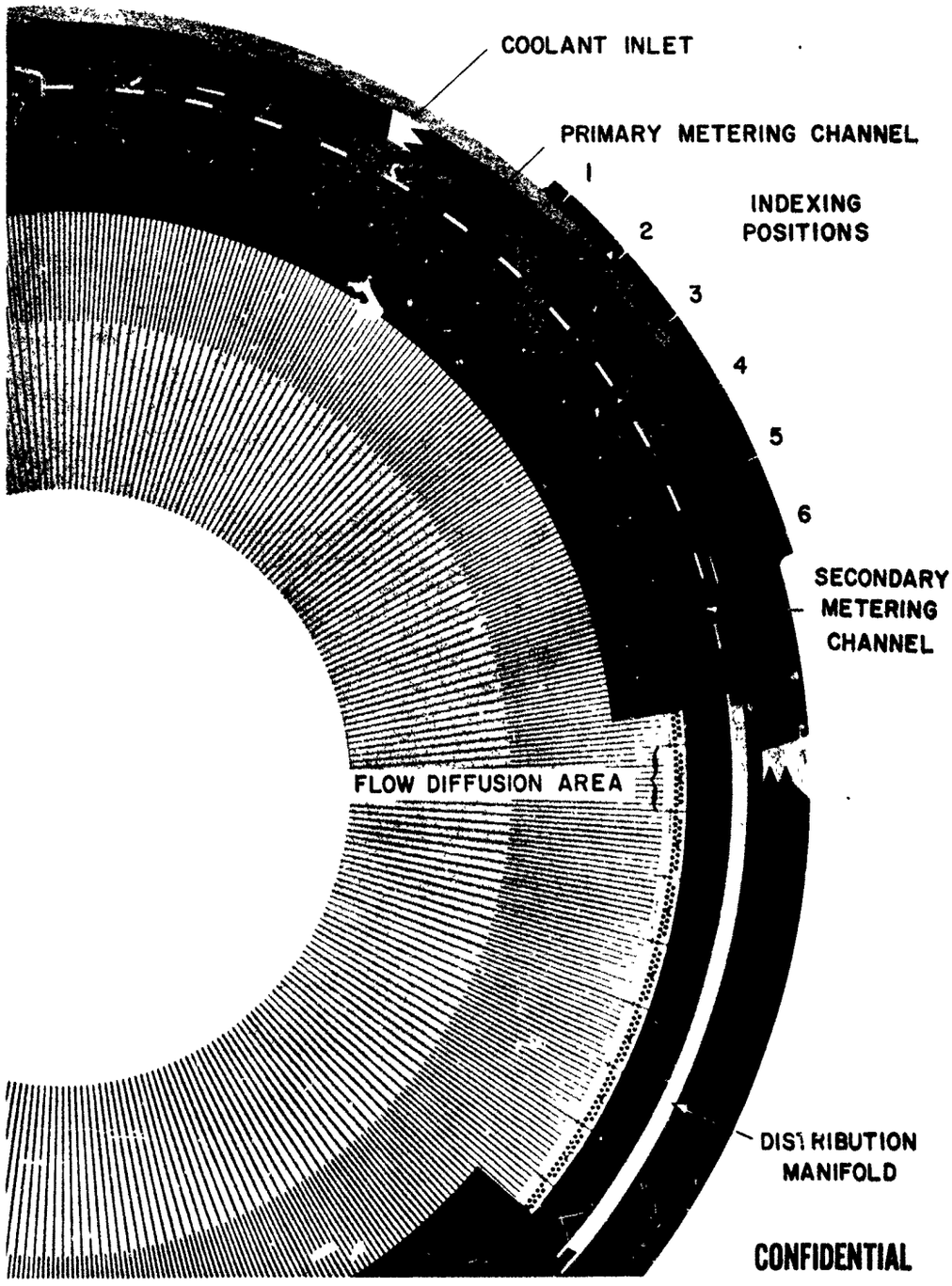

Sectional Washer Pairs for Transpiration Chambers (u)

Figure VI-66

CHAMBER COMPARTMENT NUMBER

ITEM	1	2	3	4	5	6	7	8	9	10	11	12	TOTAL
COMPARTMENT LENGTH (IN.)	0.986	2.331	2.331	1.680	1.932	2.035	1.133	0.484	0.528	0.781	1.375	2.289	
PLATELET THICKNESS (IN.)	0.021	←	←	→	0.021	0.011	←	←	←	→	0.011	0.021	
PLENUM PRESSURE (PSIA)	3320	3320	3320	3370	3890	3693	3503	3080	3000	2480	1525	1490	
WEIGHT FLOW FOR 1900°F NOMINAL WALL TEMP, LB/SEC	0.60	1.42	1.42	1.11	2.06	2.24	1.37	0.65	0.69	0.95	1.11	1.19	14.81
MAXIMUM WEIGHT FLOW (PLENUM PRESSURE 4500 PSIA)	1.83	4.28	4.28	3.10	3.10	3.73	2.28	1.28	1.28	1.99	3.79	3.90	34.84
ESTIMATED WALL TEMP. RANGE, °F MIN	970	970	970	760	1280	1270	1160	950	1070	820	680	760	
TEMP. RANGE, °F MAX	970	970	970	790	1420	1450	1330	1220	1310	1190	870	790	
PLATELET INDEXING POSITION NUMBER OF PLATELETS	1 47	1 111	1 111	1 80	4 15 3 18 2 31 1 28	1 103 2 82	1 13 2 69 3 21	1 22 2 22	2 24 3 12 4 12	1 6 2 10 3 13 4 14 5 14 6 14	1 22 2 17 3 16 4 15 5 12 6 43	1 27 2 14 3 19 4 13 5 11 6 25	

Summary of ARES Transpiration-Cooled Chamber Assembly
(Flow Rates, Supply Pressure and Wall Temperatures) (u)

CONFIDENTIAL

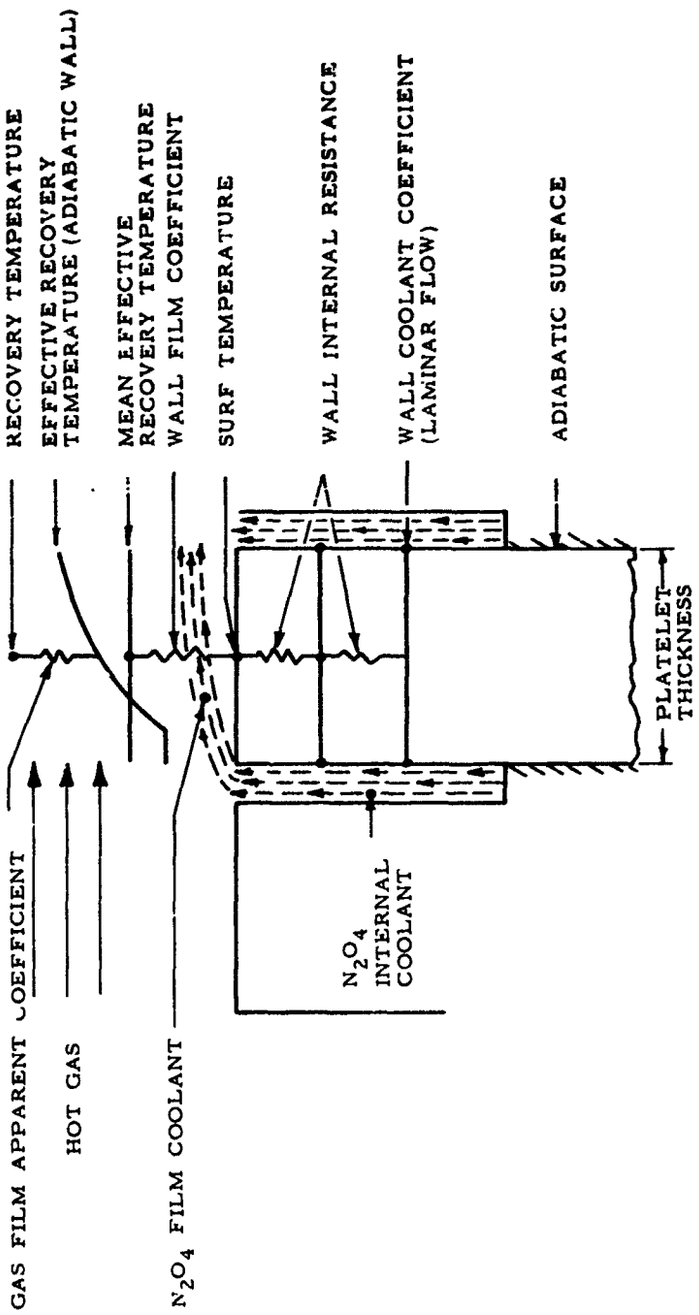

Advanced Thermal Model

Figure VI-68

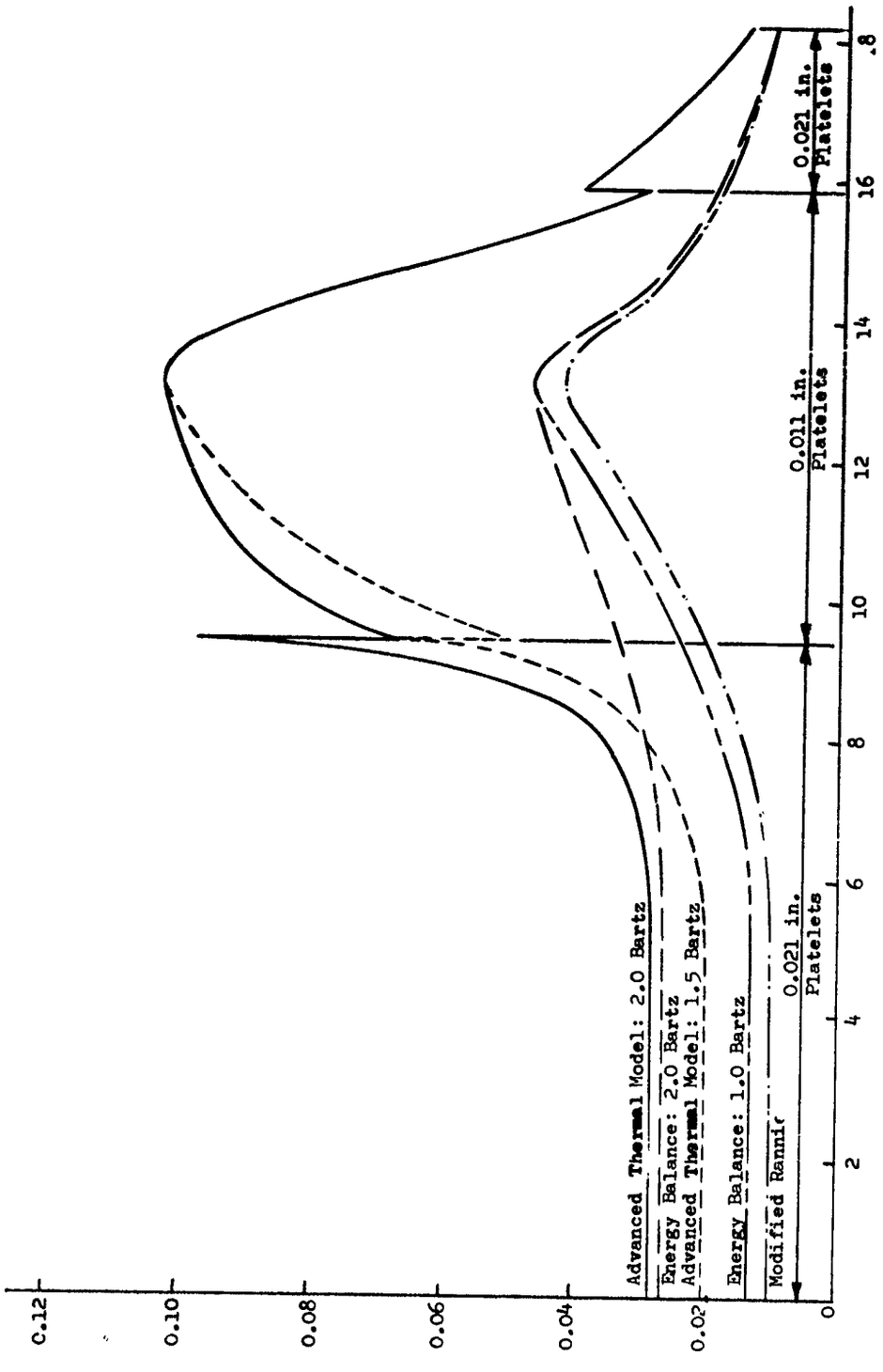

Transpiration Coolant Flow Rates vs Axial Distance (L
(1500°F Wall)

Figure VI-69

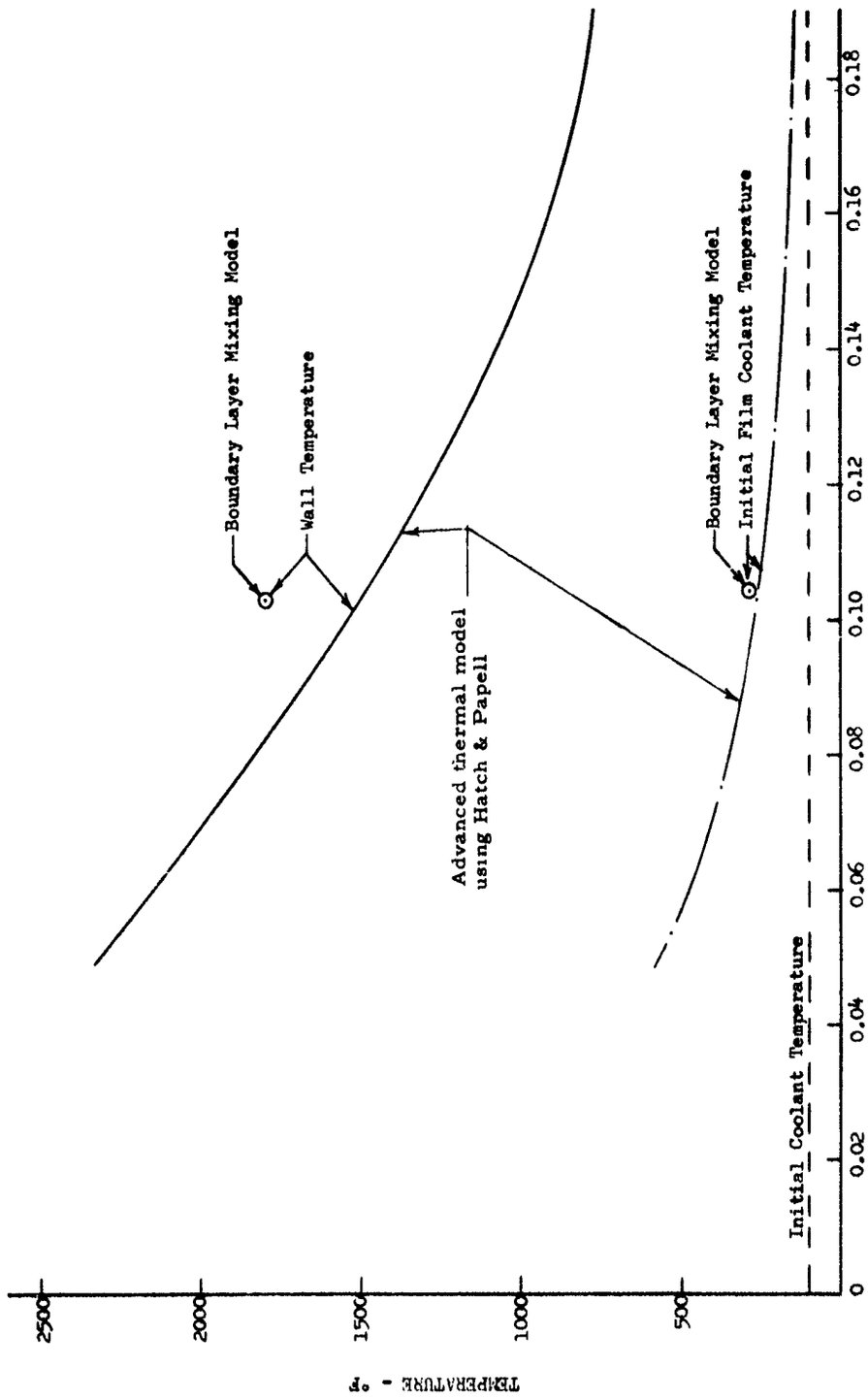

Throat Wall and Coolant Temperatures vs Transpiration Coolant Flow Rates

Figure VI-70

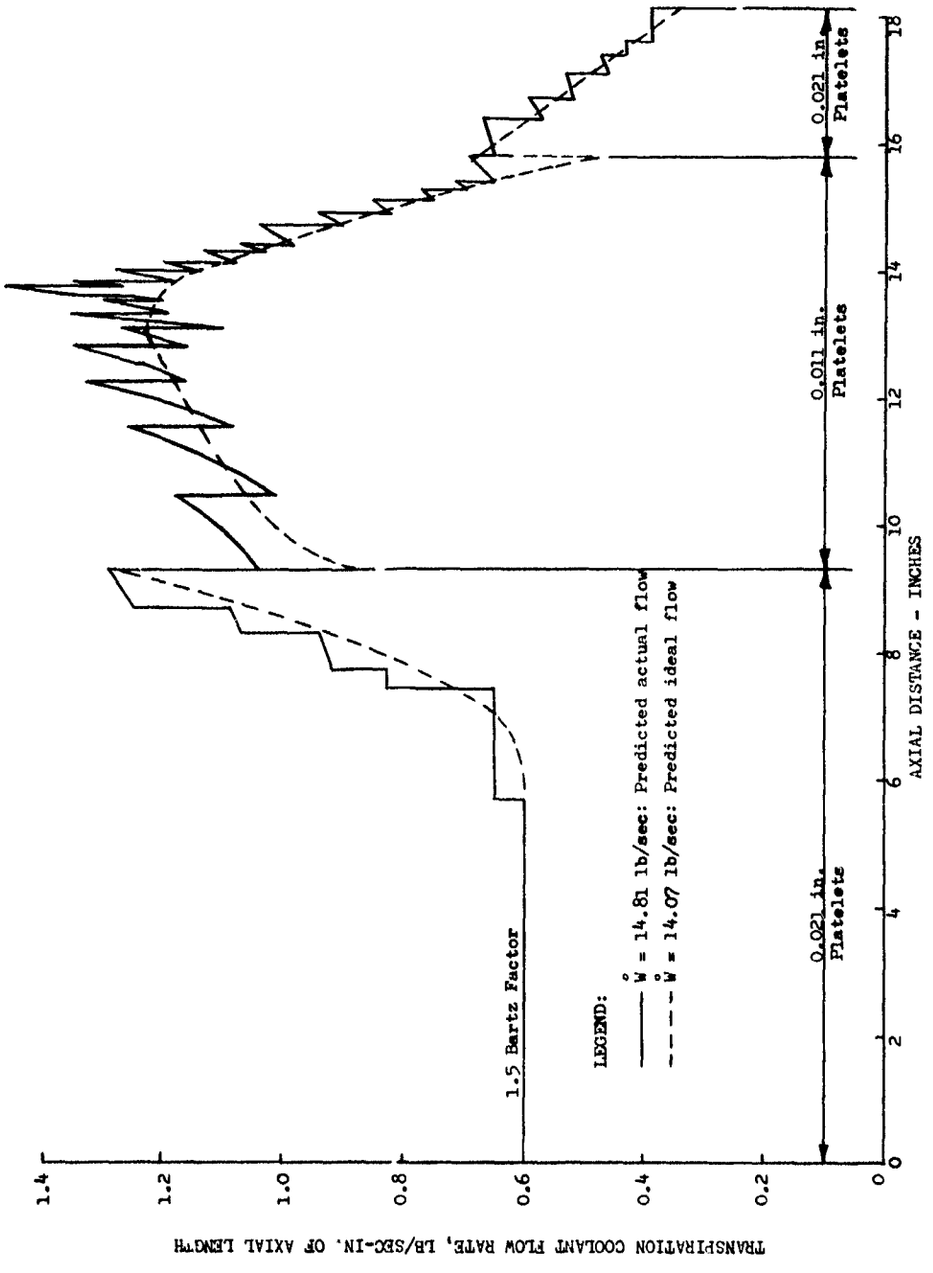

Transpiration-Coolant Flow Rates vs Axial Distance
(1900°F Wall)

Figure VI-71

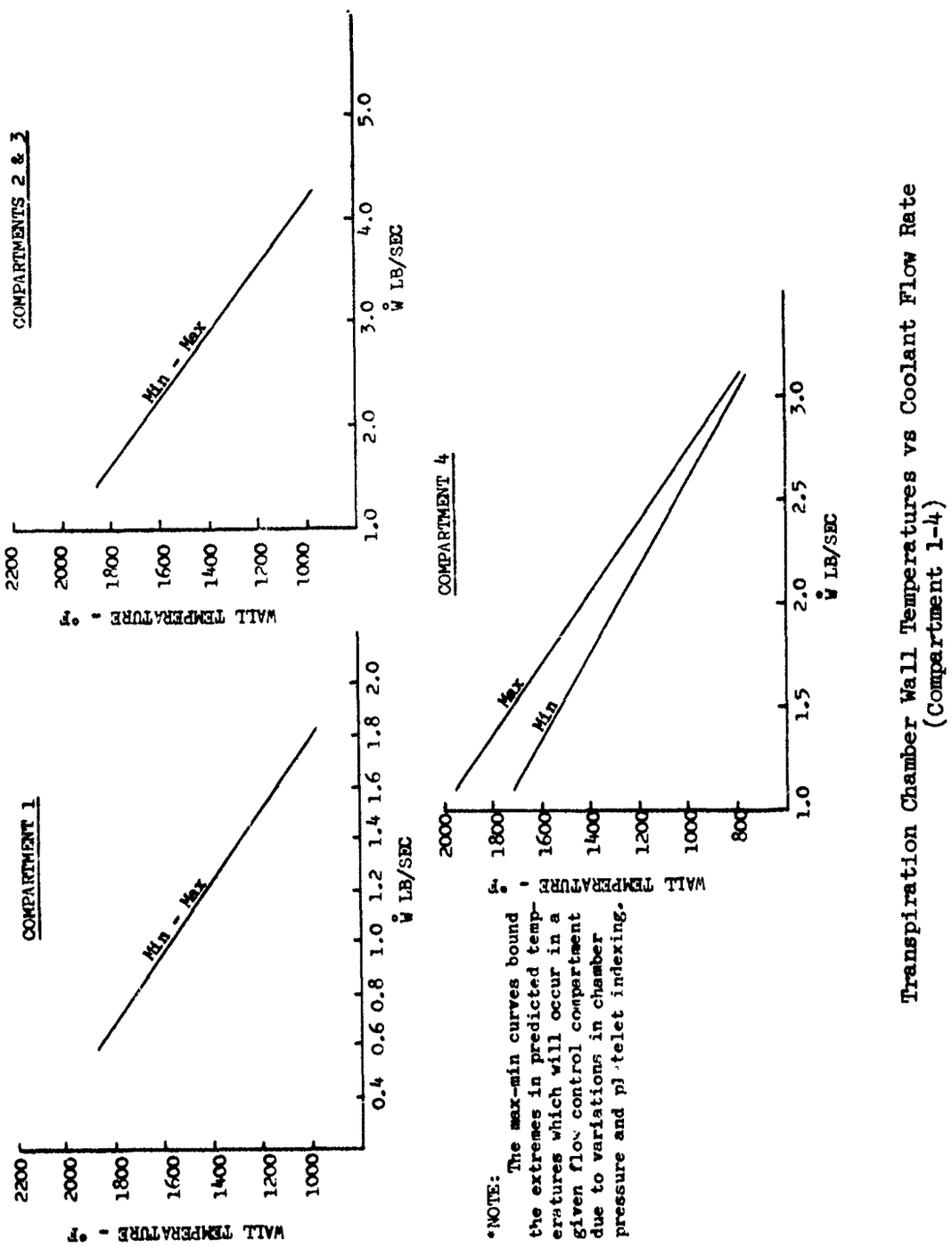

*NOTE:
The max-min curves bound the extremes in predicted temperatures which will occur in a given flow control compartment due to variations in chamber pressure and pintelet indexing.

Transpiration Chamber Wall Temperatures vs Coolant Flow Rate
(Compartment 1-4)

Figure VI-72

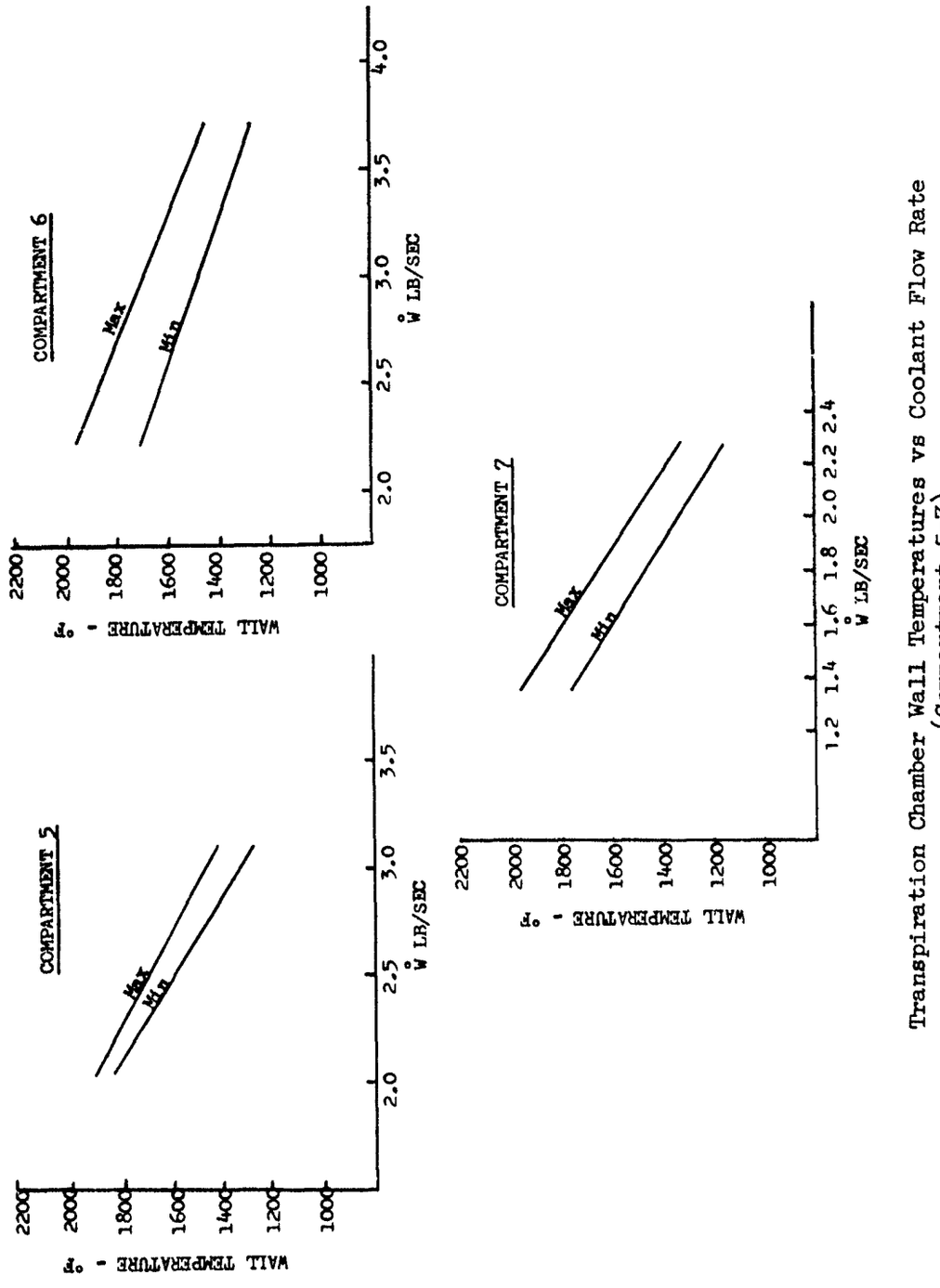

Transpiration Chamber Wall Temperatures vs Coolant Flow Rate
(Compartment 5-7)

Figure VI-73

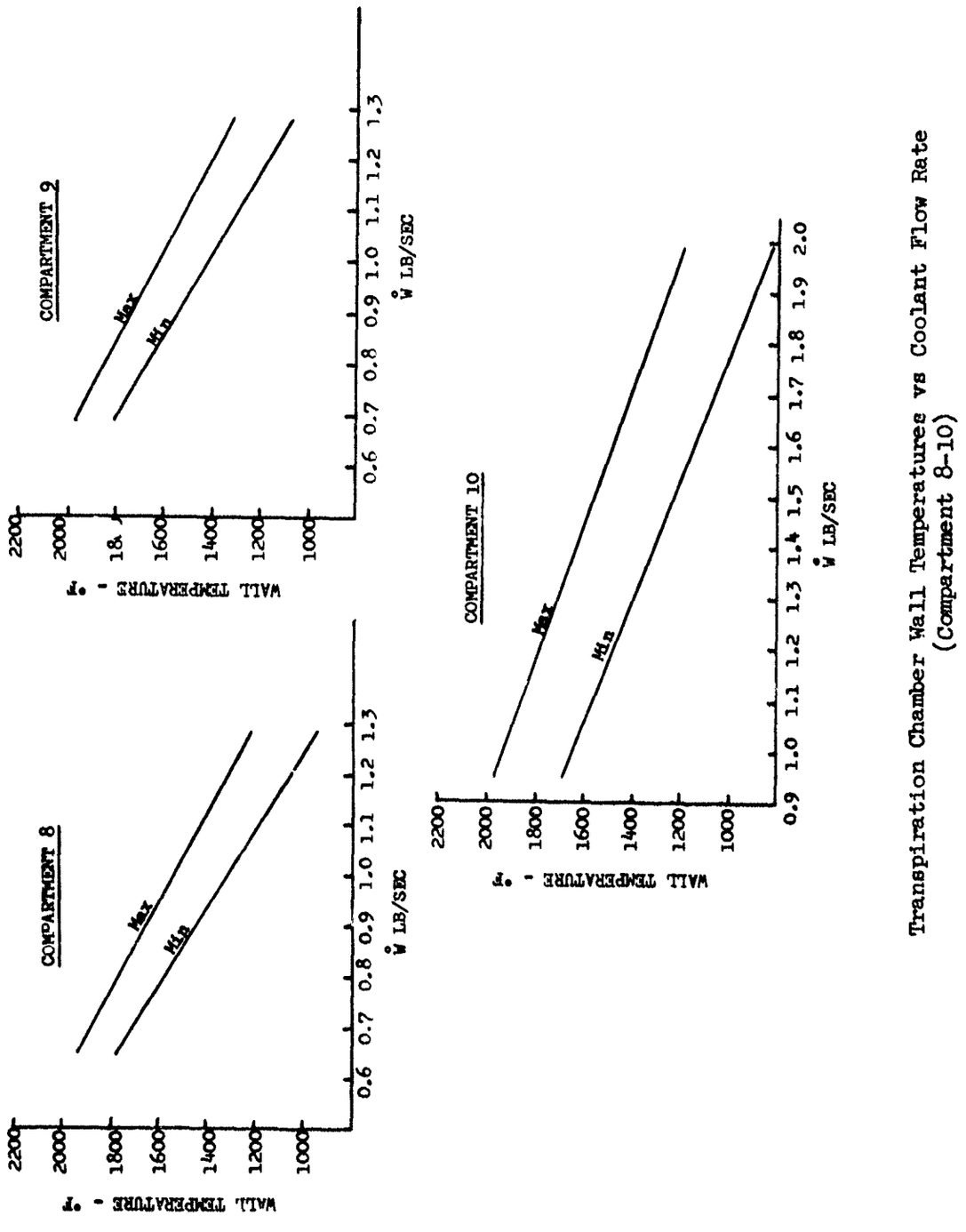

Transpiration Chamber Wall Temperatures vs Coolant Flow Rate
(Compartment 8-10)

Figure VI-74

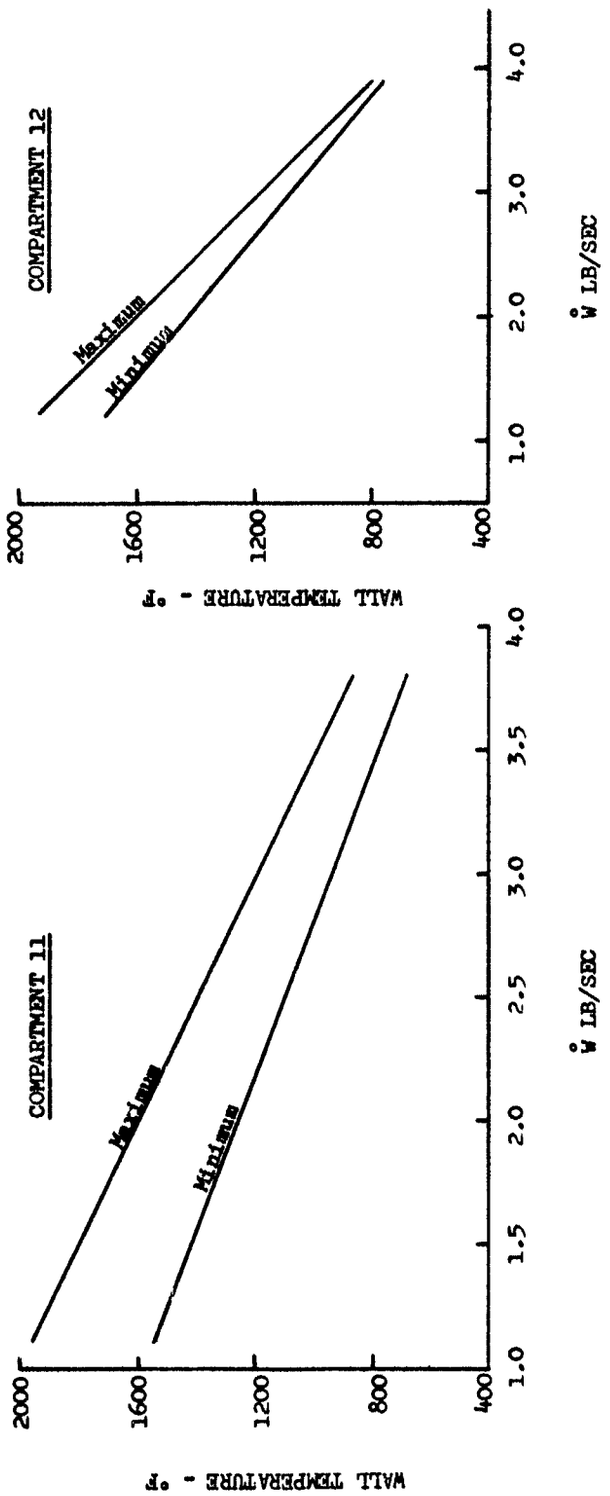

Transpiration Chamber Wall Temperatures vs Coolant Flow Rate
(Compartment 11 and 12)

Figure VI-75

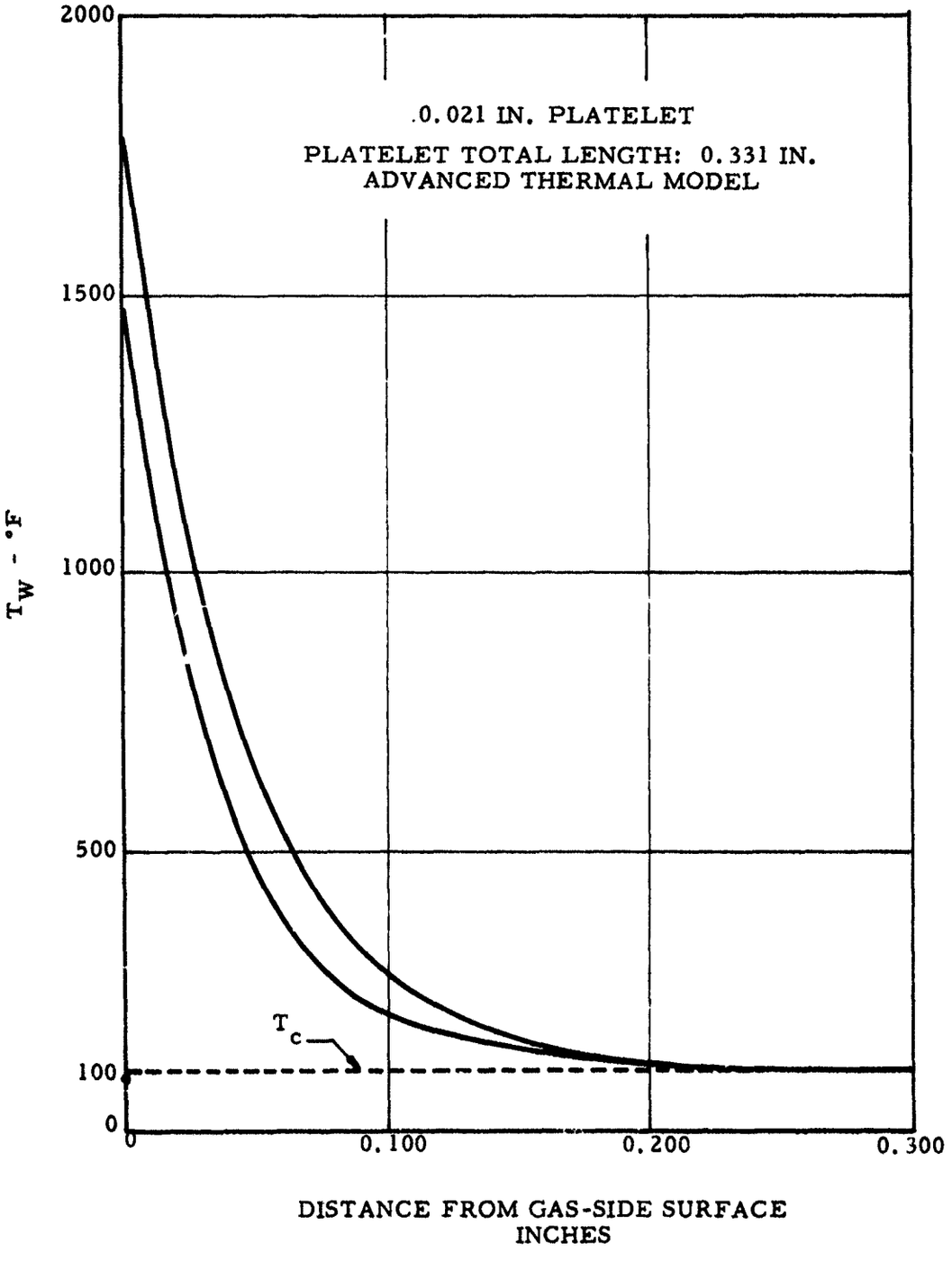

Radial Wall Temperature Distribution in ARES Transpiration-Cooled Chamber

Figure VI-76

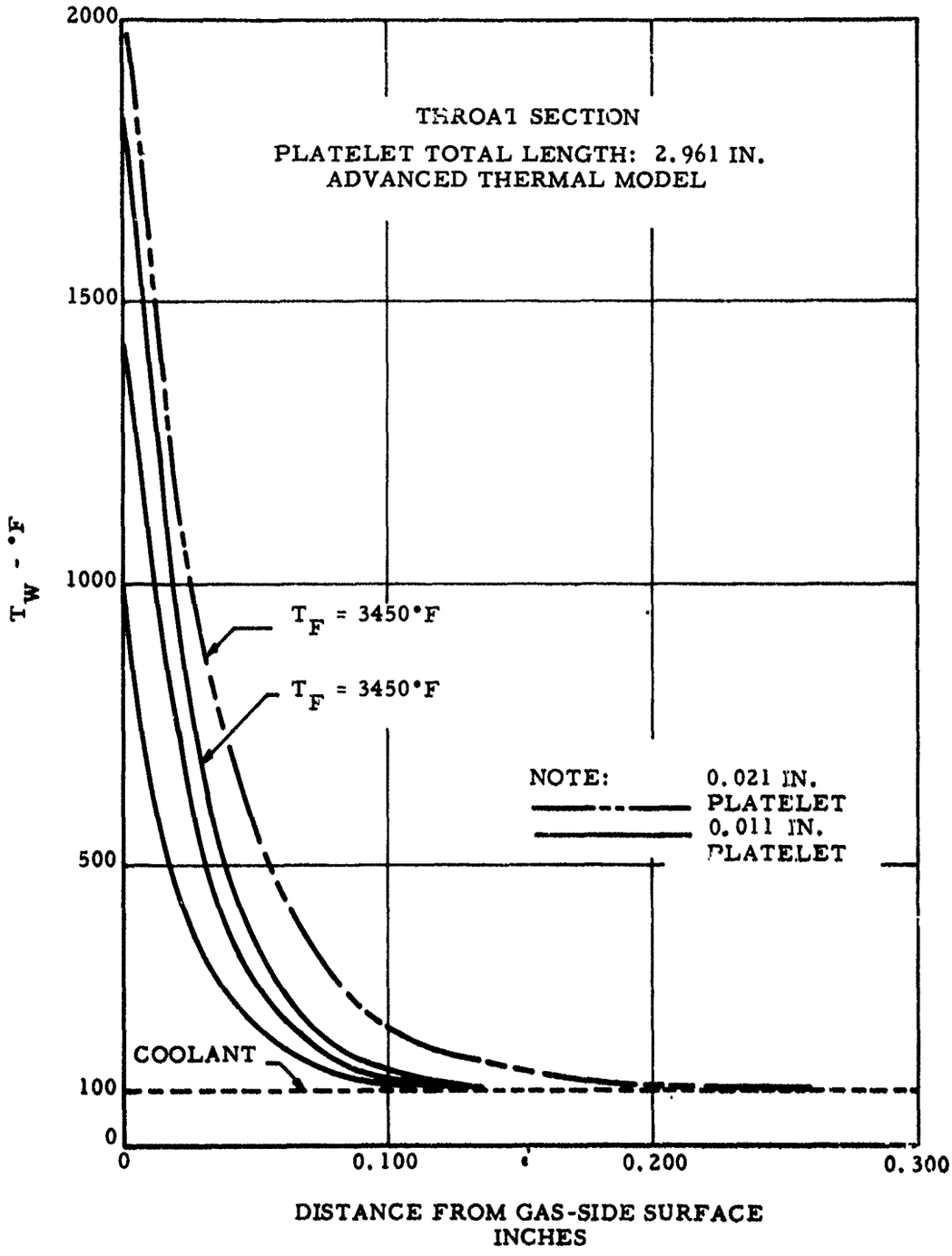

Radial Wall Temperature Distribution in ARES Transpiration-Cooled Chamber

Figure VI-77

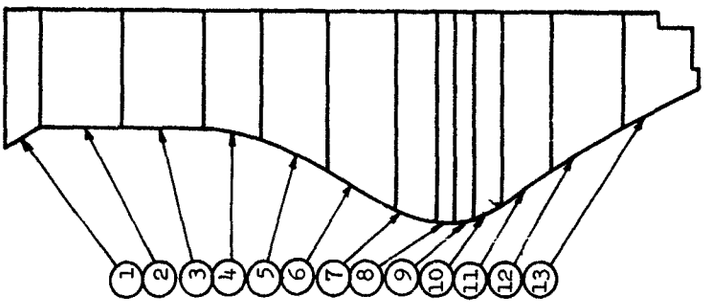

Transpiration Chamber Flow Data Summary (Chamber SN 001)

TEST SERIES 1.2-12-WAM

FILM COOLANT SEGMENT WEIGHT FLOW W_{ORC} (lb/sec) N_2O_4 DURATION	001	002	003	004	005	006	007	008	009	010	011	012
①	1.59	1.61	0.71	1.66	2.41	1.65	3.00	3.02	3.01	3.00	2.99	2.99
②	2.03	1.93	TEST STAND MALFUNCTION	1.80	2.00	2.05	1.98	2.03	2.05	1.95	2.02	1.83
③	5.86	6.23		5.80	6.07	6.25	6.02	6.04	6.05	5.28	6.12	5.78
④	5.86	6.06		5.45	5.98	6.08	5.97	5.18*	4.78	4.68	6.09Δ	4.20*
⑤	4.16	4.02		3.68	4.10	4.18	4.07	3.63*	3.61	3.40	4.14Δ	3.31*
⑥	4.07	4.06		3.70	4.08	4.05	4.05	4.17	4.09	4.17	4.10	3.75
⑦	4.76	4.72		9.92Δ	10.70	10.70	11.10	11.41	11.08	11.26	10.74	10.72
⑧	2.62	2.49		4.43Δ	4.59	4.58	4.57	4.68	4.70	4.70	4.67	4.43
⑨	1.34	1.30		1.84Δ	1.93	1.91	1.91	1.97	1.93	1.95	1.94	1.84
⑩	1.28	1.28		2.32Δ	2.44	2.40	2.43	2.49	2.45	2.46	2.45	2.33
⑪	1.93	1.94		1.84Δ	2.02	1.97	2.00	1.99	2.06	2.05	2.01	1.79
⑫	4.28	4.21		4.01	4.25	4.20	4.25	3.54*	3.52	3.56	4.35Δ	3.20*
⑬	4.63	4.59		4.34	4.70	4.50	4.67	3.23*	3.18	3.23	4.70Δ	2.89*
	5.14	5.14		5.05	5.23	0	4.24	0	0	0	5.15	0
TOTAL ORIFICE	47.94	47.97	--	54.18	58.10	52.87	57.26	50.36	49.50	48.70	58.47	46.07
TOTAL FLOWMETER	48.4	47.6	--	57.4	59.4	52.4	57.4	58.3	53.1	52.8	58.5	--

S/N 001 ——— S/N 001A

Δ INDICATES ORIFICE CHANGE TO INCREASE FLOW.

* INDICATES ORIFICE CHANGE TO DECREASE FLOW.

Figure VI-78

TEST SERIES 1.2-12-WAM-

	013	014	015	016	017	018	019	020	021	022	023	024	025	026	027	028	029	030
DURATION	1.32	1.75	2.01	3.03	3.03	3.03	1.13	1.12	2.22	3.04	1.76	1.76	1.75	3.01	1.76	3.02	1.76	3.02
FILM COOLANT SEGMENT WEIGHT FLOW $*W_{FC}$ (lb/sec) N_2O_4 1	1.98	1.94	1.98	1.84	1.96	2.33	TEST STAND MALFUNCTION	TEST STAND MALFUNCTION	2.56	2.32	2.87	3.07	2.58	2.10	2.70	2.69	3.07	3.09
2	3.14*	4.28	4.50	4.27	4.56	3.18*			3.20	3.13	3.24	3.36	5.81Δ	5.13	3.30*	3.30	2.55*	2.56
3	3.73*	5.20	4.45	4.23	3.72*	2.50*			2.52	2.46	2.55	2.59	4.12Δ	3.83	2.59*	2.49	2.58	2.57
4	2.84*	3.92	4.06	3.74	3.14*	2.44*			2.37	2.29	2.37	2.38	3.34Δ	3.20	2.35*	2.33	2.38	2.38
5	3.99Δ	4.60	5.97	5.23	5.71	6.03			5.73*	5.34	6.22	6.74	7.56Δ	6.61	7.79	7.25	7.24*	7.61
6	7.82	8.67	7.81	7.53	7.52	7.42			7.21	7.09	8.59	8.27	8.11	8.33	8.64	8.73	6.36*	6.53
7	4.36	4.03	3.86	3.71	3.65	3.64			3.69	3.37	3.82	4.38	3.70	3.51	3.90	3.2	4.60	4.75
8	1.47	1.44	1.39	1.27	1.12	1.29			2.21Δ	2.19	2.29	2.30	2.38	2.40	2.38	2.41	2.42	2.46
9	2.21	1.77	1.60	1.35	1.20	1.29			2.04	1.61	2.25	2.30	2.01	1.84	1.87	2.02	2.48	2.53
10	2.47	2.02	1.85	2.08	2.07	2.08			2.01	1.98	INVALID	2.23	INVALIDΔ	2.47	2.66	2.41	2.11*	2.37
11	3.20	2.38	3.62	3.09	2.64*	2.74			1.86*	1.80	1.87	1.83	2.72Δ	2.87	2.87	2.87	1.82*	1.82
12	2.50	2.95	3.12	2.67	2.82*	2.42			2.06*	2.04	2.82	2.81	2.39Δ	2.43	2.43	2.44	2.07*	2.07
13	0	0	0	0	0	0			0	0	0	0	0	0	0	0	0	0
TOTAL ORIFICE	39.71	43.13	44.21	41.01	40.20	37.36	--	--	37.46	35.62	--	42.26	--	44.77	43.48	42.95	39.68	40.74
TOTAL FLOWMETER	--	56.2	45.6	43.7	41.3	38.8	--	--	38.5	36.6	40.8	42.3	--	44.8	--	42.8	--	--
	S/N 002								S/N 002A									

Δ INDICATES ORIFICE CHANGES TO INCREASE FLOW.
* INDICATES ORIFICE CHANGE TO DECREASE FLOW.

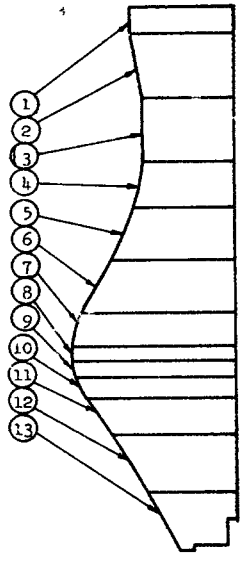

UNCLASSIFIED

Figure VI-79

Transpiration Chamber Flow Data Summary (Chamber SN-002)

	GENERAL DATA								MEASURED DATA					
	DATE	DURATION FS_1	DURATION FS_2	DATA PERIOD FS_1 +	INJECTOR SERIAL NUMBER	CHAMBER SERIAL NUMBER	THROAT AREA	AREA RATIO	CHAR-ACTERISTIC LENGTH	CHAMBER PRESSURE	INJECTOR MIXTURE RATIO	FILM COOLANT FLOW RATE	VACUUM THRUST	ENGINE WEIGHT FLOW	MEASI SEA L SPECI IMPUL
SYMBOLS							A_T		L^*	P_C	MR_J	$\dot{W}_{FC}$	F_V	$\dot{W}_T$	I_{sp}
UNITS	---	SEC		SEC	---	---	IN.^{2}	---	IN.	PSIA	---	LB/SEC	LB	LB/SEC	SEC
TEST															
1.2-12-WAM-001	8-4-66	1.590		1.56-1.64	2	1	21.35	5.70	40.0	2678	2.44	48.4	86,285	387.8	217.
002	8-17-66	1.605		1.57-1.62	2	1	21.58	19.60	40.0	2690	2.70	47.6	102,760	383.2	252.
003	9-10-66	.708		NONE	4	1A	22.2	19.60	38.4	MALFUNCTION - NO VALID PERFORMANCE DATA					
004	9-12-66	1.664		1.65-1.75	4	1A	22.2	19.10	38.4	2730	2.39	57.4	104,560	385.0	254.
005	9-13-66	2.410		1.86-2.36	1	1A	22.2	19.10	38.4	2810	2.70	59.4	107,275	400.5	252.
006	9-20-66	1.653		1.55-1.65	1	1A	22.2	19.10	38.4	2490	2.36	52.4	98,190	370.0	248.
007	9-21-66	3.002		2.00-2.90	3	1A	22.2	19.10	38.4	2754	2.15	57.4	106,556	399.0	249.
008	9-26-66	3.018		1.98-2.98	3	1A	22.2	19.10	38.4	2770	2.20	58.3	105,190	403.2	245.
009	9-27-66	3.004		1.95-2.95	3	1A	22.2	19.10	38.4	2750	2.17	53.1	103,697	394.4	247.
010	9-27-66	2.998		1.95-2.95	3	1A	22.2	19.10	38.4	2800	2.21	52.8	105,140	394.2	251.
011	9-28-66	2.993		1.94-2.94	4	1A	22.2	19.00	38.4	2828	2.24	58.5	108,209	395.4	258.
012	9-30-66	2.993		NONE	4	1A	22.2	19.10	38.4	HARDWARE DAMAGE - NO VALID PERFORMANCE DATA					
013	10-22-66	1.315		NONE	3	2	21.35	19.90	40.0	SHORT DURATION - NO VALID PERFORMANCE DATA					
014	10-25-66	1.749		1.70-1.75	3	2	21.35	19.90	40.0	2880	2.38	56.2	104,527	376.0	261.
015	10-25-66	2.005		1.76-1.96	3	2	21.35	19.90	40.0	2930	2.36	45.6	105,615	380.0	261.
016	10-25-66	3.027		1.98-2.98	3	2	21.35	19.90	40.0	2860	2.34	43.7	104,210	376.0	260.
017	10-26-66	3.026		2.53-2.93	3	2	21.35	19.90	40.0	2910	2.17	41.3	105,719	376.0	264.
018	10-26-66	3.025		2.58-2.98	3	2	21.35	19.90	40.0	2900	2.18	38.8	104,921	372.2	265.
019	10-26-66	1.132		NONE	3	2	21.35	19.90	40.0	MALFUNCTION - NO VALID PERFORMANCE DATA					
020	10-26-66	1.120		NONE	3	2	21.35	19.90	40.0	MALFUNCTION - NO VALID PERFORMANCE DATA					
021	10-29-66	2.217		2.07-2.17	3	2A	21.35	19.90	40.0	2900	2.38	38.5	104,972	374.0	263.
022	10-31-66	3.040		1.99-2.99	3	2A	21.35	19.90	40.0	2960	2.21	36.6	104,513	367.0	267.
023	11-1-66	1.764		1.66-1.76	2	2A	21.35	19.90	40.0	2940	2.40	40.8	108,479	377.0	271.
024	11-2-66	1.763		1.66-1.76	2	2A	21.35	19.90	40.0	2890	2.32	42.3	109,872	383.0	270.
025	11-13-66	1.750		NONE	5	2A	21.35	19.90	40.0	SHORT DURATION - NO VALID PERFORMANCE DATA					
026	11-14-66	3.007		2.66-2.96	5	2A	21.35	19.90	40.0	2890	2.17	44.8	106,280	376.0	266.
027	11-14-66	1.760		NONE	5	2A	21.35	19.90	40.0	SHORT DURATION - NO VALID PERFORMANCE DATA					
028	11-14-66	3.018		2.51-3.01	5	2A	21.35	19.90	40.0	2920	2.18	42.8	105,380	374.0	265.
029	11-14-66	1.756		NONE	5	2A	21.35	19.90	40.0	SHORT DURATION - NO VALID PERFORMANCE DATA					
030	11-14-66	3.022		NONE	5	2A	21.35	19.90	40.0	HARDWARE DAMAGE - NO VALID PERFORMANCE DATA					

MEASURED DATA					PERFORMANCE							PERCENT PERFORMANCE		
INJECTOR MIXTURE RATIO	FILM COOLANT FLOW RATE	VACUUM THRUST	ENGINE WEIGHT FLOW	MEASURED SEA LEVEL SPECIFIC IMPULSE	VACUUM SPECIFIC IMPULSE	MIXTURE RATIO DISTRIBUTION LOSS	NOZZLE GEOMETRY LOSS	NOZZLE FRICTION LOSS	FILM COOLING LOSS	COMBUSTION LOSS	THEORETICAL VACUUM SPECIFIC IMPULSE	PERCENT COOLANT	PERCENT COOLANT LOSS	PERCENT VACUUM SPECIFIC IMPULSE
MR_o	$\dot{W}_{OFC}$	F_v	$\dot{W}_T$	Is_{SL}	Is_v	MRDL	NGL	NFL	FCL	ERL	Is_{VT}	$\%\dot{W}_{OFC}$	$\%Is_{FC}$	$\%Is_v$
---	LB/SEC	LB	LB/SEC	SEC	SEC	SEC	SEC	SEC	SEC	SEC	SEC	%	%	%
2.44	48.4	86,285	387.8	217.9	222.5	17.4	10.5	.9	21.3	10.8	293.8	12.5	7.35	75.5
2.70	47.6	102,760	383.2	252.0	268.2	9.7	2.4	3.0	22.0	10.7	316.0	12.4	6.94	84.9
TION - NO VALID PERFORMANCE DATA														
2.39	57.4	104,560	385.0	254.7	271.6	0	2.6	3.0	22.5	11.2	323.8	14.9	6.95	83.9
2.70	59.4	107,275	400.5	252.3	267.9	0	2.5	3.0	19.8	11.0	315.7	14.8	6.27	84.9
2.36	52.4	98,190	370.0	248.6	265.4	9.9	2.5	3.[illegible]	23.2	11.3	324.7	14.1	7.11	81.7
2.15	57.4	106,556	399.0	249.7	265.3	10.6	2.5	3.1	23.1	11.5	329.3	14.3	7.02	80.6
2.20	58.3	105,190	403.2	245.5	261.0	13.9	2.5	3.1	24.0	11.4	328.6	14.5	7.28	79.4
2.17	53.1	103,697	394.4	247.2	263.0	16.3	2.5	3.1	24.4	11.4	329.0	13.5	7.41	79.9
2.21	52.8	105,140	394.2	251.2	267.0	11.9	2.6	3.0	24.2	11.4	328.3	13.5	7.35	81.2
2.24	58.5	108,209	395.4	258.2	274.0	0	2.6	3.0	23.5	11.4	327.6	14.8	7.17	83.6
E DAMAGE - NO VALID PERFORMANCE DATA														
URATION - NO VALID PERFORMANCE DATA														
2.38	56.2	104,527	376.0	261.5	278.0	6.0	2.6	3.0	23.4	11.3	324.3	14.9	7.2	85.7
2.36	45.6	105,615	380.0	261.6	277.9	6.0	2.6	3.0	24.1	11.3	324.9	12.0	7.4	85.5
2.34	43.7	104,210	376.0	260.5	277.1	6.0	2.6	3.0	25.6	11.3	325.6	11.6	7.9	85.1
2.17	41.3	105,719	376.0	264.4	281.2	6.0	2.7	3.0	25.4	11.4	329.7	11.0	7.7	85.3
2.18	38.8	104,921	372.2	265.0	281.9	6.0	2.7	3.0	24.6	11.4	329.6	10.4	7.5	85.6
TION - NO VALID PERFORMANCE DATA														
TION - NO VALID PERFORMANCE DATA														
2.38	38.5	104,972	374.0	263.9	280.7	6.0	2.7	3.0	20.6	11.3	324.3	10.3	6.4	86.6
2.21	36.6	104,513	367.0	267.6	284.8	6.0	2.7	3.0	21.3	11.4	329.2	10.0	6.5	86.5
2.40	40.8	108,479	377.0	271.1	287.7	0	2.7	3.0	19.0	11.3	323.7	10.8	5.9	88.9
2.32	42.3	109,872	383.0	270.6	286.9	0	2.7	3.0	22.3	11.3	326.2	11.1	6.8	88.0
URATION - NO VALID PERFORMANCE DATA														
2.17	44.8	106,280	376.0	266.0	282.7	3.0	2.7	3.0	26.9	11.4	329.7	11.9	8.2	85.7
URATION - NO VALID PERFORMANCE DATA														
2.18	42.8	105,380	374.0	265.0	281.8	3.0	2.7	3.0	27.7	11.4	329.6	11.5	8.4	85.5
URATION - NO VALID PERFORMANCE DATA														
E DAMAGE - NO VALID PERFORMANCE DATA														

Transpiration Chamber Test Data and Performance Summary

Figure VI-80

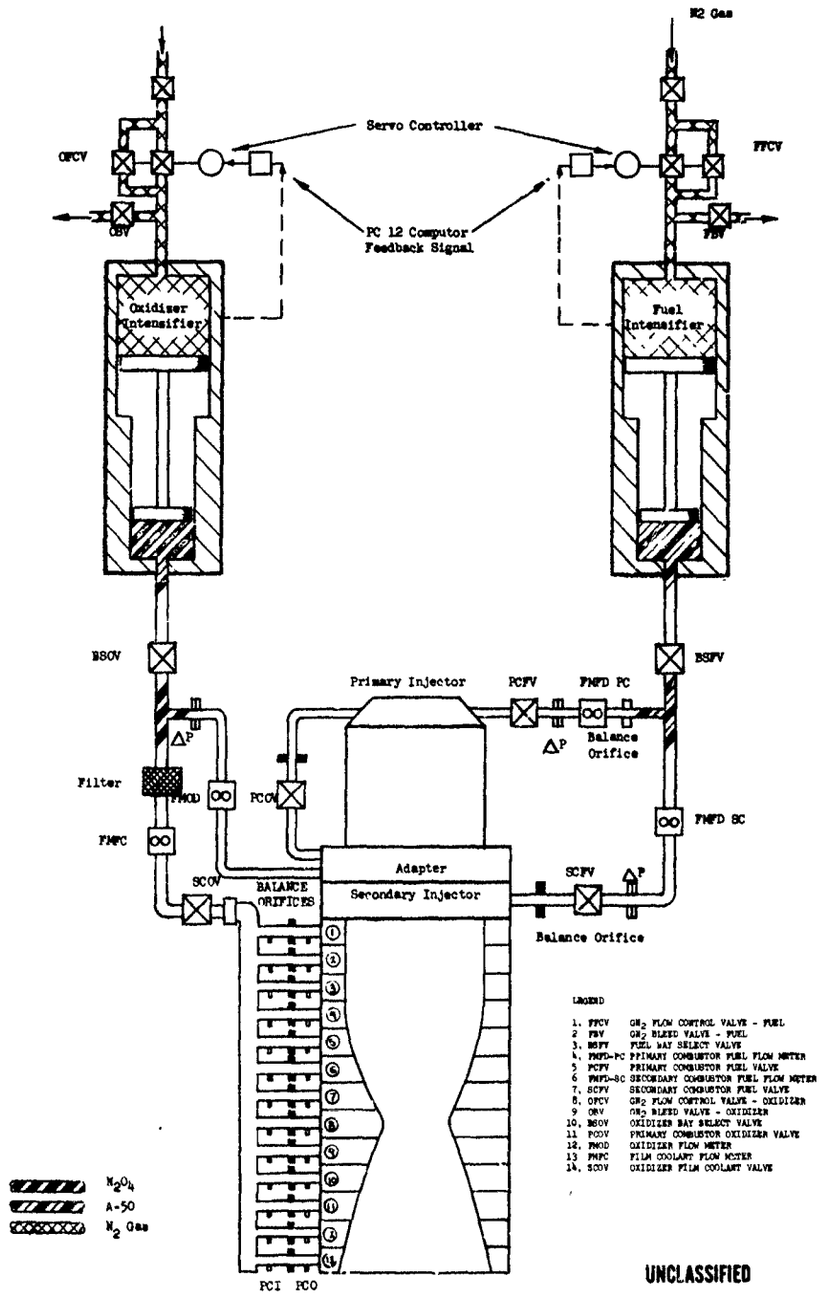

Transpiration Cooled Chamber Intensifier Fed Test Schematic

Figure VI-81

Transpiration Chamber Postfire Condition (Test 1.2-12-WAM-002) (u)

Figure VI-82

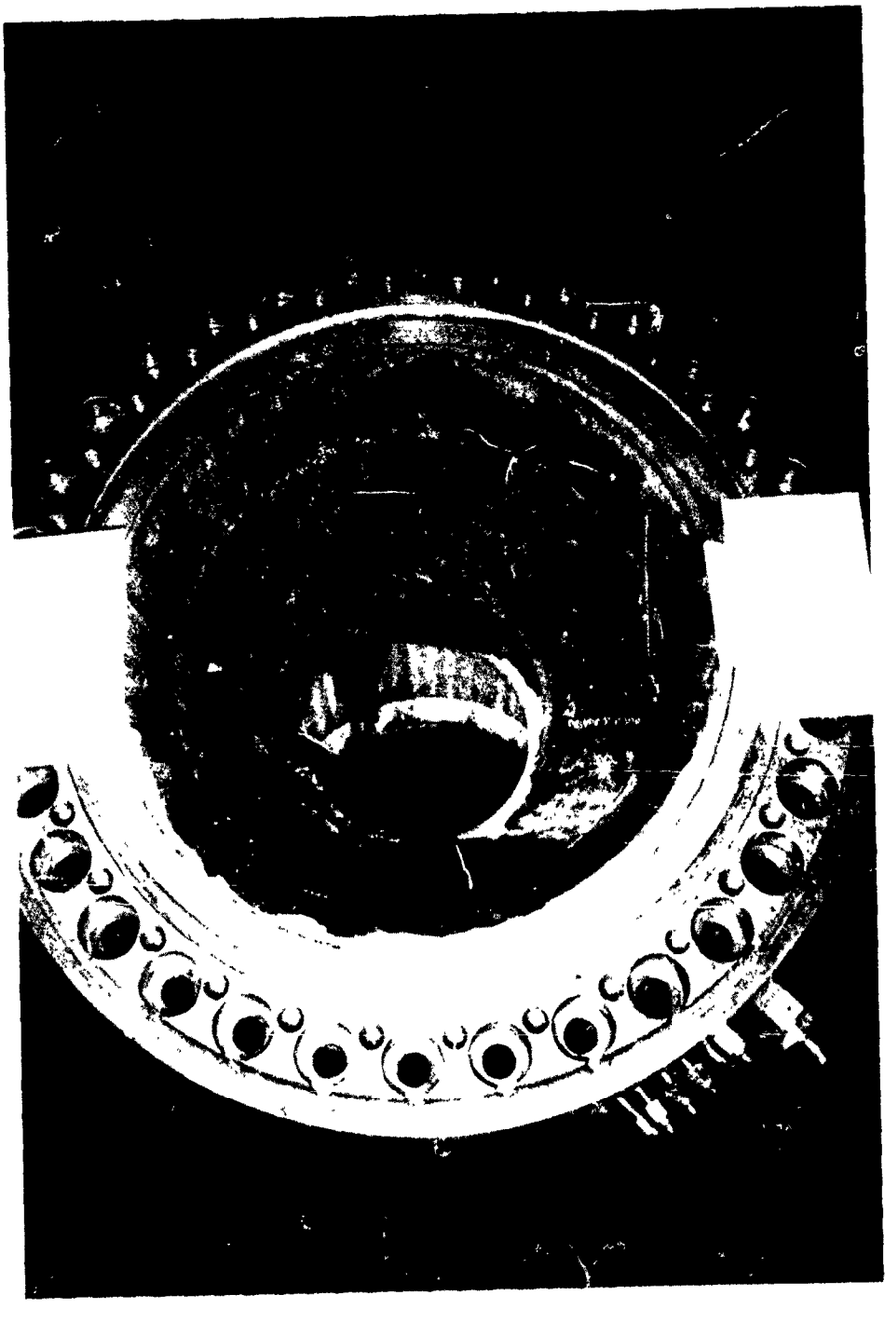

Transpiration Chamber Postfire Conditions (Test 1.2-12-WAM-012)

Figure VI-83

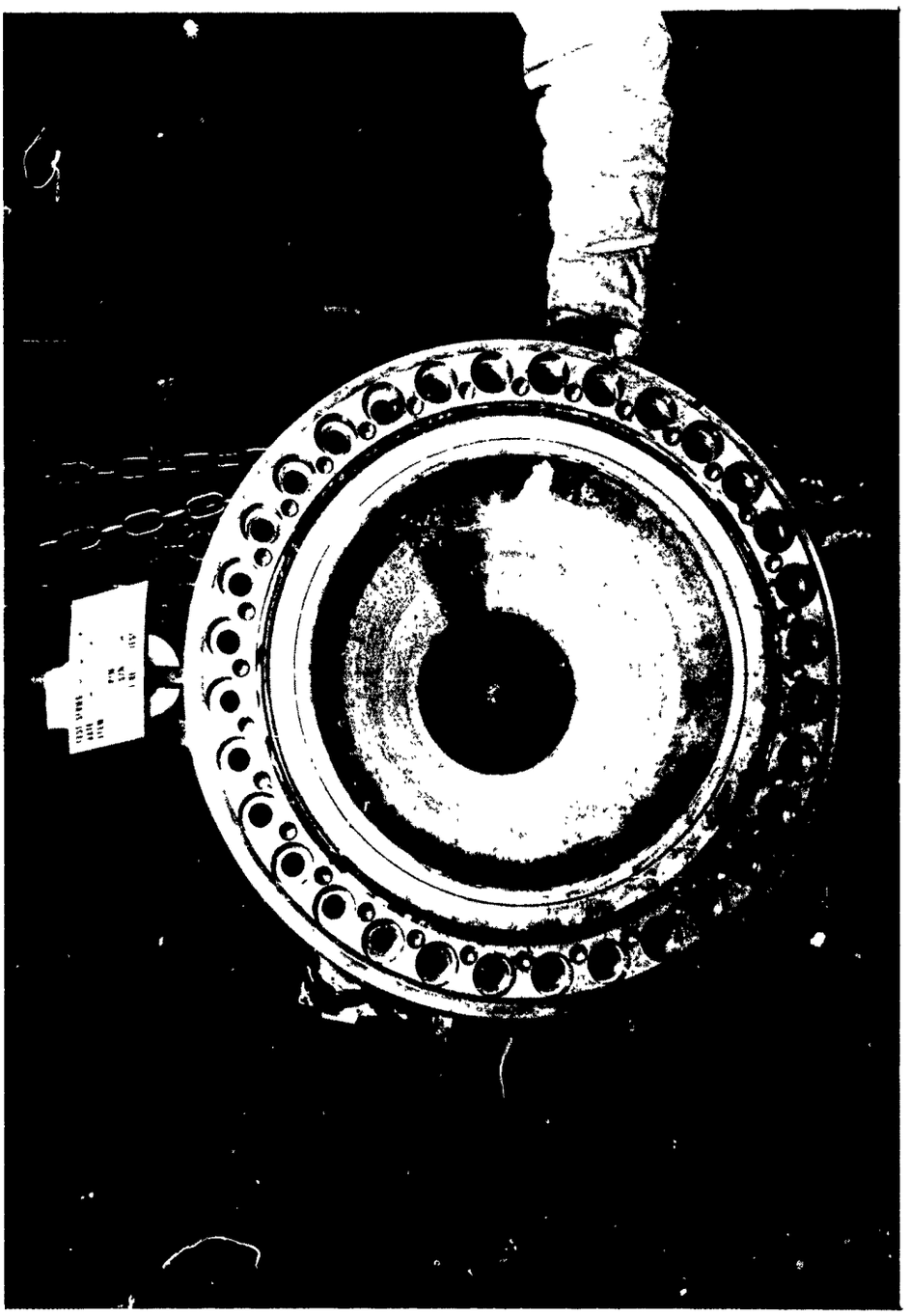

Transpiration Chamber Postfire Conditions (Test 1.2-12-WAM-024)

Figure VI-84

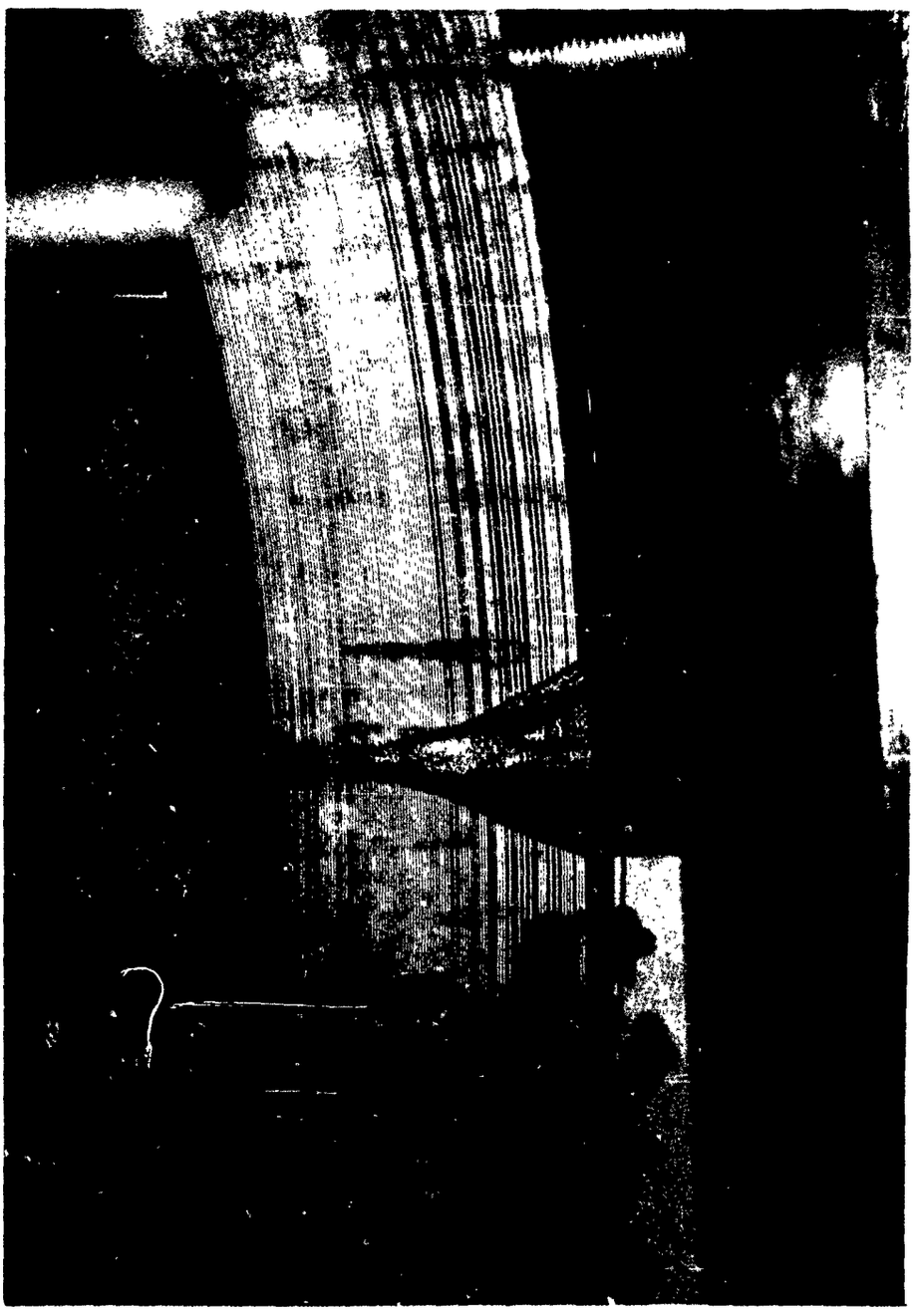

Transpiration Chamber Postfire Conditions (Test 1.2-12-WAM-030)

Figure VI-85

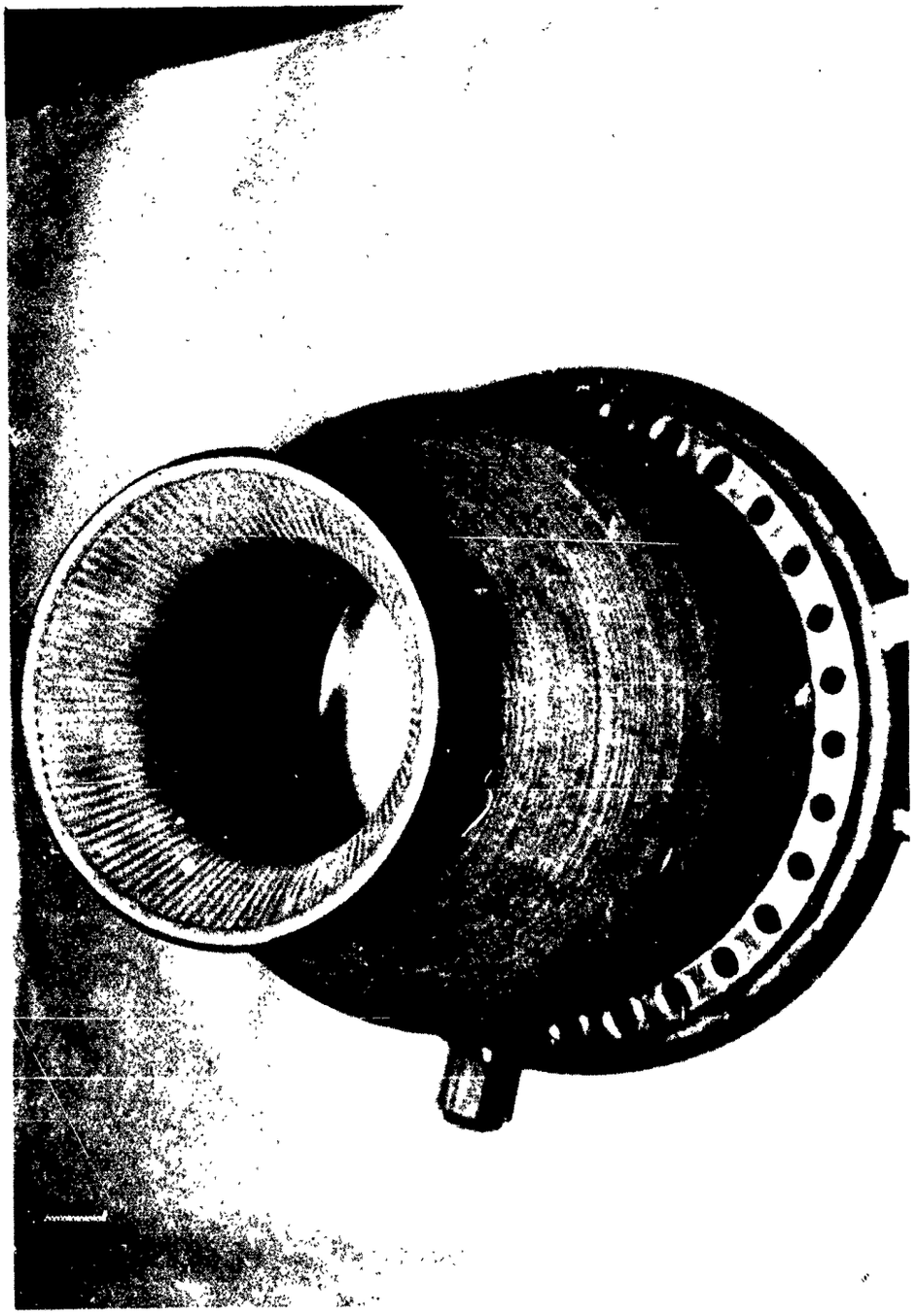

Regenerative Chamber Postfire Conditions (Test 1.2-14-WAM-002)

Figure VI-86

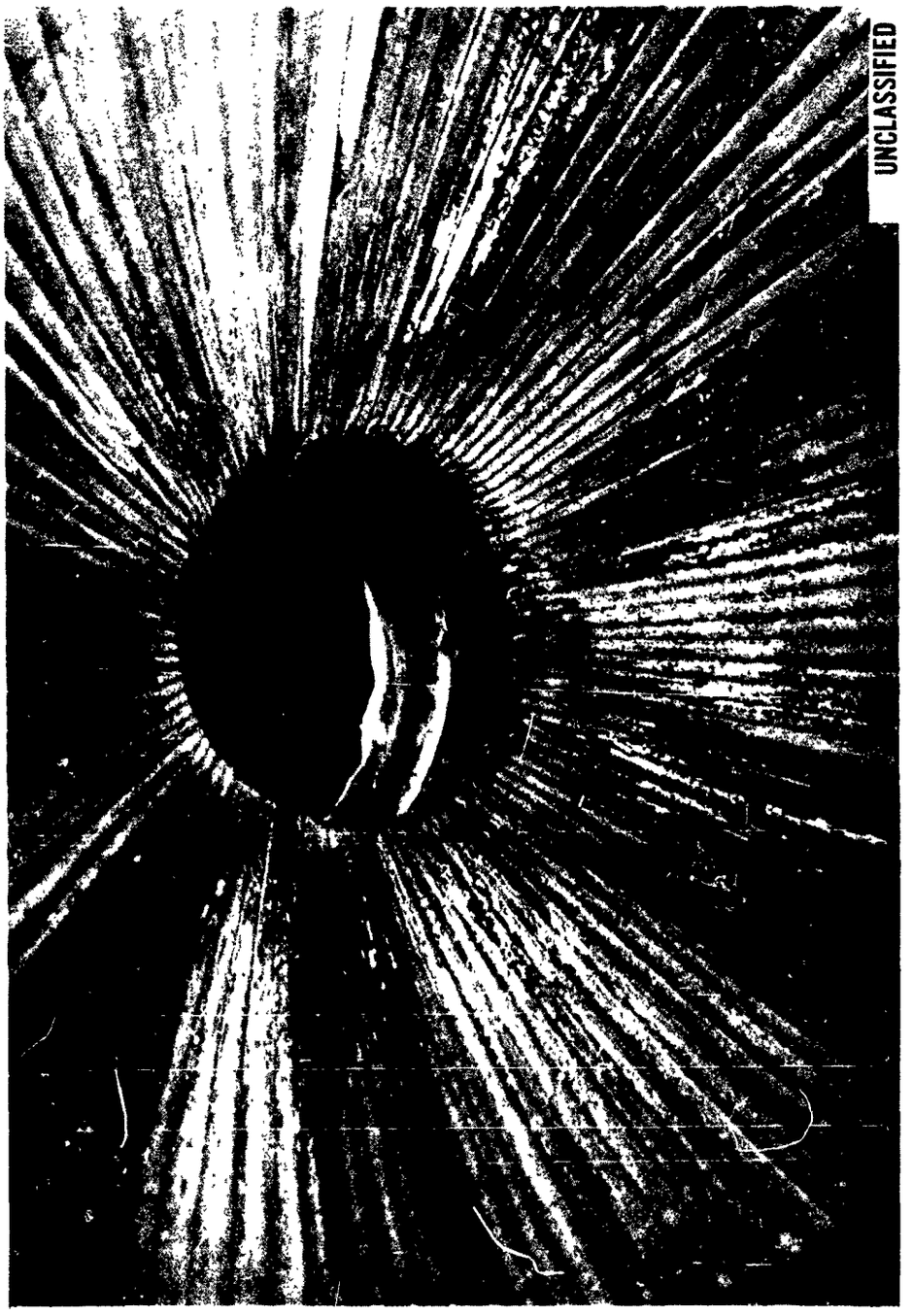

Regenerative Chamber Postfire Conditions (Test 1.2-14-WAM-005)

Figure VI-87

COOLED CHAMBER, A_e/A_t 20:1: L* = 39

P_c = 2800 PSIA, MR_{in} - 2.2

	PHASE I REQ'T. SECONDS	PHASE I REQ'T. PERCENT	PHASE II REQ'T. SECONDS	PHASE II REQ'T. PERCENT
1. THEORETICAL PERFORMANCE				
I_s VAC	329.5	100.0	329.5	100.0
2. PERFORMANCE LOSSES				
MIXTURE RATIO DISTRIBUTION LOSS	0.0	0.0	0.0	0.0
COMBUSTION LOSS*	11.2	3.4	8.0	2.4
NOZZLE FRICTION LOSS	3.1	1.0	3.1	1.0
NOZZLE GEOMETRY LOSS	2.9	0.9	2.9	0.9
OXIDIZER FILM COOLING LOSS	13.7	4.2	11.9	3.6
3. PREDICTED DELIVERED PERFORMANCE				
I_s VAC	298.6		303.6	
I_s SEA LEVEL	280.0	90.0	285.0	91.6
4. ALLOWABLE SUPPLEMENTAL COOLING				
REGENERATIVE CHAMBER, LB/SEC	29.2		25.2	
TRANSPIRATION CHAMBER, LB/SEC	25.0		21.0	

*BASED ON CURRENT MARK 125 INJECTOR FOR PHASE I; ASSUMES 1% PERFORMANCE IMPROVEMENT IN PHASE II

CONFIDENTIAL

Predicted ARES Performance (u)

CONFIDENTIAL

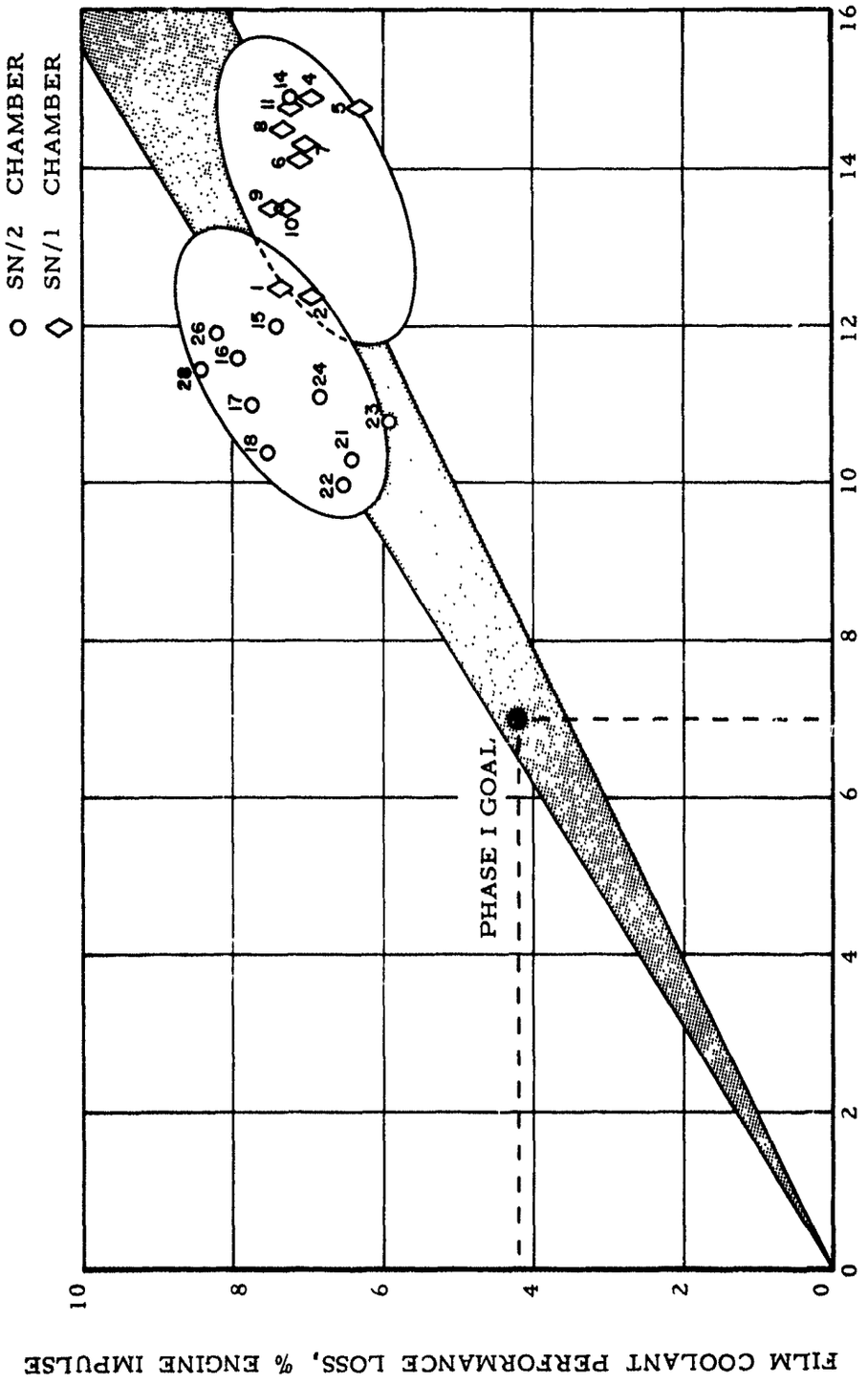

Percent Film Coolant Loss vs Percent Collant Flow
(Test Series 1.2-12-WAM)

Figure VI-89

Injector-Chamber Configuration for Transpiration Chamber SN 001
(Test Series 1.2-12-WAM)

Figure VI-90

TEST	014	015	016	017	018	021	022
INJECTOR	S/N-3	S/N-3	S/N-3	S/N-3	S/N-3	S/N-3	S/N-3
FCL (sec)	25.4	26.0	27.6	25.6	24.5	20.1	21.1
MRDL (sec)	6.0	6.0	6.0	6.0	6.0	6.0	6.0

TEST	023	024
INJECTOR	S/N-2	S/N-2
FCL (sec)	19.7	22.0
MRDL (sec)	0	0

TEST	026	028
INJECTOR	S/N-5	S/N-5
FCL (sec)	26.6	26.7
MRDL (sec)	3.0	3.0

Injector-Chamber Configuration for Transpiration Chamber SN 002
(Test Series 1.2-12-WAM)

Figure VI-91

	GENERAL DATA								MEASURED DATA					
	DATE	DURATION PS_1-PS_2	DATA PERIOD PS_1 +	INJ. SERIAL NUMBER	CHAMBER SERIAL NUMBER	THROAT AREA	AREA RATIO	CHAR. LENGTH	CHAMBER PRESSURE	INJECTOR MIXTURE RATIO	FILM COOLANT FLOW	VACUUM THRUST	ENGINE WEIGHT FLOW	MEA SEA SPE
SYMBOLS	---	---	---	---	---	A_t	---	L^*	P_c	MR_j	%OFC	F_v	$\dot{w}_t$	Is
UNITS	---	sec.	sec.	---	---	$in.^2$	---	in.	psia	---	lbs/sec	lbs	lbs/sec	s
TEST														
1.2-14-WAM-001	11-4-66	1.613		SN-1	SN-2	21.4	1.86	40	TRANSIENT TEST ONLY. NO PERFORMANCE INFORMATION.					
-002	11-4-66	2.011	1.857 1.957	SN-1	SN-2	21.4	1.86	40	2910	2.53	49.5	72,878	387	1
-003	11-4-66	1.616		SN-1	SN-3	19.61	21.75	42.3	TRANSIENT TEST ONLY. NO PERFORMANCE INFORMATION					
-004	11-5-66	2.050	1.895 1.995	SN-1	SN-3	19.61	21.75	42.3	2850	2.79	56.9	92,420	364	2
-005	11-10-66	1.734		SN-5	MALFUNCTION RESULTING IN INJECTOR AND CHAMBER DESTRUCTION									

DATA				PERFORMANCE							PERCENT PERFORMANCE		
ILM OLANT LOW	VACUUM THRUST	ENGINE WEIGHT FLOW	MEASURED SEA-LEVEL SPECIFIC	VACUUM SPECIFIC	MIXTURE RATIO DISTR.	NOZZLE GEOMETRY LOSS	NOZZLE FRICTION LOSS	FILM COOLING LOSS	COMB. LOSS	THEO. VACUUM SPECIFIC IMPULSE	PERCENT COOLANT	PERCENT COOLANT LOSS	PERCENT VACUUM SPECIFIC IMPULSE
WOFC #/sec	F_v lbs	$\dot{w}_t$ lbs/sec	$I_{s_{S.L.}}$ sec.	I_{sv} sec.	MRDL sec.	NGL sec.	NFL sec.	FCL sec.	ERL sec.	I_{sV_t} sec.	% WOFC %	% IsPc %	% Is_V %
O PERFORMANCE INFORMATION.													
9.5	72,878	387	187	188	5.2	13.5	0.2	17.7	6.4	231	12.8	7.68	81.4
O PERFORMANCE INFORMATION													
6.9	92,420	364	237	254	14.1	2.3	2.8	28.2	9.6	311	15.6	9.07	81.8
ON													

Regenerative Chamber Test Data and Performance Summary (u)

Figure VI-92

CHAMBER S/N-1	TEST 1.2-12-WAM- 001	002	005	THERM. DEPTH
Compartment #1				
$\dot{W}_{FC-1}$	2.03	1.93	2.00	
T_{CSC-1}	380	321		.006
T_{CSC-2}	260	362		.015
T_{CSC-3}	350	294		.007
T_{CSC-4}	260			.017
T_{CSC-5}	292			.007
T_{CSC-}	197	369		.006
Compartment #2				
$\dot{W}_{FC-2}$	5.86	6.23	6.07	
T_{CSC-9}	320			.005
T_{CSC-10}	370	454		.005
T_{CSC-11}	407		345	.006
Compartment #3				
$\dot{W}_{FC-3}$	5.86	6.06	5.98	
T_{CSC-13}	378	393		.005
T_{CSC-14}	158	179		.072
Compartment #4				
$\dot{W}_{FC-4}$	4.16	4.02	4.10	
T_{CSC-20}				.006
T_{CSC-21}	140	227		.059
T_{CSC-22}	368	536		.005
T_{CSC-23}	418	298		.004
T_{CSC-24}	342			.016
Compartment #5				
$\dot{W}_{FC-5}$	4.07	4.06	4.08	
T_{CSC-25}	748			.007
T_{CSC-28}	882			.006
Compartment #6				
$\dot{W}_{FC-6}$	4.76	4.72	10.70	
T_{CSC-32}	1140	2410		.005
T_{CSC-36}	1561			.006

CHAMBER S/N-1	TEST 1.2-12-WAM- 001	002	005	THERM. DEPTH
Compartment #7				
$\dot{W}_{FC-7}$	2.62	2.49	4.59	
T_{CSC-37}	1518			.005
T_{CSC-38}	955			.006
T_{CSC-40}	1079			.005
T_{CSC-41}	1120			.004
T_{CSC-42}	1050			.005
Compartment #8				
$\dot{W}_{FC-8}$	1.34	1.30	1.93	
T_{CSC-43}	1803			.005
T_{CSC-44}	2245			.021
T_{CSC-45}	900			.006
Compartment #9				
$\dot{W}_{FC-9}$	1.28	1.28	2.44	
T_{CSC-51}	587			.008
T_{CSC-53}	525			.005
T_{CSC-54}	605			.005
Compartment #10				
$\dot{W}_{FC-10}$	1.93	1.94	2.02	
T_{CSC-57}	300			.006
T_{CSC-58}	418			.007
T_{CSC-59}	292			.007
T_{CSC-60}	438	105		.006
Compartment #11				
$\dot{W}_{FC-11}$	4.28	4.21	4.25	
T_{CSC-61}	1150	2095		.006
T_{CSC-62}	395	660		.007
T_{CSC-63}	407			.005

NOTE: 1. All temperatures (T_{CSC-N}), °F

2. Weight Flows ($\dot{W}_{FC-N}$), lb/sec N_2O_4

3. Thermocouple Depths, in.

4. Test -001 & 002 do not reach steady state.

Transpiration Chamber SN-001 Temperature Summary

Figure VI-93

Report 10830-F-1, Phase I

CHAMBER S/N-2	TEST 1.2-12-WAM- 014	015	016	017	018	021	022	023	024	THERM. DEPTH
Compartment #1										
$\dot{W}_{FC-1}$	1.94	1.98	1.94	1.96	2.33	2.56	2.32	2.87	3.07	
T_{CSC-1}	384	383	440	471						.005
T_{CSC-3}	425	475	448	524	548		600	530	480	.005
T_{CSC-4}	326									.008
Compartment #2										
$\dot{W}_{FC-2}$	4.28	4.50	4.27	4.56	3.18	3.20	3.13	3.24	3.36	
T_{CSC-7}	366									.006
T_{CSC-8}	396	422	455	370	546					.005
T_{CSC-9}	541	556	630	521	709	565	570			.002
T_{CSC-10}	583	761	800	897	1565					.006
T_{CSC-11}	552	584	709	598	839					.006
Compartment #3										
$\dot{W}_{FC-4}$	5.20	4.45	4.23	3.72	2.50	2.52	2.46	2.55	2.59	
T_{CSC-13}						950	1038	1419	1042	.007
T_{CSC-14}	238	318	427	428	630	507	570	514	370	.053
T_{CSC-15}	380	403	430	414	658	742	731	962	813	.006
T_{CSC-17}	480	481	515	554	749	830	817	842	841	.005
T_{CSC-18}	462	506	572	704	1034					.006
Compartment #4										
$\dot{W}_{FC-4}$	3.92	4.06	3.74	3.14	2.44	2.37	2.29	2.37	2.38	
T_{CSC-20}		393	438		1119					.005
T_{CSC-23}	300	300	332	561	424					.006
Compartment #5										
$\dot{W}_{FC-5}$	4.60	5.97	5.23	5.71	6.03	5.73	5.34	6.22	6.74	
T_{CSC-25}	290	281	281	290	320					.005
T_{CSC-26}	293	405	563	473	583					.014
T_{CSC-29}	162	178	158	167	189	234	185	211	190	.020
Compartment #6										
$\dot{W}_{FC-6}$	8.67	7.81	7.53	7.52	7.42	7.21	7.09	8.59	8.27	
T_{CSC-31}	575	574	538	555	1544					.014
T_{CSC-33}		459	570	586	660					.010
T_{CSC-35}	307	324	309	528	331					.009
T_{CSC-36}	560	645	600	647	549	421	709	491	380	.007

NOTE:

1. All temperature (T_{CSC-N}), °F
2. Weight Flows ($\dot{W}_{FC-N}$), $lb/sec_{N_2O_4}$
3. Thermocouple depth, in.

Transpiration Chamber SN 002 Temperature Summary

Figure VI-94, Sheet 1 of 2

Report 10830-F-1, Phase I

CHAMBER S/N-2	014	015	016	TEST 1.2-12-WAM-017	018	021	022	023	024	THERM. DEPTH
Compartment #7										
$\dot{W}_{FC-7}$	4.03	3.86	3.71	3.65	3.64	3.69	3.37	3.82	4.38	
T_{CSC-37}	533	590	655	716	691					.009
T_{CSC-38}	677	720	704	767						.008
T_{CSC-39}	438	495	648	639						.007
T_{CSC-42}	858									
Compartment #8										
$\dot{W}_{FC-8}$	1.44	1.39	1.27	1.12	1.29	2.21	2.19	2.29	2.30	
T_{CSC-43}		943	900	901	934					.007
T_{CSC-44}	989	701	765	849	801					.016
T_{CSC-47}	1531	1485	1489	1566	1408					.006
T_{CSC-48}		1042	500	212	1440					.010
Compartment #9										
$\dot{W}_{FC-9}$	1.77	1.60	1.35	1.20	1.29	2.04	1.61	2.25	2.30	
T_{CSC-50}	165	203	208	234	281					.021
T_{CSC-52}	1053	1115	1150	1189	1145					.005
T_{CSC-54}	839									.005
Compartment #10										
$\dot{W}_{FC-10}$	2.02	1.85	2.08	2.07	2.08	2.01	1.98	Invalid	2.23	
T_{CSC-57}	398	430	485	552	584					.005
T_{CSC-59}	673	687	700	831						.006
T_{CSC-60}	527	551	620	748	770					.006
Compartment #11										
$\dot{W}_{FC-11}$	2.38	3.62	3.09	2.64	2.74	1.86	1.80	1.87	1.83	
T_{CSC-61}	135	151	150	164	153					.006
T_{CSC-62}	229	245	263	337						.006
T_{CSC-64}	321	367	401	533						.006
T_{CSC-65}	149	158	162	166	154					.007
T_{CSC-66}	70	90	100	99	99					.071

NOTE: 1. Temperatures (TCSC-N), °F
2. Weight Flows ($\dot{W}_{FC-N}$), lb/sec$_{N_2O_4}$
3. Thermocouple Depth, in.

Transpiration Chamber SN 002 Temperature Summary

Figure VI-94, Sheet 2 of 2

Compartment No.	Test No. -016	-017	-018	Clock Location	TC No.
1.	615	645		4:30	TCSC-1
	623	699	723	12:20	-3
2.	630	545	721	6:00	-8
	700	591	779	3:00	-9
	1010	1107	1775	2:30	-10
	919	708	1059	12:40	-11
3.	640	624	868	4:20	-15
	690	729	924	4:20	-17
	782	914	1254	8:15	-18
4.	613		1294	4:40	-20
	542	771	634	10:40	-23
5.	481	490	520	6:20	-25
6.	1020	1036	1110	2:40	-33
	714	733	736	10:40	-35
	915	962	864	9:30	-36
7.	1105	1166	1141	7:15	-37
	1104	1167		3:20	-38
	998	989		12:20	-39
8.	1250	1251	1284	7:30	-43
	1789	1866	1708	10:40	-47
	1000	712	1940	8:40	-48
9.	1400	1439	1395	10:20	-52
10.	735	802	834	3:40	-57
	1000	1131		1:30	-59
	920	1048	1070	11:30	-60
11.	450	464	453	7:15	-61
	563	637		3:15	-62
	701	833		12:20	-64
	512	516	504	8:15	-65

Transpiration Chamber SN 002 Surface Temperatures
(Tests 1.2-12-WAM-016 to 018)

Figure VI-95

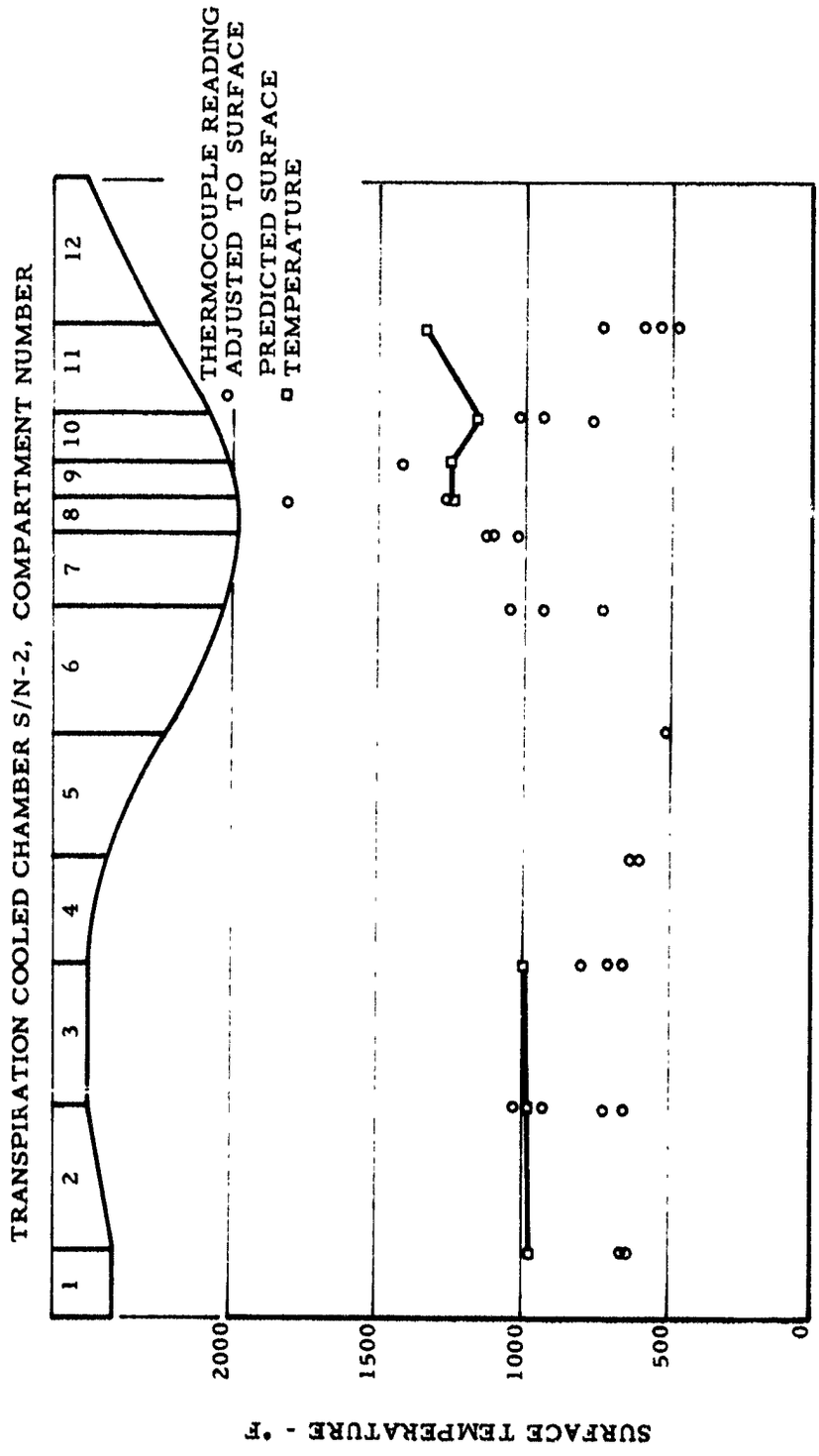

Measured and Predicted Temperatures for Test 1.2-12-WAM-016

Figure VI-96

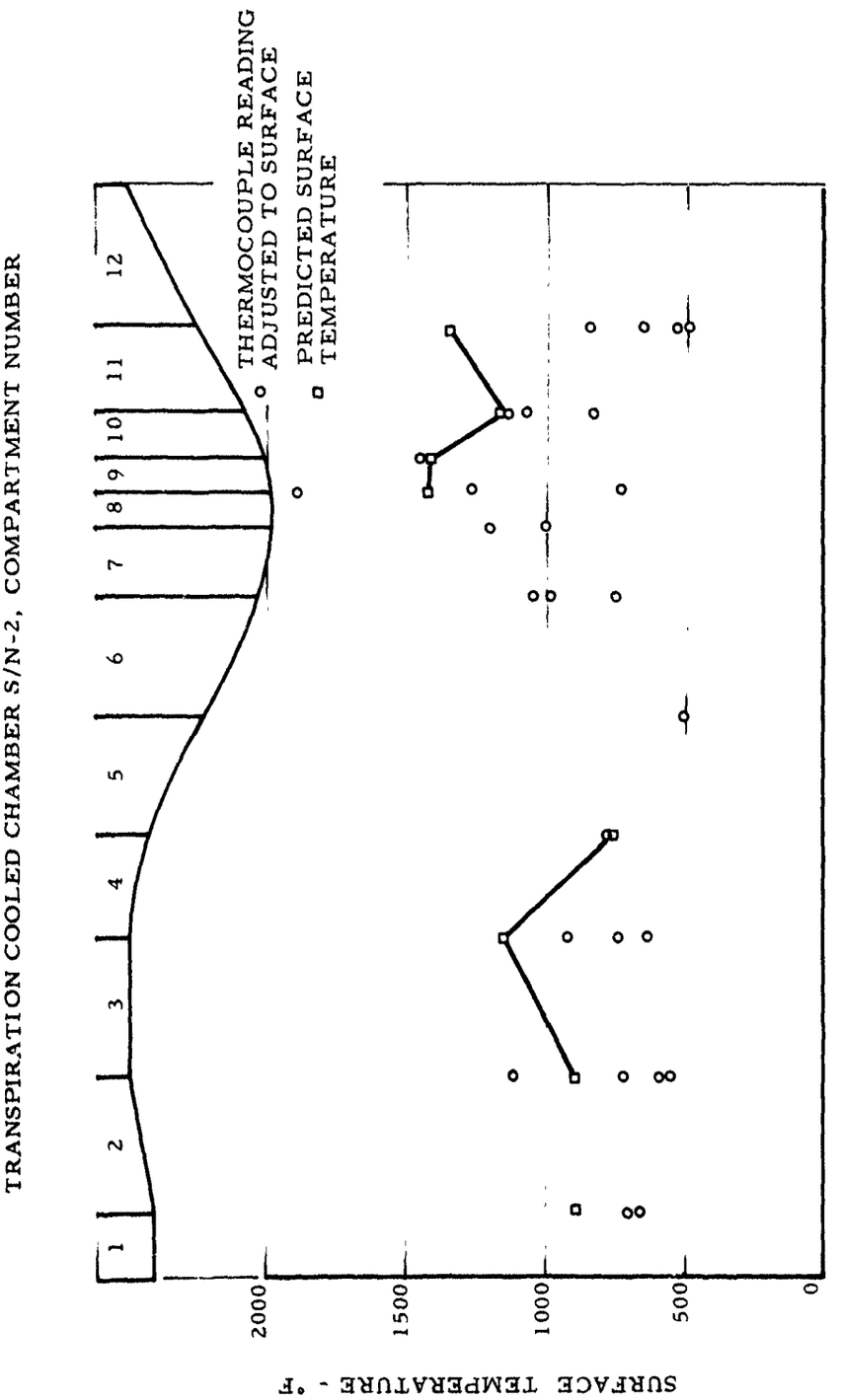

Measured and Predicted Temperatures for Test 1.2-12-WAM-017

Figure VI-97

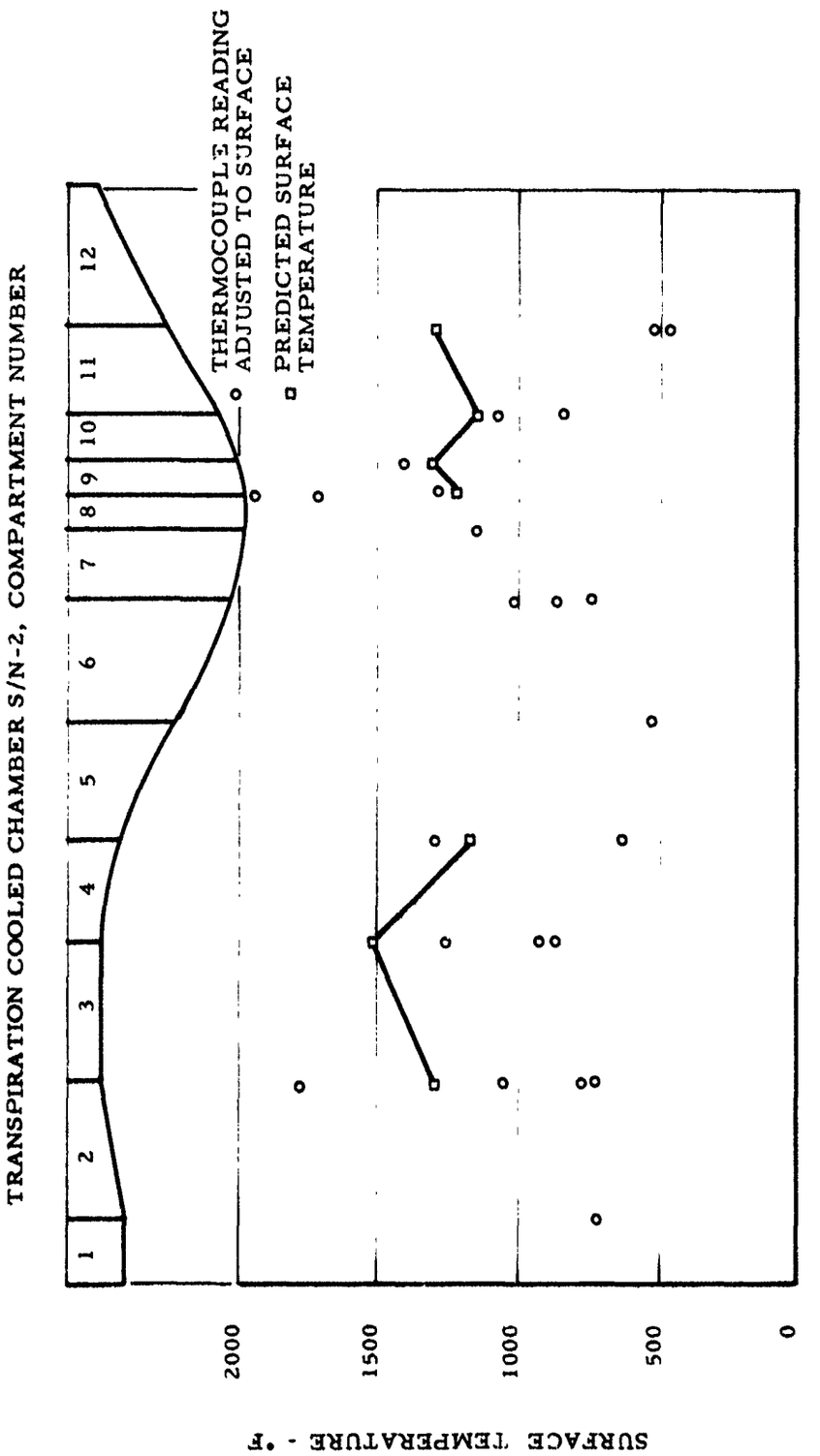

Measured and Predicted Temperatures for Test 1.2-12-WAM-018

Figure VI-98

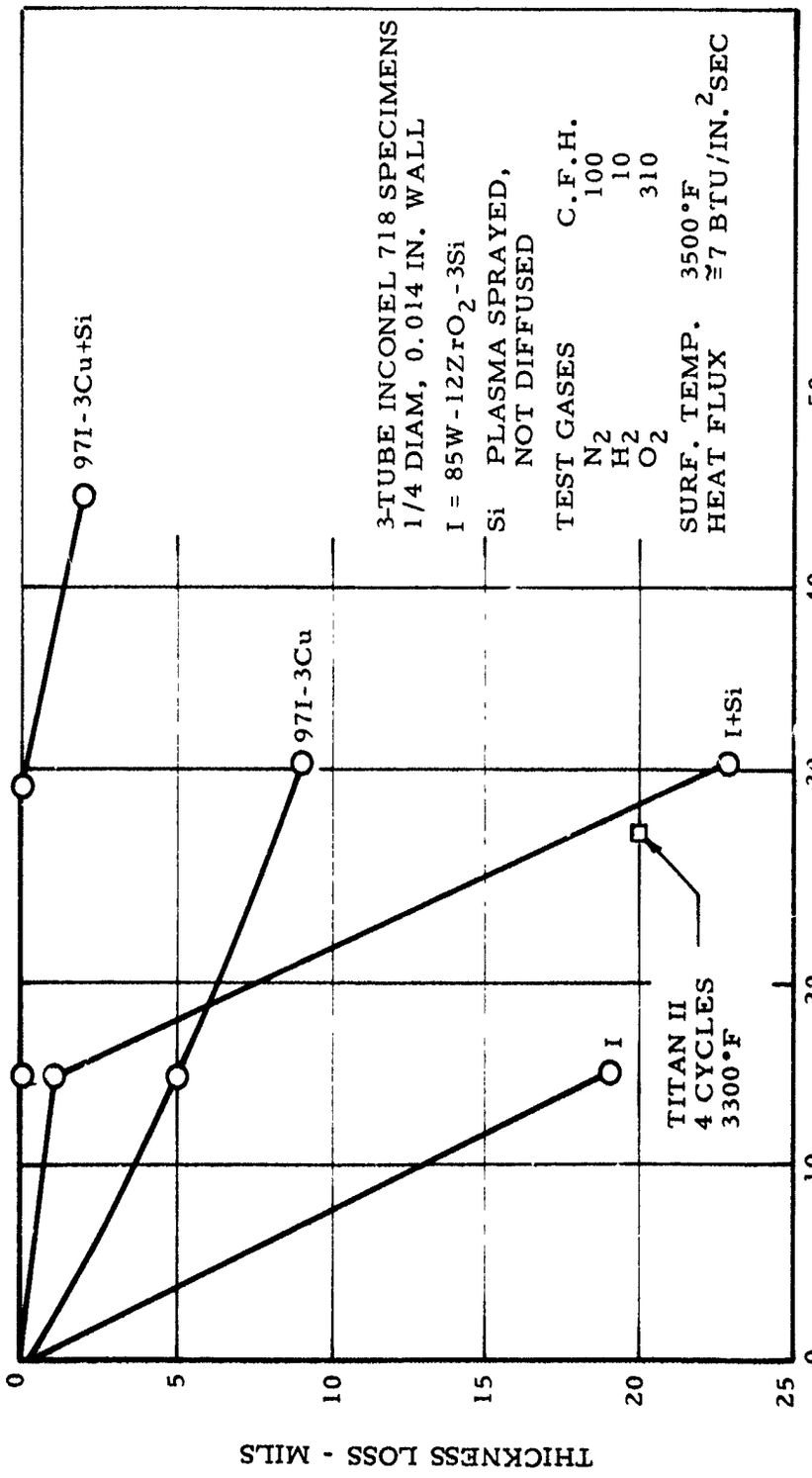

Plasma Thermal Shock/Oxidation Test Results

Figure VI-99

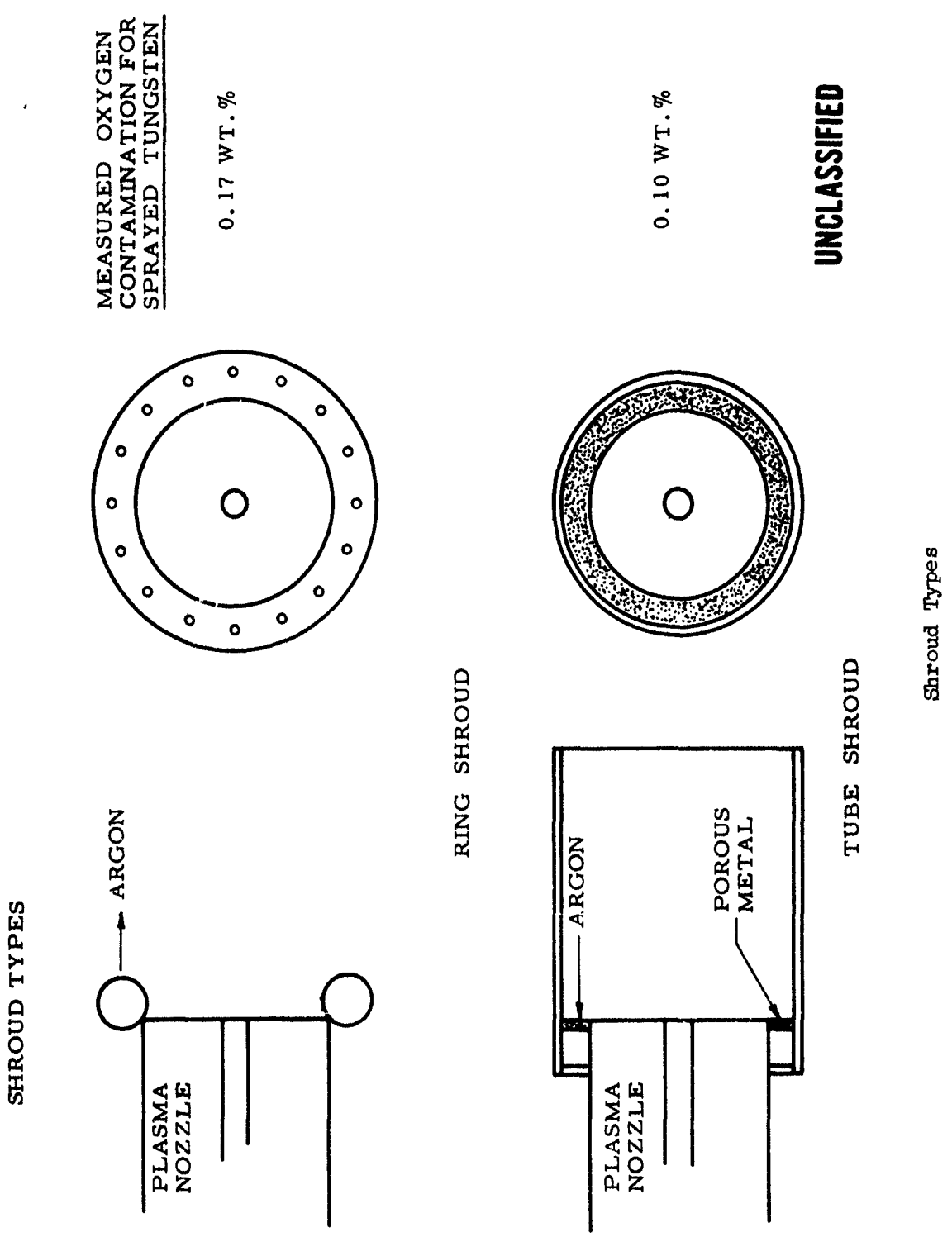

Figure VI-100

Brazed Bonded Laminated Tungsten Cermet Thermal Barrier (u)

Figure VI-101

As sprayed 95W-5 gold alloy on stainless steel 400X Iodine Etch

Braze bonded two hours at 1730°F in vacuum 400X Iodine Etch

Braze Bonding Microstructure (u)

Figure VI-102

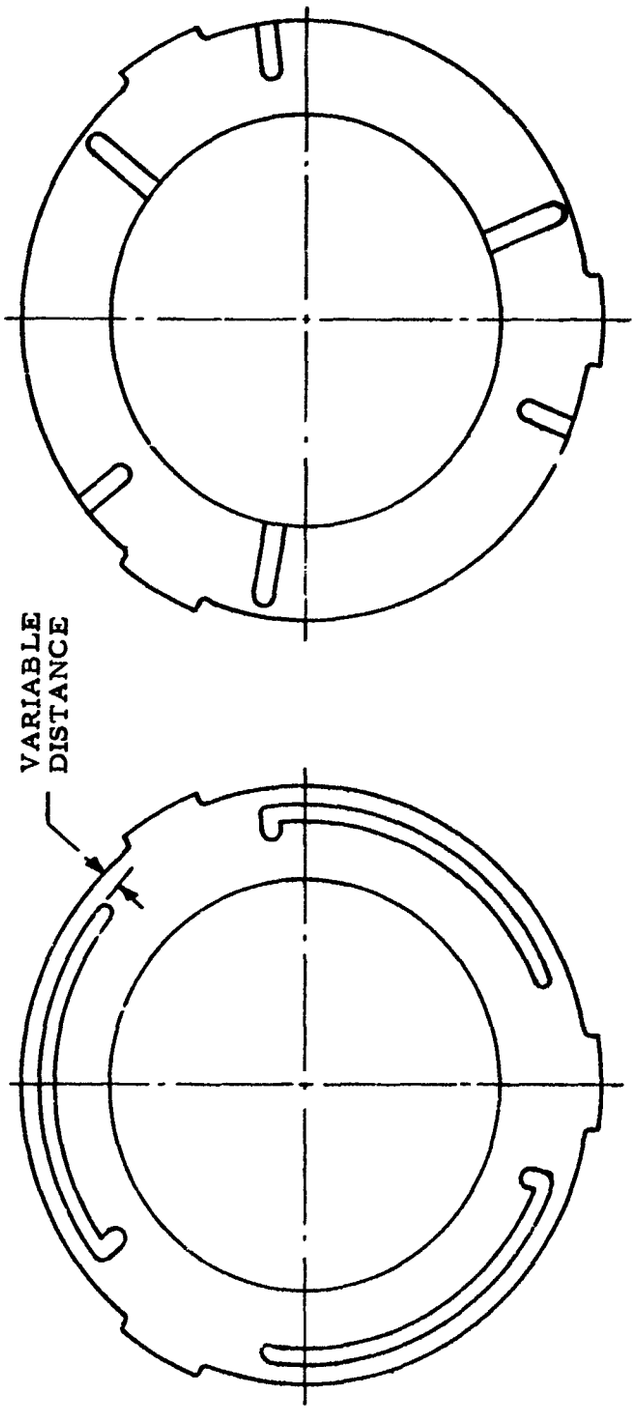

Transpiration Laboratory Program, Subscale Washers

Figure VI-103

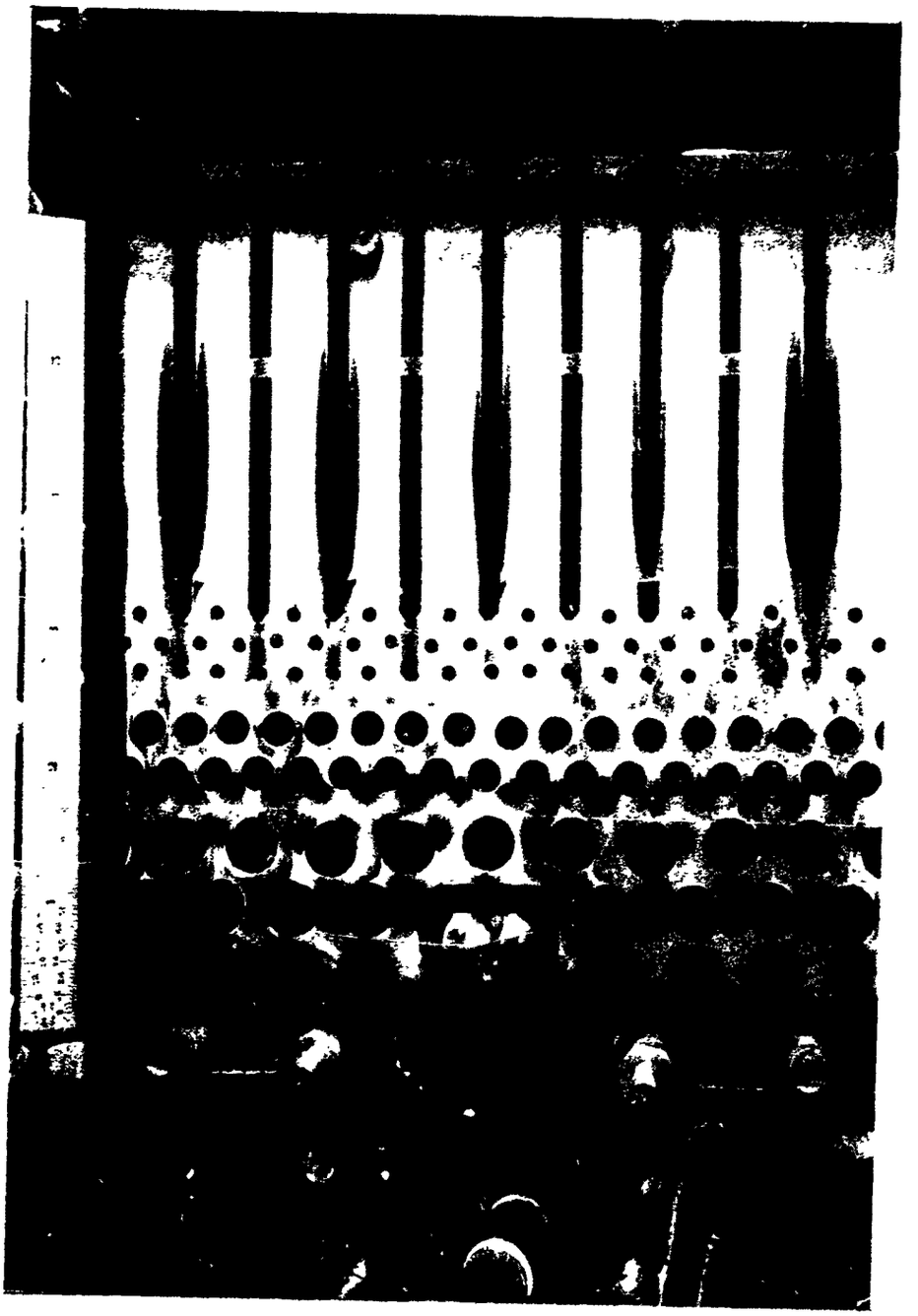

Photograph of Transparant Scale Model Simulating Diffusion Area

Figure VI-104

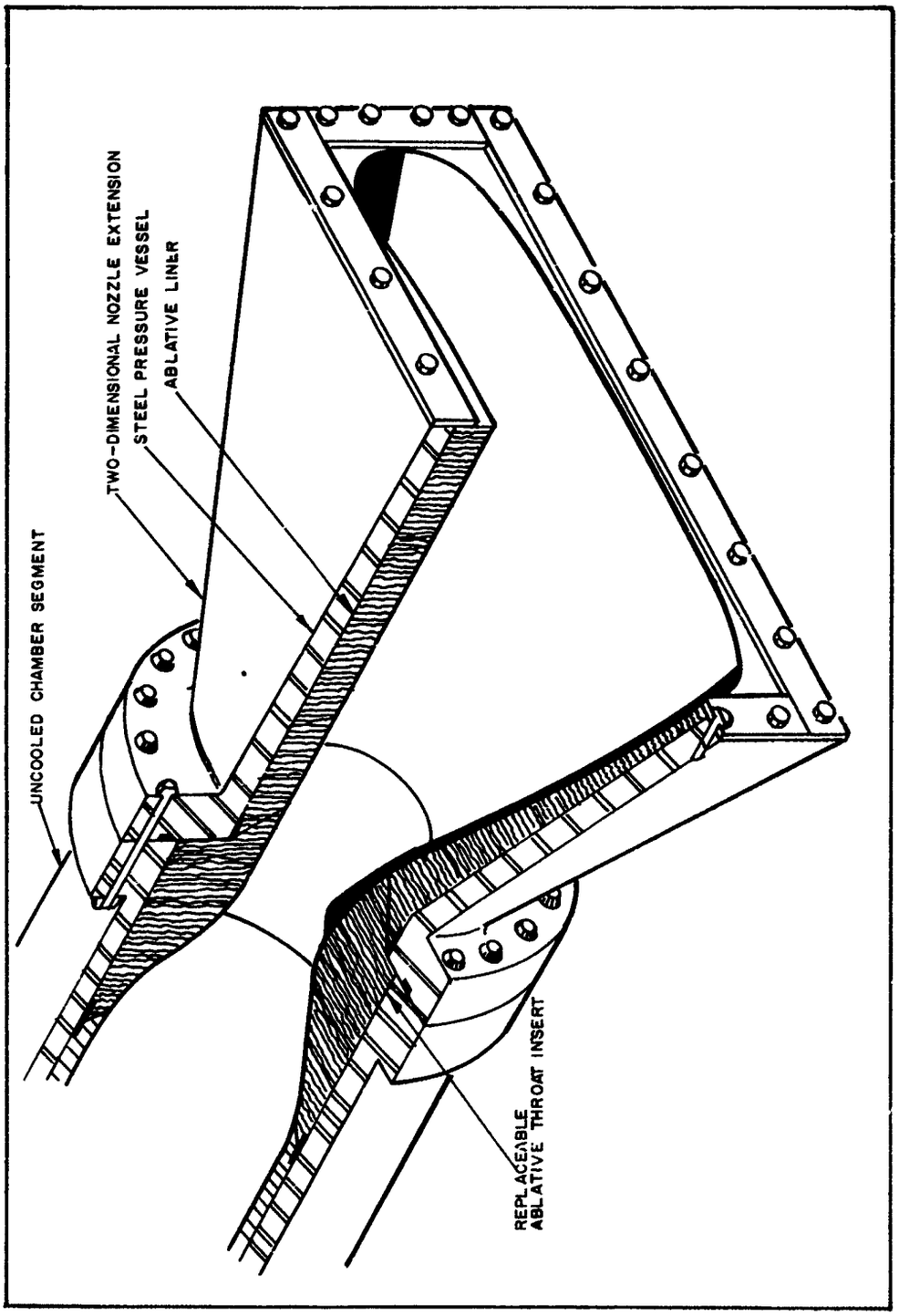

Two-Dimensional Nozzle Design

Figure VI-105

Two-Dimensional Nozzle Assembly

Figure VI-106

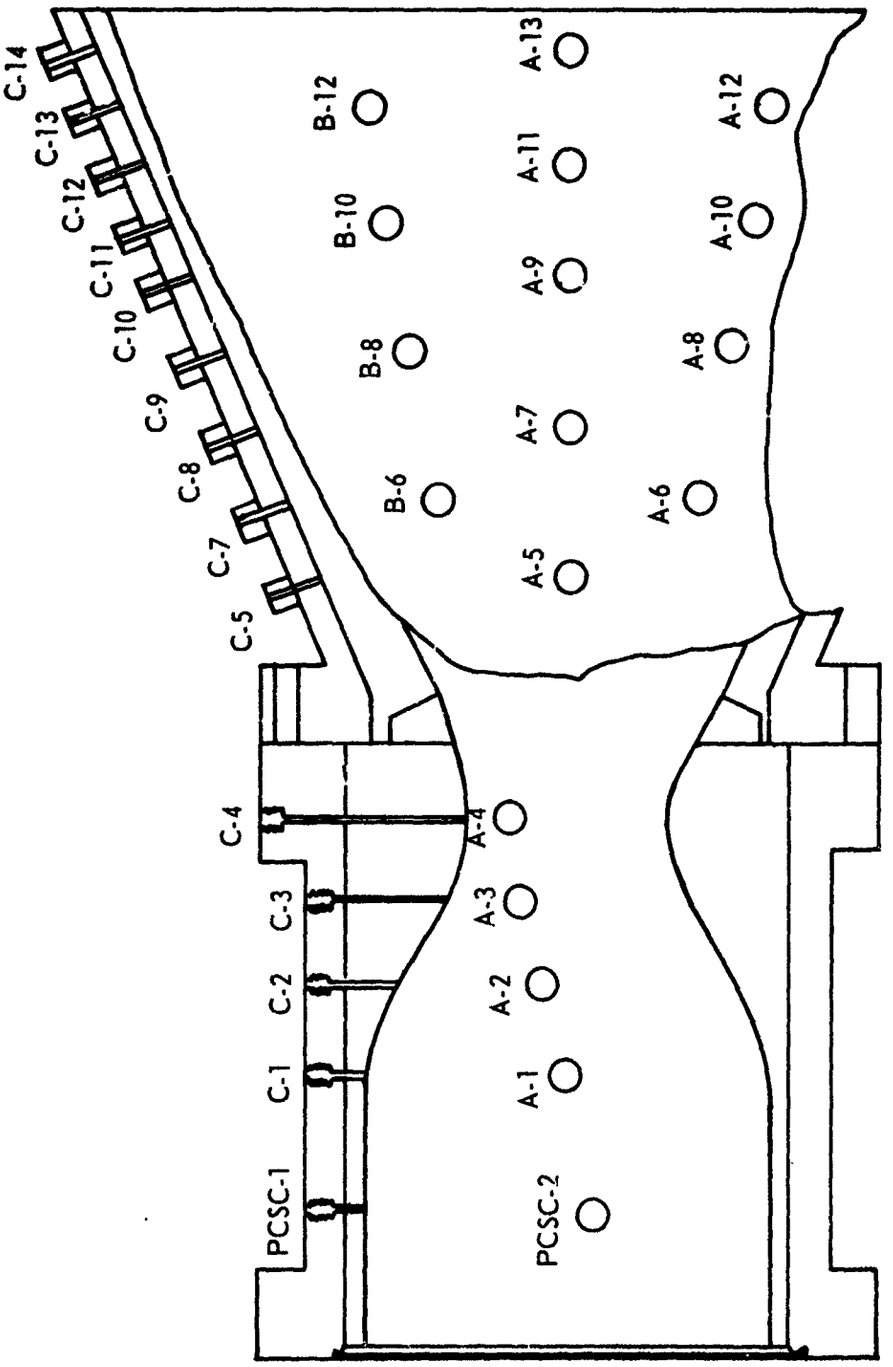

Chamber-Nozzle Instrumentation Schematic

Figure VI-107

	GENERAL DATA								MEASURED DATA					
	DATE	DURATION FS_1-FS_2	DATA PERIOD FS_1 +	INJ. SERIAL NUMBER	CHAMBER CONFIG.	THROAT AREA	AREA RATIO	CHAR. LENGTH	CHAMBER PRESS.	INJECTOR MIXTURE RATIO	FILM COOLANT FLOW RATE	VACUUM THRUST	ENGINE WEIGHT FLOW	M SE SI I
SYMBOLS / UNITS	---	sec.	sec.	---	--	A_t $in.^2$	---	L^* in.	Pc psia	MR_j ---	WOFC lbs/sec	Fv lbs	Wt lbs/sec	Is s
TEST														
1.2-11-WAM-023	10-18-66	3.012	1.96-2.96	3	2-D	21.712	4.77	30	2775	2.19	55.4	89,310	377.0	
1.2-11-WAM-025	11-18-66	2.263	2.11-2.21	5	2-D	23.486	4.4	27.7	2720	2.23	61.2	95,010	401.9	

DATA				PERFORMANCE							PERCENT PERFORMANCE		
LM LANT OW TE	VACUUM THRUST	ENGINE WEIGHT FLOW	MEASURED SEA-LEVEL SPECIFIC IMPULSE	VACUUM SPECIFIC IMPULSE	MIXTURE RATIO DIST. LOSS	NOZZLE GEOMETRY LOSS	NOZZLE FRICTION LOSS	FILM COOLING LOSS	COMB. LOSS	THEO. VACUUM SPECIFIC IMPULSE	PERCENT COOLANT	PERCENT COOLANT LOSS	PERCENT VACUUM SPECIFIC IMPULSE
C /sec	F_V lbs	$\dot{W}_t$ lbs/sec	$Is_{S.L.}$ sec.	Is_V sec.	MRDL sec.	NGL sec.	NFL sec.	FCL sec.	ERL sec.	IsV_t sec.	% $\dot{W}_{OFC}$ %	% Is_{FC} %	% IsV %
.4	89,310	377.0	233	237	Loss data compromised by nozzle configuration.					291	14.65	-	81.5
.2	95,010	401.9	233	237	Loss data compromised by nozzle configuration.					283.3	15.2	-	83.8

Test Data Summary (u)

Figure VI-.08

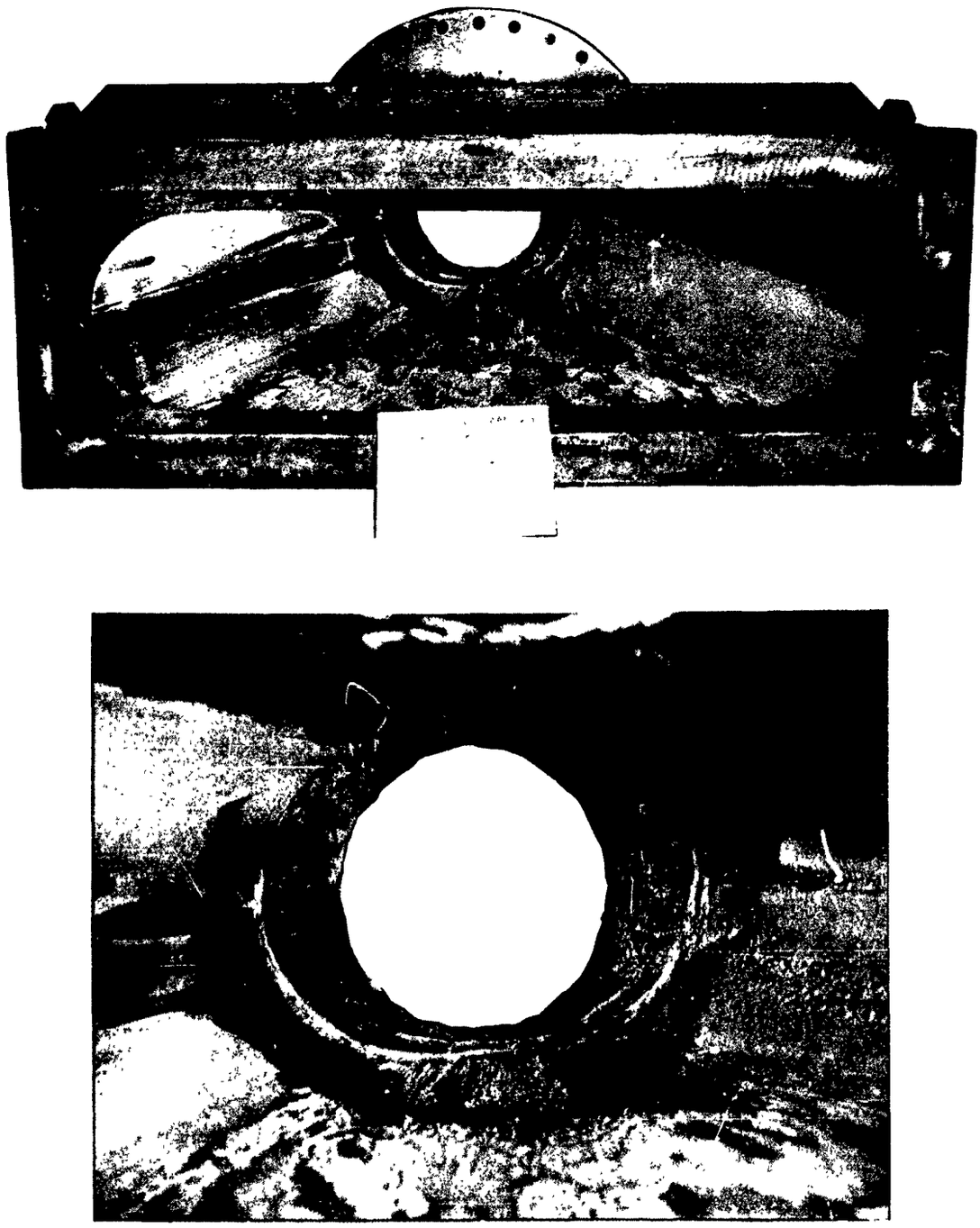

Condition of Nozzle After Test 1.2-11-WAM-025

Figure VI-109

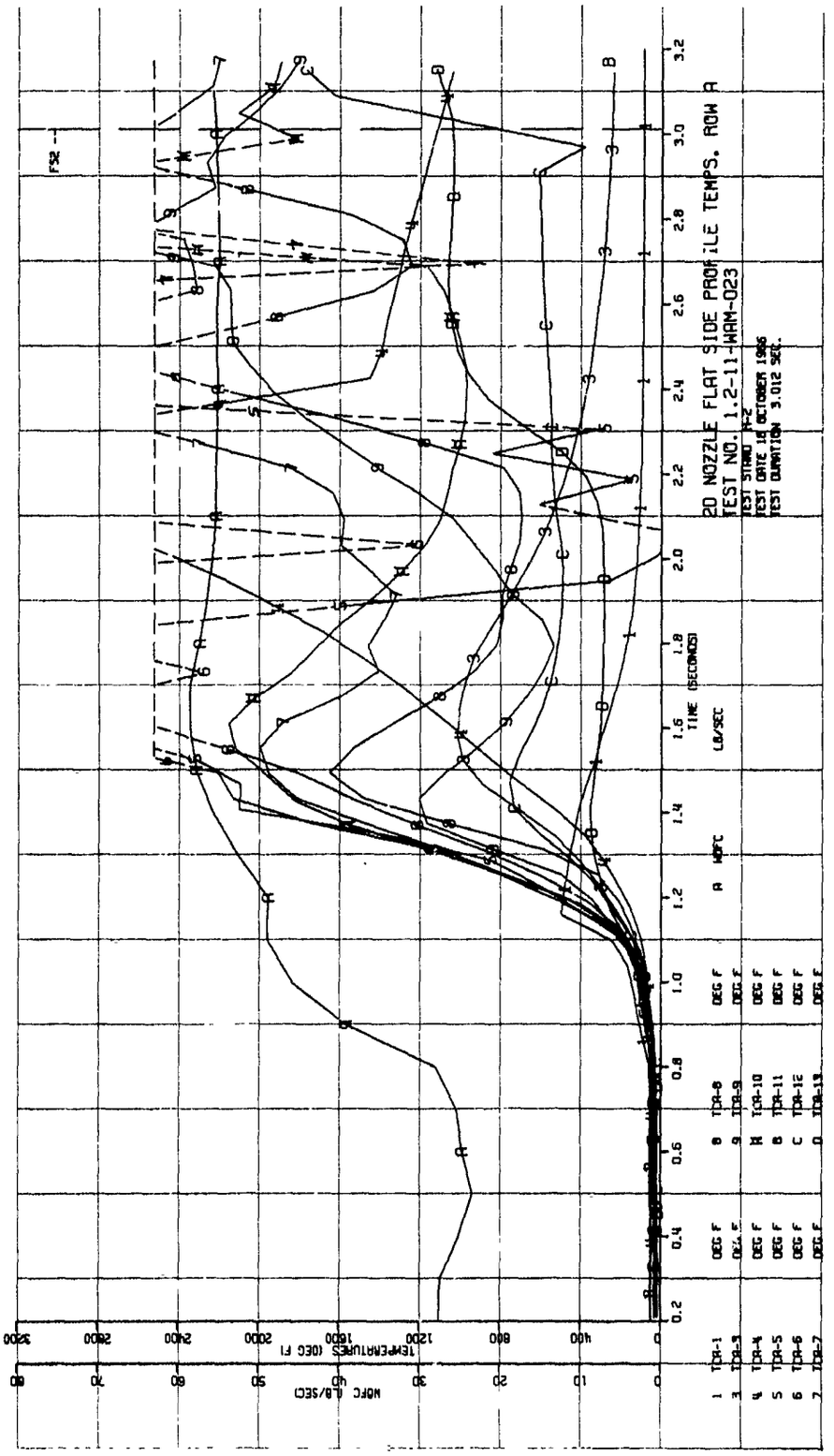

Nozzle Temperature Data, Test 1.2-11-WAM-023

Figure VI-110, Sheet 1 of 3

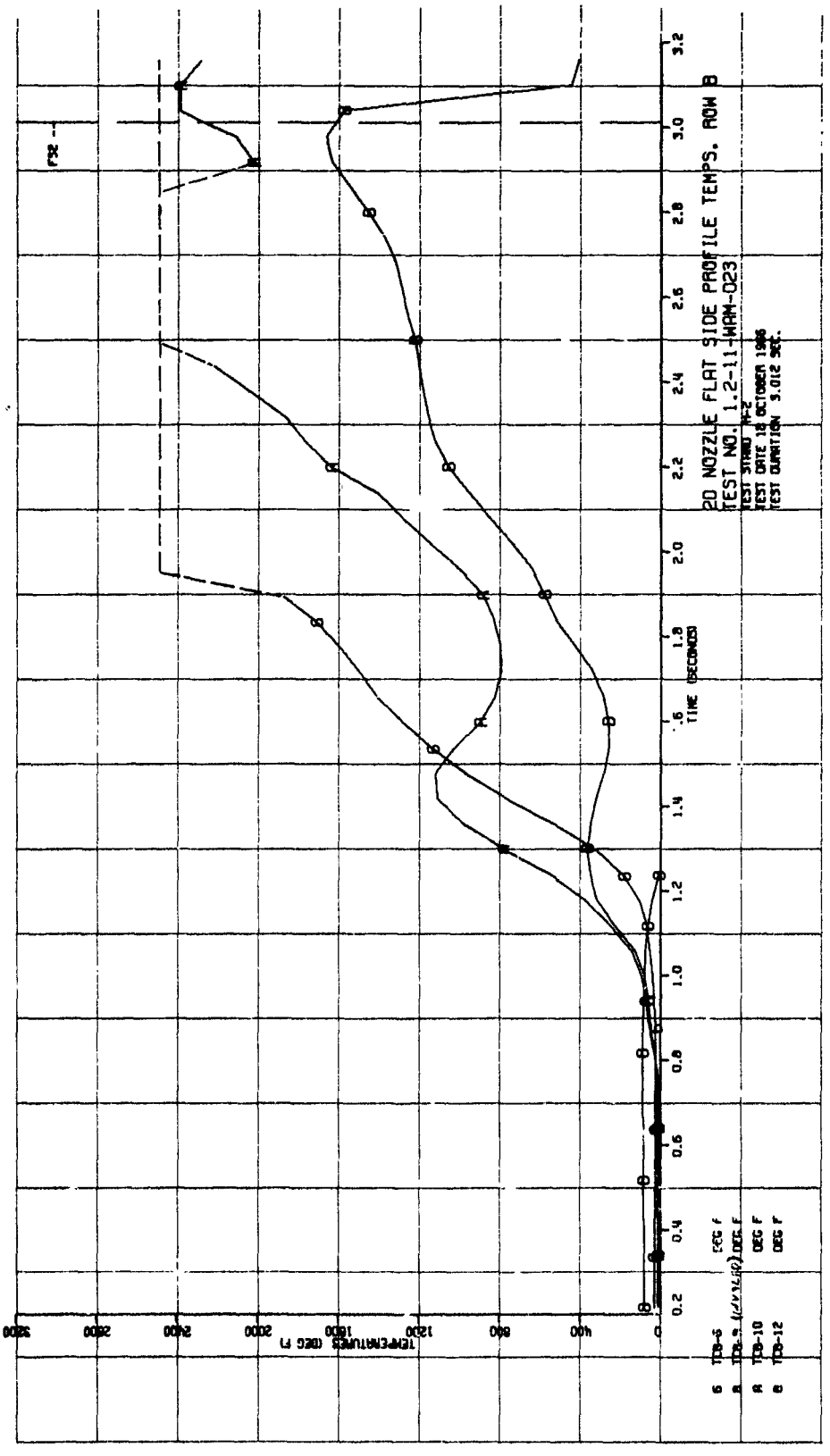

Nozzle Temperature Data, Test 1.2-11-WAM-023

Figure VI-110, Sheet 2 of 3

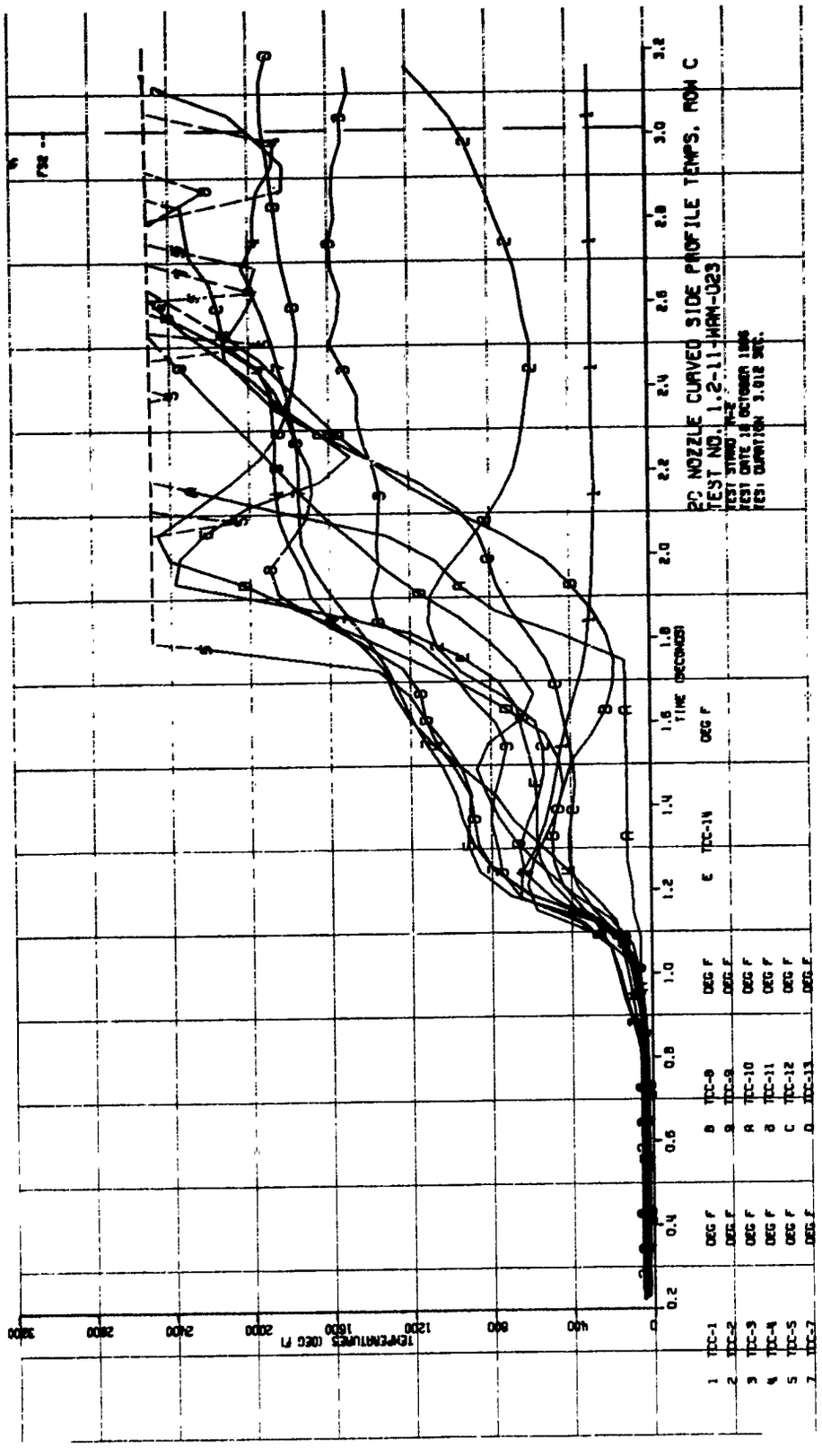

Nozzle Temperature Data, Test 1.2-11-WAM-023

Figure VI-110, Sheet 3 of 3

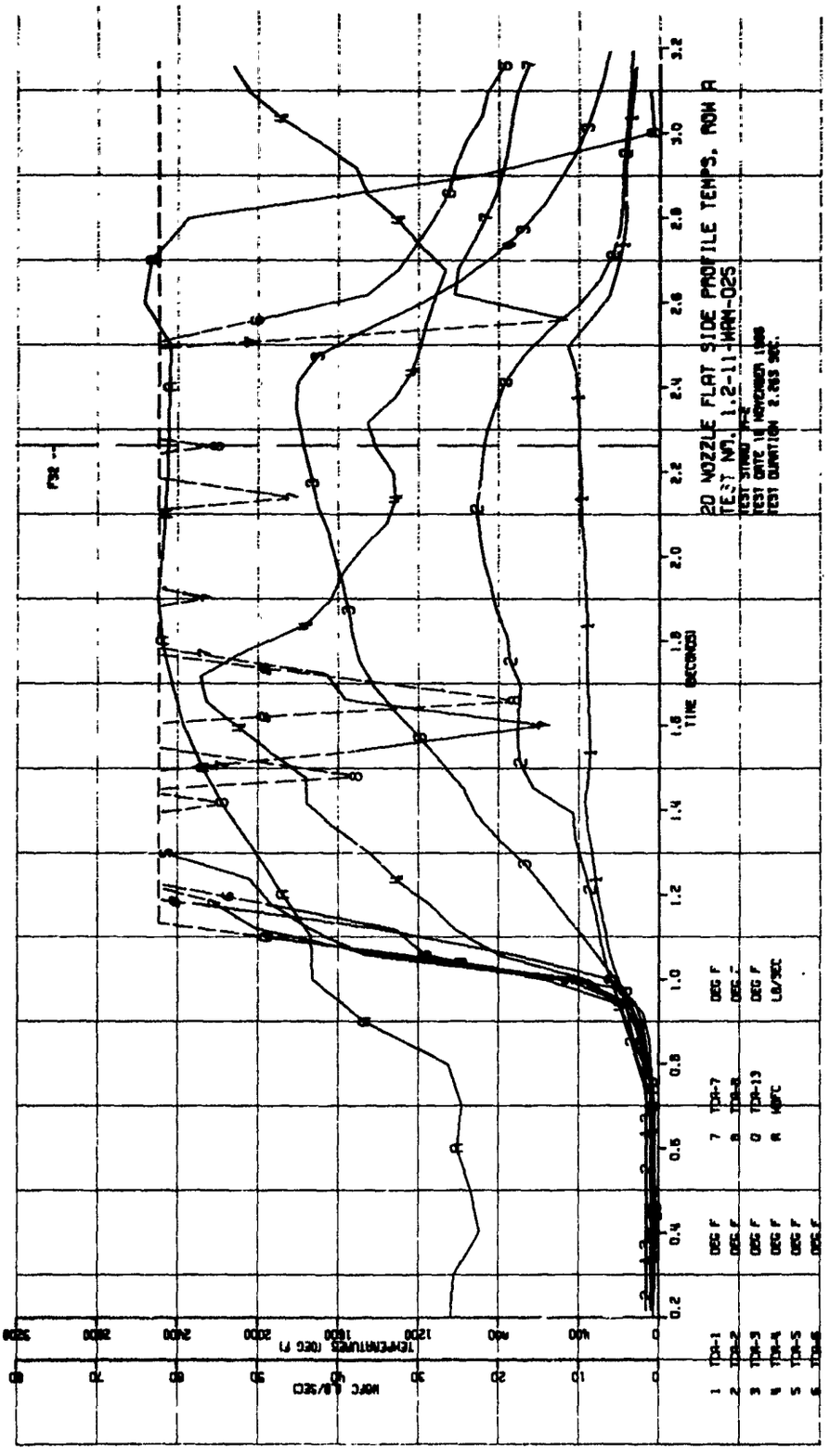

Nozzle Temperature Data, Test 1.2-11-WAM-025

Figure VI-111, Sheet 1 of 3

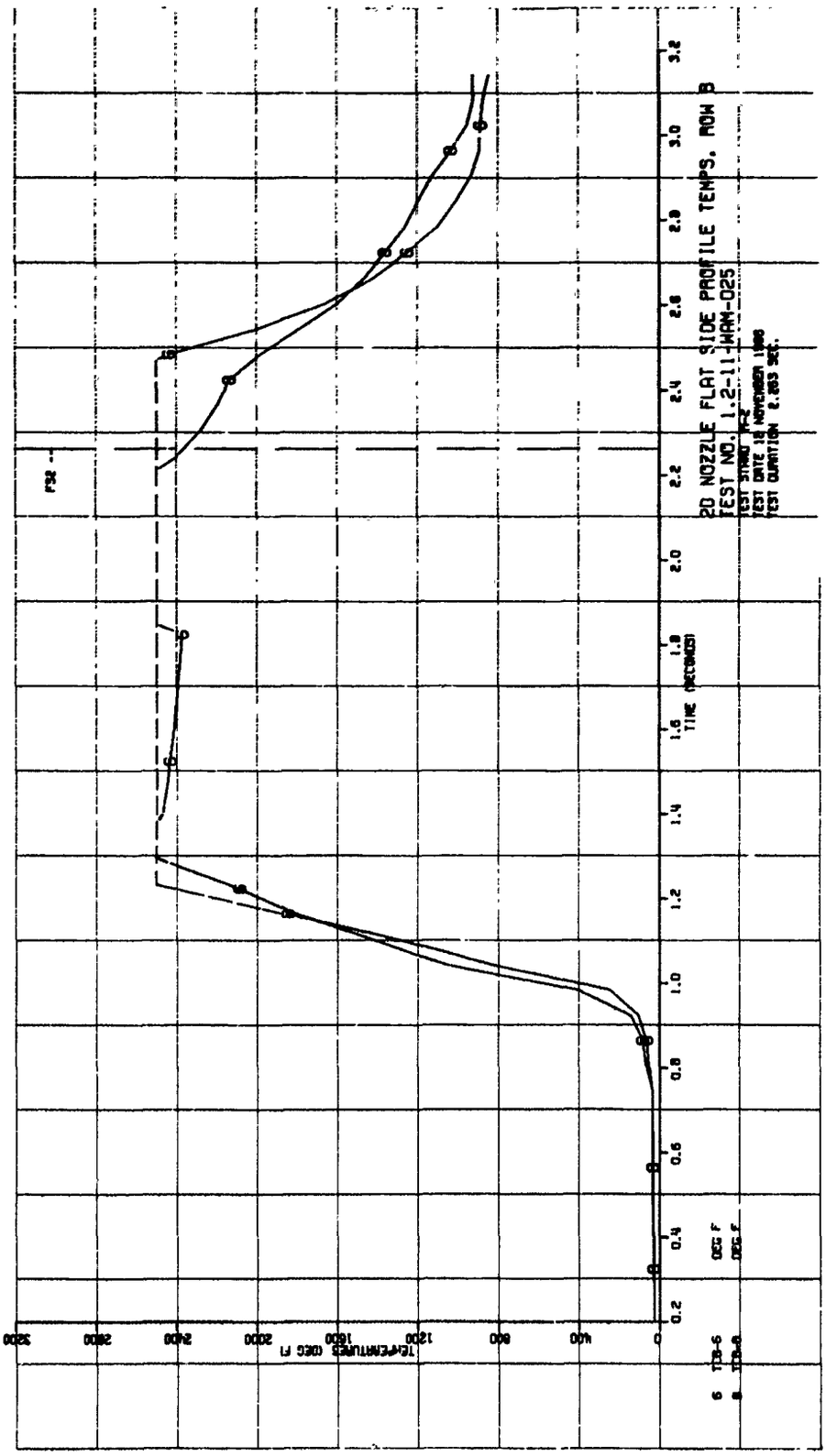

Nozzle Temperature Data, Test 1.2-11-WAM-025

Figure VI-111, Sheet 2 of 3

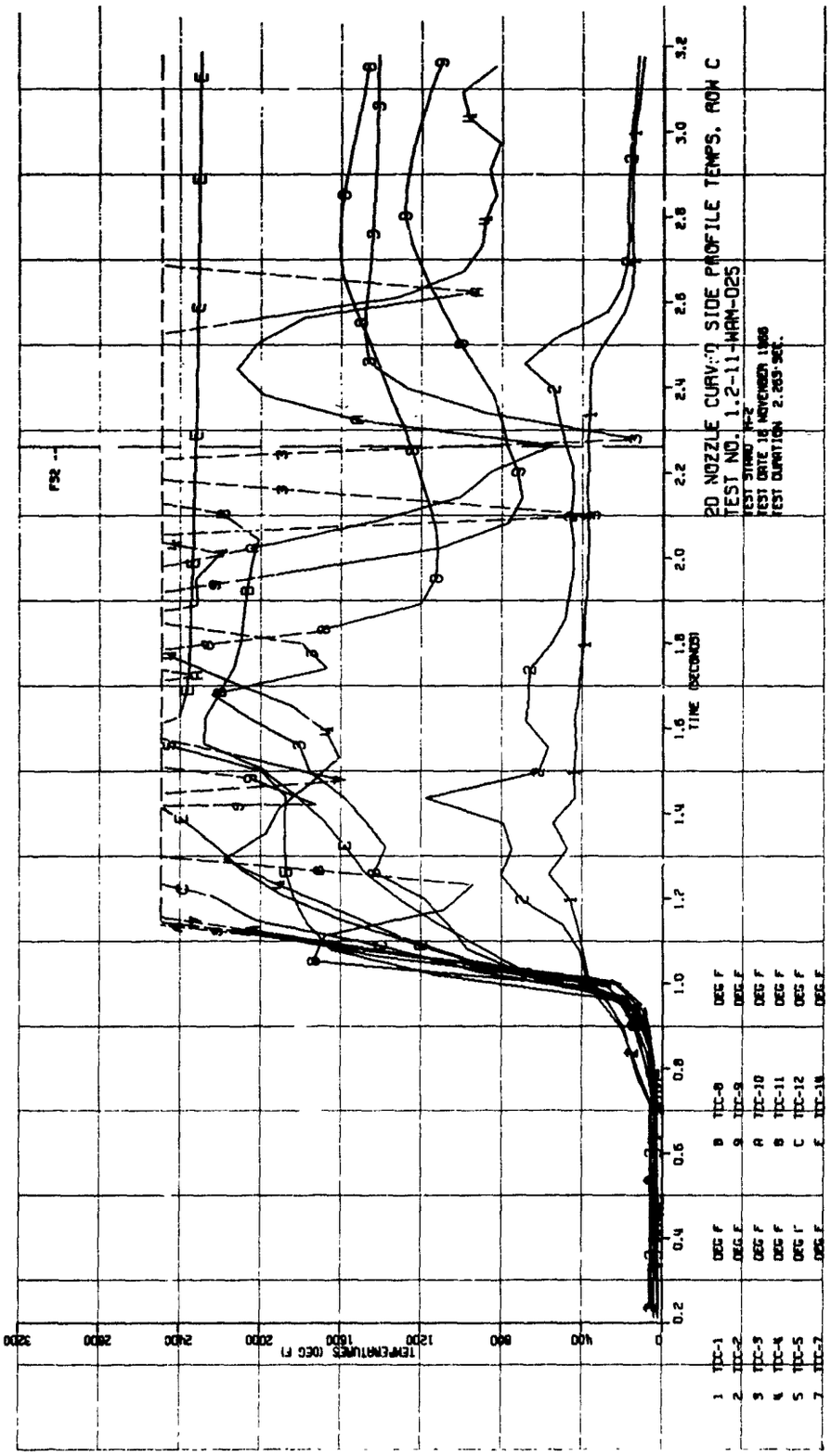

Figure VI-111, Sheet 3 of 3

Nozzle Temperature Data, Test 1.2-11-WAM-025

VII.

CONTROLS

VII.

CONTROLS

A. INTRODUCTION

(U) A review of the ARES moduls control requirements showed that the key control system functions requiring feasibility demonstration under this program phase were propellant shutoff and primary and secondary combustion chamber fuel flow control. The principal activities pursued under the Controls Task included initial development of the oxidizer and fuel suction (shutoff) valves, primary and secondary combustor fuel control valves, and developmental controllers and actuators for the valves. A secondary activity was associated with design of main pump suction lines and boost pump feed lines.

(U) Analyses of the ARES propellant supply system and proposed mission requirements dictated the need for propellant shutoff valves which: (1) were closely coupled to the engine to minimize propellant residual volume at shutoff; (2) would provide near zero leakage for long-term storage; and (3) would provide effective shutoff after initial actuation. Additionally, they must be capable of opening and closing in less than 0.400 sec with minimum "on-board" power.

(U) Dynamic analyses of the engine demonstrated the need for accurate flow control of the fuel to both the primary and secondary combustors during transient operation to provide safe start and shutdown and during steady-state operation to provide engine balance and operating efficiency. Accurate sequencing of the fuel flow to each combustion chamber with some method of interlocking the two fuel controls was needed to prevent excessive turbopump acceleration rates and primary combustor gas temperatures during the start and shutdown transients. Operating response requirements for the control valves of 0.025 to 0.040 sec were determined to be adequate for engine module operation; however, certain failure modes which may occur during development of the TPA indicated a possible need for a 0.005/0.008 sec shutoff of the primary combustor fuel control valve.

VII, Controls (cont.)

B. SUCTION VALVE

1. Objective and Approach

a. Objective

(U) The main objective of this effort was to develop propellant valves that would have (1) both a long-term storage seal and a positive shut-off operational seal, (2) a response capability to open or close in less than 0.400 sec, and (3) an unobstructed flow passage to permit close coupling of the valve to the main pump inlet minimizing residual propellant flow after shutdown. Secondary objectives were minimum size, weight, and operating torque, and maximum interchangeability of components between the fuel and oxidizer suction valves.

(U) Specific design objectives for the suction valves were:

Operating Pressure, psi	
Storage seal	100
Operational seal	150
Valve housing	350
Proof Pressure, psi	
Storage seal	150
Operational seal	225
Valve housing	525
External Leakage	
Storage	$<1 \times 10^{-4}$ std cc of He/sec at 100 psi inlet pressure
Operational	<5 cc/hr of propellant from actuation shaft only - none discernible from other interfaces at 350 psi internal pressure

VII, B, Suction Valve (cont.)

Internal Leakage

Storage	$<1 \times 10^{-4}$ std cc of He/sec at 100 psi inlet pressure
Operational	
Fuel	<1 cc/min at 100 psi inlet pressure
Oxidizer	<10 cc/min at 100 psi inlet pressure

Response

Both the fuel and oxidizer valves must be capable of opening or closing in less than 0.400 sec.

Endurance

The foregoing storage leakage requirements must be met after the valve inlet is subjected to 100 pressure cycles from 0 to 100 to 0 psi.

The response and operational leakage requirements must be met after the valve is subjected to 500 operations open to closed to open under flow and pressure conditions simulating actual operation.

b. Approach

(U) A survey of available valve designs disclosed that poppet and butterfly valves with metal seals for long-term storage were incompatible with the design requirement because the flow passages were obstructed and the actuating torque for both types of valves was too high. Valves with obstructed flow passages could not be close-coupled to pump inlets and the high torques of ball valves required large actuators and excessive "on board" power. All of these factors adversely affect envelope size and operational flight weight.

(U) By integrating desirable features of the poppet and ball valves, a segmented ball gate was developed that lifts from the operational (lip) seal and rotates entirely out of the flow path. The linear lifting motion permits a metal foil long-term-storage seal to be welded to the gate and to the valve inlet. This metal foil seal, which shears cleanly out of the flow path at the initial motion of the valve, is easy to fabricate, provides minimum exposure to corrosive fluids, and is capable of withstanding high differential pressure.

(U) The spring-loaded Teflon lip seal was selected after evaluation of trapped O-ring seals and of various other shapes of molded seals. Criteria for selection were ease of fabrication and ability to effect a positive seal on the spherical gate surface without requiring precise positioning of the gate.

(U) The operating mechanism of the valve, consisting of two interacting cams to effect both rotation and linear translation of the gate, was selected after evaluation of cam, gear, scissor, and linkage type designs. The cam design selected required the least operating torque and indicated the highest inherent reliability for the response required.

2. Design and Analysis

a. Design

(1) Approach

(U) The valves were sized to meet the flow and interface requirements resulting in internal exit diameters of 3.35 and 3.00 in. for the oxidizer and fuel valves, respectively. Since the larger oxidizer

VII, B, Suction Valve (cont.)

valve would have the greater stresses, both valves were designed to meet the oxidizer envelope and stresses. This approach reduced design and fabrication costs by providing maximum interchangeability of parts, and the fuel pump inducer shroud provided a tapered reduction section to the 3.00-in.-dia.

(U) Initial design efforts were directed toward the design of a functionally sound seal and operating mechanism meeting the main objectives without regard to weight or interface considerations. This experimental design, which consisted of a two-part housing with provisions for adjusting the location of the seals, and for testing different seals, was released for fabrication in January 1966. Continued effort resulted in a prototype design (Figure VII-1) incorporating the ARES module interface requirements and approaching flight weight. This design was released for fabrication in May 1966.

(U) In the prototype design weight was reduced from 32 to less than 15 lb, and fabrication costs were appreciably lower than for the experimental design.

(2) Layout

(U) Layout drawings were made to establish the method of seal installation and the kinematics required of the gate for the various operations, i.e., to shear the storage seal and rotate out of the flow path, then, on closing, to rotate into position and translate for a positive-shutoff seal. Tolerance requirements were established from precise layout drawings by analysis of the clearances observed during simulated valve operation.

VII, A, Suction Valve (cont.)

(3) Cam Design

(U) The gate loading at various positions, based on a 250 psi static inlet pressure at shutoff, was used to design a constant-torque cam within the required limits of rotation. This cam applies both the shearing force for the storage seal and the force to close the gate against fluid pressure and thus to effect an operational seal. Fabrication of the constant-torque cam was simplified by modifying the cam shape to a series of circular arcs. Clearance was provided for 10 degrees of actuator over-travel during operation of the valve. The last 15 degrees of the cam form a circular arc with the actuating axis. This portion of the cam takes the inlet pressure load while the valve is closed, causes no moment on the actuating shaft, and also locates the gate to the same axial position on closing. The spring-loaded lip seal will effect positive seal over a deflection range from 0.015 to 0.075 in., permitting reasonable manufacturing tolerances on the housing, cams, and gate.

(4) Shear-Seal and Cutter Design

(U) Several cutters were designed, fabricated, and tested to establish the configuration of the cutter, the diametral clearance between the moving cutter and the fixed inlet sleeve, and the axial location of the cutter edge with respect to the surface of the metal foil seal. Appendix II shows more detail on the seal and cutter design and development.

(U) Minimum thickness of the 304L annealed CRES-foil shear seal was established at 0.002 in. by stress and corrosion requirements. A 0.003-in.-thick foil was selected to provide a margin of safety. The foil seal was sandwiched between thicker metal sections (rings) to facilitate welding. The rings are tapered to guide and position the gate as it approaches the seal, thereby alleviating the need for precision tolerances on the cams to position the gate during translation.

VII, B, Suction Valve (cont.)

b. Analysis

(1) Dynamic Analysis

(U) A dynamic analysis was made to establish the power requirements and the cam and cam-follower stresses that would occur during high-response operations. The load-carrying members were designed to operate safely at response times less than 0.300 sec with a static inlet pressure of 250 psi. The anticipated peak torques were calculated to be less than 400 in.-lb.

(2) Stress Analysis

(U) A complete stress analysis was performed on all critical members of both the experimental valve design and the prototype design. Both analyses showed all components were within design allowable stresses, and testing verified the analyses were sound.

(3) Material Selection

(U) Material studies were made to select functionally capable metals having maximum compatibility with the propellants. Hardenable stainless steels were required for the cams, bearing, and cutter. The main cams were made of 440A steel with a Rockwell hardness (RC) of 50 to 52 to obtain maximum toughness at the required hardness, and the bearings were made of 440C steel hardened to RC 58 to 60, which is the industry standard material for CRES anti-friction bearings. Cold drawn (half hard) Type 304L steel was selected for the cutter since it must withstand long-term exposure to the propellants, and the "half hard" condition provides the necessary hardness to ensure a good cutting edge. The valve inlet sleeve, metal foil seal, and weld rings are all Type 304L steel to minimize weld cracking and carbide precipitation during electron beam welding.

VII, B, Suction Valve (cont.)

(U) The experimental and demonstration valve housings were made of A-356 aluminum, and a stainless-steel inlet sleeve was shrunk into the housing. This choice of material should be acceptable for flight hardware; however, it is planned to use Type 304L stainless steel for the oxidizer valve housing intended for extended ARES module testing. The reason for this is to eliminate the possibility of formation of aluminum nitrate, oxide, and hydroxide salts during periods between tests.

(U) During disassembly after oxidizer leak testing some salt formation was found retained in a recessed area of that suction valve where N_2O_4 and H_2O were probably trapped for considerable periods between the time the valve was flushed and dehydrated. A solution to this problem would be to thoroughly dehydrate the valve immediately after flushing with H_2O.

(U) The salts observed were identical to salts found in Titan hardware using aluminum and CRES in combination. Previous analyses have proven that considerable water must be present with N_2O_4 to provide these salts. The valve in question was removed from the test stand, two separate times flushed, reworked, dehydrated, and then replaced in the stand. The elapsed time between each flushing and dehydrating was approximately 15 to 18 hours, while the valve was being reworked, which would be sufficient time for salts to form. Since the ARES module testing will include elapsed time between firings, during which moisture could get into the valve, it is recommended that the oxidizer housing be CRES. Conversely, flight hardware will not be exposed to H_2O between shutdowns in space, so the aluminum housing is recommended in view of its considerable weight advantage.

(U) Teflon was used for the lip seal since it is only lightly spring-loaded during storage and is compatible with both the fuel and the oxidizer. Local bearing stresses at the seal contact area were determined to be less than the stress which causes cold flow.

VII, B, Suction Valve (cont.)

3. Fabrication

(U) All components for two experimental and four prototype suction valves were fabricated with available tooling at Aerojet-General facilities. One spare housing and spares of all critical parts were fabricated to provide for normal attrition during development testing. The only special tooling fabricated were the valve housing casting patterns. No major fabrication or assembly problems were encountered.

(U) Several storage-seal cutters and test specimens of various designs were fabricated for the electron-beam welding program during development of the cutter configuration and of the welding technique for installation of the metal-foil shear seal.

(U) Figure VII-2 shows the location and configuration of the three electron-beam welds developed to retain the metal storage seal and secure the inlet subassembly to the body of the suction valve. The actual parameters used to control the weld character and the penetration for each weld are also shown. Additional development information on the electron-beam welding program is available in Aerojet Report No. FSC66-246, dated 23 January 1967, which is included in Appendix II.

(U) Actual development data other than that shown in Figure VII-2 would be of little value to anyone having a different E.B. welder since different welders of the same model usually require different electrode spacing and have different focal lengths, requiring different voltage and current inputs to duplicate a specific weld.

VII, B, Suction Valve (cont.)

4. Testing

a. Cutter and Shear-Seal Development

(U) The cutter configuration, radial-clearance tolerance band, and the cutter axial location from the surface of the metal shear seal were established empirically by extensive testing to ensure shearing the metal foil seal cleanly without generating contaminants.

b. Experimental Suction-Valve Testing

(U) Testing on the experimental suction valves was initiated in April 1966 and continued through July 1966.

(U) Two valves, SN 001 and 002, successfully demonstrated the requirements of proof pressure, internal and external leak, flow factor (K_W), response, and torque. The secondary seal failed in both valves during endurance cycling. The failure was caused by inadequate support of the lip seal to effect a closure against a 250 psi inlet pressure. The seal support was redesigned and the modified seal support installed in valve SN 002. Endurance and leak test requirements were successfully met with this valve.

(U) After initial flow-testing, the inlet of experimental valve SN 001 was modified for storage seal-shearing tests. The final configuration of the cutter was established from tests made with this valve.

c. Demonstration Testing

(U) Testing of the prototype suction valves to demonstrate compliance to the contract was initiated on 15 August 1966. Structural and functional integrity requirements were satisfied by performing proof pressure,

operational leakage, response, and endurance tests with water. Tests were performed using an adapter sleeve prior to welding the inlet sleeve and storage seal into the valves. The original adapter sleeve was incorrectly designed and caused the first valve tested to fail during endurance cycling. This valve was rebuilt using the spare housing and a redesigned adapter sleeve, and all the tests were satisfactorily completed. No internal or external leakage was observed, and all valves were operated at response rates of less than 0.400 sec after having been operated over 500 cycles under simulated operating conditions.

(U) After the structural and functional integrity tests, the inlet sleeves and storage seals were welded in place. The internal and external storage leak rate requirements were successfully demonstrated on 9 September 1966. The leakage was less than 1×10^{-8} std cc of He/sec.

(U) Opening response rate while shearing the storage seal was demonstrated at 0.360 sec 21 September 1966.

(U) The contract work statement called for allowable operational leakage in quantities of fuel and oxidizer. The valves were subjected to endurance cycling with both water and propellants and then leak tested. Performance exceeded contract requirements for both propellant applications.

(U) The actual test results are summarized as follows: These results were obtained during demonstration of compliance to the work statement.

TABLE VII-I

TEST REQUIREMENTS AND RESULTS OF THE SUCTION VALVES

Item	Test Performed	Test Value Required	Test Value Obtained
1	Proof pressure - Oxidizer valve and fuel valve SN 0000001 15 August 1966	1 5 x 350 psi	540 psig applied for 1 min - 4 times. No discernible leakage or malfunction during or after application.
2-a	Leakage - External, operational, fuel valve SN 0000001 15 August 1966	<5 cc/hr water @ 150 psi (Actuator shaft seal only)	None discernible in 5 min @ 150 psig. (Test fluid - H_2O)
2-b	Leakage - External, operational, oxidizer valve SN 0000001 15 August 1966	<5 cc/hr water @ 350 psi (Actuator shaft seal only)	None discernible in 5 min @ 350 psig. (Test fluid - H_2O)
3-a	Leakage - Internal, operational, fuel valve SN 0000001 15 August 1966	<1 cc/min of water @ 20 psig inlet pressure	None discernible in 5 min @ 20 psig inlet pressure. (Test fluid - H_2O)
		<1 cc/min of water @ 100 psig inlet pressure	None discernible in 5 min @ 105 psig inlet pressure.
3-b	Leakage - Internal, operational, oxidizer valve SN 0000001 15 August 1966	<10 cc/min of water @ 100 psig inlet pressure	Note: Both valves are similar physically and functionally and use interchangeable parts; therefore the more severe leakage requirement of the fuel valve was demonstrated.
4	Response capability, opening with 100 psi inlet pressure and not shearing 5-yr seal. SN 0000005 25 August 1966	<0.400 sec	Valve opened in 0.380 sec with *4.5 MA signal to servovalve.
5	Response capability, closing with 100 psi inlet pressure Note: Test performed with 180 psig inlet and 40 psig back pressure to develop 100 psi ΔP across valve during closing. SN 0000005 25 August 1966	<0.400 sec	Valve closed in 0.380 sec with *7.0 MA to servovalve. Differential pressure across valve was greater than 100 psid during closure at the 10% open position.
6	Determine K_w of one valve		
	% Open is based on % shaft rotation average values of K_w taken from two valves, SN 0000002 and SN 0000004	% Open: 0, 100 — K_w: 0, 120	% Open*: 0, 10, 20, 30, 40, 50, 60, 70, 80, 85, 90, 95, 100 — K_w: 0, 0, 0.5, 1.5, 2.0, 3.0, 5.0, 10.0, 18.0, 24.0, 45.0, 83.0, 127.0

*Actuation rate was controlled by variable signal amplitude to an "open loop" servo actuator.

TABLE VII-I (cont.)

Item	Test Performed	Test Value Required	Test Value Obtained
7	Endurance - Cycle valve open and closed 500 times at a response rate of 0.5 + 0.1 sec with 150 psi inlet and 30 psi back pressure to obtain 100 psid ΔP @ 10% valve open, while closing.	500 cycles under simulated operating conditions	Precycle leak test Internal @ 20 psi = 0 Internal @ 100 psi = 0 External @ 150 psi = 0 510 cycles performed and 100 psid ΔP across valve @ 10% open, while closing.
	Test performed with water.		Post cycle leak test Internal @ 20 psi = 0 Internal @ 100 psi = 0 External @ 150 psi = 0
	Internal leakage after cycling.	<10 cc/min of H_2O at 100 psig inlet pressure	None discernible @ 100 psig inlet pressure.
	External leakage after cycling.	<5 cc/hr of H_2O at 350 psig inlet pressure (Actuator shaft seal only)	No discernible leakage @ 350 psi internal pressure.
	Response after cycling: Open Close	<0.400 sec <0.400 sec	0.370 sec @ 4.5 MA input 0.390 sec @ 7.0 MA input
	Endurance test performed on valve SN 0000005 25 Aug 1966		
8	Leakage, internal, storage fuel valve Leakage, internal, storage oxidizer valve Leakage, external, storage fuel valve Leakage, external, storage oxidizer valve	Atmospheric cc/sec of He at 100 psi <1 x 10^{-4} cc/sec	MR Calib. 7.5 Background 0.64 1st cycle 0.42 100 cycles 0.35 5 min leak test after cycle test 0.34
	Calibrator LR = 3.4 x 10^{-7} std cc/sec MR = Meter Reading LR = Leak Rate in std cc/sec Vac on test piece - start 75 microns - end 48 microns $LR = \frac{MR - Background}{Calib.\ Meter\ Reading} \times Calibrator\ LR =$ $LR = \frac{0}{7.50} \times 3.4 \times 10^{-7}$ cc/sec = 0 Test performed on valve SN 0000005 9 September 1966.		No measurable leakage Note: 1. Internal and external cumulative leakage was measured simultaneously. 2. Cycling was performed at gage pressure 0 to 100 psig to 0 - Valve except inlet port was in a vacuum creating a differential across the foil seal of 15 to 115 psid.
9	Response capability, opening with 20 psi inlet pressure and shearing 5-year seal. Test performed on valve SN 0000002 21 August 1966.	<0.400 sec	.lve opened in 0.360 sec with 5 MA signal to servovalve.

TABLE VII-I (cont.)

Item	Test Performed	Test Value Required	Test Value Obtained
10-a	Endurance - Cycle valve open and closed 500 times at a response rate of 0.5 + 0.1 sec with 150 psi inlet, and 30 psi back pressure to obtain 100 psid ΔP @ 10% valve open, while closing. Test performed on valves using water. SN 0000003, 28 October 1966 SN 0000004, 2 November 1966 Following these tests, valves were installed in fuel and oxidizer test bays.	500 cycles under simulated operating conditions	510 cycles performed @ 0.56 sec opening and 0.57 sec closing while closing against 95 to 100 psid ΔP using water. Post cycle: External leakage @ 150 psig = 0 Internal leakage @ 20 psig = 0 Internal leakage @ 100 psig = 0
10-b	Cycle valve 25 times with fuel at 100 psi inlet pressure. Internal leakage after cycling. External leakage after cycling. Test performed on valve SN 0000003, 2 November 1966 Note: 500 cycles of simulated operation certified on this valve 28 Oct 1966 (10-a)	25 additional cycles in fuel test setup: <1 cc/min of fuel at 20 psig inlet pressure <1 cc/min of fuel at 100 psig inlet pressure <5 cc/min of fuel at 150 psig (Actuator shaft seal only)	Precycle leak test: Internal @ 20 psi = 0 Internal @ 100 psi = 0 External @ 150 psi = 0 25 cycles performed at valve ΔP = 110 to 115 psi Post leat test: Internal @ 20 psi = 0 Internal @ 100 psi = 0 External @ 150 psi = 0
10-c	Cycle valve 25 cycles with oxidizer at 100 psi inlet pressure. Internal leakage after cycling External leakage after cycling Test performed on valve SN 0000004, 17 November 1966. Note: 500 cycles of simulated operation certified on this valve 2 November 1966 (10-a)	25 additional cycles in oxidizer test setup <10 cc/min of oxidizer @ 100 psig inlet pressure <5 cc/hr of oxidizer @ 350 psig inlet pressure (Actuator shaft seal only)	25 cycles performed, pressure and rate of closure adjusted to obtain 150 psi propellant pressure drop across valve gate at the 10% position while closing the valve. No discernible leakage @ 100 psig inlet pressure. No discernible leakage @ 350 psig internal pressure.

VII, Controls (cont.)

C. FUEL CONTROLS

1. Primary Combustor Fuel Control Valve (PCFCV)

a. Objective and Approach

(U) The objective of this task was to develop a flow control valve to accurately control the fuel flow rate to the primary combustor. Prime requisites were that the valve have (1) a maximum control range with a minimum range of 25 to 1 and flow factor (K_w) repeatibility at any preselected position within the control range; (2) that it have a response capability to shut off from any control position in less than 0.025 sec while operating in a 6000 psi fuel system; and (3) that it be a modular design compatible with the ARES engine design.

(U) Since the control range indicated the need for a precise metering valve, prime consideration was given to poppet and rotary sleeve valves with contoured radial control ports. The rotary sleeve valve was selected after evaluation of conceptual designs of both types because it provided a greater control range and was inherently easier to pressure balance and control in the 6000-psi system.

(U) Fuel valve flow control requirements were reduced to a flow proportional admittance factor ("K_w"), which has the following relationship to flow rate and pressure differential

$$K_w = \frac{\dot{w}}{\sqrt{\Delta P \times SG}} \quad \text{where}$$

$\dot{w}$ = flow rate in lb/sec

ΔP = pressure drop in $lb/in.^2$

SG = specific gravity of fluid flowing

VII, C, Fuel Controls (cont.)

b. Design and Analysis

(U) The modular configuration and envelope size of the valve (Figure 7.1.1-1 of Appendix I) were established from ARES module installation layouts.

(U) The control range and accuracy required were established from the transient and steady-state computer studies of the ARES engine model.

(U) For example, the start transient shown in Figure I-2.4.3-1 of Appendix I required an initial opening and dwell of the primary fuel control valve at a K_w of 0.055 $\pm$ 0.005. The steady-state K_w requirement of the same valve was 0.92 $\pm$ 0.01, and the full open K_w required was established at 1.4 to provide flexibility for off-design pump operation during engine development testing. The valve ports were contoured to provide a low gain (K_w to position) and high accuracy below a K_w of 0.10, and a higher gain for the rest of the stroke to obtain the maximum capacity at the full-open position. The changes in gain were made gradually and the gain was made sufficiently linear to permit easy programing of position to meet K_w requirements.

(U) Figure VII-3 shows the calculated performance characteristics (flow factor "K_w" versus position). Because of the accurate position control ($\pm$0.015% of full actuator stroke), this valve meets the engine primary fuel control requirements. Discharge coefficients were assumed for several valve positions between shutoff and full open and the radial control ports were contoured as shown in Figure VII-4 to approach the calculated flow characteristics shown.

(U) To reduce the actuation force, the valve is pressure balanced except for the actuation shaft; this pressure load is taken by a radial thrust bearing. This bearing also maintains concentricity between the

VII, C, Fuel Controls (cont.)

rotating and stationary control sleeves, thereby controlling the leakage path between these closely fitted sleeves and eliminating friction through rubbing.

(U) Two test-valve housing configurations were designed and released for fabrication. One housing was designed for use in high pressure intensifier testing and had flanges to interface with the test complex in Area H; the other was designed for functional development testing and simulated the actual engine module inlet and outlet flow conditions. Both valves had identical modular control assemblies but the functional development configuration had a considerably greater control range because of the chamfered control port inlets and the improved housing inlet and outlet flow passages. The only change made to the control ports during development was to chamfer the port inlets which increased the full-open capacity of the valve.

(U) All high-pressure dynamic seals were made of Teflon to reduce friction. Both static and dynamic leak paths were vented to pump suction so that only low-pressure external seals are needed. The sleeve and shaft were made from 17-4 PH CRES. The sleeve was hardened to RC 38-41 and the shaft was hardened to RC 44-47.

c. Fabrication

(U) Fabrication of two high-pressure test valves was initiated in November 1965 and completed in January 1966. Later in the program, the valve housing simulating module flow passages was fabricated and one of the modular sleeve and shaft assemblies was modified to chamfer the inlets to the control ports.

VII, C, Fuel Controls (cont.)

d. Testing

(U) Initial proof-pressure and differential proof-pressure testing performed on the high-pressure intensifier test units verified the functional and structural integrity of the PCFCV design.

(U) The functional control characteristics (K_w versus valve position) were determined for three valve configurations during the development period and these three performance curves are shown with the calculated curve on Figure VII-3. Curve 1 shows the choking effect which occurred at high flow rates because of the sharp-edged control ports and the restricted inlet and outlet flow passages of the high-pressure test valve housing. Curve 2 shows some improvement obtained by partially chamfering the control port inlets. Curve 3 represents the characteristics of the valve with fully chamfered control port inlets operating in the housing which simulated flow conditions expected in the ARES engine. The predicted performance for the engine module valve, Figure 7.1.1-1 Appendix I, was based on Curve 3 shown in Figure VII-3.

(U) Examination of all three curves shows excellent correlation of control characteristics in the critical control range up to the point where choking occurred. This correlation verified that the modular control valve can be accurately precalibrated in a test housing before installation in the engine housing.

(U) All testing was conducted in the Aerojet Engineering Components Laboratory using water as the test fluid.

(U) All the design criteria were met or exceeded and the maximum capacity and control range greatly exceeded requirements. The maximum

VII, C, Fuel Controls (cont.)

K_w attained was 2.1 as against a requirement of 1.45. The control range demonstrated was from a K_w of 0.025 to 2.0 giving a range of 80 to 1 as against a minimum required range of 25 to 1.

2. Secondary Combustor Fuel Control Valve

a. Objective and Approach

(U) The objective was to develop a flow control valve to accurately control the fuel flow rate to the secondary combustor. The prime requisites were the same as for the PCFCV (see Section VII,C,1,a) except that the SCFCV capacity was greater and the system operating pressure was 4000 psi. An additional design requirement imposed was that actuators for both valves be identical and interchangeable.

(U) The rotary sleeve valve concept with an identical angular stroke was selected for this application on the basis of the same reasoning which influenced its selection for the PCFCV.

b. Design and Analysis

(U) The size and modular configuration of the valve were established from the ARES engine layouts and the functional performance characteristics were determined from transient and steady-state computer studies of the engine secondary fuel flow requirements. Figure I-7.1.2-1 of Appendix I shows the configuration of the module valve and Figure VII-5 shows the calculated performance characteristics (K_w versus position) which coupled with accurate positioning met the engine secondary fuel control requirements.

VII, C, Fuel Controls (cont.)

(U) Two test valves, one for high-pressure intensifier combustor testing and one simulating module flow conditions, were designed and released for fabrication. The control ports were contoured to meet the calculated performance characteristics shown in Figure VII-5, utilizing the information gained during the development testing of the PCFCV. Figure VII-6 is a photograph of the exploded view of the development test valve which was flow tested to establish predicted performance characteristics. The control port inlets were chamfered as on the PCFCV and the same materials and design concepts were employed to reduce friction and eliminate any high-pressure external seals. The direction of the applied stresses permitted the sleeve of this valve to be made from 7075-T73 aluminum, realizing a considerable weight reduction.

c. Fabrication

(U) Three sleeve and shaft modular control assemblies were fabricated. Two valve housings were assembled, one meeting the interface requirements for high-pressure intensifier testing and a second configuration for development flow testing with simulated engine flow passages.

d. Testing

(U) Two modular control assemblies consisting of the sleeve and shaft were tested in the development test valve housing. Both were subjected to proof-pressure static testing and functional testing to establish the flow characteristics (K_w versus position). Both assemblies were identical except the internal bore diameter of one was 1.850 in. and the other had a 1.700-in. diameter bore to provide structural strength to withstand a 6000-psi differential pressure without danger of binding. The flow characteristic curves for both valves are superimposed on the calculated curve in Figure VII-5

and illustrate the excellent correlation over the major portion of the control range. Curve 1 shows the characteristics of the valve with the 1.700-in. inside diameter which was the diameter assumed for the calculated values. Curve 2 showing the characteristics of the valve with the 1.850-in. inside diameter was used to establish the predicted performance curves, Figure I-7.3.2-1 of Appendix I.

(U) All of the testing was conducted in the Aerojet Engineering Components Test Laboratory using water as the test fluid.

(U) All design criteria were met or exceeded especially in the range of control. The actual control range demonstrated was from a K_w of 0.10 to 7.5 giving a range of 75 to 1 against a minimum design requirement of 25 to 1.

3. Control System

a. Objective and Approach

(U) (1) The control systems must provide the ARES fuel control valves with required response and position accuracy by controlling the actuation stroke and providing an adjustable response opening and closing actuation system for the suction valves.

(2) Approach

(a) Suction Valves

(U) The suction valves as designed for the engine are required to be either fully opened or fully closed at a predetermined rate. An open loop actuation control system, using a proportional flow

servovalve as the control element, was deemed adequate to meet this requirement. The actuator was also provided with closed loop position control capability to permit the evaluation of valve flow characteristics at any position.

(b) Fuel Flow Controllers

1 Mixture Ratio

(U) Preliminary investigation of engine operating modes suggested the use of a closed loop bipropellant flow-rate feedback servo system to control primary combustor mixture ratio. After careful weighing of advantages and disadvantages of such a system it was abandoned in favor of a time subordinated position control servo system for the two fuel control valves with a simple sequencing interlock. Some of the factors that led to this decision were:

(U) a Evaluation of transducer resolution requirements over a wide range and limitations of flowmeter response accuracies suggested that feedback signals during transient operation would either be inaccurate or late in establishing the required injector mixture ratios.

(U) b There was insufficient data available from digital computer studies on the actual mixture ratio changes occurring during transient operation to ensure an intelligent input to the servo controller. These simulation runs indicated, however, that the temperature of the primary combustor and TPA acceleration can be adequately controlled during the start transient by relative position with respect to time and opening rate control of the two fuel valves.

2 Position Feedback

(U) Two principal requirements led to the consideration of closed-loop position control for the two fuel control valves. First, precise metering and sequencing of fuel flow during transient operation is mandatory. Second, precise adjustments in nominal operating position of the fuel valves may be necessary in the engine development phase to obtain engine balance for steady-state operation by compensating for variations in the performance of other engine subsystems. A simple position control servo system permits the accurate tracking of the desired valve motion and attainment of the required terminal position with maximum stability.

b. Design and Analysis

(1) Design

(a) Actuators

(U) The actuators for both suction and fuel control valves were selected to operate with MIL-O-5606 hydraulic fluid and were sized to meet the response and control requirements with a common 2500-psi hydraulic supply system.

1 Suction Valves

(U) Off-the-shelf commercial rotary actuators of the hydraulic rack and pinion type were selected for the suction valves. The actuators were modified to incorporate limit switches, a position potentiometer and a proportional control servo valve. The actuator stops were factory adjusted to provide 227 degrees of rotation (full rotation of the suction valve actuating shaft) at the output shaft.

VII, C, Fuel Controls (cont.)

2 Fuel Valves

(U) Aerojet-furnished linear, electro-hydraulic servo actuators were modified to incorporate a fail-safe spring, which closes the fuel valve in the event of actuator hydraulic power failure; a micrometer stroke adjustment was provided so that a positive steady-state operation position can be preset on each fuel-control valve; infinite resolution potentiometers were incorporated compatible with the electrical control system. The actuator-valve interface was designed so that full valve stroke corresponded to 0.600-in. linear actuator stroke.

(b) Control Systems

1 Suction Valves

(U) Control mode of the suction valves in the engine is an open loop. A signal to these valves simply shuttles them full open or closed depending on the polarity of the command signal. Response rate is dependent on the signal amplitude to the servovalve and hydraulic supply pressure. To aid development of the valves, however, a selective control circuit was developed that permitted normal open-loop operation with adjustable rates of opening and closing, or closed loop with position control to determine the flow characteristics of the valves at intermediate positions. Figure VII-7 shows the combined control circuits.

2 Fuel Valves

( ) To satisfy the critical sequencing, response and position control requirements of the two fuel valves a modular servo controller was designed and developed. The controller is a self-contained unit which provides all necessary regulated power and control signals

to an electro-hydraulic actuator to obtain position control. The only requirement for activation is a source of 115-vac, command signal sources and wiring to the actuator servovalve and position feedback potentiometer.

(U) Figure VII-8 is the schematic of a single-valve controller which has two modes of operation: manual for adjustment during test setup and automatic for use during a firing test. In the manual mode a calibrated ten-revolution precision potentiometer on the front panel can be adjusted to command any valve position from fully closed to fully open. In the automatic mode, on receipt of a command signal from the test facility (FS-1 plus an elapsed time, t), the function generator increases a positive input voltage to the servo amplifier at an adjustable rate. This command voltage increases to a preselected amplitude determined by the adjustable diode clamp. The valve opens at a rate corresponding to the rate of voltage rise and to a position corresponding to amplitude. Position is maintained until another command signal either commands it to open further or to close.

(U) On receipt of a shutdown signal the function generator decreases amplifier input voltage at an independently adjustable rate. The valve closes at a rate corresponding to rate of voltage decay.

(U) The valve can be controlled to open and dwell at any number of predetermined intermediate positions simply by cascading additional adjustable diode clamps and providing command signals to release the clamps when desired.

(c) Interlocks

(U) The flexibility of the control design permits easy expansion to incorporate functional interlocks and to produce sequenced

control of two or more valves. Additionally, safety shutdown signals can effect a controlled shutdown through the function generator. If an emergency condition demanded it, a shutdown signal can actuate a switching transistor and produce a direct ground at the input to the servo amplifier, thereby causing an instantaneous signal for step shutdown.

(2) Analysis

(a) Transients Program

1 Valve Sequencing

(U) A digital computer program was used to define the sequencing requirements of the engine valves. The oxidizer suction valve is signaled open at the fire switch. The fuel suction valve is delayed 0.5 sec to fill the fuel pumps and discharge lines. At 1.95 sec into the transient, the primary fuel valve opens to a dwell position at 6% of operating K_w. The secondary fuel valve is signaled open at primary ignition. The primary fuel valve is interlocked to open after the secondary is at the 100% position. If the fuel valve sequence is interrupted at any position the engine will continue to operate in a safe manner. For example, if the primary fuel valve does not open to its 100% position from the dwell position, the engine will seek an operating point at approximately 7000 rpm. If the secondary fuel valve fails to open, the engine will operate safely at approximately 25,000 rpm.

2 Tolerances

(U) Tolerance requirements were studied for two servo controller performance parameters, namely, time and position. Digital computer analysis of the start transient indicated that if valve

VII, C, Fuel Controls (cont.)

initiation timing can be controlled within +150 and -300 millisec a safe operational sequence will result. State-of-the-art timing techniques will adequately meet this requirement.

(U) Positional tolerance requirements were also established from the start-transient digital computer program. Safe operation required a K_w value of 0.06 $\pm$ 0.006 at the dwell position. Translated into positional accuracy, this meant $\pm$ 0.015% of the full actuator stroke. The position servo controller was designed to this requirement.

(b) Fuel Valve Control System

(U) An extensive modes-of-failure analysis was conducted on the fuel-valve control system to determine the optimum interlock concept. The analysis concluded that an electrical interlock has distinct advantages over mechanical or hydraulic interlocks. Either of the latter concepts would cost more to provide than the hardware they would protect, if residual components were used during the test program. Should it be necessary to use new components for each test, the mechanical option would be competitive and should be considered in the engine design as a backup option.

c. Fabrication

(1) Actuators

(a) Suction Valves

(U) Commercially available fixed-stroke rotary actuators were used. The actuators were modified in-house to interface with the valves and to incorporate limit switches, position potentiometers, and proportional-control servo valves.

(b) Fuel Valves

(U) The servo actuators were available from another Aerojet program. They were modified in-house to interface with the fuel valves. The modification incorporated a fail-safe spring, a micrometer stroke adjustment and an infinite resolution potentiometer. The actuator stroke was mechanically adjusted to 0.600 in., and the position feedback potentiometers were positioned and electrically balanced to that stroke.

(2) Control System

(a) Suction Valves

(U) All parts required to fabricate the control system shown schematically in Figure VII-7 were standard commercial components available in the test laboratory.

(b) Fuel Valves

(U) The controller (Figure VII-8) was fabricated in the Engineering Components Laboratory using standard commercially available components.

d. Testing

(1) Suction Valve Control System

(U) All open-loop functions were performed satisfactorily. Valve opening and closing control capabilities were within specification. Opening and closing rates were adjustable from < 0.200 sec to > 1.000 sec, and repeatability for a particular input signal was within $\pm$0.010 sec.

Operating in the closed loop, the control system provided adequate position control for the predicted K_w-versus-position of the valves.

(2) Fuel Valves

(U) A calibration curve of valve position (measured with a micrometer attached to the valve) versus manual-position-potentiometer setting was made. Checks showed the position commanded to repeat better than 0.001 in. The repeatability of ramping open to the same position or closing to shutoff was also better than 0.001 in. No instability occurred during any of the testing. Control system performance was also checked during water flow testing of the fuel valves. Data showed position selection and repeatability consistently better than 0.001 in. In terms of valve K_w, the controller demonstrated that the primary fuel control test valve can be adjusted to a preselected K_w anywhere within the range of 0.025 to 2.00 with an accuracy of $\pm$0.3% of the full K_w range. The repeatability after flow adjustment was within $\pm$0.2%. Similar accuracies and repeatability were demonstrated with the secondary fuel control valve.

D. SUCTION AND FEED LINES

1. Suction Lines

a. Objective

(U) Objectives of this effort were to size the propellant suction lines between the boost pumps and the suction valves and to establish satisfactory interface designs at the boost pump discharges and the suction valve inlets.

VII, D, Suction and Feed Lines (cont.)

b. Design and Analysis

(U) The suction line configuration contained one 90-degree short radius bend. Length between interfaces was assumed to be 6 ft. Flow rates and allowable pressure drops were obtained from the digital computer studies of the engine. Limiting values for the main-pump inducer inlet approach velocities were established by the inducer design characteristics.

(U) Minimum internal diameters of the oxidizer and fuel lines, respectively, were established at 3.35 and 3.00 in. It was also established that smooth bore lines were necessary to meet the allowable pressure schedules at the minimum diameters. If flexible joints or lines are used, these sections must be lined.

(U) It is recommended from a standpoint of maximum interchangeability that both the fuel and oxidizer suction lines have a 3.35-in. inside diameter.

2. Feed Lines

a. Objective

(U) The objective of the effort was to design high-pressure lines to supply power to the boost pump hydraulic turbines from the respective main-pump discharge.

b. Design and Analysis

(U) Feed-line configurations contained two 90-degree bends. The length between interfaces was assumed to be 6 ft. Flow rates and pressure schedules were established by the engine steady-state digital computer studies.

VII, D, Suction and Feed Lines (cont.)

Interface configurations and locations were established by consideration of (1) main pump discharge pressure and flow characteristics, (2) turbine entrance flow conditions, and (3) the basic criteria of weight, stress, and physical interference with other components.

(U) The feed lines required check valves to prevent reverse flow from the boost pumps to the main pumps at shutdown. Valves from two suppliers were evaluated and both were determined to be acceptable. The minimum flow-passage diameter for smooth tubing was determined to be 1.00 and 0.87 in., respectively, for the oxidizer and fuel feed lines. Minimum acceptable check-valve sizes were 1.25 and 1.00 in., respectively, based on tubing outside diameters.

(U) Tubing made from Type 304 CRES, meeting specification MIL-T-6845, will provide the minimum weight installation to meet the pressure stress requirements. A further analysis will be needed to consider transient vibration loads when more information on the engine installation is available.

E. CONCLUSIONS

(U) The control valves for the ARES module performed satisfactorily. In each test, the valve exceeded the specified requirement, in favor of the valve. Response times were faster, leakage rates were less than allowable, and life-cycle tests were easily exceeded. The fuel flow-control valves are capable of throttling the module over a range greater than ten to one should this feature be required.

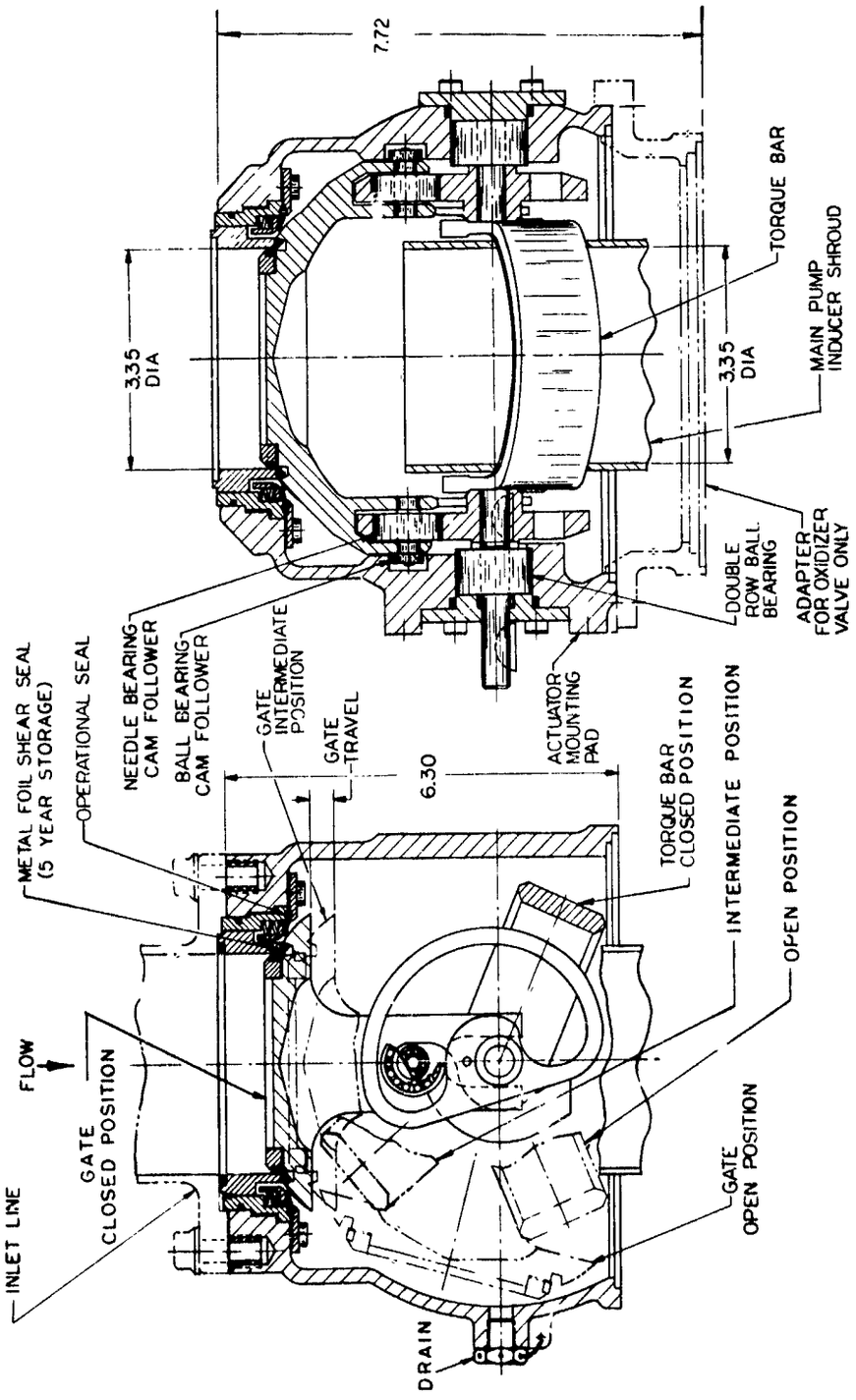

Suction Valve Configuration

Figure VII-1

NO.	WELD PENETRATION (IN.)	TYPE OF MTL.	TYPE OF JOINT	DIST. GUN TO WORK (IN.)	BEAM CURRENT M.A.	VOLTAGE K.V.	FOCUS CURRENT AMP.	FILAMENT CURRENT M.A.	WELD RATE 1 PM	FILAMENT SIZE MA	FILAMENT TO CATHOL DIST. (I..)	SPACER ANODE TO CATH. (IN.)	GUN TYPE KV
1	0.10	304	BUTT	2.25	54	28	4.7	50	100	500	0.37½	0.550	60
2	0.16	304	BEAD ON PLATE	2.50	80	38	5.4	53	100	500	0.37½	0.550	60
3a	-	304	SEAL WELD	4.25	55	12	3.0	53	55	500	0.37½	-	60
3b	0.153	304	BUTT	4.25	95	17	3.5	53	55	500	0.37½	-	60

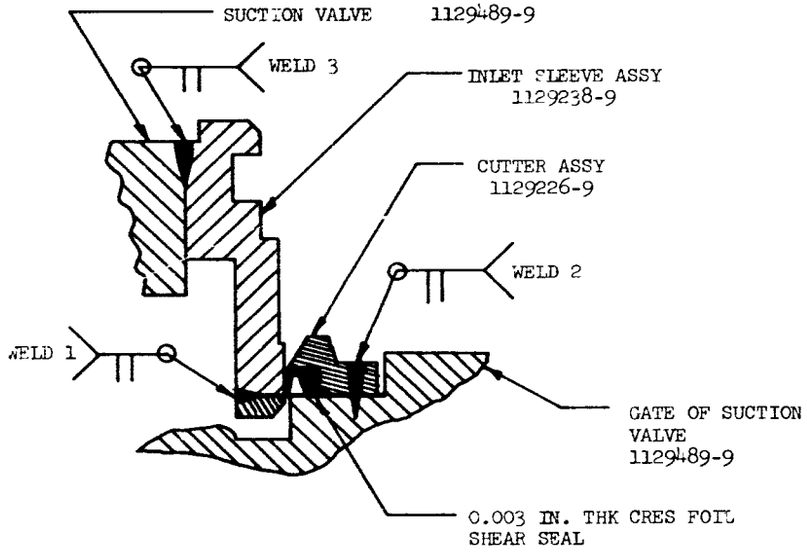

REMARKS

WELD 1 - PREHEAT HOLDING FIXTURE TO 400°F IMMEDIATELY BEFOFE WELDING. GUN IN HORIZONTAL POSITION. TWO PASSES 0.025 IN. PART.

WELD 2 - INSTALL INLET SLEEVE INTO VALVE BODY AND POSITION FOR UNIFORM RADIAL CLEARANCE WITH GATE.

WELD 3a,b - PRELOAD INLET SLEEVE TO 575 ± 50 LB.

Figure VII-2

Electron Beam Welding Parameters

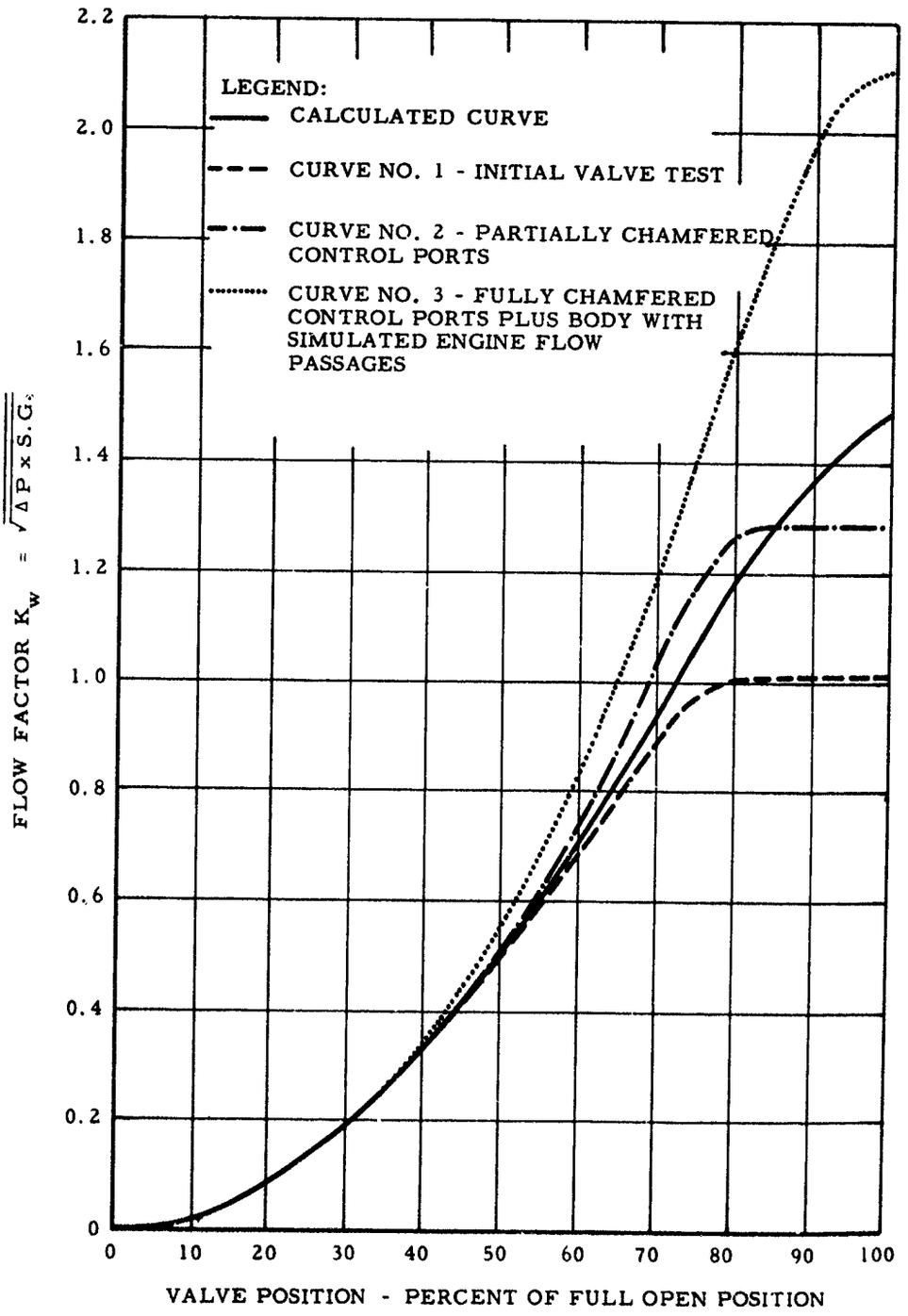

PCFCV Flow Characteristics

Figure VII-3

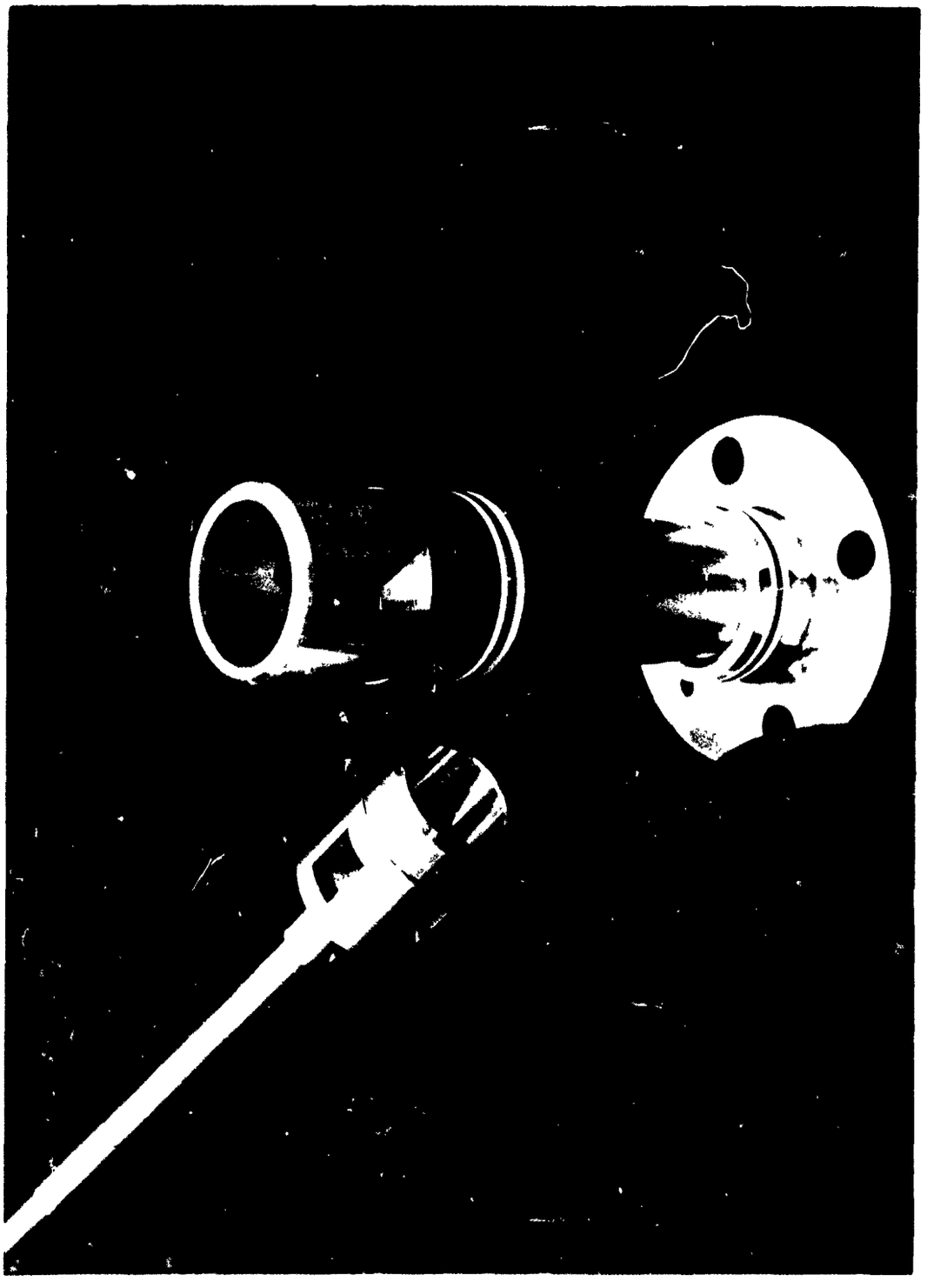

PCFCV Control Port Configurations

Figure VII-4

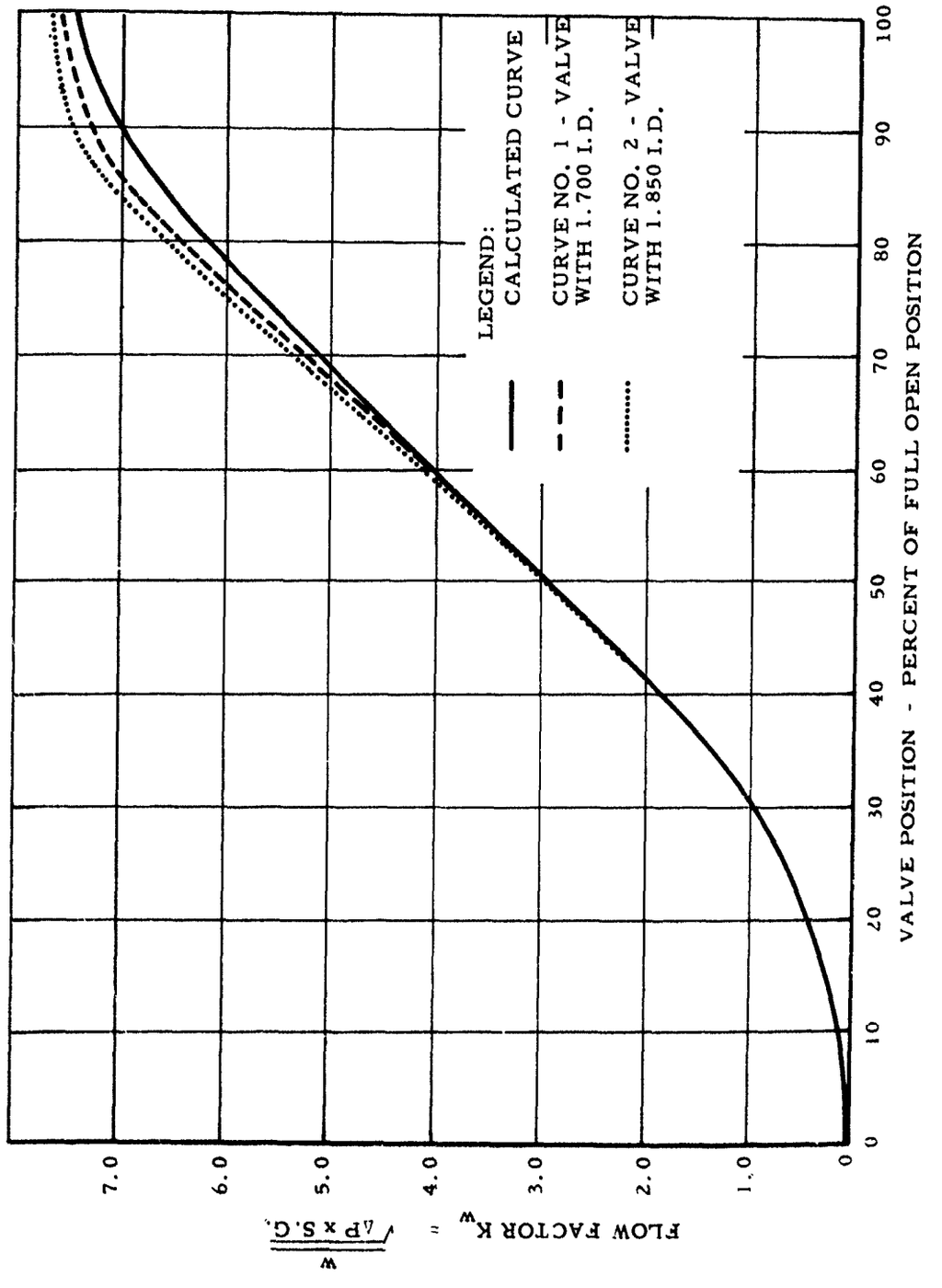

SCFCV Flow Characteristics

Figure VII-5

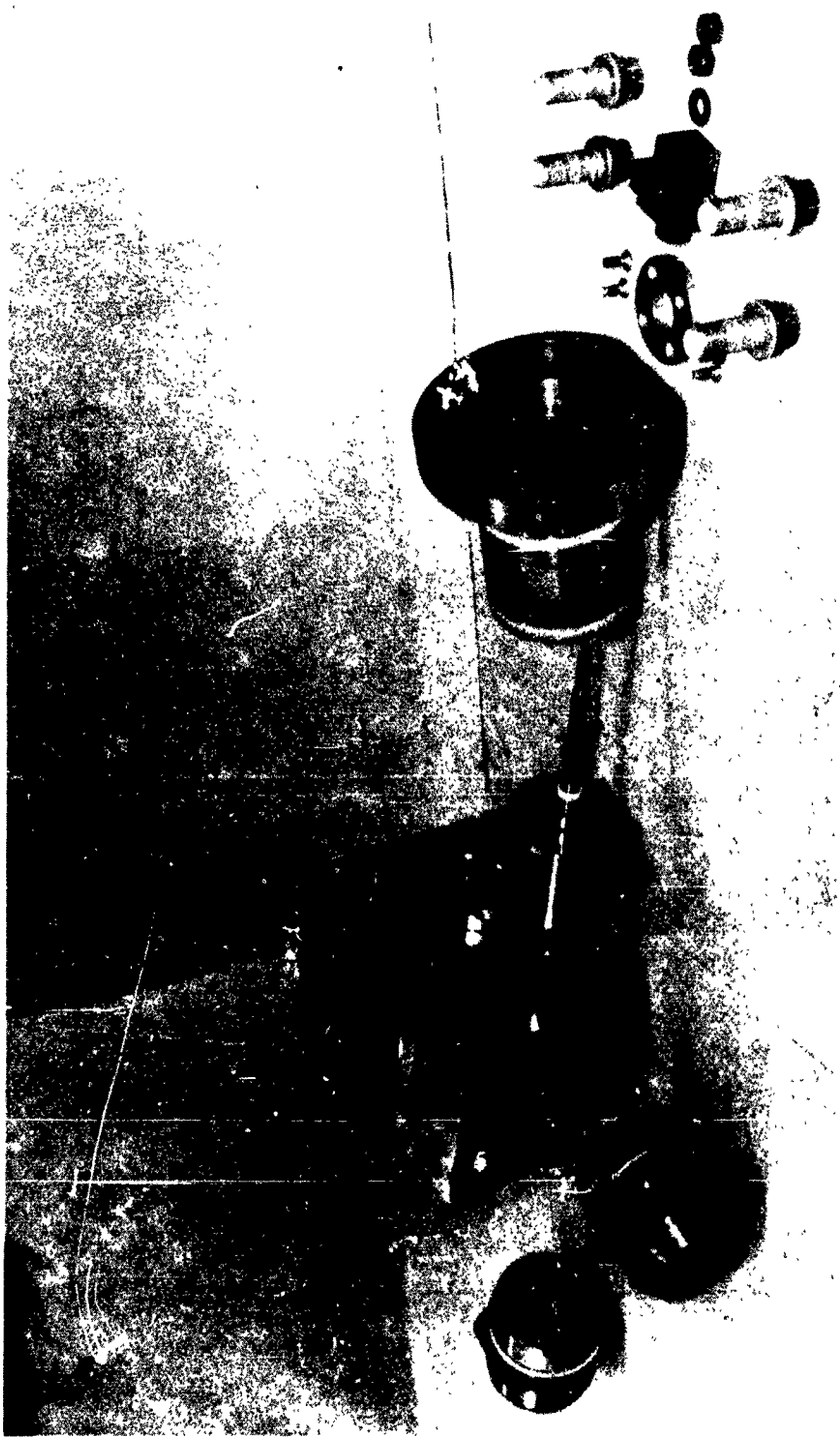

SCFCV Exploded View

Figure VII-6

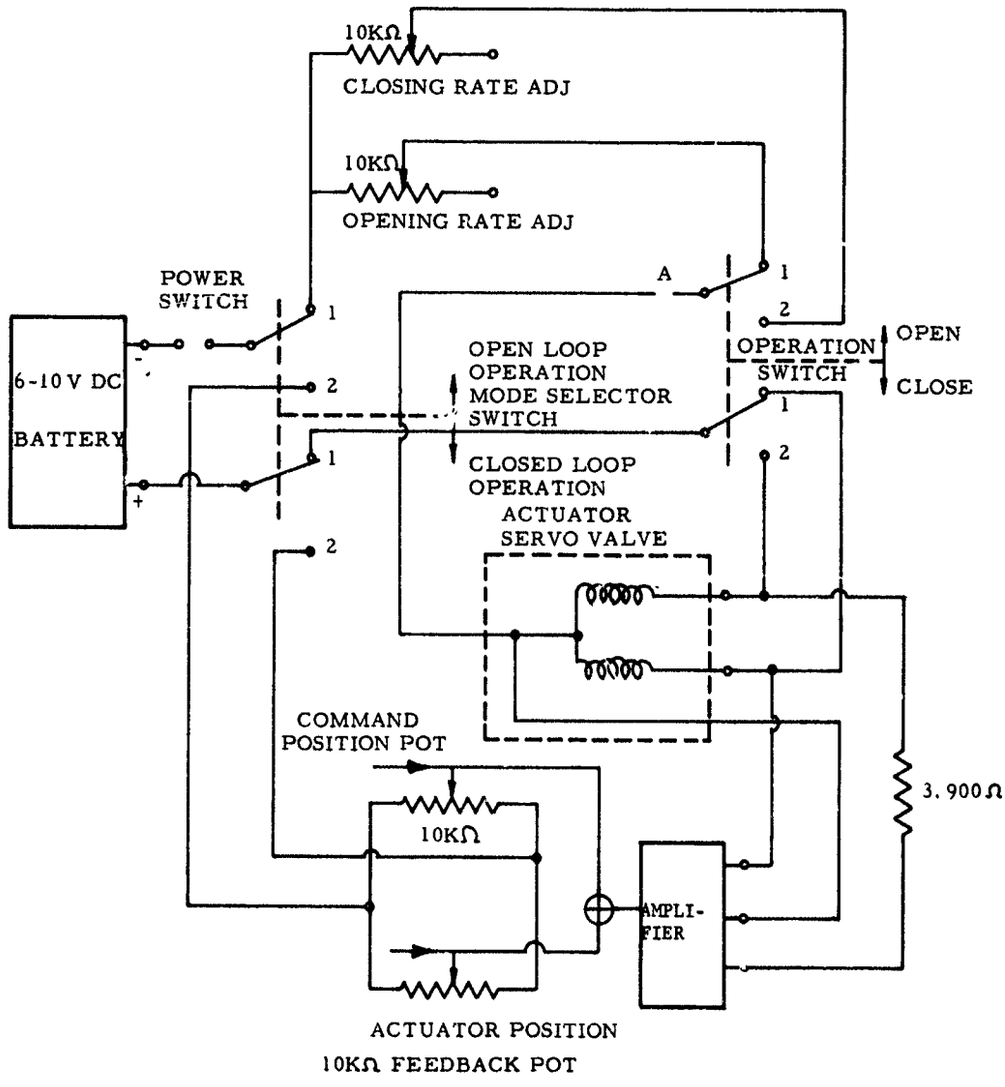

Suction Valve Selective Control Circuit

Figure VII-7

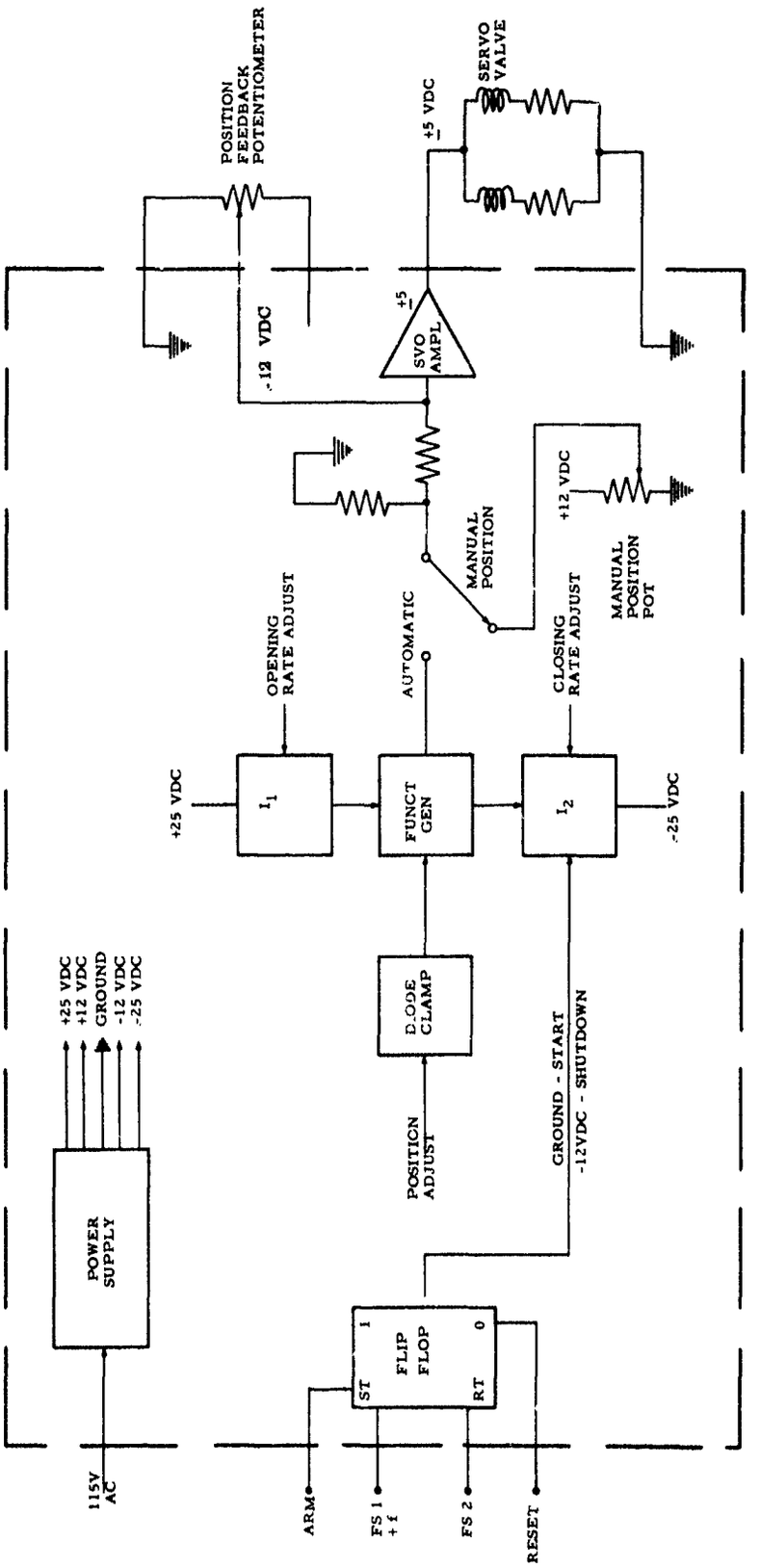

Fuel Valve Servo Controller (Schematic)

Figure VII-8

VIII.

SUPPORTING STUDIES

VIII.

SUPPORTING STUDIES

A. MODULE FLUID DYNAMIC TESTING

1. Introduction

(U) The structural components of the ARES are used to distribute propellant flow through the engine. The primary combustor and turbine exhaust configurations are contained within the available space of the turbopump housing. The resultant configuration of many of the flow passages are such that purely analytical techniques are inadequate to predict pressure drop and flow distribution. Consequently, a program was undertaken to experimentally analyze these flow passages by means of air-flow testing models. Careful examination of the engine revealed that four flow passages should be experimentally analyzed to properly predict their performance:

(a) Oxidizer pump discharge to thrust chamber flange.
(b) Thrust chamber flange to primary injector face (oxidizer).
(c) Primary injector to turbine inlet.
(d) Turbine exhaust to secondary injector face.

Therefore four full-scale models were built and tested, each geometrically similar to one of the above flow passages. The program conducted on these models is described in Section 4 below.

2. Conclusions and Recommendations

(U) The results of the air-flow testing gave sufficient information to confidently design all of the flow passages with the exception of the turbine exhaust to injector face passage. In the case of this turbine exhaust passage, a program is needed to optimize the design for uniform flow to the secondary injector.

VIII, A, Module Fluid Dynamic Testing (cont.)

3. Test Facility

(U) This program was conducted at the Aeronautical Engineering Laboratories, Naval Post Graduate School in Monterey, California, under the direction of Dr. M. H. Vavra. The air-test facility consisted of a compressor, cooler, plenum chambers, flow straightener, and instrumentation to measure flow rate, pressure, and temperature of the incoming air. This is shown schematically in Figure VIII-1. In addition, water and mercury manometer banks were available for measuring pressures in the models.

4. Accomplishments

a. Oxidizer Discharge Passage Model

(1) Objectives

(U) The oxidizer discharge housing receives oxidizer from pump discharge and distributes oxidizer to the thrust chamber regenerative cooling tubes. Housing pressure drop must be no greater than 125 psi to satisfy the design specification. Flow distribution at the thrust chamber coolant-tube inlet must be such that all coolant tubes receive adequate flow for regenerative cooling. Flow and pressure distribution at the pump discharge must be such that excessive radial thrust in the pump is avoided. Therefore, the test objectives were established as follows:

(a) Determine the pressure loss across the passages from the discharge of the oxidizer pump to the exit flange of the turbopump housing.

(b) Determine the flow distribution at the exit flange of the turbopump housing.

VIII, A, Module Fluid Dynamic Testing (cont.)

(c) Determine the flow distribution at the oxidizer pump discharge plane.

(2) Approach

(U) These objectives were accomplished by air testing a plastic full-scale model that simulated the flow passages from oxidizer pump discharge to the interface between the TPA housing and the thrust chamber. Upstream conditions were simulated by a swirl device installed in the location of the oxidizer pump. Downstream pressure drop was simulated by orifices.

(U) The model was constructed largely of Plexiglas, for visual observation during testing, with vanes fabricated from rubber strips. The assembly is shown installed for test in Figure VIII-2. Total flow was measured with a standard sharp-edged orifice, with the pressure differential recorded on a mercury micro-manometer. Inlet total pressure and distribution were measured with pitot probes while outlet pressure and flow distribution were measured on a specially designed orifice plate.

(U) Thread tufts were installed at several locations. The pattern and behavior of the tufts were useful for interpreting the flow distribution in the model. Initial testing was accomplished on a model which simulated Turbopump Housing Design B. Testing of the model revealed high-pressure drop and poor flow distribution. Therefore, flow passage height was increased from 1/4- to 3/8-in., the vanes were revised and holes in the T-portion were increased in size. The model then simulated the significant features of Turbopump Housing Design C with the exception of the cross flow manifold at the base of the housing just upstream of the thrust chamber.

(U) The vane configuration is shown on the developed view of the oxidizer flow passages in Figure VIII-3.

VIII, A, Module Fluid Dynamic Testing (cont.)

(3) Results

(U) The air pressure-drop-parameter K, calculated from the test data at the various stations is shown in Figure VIII-4. From this data, the equivalent housing pressure drop in terms of N_2O_4 propellant is 167 psi, compared to 125 psi allowable.

(U) The flow distribution at the entrance to the flow vanes and at the thrust chamber flange is shown in the top plot of Figure VIII-5. In general, the data lies in a $\pm$ 6% band with the exception of a few points which lie outside this band. The cross-flow manifold incorporated in the TPA Housing Design C, but not included in this model, will further improve the distribution of flow to the thrust chamber tubes, and also reduce the housing pressure drop.

(U) The flow distribution at the pump discharge is shown in the bottom plot in Figure VIII-5. The connected data points show that the flow into adjacent passages is severely nonuniform. This can be corrected by redesign of the fifteen short curved vanes (see Figure VIII-3). The flow distribution from the pump discharge is represented by the average flow into each pair of passages. This is shown dotted on Figure VIII-5. The effect of nonuniform flow distribution on radial thrust can be determined from a detailed analysis of the pump design. If improvement is needed, tailored orificing of selected passages would provide a satisfactory solution.

b. Oxidizer Return Passages Model

(1) Objectives

(U) The oxidizer return passages receive oxidizer from the thrust chamber regenerative cooling tubes at the TCA flange and duct this

oxidizer to the primary injector. Flow leaving the regenerative cooling tubes should be nearly uniform and hence the housing must be able to accept this flow. Uniform flow is also needed at the primary injector to avoid streaking. The specified pressure drop for the oxidizer return passages is 125 psi. Therefore, test objectives were established as follows.

(U) (a) Determine the pressure drop from the thrust chamber flange to the primary injector.

(U) (b) Determine the flow distribution at the TCA flange.

(U) (c) Determine the flow distribution at the primary combustor injector.

(2) Approach

(U) These objectives were accomplished by air testing a full-scale plastic model that simulates the flow passages from the thrust chamber flange to the primary injector. Upstream conditions were established by a fixture that simulated the thrust chamber coolant-tube passages and the passages in the thrust chamber flange. Downstream conditions were simulated by a fixture containing flow passages similar to those in the primary injector. Vanes in the flow passages were fabricated from rubber strips and glued in place. Figure VIII-6 shows a developed view of the cylindrical portion of the "C" design TPA housing, with vanes and primary injector feed holes. Static pressure probes were located circumferentially around the model planes D, E, X, F & H (see sketch on Figure VIII-7). In addition a rotating total pressure probe assembly was located to measure the flow at the exit holes from the simulated primary injector.

VIII, A, Module Fluid Dynamic Testing (cont.)

(3) Results

(U) Results of this testing are shown in Figures VIII-7 and 8. Figure VIII-7 shows the measured air pressure-drop-parameter K at the various planes. The variation in flow velocity entering the return passages was estimated by taking the square root of the pressure drop variation vetween planes D and X. This resulted in a velocity variation of approximately ± 1.7%, which is within the allowable variation for thrust chamber coolant flow distribution. The pressure drop across the housing between planes G and H is 100 psi compared to 125 psi allowable, in terms of N_2O_4 propellant. Flow distribution from the primary injector is plotted in Figure VIII-8. Considering the extremes of the two tests, a circumferential flow distribution of approximately ± 20% about the nominal is predicted. This can be improved if needed by selectively orificing the injector feed holes.

c. Turbine-Inlet Model

(1) Objective

(U) The turbine-inlet model represents the primary combustor from the injector face to the turbine nozzle inlet. This component must have characteristics so that overall pressure drop is within design specifications and flow at the turbine entrance is uniform. Most of the pressure drop in the primary combustor occurs as a result of the combustion process. Therefore, the measured pressure drop in cold-flow testing must be significantly less than that allowable in the engine specification. The turbine is designed for uniform flow at its entrance. Turbine efficiency is affected if the flow is severely nonuniform. Hence he objectives established for this testing were:

(U) (a) Determine the pressure drop as a result of gas flow only (no combustion).

(U) (b) Determine the flow distribution at the turbine inlet.

(2) Approach

(U) These objectives were accomplished by air testing a full-scale plastic model which is geometrically similar to the primary combustor. Upstream conditions were established by flow through an injector-simulating plate and straightening vanes. The downstream conditions at the entrance of the turbine were simulated by radial vanes. The test setup is shown in Figure VIII-9. Flow distribution was measured by traversing the flow stream with probes at various planes as shown in Figure VIII-10 and locations shown in Figure VIII-11. Visual observation of the qualitative flow was provided by radial plates coated with oil and lamp black.

(3) Results

(U) Initial testing indicated that severe flow separation occurred as the gas turned around the annular divider. This flow separation extended sufficiently far downstream that it could have been detrimental to turbine performance. Subsequently, a rounded annular nose was added as shown by the cross-hatched section in Figure VIII-11. Flow direction at the turbine entrance with and without the primary injector simulator orifice plate is shown in Figure VIII-12. The difference noted with and without the injector simulator orifice plate can be attributed to the difference in uniformity of conditions at the inlet. The disagreement between the results obtained with the pressure probes and results obtained by visual observation is caused by

the different flow conditions that occur in the boundary layer on a radial surface as opposed to free stream conditions. For this reason, the visual data is considered qualitative only and the measured data is considered valid. The velocity distribution can be determined from Figure VIII-13; a plot of dynamic pressure ratio as a function of radial position at the turbine inlet. In the free stream, the dynamic pressure ratio varies approximately ± 21% which results in a velocity variation of ± 10%. The effect of this variation on turbine performance is negligible.

(U) During primary combustor development (hot testing) the primary combustor design evolved into a configuration in which turbulence rings were used to enhance mixing. The nose piece discussed above was not incorporated. Subsequent testing of a wedge model of this new configuration verified that the resultant flow conditions would be very similar to those resulting from the configuration discussed above. (See Figure V-8, Sheet 10 of 11).

(U) Air test data was converted to engine conditions to determine the predicted pressure drop in the primary combustor. Predicted pressure drop is 8 psi without including combustion effects.

d. Turbine Exhaust Passage Model

(1) Objective

(U) The turbine exhaust passage carries the turbine discharge gas from the turbine exit to the secondary injector. The secondary injector requires uniform gas flow to avoid mixture ratio distribution combustion losses and streaking on the wall. It has been estimated that flow distribution should be within a band of ± 5% in the center and + 5%, -0%, at the wall to satisfy these requirements. The objective of this testing was to determine the flow distribution at the injector face.

VIII, A, Module Fluid Dynamic Testing (cont.)

(2) Approach

(U) This objective was accomplished by air testing a full-scale model that simulated the flow passage from the turbine exhaust to the injector face in the "B" TPA design. This model used the turbine inlet model as a test fixture to simulate inlet conditions at the turbine exhaust. The vanes used to simulate the turbine in the turbine inlet testing were retained to simulate flow from the turbine. Exit conditions at the injector face were simulated by a screen designed to produce the pressure drop caused by combustion in the secondary combustor. The test setup is shown with the combustion-simulation screen installed in Figure VIII-14. Flow distribution was measured by traversing the face of the injector with a five-element pressure probe. Two different concepts for distributing the flow to the secondary injector were tested; one was a set of vanes located in the vertical region of the turbine exhaust duct; the other was a waffle-type pressure drop plate located just upstream of the secondary injector. These are shown in Figure VIII-15. The waffle plate was designed to simulate 100 psi pressure drop in the engine.

(3) Results

(U) The model was tested six different ways:

(a) Without distributing devices in the turbine exhaust passage, but with the secondary combustion-simulator screen installed.

(b) Same as (a) except without combustion simulator.

(c) Vanes in turbine exhaust passage, with combustion-simulator screen.

(d) Same as (c) except without combustion-simulator screen.

VIII, A, Module Fluid Dynamic Testing (cont.)

(e) Waffle plate upstream of secondary injector, with combustion-simulator screen.

(f) Same as (e) except without combustion-simulator screen.

(U) Results of testing these configurations are shown in Figure VIII-16. Relative velocities are noted at the locations where the measurements were taken. Velocity distributions in all cases were unsatisfactory from an injector standpoint. Velocity variations of a factor of approximately 3:1 occurred in all cases. However, methods of improvement are indicated by the test results. The introduction of a pressure drop tended to reduce the variation in flow in all cases. Increasing the pressure drop can be expected to further improve the flow distribution. The effect on flow distribution by addition of vanes was disappointing. However, the vanes were designed to divide the flow area equally at inlet and outlet. Consequently, if the distribution entering the vanes is poor, the distribution leaving the vanes will be equally poor. Therefore, an improved vane design to create equal flow at the inlet is required. It is believed that if the vane design is carefully optimized, the addition of 100 to 200 psi pressure drop will be adequate to satisfactorily distribute the flow to the secondary injector. Therefore additional airflow testing to optimize the turbine-exhaust passage is recommended.

VIII, Supporting Studies (cont.)

B. SUBSCALE NOZZLE PROGRAM

1. Introduction and Objectives

(U) The ARES engine is designed as a modular engine which can be clustered into large forced-deflection or plug nozzles. When clustered into large single nozzles, practical considerations normally dictate the introduction of discontinuities where the individual modules exhaust onto the common skirt. Also, in the forced-deflection nozzle, a base heat shield is needed to prevent base recirculation from damaging the bottom of the vehicle. In regions of discontinuities in flow, purely analytical techniques for optimizing performance and determining heat transfer rates cannot be applied with confidence, and experimental data is needed. Therefore, a subscale program was conducted to obtain this information. Objectives of this program were to obtain specific design criteria for a 2-million-lb-thrust engine employing twenty 100K modules exhausting into a single forced deflection nozzle skirt. The engine was to be installed in a vehicle approximately 18 ft in diameter. The program was conducted in two parts. The first part was to determine the performance potential of the nozzle and evaluate the effect of various design choices on the performance. The second part was to obtain heat transfer data in regions of the nozzle where flow conditions are such that purely analytical techniques would not be expected to apply.

2. Conclusions

(C) a. Forced-deflection and plug nozzles using 20 modules perform better with axisymmetric Internal Expansion Sections (IES) than with contoured wedge IES's.

VIII, B, Subscale Nozzle Program (cont.)

(C) b. With respect to design variations with the 20-module forced-deflection nozzle using axisymmetric IES's the following conclusions apply:

(C) (1) Ambient base bleed offers between 2.5% and 3.5% performance improvement over nonvented performance within the atmosphere.

(C) (2) Variations in IES area ratio from approximately 13 to 20 (based on engine gas properties) has an insignificant effect on nozzle performance.

(C) (3) The angle between a tangent to the IES exit wall and the nozzle skirt can be as high as 12.5 degrees without affecting performance.

(C) (4) Shortening the nozzle skirt by 18% results in a 0.6% performance loss.

(C) (5) Module cant angle can be reduced 5 degrees below theoretical optimum without performance loss. Increasing module cant angle results in performance loss.

(C) (6) Performance with two adjacent modules out is approximately 0.5% lower than performance with all modules operating. Resultant thrust vector angle is 1.2 degrees.

(C) c. Throttling by module shutdown results in a performance loss of approximately 0.5% for forced deflection nozzles employing either axisymmetric IES's or contoured wedge IES's.

VIII, B, Subscale Nozzle Program (cont.)

(U) d. The heat transfer coefficient in the region where the IES's flow onto the skirt is higher than would be predicted for a continuous wall with no discontinuities. The magnitude of the increase is strongly dependent on the IES geometry and spacing.

(C) (1) Axisymmetric IES's result in the lowest heat-transfer rate of the cases tested.

(U) (2) Use of contoured wedge IES's (gapped) result in heat-transfer rates which are nearly twice as great as for axisymmetric IES's. If no gap is used. heat transfer rates are further increased by approximately 40%.

(U) e. Heat transfer rates on the base heat shield are less than 10% of the maximum heat transfer rate measured at low ambient pressures on the nozzle skirt using axisymmetric IES's. The heat transfer rate on the base heat shield at sea-level atmospheric conditions is approximately four times as high as at vacuum.

(U) f. The heat transfer rate inside a shutdown module is approximately the same as on the base heat shield.

3. Nozzle Performance

a. Objectives

(U) The basic 20-module engine installation incorporates axisymmetric IES's exhausting into a single forced-deflection nozzle skirt. Other choices include (1) use of contoured wedge IES's, (2) use of a plug nozzle with axisymmetric IES's, (3) use of a plug nozzle with contoured wedge IES's. Sufficient information is available on performance potential of plug

VIII, B, Subscale Nozzle Program (cont.)

nozzles with axisymmetric IES's from other programs (References 26 and 27). Therefore, only the other choices were considered in this program. Practical considerations dictate that the 20-module axisymmetric IES forced-deflection nozzle have a discontinuity where the module IES's exhaust into the nozzle skirt. Therefore, experimental data is needed to establish design criteria for the skirt contour, skirt length, IES area ratio and IES cant angle. In addition the degree to which base bleed can improve performance in this configuration is not known. Application of this engine system to a practical launch vehicle makes considerations of operating, with modules out, for reliability with throttling important. Data is needed on performance and thrust vector angle produced when modules are shut down. Therefore the following objectives were defined for the nozzle performance program.

(U) (1) Determine the performance characteristics of a 20-module FD nozzle design using axially symmetric IES's and contoured wedge IES's.

(U) (2) Determine the performance characteristics a plug nozzle with 20 contoured wedge IES's for the same installation as for the FD nozzles.

(U) (3) Investigate the effects of variations in skirt contour, skirt length, IES area ratio, IES cant angle, and base bleed on the performance of the FD nozzle with axially symmetric IES's.

(U) (4) Determine the effect of module failure and engine throttling by module shutdown on the performance of the FD nozzles.

VIII, B, Subscale Nozzle Program (cont.)

b. Approach

(U) These objectives were accomplished by air testing scale models of the full-scale engine configuration over a range of pressure ratios representative of sea level to near vacuum operating conditions. Four basic models were fabricated for this testing,

(U) (1) Model 1a, FD nozzle using contoured wedge IES's.
(U) (2) Model 2, FD nozzle using axisymmetric IES's.
(U) (3) Model 3, FD nozzle using axisymmetric IES's.
(U) (3) Model 4, Plug nozzle using contoured wedge IES's.

(U) The first two objectives were accomplished by air testing three of these four basic models, with Model 4 tested as both a zero length plug and as an 18% plug. The third objective was accomplished by testing Models 2 and 3 with design variations to simulate each of the parameters of interest. The fourth objective was accomplished by testing Models 1a and 2 with selected module throats plugged. The specific test points obtained on each model are summarized in Figure VIII-17. Specific design parameters for each model are summarized in Figure VIII-18. Photographs of these models are shown in Figure VIII-19.

(U) The test program was conducted by FluiDyne Engineering Corporation. The greater portion of the cold-flow testing was conducted in Channel 8 of the Elk River Aerodynamics Laboratory. The design pressure ratio requirements of several configurations (Models 1a and 2 at high throttle ratios, for instance) exceeded the performance capability of the Channel 8 static thrust stand. For these models the hypersonic wind tunnel of FluiDyne's Medicine Lake Laboratory was used.

(This page is Unclassified)

VIII, B, Subscale Nozzle Program (cont.)

c. Results

(1) Nozzle Comparison

(U) Nozzle performance characteristics for the three basic nozzle configurations tested are presented in Figure VIII-20. The nozzle performance corrected to the combustion gas properties of the full-scale engine is shown in Figure VIII-21.

(C) The zero-length plug nozzle with no base bleed exhibited far poorer performance than the other nozzles tested. Of the other three, the FD nozzles showed better performance than the plug nozzle at altitude and lower performance at sea level. The FD nozzle using the axisymmetric IES's was slightly superior to the FD nozzle with contoured wedge IES's. It can further be concluded that the plug nozzle performance would be improved if axixymmetric IES's were used. This is further substantiated in References 26 and 27.

(2) Base Bleed

(C) Performance of Model 2 with and without ambient base bleed is shown in Figure VIII-22. This figure shows that a substantial performance gain is available through use of base bleed. Forced bleed was also examined but was found to offer less performance gain than with ambient base bleed.

(3) IES Area Ratio

(C) The effect of IES area ratio was investigated with Model 3. An IES area ratio of 7.59 was used on the basic model. The purpose of this portion of the program was to determine the effect of using an area

VIII, B, Subscale Nozzle Program (cont.)

ratio of 9.72 which would have a design pressure ratio equal to model sea-level optimum pressure ratio. Results of testing with the higher IES area ratio are shown in Figure VIII-23. Use of the higher area ratio IES offers some improvement at low pressure ratios. However, performance differences are slight over most of the range of operation. It should be pointed out that the larger area ratio IES's require greater base area ratio. Therefore, base bleed could be expected to yield greater improvement for this model than for the basic Model 2.

(4) Module-Skirt Merging Angle

(C) The region where the modules exhaust onto the forced deflection nozzle skirt does not lend itself to rigorous analysis. Therefore, Model 2a incorporated an abrupt zero-radius turn of 12.5 degrees where the IES skirt joined the wall as opposed to a smooth transition employed in Model 2. Thrust efficiency of Models 2 and 2a are shown as a function of pressure ratio in Figure VIII-24. Thrust efficiency was unaffected within the range of instrumentation by this change in the module-skirt merging angle.

(5) Skirt Length

(C) The effect of skirt length on nozzle performance was investigated with Model 2b. This model employed the same modules as Model 2a but used a parabolic skirt which was approximately 18% shorter. Theoretically, this modification would cause a 1% loss in performance. However, results of testing (Figure VIII-25) showed the performance to be only 0.6% lower over most of the pressure ratio range. Sea-level performance was unchanged.

VIII, B, Subscale Nozzle Program (cont.)

(6) Module Cant Angle

(C) The effect of module cant angle was investigated to determine the sensitivity of the nozzle to this parameter. Two cant angles were investigated with two different models. Model 2c was a modification of Model 2a with a cant angle of 15 degrees which is 5 degrees less than nominal. Model 2d was a modification of Model 2a with a cant angle of 25 degrees which is 5 degrees greater than nominal. Test results in Figure VIII-26 show that a reduced cant angle, 5 degrees less than nominal, results in no performance loss over the range of pressure ratios of interest. A cant angle 5 degrees greater than nominal caused a loss of approximately 0.5%.

(7) Module Out

(C) Model 2 was tested with several combinations of module throats plugged to investigate the effect of module-out on performance and thrust vector angle. Three test series were conducted with different combinations of throats plugged.

One module plugged
Two adjacent modules plugged
Two opposing modules plugged

Results of this testing, showing the effect of plugging module throats on thrust efficiency and thrust vector angle, are shown in Figures VIII-27 and VIII-28. Performance loss averages less than 0.5% for all three cases tested. Equivalent gimbal angle is a maximum 1.2° if two adjacent modules are shut down. Shutting down one module results in a gimbal angle of 0.6 degrees and as expected shutting down opposing modules results in no thrust vector change.

VIII, B, Subscale Nozzle Program (cont.)

(8) Throttling by Module Shutdown

(C) The effect of throttling, by shutting off modules, on nozzle performance was investigated by testing Models 1a and 2 with various numbers of throats symmetrically plugged. Results of this testing, shown in Figure VIII-29, show that performance loss is very small at 50% throttling. However, at 25 and 75% throttling, losses of approximately 0.5% can be expected.

(U) There are three effects that contribute to the performance change when modules are shut off for throttling. As the number of modules operating is reduced, the effective nozzle area ratio increases thus increasing performance. However, interaction effects of the exhaust streams impinging on one another tends to reduce performance. If very few modules are operating, large gaps exist between the exhaust streams and base pressure is lost. With half the modules operating, the effect of larger area ratio is apparently compensated for by the larger jet interaction losses and very little effect on overall performance is observed. With more than half the modules operating, the operating modules that are next to each other are unable to expand to take full advantage of the increased area ratio and the interaction effects are predominent. With only 20% of the modules operating base pressure is apparently lost because of the large gaps in the flow stream thus reducing performance.

4. Nozzle Heat Transfer

a. Objectives

(U) This program was conducted to determine the heat transfer rates that can be expected in the 20-module forced-deflection nozzle. Two

VIII, B, Subscale Nozzle Program (cont.)

areas are of interest; the region where the flows from individual modules merge on the forced deflection skirt, and the heat shield. There are two contending designs for the internal expansion section, the axisymmetric and the contoured wedge designs. Also there is some flexibility as to the spacing between module nozzle exits. Under module out conditions, environmental conditions are somewhat different than under normal operating conditions. Also, the module that is out is subjected to an environment that is not predictable by analytical means. Therefore, the objectives established for this program are as follows:

(1) Determine the heat transfer rate in the region of discontinuity where the module flow enters the forced-deflection nozzle skirt.

(2) Determine the heat transfer rate on the base heat shield.

(3) Determine the effect of the internal expansion geometry (axisymmetric or contoured wedge) on heat transfer rate.

(4) Determine the effect of IES spacing on heat transfer rate.

(5) Under module out conditions, determine the heat transfer rates on the skirt and in the IES that is shut off.

b. Approach

(U) The above objectives were accomplished by warm air testing of nozzle models. Testing was conducted in FluiDyne's Elk River Aerodynamics Laboratory in the Channel 8 static thrust stand. This facility used

an alumina pebble-bed heater preheated to 900°R by superheated steam to heat the incoming air. Air temperature was controlled by mixing heated air with ambient air.

(U) Three models were used:

(1) A forced-deflection nozzle using contoured wedge internal expansion sections.

(2) A forced-deflection nozzle using axisymmetric internal expansion sections.

(3) A two-dimensional model of the forced-deflection nozzle using contoured wedge internal expansion sections.

(U) The first two models used in the warm flow program were modified versions of Models 1a and 2 used in the nozzle system performance program. A thin wall was machined on one of the modules and three thermocouples installed on this wall. Thermocouples and pressure taps were installed on the existing nozzle skirt. A special centerbody of thin wall design, in the form of a convex spherical segment, replaced the flat base used in the performance tests. Thermocouples and pressure taps were installed on this simulated heat shield. Inlet sections were roughened to promote turbulent boundary layer conditions along the wall of the modules and the skirt.

(U) The third model, 2-D, was a flat development of five internal expansion sections of cold flow Model 1a. The module contour and flow interaction angles of Model 2-D were geometrically similar to those of Model 1a. The five-module sector was selected for this model (1) to permit a larger model for better flow visualization and (2) to have sufficient aspect

VIII, B, Subscale Nozzle Program (cont.)

ratio to avoid wall effects on the shock patterns in the module under examination. Two modules on one side had intersecting exit wall contours while the two modules on the opposite side had gapped module exits. The center module had one wall of each type. These differences in module geometry are clearly shown on Figure VIII-30 (exit view).

(U) The throats of Model 2-D were axially symmetrical with machine roughened walls to promote turbulent flow in the modules. Figure VIII-30 also includes a side view of this model with glass walls for flow visualization. Additional side walls for this model included a wall instrumented with pressure taps and a thin-skin wall with thermocouples attached to the back side. The pressure taps and thermocouples were concentrated in the flow interaction region downstream of the two modules adjacent to the center module. Tests were conducted with these two modules closed off and with all five modules operating.

(U) A summary of all the warm flow program test conditions is shown on Figure VIII-31. Tests of the three-dimensional models were run over a range of pressure ratios (P_c/P_a) but the two-dimensional model was tested at essentially constant pressure ratio. By examining a range of pressure ratios it was possible to determine the effect of altitude compensation on both nozzle skirt and base region heat transfer. Since the two-dimensional model had its exhaust confined on all sides and was of small area ratio, ambient pressure effects on its skirt heat transfer were not present. In the following sections, results for each of the models will be discussed in detail.

c. Results

(1) Model 2-D

(U) The purpose of this model was to provide qualitative information by flow visualization and quantative results from heat flux

measurements in (1) the flow interaction region downstream of the module exits and (2) the flow recirculation patterns behind a shutdown module. Two types of flow visualization were used for these tests. The first was a fluorescent oil mixture applied to the far wall and photographed through a glass near wall to show the flow patterns in the boundary layer. These were color photographs taken with an ultraviolet light source and variations in color from a light yellow to a dark green permitted a qualitative evaluation of the region of interest. The flow field was also photographed with the shadowgraph technique and these results are shown in Figure VIII-32. Model operation under both full flow and module-out conditions is shown here and the shock patterns caused by the flow interaction are clearly evident. The effect of module exit gaps on the shock pattern is sharply defined by the shadowgraph. Referring to Figure VIII-30, the upper and middle modules are separated by a finite base width (gapped) while the lower and middle modules converge to a point at the module exit plane. The two base regions are labeled A and B, respectively, on Figures VIII-30 and 32. The flow patterns during module-out operation are not clearly defined by the shadowgraph technique although the outline of the converging flow is distinguishable on Figure VIII-32, where the throat plugs used to shut off the modules are visible.

(U) The heat transfer coefficients in the module and on the nozzle skirt are correlated to a modified form of "Reynolds Analogy" for turbulent flows on Figure VIII-33. Calculated coefficients on Figure VIII-33 are based on the measured Mach number distribution along the particular flow paths of interest. The solid line represents data down the module centerline. Relatively good agreement was obtained for the calculated and measured coefficients along this path. The broken lines on Figure VIII-33 represent calculated heat transfer coefficients along the interaction streamlines and clearly show that module gapping reduces heat transfer to the nozzle skirt.

VIII, B, Subscale Nozzle Program (cont.)

(U) Model 2-D was also tested during module-out operation. Experimental data indicated that the static wall pressure in the shutdown module was essentially constant, signifying low recirculation velocities. Flow from adjacent operating modules continued to expand along the skirt converging at the centerline of the dead module a considerable distance downstream. With a module out, the heat transfer rate near the module exits was relatively low because of expansion in the absence of adjacent flow. Heat transfer coefficients in the dead module were very low (1 to 4 Btu/ft^2-hr-$^\circ$R). In the convergence region downstream of the dead module the coefficients ranged from 13 to 32 Btu/ft^2-hr-$^\circ$R.

(2) Model 1a

(U) This model employed 20 two-dimensional, contoured wedges IES modules exhausting onto a common forced-deflection nozzle skirt. The experimental Mach number distribution as well as calculated and measured heat transfer coefficients on the nozzle skirt (at high pressure ratio) are shown on Figure VIII-34. The discontinuity in Mach numbers along the module centerline is a result of the variation in wall slopes necessary to mechanically match the modules to the skirt; however, a considerably greater variation in Mach number was experienced along the interaction streamline, as evidenced by this figure. Mach numbers were calculated at each point by assuming the total pressure was constant (at its stagnation value) and using measured static pressures. Some error is introduced by this method since total pressure is not constant in the shock interaction region. However, the oblique shock angles generated by the flow interaction are relatively low so that the error introduced by assuming constant stagnation pressure is quite small.

(U) In the comparison of measured and calculated heat transfer coefficients shown on Figure VIII-34, the same trends as experienced

VIII, B, Subscale Nozzle Program (cont.)

with Model 2-D were observed. Module centerline heat transfer is predicted satisfactorily but that in the initial portion of the flow interaction streamline is over-estimated.

(U) Both heat transfer and static pressure data were obtained from Model 1a over a range of pressure ratios. At the lower pressure ratios, where altitude compensation begins to affect the pressure distribution on the nozzle skirt, there is an increase in heat flux to the wall due to the higher local pressure. In fact, at a pressure ratio of 60, the heat transfer coefficient near the skirt exit was approximately double that exhibited at the higher pressure ratios.

(U) Module-out heat transfer with Model 1a followed the same general trends as observed in Model 2-D; very low heat transfer rates just downstream of the dead module progressing to higher rates at the point where the flows from adjacent modules merged. The effect of pressure ratio on heat transfer rate was somewhat greater for the module-out case than with full flow operation. In fact, the heat transfer coefficient at the nozzle exit for the low pressure ratio case was greater than that measured with fully developed flow. This is a result of the relatively high static pressure (or low Mach number) that exists in this region at this off design condition.

(U) Experimental heat transfer coefficients for the base heat shield on Model 1a are shown on Figure VIII-35 where the several data points at one radial location represent different angular locations, ranging from those in line with the module centerline to those in line with the module exits. Some effect of radial location is noted; however, angular variations are too small to draw any significant conclusions. This data represents the average measured coefficients from the three highest pressure ratio tests, where the base pressure had stabilized at a constant value.

VIII, B, Subscale Nozzle Program (cont.)

Below a pressure ratio of 250, the base pressure and heat transfer coefficients are no longer constant but increase steadily with decreasing pressure ratio. This variation in average heat transfer coefficient at the center of the base heat shield as a function of pressure ratio is given below.

Pressure Ratio (P_c/P_a)	$\overline{h_g}$ (Btu/hr-ft^2-°R)
1500 to 250	2.5
170	7.5
60	13.0

(U) Also included on Figure VIII-35 is the radial base pressure distribution across the base heat shield. The cold-flow performance model had a flat base, while that on the heat transfer model was a convex spherical segment. Both pressure distributions are shown on this figure and, since base pressure increased with the convex base, heat transfer should be greater than that on the corresponding flat base. However, the higher base pressure should also increase overall nozzle performance, in this case, on the order of 0.25%.

(3) Model 2

(U) This model was a cluster of 20 axisymmetric IES modules in a circular arrangement, exhausting onto a common skirt. The complex nature of the merging flow pattern is illustrated on Figure VIII-36, which shows the Mach number distribution down the nozzle skirt for a streamline along the module centerline and for the interaction streamline between adjacent modules. Along the module centerline the flow initially expands, is compressed, and then expands again. The effect of these complex flow

VIII, B, Subscale Nozzle Program (cont.)

patterns on the heat transfer coefficients is also included on Figure VIII-36, where, as the flow is compressed, the heat transfer coefficients increase, followed by a decrease during further expansion. Comparison of measured and calculated heat transfer coefficient values can be considered satisfactory for the most part, though some problems were again encountered in trying to correlate data over the initial portion of the skirt flow.

(U) Comparing the results on Figure VIII-36, with those on Figure VIII-34, it is evident that the nozzle with axisymmetric modules (Model 2) has less of a heat transfer problem than the one with two-dimensional modules (Model 1a), as the peak heat flux on the nozzle skirt of Model 1a is approximately twice that measured with Model 2. Pertinent geometric variables for these two models are listed below:

	Model 1a	Model 2
Module area ratio	3.6:1	7.6:1
Base area ratio	22.6:1	14.5:1
Nozzle area ratio	38.9:1	39.6:1

Notice that the module area ratio for Model 1a is less than one-half that of Model 2. Thus the associated higher exit Mach number of the axisymmetric modules would be expected to result in lower heat transfer coefficients on the skirt. Both nozzle designs have been optimized for these respective module configurations. Therefore, this is a reasonable representation of the heat transfer differences.

(U) Model 2 was also tested with modules shutdown to determine the heat transfer coefficient in the shutdown module. Data indicated a heat transfer coefficient profile along the shutdown module centerline of from 2 Btu/hr-ft^2-°R at the module exit to about 20 Btu/hr-ft^2-°R at the skirt exit. In this case very little variation was observed with pressure ratio.

VIII, B, Subscale Nozzle Program (cont.)

(U) Base heat-shield heat transfer coefficients for Model 2 were on the order of 2 Btu/hr-ft^2-°R, or approximately the same as measured with Model 1a. Again, these showed considerable variation with pressure ratio below a pressure ratio of 250. The average measured base heat transfer coefficients for this model are listed below:

Pressure Ratio (P_c/P_a)	$\overline{h_g}$ (Btu/hr-ft^2-°R)
1600 to 250	2.0
130	6.0
70	9.0

The data also showed some radial as well as angular variation in measured heat transfer coefficients on the center base, similar to that observed on Model 1a.

VIII, Supporting Studies (cont.)

C. ADVANCED PROPELLANTS

1. Objective

(U) This program was to determine the necessary changes in the ARES engine incorporating the advanced turbopump so that the engine would be suitable for use with advanced propellants.

2. Summary

(U) A complete report on the advanced propellant design evaluation program was published as Section XIX of Quarterly Technical Report AFRPL-TR-66-1 (Aerojet Report 10830-Q-2) dated January 1966, and is republished with only minor revisions for clarification as Appendix III of this report. A summary follows.

(U) The ARES module design, pressure schedule, list of materials, etc., as defined in September 1965, the time of the study, were evaluated to determine their compatibility and the changes that would be required to accommodate each of three sets of advanced propellants: N_2O_4/Alumizine 43, 98% H_2O_2/Alumizine 43, and Compound-A/N_2H_4.

(U) Results of this study showed that conversion of the ARES module to the use of advanced propellants at the 100,000-lb thrust level would change the flow schedule of the module significantly. The major components were classified as to their usability in the conversion, as follows: (1) could be used directly with no design change, (2) could be used directly with recommended design changes, (3) could be used after rework, and (4) could not be used, and must be resized to be satisfactory.

VIII, C, Advanced Propellants (cont.)

(U) The following ARES components were established as being usable directly with no design change: (1) boost pumps*, (2) suction lines*, (3) suction valves*, and (4) primary combustor fuel valve when used for the control valve in the bipropellant primary combustor. The turbopump oxidizer housing design is adequate for two advanced propellant combinations, N_2O_4/Alumizine 43 and H_2O_2/Alumizine 43. The housing can be made adequate for the third combination analyzed, Compound-A/N_2H_4, provided shaft speed is increased, or operating pressure of the secondary combustor is reduced, or the housing is modified to accommodate a larger diameter pump impeller.

(U) Components that can be reworked from the ARES configuration to accommodate a specific propellant are:

(1) The oxidizer impeller
(2) The second-stage fuel impeller (where required for bipropellant use)

(U) The other major components are not acceptable because of the increased liquid flow to the secondary combustor. These components will have to be resized.

(U) Greater convertibility could be achieved by using an N_2O_4/AeroZINE 50 cycle based on a fuel-rich rather than an oxidizer-rich primary combustor. However, conversion to this cycle would demand the development of a high-temperature turbine as well as new primary and secondary combustors. Therefore, the fuel-rich primary combustor cycle with N_2O_4/AeroZINE 50 is not recommended in the current program.

*These items require change of location, i.e., reversal of fuel and oxidizer parts.

VIII, C, Advanced Propellants (cont.)

3. Technical Results

(U) As noted in the summary above, a complete report including the technical results is in Appendix III of this report.

VIII, Supporting Studies (cont.)

D. ANALYTICAL MODELS

(U) The objective of this task is to establish the engine module operating point and transient operation and to define system stability characteristics. To accomplish this task three engine simulation computer programs were developed.

(U) The steady state program is used to establish the engine operating point. It is also used in determining off-design operating characteristics (the ability of the engine to seek a design point when perturbed) and the influence of changes in component characteristics of the engine parameters.

(U) In the transient program, the transient operation of the engine was determined. Water hammer equations are incorporated into the model. Hence, results from this program will show the oscillatory behavior of the engine during start, steady state and shutdown operations.

(U) The low-frequency analysis program is used for studying the system stability characteristics during steady state operation.

(U) These three analytical models are further described in this section. Similar models were prepared for use with the component test hardware. These used basically the same equations, but their solutions were varied to suit the particular test setup.

1. Steady State

A steady state model of the ARES engine was prepared and programed for use on the IBM 7094 digital computer. This program is based on Aerojet-General's Liquid Engine Design Program--Job 102, which is a general

VIII, D, Analytical Models (cont.)

purpose digital simulation program written originally for Titan I engines. Job 102 has been used for engineering analysis of Titan II/Gemini, M-1, Apollo, Transtage, and many proposed engines, as well as ARES.

a. Description

(U) The Program is used to determine the steady state operating point by iterative solution of a system of equations representing the performance of system components (thrust chamber, pumps, turbine, gas generator, injectors, lines, valves, etc). The program provides great flexibility in the number of variables which can be iterated. It can be used to predict engine performance given all component performances or to determine required component performance (valve admittance, pump curves, etc.) when the engine operating point is specified.

(U) Special routines are available to determine linear influence coefficients to show the effects of either interface parameters or of individual component performances.

(U) Another special routine makes use of a Monte Carlo approach to predict the effect of combined component and interface tolerances. By specifying the distribution of each component parameter, the engineer can use the program to generate a statistical sample of engines having random combinations of components. The sample of engines can be used to predict performance tolerances without calibration, or to determine orifice ranges needed to permit engine calibration to specified tolerance.

b. Results

(U) This program was used to arrive at the steady state operating data presented in the engine handbook (Appendix I). This includes

the operating point, the performance maps and the engine influence coefficients. These are also discussed in the engine design task (Section III).

2. Transient and Waterhammer

Start transients are calculated with digital computer program No. 109 programmed on the IBM 360 computer that uses water-hammer equations to represent the hydraulic lines between the various other components, such as tanks and pumps. All of the components are treated as being one-dimensional. With the exception of lines, manifolds that are being filled, and combustors, the flows into and out of a component at any instant of time are considered to be equal. Where the necessary data for the computations are available in the form of curves, these curves are put into the program as tables, and interpolation in the tables is performed by the program as needed. In most cases, the sets of equations representing the components are nonlinear, and an iterative procedure is usually necessary to solve each set.

a. Description

(1) Hydraulic Lines

(U) The flows and pressures in the liquid lines are computed by using water-hammer equations, which account for the elasticity of the "pipe" and the elasticity of the liquid in the transmission of disturbances through the system. The water-hammer equations provide a better representation of flows in the engine than did the rigid column theory formerly used. Also, distinct computational advantages result. Using the rigid column theory, all of the equations representing the entire system must be solved simultaneously at each new point in time. With water-hammer theory, it is only necessary to solve, as a simultaneous set, the equations representing one component and one or two water-hammer equations. In general, it is much easier to solve several

small sets of simultaneous equations than one large set. Further, it is much simpler to identify performance anomalies when each component is considered separately.

(2) Combustion Chamber

(U) An instantaneous mixing model is used for the primary and secondary combustion chambers. In this model, the propellants flowing into the chamber burn and mix instantaneously with the combustion products already present in the chamber. The mixture ratio of the gases leaving the chamber is then equal to the mixture ratio of the gases residing in the chamber. A different model could be used which sets the chamber mixture ratio equal to the incoming propellant mixture ratio at all times; however, problems arise with such a model when the incoming propellant mixture ratio is fluctuating badly. For example, if the oxidizer flow should be nearly cut off in the latter model, the chamber mixture ratio would approach zero instantaneously; this would result in the chamber temperature (and pressure) declining at the same rate as the mixture ratio. Such a situation does not seem likely in a real engine, because there is hot gas residing in the chamber to be accounted for.

(U) The total temperature and molecular weight of the gas are found from curves which are plotted as functions of mixture ratio. The effect of pressure on chamber temperature is ignored. The density of the gas in the chamber is the average density, or the quotient of the quantity of gas residing in the chamber and the chamber volume. The gas density, temperature, and molecular weight are used in the ideal gas law to obtain the chamber pressure. The gas flow out of the chamber is computed using the steady state perfect gas flow relation.

(U) During the early periods of the transient, very high mixture ratios exist (>>100). At these mixture ratios, it is believed that complete mixing cannot occur and therefore considerable liquid at ambient temperature exists. Therefore, with the combustion model it is assumed that combustion of all the fuel will take place and reach equilibrium conditions with oxidizer at mixture ratios below an input maximum. Excess oxidizer is transferred unheated to the secondary combustor in the case of the primary combustor and overboard in the case of the secondary combustor.

(3) Filling of Lines and Manifolds

(U) One of the most difficult parts of the start sequence to simulate accurately is the filling of the lines downstream of the propellant valve and the filling of the injector manifold. For the filling of lines, it is assumed that any cross section containing liquid is completely filled. The resistance of the line is taken to be proportional to the volume filled. The filled portion of the line is then treated using standard water-hammer techniques. For the injector manifolds, a model is used that permits liquid to flow out of the injector before it is completely filled. A curve of the ratio of "flow out" to "flow in" versus the ratio of volume filled to volume of the manifold is used to determine flow out. The injector resistance is then proportional to the flow ratio.

(4) Turbines

(U) The behavior of the gas turbines is found using two steady state plots. The first plot is torque versus two parameters, (1) speed divided by the square root of the product of the inlet total temperature and gas constant, and (2) pressure ratio. The second plot is flow rate versus the above described speed parameter and versus pressure ratio. The rotor acceleration is then balanced against the difference between the turbine torque and

VIII, D, Analytical Models (cont.)

the pump torque divided by the moment of inertia of the rotor. Essentially the same procedure is used for the hydraulic turbines, the principal difference being that the temperature and gas constant does not enter into the computations.

(5) Pumps

(U) The pump performance is found from steady-state plots of head-to-speed ratio and torque-to-speed ratio versus flow rate, and the cavitating head loss versus suction specific speed.

(6) Valves

(U) Valve positions are programmed as a function of time. The valve admittances as a function of position are also programed.

b. Application to ARES Module

(1) Differences between Engine and Model Used in Transient Program

The schematic diagram used for the program is shown in Figure 2.6-1, Appendix I, except that minor flow circuits with a negligible effect on the engine dynamics were neglected to keep the transient program to a manageable size. These are the bearing and seal flows ($\dot{W}_{OBOS-1}$, $\dot{W}_{OBOS-2}$, $\dot{W}_{FBOS}$ and $\dot{W}_{OTS}$) and the fuel returned to first-stage fuel pump suction ($\dot{W}_{FRTS}$). The elimination of these flows was compensated for by reducing the efficiency of the turbine and increasing the turbine nozzle area to maintain the proper pressure drop across the turbine. Also, the second-stage fuel-pump performance was adjusted to increase flow to the primary combustor.

VIII, D, Analytical Models (cont.)

(2) Valve Sequencing

(U) The predicted nominal valve sequence for the ARES module is shown in Figure 2.4.3-1, Appendix I. The oxidizer suction valve is signaled open at fire switch. The fuel suction valve is opened at 0.5 sec to fill the fuel pumps and discharge lines. At 1.95 sec in the transient, the primary fuel valve opens to the initial step position currently set at 6% of operating K_w. With the assumed 60 psia boost-pump inlet pressure, the oxidizer manifold fills at 2.67 sec. The primary fuel manifold fills at 3.0 sec and combustion in the primary combustor occurs at 3 sec. The secondary fuel valve is signaled open at primary ignition. After the secondary valve is at the nominal open position, the primary fuel valve is opened to its nominal position. If the fuel valve sequence is interrupted at any position, the engine will continue to operate in a safe manner. For example, if the primary fuel valve does not open beyond 25% of nominal position, the engine will seek a low-speed operating point of approximately 7000 rpm. If the secondary fuel valve fails to open, the engine will run with the primary combustor at approximately 25,000 rpm.

(3) Preducted Nominal Start Transient

(U) Several engine parameters for the nominal start transient are also shown in Figure 2.4.3-1, Appendix I. Many more parameters than those shown were computed and plotted in the program. The nominal sequence is to be viewed as the present prediction based on the current engine component parameters.

(U) Primary combustor ignition occurs at 3.0 sec. The combustor model limits primary mixture ratio to an input maximum (25 in this case) and dumps any oxidizer over the mixture ratio limit into the secondary

combustor. The turbopump accelerates to 8000 rpm at 3.3 sec. The secondary fuel manifold fills and the secondary combustor ignites at 3.25 sec. The turbine speed drops slightly to 7000 rpm and then increases as the primary fuel valve is sequenced open. At 3.55 sec the primary mixture ratio drops below the input maximum and approaches the steady state value.

(4) Oxidizer Manifold Filling Time

(U) The oxidizer-manifold filling time for the nominal transient is 2.67 sec with a 60 psia initial boost pump suction pressure. At 90 psia the filling time is decreased to 2.02 sec and at 30 psia the filling time increases to 4.11 sec. Figure VIII-37 shows the effects of tank pressures on the filling times of both primary propellant circuits. An additional line on the graph shows what the oxidizer circuit fill time would be if the pump head loss were neglected. The head loss through the pump causes the turbopump to windmill at low rpm (0 to 1000). The pump operating point is as high as $(Q/N)/(Q/N)_D = 24$. The head and torque characteristics in the region beyond the zero head point were determined by extrapolating the curves linearly at the slope indicated by Reference 23, Figure 13.1, Page 270. Therefore, the analysis indicates a need for flow tests of the turbopump prior to optimizing the final transient for the engine. This was also concluded in the ICP breadboard engine test program (Contract AF 04(611)8548). Note that the nominal sequence would fill in 1.18 instead of 2.67 sec.

(5) Primary Fuel Manifold Filling Time

(U) The primary-fuel-manifold filling time for the nominal transient is 1.0 sec. Unlike the oxidizer circuit the primary fuel circuit filling time is controlled by the primary fuel discharge valve. Pump losses are less than 1 psia during the worst operating point and just prior to primary ignition the windmilling pump actually produces a 1.8 psia pressure

rise in the second stage of the fuel pump. The initial step K_W of the primary fuel valve has tentatively been set at 0.0552 (6% of the operating K_W of 0.092). A higher K_W reduces the fill time but also over-accelerates the turbopump for a condition where only the primary fuel valve is opened. A lower K_W setting will increase the fill time and lower the initial acceleration.

(6) Secondary Fuel Manifold Filling Time

(U) The secondary fuel circuit fills in 0.3 sec with a 0.3-sec valve opening time. With a 0.15-sec opening time, the fill time is reduced to 0.22 sec. With the faster opening valve, secondary ignition occurred at 4000 rpm instead of the nominal 8000 rpm. The major portion of the transient (after the primary valve begins to open) remains unchanged.

(7) Fuel Valve Tolerance

(U) The effect of variation in the point at which the secondary fuel valve opens was investigated by moving the initiation point $\pm$ 0.3 sec from the nominal case. In all cases, the primary valve was assumed to actuate just as the secondary fuel valve reached its 100% open position.

(U) Initiating the valves 0.3 sec prior to the nominal point is the extreme case, because primary and secondary ignition are only 0.04 sec apart. The primary ignites at 2.7 sec and the secondary at 2.74 sec. As a result, the turbine pressure ratio is reduced before the turbopump has reached 8000 rpm, which results in slow acceleration up to 3.0 sec. By 3.0 sec, the primary fuel valve has opened to the point where the primary mixture ratio is below 25. The turbopump acceleration then exceeds the design limit of 80,000 rpm/sec, established to prevent bearing skidding, for a period of 0.14 sec and then approaches steady state at a safe rate. A safe tolerance will be approximately + 0.15 sec.

VIII, D, Analytical Models (cont.)

(U) When fuel valve initiation is delayed 0.3 sec, the primary ignites at the same time as the nominal case. Secondary ignition is delayed from 3.0 sec to 3.2 sec. The delay in secondary fuel valve opening allows the turbopump to accelerate faster and to a higher rpm than the nominal case. The initial acceleration does not exceed the maximum limit because it is controlled by the primary valve initial step K_W.

(U) These results indicate that the tolerance will be from + 0.15 to - 0.3 sec about the nominal initiation point.

(8) Nominal Shutdown

(U) The nominal shutdown transient is shown in Figure 2.4.4-1, Appendix I. The primary fuel discharge valve closes first, followed by the secondary fuel valve, fuel suction valve, and oxidizer suction valve. Turbine speed deceleration is controlled by the primary fuel discharge valve closing rate. Variations in the valve closing rate only affect allowable shutdown impulse. The closing of 0.7 sec was selected to limit the deceleration of the turbopump below 8000 rpm/sec.

VIII, D, Analytical Models (cont.)

3. Low-Frequency Stability Analysis

a. Introduction

(U) In the low-frequency stability analysis, the dynamic interaction of components which arises from the transfer of mass and energy through hydraulic passages and power transmission systems was considered. These effects are most pronounced in a frequency range from 10 to 500 cycles/sec. Effects such as structural dynamics and high-frequency combustion stability are not included, because these effects are not usually a key factor in engine cycle stability. (When the vehicle system is included, structural coupling can become important.)

(U) To investigate cycle stability analytically, it is first necessary to formulate a suitable mathematical model. Subsequently, the methods of feedback control system analysis are used to establish the characteristics of the model. Completely general and reliable mathematical models of rocket engine components do not presently exist; therefore, a necessary part of the complete anlysis consists of correlation of analytical results with component test data. In this way, the analytical results can be made much more reliable for predictions of stability of the integrated system. The objective of the Phase I effort was to establish a mathematical model of the ARES engine system that can be used for low-frequency stability analysis. This model is based on predicted component characteristics based on design, but can be modified to incorporate change when component test-data become available.

VIII, D, Analytical Models (cont.)

b. Mathematical Model

(U) Mathematical models for the engine components were derived by applying the laws of classical mechanics and thermodynamics. The general model equations include many nonlinear terms and effects. The methods of dynamic system analysis are not well developed for nonlinear systems and, consequently, the small perturbation theory must be used to remove the nonlinearities. In general, the process of linearization does not reduce the usefulness of the model because the process can be viewed as obtaining the stability characteristics of the nonlinear model as the magnitude of the disturbance tends to zero. The linearized model can be solved in a very general way and provides a maximum of dynamic information.

(U) A lumped-parameter mathematical model was used to describe the engine sytem. The system components are closely coupled, and distributed characteristics such as line transmission delay can be approximated adequately by lumped-parameter models for the frequency range of interest. Where necessary, multisegment lumped-parameter models can be used in series to more closely approximate distributed effects. Lumped-parameter elements are described mathematically by systems of ordinary differential equations. The general differential equations may be nonlinear, because any nonlinearities are removed by the application of small perturbation theory. The net result is a system of simultaneous linear differential equations with constant coefficients.

(U) For purposes of dynamic analysis, only six fundamentally different components are contained in the ARES engine. These six components are (1) the primary combustor, (2) the secondary combustor, (3) the main turbopump, (4) the boost pumps, (5), the valves and injectors, and (6) the

hydraulic lines. The lumped-parameter models which are used for components given in (3) through (6) above are straightforward applications of the principles of classical mechanics (Reference 29). The models which were used to describe the primary and secondary combustor characteristics are unique and will be described. The ARES primary combustor consists of injection of supercritical liquid (less than critical temperature but greater than critical pressure) fuel and oxidizer, mixing and combustion throughout the combustor, and discharge of combustion products through subcritical turbine nozzles (Mach number less than 1 at nozzle discharge). It is assumed that the contents of the combustion chamber consist of three species: unburned fuel, unburned oxidizer, and combustion products. The combustion products are further characterized by assuming the temperature and gas content to be a function of the ratio of burned oxidizer to burned fuel species present at any time as combustion products. It is assumed that only the combustion products contribute to the chamber pressure, and that the ideal gas law can be used to relate pressure, temperature, and density. The remaining relationships necessary to completely characterize the primary combustor are equations to express the rate at which the unburned propellants are converted to combustion products. A mass action law with a temperature- and pressure-dependent rate constant is deduced from chemical kinetics and energy transport considerations (Reference 30). The final form of the equation which is applied to both unburned fuel and unburned oxidizer is:

$$\dot{w}_i = K_i P_c^{n_i} (T_{pc} - T_i) M_i \quad ,$$

where,

W_i = rate of combustion of i^{th} species
M_i = mass of i^{th} species at any time

VIII, D, Analytical Models (cont.)

T_i = injection temperature of i^{th} species
K_i = proportionality constant for i^{th} species
n_i = pressure exponent for i^{th} species
T_{pc} = combustion products temperature
P_{pc} = combustion pressure

(U) The constants K_i and n_i are estimated on the basis of propellant thermodynamic data and injector geometry. These constants can best be established from experimental data for transient performance of the combustor when available. The values of n_i and K_i directly affect the response characteristics of the combustor and by means of varying n_i and K_i any assumed combustor response characteristic can be produced, ranging from critically damped to unstable for the purpose of studying the effect of combustor stability on overall system stability.

(U) The secondary combustor model is similar to the primary combustor with two exceptions. First, only fuel is assumed to exist in an unburned state, because the oxidizer enters the combustor in a precombusted state. Only a rate-of-fuel combustion equation is used. Second, the combustion products are exhausted through a choked nozzle; therefore, the secondary combustor operation is independent of ambient conditions.

c. Stability Analyses

(U) The numerical determination of stability for a multiple-feedback loop system such as the ARES engine is a complex procedure. Therefore, a computer program (Number 48066) was produced that uses matrix methods to obtain the solution for a system of up to 88 Laplace transformed linear differential equations having constant coefficients. The program requires approximately three minutes of IBM 7094 computer time to obtain a solution for 87 equations and to obtain one transfer function.

VIII, D, Analytical Models (cont.)

(U) The computer program makes use of the procedure for reducing a system of linear first-order differential equations to a standard eigenvalue problem. An existing eigenvalue subroutine was used to obtain the poles and zeros of the system transfer or transmittance functions. System stability is assured if none of the system poles are located in the right half of the complex plane. The absence of poles in the right half plane means that any and all disturbances throughout the engine system will decay exponentially with time. The presence of poles in the right half plane almost always means that disturbances will grow exponentially with time.

d. Application to ARES

(U) The basic engine model is illustrated in Figure VIII-38, showing the components of the engine which are represented mathematically in the model. The basic model consisted of 87 equations with 87 dependent variables and six independent variables or forcing functions. Forty-six of the equations were first-order differential equations and the remainder were algebraic equations. The six independent variables are the two suction pressures and the four valve positions. In the course of development of the computer program for solution of the linearized equations, numerical problems necessitated the elimination of terms which produce very high frequency effects. No compoents were removed; however, some effects (such as inertance and compressibility in short fluid lines and inertance effects in gas ducts) were neglected. The system of equations used in the stability analysis consisted of 57 equations, 57 dependent variables, and six independent variables.

(U) In the course of developing the basic computer program, two other programs were prepared to facilitate the use of the program and to

enhance the usefullness of results. Program No. 53022 is used to calculate the coefficients for the basic system equations directly from engine specifications. Program Number AS71U is used to calculate system influence coefficients.

(U) Analysis of the engine using this model showed the engine is stable.

E. RELIABILITY

(U) The ultimate objective of the reliability effort is to assure that an engine of sufficiently high operational reliability is developed. This objective would normally be accomplished by implementing the seven different reliability tasks called out in the work statement. Because of the nature of the Phase I portion of the contract, the reliability effort was focused on the design aspects of engine and component reliability. As a result, most effort was concentrated in the areas of failure-mode analysis and design review, with limited effort devoted to such tasks as maintainability and reliability prediction. The accomplishments under each task are discussed below, together with the efforts anticipated during the Phase I extension program.

1. Related Data

(U) One of the tasks of this program was to obtain applicable failure data from related programs. This task was completed early in the program and provided essential inputs for the failure mode analyses, maintainability reviews, and various comparison studies.

VIII, E, Reliability (cont.)

(U) The data were obtained from the Titan II, Titan III, and Gemini programs. The data consist of the following:

a. The component failure modes, causes, and effects that were anticipated or were actually experienced during the testing of the Titan and Gemini engines.

b. The frequency of occurrence of failures experienced during testing by component, failure mode, and cause.

c. The reliability of each component.

In these groupings, the data were in a convenient form for the various studies and analyses performed during the program.

2. Failure-Mode Analysis

(U) During the course of the Phase I program, several failure mode analyses were performed on the various components. The analyses provided useful inputs for the designers and the design review meetings.

(U) Recently, a comprehensive failure model analysis was completed and documented (Reference 31). It represents an updating of the previous analyses in terms of the most recent designs and was extended to cover all of the ARES engine components. Each component was analyzed to identify the potential failure modes, the causes of those failures, and the anticipated effects of those failures on the engine. Each failure cause was classified as resulting from the considerations of environment and design, manufacturing and inspection, or handling and use. The failure effects were classified as critical (resulting in major hardware damage), major (producing a significant performance deviation), or safety (representing a potential safety hazard to technicians

through exposure to the toxic propellants during engine or component tear-down after testing). From that analysis it is concluded that, even though a significant effort must be directed toward the solution of design problems per se, much greater emphasis must be placed in such non-design areas as fabrication, assembly, inspection, transportation, checkout, cleaning, and testing. Furthermore, there are several cases in which trapped propellants pose a potential safety hazard; these areas should be carefully analyzed and the designs changed to eliminate any possibility of injury to technicians as a result of exposure to the propellants.

3. Design Review

(U) Throughout the Phase I portion of the contract, formal and informal reviews of the conceptual and working designs of the ARES engine and components have been held. Because of the contributions of experts in such fields as turbopump design, combustion dynamics, heat transfer, metallurgy and stress analysis, the design reviews have resulted in a large number of design improvements.

(U) Reliability contributions to the design review function have come about primarily as a result of the detailed engine and component failure mode analysis that were performed, revised, and updated during the course of the program. A few of the most important contributions are summarized below.

(U) One of the areas of concern was the suction valve. The initial design of that valve was judged to be too complex because of the multitude of parts required for actuation--the cams, springs, bumpers, latches, and latch releases. Because of an interchange of ideas between reliability and controls design personnel, the design evolved to a very much simplified two-cam design.

VIII, E, Reliability (cont.)

Testing of valves manufactured according to the simplified design has demonstrated its fabricability and its ability to comply with the imposed functional requirements.

(U) Another area of concern was that of the rotary sleeve valves used to control the flow of fuel to the primary and secondary combustors. A dynamic analysis was performed for the initial conceptual drawings of each valve. This revealed that the flow of propellant through the valve would produce high axial loading of the sleeve. Calculations indicated that the resultant friction force between the housing and sleeve would produce a resisting torque exceeding the planned actuation torque. For this reason, the valve was designed to incorporate a ball bearing to carry the thrust loading and reduce the friction-induced resisting torque to an acceptable level to meet the response requirements with minimum power.

(U) An investigation was made to define the fail-safe requirements of the primary and secondary combustor fuel control valves when used in module testing durirg Phase II (Reference 32). Several alternative concepts were considered: no interlock, hydraulic interlock, mechanical interlock, and electrical interlock. Based on the results of this study, an electrical interlock would result in a lower total program cost than testing without an interlock if components remaining from component tests are used to make up Phase II test modules. The hydraulic and mechanical interlocks would result in higher total program costs than tests without an interlock. However, if it should be necessary to purchase new components for Phase II module tests, then the mechanical interlock might be competitive with the electrical interlock, depending upon expected component costs.

VIII, E, Reliability (cont.)

(U) In the area of the primary combustor injector, an exchange of ideas between reliability and design personnel culminated in improved designs. In the case of the pentad injector, the sizes of the oxidizer injection orifices were modified to produce a uniform injection velocity across the face of the injector. Furthermore, changes were made to simplify injector manufacture, and an improved sealing concept was developed for the injector insert.

4. Review of Explosion Hazards

(U) Very little effort was directed by reliability personnel to the review of the potential explosion hazard arising from main stage and boost pump rub. However, a preliminary review has indicated little or no possibility of an explosion hazard because of the use of such inert materials as Kynar and Kel-F for inserts in the wear-ring designs. Testing performed to date tends to confirm this conclusion.

5. Test Data Review

(U) A review of the overall test program indicated that the test plans were basically sound. No changes were required except in the case of the housing. Analysis revealed that some of the different phases of housing testing could subject the housing walls to more severe structural loading than would normally be imposed. As a result, a housing that would be structurally adequate under normal conditions might fail during one of the phases of testing. For this reason, the test program was changed so that structural loading would be commensurate with that of normal usage.

(U) Because of the concentration of reliability effort in the areas of the failure mode analysis and design review, little effort was

VIII, E, Reliability (cont.)

expended on test data review. However, effort during the Phase I extension will be directed toward the review of the accumulated component test histories. Failures will be classified in such basic categories as design, fabrication, assembly, inspection, test, human error, an/procedure, and trends in the failure and performance characteristics of the hardware will be established. This information will serve as a basis for channeling development effort to bring about the most effective and efficient improvement in hardware reliability during Phase II.

6. Maintainability Review

(U) While no maintenance criteria are currently specified for the operational ARES engine, it is clear that the maintenance objectives during development must be to provide for the safe and easy inspection, removal, and replacement of all components in the development engine; to eliminate as many design features as possible that could impose any requirements for maintenance on the operational engine; and to provide for rapid repair or replacement of those components of the operational engine that cannot be made maintenance free or that may require retrofit for configuration changes in the future.

(U) A review of the "T" engine design was made with respect to maintainability. While the design provides for the necessary removal of components from the developmental engine, it was concluded that the inspection and replacement of some components are not easily accomplished. These components are the hydrostatic combustion seal, the oxidizer roller bearing, and the film coolant ring in the secondary combustion chamber. The only apparent obstacles to the achievement of a completely maintenance-free operational engine are external corrosion from tank leakage, boost pumps immersed in propellants (during storage), the possible use of soft goods in

VIII, E, Reliability (cont.)

the valves, bearings, and wear rings, and corrosion resulting from the possible requirement for test-firing of production engines for calibration and acceptance. The problem of N_2O_4-aluminum salting will require further consideration. Possibly an inhibitor can be added to the oxidizer. If not, aluminum parts may have to be replaced with steel ones.

(U) The complete maintainability analysis has been documented and is available for review (Reference 33). A separate analysis has been made of requirements for cold-flow acceptance testing; this analysis is also available for review (Reference 34).

7. Reliability Prediction

(U) Because of the concentration of the reliability effort in the areas of failure mode analysis and design review, little effort was expended on reliability prediction. During the Phase I extension, a first cut prediction will be made. The prediction will be based on the reliability trends of previous programs and tempered, as deemed necessary, by the testing results of the ARES program.

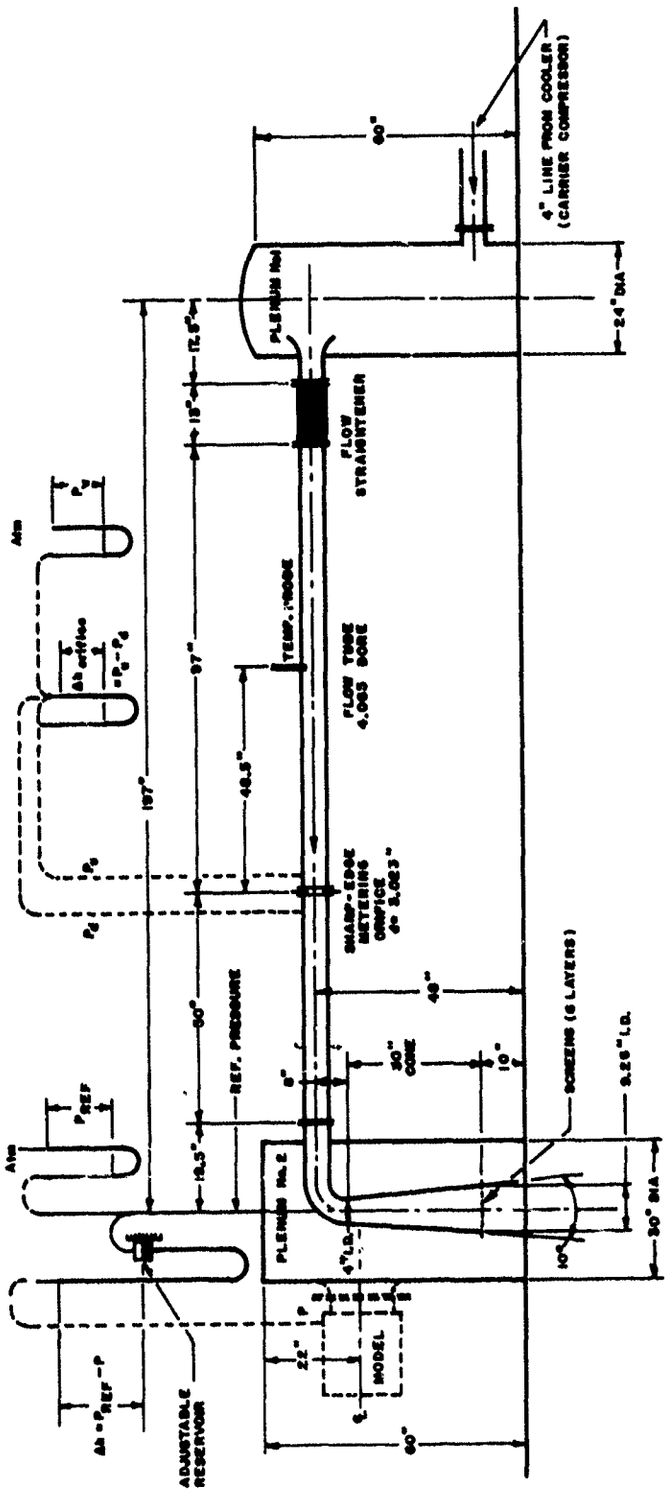

Air Test Facility Schematic

Figure VIII-1

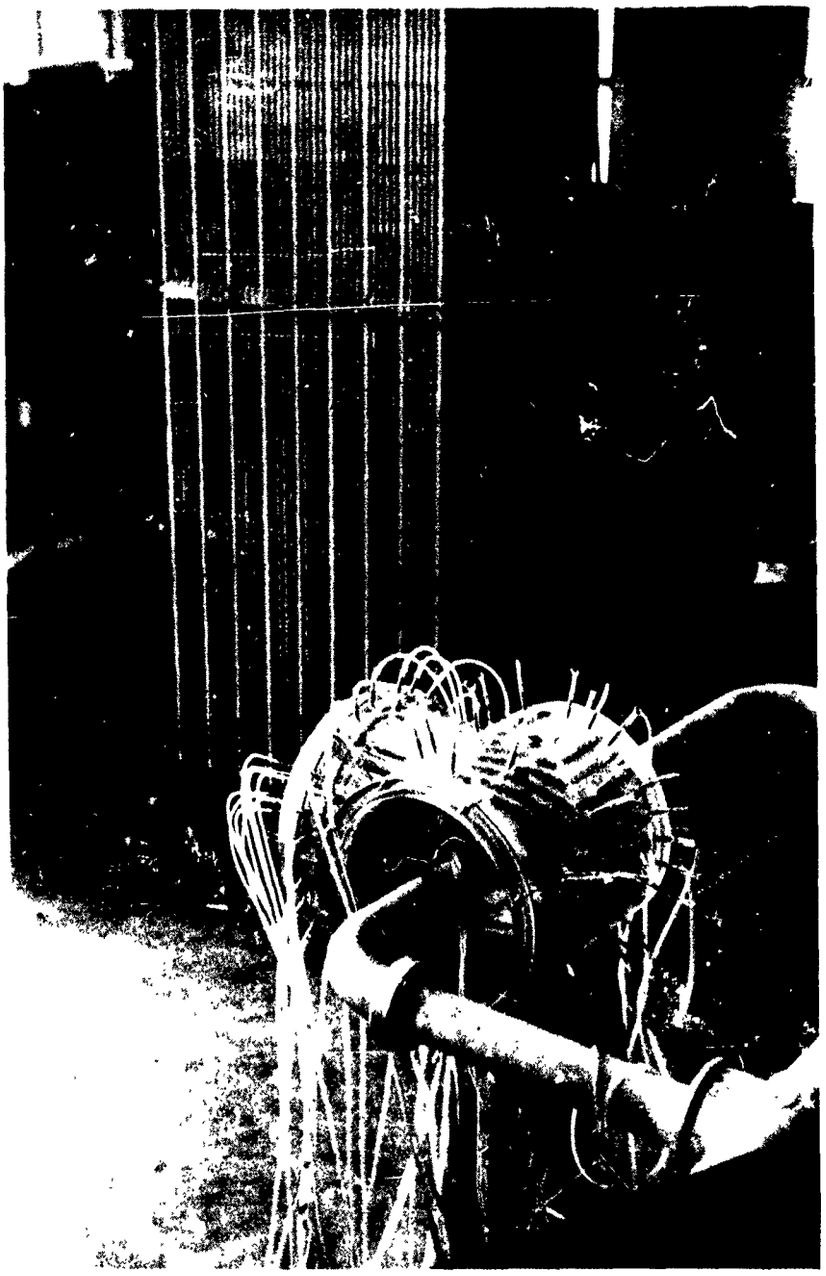

Oxidizer Discharge Model

Figure VIII-2

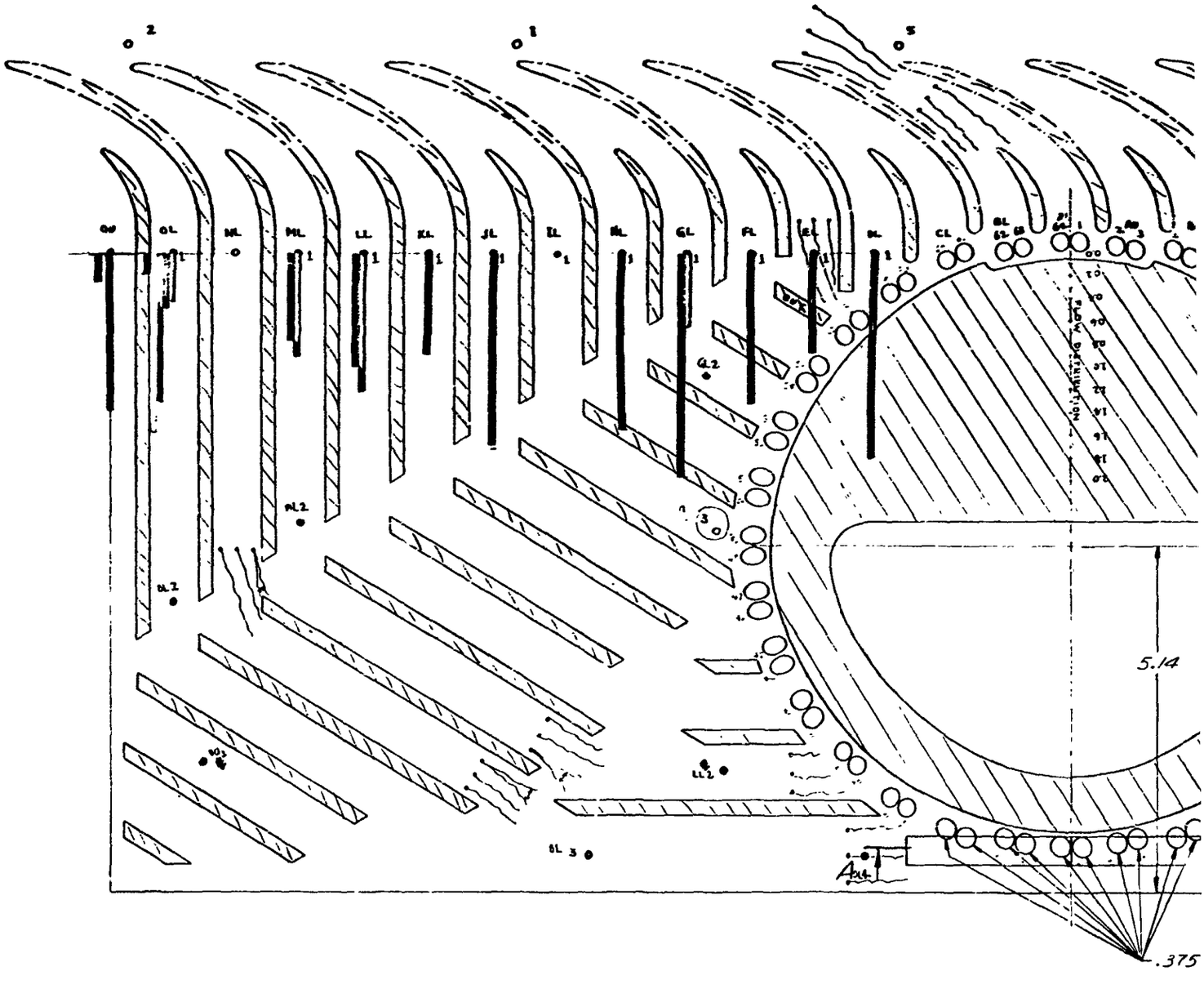
2
1
5
OL
ML
PML
LL
KL
JL
EL
HL
GL
FL
EL
DL
CL
BL
AL
PL2
QL2
OL2
LL2
5.14
.375

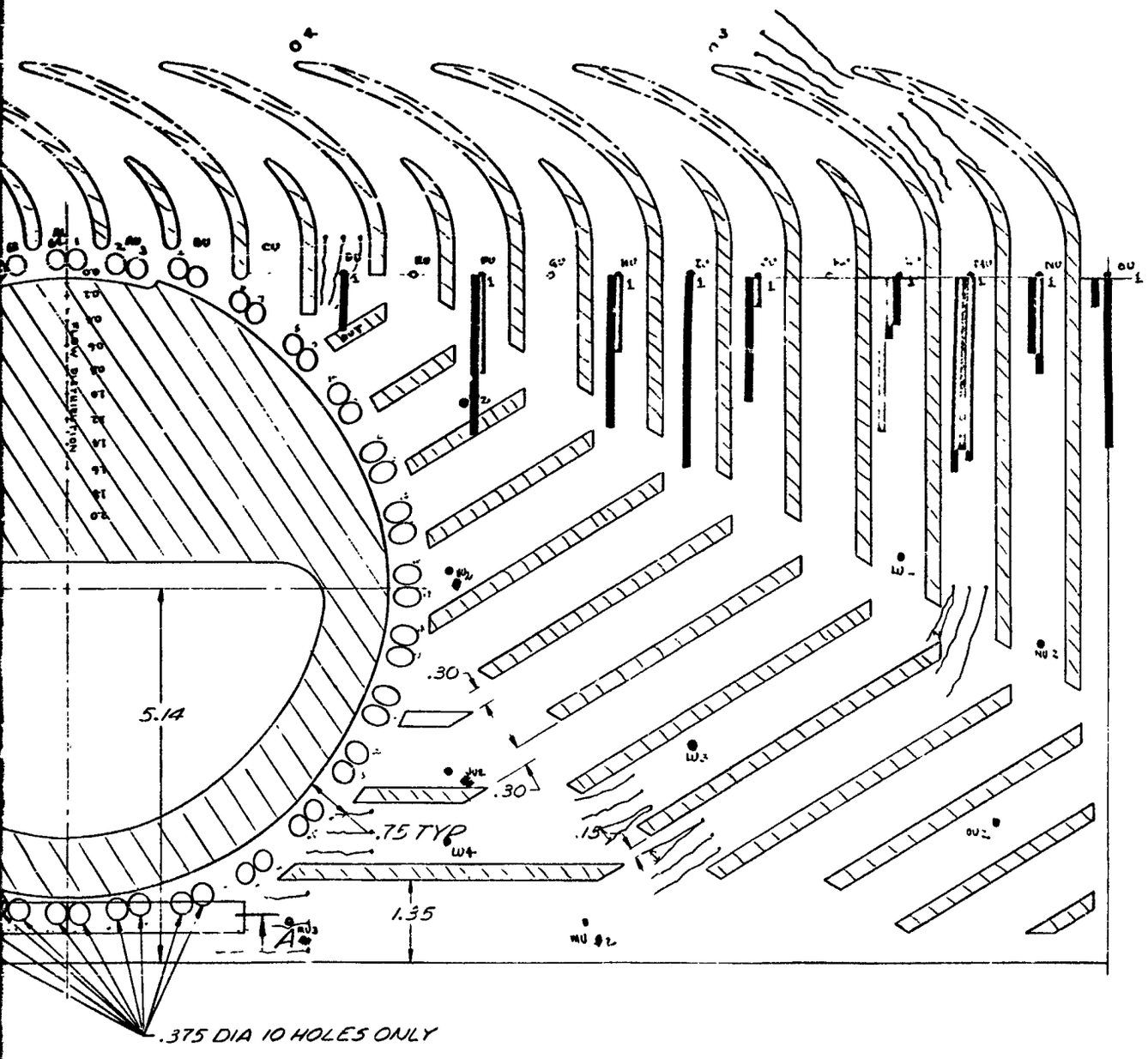

Oxidizer Discharge Housing Rib Pattern

Figure VIII-3

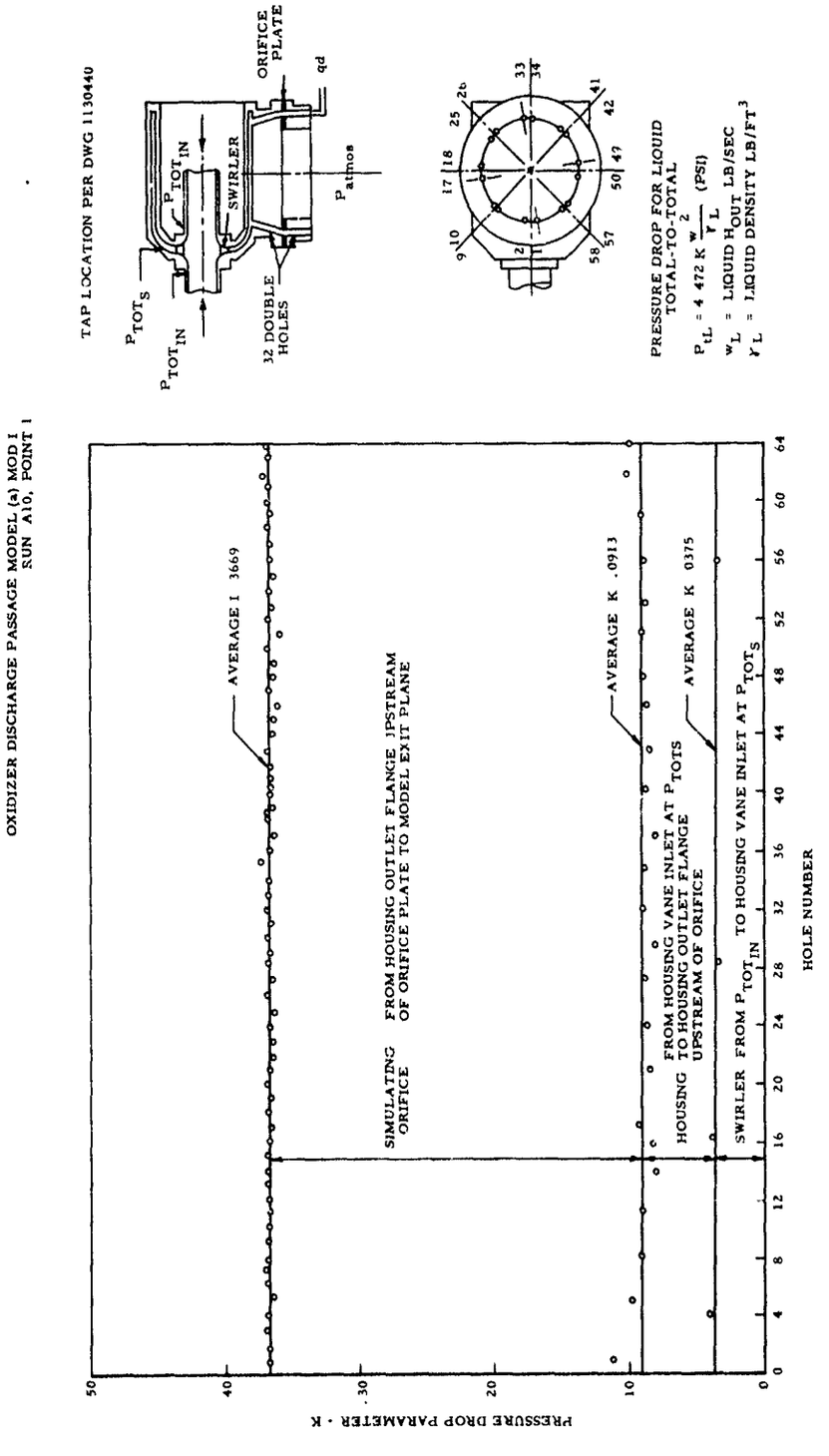

Pressure Drop Parameter vs Hole Number

Figure VIII-4

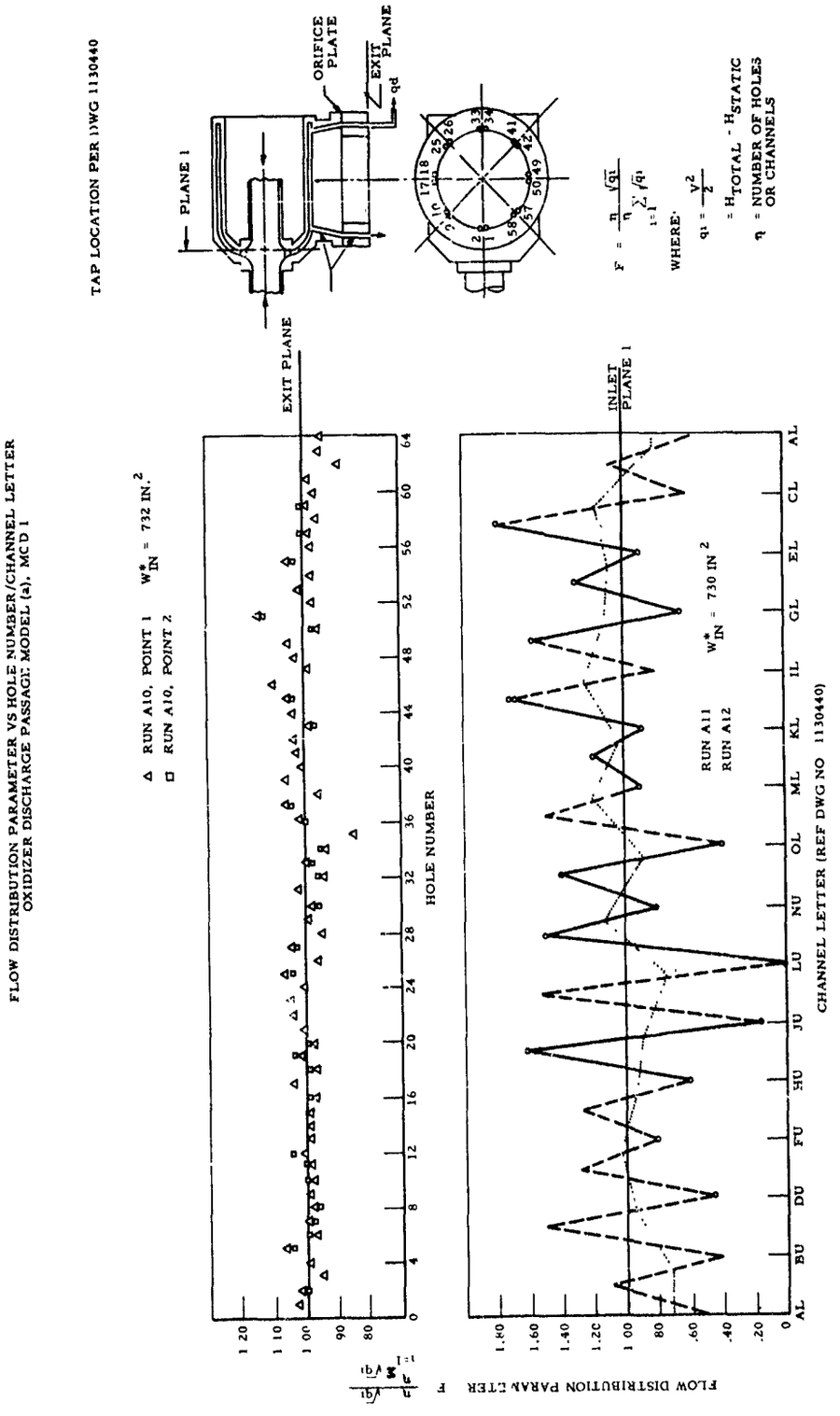

Flow Distribution Parameter vs Hole Number

Figure VIII-5

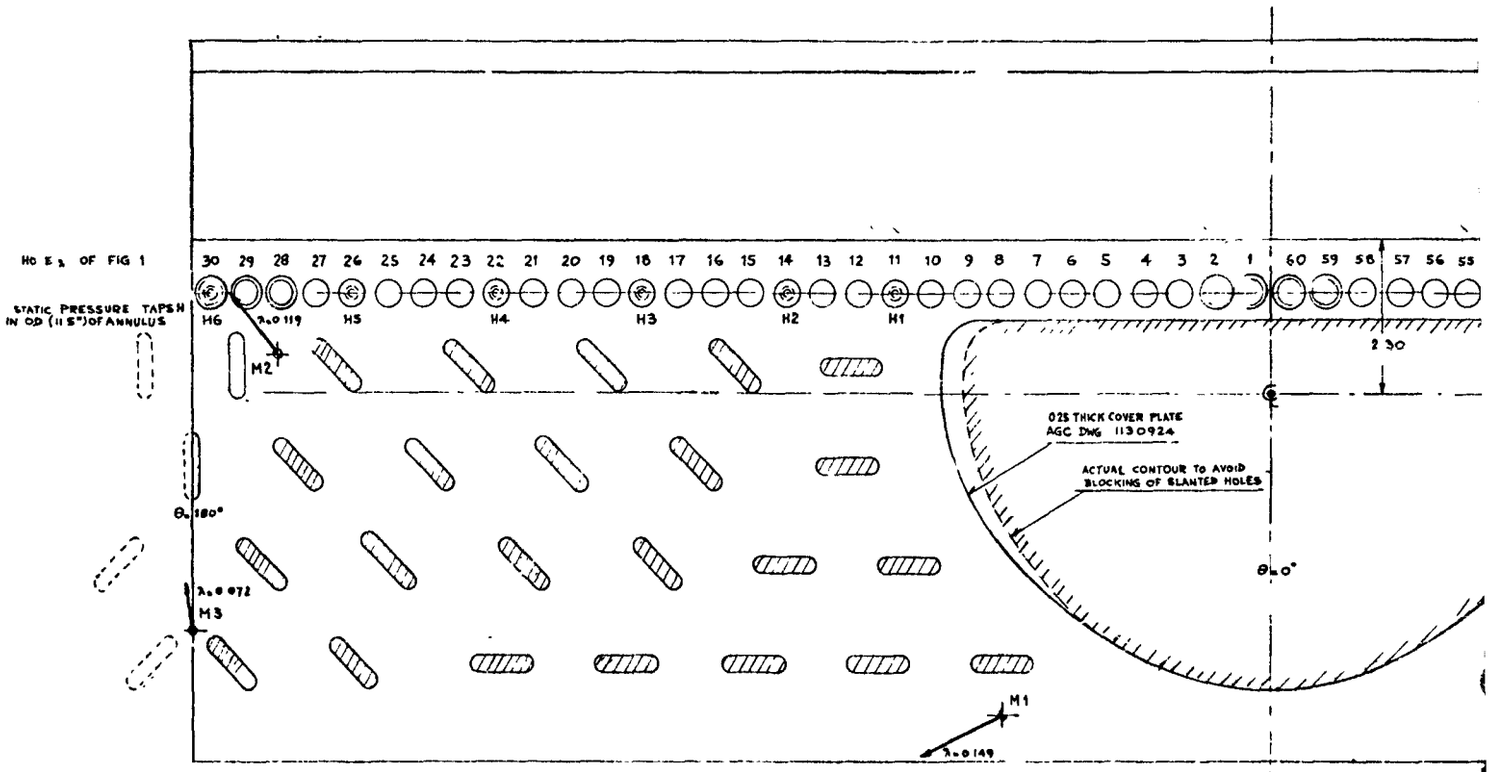

M1 TO M7 = LOCATIONS OF MINIATURE TOTAL-STATIC PROBE WITH APPROXIMATE FLOW DIRECTIONS. LENGTHS OF VECTORS ARE PROPORTIONAL TO λ (TEST B-6) OF TABLE VII

FLAT P
PLATES
DEVELOP
OF RADIA
"H" OF FIG.

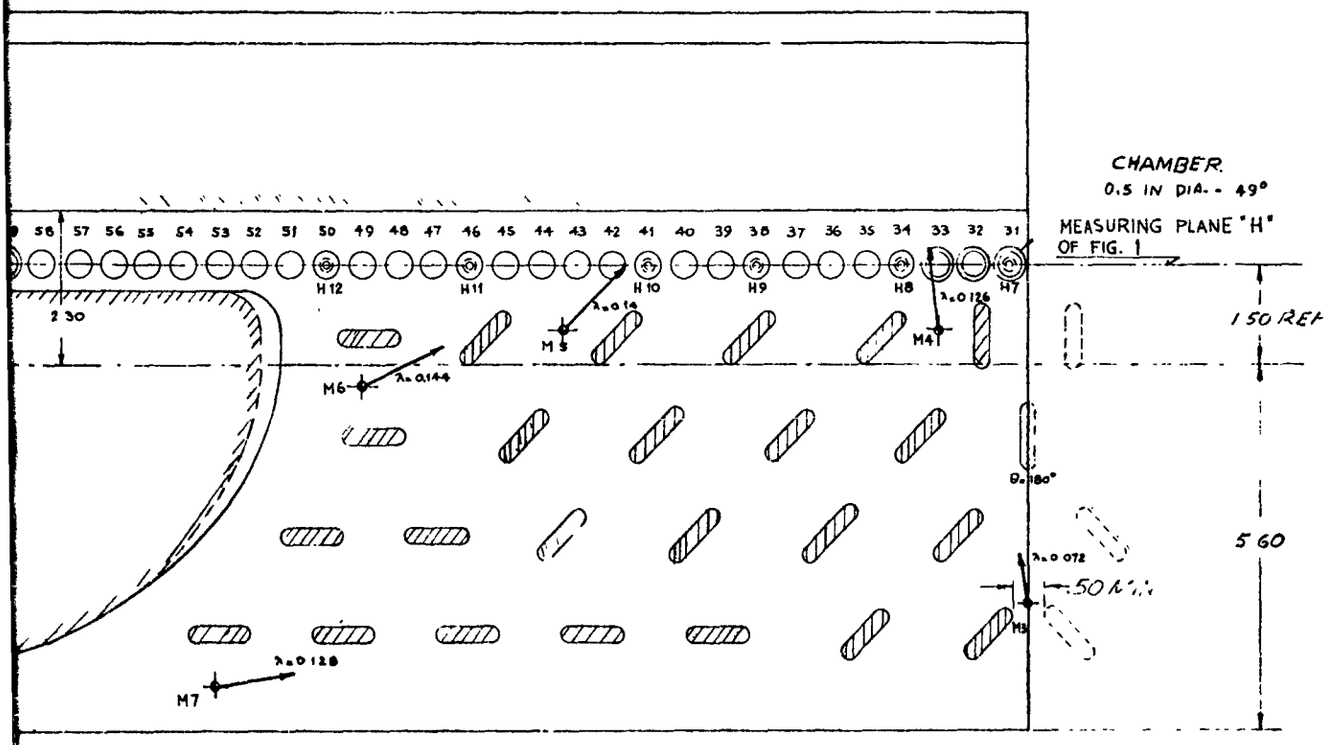

FLAT PATTERN OF RIBS AND COVER PLATES IN ANNULUS AT 11.0 DIAMETER DEVELOPED INTO PLANE, WITH LOCATIONS OF RADIAL HOLES AND STATIC TAPS IN PLANE "H" OF FIG 1. (ADAPTED FROM AGC DWG 1130924)

Oxidizer Return Housing Rib Pattern

Figure VIII-6

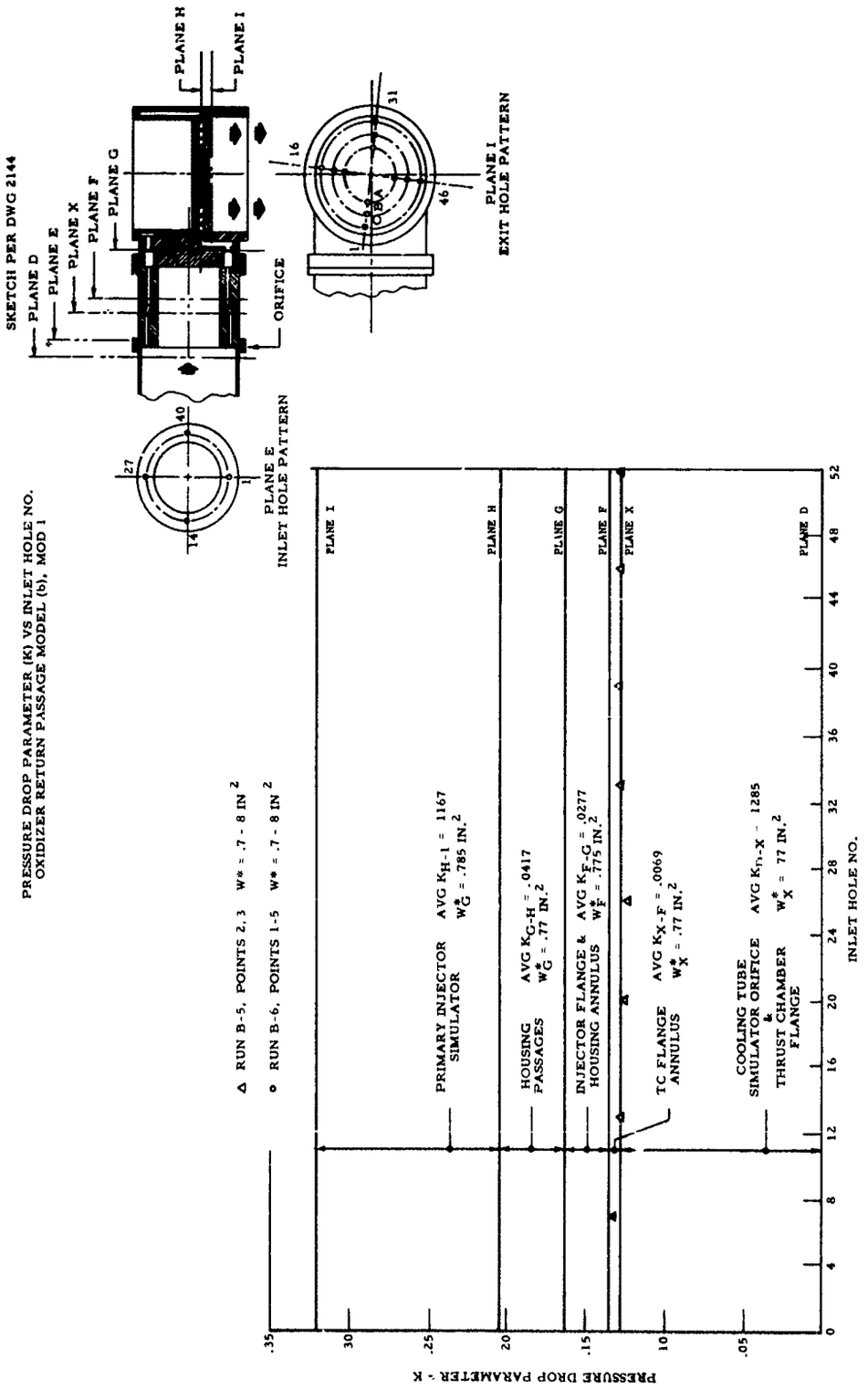

Pressure Drop Parameter vs Inlet Hole Number

Figure VIII-7

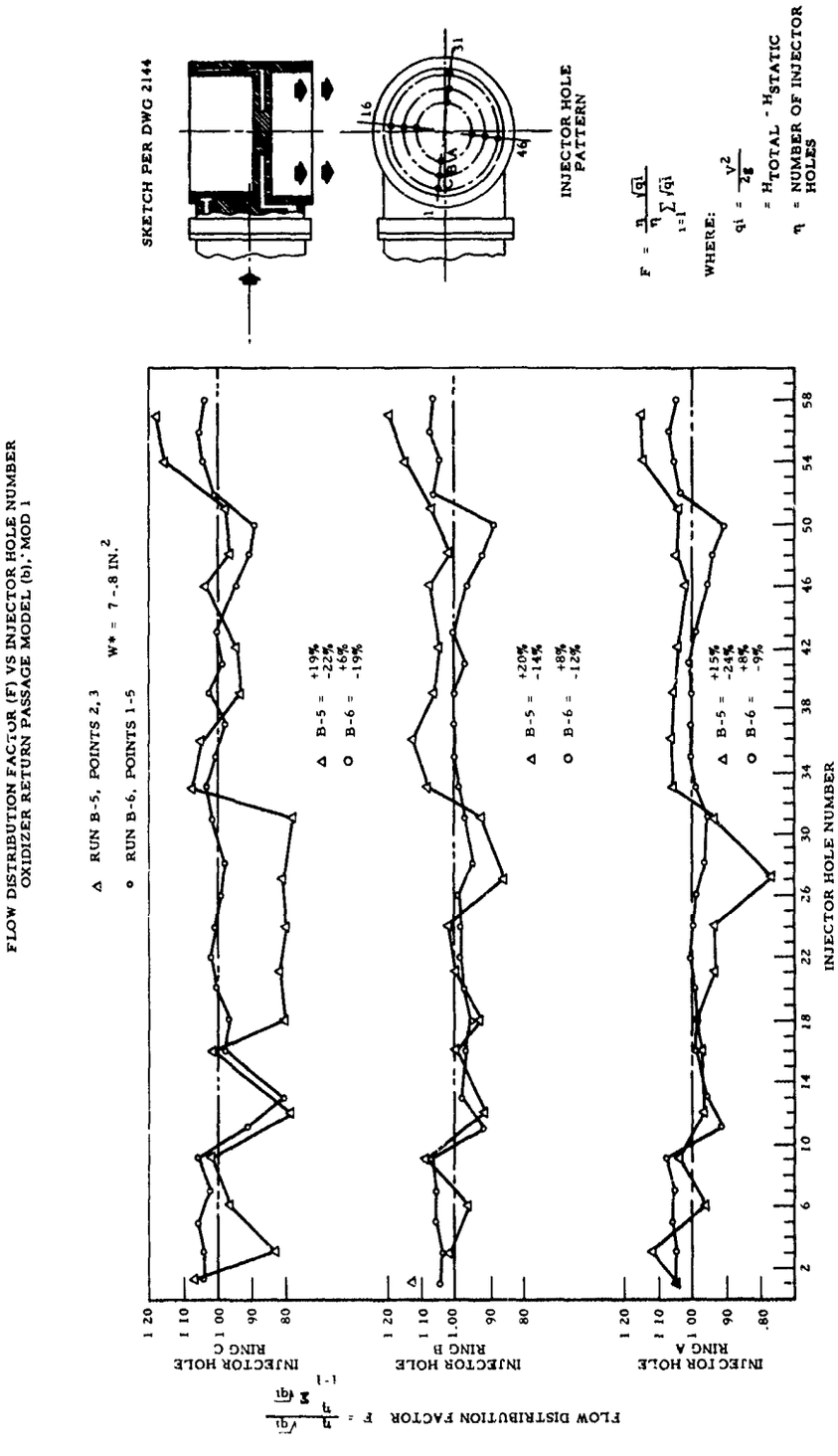

Flow Distribution Parameter vs Injector Hole Number

Figure VIII-8

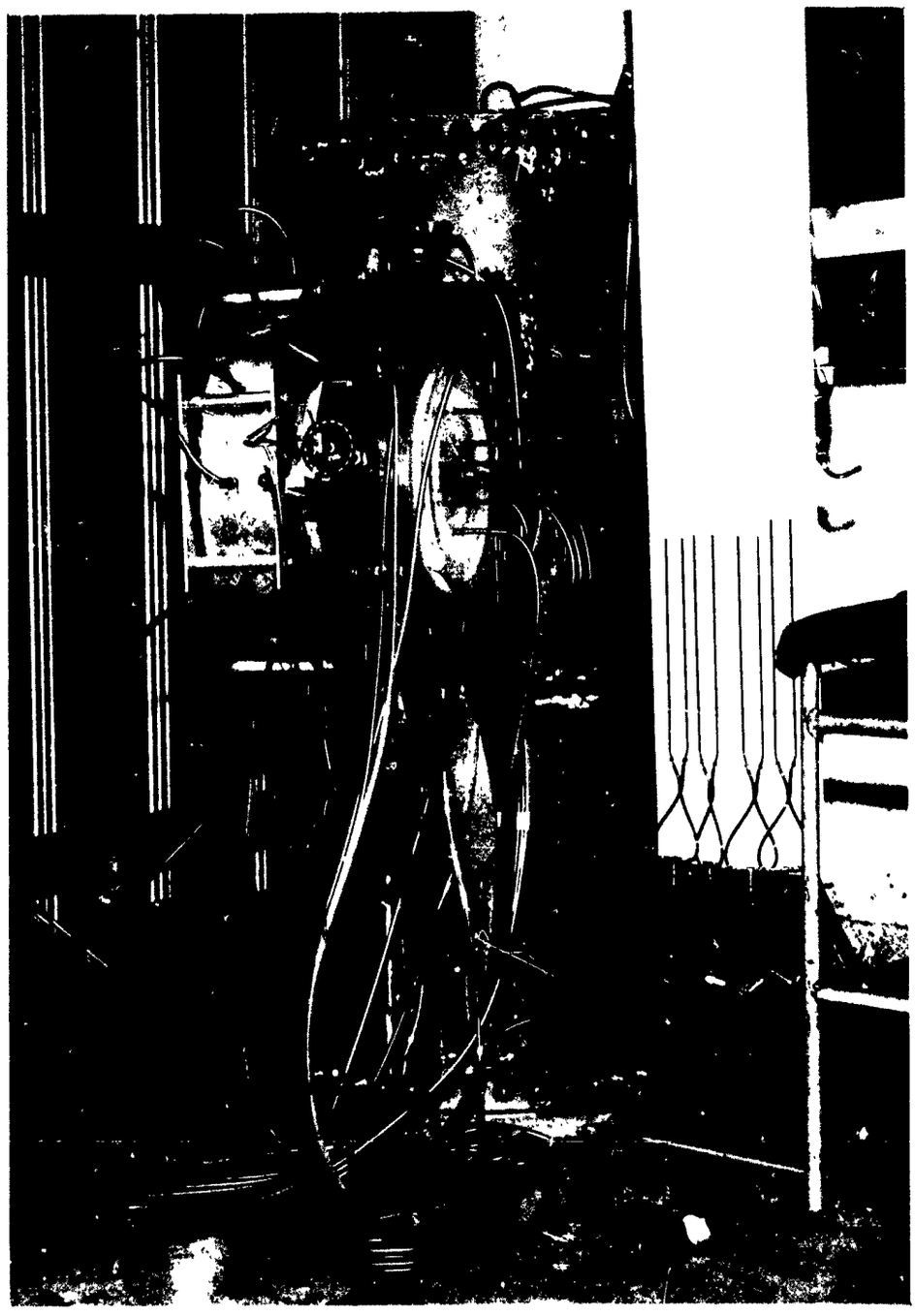

Turbine Inlet Model

Figure VIII-9

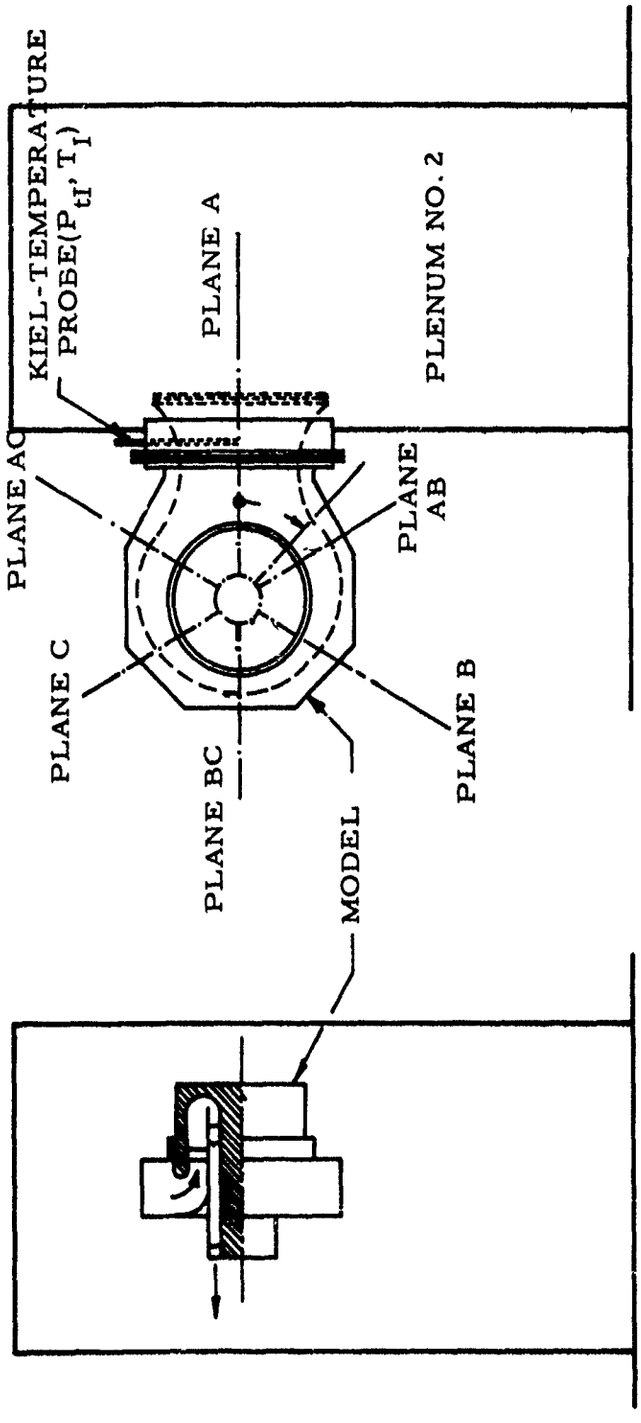

Instrumentation Planes

Figure VIII-10

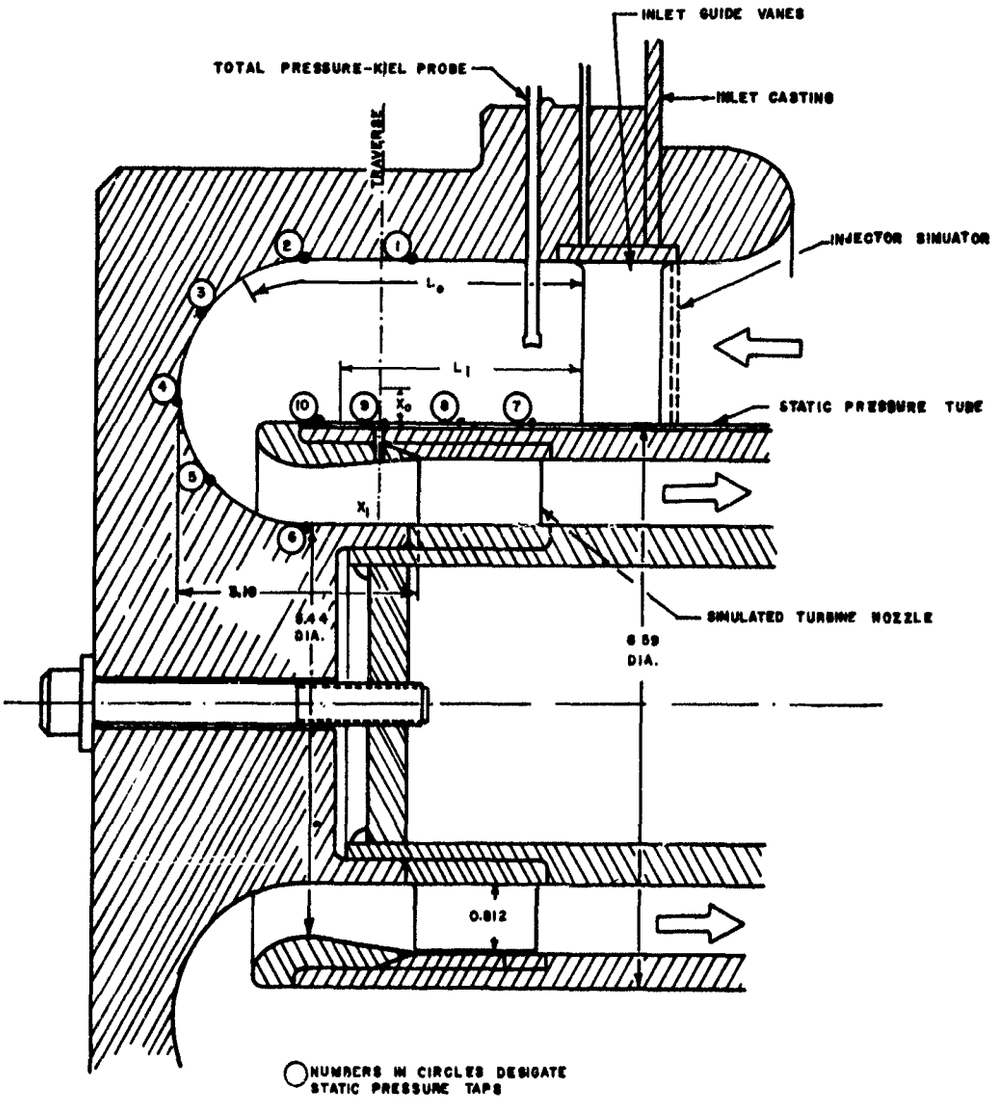

Turbine Inlet Passage

Figure VIII-11

δ= PITCH ANGLE (°) OF FLOW IN MERIDIAN PLANES (POSITIVE PITCH ANGLES δ INDICATE FLOW DIRECTIONS AWAY FROM AXIS)

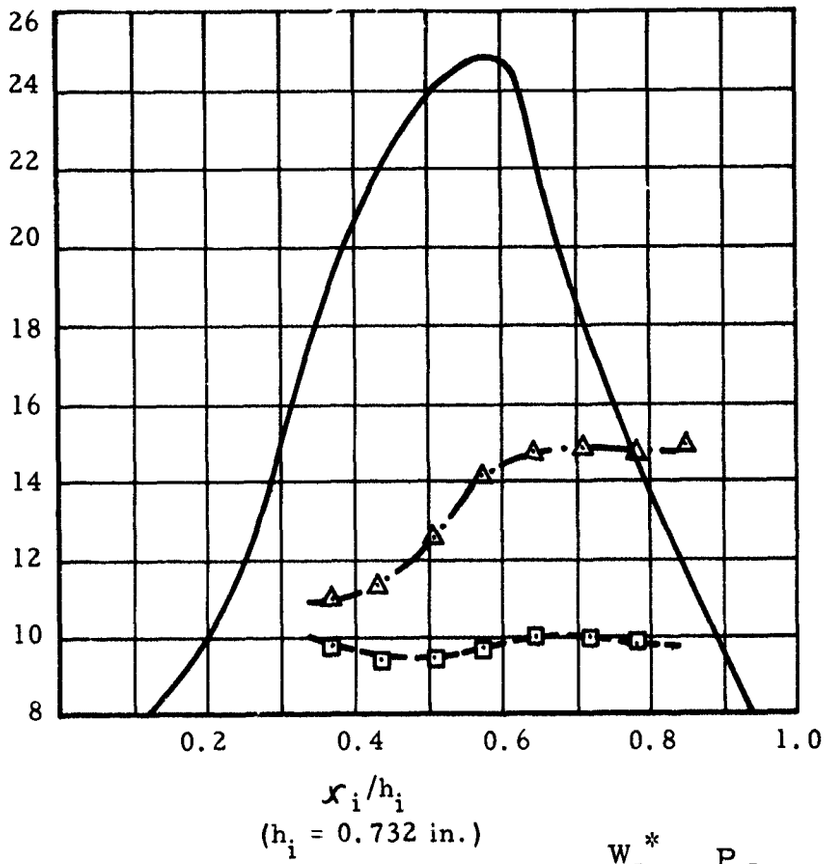

	W_I* (in.^{2})	P_{tI} (PSIA)	T_I (°F)
--□-- WITHOUT INJECTOR SIMULATOR	2.687	15.994	78
—◇— WITH INJECTOR SIMULATOR	2.782	16.475	78

——— WITH INJECTOR SIMULATOR ESTIMATED FROM PHOTOGRAPH OF LAMP BLACK TRACES

Flow Pitch Angle at Turbine Inlet

Figure VIII-12

$W_o^* = 2.697\ IN^2$ $P_{to} = 15.992$ PSIA $T_o = 78°F$

P_{to} = AVERAGE TOTAL PRESSURE IN OUTER ANNULUS

P_t = LOCAL TOTAL PRESSURE IN INNER ANNULUS

$h_i = 0.732$ IN.

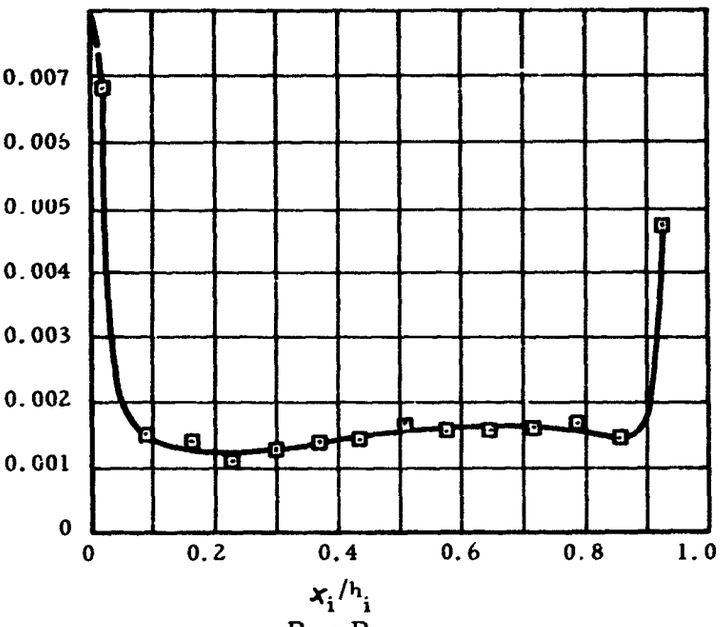

AVERAGE VALUE OF $\frac{P_{to} - P_t}{P_{to}} = 0.0022$

AVERAGE VALUE OF $K = (\frac{P_{to} - P_t}{P_{to}})/(W_o^*)^2 = 0.0003$

Total Pressure Distribution at Turbine Inlet

Figure VIII-13

Turbine Exhaust Model

Figure VIII-14

Flow Distribution Concepts

Figure VIII-15

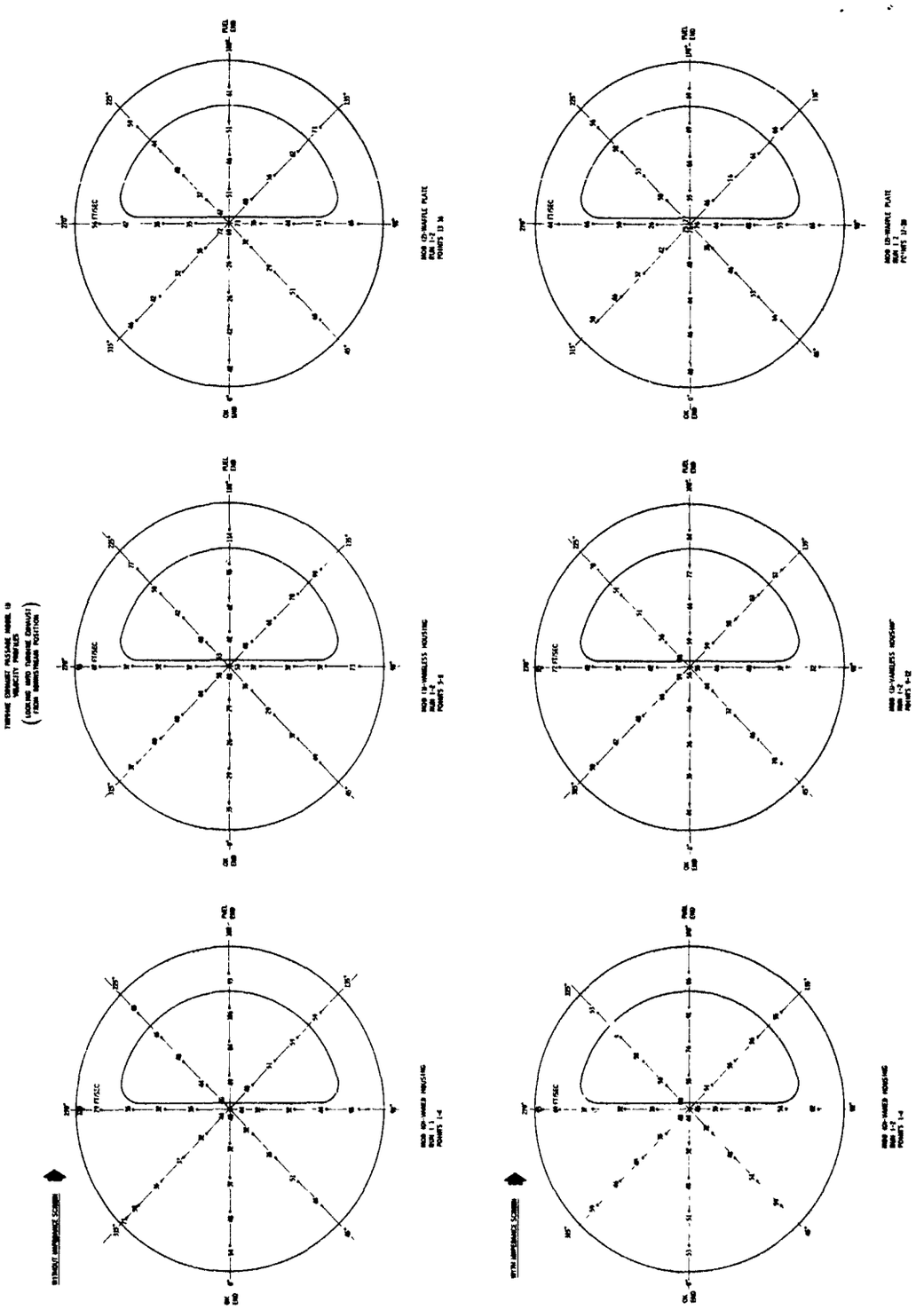

Flow Distribution

Figure VIII-16

Nozzle Performance Program Summary

MODULE FAILURE

MODEL / λ	60	120	250	500	1000	CONFIGURATION
2	0	0	0	0	0	ONE OUT
2	0	0	0	0	0	TWO OPPOSED OUT
2	0	0	0	0	0	TWO ADJACENT OUT

15 TESTS

ENGINE THROTTLING

MODEL	MODULES OUT	THROTTLE RATIO	MAX AVAILABLE
1A	8	0.4	○○○
	12	0.6	○○○
	16	0.8	○○○
2	4	0.2	○○○
	8	0.4	○○○
	12	0.6	○○○
	16	0.8	○○○

21 TESTS

PERFORMANCE SIMULATION AND OPTIMIZATION

MODEL / T	60	120	250	500	1000	2000	OBJECTIVE
1A	○	○	○	○	○	○	CONTOURED-WEDGE IES
2	○□	○□	△△△○□	○□	△△△○□	○□	AXISYMMETRIC IES
2A	○	○	○	○	○	○	IES-SKIRT MERGING STUDY
2B	○	○	○	○	○	○	SHORTENED-SKIRT STUDY
2C	○	○	○	○	○	○	CANT-ANGLE STUDY < MODEL 2
2D	○	○	○	○	○	○	CANT-ANGLE STUDY > MODEL 2
3	○	○	○	○	○	○	IES AREA-RATIO STUDY
4	○	○	○	○	○	○	CONTOURED-WEDGE PLUG ZERO LENGTH
4A	○	○	○	○	○	○	CONTOURED-WEDGE PLUG FINITE LENGTH

○ NO BASE BLEED 54
□ AMBIENT BASE BLEED 6
△ FORCED BASE BLEED 6
TOTAL NO. OF TEST 66

UNCLASSIFIED

Figure VIII-17

DESIGN PARAMETERS	AEDC PROTOTYPE NOZZLES				SUBSCALE COLD FLOW NOZZLES								
① NOT REQUIRED FOR SUBSCALE PERFORMANCE SIMULATION	CONTOURED WEDGE IES FD	DeLAVAL IES FD	CONTOURED WEDGE IES PLUG		CW IES FD	DeLAVAL IES FD						CW IES PLUG	
② NOT APPLICABLE					1A	2	2A	2B	2C	2D	3	4	4A
③ NOT AVAILABLE			0% ISEN-TROPIC	18.5% ISFN-TROPIC								5% ISFN-TROPIC	13.7% ISFN-TROPIC
N	20	20	20	20	20	20	20	20	20	20	20	20	20
ϵ_0	70.11	64.99	69.86	69.86	36.90	39.55	39.55	39.59	39.55	39.55	39.67	39.59	39.59
ϵ_c	29.38	44.23	②	②	18.31	25.03	25.03	25.07	25.30	24.76	21.22	③	②
ϵ_t	40.73	25.76	63.86	22.04	22.61	14.52	14.52	14.52	14.25	14.79	18.45	34.75	15.15
ϵ_{t1}	5.00	13.39	③	③	3.66	7.63	7.63	7.63	7.39	7.58	9.74	4.64	4.64
ϵ_v	①	①	②	②	②	9.62	②	②	②	②	②	②	②
θ_e	12.77°	14.46°	-34.84°	-13.55°	10.33°	11.19°	11.19°	11.19°	11.19°	11.19°	6.50°	-27.36°	-13.91°
θ_{e1}	33.00°	22.42°	-34.84°	-34.84°	25.00°	19.65°	19.65°	19.65°	15.00°	25.00°	13.20°	-27.36°	-27.36°
IES EQUIV. FLOW MERGING ANGLE	18.30°	②	③	③	18.30°	②	②	②	②	②	②	32.06°	32.06°
IES EFF. FLOW MERGING ANGLE	10.54°	②	③	③	12.65°	②	②	②	②	②	②	17.27°	17.27°
IES INITIAL FLOW EXPANSION ANGLE	33.00°	③	③	③	29.00°	23.89°	23.89°	23.89°	23.89°	23.89°	25.06°	35.00°	35.00°
IES EXIT WALL ANGLE	15.00°	14.63°	③	③	16.00°	12.49°	12.49°	12.49°	12.49°	12.49°	11.66°	21.00°	21.00°
GAP_{IES}/D_{e1}	0.4220	0.1153	③	③	0.4220	0.1153	0.1153	0.1153	0.1123	0.1230	0.1153	0.4220	0.4220
L/R_e	0.4225	0.6397	0.0000	0.8318	0.4919	0.7826	0.7826	0.6452	0.7978	0.7657	0.5909	0.0000	0.7582
L_{e1}/R_e	0.2036	0.1654	③	③	0.1870	0.1803	0.1803	0.1803	0.1803	0.1803	0.2198	0.1872	0.1872
R_b/R_e	0.7622	0.6066	0.9561	0.5567	0.7623	0.6058	0.6058	0.6056	0.6002	0.6126	0.6821	0.9369	0.6186
D_T/R_e	0.0531	0.0534	0.0535	0.0535	0.0717	0.0711	0.0711	0.0711	0.0711	0.0712	0.0710	0.0711	0.0711

CONFIDENTIAL

Figure VIII-18

Nozzle Design Parameters (u)

MODEL 4

MODEL 4A

UNCLASSIFIED

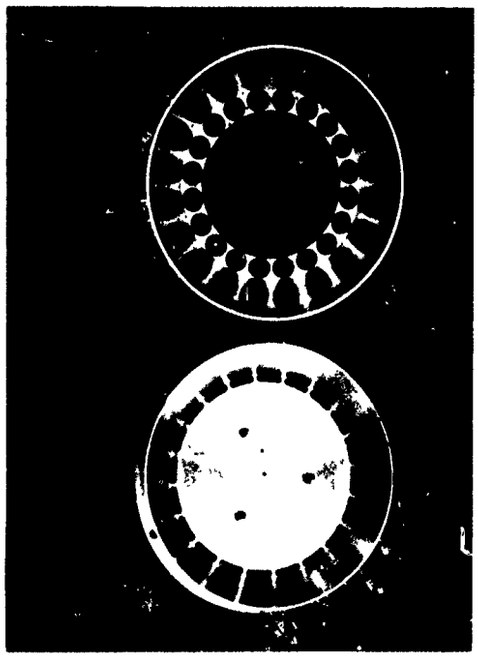

MODELS 1A & 2

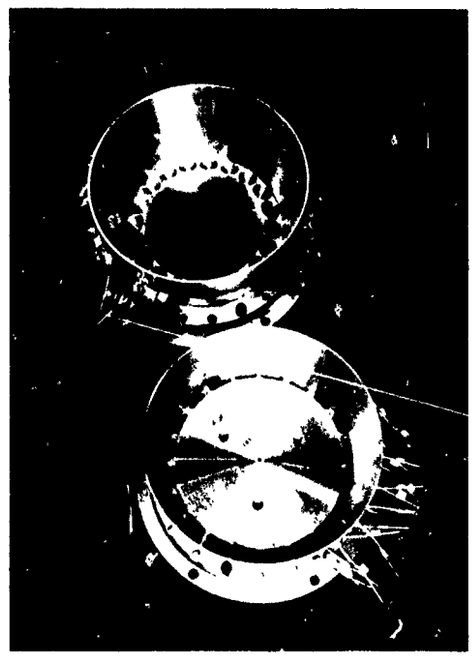

MODELS 1A & 2

Nozzle Performance Models

Figure VIII-19

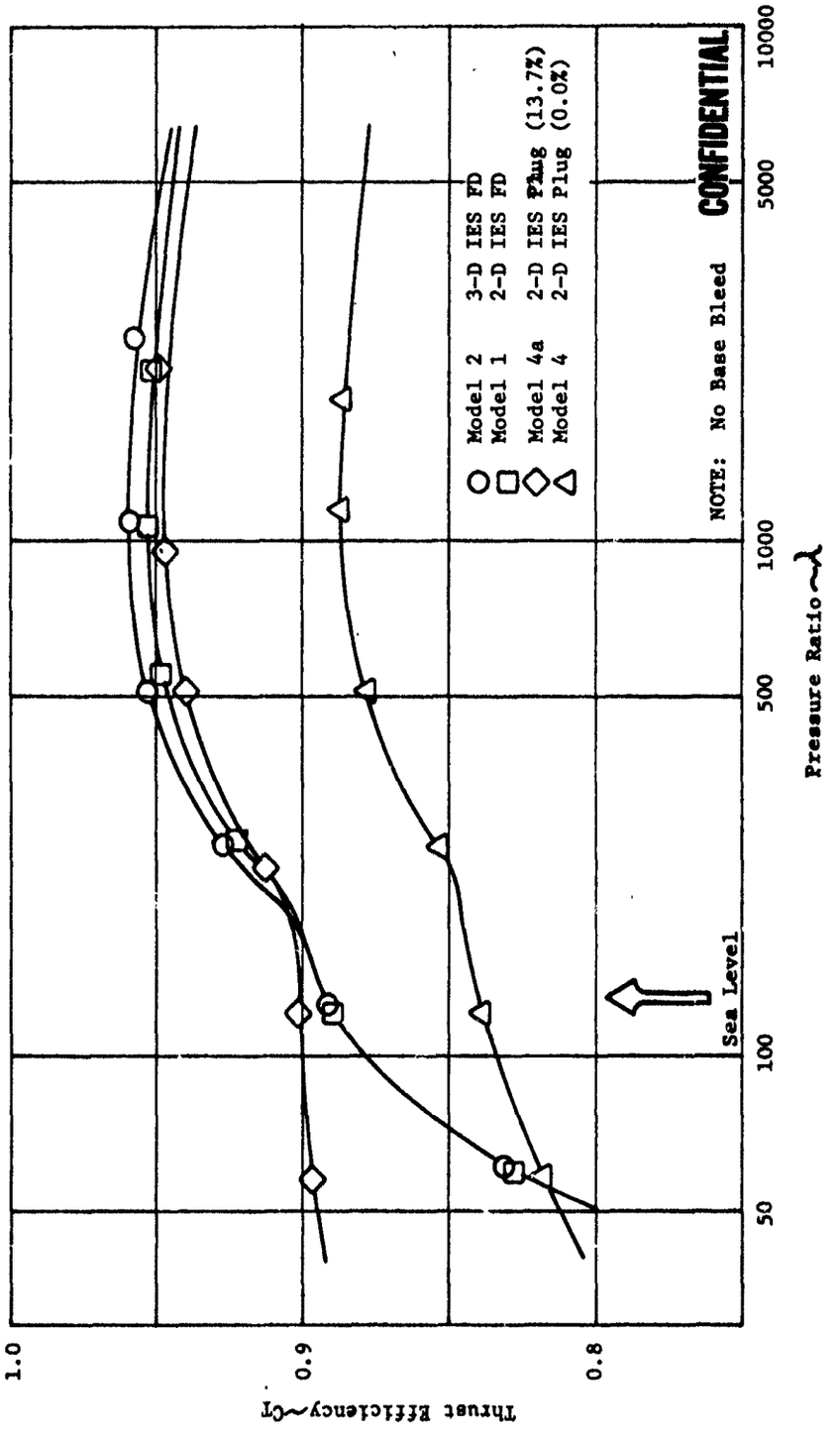

Subscale Nozzle Performance (u)

Figure VIII-20

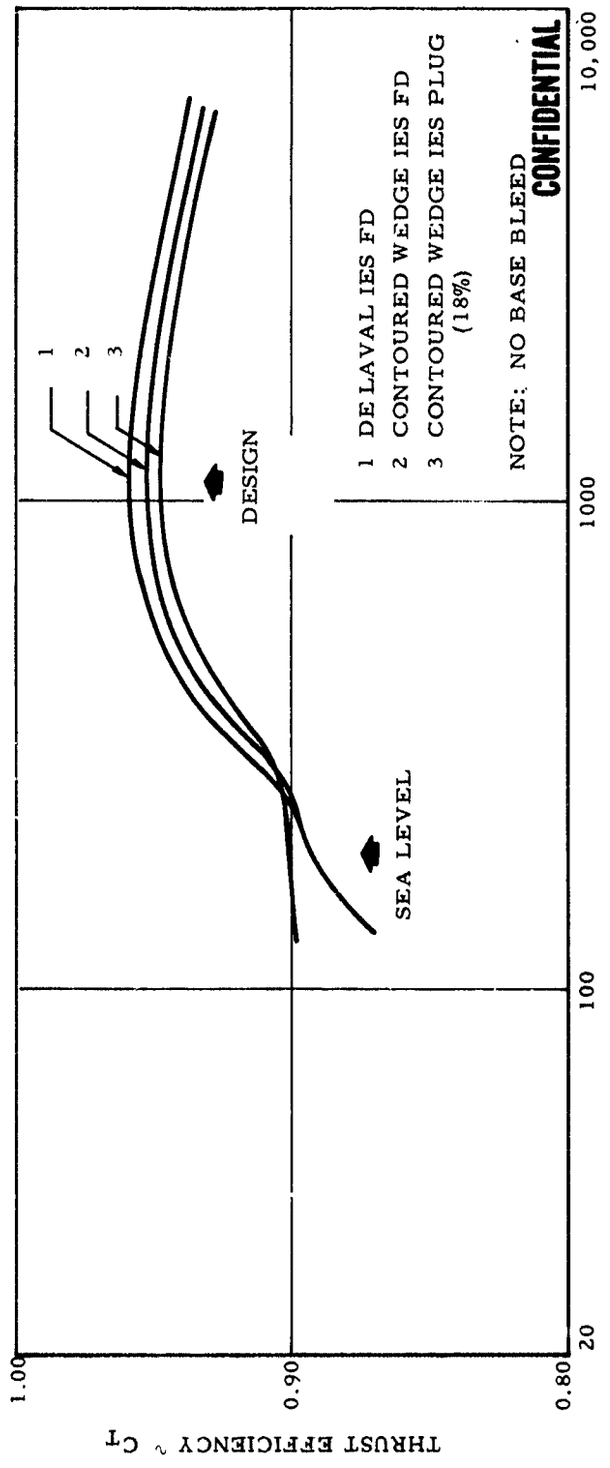

Full-Scale Nozzle Performance (u)

Figure VIII-21

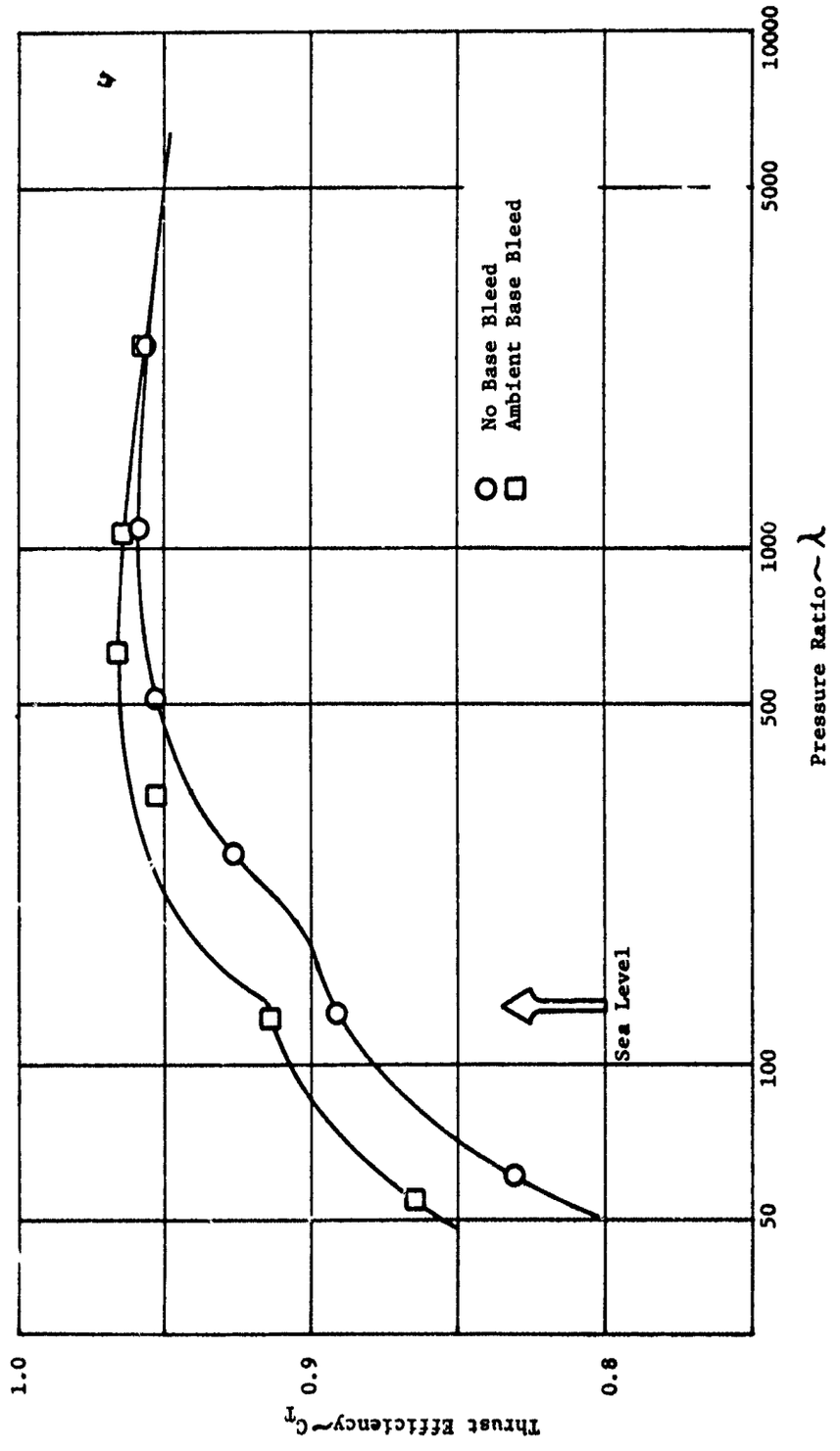

Ambient Base Bleed Effects (u)

Figure VIII-22

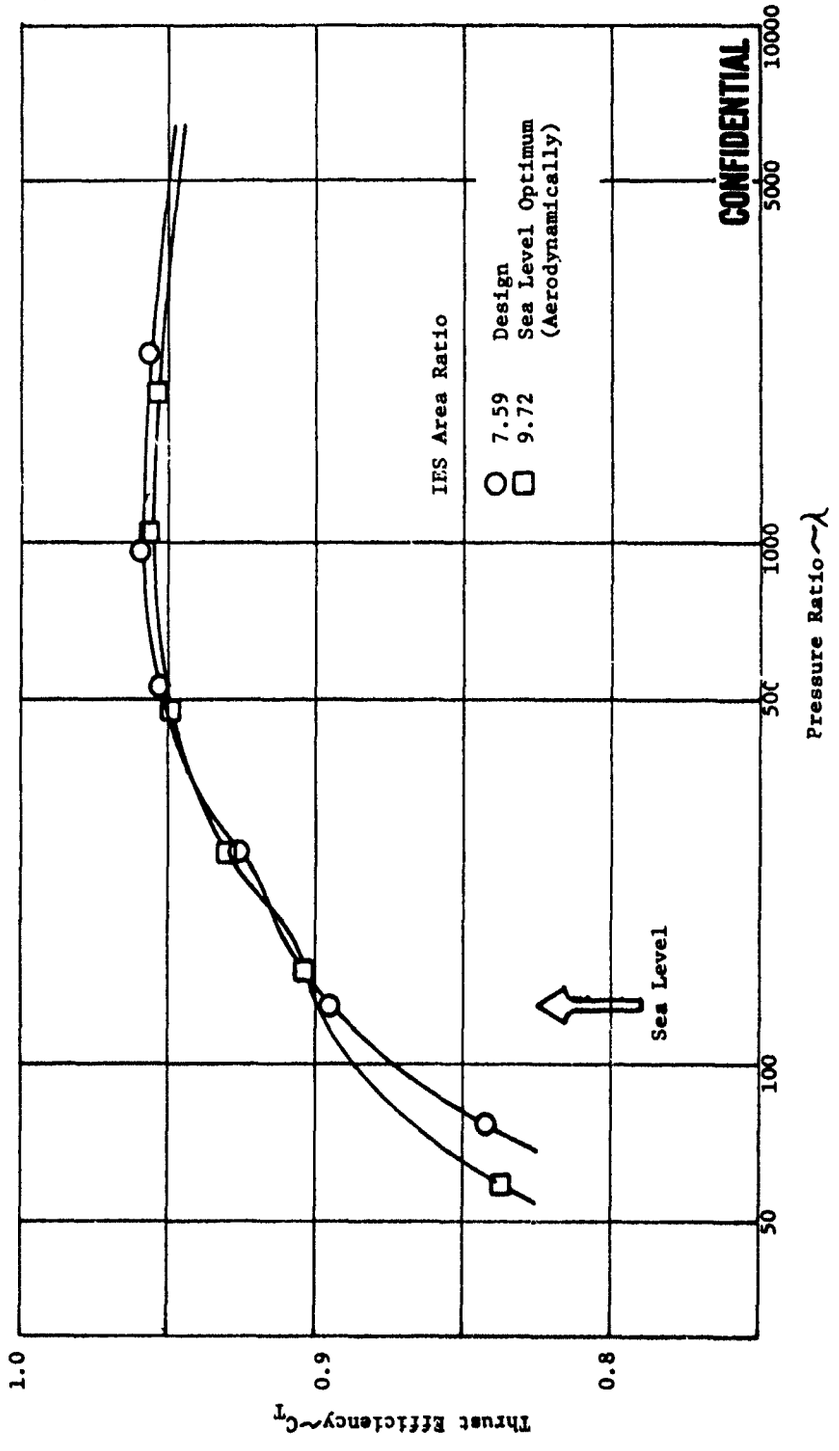

IES Area Ratio Effects (u)

Figure VIII-23

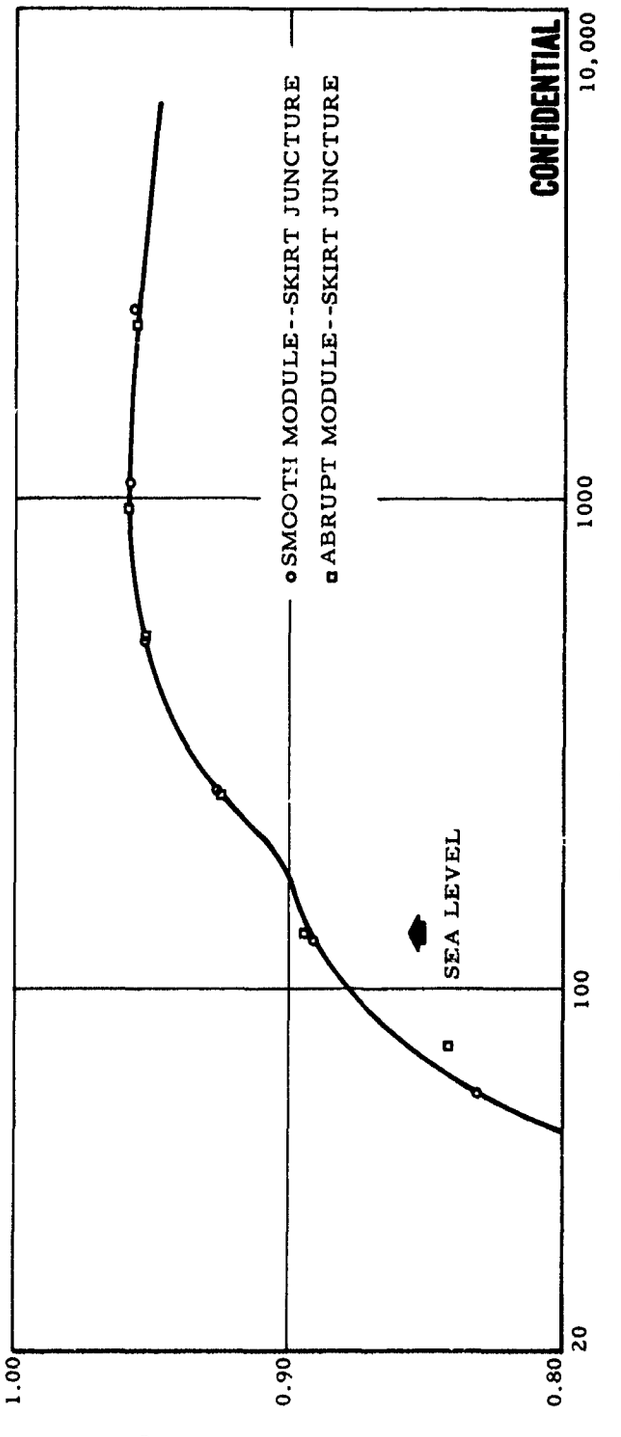

Module-Skirt Merging Angle Effects (u)

Figure VIII-24

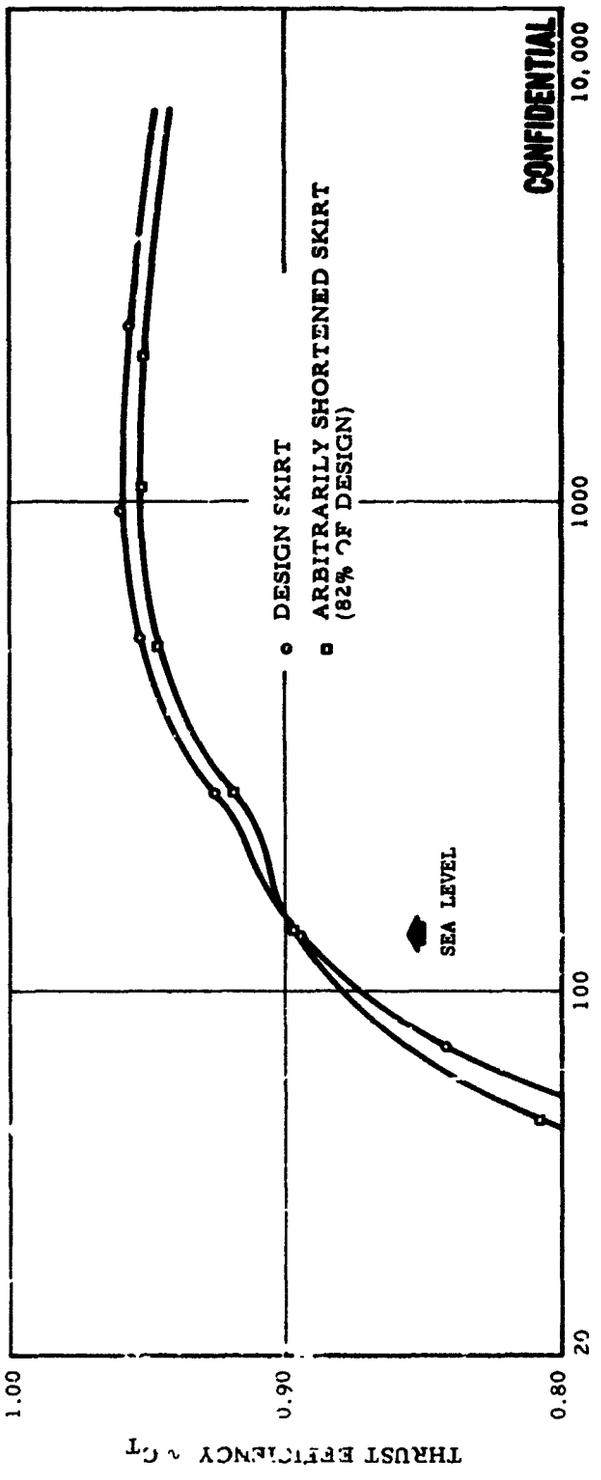

Skirt Length Effects (u)

Figure VIII-25

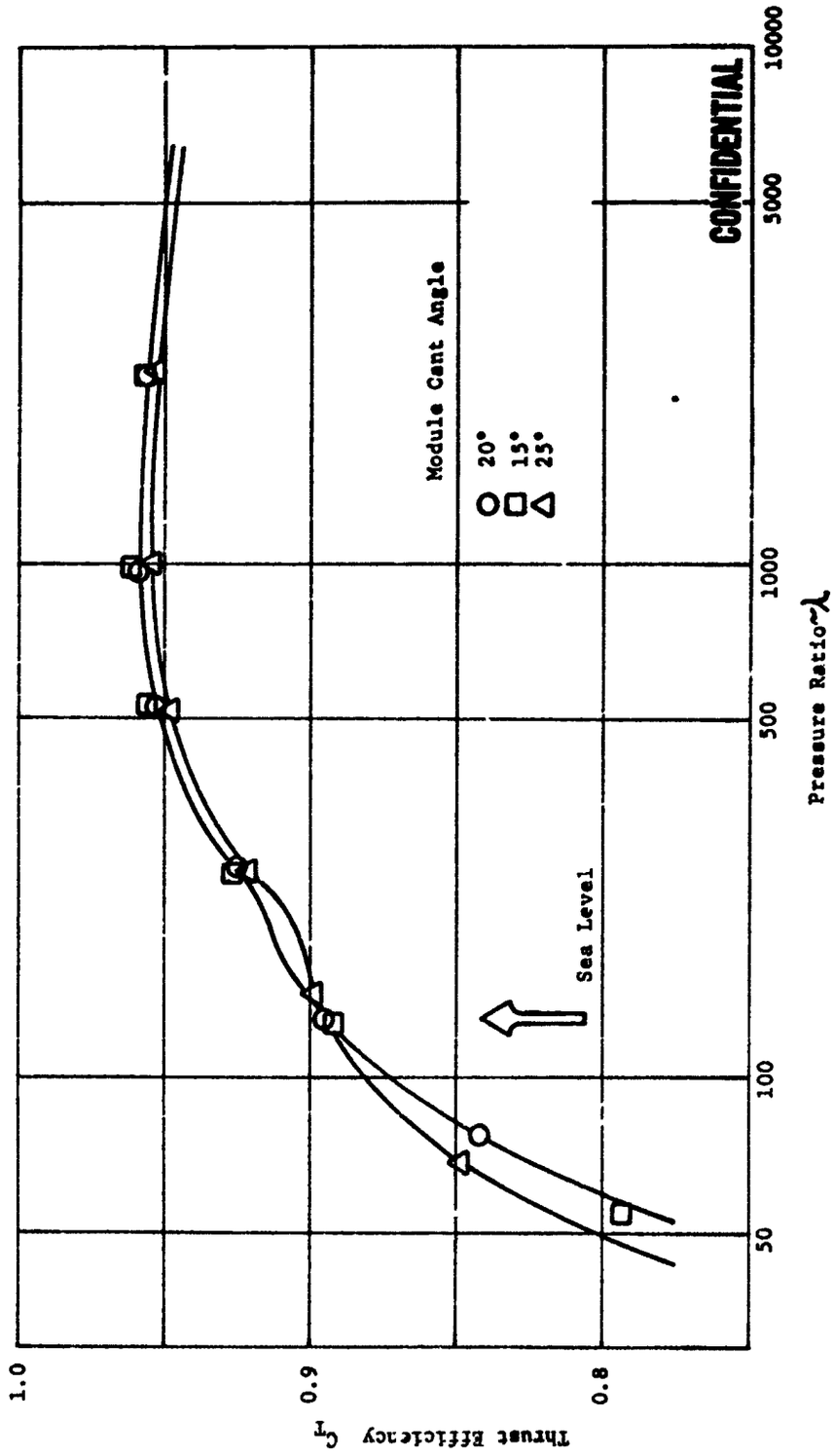

Module Cant Angle Effects (u)

Figure VIII-26

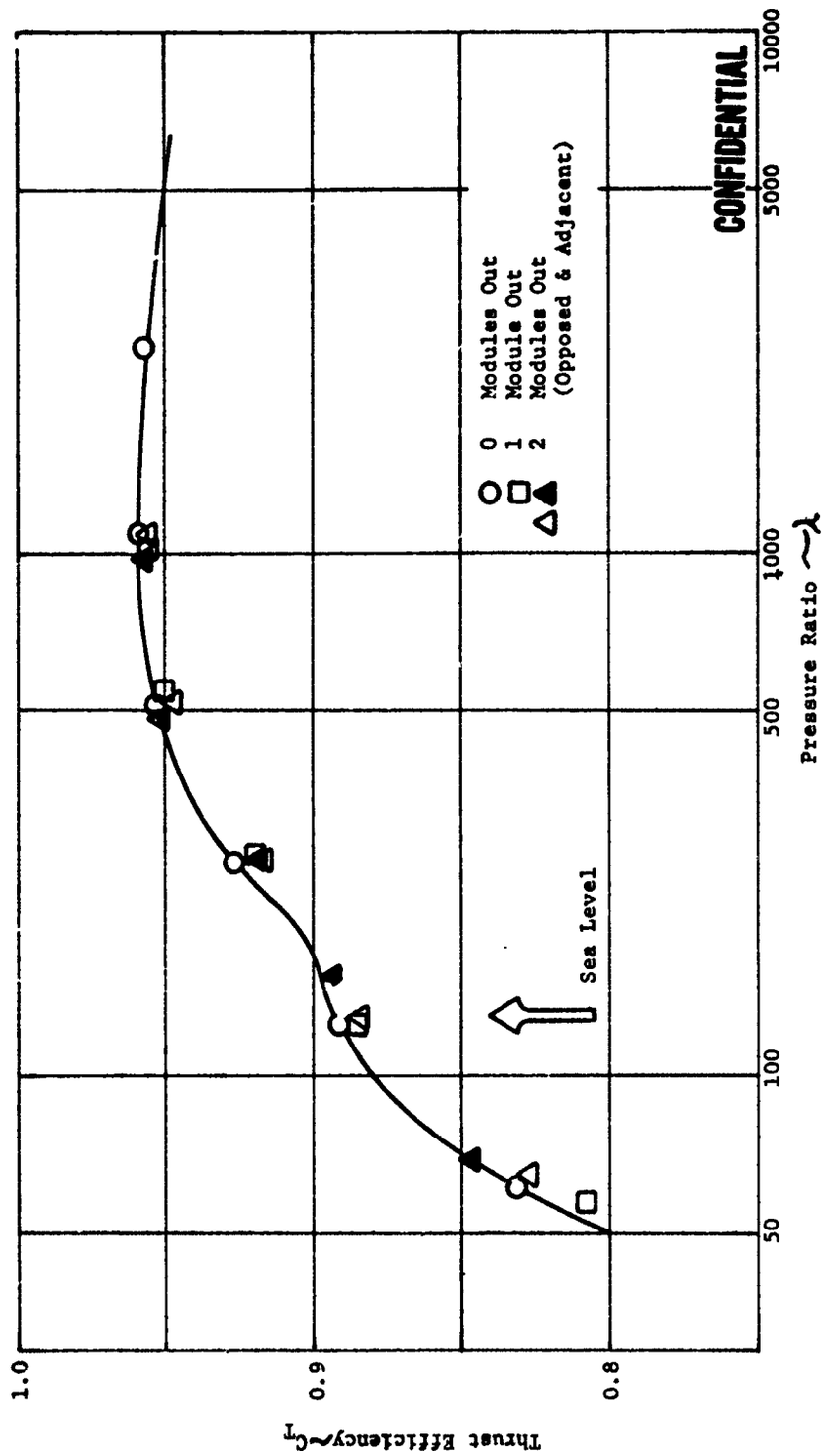

Module-Out Effects on Performance (u)

Figure VIII-27

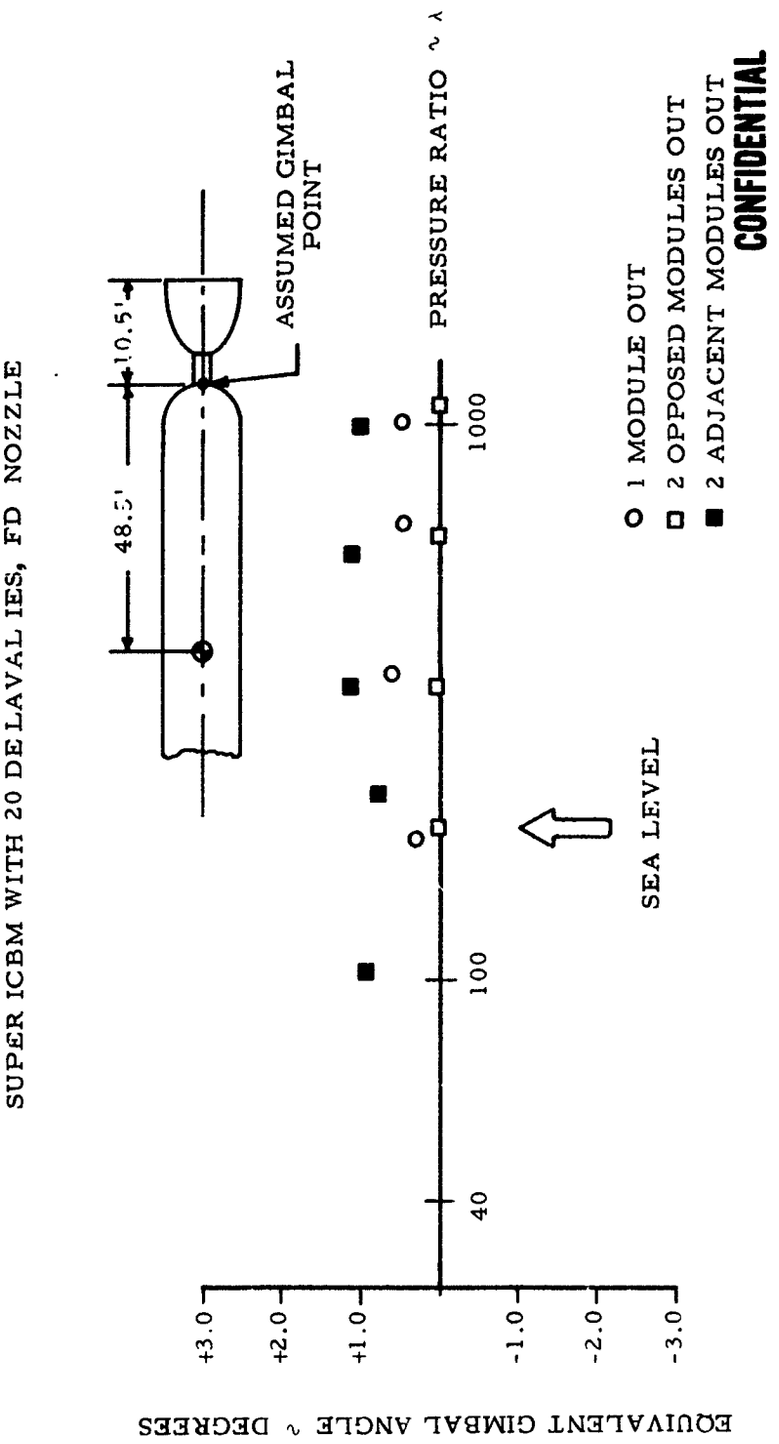

Module-Out Effects on Thrust Vector Angle (u)

Figure VIII-28

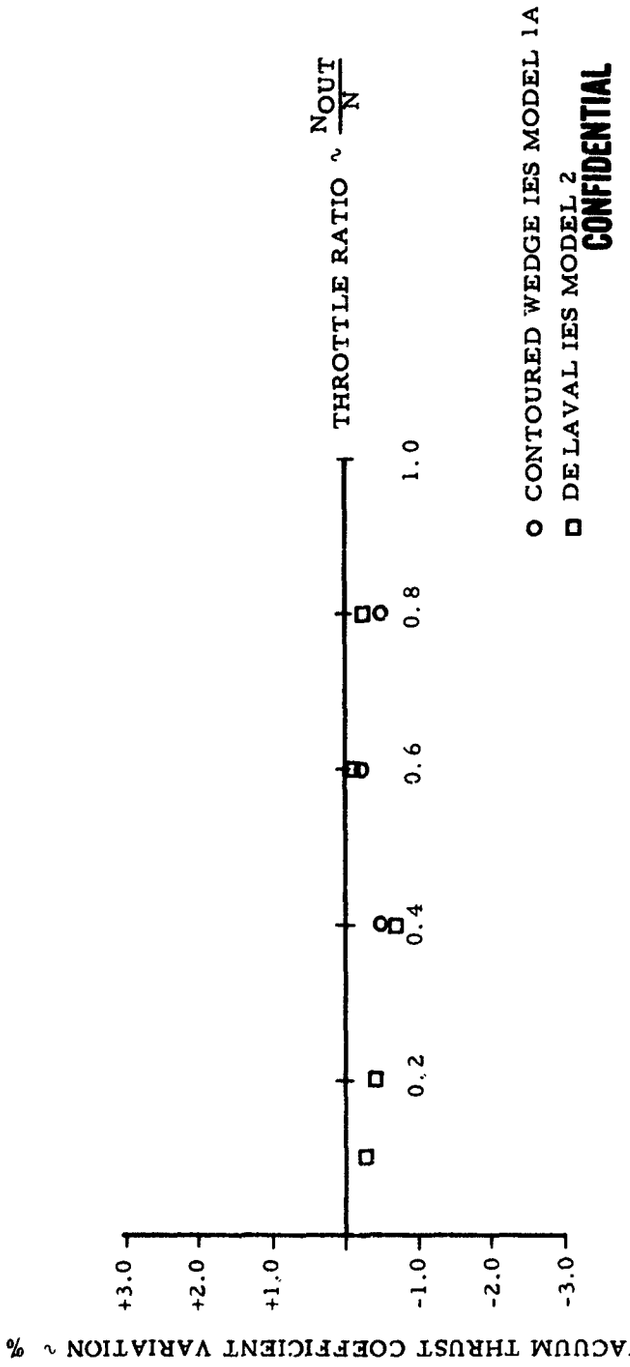

Engine Throttling by Module Shutdown (u)

Figure VIII-29

INLET VIEW

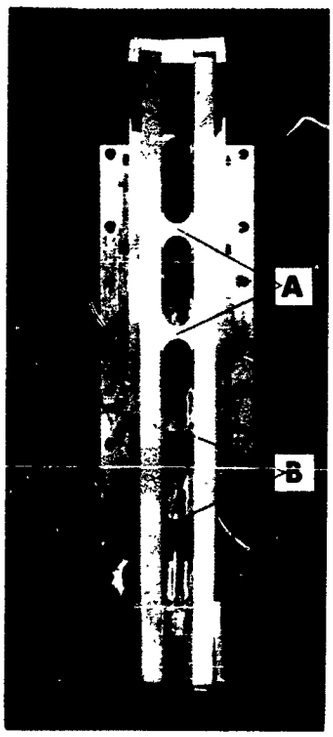

EXIT VIEW

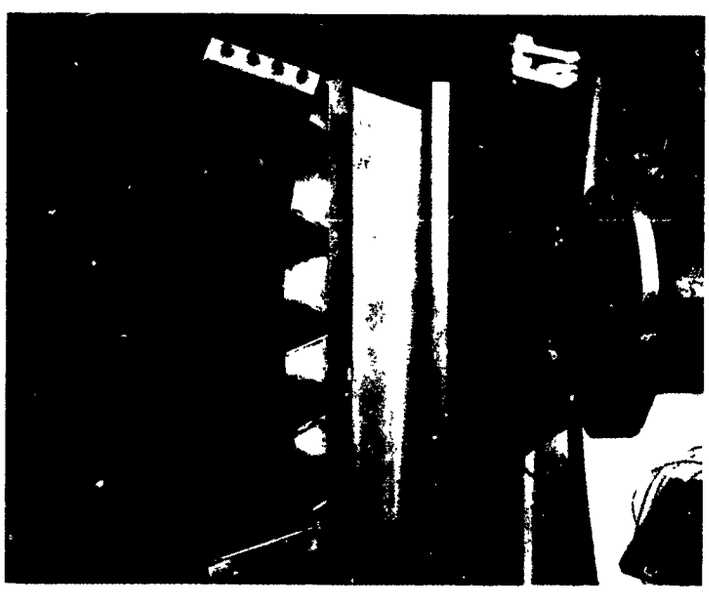

SIDE VIEW

Model 2-D

Figure VIII-30

RUN NO.	P_t PSIA	T_t °R	$Re^* \times 10^{-6}$	PRESSURE RATIO λ	MODULE FLOW CONDITION
			MODEL 1A		
1	102.17	856	.370	62.3	
2	101.13	833	.385	173.1	
3	99.56	847	.369	319.8	FULL FLOW
4	100.11	850	.371	543.9	
5	99.96	844	.379	969.5	
6	100.81	855	.368	1453.0	
7	100.26	847	.372	54.7	
8	101.00	855	.373	112.9	
9	103.00	860	.376	275.5	MODULE OUT
10	101.60	841	.379	481.5	
11	101.05	852	.375	1140.0	
12	100.64	860	.367	1393.0	
			MODEL 2		
1	102.35	855	.374	67.2	
2	100.85	822	.384	128.9	
3	100.91	838	.378	254.8	FULL FLOW
4	100.55	826	.381	527.0	
5	97.54	824	.369	1125.0	
6	92.84	825	.351	1661.0	
7	103.14	814	.399	67.7	
8	101.49	825	.384	167.2	
9	99.74	850	.367	247.0	MODULE OUT
10	100.24	840	.375	547.5	
11	96.59	833	.364	1044.0	
12	101.84	819	.388	1601.0	
			MODEL 2-D		
1	44.74	892	.439	65.79	
2	45.50	908	.433	61.01	FULL FLOW
3	45.26	896	.444	63.47	
6	56.63	877	.566	94.79	
7	53.43	890	.525	88.01	MODULE OUT
8	56.33	893	.553	95.52	

Heat Transfer Test Conditions

Figure VIII-31

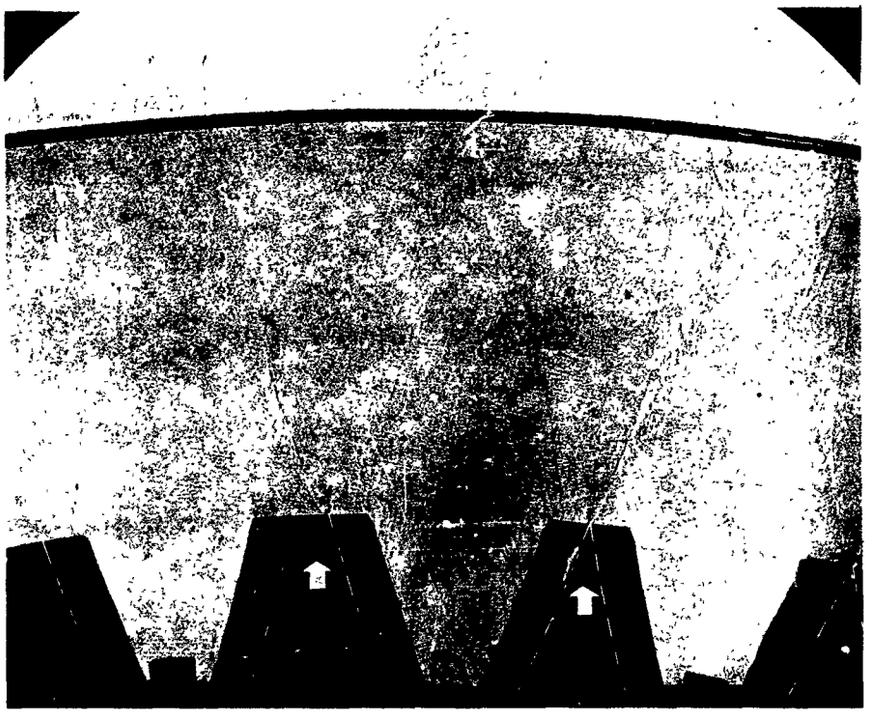

MODULE OUT

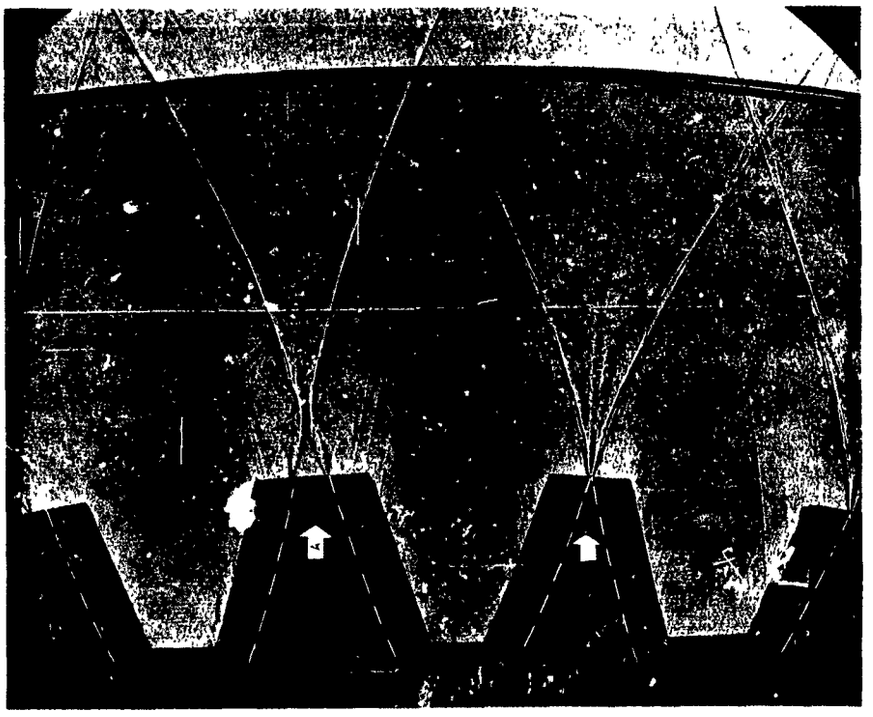

FULL FLOW

Model 2-D Shadowgraphs

Figure VIII-32

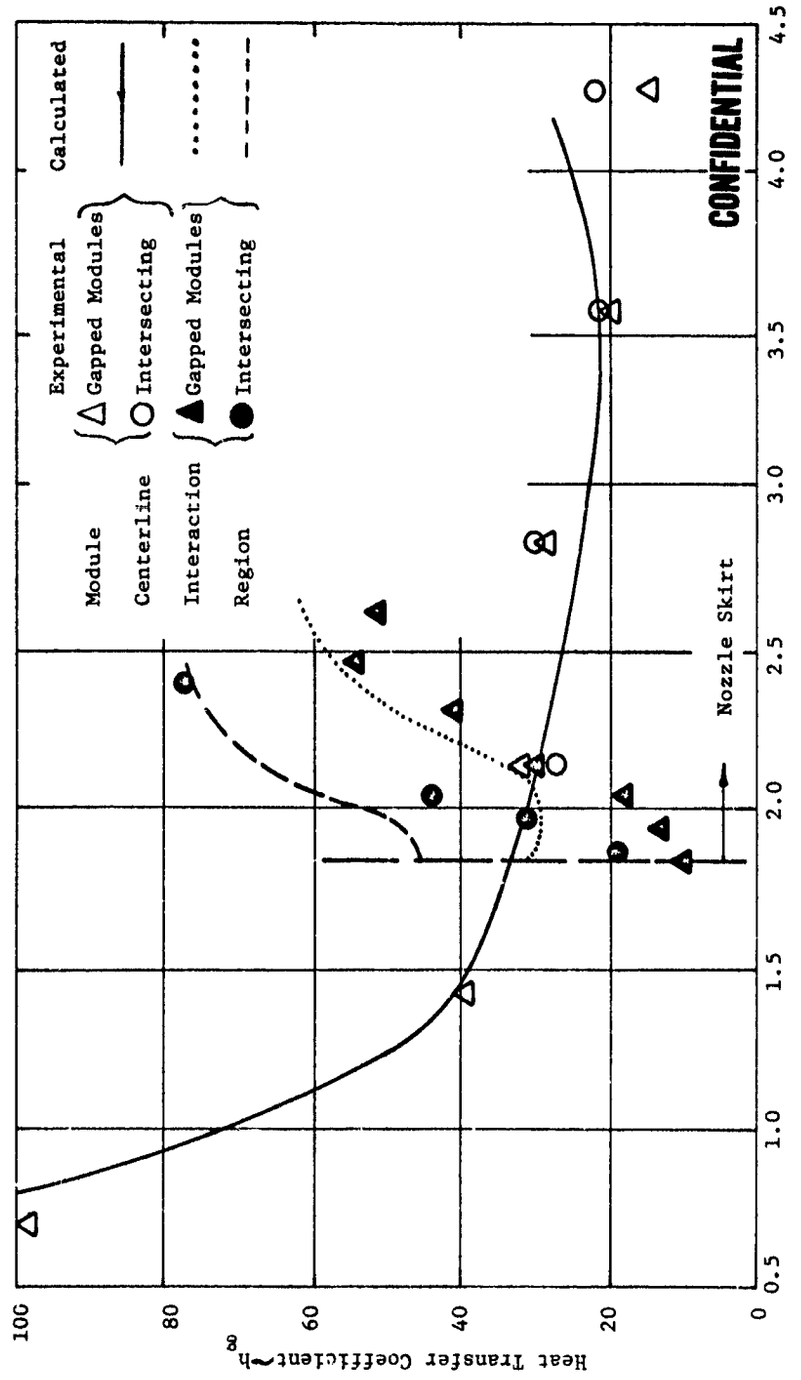

Model 2-D Heat Transfer Coefficients (u)

Figure VIII-33

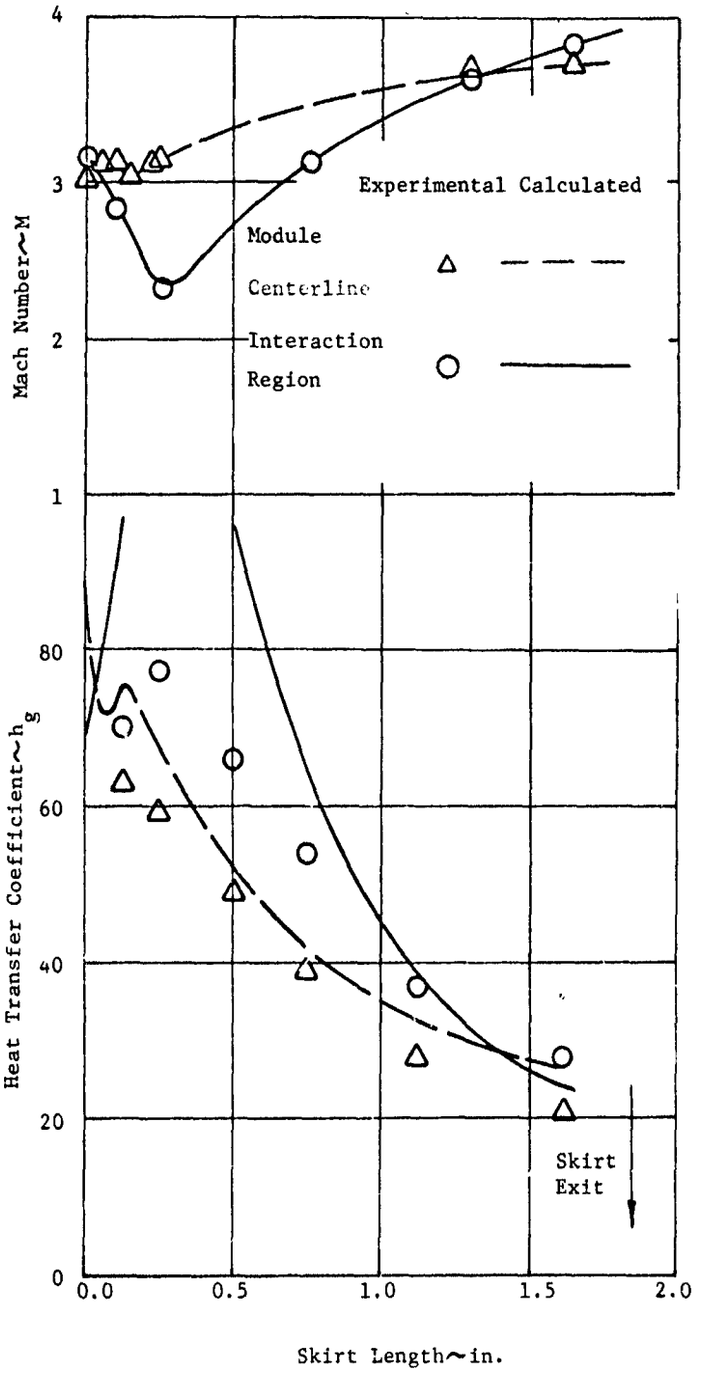

Heat Transfer Model 1a, Skirt (u)

Figure VIII-34

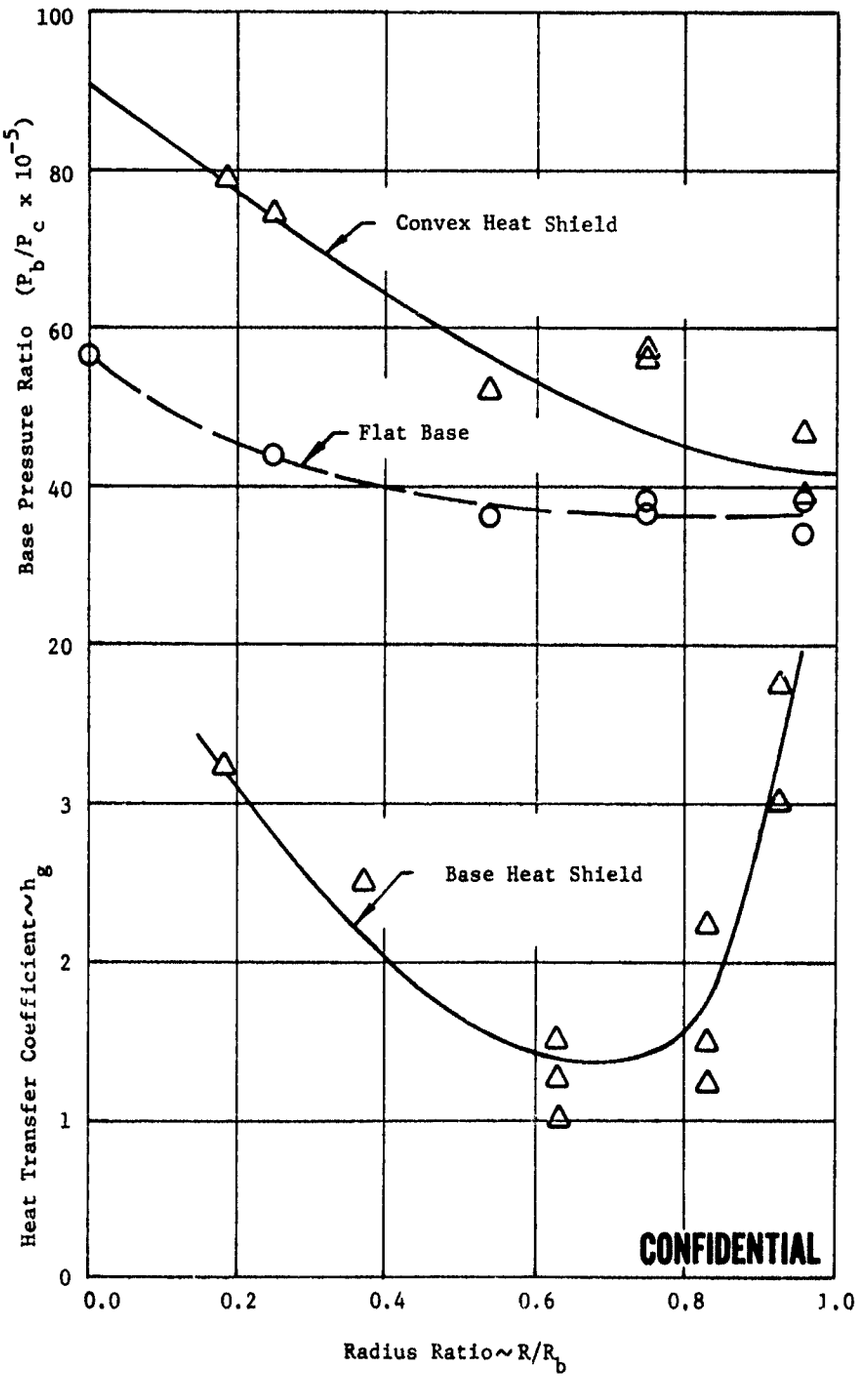

Heat Transfer Model 1a, Heat Shield (u)

Figure VIII-35

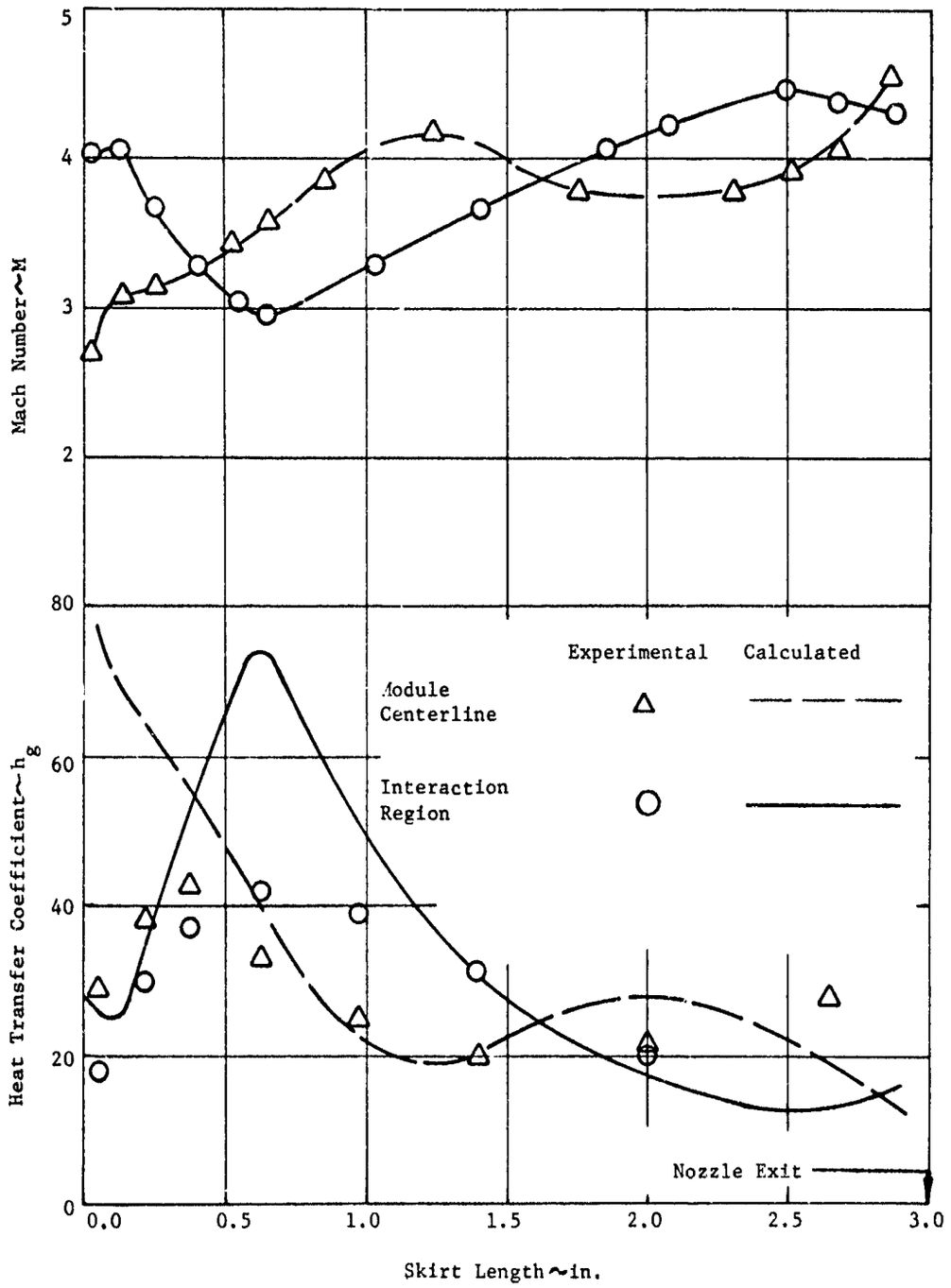

Heat Transfer Model 2 (u)

Figure VIII-36

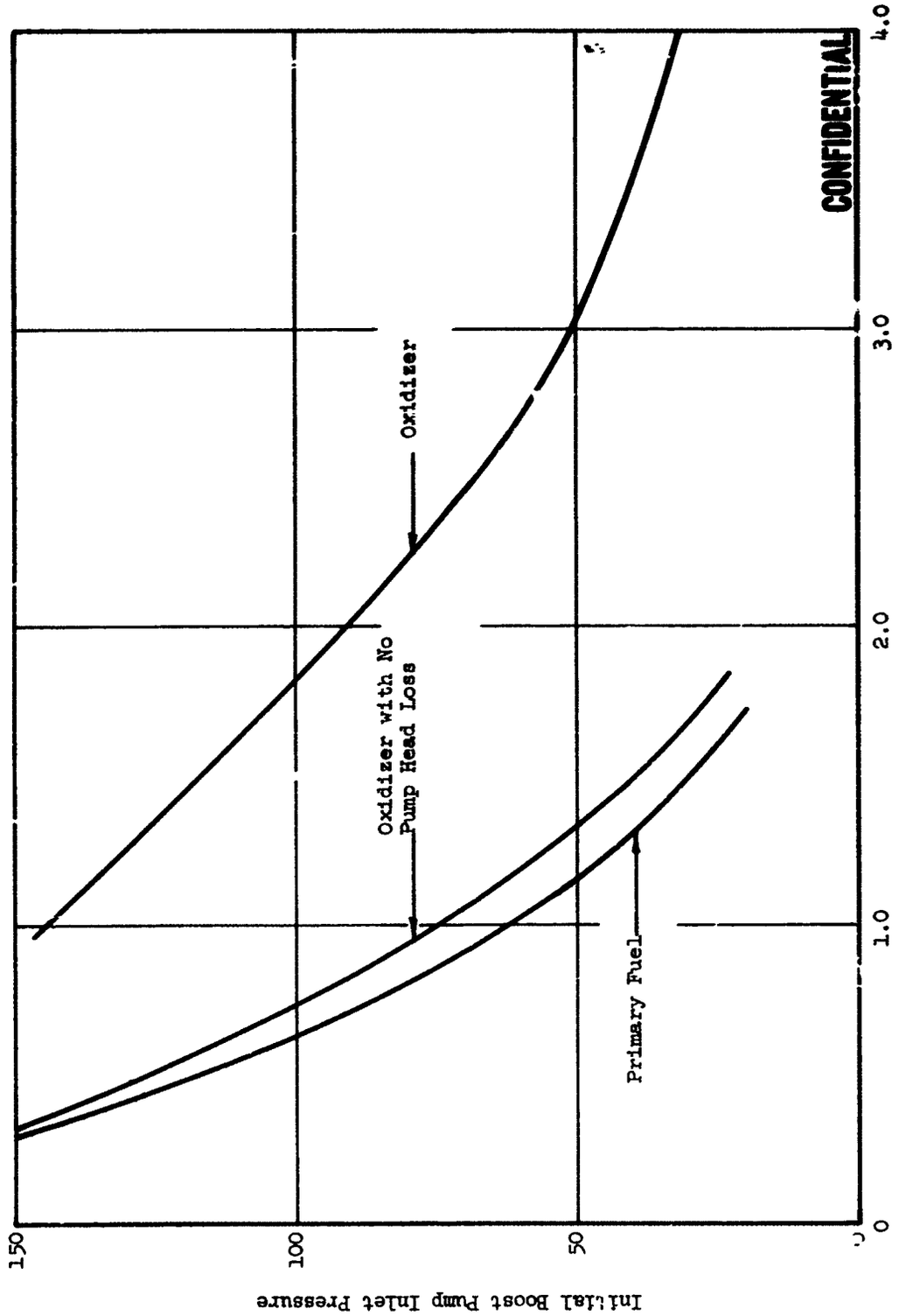

Time from Initial Valve Motion to Partial Outflow from Injector Manifold (u)

Figure VIII-37

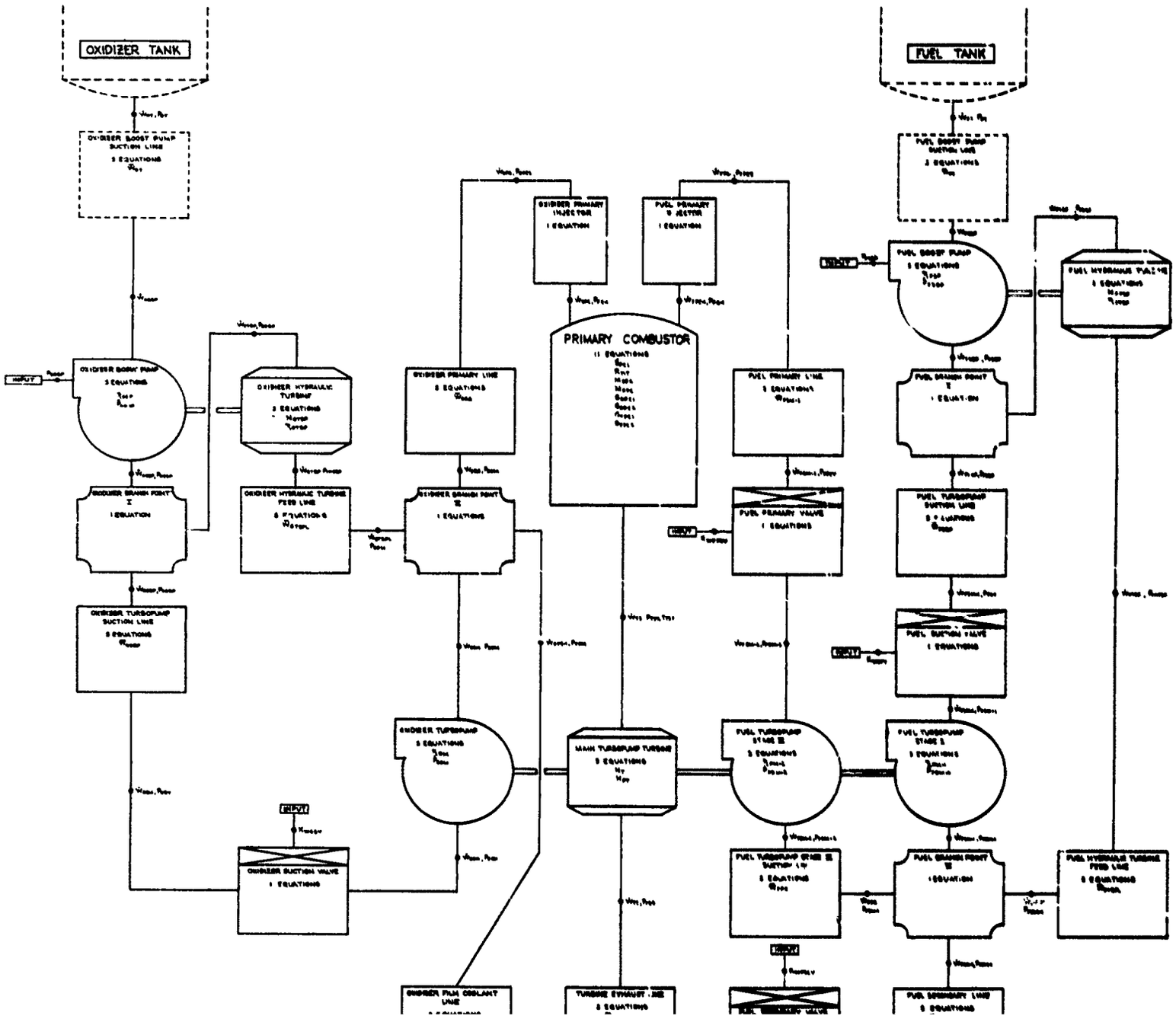
OXIDIZER TANK
FUEL TANK
PRIMARY COMBUSTOR
INPUT

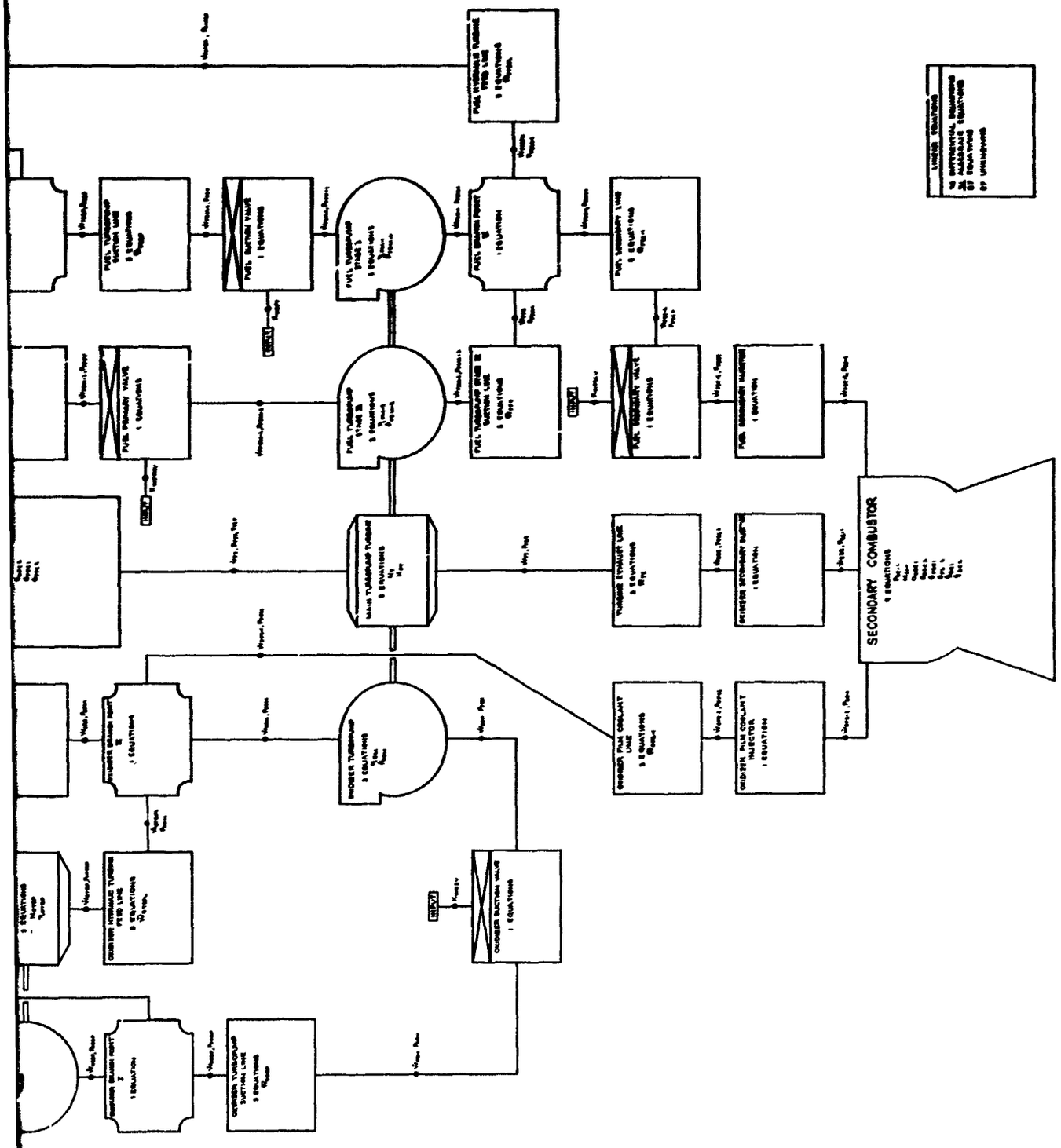

Engine Model Flow Chart

Figure VIII-38